University of Nottingham
UK | CHINA | MALAYSIA

School of Chemistry

Pillar[5]arene based Molecular Machines

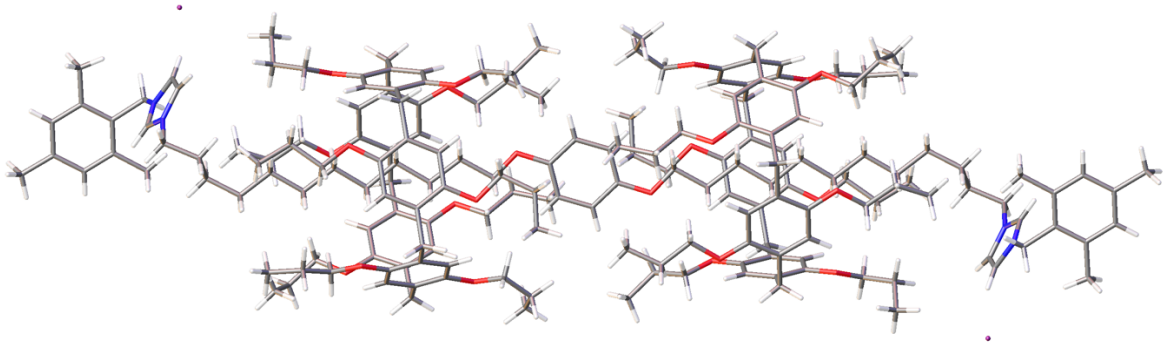

Arjun Patel

Pillar[5]arene based Molecular Machines

Thesis submitted to The University of Nottingham for the Degree of Doctor of Philosophy

Arjun Patel, MSci

2020

Declaration

Except where specific reference has been made to other sources, the work presented in this thesis is the original work of the author. It has not been submitted, either in whole or in part, for any other degree.

Signed: 

Arjun Patel

Date: 25/11/2020

Abstract

Scientists have been trying to shrink large scale technologies into smaller, molecular scales. One such pursuit is that of molecular machines. By utilising a mechanical bond, molecules can be made to perform a task. Examples such as molecular shuttles, motors and switches have been produced and are usually composed of mechanically interlocked molecules (MIMs) such as rotaxanes and catenanes. Due to the lack of chemical bonds between the components, these molecules possess translational and rotational motions with respect to one another, a key aspect as to why MIMs are ideal candidates for molecular machines. A relatively new class of macrocycle, pillararenes have been of interest for the past decade in the construction of mechanically interlocked molecules. This thesis aims to bridge the gap between pillararene based MIMs and their corresponding machine-like behaviour.

On the nanoscale, molecules are constantly in motion and inputting energy does not necessarily equate to fuel being consumed. From the impact of Brownian motion on each individual molecule, controlling the relative positions of components on a MIM is crucial in order for a molecule to perform a task. A series of [3]rotaxanes, when two rings are locked onto a single axle, were synthesised for this purpose using pillar[5]arene as macrocycles through their interactions with imidazolium moieties. Shuttling studies have been conducted on this series and their shuttling motions have been identified in polar and non-polar solvents. Non-polar solvents allow the pillar[5]arene-imidazolium interactions to be enhanced, where pillar[5]arene are found to be situated over these favourable stations on average. Polar solvents disrupt these favourable interactions and the macrocycles are forced into close proximity to each other.

This has been taken a step further with regards to controlling the ring's motion across an axle. A series of [2]rotaxane analogues, when only one ring is locked onto an axle, of the [3]rotaxane series which uses the same pillar[5]arene macrocycles have also been synthesised and their shuttling motions analysed. By freeing up space along the axle, a larger proportion of the track is accessible to the macrocycle. This however, it not necessarily the case when a steric barrier is introduced into the centre of the axle,

meaning the macrocycle has to be pushed energetically uphill to travel along this track. When in non-polar solvents, such as chloroform, the macrocycle is locked onto one side of the axle via the steric barrier. When in polar solvents such as DMSO, the macrocycle is forced closer to the steric barrier via the disruption of the pillar[5]arene-imidazolium interactions and is allowed to hop over the steric barrier without any additional fuel.

A threading and stoppering approach has been taken to assemble the rotaxanes reported in this thesis. By doing so, the number of components required to synthesise a rotaxane is three: a pillar[5]arene macrocycle, an axle and a stopper group. By swapping out components, a toolkit can be adopted to fabricate rotaxanes in order to be photopolymerised. A series of shorter, anthracene stoppered [2]rotaxanes have additionally been synthesised utilising the same pillar[5]arene-imidazole interactions to assemble. The terminal anthracene moieties possess the ability to undergo a [4 + 4] cycloaddition via photoirradiation and thus a polyrotaxanation of the [2]rotaxane species was attempted. In addition, the shuttling ability of the macrocycle was evaluated electrochemically across the series of [2]rotaxanes and the fluorescence of the products probed.

Acknowledgements

I have to start off by thanking my supervisor, Professor Neil Champness for allowing me to work in his lab, pursue a PhD with the freedom of choice for the project and for all the helpful advice provided during my time in B52.

I would not have dreamt of undertaking a PhD had it not been for the advice given to me by members of the lab during my masters year in the group, so I have to thank Nic, Tim, Harry Mac, Ben and Sam for setting me on my endeavours. The friendly atmosphere of B52 at the time made it an obvious choice to stay on but my passion for synthesising rotaxanes was drilled into me by Dr Lixu Yang, and a lot of this project would not have been possible without her handcuff synthesis before the start of this project.

The smooth start during my first few weeks in the lab as a PhD student would not have been possible if it wasn't for Sam, Charlie, Harry Martin, and Connie who made sure I had a space to work in and answered all of my stupid questions after spending the six summer months not using my brain.

The postdocs during my time made sure the lab ran like a well-oiled machine; from the start with Connie and in the end with Sarah and Georgia, but I especially have to thank Nic, for dealing with less than cooperative members of the lab on a near daily basis to keep the ship afloat and also being instrumental in the strides I have made during my time in the lab from his serious discussions about chemistry to terrible puns, but if there is anything I have learnt from Nic, it is this: never skip leg day.

None of the crystallographic work in this thesis would have been possible had it not been for without the talented crystallographers in the department. Dr Will Lewis and Dr Connie Pfeiffer set me on my ways. I especially have to thank Rosemary Young and Dr Stephen Argent for running and solving many of my highly awkward structures.

All of the electrochemical and fluorescence measurements were conducted by Dr Stephen Davies and his expertise helped to flesh out some of the experimental work. Project student Catherine Lee also contributed to some of the electrochemical findings.

The technical staff have been an asset in finishing this thesis. The NMR staff, Kevin Butler and Shazad Aslam, were indispensable in getting quality data, in addition to the long periods of time they spent setting up and running variable temperature NMR studies.

Team rotaxane has been a tremendous help to me over the years and made coming into work on the less bearable days a lot more enjoyable. Phil was a great help to me over the years even though he was deprived of banter when he was younger. Keeping up with Mark and Alex's wittiness was a challenge, but one that worth it. The long conversations about videogames and anime with Nathan and Marysia were always welcomed. A fun fact about them was the one of them is afraid of bread and the other murdered many rats.

I cannot forget the project students I've mentored in my time and I hope Will, Catherine and Sam learnt at least a thing under my wing.

Joe, Jen, Claire, Alessandra and everyone else I encountered over the course of my PhD played a huge roll in my development as a person so I am forever grateful.

Finally I'd like to thank my housemates Adam and Sharad for putting up with me for three and a half years.

Contents

Δ	Heat
ε	Extinction Coefficient
E_{act}	Activation Energy
Φ_f	Fluorescence Quantum Yield
$h\nu$	Photon
λ	Wavelength
24C8	[24]Crown-8
4,4-bipy	4,4-Bipyridinium
Ar	Aryl
B30C8	Benzo[30]crown-8
B42C8	Benzo[42]crown-8
CB-AAC	Cucurbituril-Catalysed Azide Alkyne Cycloaddition
CBPQT^{4+}	Cyclobis(paraquat-*p*-phenylene)
CD	Cyclodextrin
COSY	Correlated Spectroscopy
Cu-AAC	Copper(I)-Catalysed Azide Alkyne Cycloaddition
DCM	Dichloromethane
DEP5A	Diethoxypillar[5]arene
DHP5A	Dihexyloxypillar[5]arene
DMF	Dimethylformamide
DMP5A	Dimethoxypillar[5]arene
DMSO	Dimethyl Sulfoxide
DPP5A	Dipropoxypillar[5]arene
ESI	Electrospray Ionisation
Et	Ethyl
EtOH	Ethanol
EXSY	Exchange Spectroscopy
Fc/Fc$^+$	Ferrocene/Ferrocenium
GOF	Goodness of Fit
HPLC	High Performance Liquid Chromatography

Me	Methyl
MeCN	Acetonitrile
MIMs	Mechanically Interlocked Molecules
MOF	Metal Organic Framework
MS	Mass Spectrometry
NDI	Naphthalene Diimide
NHC	N-Heterocyclic Carbene
nHex	Normal-Hexyl
NMR	Nuclear Magnetic Resonance
NOESY	Nuclear Overhauser Effect Spectroscopy
nPr	Normal-Propyl
Ox	Oxidation
PDI	Perylene Diimide
PEG	Poly(Ethylene Glycol)
Red	Reduction
SAM	Self-Assembled Monolayer
TFA	Trifluoroacetic Acid
TLC	Thin Layer Chromatography
TOF	Time of Flight
UV	Ultraviolet
Vis	Visible
Vs	Versus

Chapter 1:

Introduction

Chapter 1: Introduction

1.1 Supramolecular chemistry

Two Nobel prizes in chemistry have been award for macrocyclic supramolecular chemistry. The first was in 1987, awarded to Jean-Marie Lehn, Donald Cram and Charles Pederson:

"for their development and use of molecules with structure-specific interactions of high selectivity."

The molecules were capable of binding ions and neutral guests such as solvent molecules and their biomimetic nature allowed for specific and selective binding. Pederson's contribution was the synthesis and selective cation binding of crown ethers.[1] Lehn developed the even more selective cryptands[2] and Cram built on these principles to synthesise carcerands where the guest molecule was unable to escape from the host after complexation.[3] The principles outlined were used as the basis for host-guest chemistry for years to come, ultimately leading to a Nobel prize being awarded to Jean-Pierre Sauvage, Fraser Stoddart and Ben Feringa in 2016:

"for the design and synthesis of molecular machines."

By using macrocycles as hosts, long chain molecules could be complexed through a macrocycle and chemically reacted to produce mechanically interlocked molecular architectures. This led to the advent of the mechanical bond, where two or more components were held together by weak intermolecular forces, and in order to separate these components covalent bonds needed to be broken. The first example of these mechanically interlocked molecules were called catenanes which contained two or more interlocked rings leading to Sauvage being awarded the Nobel prize.[4] The mechanical bond was expanded upon by Stoddart through the synthesis of rotaxanes, which were axles threaded through rings.[5]

The nature of these molecules meant that they had moving parts which allowed them to behave as machines as each component could be shifted controllably along the corresponding component. Feringa showed that a machine did not necessarily need to be mechanically interlocked when he synthesised a molecular rotor which span continually in one direction. His team later expanded on this concept by designing and synthesising a nanocar.[6]

1.2 Mechanically interlocked molecules

1.2.1 Rotaxanes

The origins of the rotaxane can be traced back to 1967 when they were first reported by Harrison and Harrison (**Figure 1.1b**).[7] The name they initially suggested for the family of compounds was "hooplane" and their product was formed via statistical threading at only 6% yield, massively favouring the formation of the dumbbell instead. Since their inception rotaxanes have been used as the basis to develop more complicated molecular machines.

[n]Rotaxanes, where n denotes the number of components present within a rotaxane, consist of a macrocyclic component encircling a long chain axle molecule, which is capped on both ends by bulky stopper groups to prevent the macrocycle from slipping off. When no macrocycle is present over the end capped axle, it is known as a dumbbell molecule (**Figure 1.1**). A [2]rotaxane consists of a single macrocycle and a single dumbbell molecule, whereas a [3]rotaxane could have either two macrocyclic components and a single dumbbell or two dumbbells and a single macrocycle.

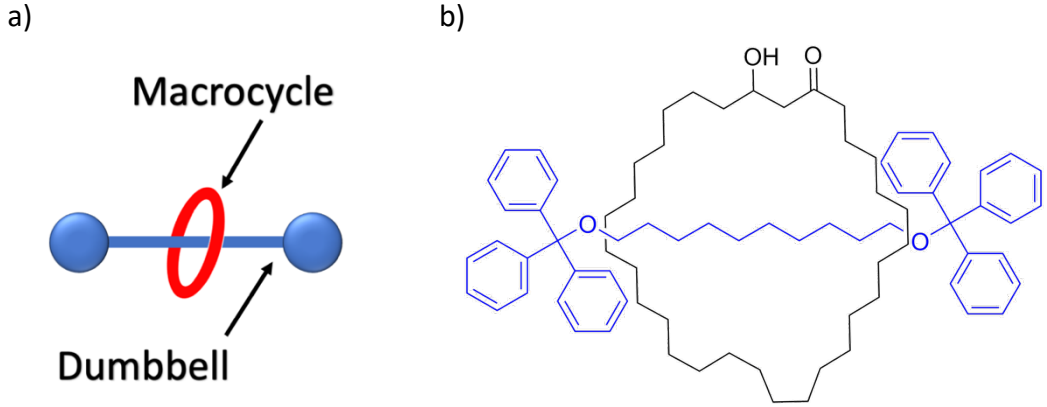

Figure 1.1. A cartoon representation of a rotaxane highlighting the macrocyclic and dumbbell components (a) and Harrison's rotaxane (b).[7]

There are four main ways of synthesising rotaxanes (**Figure 1.2**), the first of which is end-capping, also known as threading and stoppering, where the macrocycle and axle form an inclusion complex, known as a pseudorotaxane, and the ends of the axle are reacted with bulky stopper groups. When only one end of the axle is reacted with the stopper group, due to an asymmetric rod or an already present bulky moiety on one end of the axle, the assembly method is known as snapping. The third way of assembling rotaxanes is known as slipping. This is when a presynthesised macrocycle is forced over a presynthesised dumbbell molecule through heating or via other external stimuli. The fourth way of assembling rotaxanes is known as clipping and this is when a partially assembled macrocycle is complexed to a presynthesised dumbbell molecule with a recognition motif where the macrocycle is then synthesised around the dumbbell.[8]

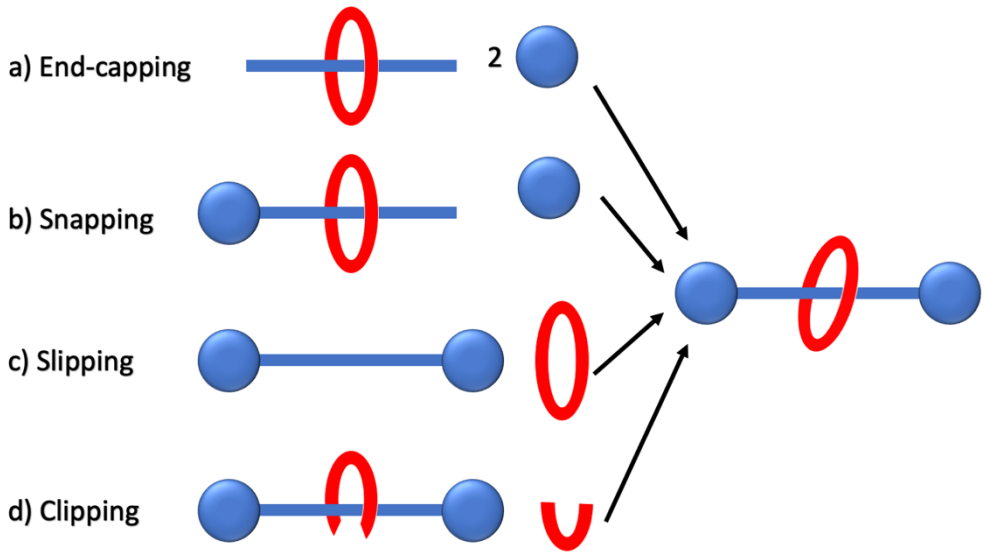

Figure 1.2. Methods of assembling rotaxanes.

More recently, alternative approaches have been taken into assembling rotaxanes. One such example is the active template method (**Figure 1.3**), where metal centres, usually copper, are used to position two halves of a dumbbell inside of macrocycle and facilitate the production of a rotaxane via the formation of new covalent bonds catalytically. The metal centres can easily be decomplexed after the formation of the desired product due to the catalytic nature of the reaction.[9]

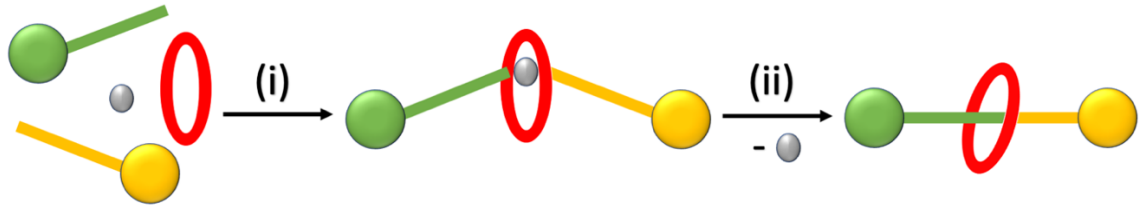

Figure 1.3. Active template method of rotaxane assembly where a catalytic metal centre prearranges the dumbbell fragments around a macrocycle (i), reacting to assemble the rotaxane via the removal of the catalytic metal centre (ii).

1.2.1.1 Molecular machines based on rotaxanes

A molecular machine is a molecule which can undergo mechanical movement in response to specific stimuli. The movement of the macrocycle within a rotaxane has the potential to perform tasks. An interlocked macrocycle has two forms of motion along an axle: the first is shuttling and this is the translational motion of the axle; and the second is pirouetting which is the rotational motion of the macrocycle along the axle.

Translational motion of the most basic form within rotaxanes is known as shuttling. This is when the macrocycle transitions between two degenerate 'stations', therefore this type of rotaxane is known as a shuttle. When these 'stations' are no longer degenerate the macrocycle can transition between them via external stimuli, thus these types of rotaxanes are known as switches. These subsets of molecular machines can be used as components in a greater array in order to build a nano-device.

An example of using the motion of a macrocycle was described by Stoddart and co-workers when they synthesised a molecular shuttle.[10] This consisted of a [2]rotaxane using a cyclobis(paraquat-*p*-phenylene) [CBPQT^{4+}] or the blue box macrocycle which was clipped over a polyether axle with two degenerate 1,4-dioxybenzene stations and stoppered by triiospropylsilyl groups at either end. As the blue box was clipped over the 1,4-dioxybenzene units, they acted as stations for the macrocycle and ^{1}H NMR showed that both aromatic units were degenerately shielded by the macrocycle, shifting their aromatic protons upfield. This suggested that the macrocycle was shuttling from one 1,4-dioxybenzene station to the other over the timeframe of a ^{1}H NMR experiment.

The work on the molecular shuttle was expanded upon by Stoddart and co-workers by developing a molecular switch (**Figure 1.4**).[11] Instead of two degenerate 1,4-dioxybenzene stations along the axle, they used one benzidine and one biphenol station which the $CBPQT^{4+}$ macrocycle can shuttle to and from. Before any alterations to the [2]rotaxane, the favourable station was the benzidine for the blue box, however on addition of trifluoroacetic acid or electrochemical oxidation, the macrocycle shuttled towards the biphenol station as the protonated benzidine become an electronic barrier towards the blue box. This process is reversible as pyridine or electrochemical reduction allowed the macrocycle to reside over the benzidine once again.

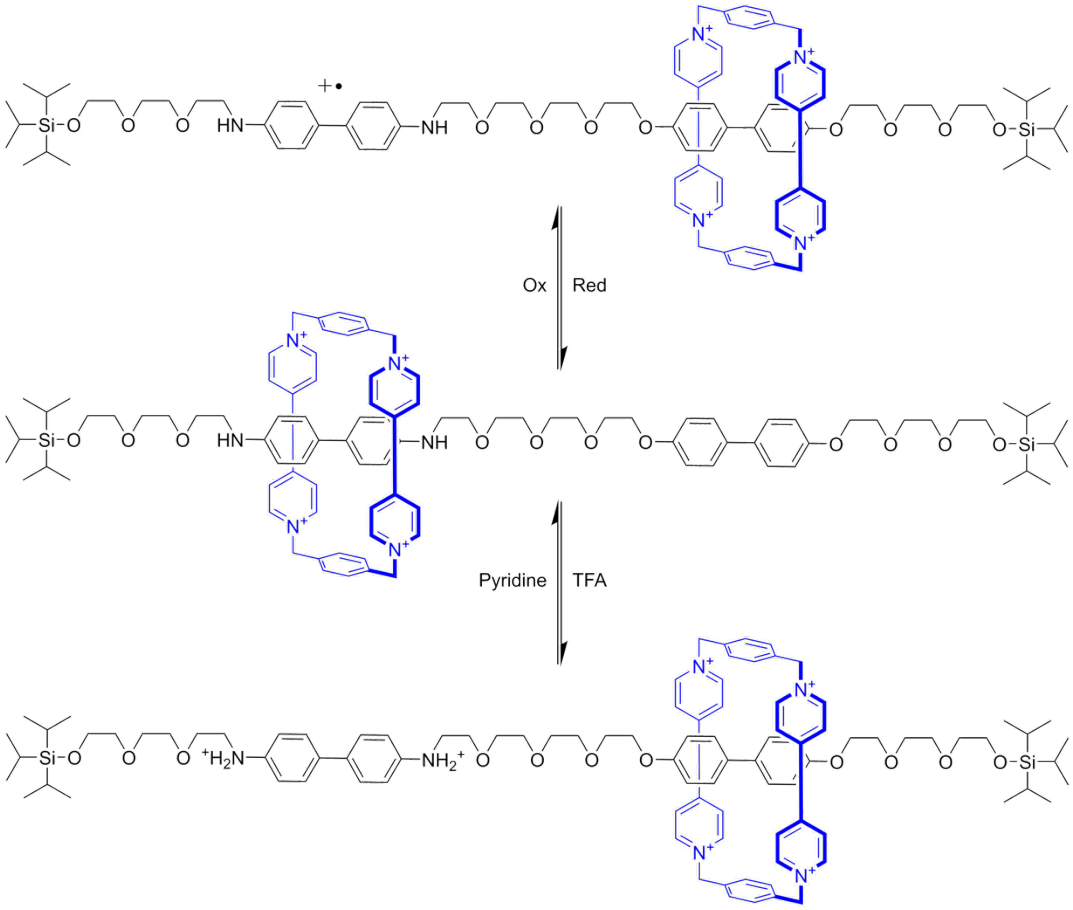

Figure 1.4. Stoddart's molecular switch. The blue box macrocycle is reversibly shifted away from its preferred binding site either chemically or electrochemically.[11]

1.2.2 Polyrotaxanes

Poly[n]rotaxanes, where n is the number of repeat units, are mechanically interlocked polymers formed by, or containing, polymeric rotaxane units. Main chain polyrotaxanes consist of either a polymer of dumbbell with macrocycles threaded over each repeated unit or a polymer of cross-linked macrocycles with dumbbells threaded through each repeated unit and these can be assembled via end capping (**Figure 1.5a**), a supramolecular interaction between preassembled rotaxane units (**Figure 1.5b**) or mechanical interlocking with a subsequent monomer unit in the form of a daisy chain (**Figure 1.5c**). Side chain polyrotaxanes consist of a branching polymer backbone which is mechanically interlocked on each of the branches (**Figure 1.5d**).[12]

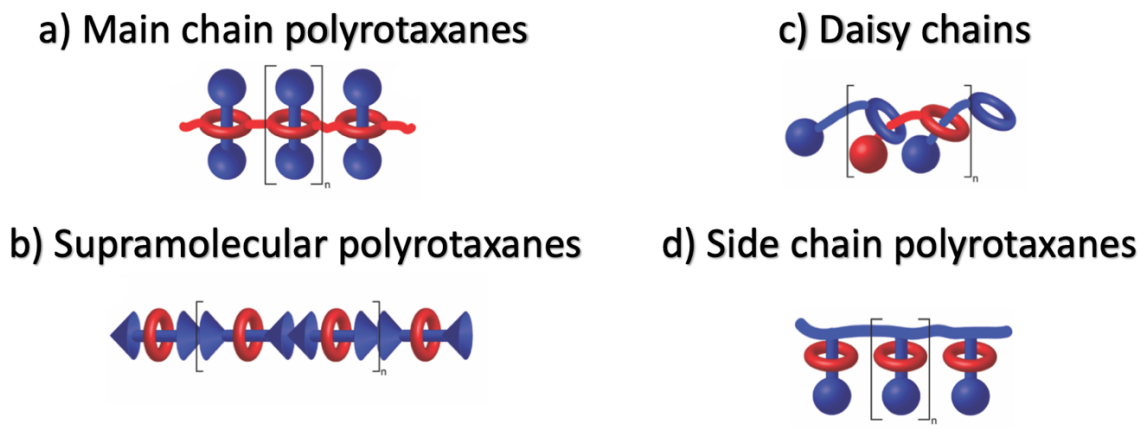

Figure 1.5. The two main types of polyrotaxanes which are main chain polyrotaxanes (a,b and c) and side chain polyrotaxanes (d). Main chain polyrotaxanes can be further subclassified where the backbone is connected covalently (a), supramolecularly (b) or mechanically (c). Adapted with permission from ref 12. Copyright 2019 The Royal Society of Chemistry.

After reporting that polymers such as poly(ethylene glycol) (PEG) form inclusion complexes with cyclodextrins (CD), specifically α-CD in this case,[13] in the form of polypseudorotaxanes, Harada and co-workers synthesised many polyrotaxanes using this recognition motif.[14] One such example used a PEG axle with amine groups terminating each end, allowing for up to twenty-three α-CD molecules to thread across the axle in water and to be stoppered with 2,4-dinitrofluorobenzene. The sheer number of macrocycles threaded through a single axle led to Harada naming the polyrotaxane "the molecular necklace."[15]

Okada and Harada used anthracene stopper groups to cap a polyrotaxane in order to either further polymerise the polyrotaxane into a poly(polyrotaxane) or cyclise the polyrotaxane into a polycatenane (**Figure 1.6**).[16] Using an asymmetric bisamine PEG axle where one side had been reacted with 9-anthracenecarboxylic acid and the other was terminal, α-CDs were used as hosts to form polypseudorotaxanes. This was then reacted with 9-anthracenecarboxylic acid to snap the polyrotaxane in place. Photoirradiation with visible light (λ>340 nm) using a Xe lamp allowed the anthracene stopper groups to photodimerise into polymers of polyrotaxanes. When the photodimerisation was conducted at a higher dilution, polycatenanes were observed. Both polymeric products could be reverted to the original polyrotaxanes via heating at 120 °C.

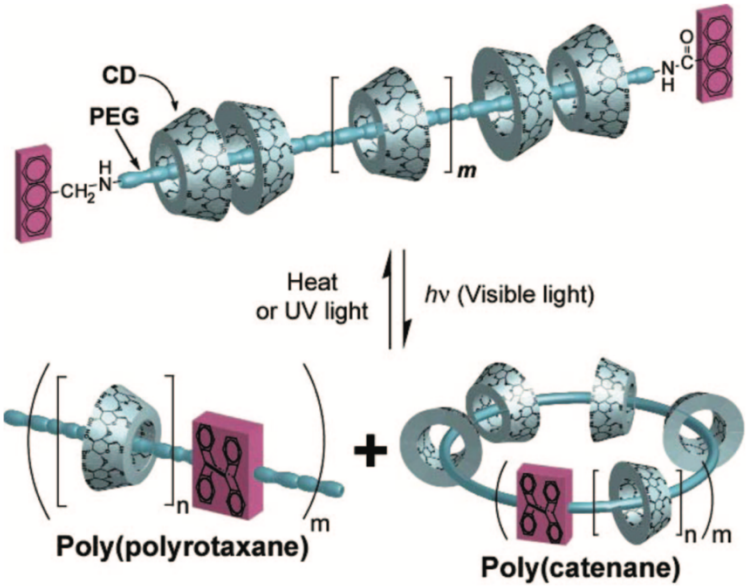

Figure 1.6. Harada's polyrotaxane using α-CD macrocycles along a PEG axle which can form poly(polyrotaxanes) and polycatenanes via photoirradiation, where n denotes the number of macrocycles and m denotes the number of repeated units. Two CDs are represented close together due to intermolecular hydrogen bond. Reprinted with permission from ref 17. Copyright 2009 American Chemical Society.

Other macrocycles such as crown ethers,[18] cucurbiturils[19] and the blue box macrocycle[20] have been used to assemble polyrotaxanes.

1.2.3 Molecular machines based on catenanes

The synthesis of catenanes can be traced back earlier than their rotaxane counterparts, to as early as 1964 by Schill and Lüttringhaus where interlocked rings which they called "catena compounds" were produced using a low yielding statistical method.[21] Whether Schill and Lüttringhaus were first could still be debated as Wasserman reported the formation of a catenane in 1960, however they proposed that only a very small percentage of catenane was produced and it was not isolated from the product mixture.[22,23] The discussion of the existence of catenanes can be traced back even further than this.[24]

[n]Catenanes, where n denotes the number of components, are interlocked rings. For example a [2]catenane consists of two interlocked rings and a [3]catenane consists of three interlocked rings. Due to the formation of mechanical bonds, rotational and translational motions are present within each ring where the rotational motion is known as pirouetting, which involves rotation of a smaller macrocycle around a larger one, and the translational motion is known as circumrotation. Therefore, these molecules can have machine-like behaviour.

Based on their original work where Sauvage and co-workers synthesised a [2]catenane using Cu(I) centres to orient symmetrical phenanthroline building blocks together to react with polyether chains,[25] Sauvage and co-workers designed an electrochemical switch using on a [2]catenane (**Figure 1.7**).[26] In the case of the electrochemical switch, the macrocycles were asymmetric so that one ring could reorient when the catenane was oxidised from Cu(I) to Cu(II). The macrocycle with a phenanthroline moiety, a bidentate ligand, and terpyridine moiety, a tridentate ligand, was initially synthesised. Another phenanthroline ligand was arranged, using Cu(I) as a template, and then ring closed with a polyether chain forming the [2]catenane. Upon oxidation, a Cu(II) cation was formed inducing instability in the initial tetrahedral site and allowing the macrocycle to rotate leading to binding of Cu(II) in a trigonal bipyramidal orientation. Another iteration of this work was a pH switching [2]catenane where a proton could coordinate with two

phenanthroline ligands of two different macrocycle and upon basification, the phenanthroline sites would slide away from each other.[27]

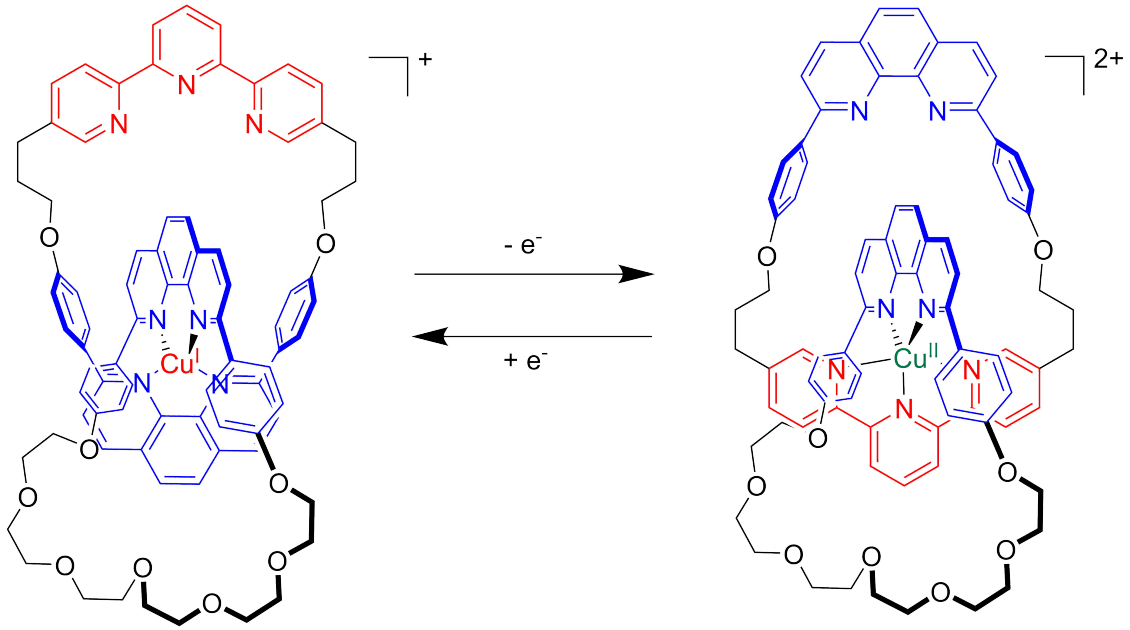

Figure 1.7. Sauvage's electrochemically triggered swinging catenane. A four coordinate Cu(I) ion can be oxidised to five coordinate Cu(II) causing circumrotation about one macrocycle.[26]

Like rotaxanes, the pirouetting motion of a macrocycle in a catenane can also be utilised in the form of mechanically interlocked rotary motors.[28,29]

1.2.4 Other molecular machines

Molecular machines have been constructed without the need of a mechanical bond. Molecular ratchets, where rotation is prohibited in one direction, have been synthesised by Kelly and co-workers where a triptycene moiety is used as a rotor and a [4]helicene as a ratchet unit which are covalently linked (**Figure 1.8**).[30] The triptycene moiety had an amine on one of the faces and the [4]helicene had a hydroxypropyl tether attached to it. The control of directionality was initiated by the reaction of the amine with carbonyl dichloride, forming an isocyanate. This isocyanate group would then react with the hydroxy tether forming a urethane link, however this can only be achieved when the triptycene moiety rotates in one direction. Once trapped, the triptycene moiety rotates unidirectionally to minimise the energy of the new bond.

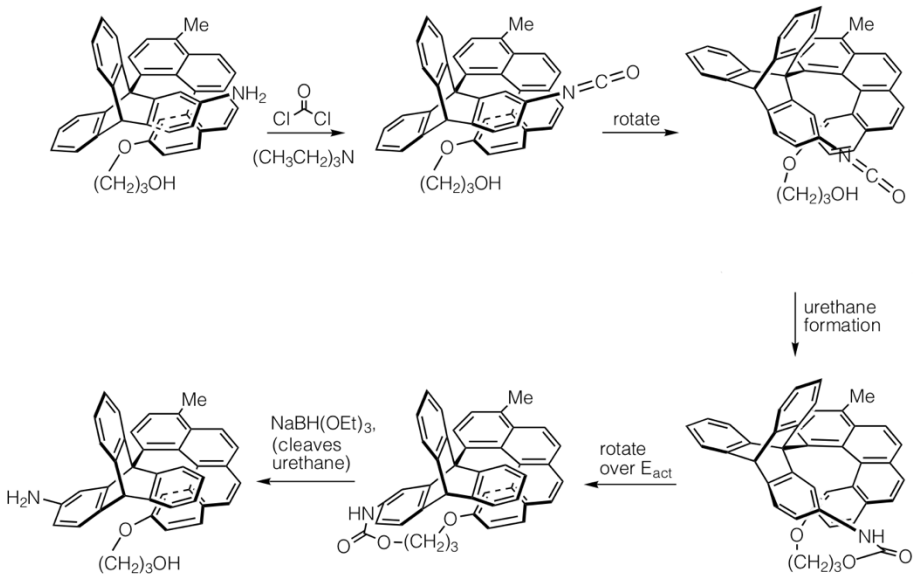

Figure 1.8. Kelly's unidirectional molecular ratchet which uses a triptycene covalently bonded to a hindered helicene. Reprinted with permission from ref 30. Copyright 1999 Springer Nature.

Another example of unidirectional motion was reported by Feringa and co-workers when they synthesised a chiral, helical alkene where rotation was initiated thermally or via UV irradiation (**Figure 1.9**).[31] Two identical, chiral and helical aromatic moieties were bridged by a carbon-carbon double bond which facilitated geometrical isomerisation. Each aromatic moiety had a stereocentre which was crucial to control the rotational process. Irradiation of the motor at -55 °C leads to the initial (*P*,*P*)-trans isomer immediately converting to the (*P*,*P*)-cis isomer, avoiding the unstable (*M*,*M*)-cis isomer. Heating the (*M*,*M*)-trans produced the (*P*,*P*)-trans isomer, completing one full motion of the motor via a helix inversion. Each of these thermally controlled helix inversions prevented the motor from rotating in the backwards directing, forcing the motion unidirectionally.

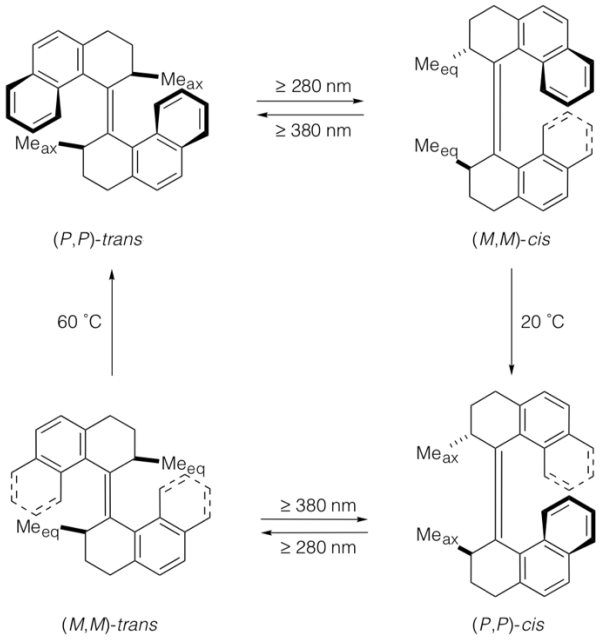

Figure 1.9. Feringa's unidirectional molecular rotor which incorporates rotation about a hindered alkene via photoirradiation. Reprinted with permission from ref 31. Copyright 1999 Springer Nature.

Subsequent iterations of the motor allowed for faster rotation around the double bond[32] and eventually was expanded upon when the same research group synthesised a nanocar where each wheel was a chiroptical unidirectional motor attached to an axle which moved along a Cu(111) surface.[33]

1.2.5 Applications of molecular machines

Advancements in molecular machinery have been iterative processes when the end goals have been to either scale down existing technologies in the form of technomimetic molecules or adapt the biological machines in the form of biomimics.[34]

Switches have been classically been used as the basis of technomimetics. A [2]rotaxne switch was used as the starting point for a molecular elevator by Stoddart and co-workers.[35] The pH driven operation of the elevator allowed the macrocyclic component to shuttle between ammonium and bipyridinium stations. Molecular switches have also been shown to produce mechanical work. The electrochemical switching of the macrocycle can cause the species of rotaxanes on a self-assembled monolayer to bend a microcantilever beam.[36–38]

Rotaxanes have also been incorporated into molecular electronics. A monolayer of a redox active [2]rotaxane species was sandwiched between metal electrodes and several of these devices were configured together to behave as AND or OR logic gates.[39] These logic gates could only function as read-only memory as the switches were singly configurable. This work was expanded by Stoddart and co-workers when they fabricated a 160 kilo-bit molecular memory patterned at 10^{11} bits per cm^2.[40] This incorporated a monolayer of a bistable [2]rotaxane switch, where the dumbbell component had two distinct stations, allowing the macrocycle to shuttle from one station to the other electrochemically, providing an output of either "1" or "0" depending on the position of the macrocycle.

Rotaxanes and their catenane counterparts have been incorporated into MOFs (metal-organic frameworks), of which there are many examples,[41–45] as a way of arranging switches in an ordered manner for molecular electronic devices.[46–48]

Different approaches have been taken in the construction of biomimetic molecules. Small molecule walkers were designed to mimic the ability of kinesin transporting itself along a microtubule.[49,50] This concept has been expanded upon in the form of mechanically interlocked structures. Rotaxanes synthesised by Leigh and co-workers have been designed to allow the macrocycle to 'pick up' amino acids in a defined sequence along a track, as it passes through each station.[51–53]

1.3 Pillararenes

Pillararenes (or pillarenes) have been a widely studied class of macrocycle since their discovery by Ogoshi and co-workers in 2008.[54] They are highly symmetrical, tubular macrocycles consisting of [n]1,4-dialkoxybenzene (or hydroquinone) units, where n is the number of repeat units present within the macrocycle, which are covalently connected in the 2 and 5 positions by methylene bridges.[55] High order pillararenes can be synthesised by ring expansion of pillar[5]arenes.[56]

1.3.1 Pillar[5]arene

Pillar[5]arenes were reported by Ogoshi and co-workers in 2008 when they synthesised dimethoxypillar[5]arene (DMP5A), where dimethoxybenzene was the repeat unit, using $BF_3{\cdot}OEt_2$ as the Lewis acid catalyst via a condensation reaction of 1,4-dimethoxybenzene with paraformaldehyde.[55] The product made was purified via recrystallisation with acetonitrile and was only sparingly soluble in organic solvents and to overcome this they then went on to react it further by fully demethoxylating the molecule with BBr_3 to produce pillar[5]arene, which was soluble in polar solvents. Since the initial report, Ogoshi's team made the synthetic process for producing DMP5A and its subsequent deprotection more efficient.[57] Additionally, the same group showed that the hydroquinone unit can be functionalised with any long chain alkane and when reacted with paraformaldehyde and a Lewis acid catalyst, would form the corresponding dialkoxypillar[5]arene.[58]

1.3.2 Pillar[5]arene synthesis

Pillar[5]arenes can be synthesised using 1,4-dialkoxybenzene monomers, paraformaldehyde and a Lewis acid catalyst in a cyclooligomerisation reaction. Lewis acid catalysts include boron trifluoride,[58] trifluroroacetric acid,[59] trifluormethanesulfonic acid,[60] ferric chloride[61] and *p*-toluenesulfonic acid.[62] When all 1,4-dialkoxybenzene monomer units are the same, a homo-cyclooligomerisation will occur, forming a symmetrical pillararene. Two different monomer units can be used at the same time to produce co-pillararenes via a co-cyclooligomerisation, however the ratio of the monomer units used must be tuned or many unwanted co-pillararenes will be formed.[63] The general ways of synthesising pillar[5]arenes have been documented by Huang and co-workers.[64]

Pillar[5]arene is the thermodynamic product of the cyclooligomerisation reaction under Friedel-Crafts conditions.[65] The high yields associated with the formation of the cyclopentamer over the oligomers or higher order pillararenes is due to the reversible cleavage of Ar-CH_2 bonds. A study by Nierengarten and co-workers[66] demonstrated that pillar[5]arene was the only cyclooligomerisation product when using a trimer of 1,4-

diethoxybenzene as the starting reagent to make pillar[6]arene however no cyclohexamer was observed.

The 1,4-dialkoxybenzene monomer has four equally reactive positions (**Scheme 1.1**) which can all react with paraformaldehyde. This reactive intermediate can then react with 1,4-dialkoxybenzene once again at any of the reactive positions. Subsequent reactions are dominated by sterics, where position 3 is blocked by the previous substitution, and the reaction at position 5 is therefore directed by symmetry.

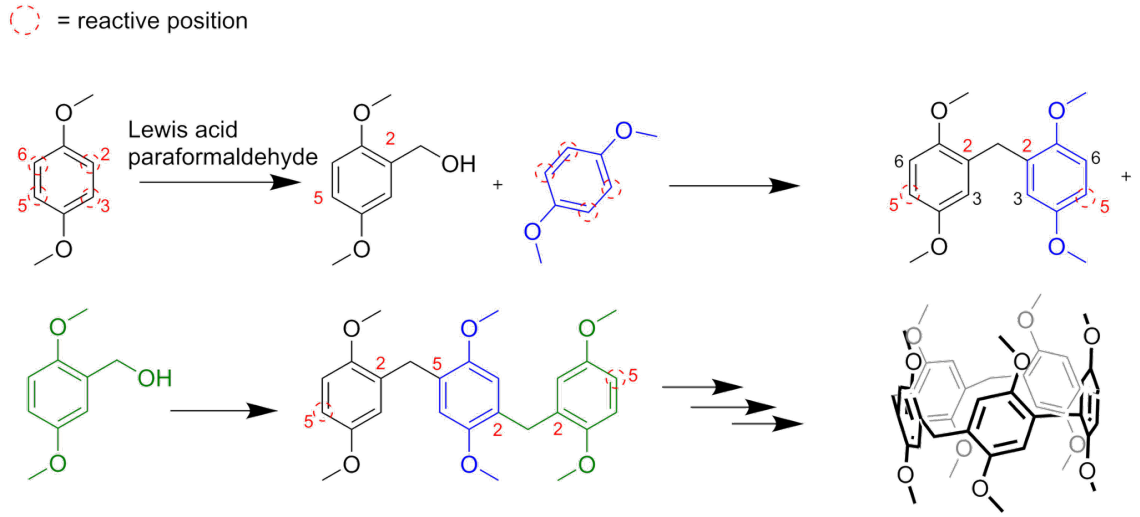

Scheme 1.1. Ogoshi's proposed reaction pathway by which pillar[5]arenes are synthesised using a Lewis acid and paraformaldehyde.[67]

Pillar[5]arenes can be post functionalised, either by producing a pillar[5]arene with reactive terminal groups, or via selective dealkoxylation of the pillar[5]arene and subsequent reaction. All of the terminal alkoxy groups can be dealkylated using excess boron tribromide, as Ogoshi showed when pillar[5]arene was first reported, producing per-hydroxylated pillar[5]arene. Smaller quantities of boron tribromide can selectively dealkylate pillar[5]arene.

Another method of synthesising pillararenes used 1,4-disubstituted 2,5-dialkoxybenzne with *p*-toluenesulfonic acid in dichloromethane, which was high yielding. Additionally, rim-differentiated pillararenes, where the substituent on one side of the macrocycle is different to the other, can be synthesised using asymmetric monomer units.[68]

1.3.3 Pillar[5]arene mechanically interlocked molecules

1.3.3.1 Host-guest properties of pillar[5]arenes

Due to their symmetrical pillar shaped structures and electron donating cavities pillar[5]arenes can be used as hosts for a multitude of molecules, including neutral and cationic guests mainly driven by solvophobic, electrostatic and weak aromatic interactions.

Cationic guests include the nitrogen containing heterocycles; pyridinium, viologen and imidazolium moieties in addition to ammonium salts. As these are all electron poor, they make great guests for the pillar[5]arene's electron rich cavity.[69] Neutral guests include long chain alkane molecules and uncharged aliphatic amines due to their shape-size selectivity, along with solvophobic effects and C-H···π interactions driving the host-guest interactions. Neutral bis(alkylimidazole) chains have also been reported as suitable guests for pillar[5]arenes.[70] It has been found that branched alkanes and cycloalkanes cannot be encapsulated by pillar[5]arene, because they are too large to fit inside the cavity.

1.3.3.2 Pillar[5]arene based rotaxanes

The first pillar[5]arene-based [2]rotaxane was reported by Stoddart and co-workers when they were trying to establish an understanding of the host-guest properties of DMP5A with alkanediamines.[71] They found that 1,8-diaminooctane had the best binding interaction with DMP5A and end capped it using 3,5-di-tert-butylbenzaldehyde to make an amide and this was then reduced using sodium borohydride to produce the subsequent amine with a low yield of 7% (**Figure 1.10**). As this was a proof of concept, formation of the rotaxane was more important than how much they produced and in addition they were keen to use commercially available reagents and all reagents other than the DMP5A were purchased.

a)

b)

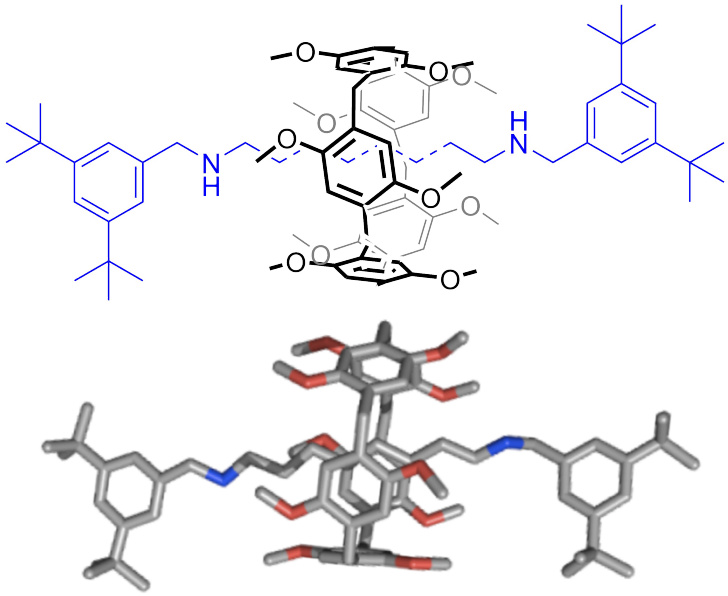

Figure 1.10. Stoddart's DMP5A bisamine rotaxane (a) and its energy minimised structure (b). Adapted with permission from ref 71. Copyright 2011 American Chemical Society.

Since the first pillar[5]arene based rotaxane was synthesised, many developments have been made to enhance the yield by utilising cation-π recognition motifs[72,73] in addition to neutral guests to form host guest complexes.[74,75]

Huang and co-workers devised a method of using triazole moieties to enhance the interaction between the axle and pillar[5]arene and after the formation of a pseudorotaxane species, it was reacted with 3,5-dinitrobenzoyl chloride via an esterification.[76] Observation of ^{1}H NMR data concluded that there were characteristic upfield shifts around the triazole region, in addition to higher yields than reported by Stoddart and co-workers.

Another approach was reported by Nierengarten and co-workers in the construction of [2]rotaxanes utilising the formation of amides via the reaction of amines and acyl chlorides.[77] Initially, sebacoyl chloride and dodecanedioyl chloride as the axles and 3,5-bis(trifluoromethyl)aniline as the stopper group, which assembled the [2]rotaxanes via the formation of an amide bond under basic and cold conditions. Other aniline based stopper groups were tested yielding the rotaxanes moderately. In addition, diamine axles

were used with acyl chloride stopper groups under the same conditions as before which produced [2]rotaxanes.

1.3.3.3 Pillar[5]arene based polyrotaxanes

Ogoshi and co-workers constructed a polypseudorotaxane utilising viologen polymers of different lengths and fully deprotected pillar[5]arenes as macrocycles.[78] In this study three different viologen polymers were used in order to test for complexation and these included a short viologen polymer where the repeat units were separated by butyl chains, a long viologen polymer separated by octyl chains and a viologen polymer terminating in adamantyl groups. Complexation was shown via ^{1}H NMR titrations for the longer polymer, however a larger concentration of pillar[5]arene was required to complex to the shorter polymer, as the bulkiness of the macrocycle required larger distances between the viologen recognition sites. The longer polymer with terminal adamantyl groups showed no polypseudorotaxane formation as they were too bulky for the pillar[5]arene to slip over and this was the basis of their polyrotaxane.[79]

The polyrotaxane was synthesised using the end-capping method where the pseudopolyrotaxane was assembled in solution, with an excess of twenty five equivalents of pillar[5]arene to viologen polymer (**Figure 1.11**). Subsequently, the adamantyl groups were added to the mixture and heated to cap the macrocycles in place. Since the pillar[5]arenes were fully dealkylated, there was an intermolecular hydrogen bonding network along the polyrotaxane making the molecule insoluble in many solvents, however this facilitated an ease of purification where it was simply washed with acetonitrile, in which all the starting reagents were soluble. The intermolecular hydrogen bonding network indicated that shuttling of the pillar[5]arenes was slow at room temperature but upon heating allowed the macrocycles to shuttle faster. This is an interesting feature of the molecule as upon oxidation the viologen radical cations were stabilised by the electron rich pillar[5]arenes. Additionally, a UV-Vis absorbance band for the polypseuodrotaxane at 540 nm seemingly diminished with increasing temperature, however for the polyrotaxane this increased, with a colour change from yellow at room temperature to violet at high temperature. This suggested that a partially formed viologen

cation species was being formed and that the intermolecular hydrogen bonding network of pillar[5]arenes was breaking apart. This in turn lead to dethreading of the polypseudorotaxane and the increased speed of macrocycle shuttling along the polyrotaxane which was stabilising the partially formed viologen cation species.

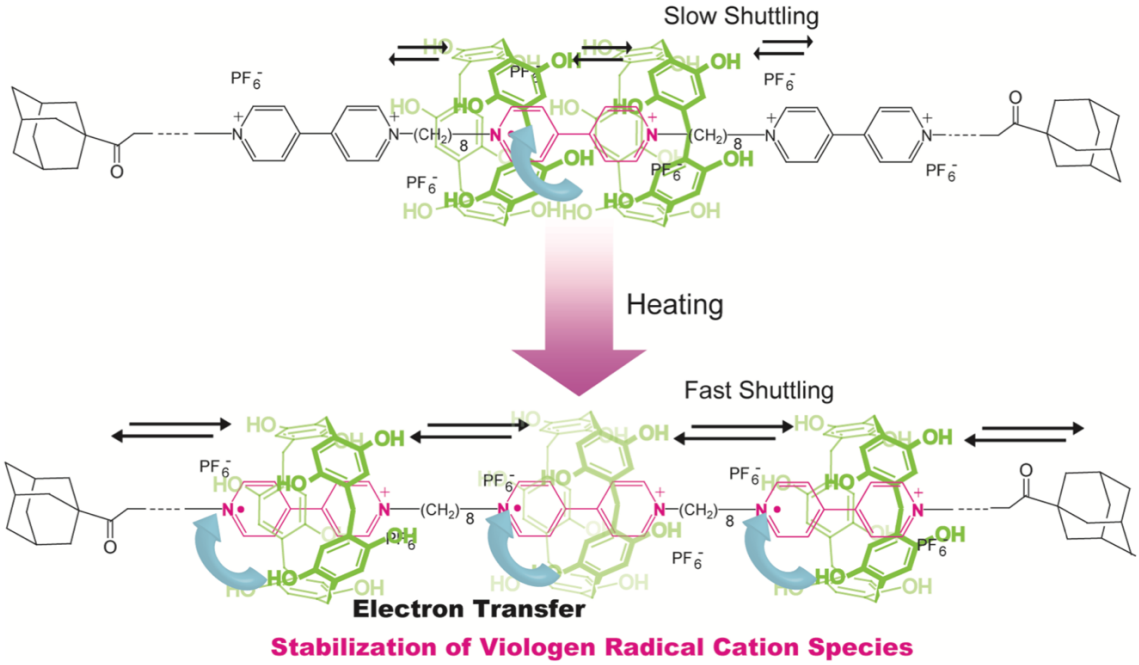

Figure 1.11. Ogoshi's pillar[5]arene based polyrotaxane capped by adamantyl moieties. Reprinted with permission from ref 79. Copyright 2010 American Chemical Society.

1.3.3.4 Other mechanically interlocked molecules using pillar[5]arenes

Ogoshi and co-workers has also synthesised a [2]catenane (**Figure 1.12**) using diethoxypillar[5]arene (DEP5A).[80] They utilised a long rod with a pyridinium moiety in the centre which terminated with alkenes on either end, where the pyridinium acted as a recognition motif for DEP5A and the alkenes could be cyclised via a ring closing metathesis process, using Grubbs first generation catalyst. In order to synthesise the catenane, a pseudorotaxane needed to form which required mixing of the components at high concentration, however when a ring closing reaction was attempted, only polymer formed. This was because the ring closing metathesis required a high dilution to afford a macrocyclic product and thus they ran the reaction at very high dilution, but in order to form a pseudorotaxane beforehand, one hundred equivalents of DEP5A were required, and this only produced the [2]catenane with a low yield of 24%.

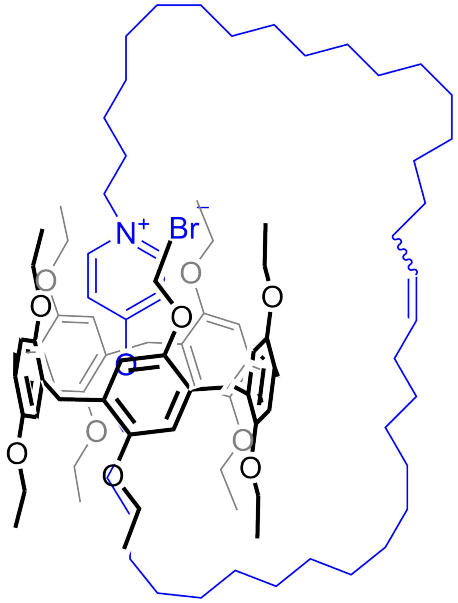

Figure 1.12. Ogoshi's pillar[5]arene based [2]catenane.[80]

Molecular [2]rotaxane handcuffs (**Figure 1.13**) have been synthesised by Champness and co-workers in order to bring together two rylene diimide moieties into close proximity to each other without being bound by covalent linkages.[81] A perylene diimide (PDI) core connected to butyl chains terminating with pillar[5]arene moieties was used as the handcuff linker which acted as the host molecule. This could then be reacted with the corresponding PDI or naphthalene diimide (NDI) rod with terminal imidazole groups which could be used as axles in a one to one ratio and subsequently end-capped using bulky mesityl stopper groups. The mechanical bonds imposed by the rotaxane forming reaction allowed the rylene cores of each component to form a co-facial arrangement, but also allowed the flexibility of the system where the rylene cores were free to separate from the lack of constraints induced by covalent linkages or coordinate bonds.

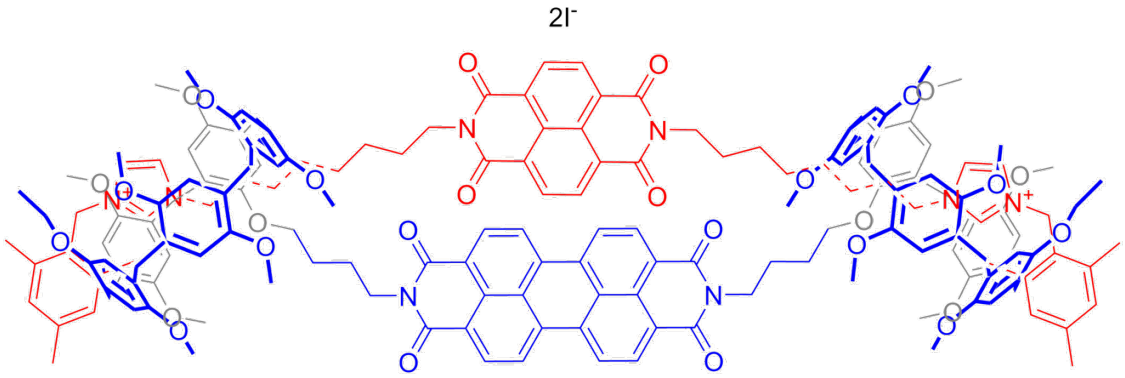

Figure 1.13. Champness' pillar[5]arene based molecular handcuff which loosely holds together rylene diimide moieties.[81]

Other examples of pillar[5]arene based MIMs include a [2]rota[2]catenane,[82] mechanically self-locked gemini-catananes[83] and a rotaxane-branched dendrimer.[84]

1.4 Thesis outline

This thesis outlines the synthesis of pillar[5]arene based [n]rotaxanes utilising the pillar[5]arene-imidazole recognition motif. Shuttling behaviour of the macrocycles have been conducted to understand where the pillararenes preferentially reside.

Chapter 2 describes the synthesis of [3]rotaxanes and the effect of increasing the lengths of the alkyl chains along the rim of pillar[5]arene. Using ^{1}H NMR spectroscopy a shielding factor can be determined to examine where the macrocycles preferentially reside across the axle. The change in polarity of the solvent the rotaxanes are subjected to is also explored, in addition of variable temperature ^{1}H NMR studies of the [3]rotaxanes.

Chapter 3 explores the shuttling effect of having a single macrocycle locked onto a long chain axle in addition to the effect of increasing the lengths of the alkyl chains along the rim of pillar[5]arene. Shuttling parameters are determined using the shielding factor and switch-like behaviour is observed when polarity of the [2]rotaxane species is changed.

Chapter 4 investigates the use of anthracene moieties as stopper groups on shorter chained [2]rotaxane species. Additionally, electrochemical and fluorescence studies of the series of rotaxanes were conducted and light-initiated photodimerisation was explored in order to produce poly[2]rotaxane species.

Chapter 5 discusses the overall conclusions made in this thesis and outlines potential avenues the expand on the research that has been conducted.

1.5 References

1 C. J. Pedersen, *Angew. Chemie Int. Ed. English*, 1988, **27**, 1021–1027.

2 J.-M. Lehn, *Angew. Chemie Int. Ed. English*, 1988, **27**, 89–112.

3 D. J. Cram, *Angew. Chemie Int. Ed. English*, 1985, **24**, 799–810.

4 J. P. Sauvage, *Angew. Chemie - Int. Ed.*, 2017, **56**, 11080–11093.

5 J. F. Stoddart, *Angew. Chemie - Int. Ed.*, 2017, **56**, 11094–11125.

6 B. L. Feringa, *Angew. Chemie - Int. Ed.*, 2017, **56**, 11060–11078.

7 I. T. Harrison and S. Harrison, *J. Am. Chem. Soc.*, 1967, **89**, 5723–5724.

8 M. Xue, Y. Yang, X. Chi, X. Yan and F. Huang, *Chem. Rev.*, 2015, **115**, 7398–7501.

9 J. D. Crowley, S. M. Goldup, A. L. Lee, D. A. Leigh and R. T. McBurney, *Chem. Soc. Rev.*, 2009, **38**, 1530–1541.

10 P. L. Anelli, N. Spencer and J. Fraser Stoddart, *J. Am. Chem. Soc.*, 1991, **113**, 5131–5133.

11 R. A. Bissell, E. Córdova, A. E. Kaifer and J. F. Stoddart, *Nature*, 1994, **369**, 133–137.

12 S. Mena-Hernando and E. M. Pérez, *Chem. Soc. Rev.*, 2019, **48**, 5016–5032.

13 A. Harada and M. Kamachi, *Macromolecules*, 1990, **23**, 2821–2823.

14 A. Harada, Y. Takashima and H. Yamaguchi, *Chem. Soc. Rev.*, 2009, **38**, 875–882.

15 A. Harada, J. Li and M. Kamachi, *Nature*, 1992, **356**, 325–327.

16 M. Okada and A. Harada, *Macromolecules*, 2003, **36**, 9701–9703.

17 A. Harada, A. Hashidzume, H. Yamaguchi and Y. Takashima, *Chem. Rev.*, 2009, **109**, 5974–6023.

18 C. Gong, Q. Ji, C. Subramaniam and H. W. Gibson, *Macromolecules*, 1998, **31**, 1814–1818.

19 C. Meschke, H. J. Buschmann and E. Schollmeyer, *Polymer*, 1999, **40**, 945–949.

20 W. Zhang, W. R. Dichtel, A. Z. Stieg, D. Benítez, J. K. Gimzewski, J. R. Heath and J. F. Stoddart, *Proc. Natl. Acad. Sci. U. S. A.*, 2008, **105**, 6514–6519.

21 G. Schill and A. Lüttringhaus, *Angew. Chemie Int. Ed. English*, 1964, **3**, 546–547.

22 E. Wasserman, *J. Am. Chem. Soc.*, 1960, **82**, 4433–4434.

23 R. Brückner, *European J. Org. Chem.*, 2019, **2019**, 3289–3319.

24 H. L. Frisch and E. Wasserman, *J. Am. Chem. Soc.*, 1961, **83**, 3789–3795.

25 C. O. Dietrich-Buchecker, J. P. Sauvage and J. P. Kintzinger, *Tetrahedron Lett.*, 1983,

24, 5095–5098.

26 A. Livoreil, C. O. Dietrich-Buchecker and J. P. Sauvage, *J. Am. Chem. Soc.*, 1994, **116**, 9399–9400.

27 D. B. Amabilino, C. O. Dietrich-Buchecker, A. Livoreil, L. Pérez-García, J. P. Sauvage and J. F. Stoddart, *J. Am. Chem. Soc.*, 1996, **118**, 3905–3913.

28 D. A. Leigh, J. K. Y. Y. Wong, F. Dehez and F. Zerbetto, *Nature*, 2003, **424**, 174–179.

29 J. V. Hernández, E. R. Kay and D. A. Leigh, *Science*, 2004, **306**, 1532–1537.

30 T. R. Kelly, H. De Silva and R. A. Silva, *Nature*, 1999, **401**, 150–152.

31 N. Koumura, R. W. J. Zijistra, R. A. Van Delden, N. Harada and B. L. Feringa, *Nature*, 1999, **401**, 152–155.

32 N. Koumura, E. M. Geertsema, M. B. Van Gelder, A. Meetsma and B. L. Feringa, *J. Am. Chem. Soc.*, 2002, **124**, 5037–5051.

33 T. Kudernac, N. Ruangsupapichat, M. Parschau, B. Maclá, N. Katsonis, S. R. Harutyunyan, K. H. Ernst and B. L. Feringa, *Nature*, 2011, **479**, 208–211.

34 L. Zhang, V. Marcos and D. A. Leigh, *Proc. Natl. Acad. Sci. U. S. A.*, 2018, **115**, 9397–9404.

35 J. D. Badjić, V. Balzani, A. Credi, S. Silvi and J. F. Stoddart, *Science*, 2004, **303**, 1845–1849.

36 T. J. Huang, B. Brough, C. M. Ho, Y. Liu, A. H. Flood, P. A. Bonvallet, H. R. Tseng, J. F. Stoddart, M. Baller and S. Magonov, *Appl. Phys. Lett.*, 2004, **85**, 5391–5393.

37 S. Silvi, M. Venturi and A. Credi, *J. Mater. Chem.*, 2009, **19**, 2279–2294.

38 S. Kassem, T. Van Leeuwen, A. S. Lubbe, M. R. Wilson, B. L. Feringa and D. A. Leigh, *Chem. Soc. Rev.*, 2017, **46**, 2592–2621.

39 C. P. Collier, E. W. Wong, M. Belohradský, F. M. Raymo, J. F. Stoddart, P. J. Kuekes, R. S. Williams and J. R. Heath, *Science*, 1999, **285**, 391–394.

40 J. E. Green, J. Wook Choi, A. Boukai, Y. Bunimovich, E. Johnston-Halperin, E. Deionno, Y. Luo, B. A. Sheriff, K. Xu, Y. Shik Shin, H. R. Tseng, J. F. Stoddart and J. R. Heath, *Nature*, 2007, **445**, 414–417.

41 V. N. Vukotic, K. J. Harris, K. Zhu, R. W. Schurko and S. J. Loeb, *Nat. Chem.*, 2012, **4**, 456–460.

42 A. Saura-Sanmartin, A. Martinez-Cuezva, D. Bautista, M. R. B. Marzari, M. A. P. Martins, M. Alajarin and J. Berna, *J. Am. Chem. Soc.*, 2020, **142**, 13442–13449.

43 G. Gholami, K. Zhu, J. S. Ward, P. E. Kruger and S. J. Loeb, *Eur. J. Inorg. Chem.*, 2016, **2016**, 4524–4529.

44 K. Zhu, V. N. Vukotic, C. A. Okeefe, R. W. Schurko and S. J. Loeb, *J. Am. Chem. Soc.*, 2014, **136**, 7403–7409.

45 N. C. Frank, D. J. Mercer and S. J. Loeb, *Chem. - A Eur. J.*, 2013, **19**, 14076–14080.

46 A. Coskun, J. M. Spruell, G. Barin, W. R. Dichtel, A. H. Flood, Y. Y. Botros and J. F. Stoddart, *Chem. Soc. Rev.*, 2012, **41**, 4827–4859.

47 Q. Chen, J. Sun, P. Li, I. Hod, P. Z. Moghadam, Z. S. Kean, R. Q. Snurr, J. T. Hupp, O. K. Farha and J. F. Stoddart, *J. Am. Chem. Soc.*, 2016, **138**, 14242–14245.

48 Q. Li, W. Zhang, O. Š. Miljanić, C. B. Knobler, J. F. Stoddart and O. M. Yaghi, *Chem. Commun.*, 2010, **46**, 380–382.

49 M. Von Delius, E. M. Geertsema and D. A. Leigh, *Nat. Chem.*, 2010, **2**, 96–101.

50 M. J. Barrell, A. G. Campaña, M. Von Delius, E. M. Geertsema and D. A. Leigh, *Angew. Chemie - Int. Ed.*, 2011, **50**, 285–290.

51 B. Lewandowski, G. De Bo, J. W. Ward, M. Papmeyer, S. Kuschel, M. J. Aldegunde, P. M. E. Gramlich, D. Heckmann, S. M. Goldup, D. M. D'Souza, A. E. Fernandes and D. a. Leigh, *Science*, 2013, **339**, 189–193.

52 G. De Bo, S. Kuschel, D. A. Leigh, B. Lewandowski, M. Papmeyer and J. W. Ward, *J. Am. Chem. Soc.*, 2014, **136**, 5811–5814.

53 G. De Bo, M. A. Y. Gall, M. O. Kitching, S. Kuschel, D. A. Leigh, D. J. Tetlow and J. W. Ward, *J. Am. Chem. Soc.*, 2017, **139**, 10875–10879.

54 H. Zhang and Y. Zhao, *Chem. - A Eur. J.*, 2013, **19**, 16862–16879.

55 T. Ogoshi, S. Kanai, S. Fujinami and T. Yamagishi, *J. Am. Chem. Soc.*, 2008, 5022–5023.

56 T. Ogoshi, N. Ueshima, F. Sakakibara, T. A. Yamagishi and T. Haino, *Org. Lett.*, 2014, **16**, 2896–2899.

57 T. Ogoshi, T. Aoki, K. Kitajima, S. Fujinami, T. A. Yamagishi and Y. Nakamoto, *J. Org. Chem.*, 2011, **76**, 328–331.

58 T. Ogoshi, K. Kitajima, T. Aoki, S. Fujinami, T. A. Yamagishi and Y. Nakamoto, *J. Org. Chem.*, 2010, **75**, 3268–3273.

59 T. Boinski and A. Szumna, *Tetrahedron*, 2012, **68**, 9419–9422.

60 K. Wang, L. L. Tan, D. X. Chen, N. Song, G. Xi, S. X. A. Zhang, C. Li and Y. W. Yang,

Org. Biomol. Chem., 2012, **10**, 9405–9409.

61 X. Wang, K. Han, J. Li, X. Jia and C. Li, *Polym. Chem.*, 2013, **4**, 3998–4003.

62 Y. Kou, D. Cao, H. Tao, L. Wang, J. Liang, Z. Chen and H. Meier, *J. Incl. Phenom. Macrocycl. Chem.*, 2013, **77**, 279–289.

63 K. Yang, Y. Pei, J. Wen and Z. Pei, *Chem. Commun.*, 2016, **52**, 9316–9326.

64 M. Xue, Y. Yang, X. Chi, Z. Zhang and F. Huang, *Acc. Chem. Res.*, 2012, **45**, 1294–1308.

65 M. Da Pian, C. A. Schalley, F. Fabris and A. Scarso, *Org. Chem. Front.*, 2019, **6**, 1044–1051.

66 M. Holler, N. Allenbach, J. Sonet and J. F. Nierengarten, *Chem. Commun.*, 2012, **48**, 2576–2578.

67 T. Ogoshi, T. A. Yamagishi and Y. Nakamoto, *Chem. Rev.*, 2016, **116**, 7937–8002.

68 Y. Kou, H. Tao, D. Cao, Z. Fu, D. Schollmeyer and H. Meier, *European J. Org. Chem.*, 2010, 6464–6470.

69 C. Li, L. Zhao, J. Li, X. Ding, S. Chen, Q. Zhang, Y. Yu and X. Jia, *Chem. Commun.*, 2010, **46**, 9016.

70 C. Li, S. Chen, J. Li, K. Han, M. Xu, B. Hu, Y. Yu and X. Jia, *Chem. Commun.*, 2011, **47**, 11294–11296.

71 N. L. Strutt, R. S. Forgan, J. M. Spruell, Y. Y. Botros and J. F. Stoddart, *J. Am. Chem. Soc.*, 2011, **133**, 5668–5671.

72 S. Dong, J. Yuan and F. Huang, *Chem. Sci.*, 2014, **5**, 247–252.

73 T. Ogoshi, D. Yamafuji, T. Aoki, K. Kitajima, T. A. Yamagishi, Y. Hayashi and S. Kawauchi, *Chem. - A Eur. J.*, 2012, **18**, 7493–7500.

74 T. Ogoshi, D. Kotera, S. Nishida, T. Kakuta, T. A. Yamagishi and A. M. Brouwer, *Chem. - A Eur. J.*, 2018, **24**, 6325–6329.

75 S. Dong, C. Han, B. Zheng, M. Zhang and F. Huang, *Tetrahedron Lett.*, 2012, **53**, 3668–3671.

76 P. Wei, X. Yan, J. Li, Y. Ma, Y. Yao and F. Huang, *Tetrahedron*, 2012, **68**, 9179–9185.

77 R. Milev, A. Lopez-Pacheco, I. Nierengarten, T. M. N. Trinh, M. Holler, R. Deschenaux and J. F. Nierengarten, *European J. Org. Chem.*, 2015, **2015**, 479–485.

78 T. Ogoshi, Y. Nishida, T. A. Yamagishi and Y. Nakamoto, *Macromolecules*, 2010, **43**, 3145–3147.

79 T. Ogoshi, Y. Nishida, T. A. Yamagishi and Y. Nakamoto, *Macromolecules*, 2010, **43**, 7068–7072.

80 K. Kitajima, T. Ogoshi and T. Yamagishi, *Chem. Commun.*, 2014, **50**, 2925.

81 L. Yang, P. Langer, E. S. Davies, M. Baldoni, K. Wickham, N. A. Besley, E. Besley and N. R. Champness, *Chem. Sci.*, 2019, **10**, 3723–3732.

82 W. B. Hu, W. J. Hu, X. L. Zhao, Y. A. Liu, J. S. Li, B. Jiang and K. Wen, *Chem. Commun.*, 2015, **51**, 13882–13885.

83 S. H. Li, H. Y. Zhang, X. Xu and Y. Liu, *Nat. Commun.*, 2015, **6**.

84 X. Q. Wang, W. Wang, W. J. Li, L. J. Chen, R. Yao, G. Q. Yin, Y. X. Wang, Y. Zhang, J. Huang, H. Tan, Y. Yu, X. Li, L. Xu and H. B. Yang, *Nat. Commun.*, 2018, **9**, 1–11.

Chapter 2:

Restrictive Shuttling of Pillar[5]arenes within [3]Rotaxane Molecular Shuttles

2.1 Introduction

2.1.1 Pillar[5]arene based [3]rotaxanes

After the discovery of pillar[5]arenes by Ogoshi and co-workers[1,2] and the synthesis of a simple [2]rotaxane utilising pillar[5]arenes as hosts by Stoddart and co-workers,[3] the field of pillararene host-guest chemistry advanced rapidly.[4–6]

Construction of a [3]rotaxane species using diethoxypillar[5]arene (DEP5A) was first reported by Ogoshi and co-workers,[7] utilising cation-π interactions of the macrocycle with pyridinium moieties along a rod molecule (**Figure 2.1**). After facilitating the formation of a pseudorotaxane, two of these host-guest complexes were joined together using a copper(I)-catalysed azide alkyne cycloaddition (Cu-AAC) reaction to afford the [3]rotaxane species. Placement of the host-guest interaction between the pillar[5]arene and the axle was crucial to end capping the rotaxane, as the pillararene blocked the alkyne when complexed to the pyridinium on the axle, so only axle molecules *not* threaded by pillararenes were able to react. To assemble the [3]rotaxane, an axle which separated the pyridinium from the alkyne using a longer decyl chain was used which could then be complexed with DEP5A to form a pseudorotaxane. The pseudorotaxane reacted with a diazide rod in a molar ratio of two to one, respectively, via a Cu-AAC reaction, where the distance between the macrocycles and the strong cation-π interactions between the axle and the pillararenes, effectively held the macrocycles at remote recognition sites and allowed two pillar[5]arenes to be co-located along the same axle. Upon analysis of the [3]rotaxanes it was concluded that the threading process is diastereoselective with respect to the pillararene, as only the conformations with the largest cavities will thread along the axle and diastereoisomers of the rotaxanes could be separated via chiral HPLC.

The pillararenes with the largest cavities denoted as (p*R*, p*R*, p*R*, p*R*, p*R*) also known as P[5]*R* and (p*S*, p*S*, p*S*, p*S*, p*S*) also known as P[5]*S* could encapsulate the axle, whereas all other conformational isomers which contained both p*R* and p*S* conformational isomer components could not as the cavity produced is too small for encapsulation.

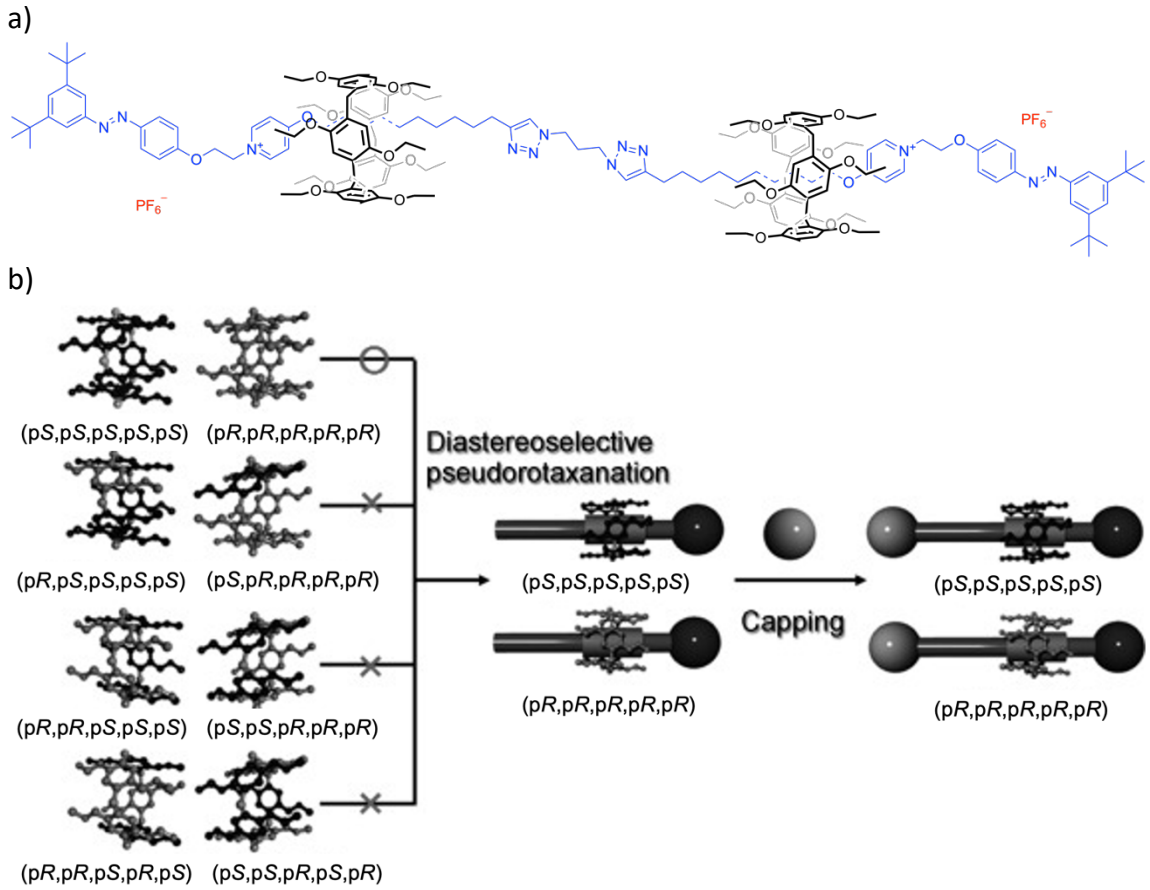

Figure 2.1. (a) is the structure of Ogoshi's [3]rotaxane. (b) the diasteroeselectivity exhibited by pseudorotaxanation between the axle and the macrocycle, where only the most symmetrical isomers of pillar[5]arene [(pS,pS,pS,pS,pS) and (pR,pR,pR,pR,pR)] will complex the axle. Adapted with permission from ref 7. Copyright 2012 Wiley-VCH Verlag GmbH & Co. KGaA, Weinheim.

This study was enhanced by Stoddart and co-workers by synthesising higher order hetero rotaxanes using pillar[5]arenes and cucurbit[6]urils.[8] After discovering that cyclodextrins have cooperative binding interactions with cucurbiturils when used in a cucurbituril-catalysed azide alkyne cycloaddition (CB-AAC) reaction to assemble MIMs,[9] they decided to extend this approach to utilise pillararenes instead of cyclodextrins (**Figure 2.2**). De-alkylated pillar[5]arene was chosen as it was a similar size to cucurbit[6]uril and allowed hydrogen-bonding between the rims of the pillararene and cucurbituril macrocycles and to behave as a "molecular gasket", stabilising the geometry of the axle and allowing rotaxane formation. Like Ogoshi's [3]rotaxane system, the pillar[5]arene threads over a positively charged axle to form a pseudorotaxane, this time bearing a double charged 4,4-bipyridinium site with diazide appendages, which were separated by alkyl chains. This pseudorotaxane would then react with a stopper group, which consisted of separate

pseudorotaxanes, composed of a secondary ammonium hexafluorophosphate salt, connected to a bulky aryl group and an alkyne, to allow both cucurbit[6]uril complexation and a CB-AAC reaction to occur. Without any pillar[5]arene the reaction did occur, but with yields of 36% for the [3]rotaxane. However, on addition of pillar[5]arene, yields were as high as 96% for the [4]rotaxane species due to cooperative hydrogen-bonding between the cucurbituril-bound-pseudorotaxane and the de-alkylated pillar[5]arene.

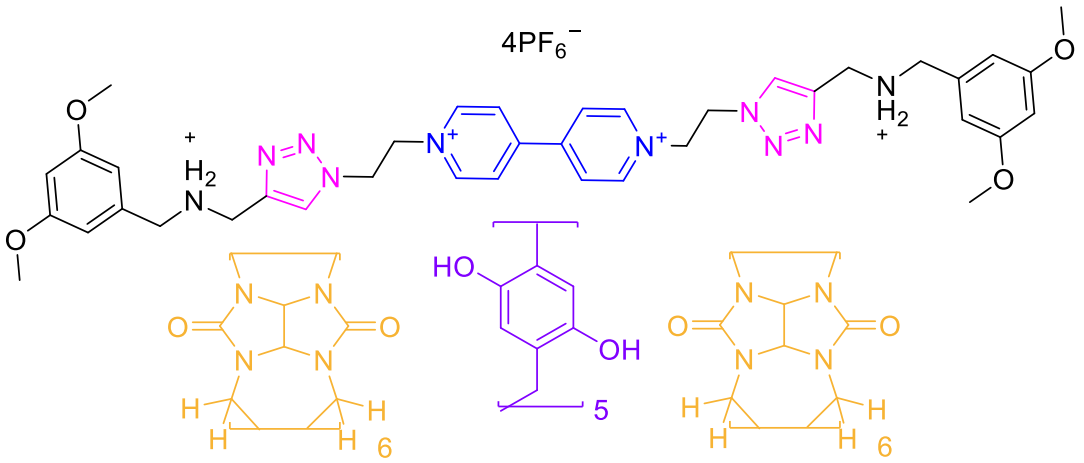

Figure 2.2. Stoddart's hetero[4]rotaxane, using pillar[5]arene and cucurbit[6]uril as the macrocycles.[8]

A [5]rotaxane was assembled as the only product using longer butyl chain spacers between the 4,4-bipyridinium and azide groups, however pentyl chains significantly reduced the yield of rotaxane formation, suggesting that the cooperative interactions between the pillararenes and the cucurbiturils were disrupted by the additional flexibility.

2.1.2 Pillar[5]arene based molecular shuttles

After synthesising two [2]rotaxanes based on the pillar[5]arene-alkane recognition motif,[10] Huang and co-workers set out to implement an imidazolium station within a [2]rotaxane to better understand the pillar[5]arene-imidazolium recognition motif, and to use the translational motion of a pillar[5]arene moiety along an axle (**Figure 2.3**). They initially determined that charged imidazolium species complex strongly with pillar[5]arene moieties,[11] which could be used to construct rotaxanes.[12] An asymmetric rod with an imidazolium component in close proximity to a stopper group was used to synthesise said rotaxane, using DEP5A as the pillar[5]arene moiety. After addition of the macrocycle and pseudorotaxane formation, an isocyanate stopper group was added to

cap the axle by reacting with the alcohol group, forming a urethane linkage. It was found that in low polarity solvents such as chloroform, the pillar[5]arene would preferentially reside over the imidazolium station due to the strong interaction between the imidazolium and the pillararene. When in high polarity solvents such as DMSO, solvophilic interactions with the imidazolium and solvophobic interactions with the alkyl chain force the macrocycle away from the imidazolium and onto the alkyl chain. Studies were also conducted at elevated temperatures (up to 115° C) where it was shown that the pillar[5]arene macrocycle shuttles back towards the imidazolium moiety and solvophobic effects are overcome. Thus, the placement of where the pillar[5]arene resides can be tuned using a solvent mix of polar/non-polar solvents and temperature.

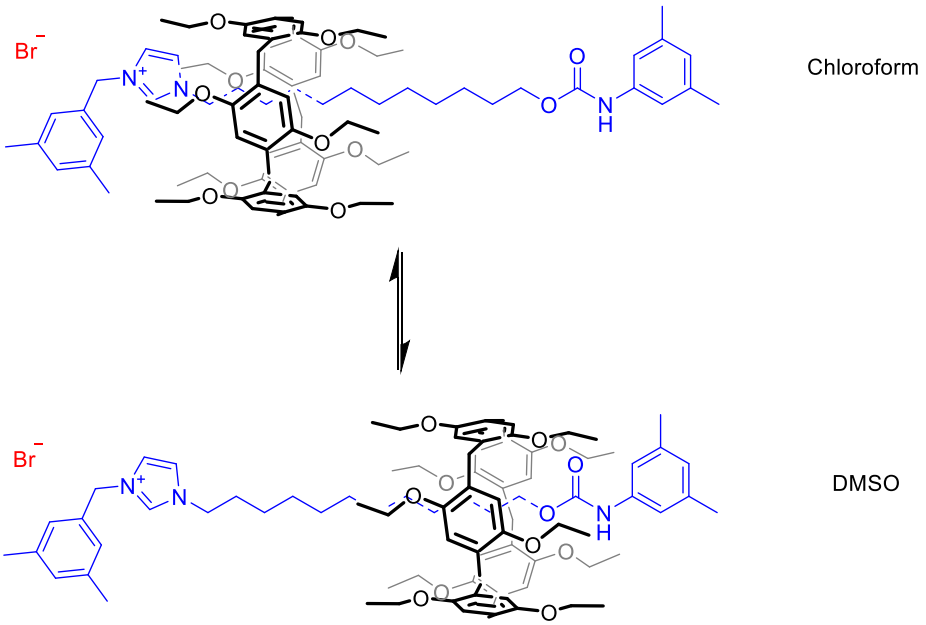

Figure 2.3. Huang's asymmetric [2]rotaxane polarity driven shuttle. The pillararene resides over the imidazolium in chloroform and closer to the urethane linkage in DMSO.[12]

The study in question uses a bromide salt of the rotaxane. Other halide salts of pillar[5]arene based [2]rotaxane systems using chloride[13] and iodide[14] have shown similar shuttling results in response to low and high polarity solvents or temperature.

2.1.3 [3]Rotaxane molecular switch

The translational motion of a macrocycle along an axle can be controlled by providing it with two distinct stations for it to shuttle between. This approach was the basis of a bistable [3]rotaxane switch designed by Stoddart and co-workers (**Figure 2.4**).[15] The

system, based on the same group's [2]rotaxane shuttles,[16] utilises four π-electron donor sites for the macrocycle which includes two tetrathiafulvalene stations and two naphthalene stations. Upon synthesis of the [3]rotaxane species, the blue box macrocycle resides over tetrathiafulvalene stations and after oxidation moved over to naphthalene stations. Reduction returns the macrocycle back to the origin. This motion was exploited to form a nanomechanical device where the macrocycles contained disulphide tethers which could attach to a gold surface to form a self-assembled monolayer deposited on silicon microcantilever beams and upon oxidation with iron(III) perchlorate of the species cause the surface to bend, whilst reduction with ascorbic acid would cause it to flatten back to origin.[17,18]

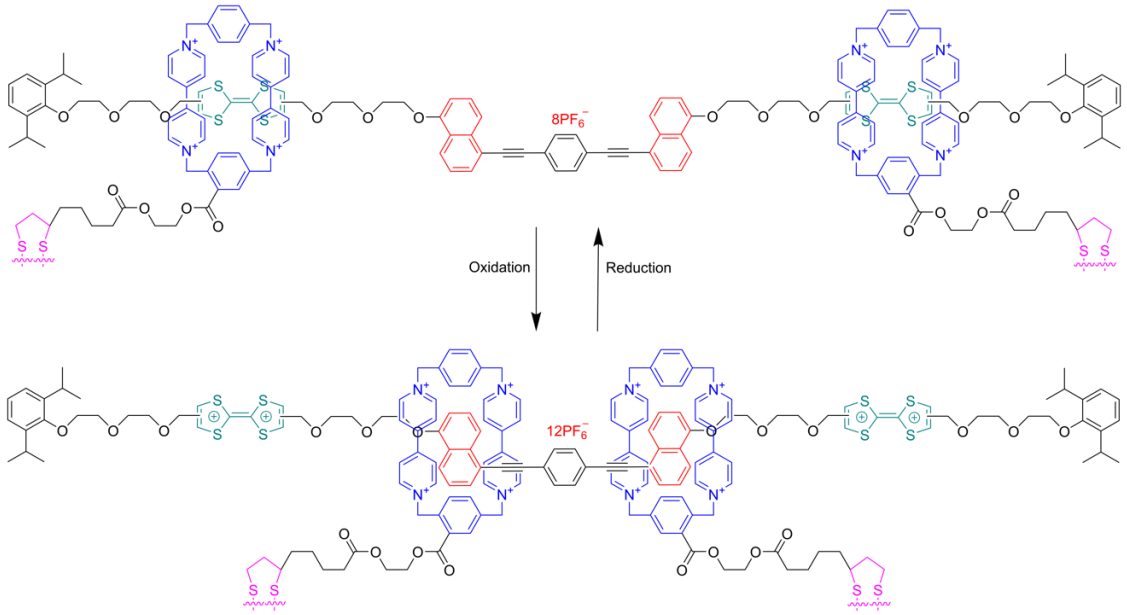

Figure 2.4. Stoddart's [3]rotaxane based molecular muscle. Thio-tethers (pink) are attached to a gold surface which is denoted by a wavy line.[15]

2.1.4 [3]Rotaxane molecular shuttle

Even more elaborate shuttling motions have been reported such as ring-through-ring shuttling. This can occur between two identical stations when two macrocycles are different within a [3]rotaxane species. This was examined when Loeb and co-workers designed a [3]rotaxane to investigate shuttling along a rigid axle when the macrocycles are of different sizes and discovered the larger macrocycle shuttles through the smaller macrocycle.[19] They started off by capping [24]crown-8 (24C8) onto a dibenzimidazole rod.

To prevent the larger macrocycle from dethreading, a larger stopper group needed to be implemented, so trityl groups were cross-coupled onto the ends of the axle via a Suzuki coupling. A larger crown ether [benzo[30]crown-8, n = 3 or benzo[42]crown-8, n = 9] was clipped onto the vacant benzimidazole site via a Grubbs catalysed ring closing reaction (**Figure 2.5**). Analysis of the of the different products using ^{1}H NMR suggested that the [24]crown-8 macrocycle on the [2]rotaxane was shuttling quickly between vacant benzimidazole sites. No shuttling was observed on the [3]rotaxane where benzo[30]crown-8 was implemented due to its similar size to 24C8, however using benzo[42]crown-8 expressed ring-through-ring shuttling behaviour, due to its larger size to pass over the smaller 24C8 and this was confirmed using 2D ^{1}H-^{1}H EXSY NMR spectroscopy.

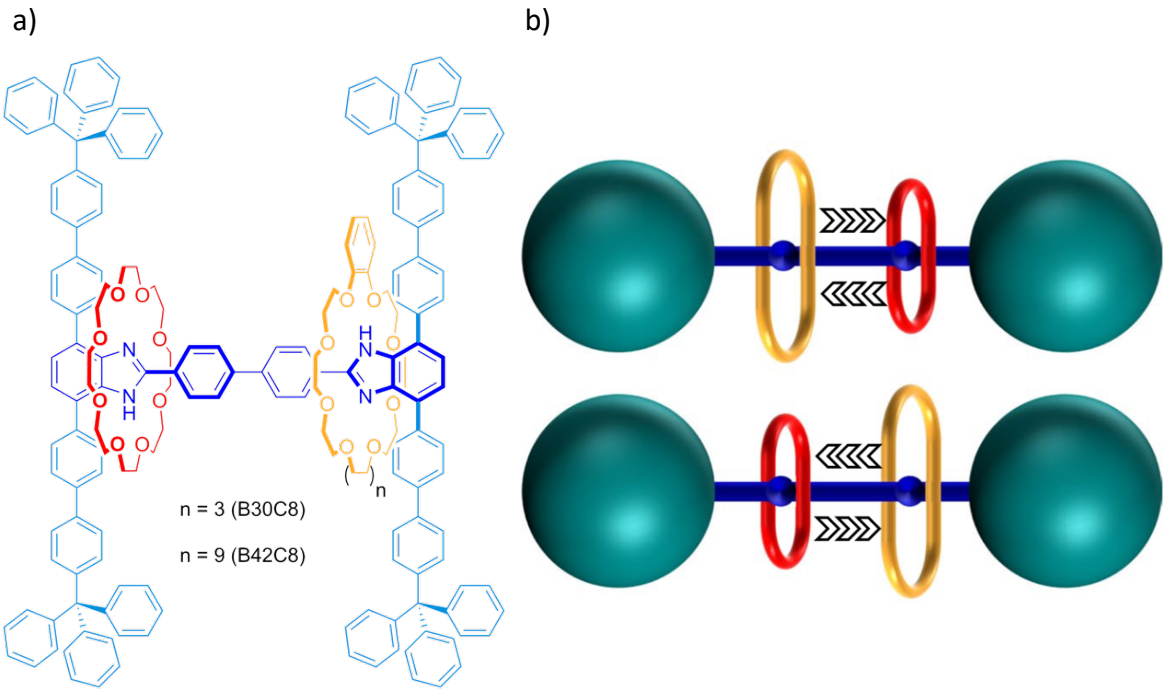

Figure 2.5. (a) is the structure of Loeb's [3]rotaxane and to the right, where no shuttling occurs when n=3, and ring-through-ring shuttling occurs when n=9. (b) is the cartoon model of ring-through-ring shuttling within the [3]rotaxane. Reprinted with permission from ref 19. Copyright 2018 Springer Nature.

2.2 Results and Discussion

The synthesis and characterisation of a series of pillar[5]arene based [3]rotaxanes, using different length alkyl chains (n=1-3, 6) along the rim of each pillararene is reported in this chapter. The rotaxanes have been characterised via ^{1}H and 2D NMR spectroscopies and shuttling behaviour has been analysed under different solvent conditions and temperatures.

2.2.1 Synthesis of toolkit

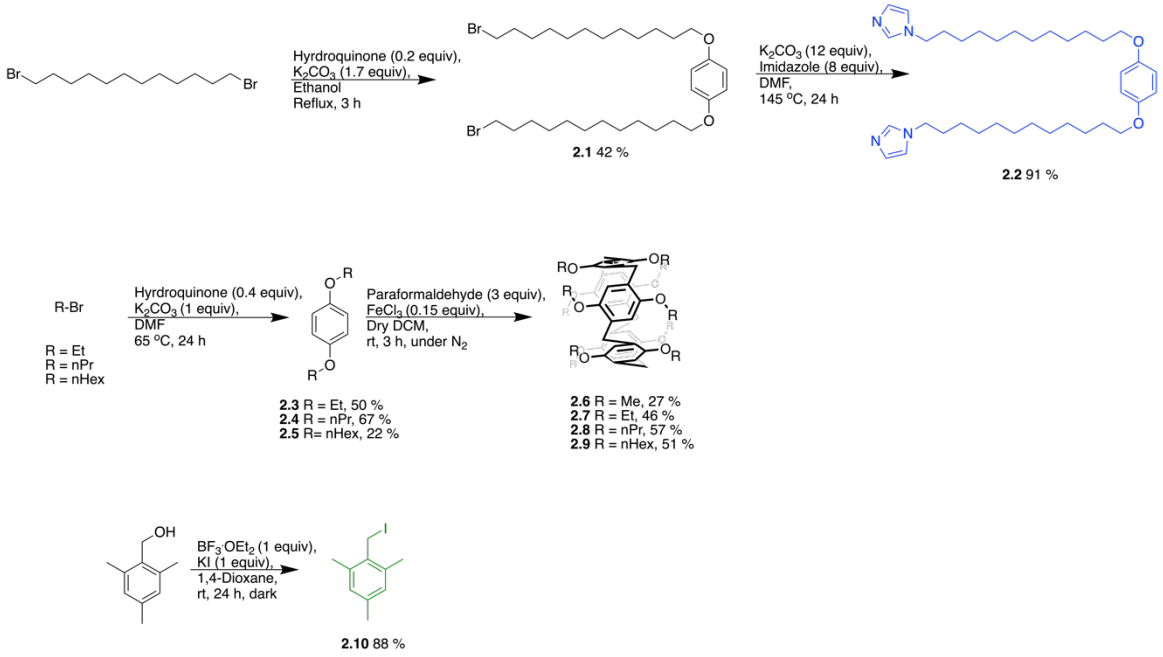

Scheme 2.1. Toolkit of components used to assemble [3]rotaxanes.

In order to assemble the rotaxanes, a toolkit of components was required. The toolkit comprises of an axle, which consisted of a bis-(alkylimidzole) hydroquinone; a macrocycle, pillar[5]arene with alkyl substituents with varying terminal chain lengths; and a mesityl stopper group to prevent dethreading (**Scheme 2.1**). Pillar[5]arene precursors (compounds **2.3**-**2.5**) were synthesised by alkylation of hydroquinone, except 1,4-dimethoxybenzene, which is commercially available. The pillararenes; DMP5A [dimethoxypillar[5]arene (n=1) **2.6**], DEP5A [diethoxypillar[5]arene (n=2) **2.7**], DPP5A [dipropoxypillar[5]arene (n=3) **2.8**] and DHP5A [dihexyloxypillar[5]arene (n=6) **2.9**] were

synthesised in moderate yields by a Friedel-Crafts alkylation under an inert N_2 atmosphere using iron(III) chloride as catalyst.

The precursor to the axle (compound **2.1**) was synthesised in a similar manner to the pillararene precursor molecules where hydroquinone was reacted with an excess of dibromoalkane, i.e more than two equivalents. This intermediate was reacted with imidazole to make the bis-imidazole rod (compound **2.2**).

The stopper group, 2-(iodomethyl)-1,3,5-trimethylbenzene (compound **2.10**), was synthesised via a one-step process[20] and was light sensitive, and therefore was stored in the dark.

2.2.2 Synthesis and characterisation of [3]rotaxanes

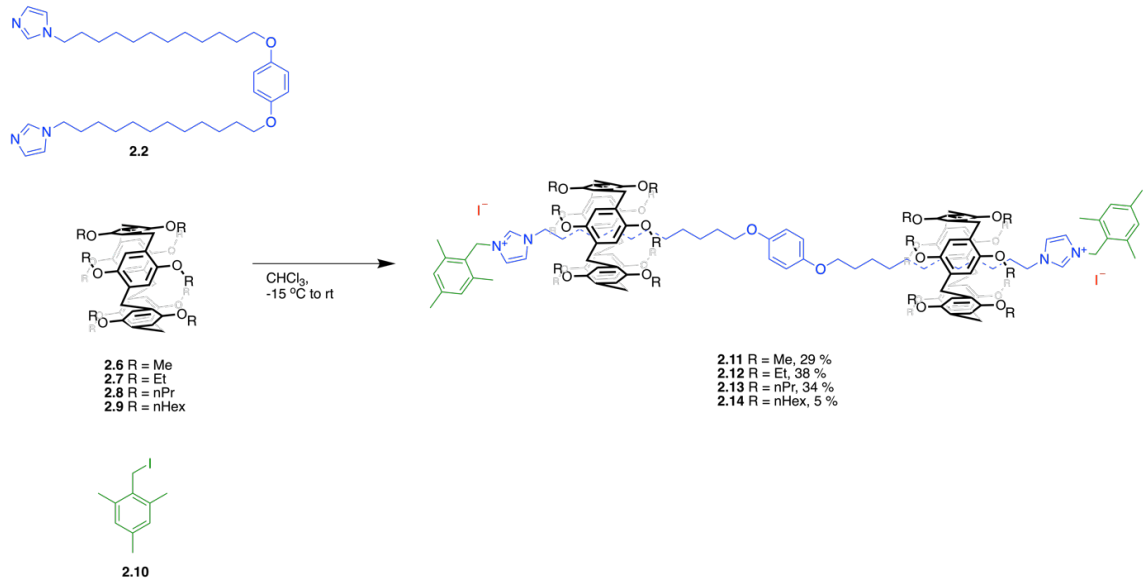

Scheme 2.2. Synthesis of [3]Rotaxanes.

Four [3]rotaxanes (compounds **2.11-2.14** on **Scheme 2.2**) were synthesised using the end-capping method, where the pillararenes were added to the axle in excess and at high concentration to encourage efficient threading and formation of pseudorotaxanes.[21] The stopper group was added last to prevent formation of the (non-threaded) dumbbell molecule. The stoppering reaction was performed in the dark, at -15 °C, to prevent the stopper group from decomposing before the reaction had taken place.

Each [3]rotaxane was purified by flash column chromatography with yields between 5 – 38%. The low yields were accounted for by the formation of [2]rotaxane by-products (**see chapter 3**). The low yield of rotaxane **2.14** could be partly accounted for by the positioning of two sterically demanding DHP5A molecules on the same rod. All [3]rotaxanes were found to be bench stable. In order to facilitate NMR characterisation and provide a reference NMR chemical shift to monitor rotaxane shuttling behaviour, a dumbbell molecule (compound **2.15**) was also synthesised by reacting the rod and stopper group in the absence of a pillararene. Characterisation was completed using ^{1}H, ^{13}C, ^{1}H-^{1}H COSY, ^{1}H-^{1}H NOESY NMR spectroscopies and electrospray ionisation mass spectrometry.

NMR analysis of the synthesised [3]rotaxanes (**2.11**–**2.14**) reveals that shuttling of the macrocycle occurs along the axle over the imidazolium stations and dodecyl chains on either end of the 1,4-dialkoxybenzene bridge. This behaviour was confirmed by changes in the chemical shift of the protons associated with imidazolium and dodecyl groups, when compared to the unthreaded dumbbell **2.15**. The shuttling of the pillar[5]arenes are restricted by bulky aromatic groups on either end of this region of the molecule, reflected by a lack of displacement in the ^{1}H NMR peaks of the aromatic stopper and hydroxyquinone linker group. The numbering used for the proton environments of the rotaxanes is shown below (**Figure 2.6**); the imidazolium region of the axle consists of protons $H_{m\text{-}q}$, the dodecyl chain consists of environments $H_{b\text{-}l}$, the 1,4-dialkoxybenzene bridge is denoted by H_a and the stopper groups are labelled $H_{r\text{-}s}$. The assignment of protons H_p and H_o was determined by the presence of cross peaks with H_q, in the COSY/NOESY NMR spectra as they were present between H_p and H_q, but not H_o and H_q (**Figures 7.1 – 7.40**). Similarly, H_b was determined via cross peaks with H_a from the ^{1}H-^{1}H NOESY NMR spectra.

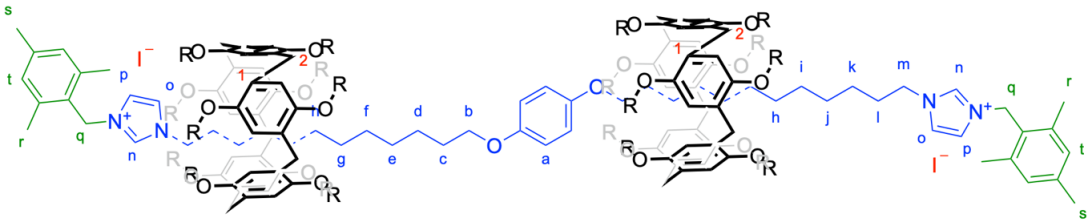

*Figure 2.6. General structure of [3]rotaxanes **2.11**-**2.14** in $CDCl_3$ where the protons are labelled for clarity.*

In order to accurately understand shuttling within the [3]rotaxane systems, a shielding factor (**Formula 2.1**) was calculated for each proton environment.

$$Shielding\ Factor = Shift\ of\ dumbbell\ (ppm) - Shift\ of\ rotaxane\ (ppm)$$

Formula 2.1. A calculated shielding factor per proton environment shows the relative change in shift on any given rotaxane from its corresponding dumbbell molecule.

A larger shielding factor implied greater pillar[5]arene residency over that particular proton environment. Due to the symmetry of the NMR spectrum, indicating that each half of the [3]rotaxane behaved similarly, plots of the shielding factors also display a mirror plane.

2.2.3 Shuttling of macrocycles on [3]rotaxanes in $CDCl_3$

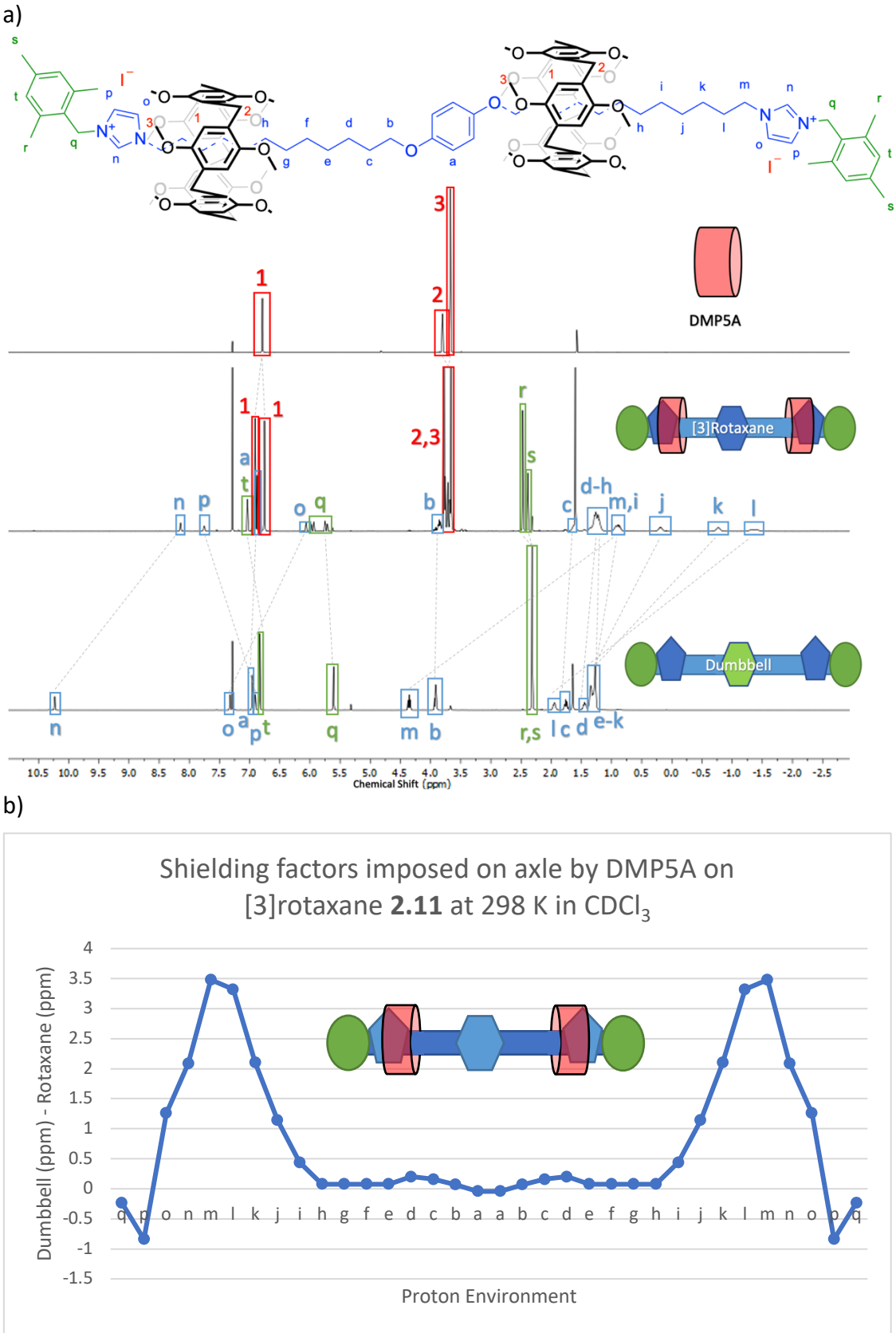

*Figure 2.7. (a) ^{1}H NMR stack of DMP5A (**2.6**), [3]rotaxane (**2.11**) and dumbbell (**2.15**) in $CDCl_3$ in descending order and (b) plot of shielding factors for [3]rotaxane **2.11** in $CDCl_3$.*

Characteristic shielding occurs across all [3]rotaxanes in chloroform, where protons on the axle which are interacting with the macrocycle component are shifted upfield. From the calculated shielding factors of **2.11** (**Figure 2.7**), peaks H_i-H_o are shielded the most as expressed by their large displacement with respect to the dumbbell molecule. This results in a maximum shielding effect around proton environment H_m which indicates the pillar[5]arene macrocycle preferentially resides close to the imidazolium moiety and neighbouring carbons along the aliphatic chain.[22] Shuttling may occur across the axle, from peaks H_o to H_b as another maximum is observed around peak H_d. However, shuttling is not observed towards the central benzene linker, with little shielding effect determined for protons H_b and H_a. This observation indicates that the benzene moiety, possibly accompanied by repulsion from the oxygen atom connecting the dodecyl chains to the benzene ring, inhibits shuttling.[23] The macrocycle does not interact with H_a on the benzene ring, with no shielding effect observed, and so the linker acts as a barrier, preventing the pillararenes from coming into direct contact with each other.

The shielding factors of peaks H_p and H_q are negative, indicating steric clashing between the pillararene and the mesityl stopper group in addition to deshielding by the oxygen atoms along the rim of the pillar[5]arene. The shielding factors from H_h to H_b, which correspond to the dodecyl chain are positive, but low, suggesting either that shuttling is either very slow or very fast along the length of the axle. These results suggest that the pillararenes are predominantly pirouetting around the imidazolium moieties.

Pillar[5]arene peak H_1 is split into two signals when threaded through the axle as a result of the asymmetry imposed onto the axle when both enantiomers of DMP5A statistically thread across the axle. Peaks H_2 and H_3 on DMP5A could not be resolved when threaded.

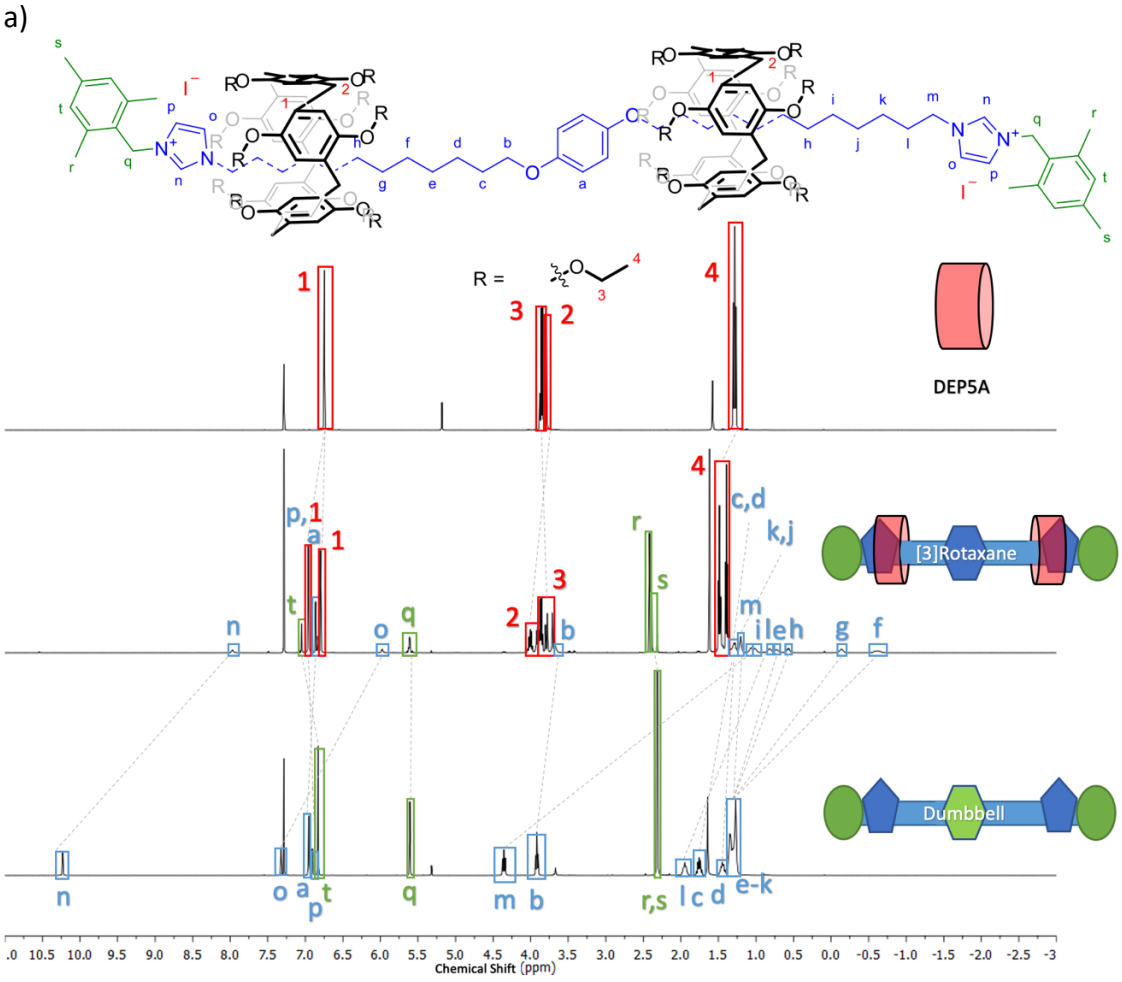

*Figure 2.8. (a) ^{1}H NMR stack of DEP5A (**2.7**), [3]rotaxane (**2.12**) and dumbbell (**2.15**) in $CDCl_3$ in descending order and (b) is the plot of shielding factors for [3]rotaxane **2.12** in $CDCl_3$.*

Shuttling occurs along the axle for [3]rotaxane **2.12** in chloroform (**Figure 2.8**), as illustrated by the three shielding factor maxima around proton environments H_m, H_f and H_c. The maximum at H_m is due to the electrostatic attraction between the pillararene and the imidazolium group, and is the most favourable position of the pillar[5]arene along the axle. Along the dodecyl chain, the maximum at peak H_c is due to H_b being the last place for the pillararene to reside before being repelled by the 1,4-dialkoxybenzene moiety (see discussion for **2.11**). The maximum at H_f is close to the centre of the dodecyl chain which is in between the repulsive 1,4-dialkoxybenzene and the favourable imidazolium moiety. This suggests that the position of the pillar[5]arene is less well defined in this instance and that favourable interactions are observed along different regions of the axle. An overall increase in shielding constants from H_a to H_m is observed, suggesting shuttling is limited closer to the central 1,4-dialkoxybenzene unit. Unlike **2.11**, the shielding factor of H_p is not negative and for H_q the magnitude of the shielding effect is not as negative, suggesting that the 1,4-dialkoxybenzene units of DEP5A are not interacting with the stopper groups as much as in **2.11**, perhaps due to the longer lengths of the terminal ethoxy chains.

Similar to **2.11**, an asymmetry is imposed by the axle and thus split H_1 peaks into two along the axle of **2.12.** Additionally, peaks H_2 and H_3 were merged, but spread across a larger area. Terminal alkyl peaks H_4 were split into two triplets in relation to a single triplet as an unthreaded ring.

a)

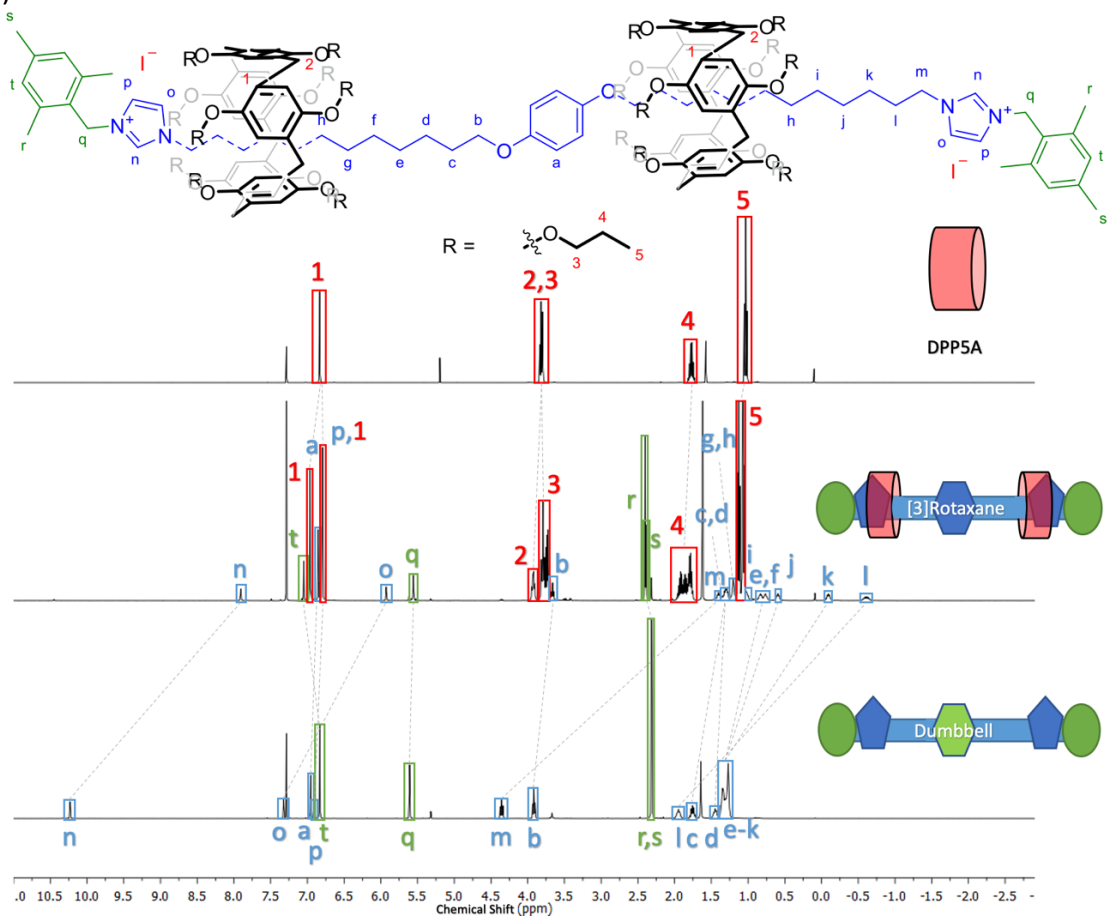

b)

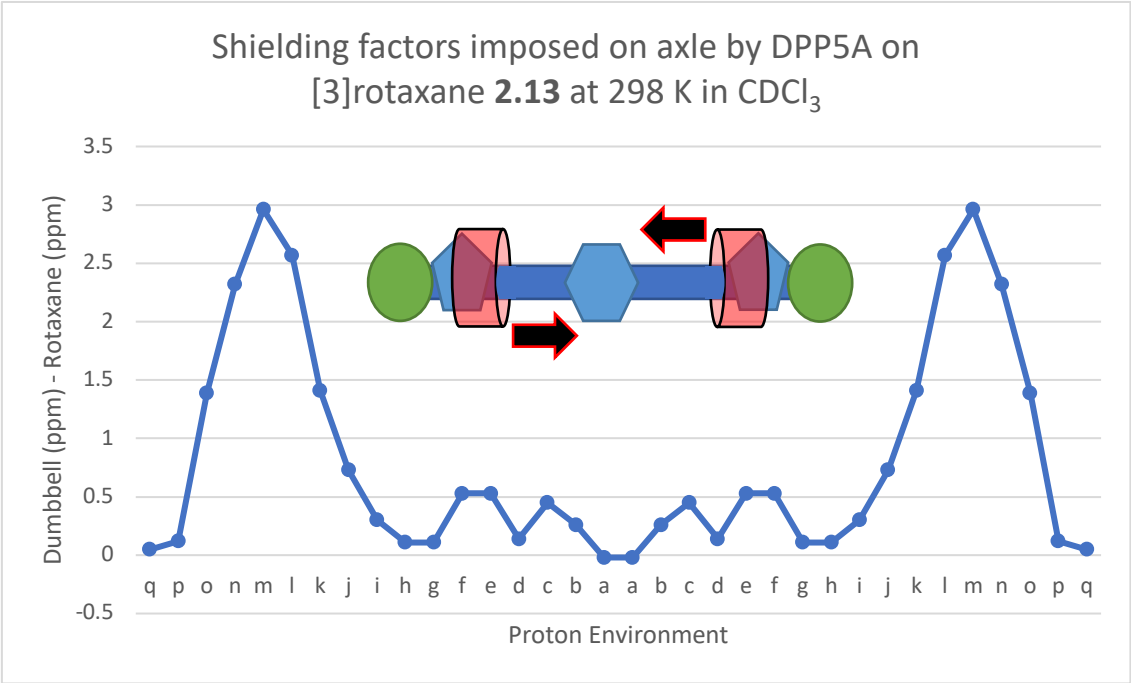

*Figure 2.9. (a) ^{1}H NMR stack of DPP5A (**2.8**), [3]rotaxane (**2.13**) and dumbbell (**2.15**) in $CDCl_3$ in descending order and (b) plot of shielding factors for [3]rotaxane **2.13** in $CDCl_3$.*

Similarly, [3]rotaxane **2.13** (**Figure 2.9**) has a maximum for its shielding factors at peak H_m due to the favourable interactions between the pillararene and the imidazolium, with shielding effects reducing either side of the imidazolium, either due to the steric effects of the stopper group or unfavourable interactions with the dodecyl chain. Shuttling across the dodecyl chain does occur, as indicated through maxima at proton environments H_f, H_e and H_c. As before, the pillararenes are sterically blocked by the 1,4-dialkoxybenzene unit in the centre of the axle. Environments H_p and H_q do not exhibit negative shielding effects, in comparison to **2.11** and **2.12**, most probably due to the longer lengths of the propoxy chains inhibiting strong interactions.

The smaller shielding factor maxima along the dodecyl chain of **2.13** is due to the odd-even effect of the pendant propoxy chains along the rim of DPP5A, where similarly depressed maxima are observed for **2.11** along the dodecyl region.[24]

Splitting of the DPP5A ^{1}H NMR signals for [3]rotaxane **2.13** are similar to those observed for **2.11** and **2.12**, where peaks H_1 are split into 2 signals. Bridging peaks $H_{2\text{-}4}$ are spread over a larger range than seen for free DPP5A and terminal alkyl peaks H_5 are split into a doublet of triplets. Like **2.12**, the splitting of the terminal peaks is accounted for by the asymmetry imposed by the axle resulting in interactions with chemically distinct environments at each terminus of the macrocycle.

a)

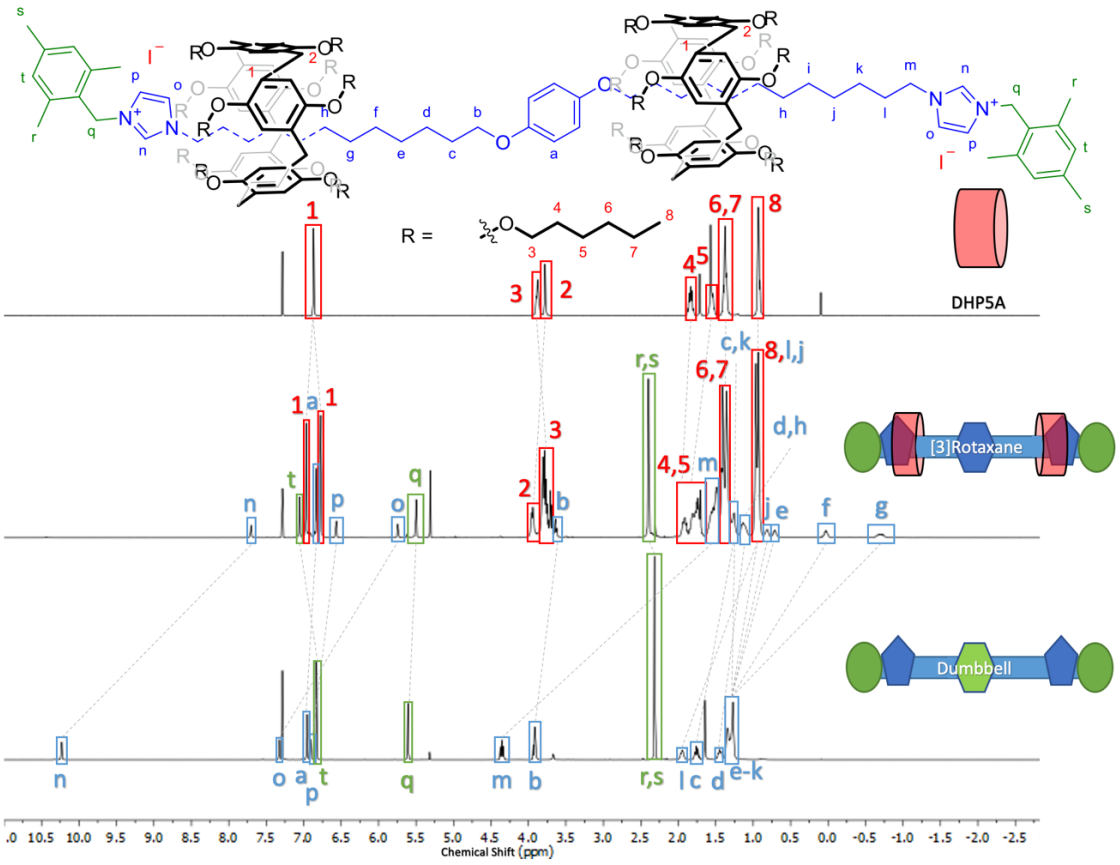

b)

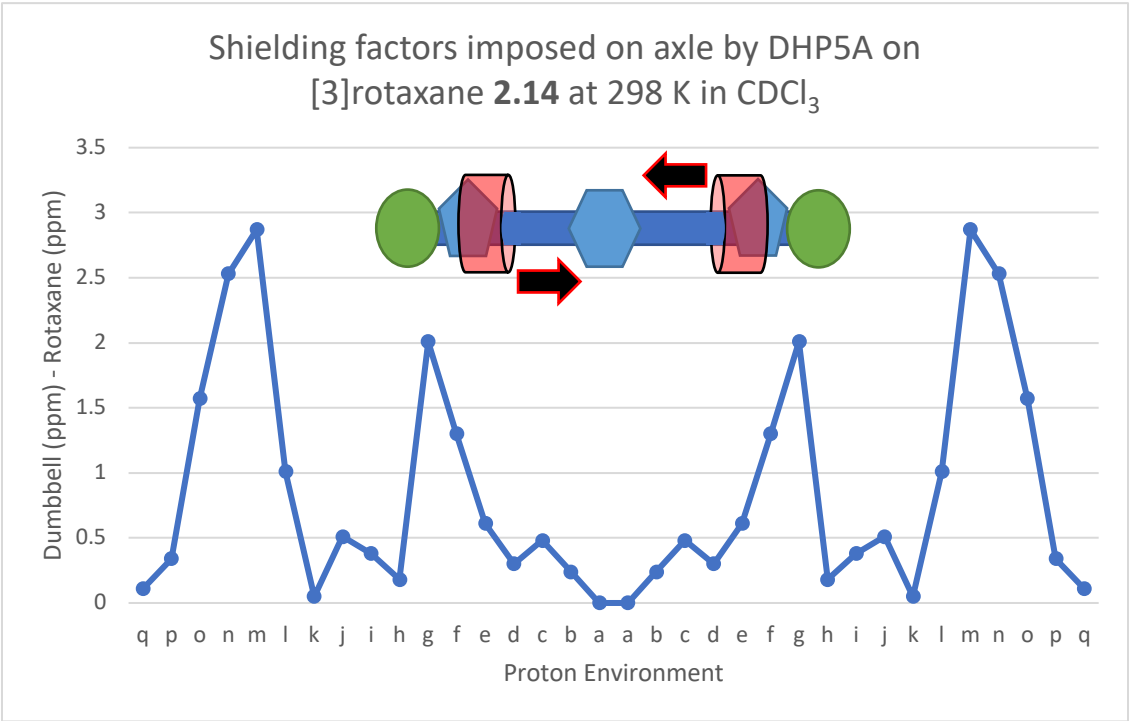

*Figure 2.10. ^{1}H NMR stack of DHP5A (**2.9**), [3]rotaxane (**2.14**) and dumbbell (**2.15**) in $CDCl_3$ in descending order and (b) plot of shielding factors for [3]rotaxane **2.14** in $CDCl_3$.*

[3]Rotaxane **2.14** (**Figure 2.10**) has a shielding factor maximum at proton environment H_m tailing off from both ends due to sterics from the stopper group and movement of the macrocycle onto the dodecyl chain. The second largest maximum is at H_g which is slightly further away from rotaxane **2.12**'s H_f maximum, probably as a result of the steric interactions of the longer hexyl chains with the stopper group, the linking dialkoxybenzene and potentially the opposing DHP5A macrocycle on the other half of the axle. Smaller maxima at H_j and H_c confirm shuttling is occurring along the rest of the axle. When threaded through the axle in **2.14**, DHP5A follows the trend of the H_1 peaks splitting into two. Central peaks $H_{3\text{-}5}$ broaden, and terminal peaks H_8 are also split into two. Peaks closest to the terminal peaks, H_6 and H_7, are no longer merged in relation to the free pillararene.

The large shielding factor maxima for **2.14** along the dodecyl chain can also be attributed to the odd-even effect where shuttling behaviour resembles **2.12** as opposed to **2.11** or **2.13**.

There may be little to no interactions between the terminal aliphatic peaks ($H_{6\text{-}8}$) along DHP5A and the axle evidenced by the lack of corresponding NOE signals, suggesting that the hexyl chains are spread away from the axle, interacting with the solvent environment (**Figure 7.30**).

a)

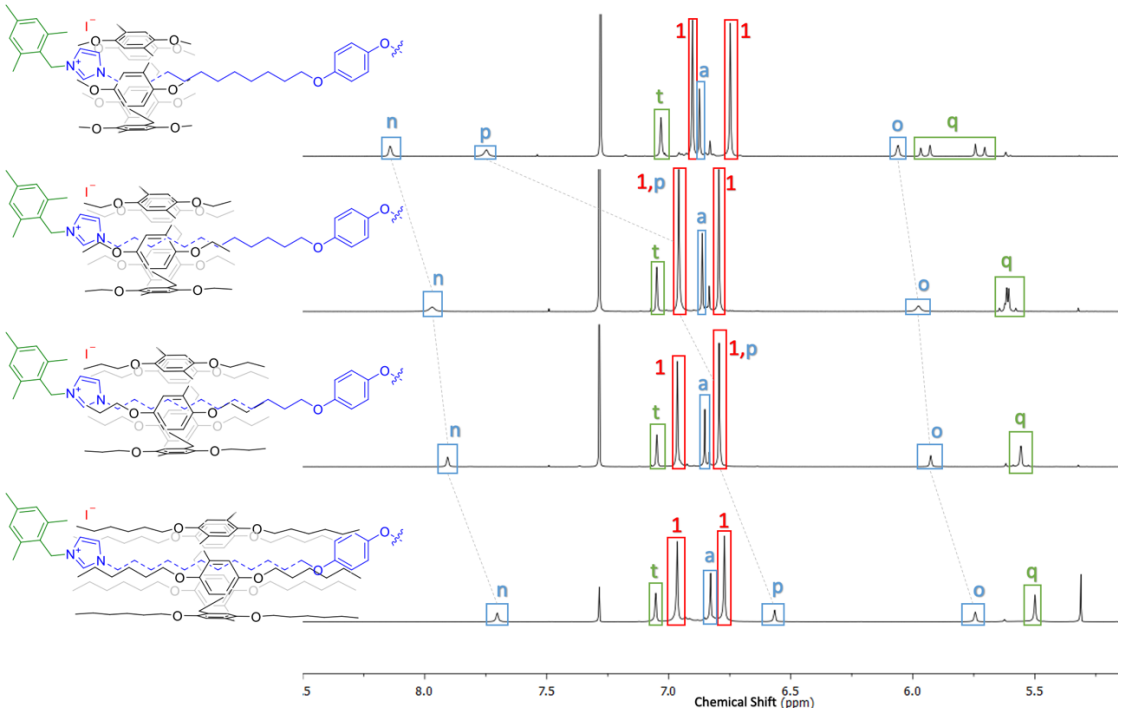

b)

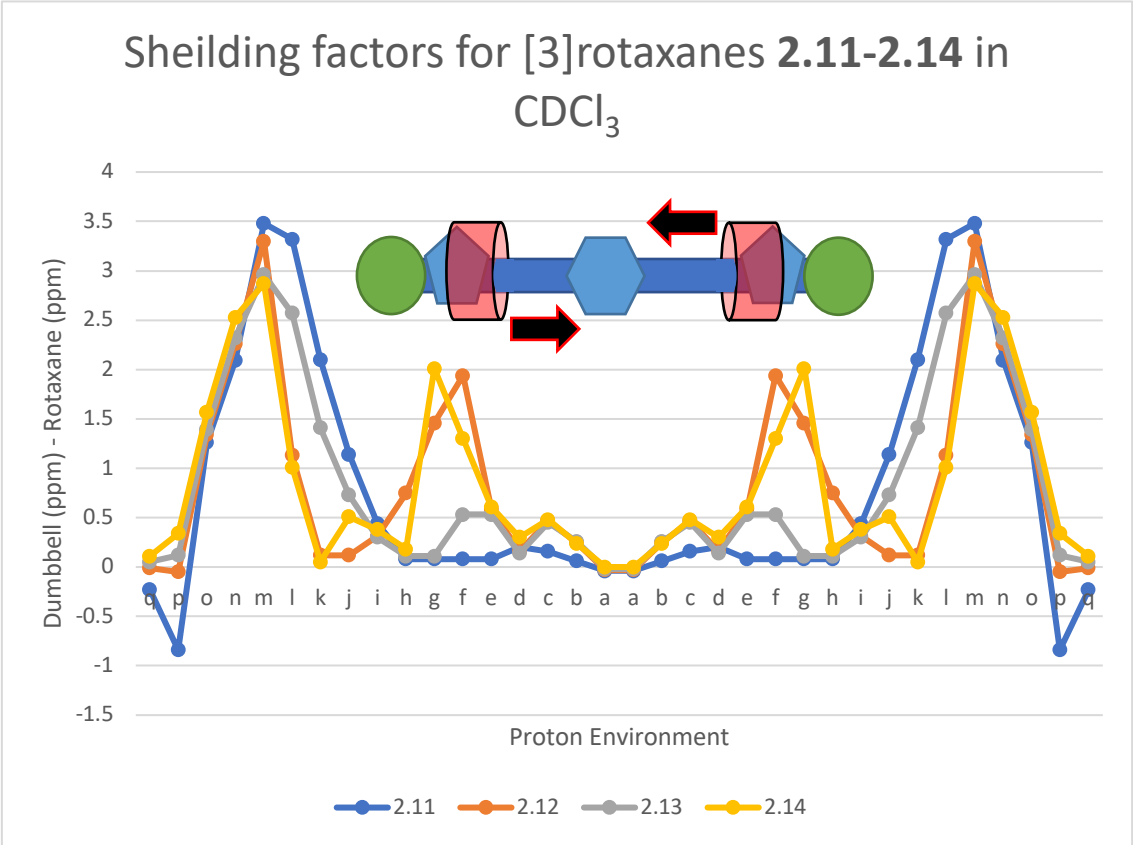

*Figure 2.11. (a) Stacked ^{1}H NMR spectra of [3]rotaxanes **2.11-2.14** in $CDCl_3$ from 8.5 ppm to 4.5 ppm in descending order and (b) overlaid plots of shielding factors of [3]rotaxanes **2.11-2.14** in $CDCl_3$.*

Trends can be seen when overlaying the ^{1}H NMR of [3]rotaxanes **2.11-2.14** in $CDCl_3$ (**Figure 2.11**). A greater spread of shielding is observed from H_n - H_q as the lengths of the alkyl chains on the pillararenes increase, a trend that is expected due to the extra surface area covered by the longer pillararenes. Peak H_q is most affected by the length of the terminal chains along the rim of the pillararene. In **2.11** the presence of diastereoisomers as a result of two DMP5A macrocycles threading across a single axle causes H_q to split into a doublet of doublets which are widely separated (**Figure 7.3**). When the lengths of the alkyl chains along the rim of the pillararene increase in **2.12**, the diasteroemeric effect had diminished into a triplet interacting with only H_3 and H_4 from the terminal ethyl chains. **2.13** enhances this effect when H_q is no longer affected by the chirality of the macrocycles, however the shielding factor still increases, so H_q only interacts with the terminal protons on DPP5A. This is exacerbated in **2.14** with its hexyl chains from DHP5A where no NOE signal can be found for H_q interacting with terminal proton H_8 (**Figure 7.30**).

2.2.4 Shuttling of macrocycles in DMSO and high temperature ^{1}H NMR studies

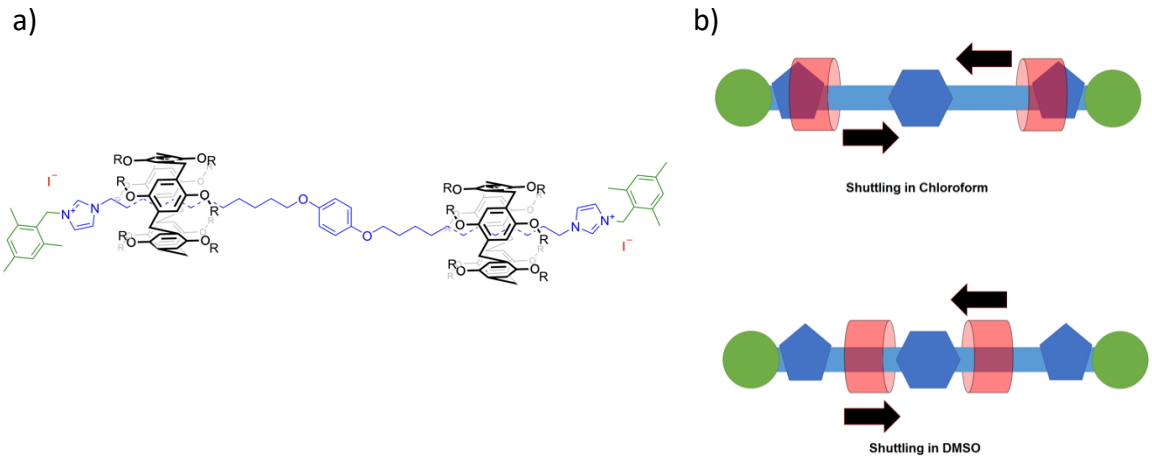

Figure 2.12. (a) general structure of the [3]rotaxanes and (b) a cartoon model of the shuttling modes observed for the [3]rotaxane systems in $CDCl_3$ and DMSO-d_6.

When the rotaxanes are dissolved in DMSO-d_6, a solvent-ion pair is stabilised, such that it becomes unfavourable for the macrocycles to reside over the imidazolium moiety. As a result, the macrocycles are pushed further onto the dodecyl chains (**Figure 2.12**).

For [3]rotaxanes **2.11**-**2.14**, proton environments H_{n-q}, which relate to the imidazolium region, experience little shielding at room temperature in DMSO-d_6, with respect to the dumbbell, as a result of interactions of the imidazolium group with the solvent.

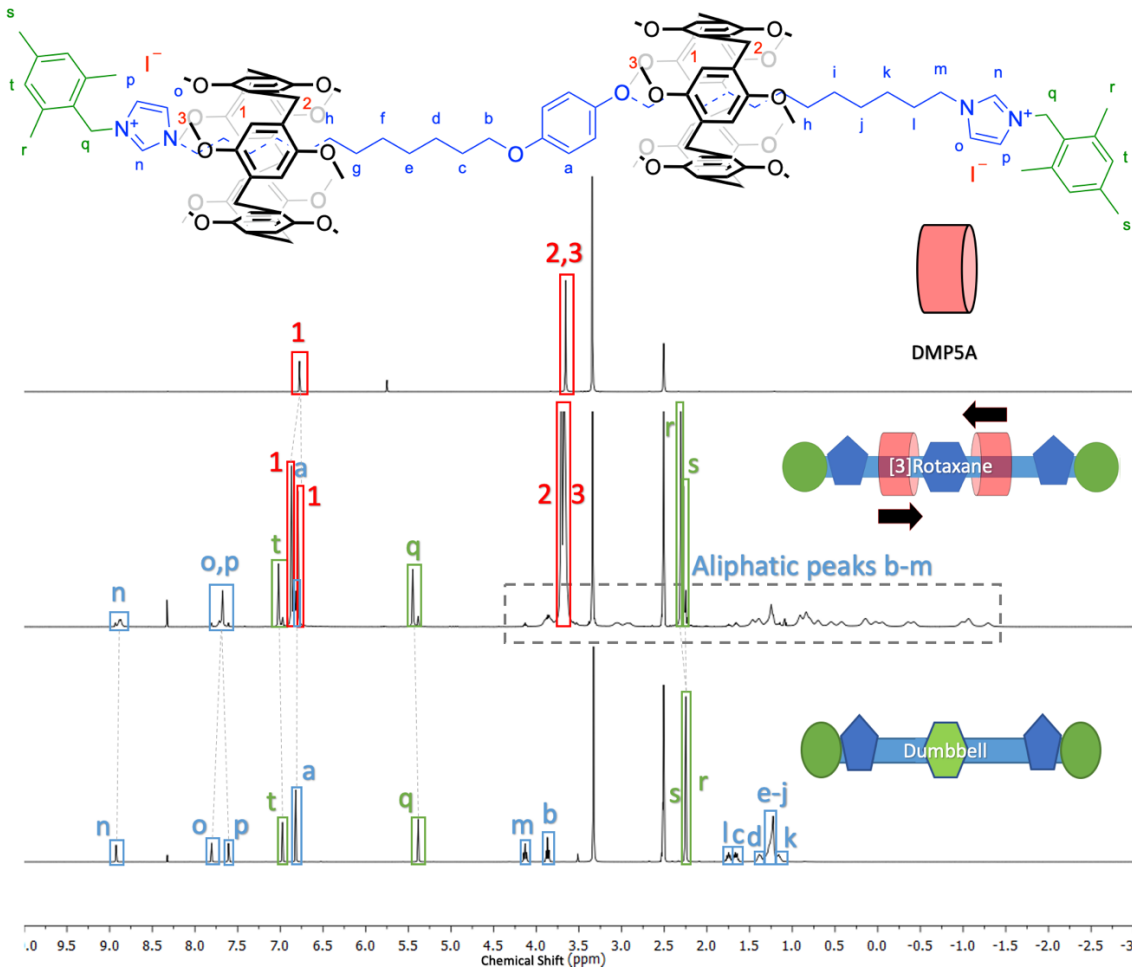

*Figure 2.13. ^{1}H NMR stack of DMP5A (**2.6**), [3]rotaxane (**2.11**) and dumbbell (**2.15**) in DMSO-d_6 at room temperature in descending order.*

The nature of the shuttling could not be quantified for [3]rotaxane **2.11** in DMSO (**Figure 2.13**), as aliphatic proton environments (H_{b-m}) could not be assigned. All other parts of the molecule could be assigned, which confirmed the DMP5A macrocycles were no longer situated over the imidazolium stations, as these environments (H_{n-q}) saw little to no upfield shift which corresponded to absence of macrocycle encirclement. Thus, similar behaviour, in terms of localisation of shielding effects was observed for **2.11** in both chloroform (**Figure 2.7**) and DMSO. Further information was provided by the 2D NMR spectroscopies ^{1}H-^{1}H COSY and ^{1}H-^{1}H NOESY (**Figure 2.14**).

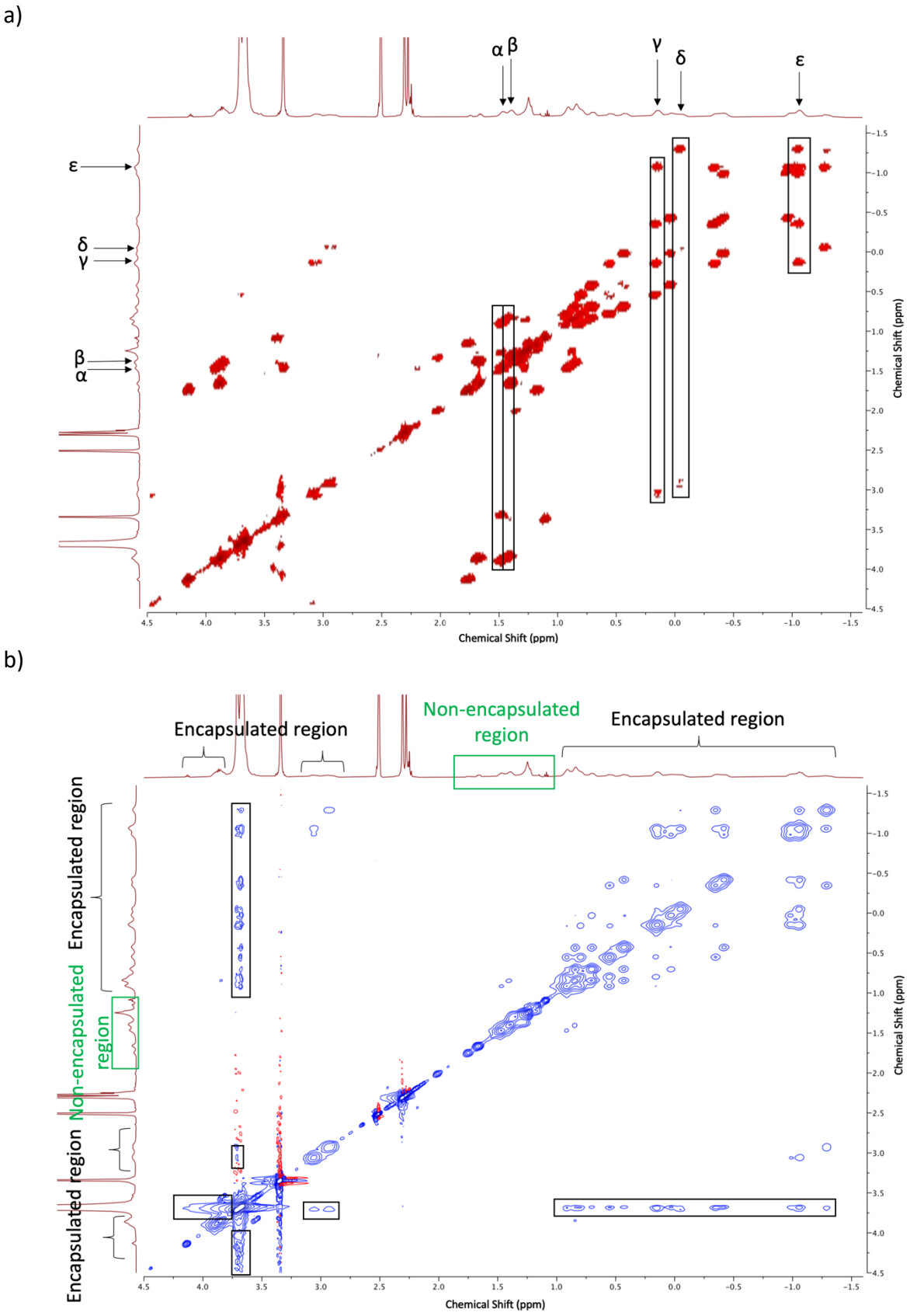

*Figure 2.14. Partial ^{1}H-^{1}H 2D spectra of [3]rotaxane **2.11** at room temperature in DMSO-d_6. (a) partial ^{1}H-^{1}H COSY and (b) partial ^{1}H-^{1}H NOESY, showing distinct encapsulated and non-encapsulated regions.*

^{1}H-^{1}H COSY data shows proton environments coupling to more than their adjacent neighbours. These environments are labelled α – ε and all possess more cross peaks than is expected for an aliphatic chain. Using information provided by ^{1}H-^{1}H NOESY through space coupling, we see that there are distinct encapsulated regions and non-encapsulated regions. The boxed cross peaks are aliphatic peaks $H_{b\text{-}m}$ on the dumbbell interacting with protons $H_{2,3}$ on the pillararene. Proton environments γ-ε are encompassed in the encapsulated region, whereas α and β do not interact with the pillararene, implying a non-encapsulated region is observed.

Summing up these deductions would suggest that shuttling along the dodecyl chains is highly limited for [3]rotaxane **2.11** at room temperature in DMSO. Another way of expressing this would be that the distribution of DMP5A along the axle is disordered resulting from the lack of a station to interact with the macrocycle.

a)

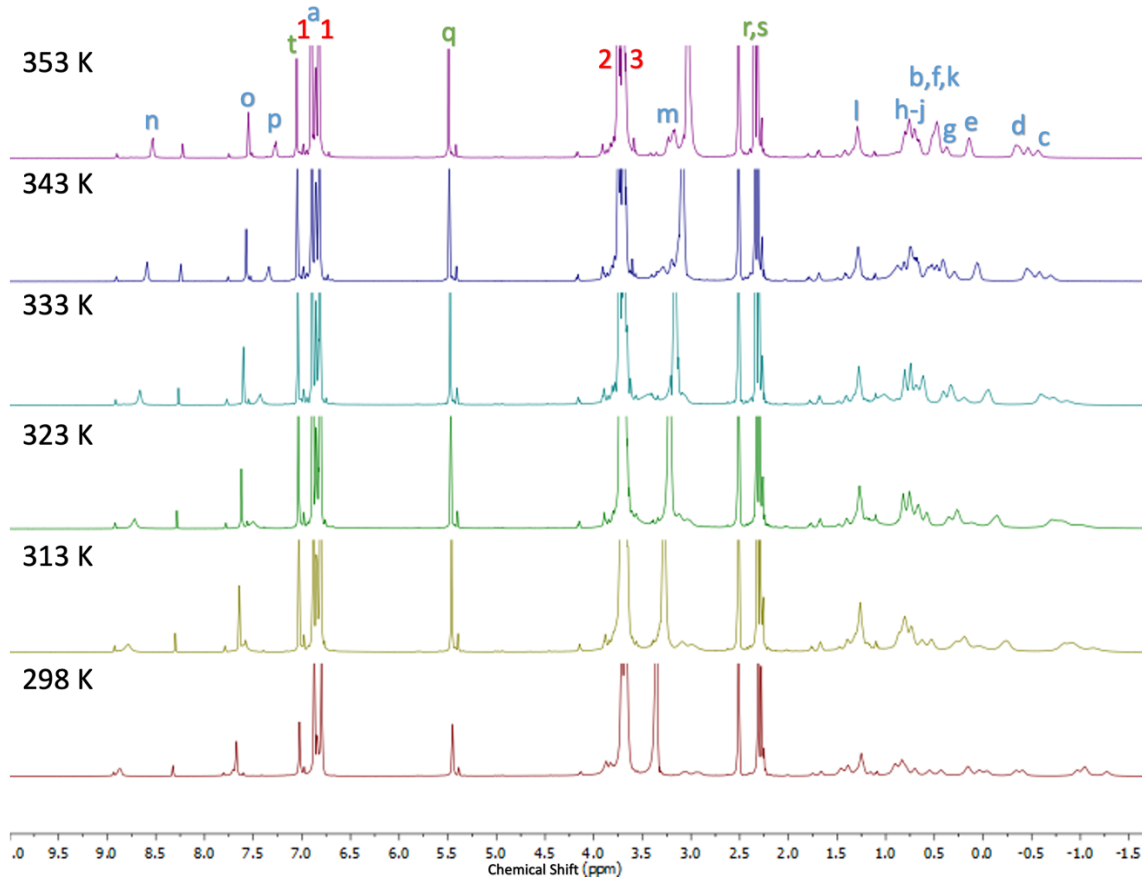

b)

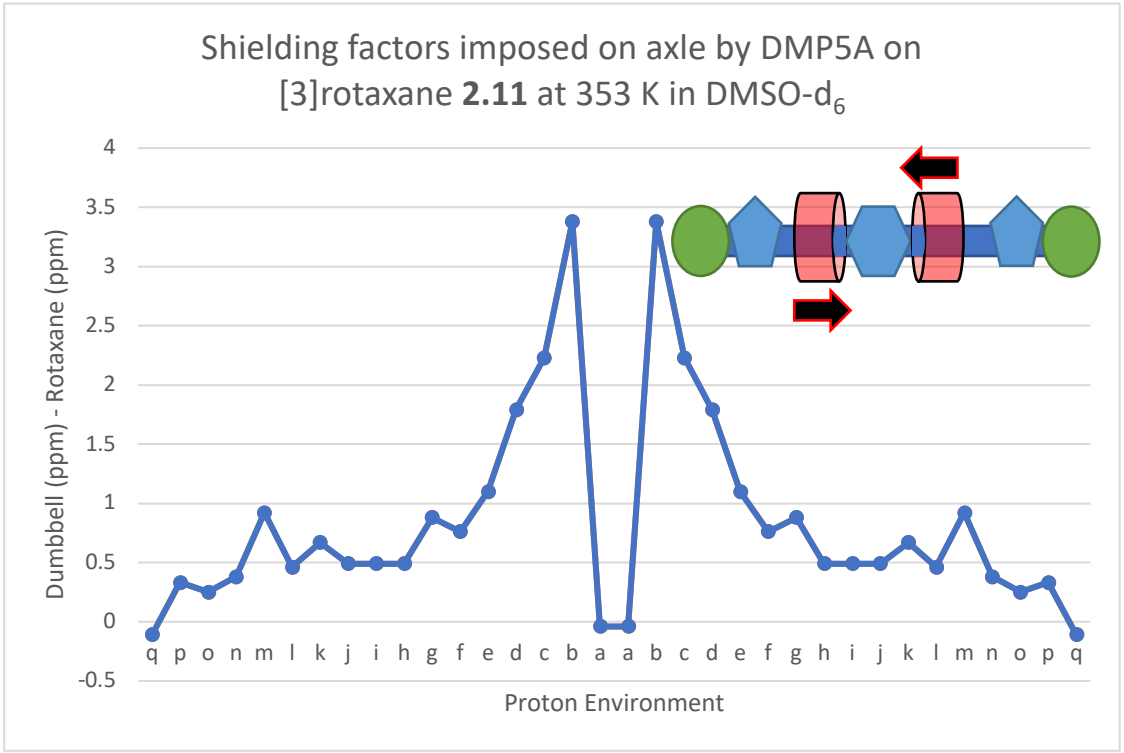

*Figure 2.15. (a) stacked variable temperature ^{1}H NMR spectra of [3]rotaxane **2.11** in DMSO-d_6 at 600 MHz and (b) corresponding shielding factors of [3]rotaxane **2.11** in DMSO-d_6 at 353 K.*

Increasing the temperature of the NMR ^{1}H NMR experiment for **2.11** in DMSO-d_6 to 353 K, rapidly increases the rate of shuttling, to faster than the timescale of the NMR experiments (**Figure 2.15**). Global maxima are about peak H_b, closest to the 1,4-dialkoxybenzene unit, with shielding factors steadily dropping as the pillararenes approach the stopper groups. Peak H_a is unaffected by shuttling of DMP5A as the macrocycles cannot reside over 1,4-dialkoxybenzene due to its larger size and poorer fit for the macrocycle.

DEP5A, DPP5A and DHP5A were all insoluble in DMSO, thus full ^{1}H NMR stacks could not be achieved, however relative shifts could still be seen and shielding factors calculated as solubility of the [3]rotaxanes (**2.12-2.14**) and the dumbbell molecule (**2.15**) in DMSO was favourable.

a)

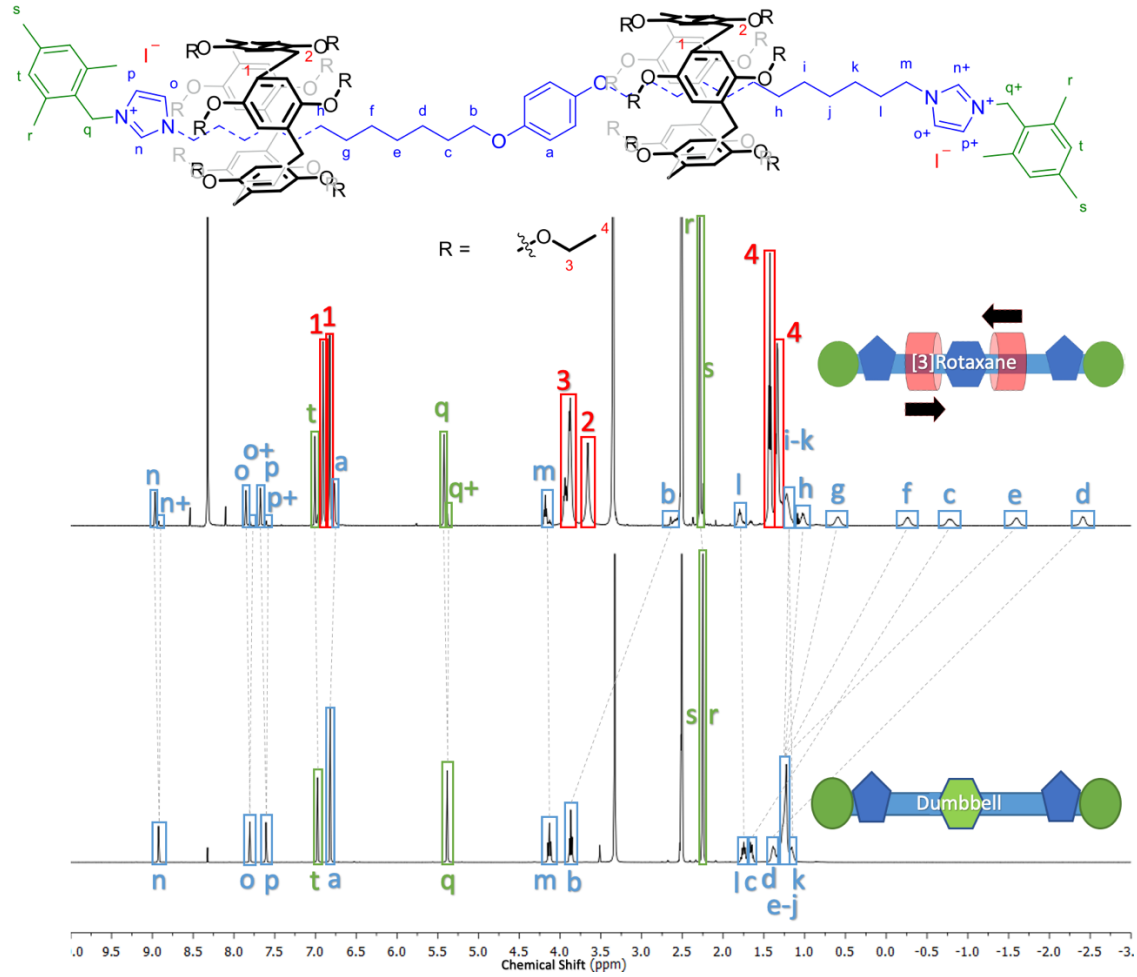

b)

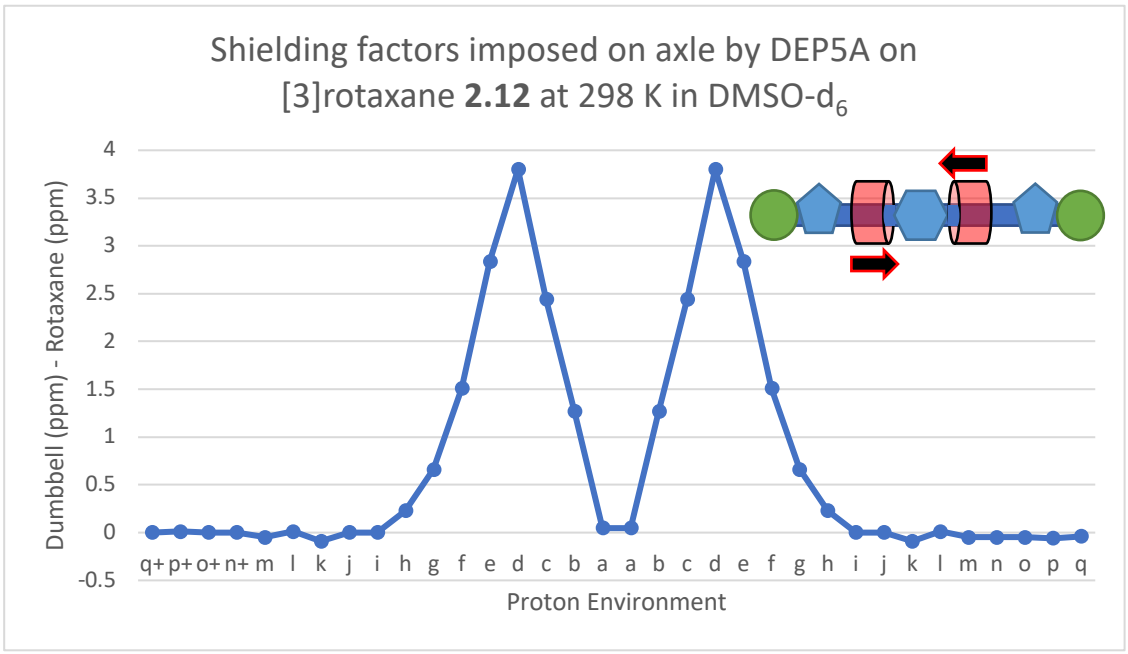

*Figure 2.16. (a) ^{1}H NMR stack of DEP5A (**2.7**), [3]rotaxane (**2.12**) and dumbbell (**2.15**) in DMSO-d_6 at room temperature in descending order and (b) plot of shielding factors of [3]rotaxane **2.12** in DMSO-d_6 at room temperature.*

[3]Rotaxane **2.12** at room temperature seemingly shuttles more conventionally in DMSO (**Figure 2.16**). The imidazolium-DMSO interaction prevents DEP5A from accessing the area affected which includes the imidazolium stations $H_{n\text{-}q}$, but also part of the dodecyl chain, as environments $H_{i\text{-}m}$ experience minimal encapsulation. A small asymmetry imposed over the imidazolium region ($H_{n\text{-}q}$ and $H_{n+\text{-}q+}$), could suggest that the macrocycles are in different positions to each other.

a)

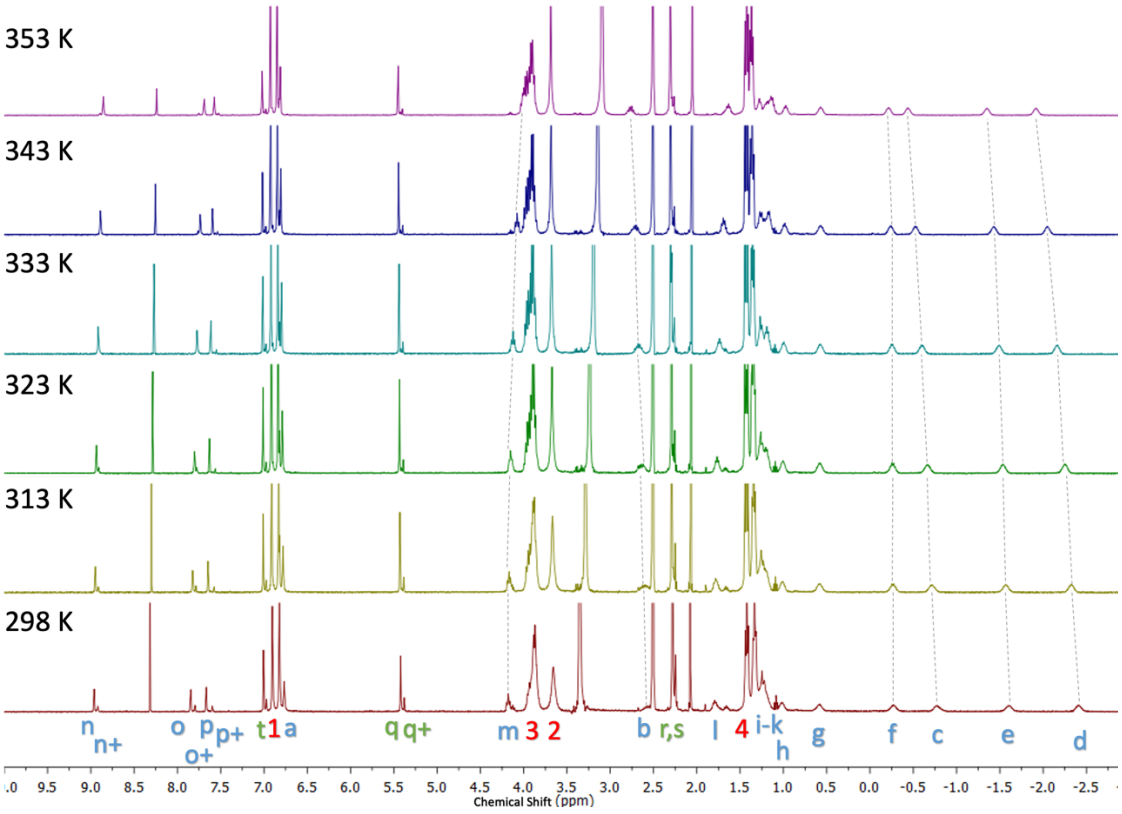

b)

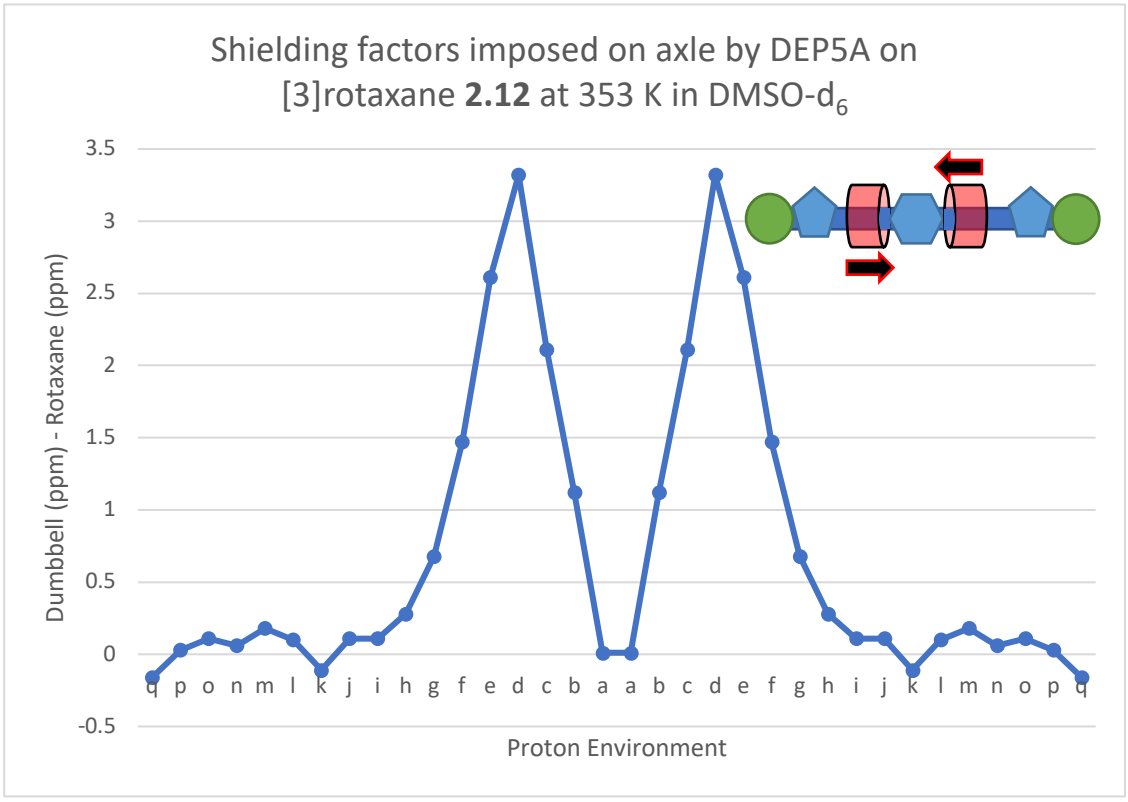

*Figure 2.17. (a) stacked variable temperature ^{1}H NMR spectra of [3]rotaxane **2.12** in DMSO-d_6 at 400 MHz and (b) corresponding shielding factors of [3]rotaxane **2.12** in DMSO-d_6 at 353 K.*

When the temperature of the ^{1}H NMR measurement for **2.12** in DMSO is increased to 353 K (**Figure 2.17**), shielding is located around the same area as at room temperature. The increase in temperature provides more energy to the DEP5A to overcome the imidazolium-solvent interactions, with peaks $H_{i\text{-}o}$ having greater shielding factors than at room temperature, however this region is only partially accessible to DEP5A.

a)

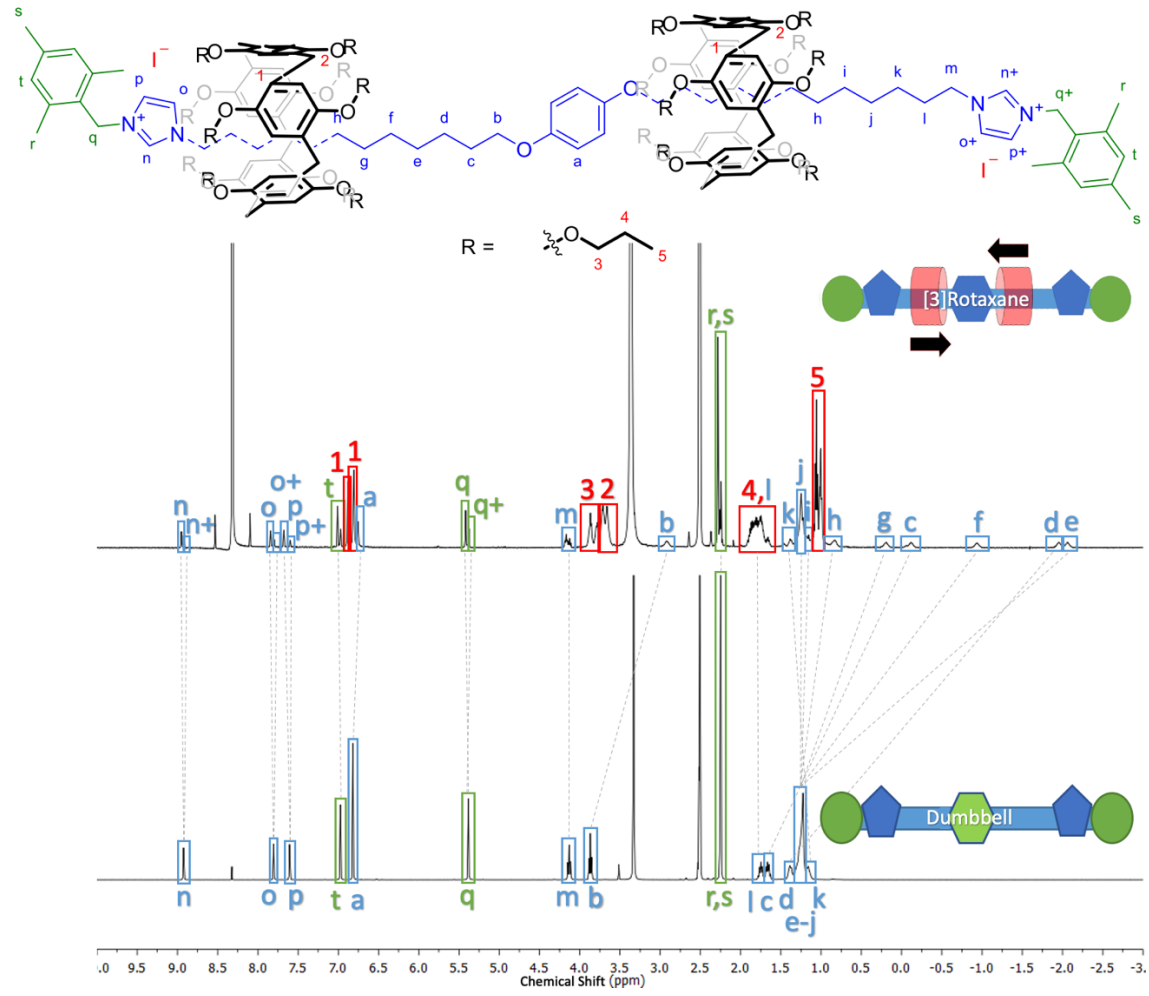

b)

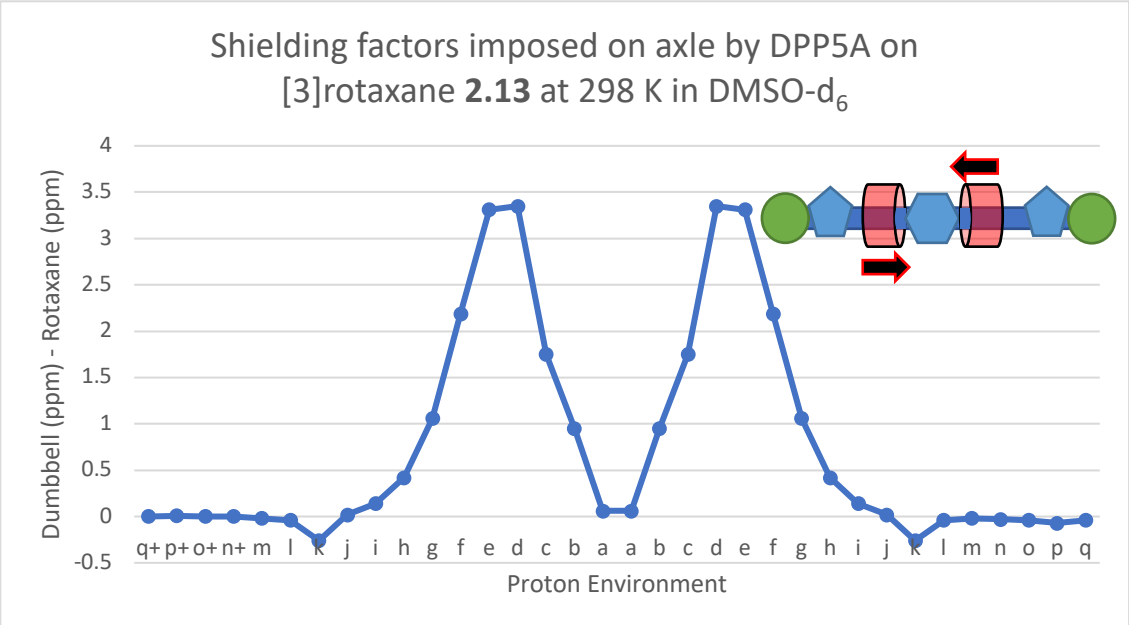

*Figure 2.18. (a) is the ^{1}H NMR stack of DPP5A (**2.8**), [3]rotaxane (**2.13**) and dumbbell (**2.15**) in DMSO-d_6 at room temperature in descending order and (b) plot of shielding factors of [3]rotaxane **2.13** in DMSO-d_6 at room temperature.*

The DPP5A macrocycles of [3]rotaxane **2.13** shuttle in a similar fashion to those of its counterpart **2.12** in DMSO (**Figure 2.18**). Shielding only occurs along the dodecyl chain, near the central 1,4-dialkoxybenzene unit, as the DMSO-imidazolium interactions push the pillararenes away from the imidazolium moieties. Due to the greater area encircled by the DPP5A macrocycles, the difference is very small between the most favourable proton environments to reside on (H_d and H_e). However, the overall shuttling area remains roughly the same with shielding mainly seen between protons $H_{a\text{-}j}$. Likewise, a small asymmetry is observed along the imidazolium regions ($H_{n\text{-}q}$) like that of [3]rotaxane **2.12**.

a)

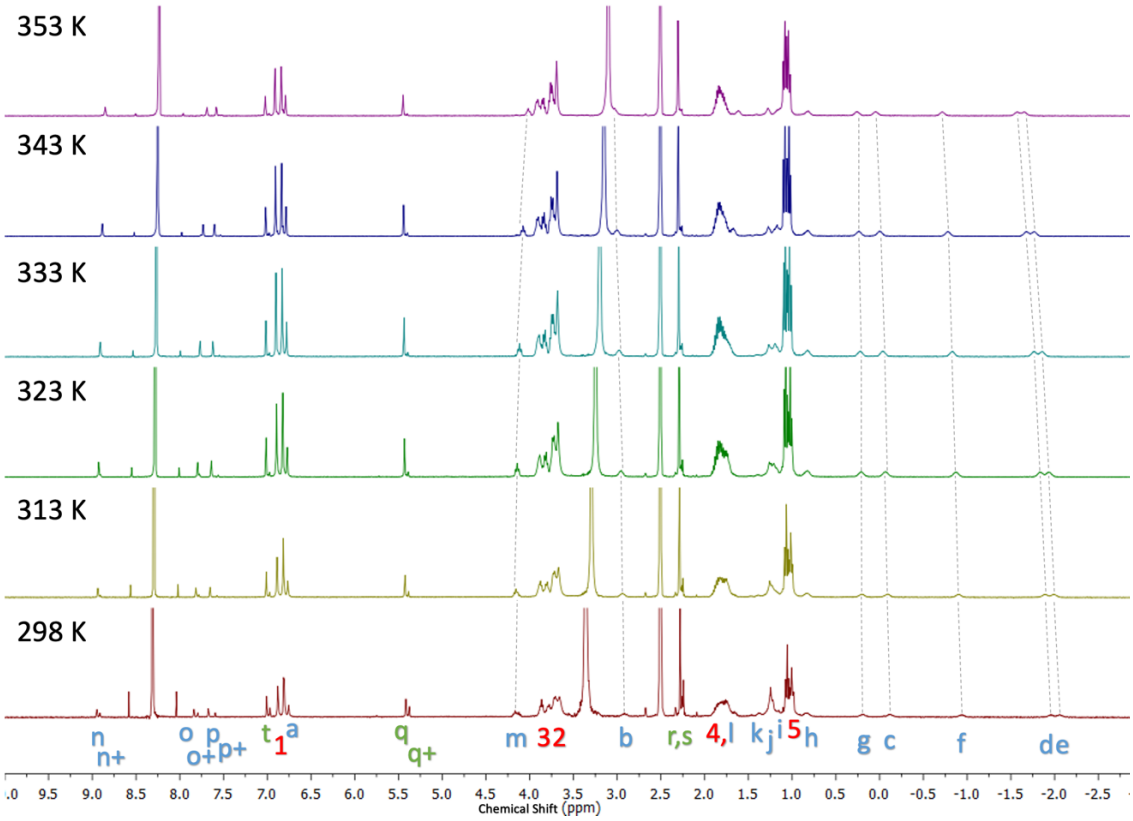

b)

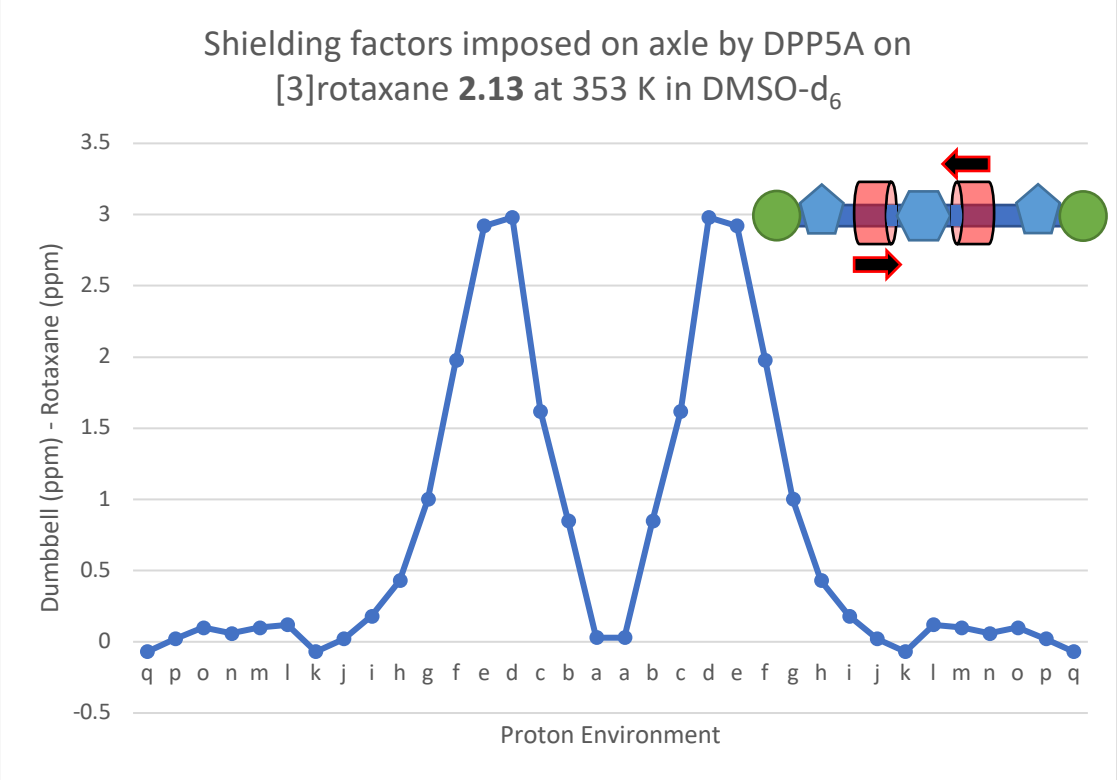

*Figure 2.19. (a) stacked variable temperature ^{1}H NMR spectra of [3]rotaxane **2.13** in DMSO-d_6 at 400 MHz and (b) corresponding shielding factors of [3]rotaxane **2.13** in DMSO-d_6 at 353 K.*

High temperature NMR studies of [3]rotaxane **2.13** in DMSO (**Figure 2.19**) confirmed the DPP5A can slightly overcome the imidazolium-DMSO interactions and can partially shuttle over protons $H_{j\text{-}o}$, shielding those proton environments, in a similar fashion to its DEP5A analogue (**2.12**).

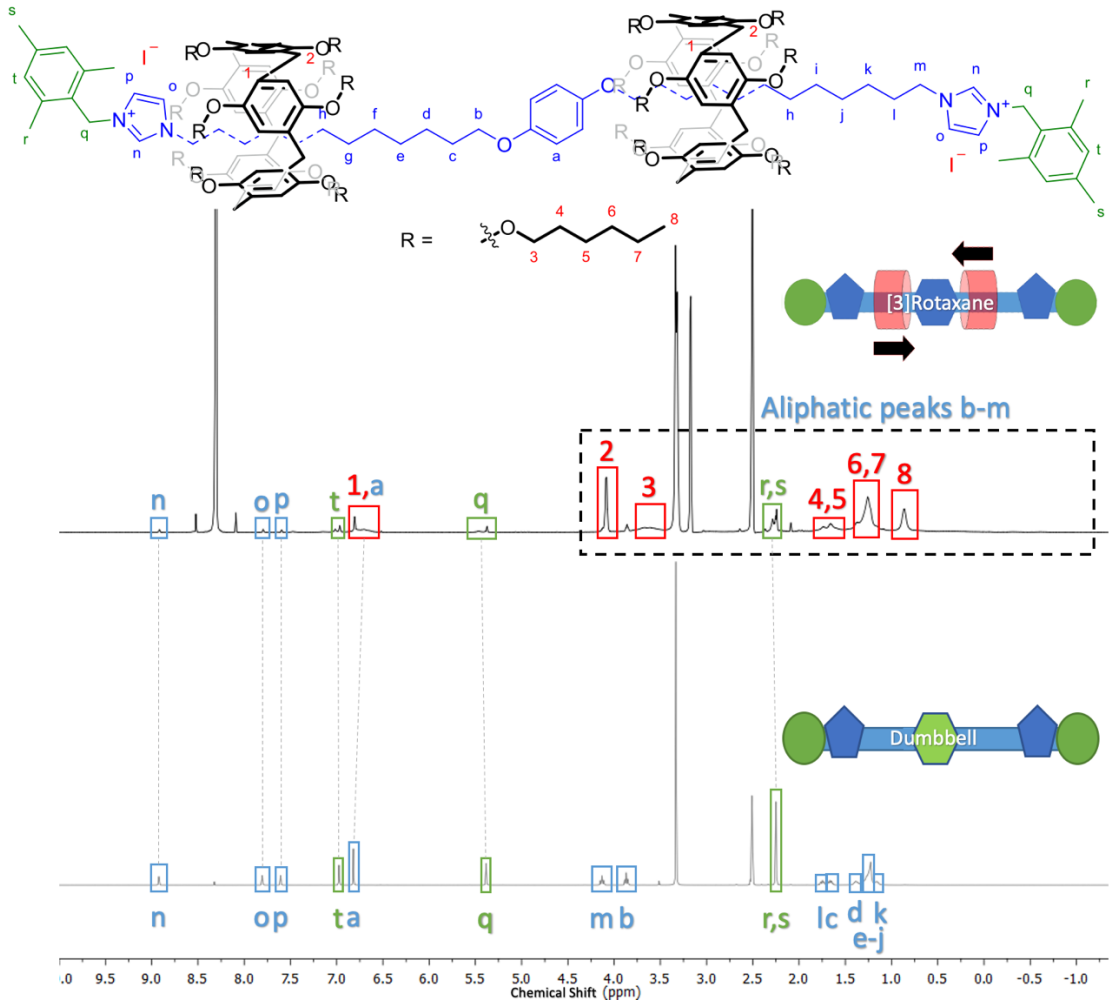

*Figure 2.20. ^{1}H NMR stack of [3]rotaxane (**2.14**) and dumbbell (**2.15**) in DMSO-d_6 at room temperature in descending order, where aliphatic peaks cannot be defined.*

Solubility of [3]rotaxane **2.14** in DMSO was low (**Figure 2.20**), a property attributed to the hexyl-functionalised DHP5A macrocycles. As such, the aliphatic region of the [3]rotaxane ($H_{b\text{-}m}$) could not be assigned at room temperature and shielding factors could not be verified. However, similarly to **2.12**, it was possible to assign the other proton environments for the room temperature measurement, identifying key pillararene regions $H_{2\text{-}8}$ as well as showing that the imidazolium region ($H_{n\text{-}q}$) was not shifted in

relation to the dumbbell molecule. This information suggested that the macrocycles had not dethreaded, but instead were forced onto the dodecyl chains of the axle.

a)

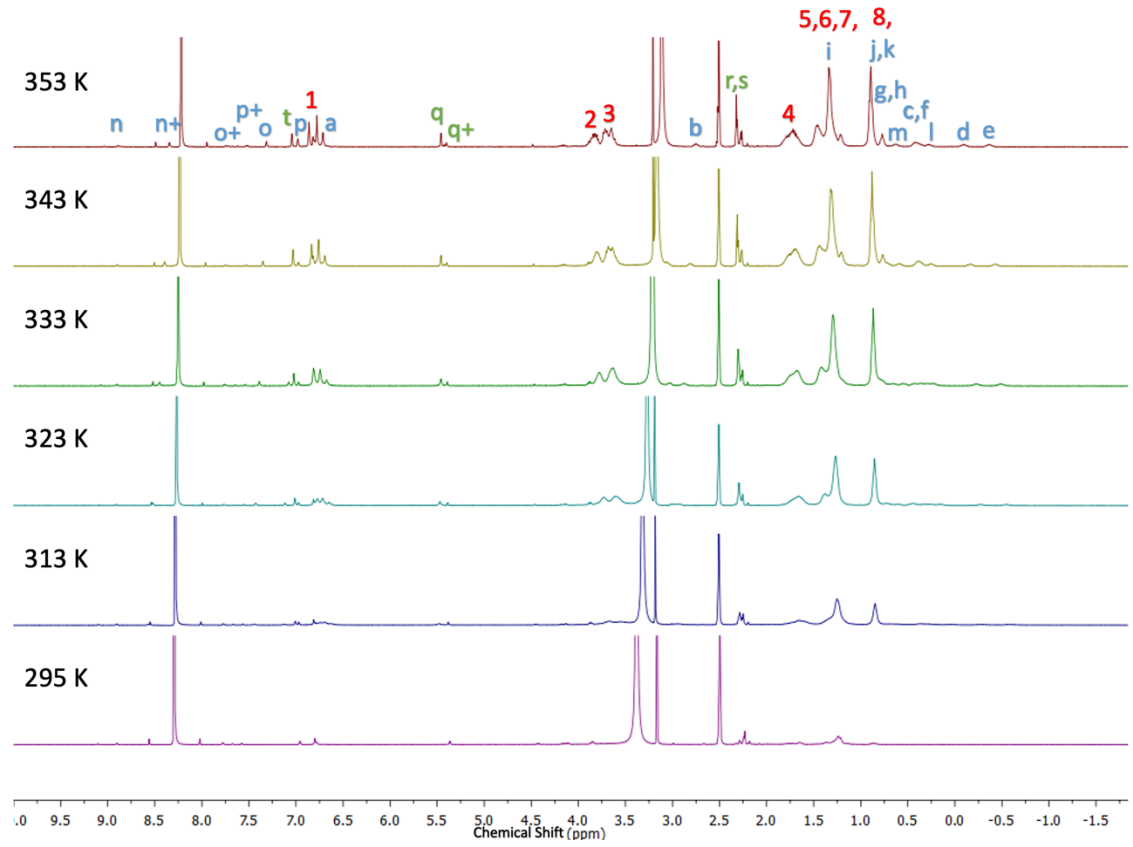

b)

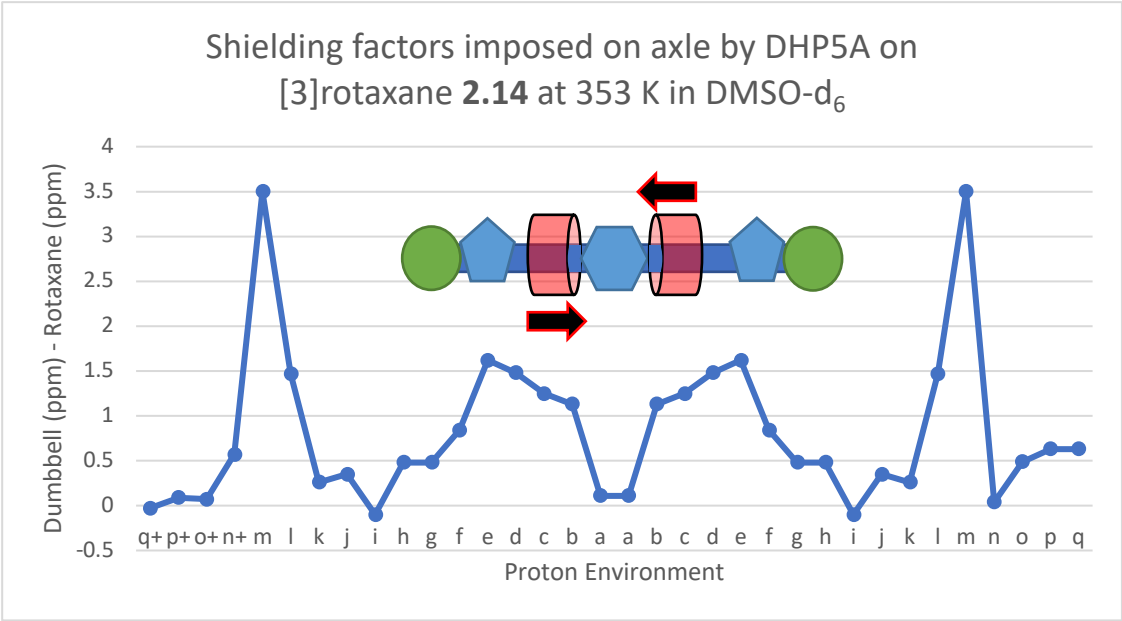

*Figure 2.21. (a) stacked variable temperature ^{1}H NMR spectra of [3]rotaxane **2.14** in DMSO-d_6 at 400 MHz and (b) corresponding shielding factors of [3]rotaxane **2.14** in DMSO-d_6 at 353 K.*

Upon heating the solution of **2.14** in DMSO (**Figure 2.21**), solubility of the rotaxane increased and as a result, the dodecyl region corresponding to aliphatic protons $H_{b\text{-}m}$ was observable. Assignments were made at 353 K with the aid of a high temperature 2D ^{1}H-^{1}H COSY experiment.

As with the other [3]rotaxanes in the series, DHP5A macrocycles on **2.14** preferentially reside over the aliphatic portion of the axle instead of over the imidazolium moiety. Proton environment H_e is the local maximum in this region which is further away from the maximum observed for **2.13**, which was at H_f. This was expected due to the longer hexyl substituents on the DHP5A pillararene. The enhanced sterics of the DHP5A macrocycles play an even more important role of the shuttling within the rotaxane, as the shielding factor for H_e is not large, with a displacement of approximately 1.5 ppm, in comparison to ~3.5 ppm for all other [3]rotaxanes in the series (where spectra are recorded in DMSO).

Perhaps surprisingly, the global maximum in shielding effects is within the imidazolium region at proton environment H_m, as DHP5A macrocycles are overcoming the solvent-ion pair interactions from the increased thermal energy.

Desymmetrisation of the imidazolium region may be occurring because, the macrocycles could be in different positions with respect to one another along the axle for extended periods of time. This may suggest that the macrocycles are in fact, not interlacing at close range. This shows that both thermal energy and the effect of favourable pillararene-imidazolium interactions overcome the barrier imposed by the solvophilic interactions of the imidazolium moieties with DMSO.

2.2.5 X-Ray crystallography

Single crystals were grown for **2.13** by vapour diffusion of hexane into a chloroform solution of the compound and crystal structures were obtained for this [3]rotaxane (**Figure 2.22**). X-ray diffraction was collected with a SuperNova GV1000, Atlas S2 diffractometer and the crystal structures were solved by Dr Stephen Argent. Crystals were grown for **2.12**, however they diffracted weakly, and no crystals could be obtained for the other [3]rotaxanes **2.11** and **2.14**.

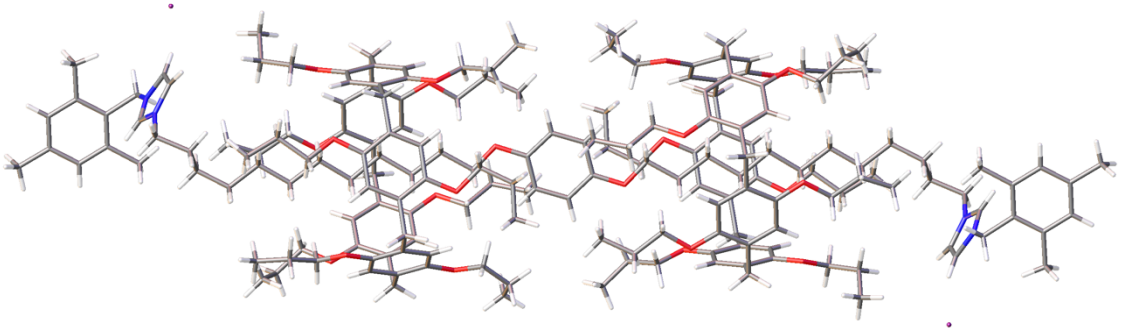

*Figure 2.22. X-ray crystal structure of a single molecule of [3]rotaxane **2.13** where solvent molecules have been omitted for clarity. Atoms C – grey, H – white, O – red, N – blue, I – purple.*

2.13 crystallises into the monoclinic space group C2/c. In the solid state, the macrocycles reside along the dodecyl chain, as opposed to over the imidazolium stations, akin to what is observed when dissolved in DMSO. The diameter of the 1,4-dialkoxybenzene unit was measured to be 2.8 Å, and corresponding protons had a distance of 4.7 Å between them. The distance between the a 1,4-dipropoxybenzene unit and a methylene bridge across the pillararene was measured to be 9 Å. The internal volume accessible to guest molecules has been previously reported to ca. 5 Å.[2] This indicates that the 1,4-dialkoxybenzene bridge is large enough to be an unfavourable position for the macrocycle to reside over.

a)

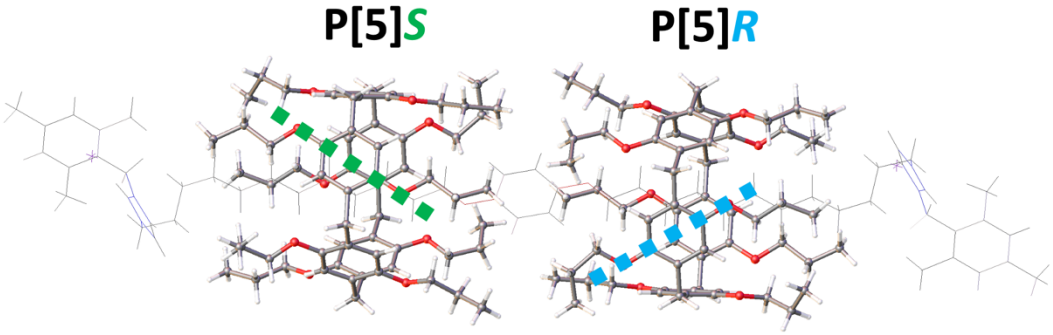

b)

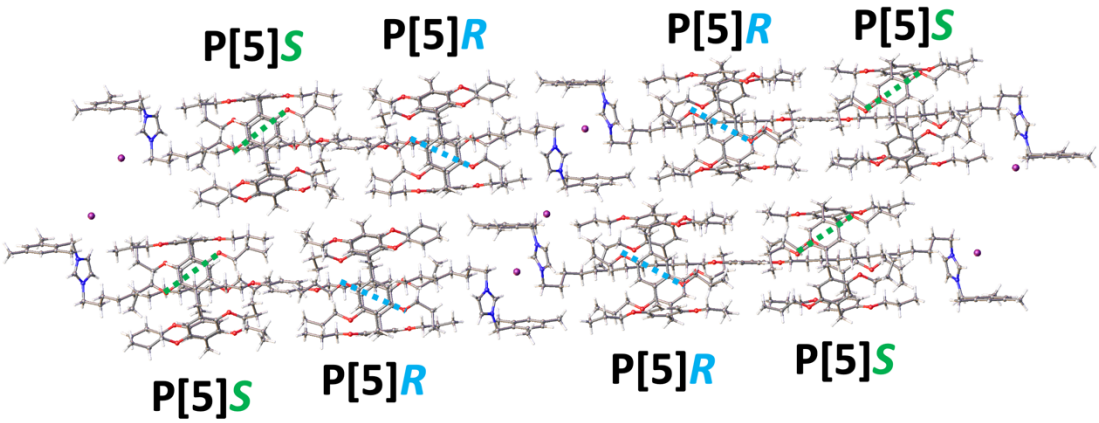

*Figure 2.23. X-ray crystal structure showing the chirality of DPP5A on [3]rotaxane **2.13** as a single molecule (a) and as multiple molecules (b). Atoms C – grey, H – white, O – red, N – blue, I – purple.*

From the statistical nature of threading, both enantiomers of pillar[5]arene, P[5]*R* and P[5]*S* are present along a single axle molecule of **2.13** (**Figure 2.23**). When more than one molecule of the [3]rotaxane is observed, it is shown that both P[5]*R* with P[5]*S* and P[5]*S* with P[5]*R* diastereoisomers of the [3]rotaxane are present within the crystal structure. These diastereoisomers alternate where a [3]rotaxane that has P[5]*R* with P[5]*S* would be next to a [3]rotaxane that has P[5]*S* with P[5]*R* horizontally, however the same diastereoisomer is repeated vertically (as pictured).

To our knowledge, this is the first example of a crystal structure for a pillar[5]arene based [3]rotaxane.

2.3 Conclusions and future work

In conclusion, a series of [3]rotaxanes have been assembled from a toolkit approach, comparing pillar[5]arene macrocycles with different terminal chain lengths. NMR studies illustrate how the macrocycles interact with the axle, including experiments conducted in solvents with different polarities, chloroform and DMSO, and in the latter case as a function of temperature.

In chloroform, high shielding factors are found around the imidazolium regions due to the pillararene's affinity for the positively charged group, and we can infer that in the solution phase the pillararene macrocycle spends more time localised around the imidazolium portion of the axle component. There is a gradual decrease in shielding constants along the dodecyl chains approaching the central 1,4-dioxybenzene unit, although the upfield shift from the dumbbell to rotaxane suggests that shuttling occurs along the entire axle for DEP5A, DPP5A and DHP5A. DMP5A behaves somewhat dissimilarly, as high shielding constants are only found around the imidazolium region, with little to no change in shift along the aliphatic backbone suggesting that the macrocycles are only pirouetting around the imidazolium stations.

When the polarity of the solvent the [3]rotaxanes are dissolved in is changed, using highly polar DMSO, the pillar[5]arenes are forced away from the favourable imidazolium stations due to the solvent-ion pair interactions being stronger than that of the pillar[5]arene-cation motif. As a result, the pillar[5]arenes are displaced from the imidazolium stations and onto the dodecyl chains. As DMP5A does not shuttle along the rod at room temperature, thermal energy was required to encourage the shuttling process of the macrocycles and at 353 K, where shuttling behaviour resembles the other [3]rotaxanes in the series.

To further enhance the conclusions observed here, the diastereoisomers produced as a consequence of the rotaxane reaction need to be separated to understand how the pirouetting motion of the macrocycles is affected when two pillararenes are forced into close proximity to each other. This would probably require separation via chiral HPLC and

circular dichroism studies of each diastereoisomer in DMSO, potentially elucidating whether the macrocycles pirouette in tandem.

In order to understand whether the alkyl chains of the macrocycles are interdigitating, or not, at close range an asymmetric [3]rotaxane would need to be synthesised. This would consist of the same symmetrical axle, but uses two different pillar[5]arene molecules on either side of the 1,4-dialkoxybenzene unit. Hypothetical rotaxane **2.Y** (**Figure 2.24**) is a hetero[3]rotaxane, utilising DPP5A and DHP5A either side of the 1,4-dialkoxybenzene barricade. Potential synthesis could require formation and purification of a pseudo[2]rotaxane (akin to the [2]rotaxanes seen in **chapter 3**) intermediate and an immediate capping reaction with the corresponding pillararene. This may also be achieved statistically via a one-pot route, however the separation may not be straight-forward. Two-dimensional NMR experiments would be required to determine the range of the interdigitation via the presence of cross peaks in the ^{1}H-^{1}H NOESY spectrum between alkyl chains along the rim of the pillararenes.

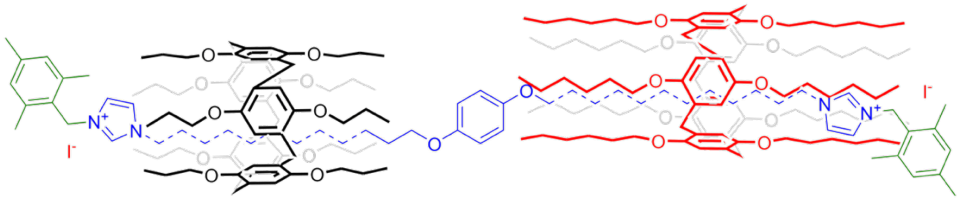

2.Y

*Figure 2.24. Hetero[3]rotaxane **2.Y** utilising DPP5A and DHP5A on either ends of the axle.*

Additionally, increasing the length of the axle with the inclusion of another 1,4-dialkoxybenzene unit would be of interest to further supplement the knowledge on how pillar[5]arenes shuttle along long axles. [3]Rotaxane **2.Z** (**Figure 2.25**) expresses this concept by showing a vacant zone, which the pillararenes should not have access to when threading onto the axle in chloroform.

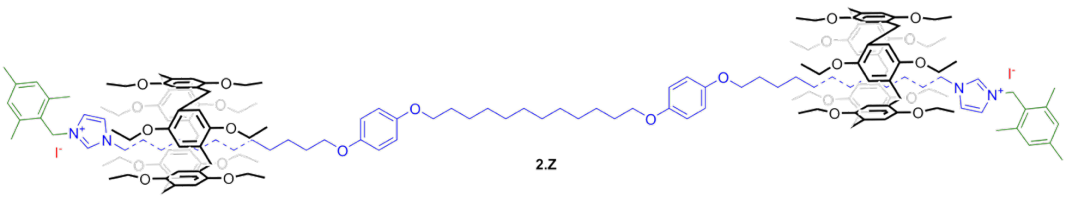

2.Z

*Figure 2.25. [3]Rotaxane **2.Z** incorporating a vacant zone inaccessible to both pillar[5]arene macrocycles.*

2.4 Materials and methods

All chemicals were obtained from commercial sources and used without further purification (see **Chapter 6**). ^{1}H and ^{13}C NMR spectra were recorded using a Bruker AV(III)400HD, Bruker AV(III)400, Bruker AV400 and Bruker AV(III)500 machines. High temperature ^{1}H NMR spectra were recorded using a Bruker AV(III)400, Bruker AV(III)400HD, or a Bruker AV(III)600 instrument. Deuterated solvents were used as specified. Chemical shifts were recorded referenced to solvent residue. ESI-MS spectra were taken using a Bruker microTOF II mass spectrometer.

2.4.1 Synthesis

Synthesis of 1,4-bis((12-bromododecyl)oxy)benzene [**2.1**][25]

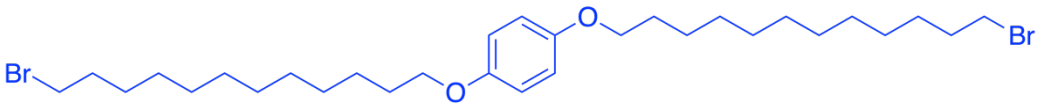

Hydroquinone (383 mg, 3.48 mmol) and 1,12-dibromododecane (5.71 g, 17.4 mmol) were dissolved in hot ethanol (20 mL). Potassium carbonate (1.44 g, 10.4 mmol) was added to the solution and was heated at reflux for 3 hours. The mixture was left to cool, extracted into dichloromethane and the organic layer was washed with water three times and then brine. The organic fractions were dried with $MgSO_4$, filtered and the solvent was removed under reduced pressure. The crude solid was dissolved in the minimum amount of dichloromethane and on addition of methanol a white solid was precipitated and was collected by vacuum filtration (886 mg, 1.47 mmol, 42 %). ^{1}H NMR (400 MHz, Chloroform-*d*) δ 6.84 (s, 4H), 3.92 (t, *J* = 6.6 Hz, 4H), 3.43 (t, *J* = 6.9 Hz, 4H), 1.88 (p, *J* = 7.0 Hz, 4H), 1.82 – 1.72 (m, 4H), 1.45 (q, *J* = 7.1 Hz, 8H), 1.32 (d, *J* = 10.2 Hz, 24H) ppm. ^{13}C NMR (101 MHz, Chloroform-*d*) δ 153.21, 115.40, 68.67, 34.08, 32.86, 29.65 – 29.33, 28.78, 28.19, 26.07 ppm. ESI-MS (positive mode) m/z calc'd. for $C_{30}H_{56}Br_2NO_2$ $[M + NH_4]^+$: 620.2672, found: 620.2656.

Synthesis of 1,4-bis((12-(1*H*-imidazol-1-yl)dodecyl)oxy)benzene [**2.2**]

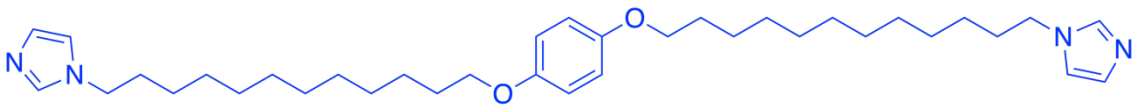

A suspension of potassium carbonate (1.85 g, 13.4 mmol), 1,4-bis((12-bromododecyl)oxy)benzene (675 mg, 1.12 mmol) and imidazole (608 mg, 8.93 mmol) in DMF (20 mL) was heated at 145 °C for 24 hours. The suspension was cooled to room temperature and the solvent was removed under reduced pressure. The crude solid was redissolved in dichloromethane and the organic layer was washed with water three times and then brine. The organic fractions were combined, dried with $MgSO_4$, filtered and the solvent was removed under reduced pressure to yield a yellow solid (589 mg, 1.02 mmol, 91 %). ^{1}H NMR (400 MHz, Chloroform-*d*) δ 7.48 (d, *J* = 1.1 Hz, 2H), 7.07 (t, *J* = 1.1 Hz, 2H), 6.92 (t, *J* = 1.3 Hz, 2H), 6.83 (s, 4H), 3.93 (dt, *J* = 9.3, 6.8 Hz, 8H), 1.85 – 1.69 (m, 12H), 1.52 – 1.41 (m, 4H), 1.37 – 1.21 (m, 24H) ppm. ^{13}C NMR (101 MHz, Chloroform-*d*) δ 153.20, 137.08, 129.38, 118.77, 115.39, 68.65, 47.05, 31.10, 29.50 - 29.41, 29.07, 26.56, 26.06 ppm. ESI-MS (positive mode) m/z calc'd. for $C_{39}H_{63}N_6O_2$ $[M + C_3H_5N_2]^+$: 647.5007, found: 647.5024.

Synthesis of 1,4-diethoxybenzene [**2.3**][26]

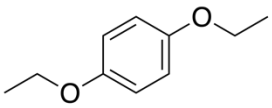

Hydroquinone (20.0 g, 181 mmol), potassium carbonate (62.7 g, 454 mmol) and bromoethane (33.8 mL, 453 mmol) were dissolved in DMF (300 mL). The mixture was heated at 65 °C for 24 hours, then allowed to cool to room temperature, and the solvent removed under reduced pressure. The brown solid was redissolved in dichloromethane and the organic layer was washed with water three times and then brine. The organic fraction was dried with $MgSO_4$, filtered and the solvent was removed under reduced pressure. The crude solid was purified by column chromatography [silica, hexane: ethyl acetate (95:5)] to yield a white solid (15.1 g, 90.8 mmol, 50 %).^{1}H NMR (400 MHz, Chloroform-*d*) δ 6.85 (s, 4H), 4.01 (q, *J* = 7.0 Hz, 4H), 1.41 (t, *J* = 7.0 Hz, 6H) ppm. ^{13}C NMR

(101 MHz, Chloroform-*d*) δ 153.04, 115.41, 64.01, 14.97 ppm. TLC: R_f = 0.60 (19:1 hexane/ethyl acetate).

Synthesis of 1,4-dipropoxybenzene [**2.4**][27]

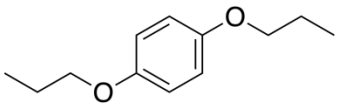

Hydroquinone (13.3 g, 121 mmol), potassium carbonate (41.8 g, 302 mmol) and 1-bromopropane (27.4 mL, 302 mmol) were dissolved in DMF (200 mL). The mixture was heated at 65 °C for 24 hours, then allowed to cool to room temperature, and the solvent removed under reduced pressure. The brown solid was redissolved in dichloromethane and the organic layer was washed with water three times and then brine. The organic fraction was dried with $MgSO_4$, filtered and the solvent was removed under reduced pressure. The crude solid was purified by column chromatography [silica, hexane: ethyl acetate (95:5)] to yield a white solid (15.9 g, 81.8 mmol, 67 %). ^{1}H NMR (400 MHz, Chloroform-*d*) δ 6.86 (s, 4H), 3.90 (t, *J* = 6.6 Hz, 4H), 1.81 (dtd, *J* = 13.9, 7.4, 6.5 Hz, 4H), 1.06 (t, *J* = 7.4 Hz, 6H) ppm. ^{13}C NMR (101 MHz, Chloroform-*d*) δ 153.22, 115.43, 70.19, 22.72, 10.55 ppm. TLC: R_f = 0.60 (19:1 hexane/ethyl acetate).

Synthesis of 1,4-dihexyloxybenzene [**2.5**][28]

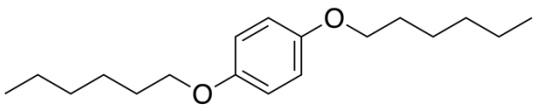

Hydroquinone (10.0 g, 90.8 mmol), potassium carbonate (32.0 g, 232 mmol) and 1-bromohexane (28.0 mL, 200 mmol) were dissolved in DMF (150 mL). The mixture was heated at 65 °C for 24 hours, then allowed to cool to room temperature, and the solvent removed under reduced pressure. The brown solid was redissolved in dichloromethane and the organic layer was washed with water three times and then brine. The organic fraction was dried with $MgSO_4$, filtered and the solvent was removed under reduced pressure. The crude solid was purified by column chromatography [silica, hexane: ethyl acetate (95:5)] to yield a yellow solid (5.63 g, 20.2 mmol, 22 %). ^{1}H NMR (400 MHz,

Chloroform-*d*) δ 6.85 (s, 4H), 3.93 (t, *J* = 6.6 Hz, 4H), 1.78 (dq, *J* = 7.9, 6.6 Hz, 4H), 1.53 – 1.43 (m, 4H), 1.37 (dtd, *J* = 7.2, 4.5, 4.0, 2.2 Hz, 8H), 0.98 – 0.90 (m, 6H) ppm. ^{13}C NMR (101 MHz, Chloroform-*d*) δ 153.22, 115.40, 68.67, 31.64, 29.40, 25.77, 22.64, 14.06 ppm. TLC: R_f = 0.50 (19:1 hexane/ethyl acetate).

Synthesis of DMP5A [**2.6**][2]

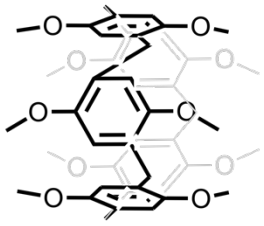

1,4-Dimethoxybenzene (6.00 g, 43.4 mmol) and paraformaldehyde (3.91 g, 130 mmol) were dissolved in dry dichloromethane (500 mL), under N_2 and stirred for 15 mins. Anhydrous iron(III)chloride (1.04 g, 6.45 mmol) was added and stirred for a further 3 hours at room temperature. The mixture was then quenched with water, and the organic phase was separated and washed with water a further five times. The organic phase was then concentrated and subjected to column chromatography [silica, dichloromethane] to yield a white solid (1.74 g, 2.32 mmol, 27 %). ^{1}H NMR (400 MHz, Chloroform-*d*) δ 6.79 (s, 10H), 3.80 (s, 10H), 3.67 (s, 30H) ppm. ^{13}C NMR (101 MHz, Chloroform-*d*) δ 150.83, 128.25, 114.12, 55.80, 29.69 ppm. ESI-MS (positive mode) m/z calc'd. for $C_{45}H_{51}O_{10}$ $[M + H]^+$: 751.3477, found: 751.3463. TLC: R_f = 0.29 (dichloromethane).

Synthesis of DEP5A [**2.7**][29]

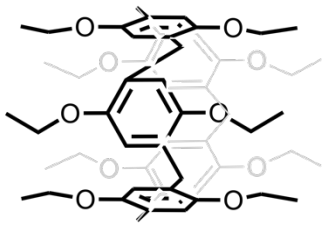

1,4-Diethoxybenzene (6.00 g, 36.1 mmol) and paraformaldehyde (3.24 g, 108 mmol) were dissolved in dry dichloromethane (500 mL), under N_2 and stirred for 15 mins. Anhydrous iron(III)chloride (876 mg, 5.40 mmol) was added and stirred for a further 3 hours at room temperature. The mixture was then quenched with water, and the organic phase was

separated and washed with water a further five times. The organic phase was then concentrated and subjected to column chromatography [silica, dichloromethane] to yield a white solid (2.94 g, 3.30 mmol, 46 %). ^{1}H NMR (400 MHz, Chloroform-*d*) δ 6.75 (s, 10H), 3.85 (q, *J* = 7.0 Hz, 20H), 3.79 (s, 10H), 1.28 (t, *J* = 7.0 Hz, 30H) ppm. ^{13}C NMR (101 MHz, Chloroform-*d*) δ 149.86, 128.53, 115.15, 63.81, 29.87, 15.07 ppm. ESI-MS (positive mode) m/z calc'd. for $C_{55}H_{74}N_4O_{10}$ $[M + NH_4]^+$: 908.5307, found: 908.5592. TLC: R_f = 0.40 (dichloromethane).

Synthesis of DPP5A [**2.8**][29]

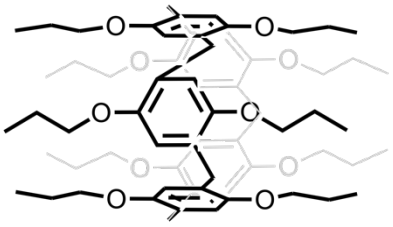

1,4-Dipropoxybenzene (6.00 g, 31.0 mmol) and paraformaldehyde (2.78 g, 92.6 mmol) were dissolved in dry dichloromethane (500 mL), under N_2 and stirred for 15 mins. Anhydrous iron(III)chloride (750 mg, 4.63 mmol) was added and stirred for a further 3 hours at room temperature. The mixture was then quenched with water, and the organic phase was separated and washed with water a further five times. The organic phase was then concentrated and subjected to column chromatography [silica, dichloromethane] to yield a white solid (3.67 g, 3.56 mmol, 57 %). ^{1}H NMR (400 MHz, Chloroform-*d*) δ 6.83 (s, 10H), 3.85 – 3.78 (m, 30H), 1.78 (hept, *J* = 6.8 Hz, 20H), 1.03 (t, *J* = 7.4 Hz, 30H) ppm. ^{13}C NMR (101 MHz, Chloroform-*d*) δ 149.82, 128.30, 115.00, 69.92, 29.59, 23.01, 10.77 ppm. ESI-MS (positive mode) m/z calc'd. for $C_{56}H_{90}O_{10}$ $[M]^+$: 1031.4250, found: 1031.6629. TLC: R_f = 0.17 (dichloromethane).

Synthesis of DHP5A [**2.9**][29]

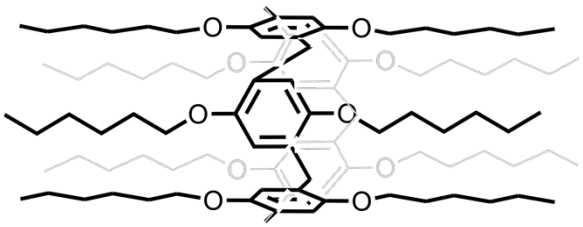

1,4-Dihexyloxybenzene (5.50 g, 19.8 mmol) and paraformaldehyde (1.78 g, 59.3 mmol) were dissolved in dry dichloromethane (500 mL), under N_2 and stirred for 15 mins. Anhydrous iron(III)chloride (480 mg, 2.96 mmol) was added and stirred for a further 3 hours at room temperature. The mixture was then quenched with water, and the organic phase was separated and washed with water a further five times. The organic phase was then concentrated and subjected to column chromatography [silica, dichloromethane] and [silica, dichloromethane: hexane (25:75)] respectively. The crude solid was washed with hot acetonitrile and vacuum filtered to afford a white solid (2.93 g, 2.02 mmol, 51 %). ^{1}H NMR (400 MHz, Chloroform-*d*) δ 6.87 (s, 10H), 3.88 (t, *J* = 6.6 Hz, 20H), 3.78 (s, 10H), 1.90 – 1.77 (m, 20H), 1.62 – 1.49 (m, 20H), 1.45 – 1.30 (m, 40H), 0.93 (td, *J* = 5.7, 4.6, 2.1 Hz, 30H) ppm. ^{13}C NMR (101 MHz, Chloroform-*d*) δ 149.82, 128.26, 114.73, 68.39, 31.83, 29.93, 26.06, 22.64, 14.07 ppm. TLC: R_f = 0.56 (1:3 dichloromethane/hexane).

Synthesis of 2-(iodomethyl)-1,3,5-trimethylbenzene [**2.10**][20]

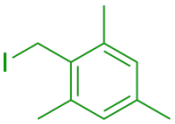

Potassium iodide (0.83 g, 5.00 mmol) and 2,4,6 trimethylbenzylalcohol (0.75 g, 5.00 mmol) were dissolved in 1,4 dioxane (10 mL) and $BF_3{\cdot}OET_2$ (0.62 mL, 5.02 mmol) was added carefully to the mixture and stirred at room temperature overnight in the dark. The reaction was quenched with cold water (10 mL) and was extracted with diethyl ether (3 x 10 mL). The combined organic phase was washed with water (3 x 10 mL) and then brine (10 mL) and subsequently dried over $MgSO_4$ and the solvent was removed under reduced pressure, which yielded a yellow solid (1.14 g, 4.39 mmol, 88 %). ^{1}H NMR (400 MHz, Chloroform-d) δ 6.85 (d, *J* = 1.3 Hz, 2H), 4.48 (s, 2H), 2.31 (d, *J* = 27.1 Hz, 6H), 2.20 (s, 3H)

ppm. ^{13}C NMR (101 MHz, Chloroform-d) δ 137.98, 137.30, 136.83, 129.42, 21.08, 19.30, 3.96 ppm.

Synthesis of [3]rotaxane [**2.11**]

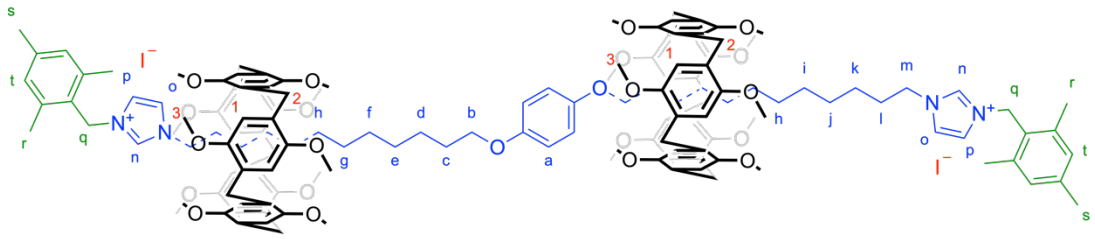

1,4-Bis((12-(1*H*-imidazol-1-yl)dodecyl)oxy)benzene (100 mg, 173 μmol) and dimethoxypillar[5]arene (324 mg, 432 μmol), were dissolved in chloroform (2.4 mL) and sonicated for 30 mins. The solution was cooled to -15°C and, under the exclusion of light, 2-(iodomethyl)-1,3,5-trimethylbenzene (158 mg, 607 μmol) was added. The mixture was left to warm to room temperature and stirred for 3 days. The crude residue was purified by column chromatography [silica, dichloromethane: methanol (96:4)] to yield a yellow solid (128 mg, 49.2 μmol, 29 %). ^{1}H NMR (400 MHz, Chloroform-*d*) δ 8.18 – 8.10 (m, 2H, H_n), 7.79 – 7.71 (m, 2H, H_p), 7.03 (s, 4H, H_t), 6.90 (s, 10H, H_1), 6.87 (s, 4H, H_a), 6.75 (s, 10H, H_1), 6.10 – 6.02 (m, 2H, H_o), 5.84 (dd, *J* = 89.6, 15.1 Hz, 4H, H_q), 3.99 – 3.82 (m, 4H, H_b), 3.80 – 3.64 (m, 80H, $H_{2,3}$), 2.47 (s, 12H, H_r), 2.38 (s, 6H, H_s), 1.41 – 1.13 (m, 20H, H_{d-h}), 0.88 (dq, *J* = 23.2, 9.1, 7.6 Hz, 8H, $H_{m,i}$), 0.18 (d, *J* = 8.6 Hz, 4H, H_j), -0.68 – -0.90 (m, 4H, H_k), -1.37 (d, *J* = 34.5 Hz, 4H, H_l) ppm. ^{13}C NMR (101 MHz, Chloroform-*d*) δ 153.24, 151.01, 150.36, 139.82, 138.14, 132.40, 129.98, 129.65, 128.80, 126.08, 122.56, 120.86, 115.66, 115.30, 113.59, 68.57, 58.08, 55.55, 48.88, 47.64, 31.01, 30.41, 30.37, 29.91, 29.53, 29.42, 29.07, 28.66, 25.99, 25.96, 25.84, 21.19, 20.20 ppm. ESI-MS (positive mode) m/z calc'd. for $C_{146}H_{184}N_4O_{22}$ $[M]^{2+}$: 1173.1712, found: 1173.1869.

Synthesis of [3]rotaxane [**2.12**]

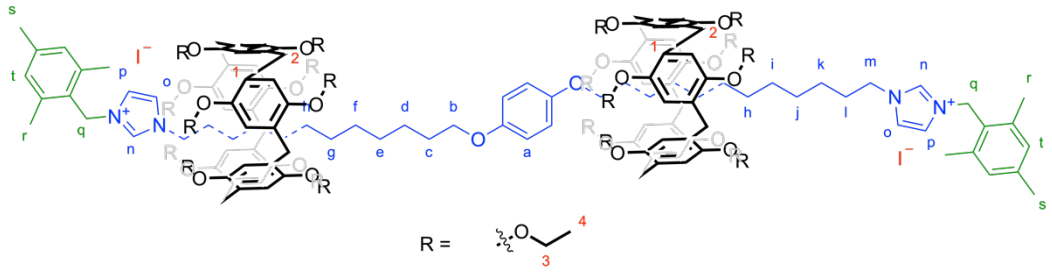

1,4-Bis((12-(1*H*-imidazol-1-yl)dodecyl)oxy)benzene (100 mg, 173 μmol) and diethoxypillar[5]arene (385 mg, 432 μmol), were dissolved in chloroform (1.6 mL) and sonicated for 30 mins. The solution was cooled to -15°C and, under the exclusion of light, 2-(iodomethyl)-1,3,5-trimethylbenzene (158 mg, 607 μmol) was added. The mixture was left to warm to room temperature and stirred for 3 days. The crude residue was purified by column chromatography [silica, dichloromethane: methanol (193:7)] to yield an orange solid (187 mg, 64.9 μmol, 38 %). ^{1}H NMR (500 MHz, Chloroform-*d*) δ 7.97 (s, 2H, H_n), 7.05 (s, 4H, H_t), 6.96 (s, 14H, $H_{p,1}$), 6.86 (s, 4H, H_a), 6.79 (s, 10H, H_1), 5.98 (s, 2H, H_o), 5.65 – 5.58 (m, 4H, H_q), 4.04 – 3.88 (m, 20H, H_2), 3.88 – 3.68 (m, 40H, H_3), 3.67 (s, 4H, H_b), 2.42 (s, 12H, H_r), 2.39 (s, 6H, H_s), 1.49 (t, *J* = 6.9 Hz, 30H, H_4), 1.39 (t, *J* = 7.0 Hz, 30H, H_4), 1.28 (p, *J* = 7.2, 6.6 Hz, 8H, $H_{c,d}$), 1.23 – 1.18 (m, 8H, $H_{j,k}$), 1.06 (s, 4H, H_m), 1.01 (d, *J* = 6.5 Hz, 4H, H_i), 0.82 (s, 4H, H_l), 0.73 (s, 4H, H_e), 0.62 – 0.51 (m, 4H, H_h), -0.14 (s, 4H, H_g), -0.62 (s, 4H, H_f) ppm. ^{13}C NMR (126 MHz, Chloroform-*d*) δ 153.25, 150.52, 149.32, 140.26, 137.87, 133.31, 130.13, 130.11, 128.85, 125.41, 121.79, 120.19, 116.90, 115.40, 115.08, 114.50, 68.63, 65.98, 63.67, 48.03, 47.92, 30.96, 30.57, 30.50, 30.01, 29.49, 29.29, 29.23, 27.45, 26.24, 25.37, 21.16, 19.97, 15.62, 15.47 ppm. ESI-MS (positive mode) m/z calc'd. for $C_{166}H_{224}N_4O_{22}$ $[M]^{2+}$: 1313.3277, found: 1313.3231.

Synthesis of [3]rotaxane [**2.13**]

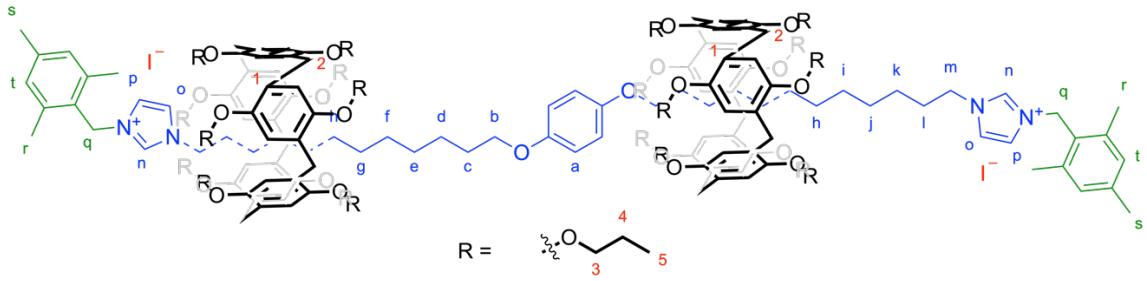

1,4-Bis((12-(1*H*-imidazol-1-yl)dodecyl)oxy)benzene (100 mg, 173 μmol) and dipropoxypillar[5]arene (445 mg, 432 μmol), were dissolved in chloroform (1.6 mL) and sonicated for 30 mins. The solution was cooled to -15°C and, under the exclusion of light, 2-(iodomethyl)-1,3,5-trimethylbenzene (158 mg, 607 μmol) was added. The mixture was left to warm to room temperature and stirred for 3 days. The crude residue was purified by column chromatography [silica, dichloromethane: methanol (193:7)] to yield a yellow solid (185 mg, 58.5 μmol, 34 %). ^{1}H NMR (500 MHz, Chloroform-*d*) δ 7.91 (s, 2H, H_n), 7.05 (s, 4H, H_t), 6.96 (s, 10H, H_1), 6.85 (s, 4H, H_a), 6.79 (s, 14H, $H_{p,1}$), 5.93 (d, *J* = 1.8 Hz, 2H, H_o), 5.56 (d, *J* = 2.0 Hz, 4H, H_q), 3.92 (ddt, *J* = 8.8, 6.5, 4.4 Hz, 20H, H_2), 3.84 – 3.69 (m, 40H, H_3), 3.66 (t, *J* = 7.0 Hz, 4H, H_b), 2.40 (s, 12H, H_r), 2.39 (s, 6H, H_s), 2.04 – 1.71 (m, 40H, H_4), 1.44 – 1.37 (m, 4H, H_m), 1.34 – 1.27 (m, 8H, $H_{c,d}$), 1.24 – 1.17 (m, 8H, $H_{g,h}$), 1.10 (dt, *J* = 30.4, 7.4 Hz, 60H, H_5), 1.04 – 0.99 (m, 4H, H_i), 0.88 – 0.72 (m, 8H, $H_{e,f}$), 0.64 – 0.56 (m, 4H, H_j), -0.09 (dt, *J* = 16.5, 8.7 Hz, 4H, H_k), -0.62 (dq, *J* = 20.8, 12.4, 10.1 Hz, 4H, H_l) ppm. ^{13}C NMR (126 MHz, Chloroform-*d*) δ 153.28, 150.69, 149.53, 140.37, 137.81, 133.31, 130.17, 128.98, 125.22, 121.90, 119.85, 117.05, 115.40, 115.14, 114.67, 72.42, 70.09, 68.67, 48.00, 47.80, 31.31, 30.86, 30.78, 30.12, 29.52, 29.45, 29.29, 29.17, 27.62, 26.36, 25.46, 23.23, 21.15, 19.97, 10.86, 10.71 ppm. ESI-MS (positive mode) m/z calc'd. for $C_{186}H_{264}N_4O_{22}$ $[M]^{2+}$: 1453.9859, found: 1453.9764.

Synthesis of [3]rotaxane [**2.14**]

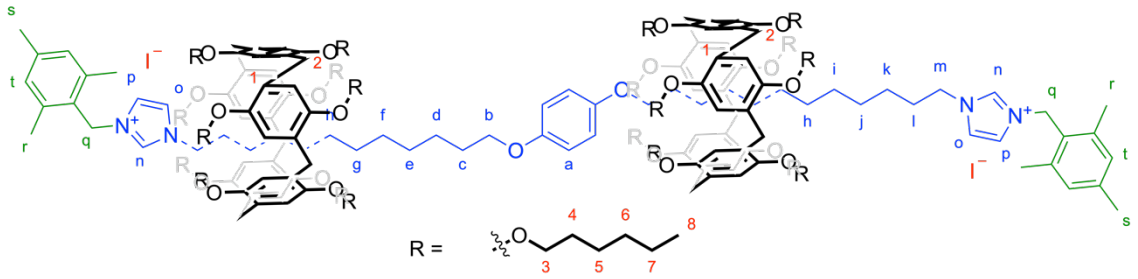

1,4-Bis((12-(1*H*-imidazol-1-yl)dodecyl)oxy)benzene (79.0 mg, 136 μmol) and dihexyloxypillar[5]arene (500 mg, 344 μmol), were dissolved in chloroform (1.7 mL) and sonicated for 30 mins. The solution was cooled to -15 °C and, under the exclusion of light, 2-(iodomethyl)-1,3,5-trimethylbenzene (134 mg, 516 μmol) was added. The mixture was left to warm to room temperature and stirred for 3 days. The crude residue was purified by column chromatography [silica, dichloromethane: methanol (193:7)] to yield a pale yellow solid (29.0 mg, 7.24 μmol, 5 %). ^{1}H NMR (500 MHz, Chloroform-*d*) δ 7.70 (s, 2H, H_n), 7.05 (s, 4H, H_t), 6.97 (s, 10H, H_1), 6.83 (s, 4H, H_a), 6.77 (s, 10H, H_1), 6.57 (d, *J* = 2.0 Hz, 2H, H_p), 5.75 (d, *J* = 1.9 Hz, 2H, H_o), 5.50 (s, 4H, H_q), 3.99 – 3.81 (m, 20H, H_2), 3.81 – 3.67 (m, 40H, H_3), 3.64 (t, *J* = 6.9 Hz, 4H, H_b), 2.39 (d, *J* = 3.6 Hz, 18H, $H_{r,s}$), 2.00 – 1.52 (m, 80H, $H_{4,5}$), 1.50 – 1.47 (m, 4H, H_m), 1.40 (dq, *J* = 7.1, 3.6 Hz, 40H, H_6), 1.35 (qd, *J* = 8.0, 7.3, 2.4 Hz, 40H, H_7), 1.32 – 1.21 (m, 8H, $H_{c,k}$), 1.21 – 1.05 (m, 8H, $H_{d,h}$), 1.02 – 0.87 (m, 68, $H_{8,i,l}$), 0.81 (tt, *J* = 10.2, 5.4 Hz, 4H, H_j), 0.76 – 0.65 (m, 4H, H_e), 0.10 – -0.03 (m, 4H, H_f), -0.69 (dtt, *J* = 30.9, 13.1, 6.2 Hz, 4H, H_g) ppm. ^{13}C NMR (126 MHz, Chloroform-*d*) δ 153.28, 150.76, 149.51, 140.41, 137.73, 133.31, 130.27, 130.20, 128.99, 125.09, 121.96, 119.26, 117.13, 115.38, 115.00, 114.63, 71.05, 68.67, 68.51, 53.47, 47.75, 47.58, 31.93, 31.73, 31.60, 31.13, 31.07, 30.48, 30.39, 30.16, 30.12, 30.06, 29.99, 29.82, 29.61, 29.42, 29.38, 29.20, 27.61, 26.60, 26.07, 26.05, 25.64, 22.72, 22.68, 21.16, 19.96, 14.10 ppm. ESI-MS (positive mode) m/z calc'd. for $C_{246}H_{384}N_4O_{22}$ $[M]^{2+}$: 1874.4554, found: 1874.4482.

Synthesis of dumbbell [**2.15**]

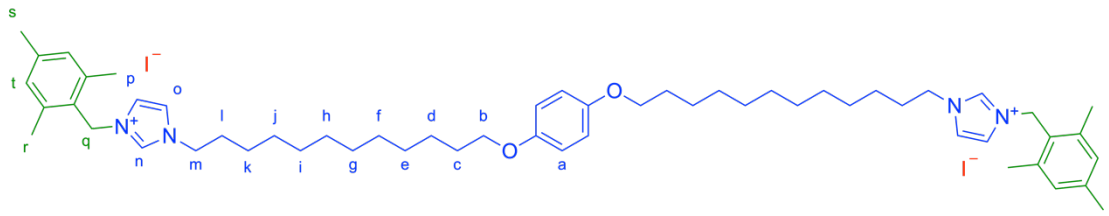

1,4-Bis((12-(1*H*-imidazol-1-yl)dodecyl)oxy)benzene (50.0 mg, 86.4 µmol) and 2-(iodomethyl)-1,3,5-trimethylbenzene (52.0 mg, 200 µmol) were dissolved in chloroform (4 mL) and were stirred at room temperature for 24 hours. The solvent was then removed under reduced pressure and the crude solid was purified by column chromatography [silica, dichloromethane: methanol (95:5)] yielding a white solid (71.0 mg, 64.6 µmol, 75 %). ^{1}H NMR (400 MHz, Chloroform-*d*) δ 10.23 (d, *J* = 1.6 Hz, 2H, H_n), 7.32 (t, *J* = 1.9 Hz, 2H, H_o), 6.95 (s, 4H, H_t), 6.91 (t, *J* = 1.8 Hz, 2H, H_p), 6.83 (s, 4H, H_a), 5.61 (s, 4H, H_q), 4.36 (t, *J* = 7.5 Hz, 4H, H_m), 3.92 (t, *J* = 6.5 Hz, 4H, H_b), 2.31 (s, 18H, $H_{r,s}$), 1.95 (p, *J* = 7.9 Hz, 4H, H_l), 1.82 – 1.71 (m, 4H, H_c), 1.44 (td, *J* = 11.4, 9.4, 4.6 Hz, 4H, H_d), 1.39 – 1.21 (m, 28H, H_{e-k}) ppm. ^{13}C NMR (101 MHz, Chloroform-d) δ 153.17, 140.11, 138.17, 136.40, 130.03, 125.13, 121.79, 120.83, 115.46, 68.64, 50.50, 48.23, 30.21, 29.47, 29.42, 29.39, 29.32, 29.29, 28.92, 26.24, 25.99, 21.09, 20.08 ppm. ESI-MS (positive mode) m/z calc'd. for $C_{56}H_{84}N_4O_2$ $[M]^{2+}$: 422.3292, found: 422.3327.

2.5 References

1 T. Ogoshi, T. Aoki, K. Kitajima, S. Fujinami, T. A. Yamagishi and Y. Nakamoto, *J. Org. Chem.*, 2011, **76**, 328–331.

2 T. Ogoshi, S. Kanai, S. Fujinami and T. Yamagishi, *J. Am. Chem. Soc.*, 2008, 5022–5023.

3 N. L. Strutt, R. S. Forgan, J. M. Spruell, Y. Y. Botros and J. F. Stoddart, *J. Am. Chem. Soc.*, 2011, **133**, 5668–5671.

4 T. Ogoshi, T. A. Yamagishi and Y. Nakamoto, *Chem. Rev.*, 2016, **116**, 7937–8002.

5 T. Ogoshi and T. Yamagishi, *Chem. Commun.*, 2014, **50**, 4776–4787.

6 M. Xue, Y. Yang, X. Chi, Z. Zhang and F. Huang, *Acc. Chem. Res.*, 2012, **45**, 1294–1308.

7 T. Ogoshi, D. Yamafuji, T. Aoki, K. Kitajima, T. A. Yamagishi, Y. Hayashi and S. Kawauchi, *Chem. - A Eur. J.*, 2012, **18**, 7493–7500.

8 C. Ke, N. L. Strutt, H. Li, X. Hou, K. J. Hartlieb, P. R. McGonigal, Z. Ma, J. Iehl, C. L. Stern, C. Cheng, Z. Zhu, N. A. Vermeulen, T. J. Meade, Y. Y. Botros and J. F. Stoddart, *J. Am. Chem. Soc.*, 2013, **135**, 17019–17030.

9 C. Ke, R. A. Smaldone, T. Kikuchi, H. Li, A. P. Davis and J. F. Stoddart, *Angew. Chemie - Int. Ed.*, 2013, **52**, 381–387.

10 S. Dong, C. Han, B. Zheng, M. Zhang and F. Huang, *Tetrahedron Lett.*, 2012, **53**, 3668–3671.

11 S. Dong, B. Zheng, Y. Yao, C. Han, J. Yuan, M. Antonietti and F. Huang, *Adv. Mater.*, 2013, **25**, 6864–6867.

12 S. Dong, J. Yuan and F. Huang, *Chem. Sci.*, 2014, **5**, 247–252.

13 N. Sun, X. Xiao, W. Li and J. Jiang, *Adv. Sci.*, 2015, **2**, 1–8.

14 P. Langer, L. Yang, C. R. Pfeiffer, W. Lewis and N. R. Champness, *Dalt. Trans.*, 2019, **48**, 58–64.

15 T. J. Huang, B. Brough, C. M. Ho, Y. Liu, A. H. Flood, P. A. Bonvallet, H. R. Tseng, J. F. Stoddart, M. Baller and S. Magonov, *Appl. Phys. Lett.*, 2004, **85**, 5391–5393.

16 S. Kang, S. A. Vignon, H. R. Tseng and J. F. Stoddart, *Chem. - A Eur. J.*, 2004, **10**, 2555–2564.

17 S. Silvi, M. Venturi and A. Credi, *J. Mater. Chem.*, 2009, **19**, 2279–2294.

18 S. Kassem, T. Van Leeuwen, A. S. Lubbe, M. R. Wilson, B. L. Feringa and D. A. Leigh, *Chem. Soc. Rev.*, 2017, **46**, 2592–2621.

19 K. Zhu, G. Baggi and S. J. Loeb, *Nat. Chem.*, 2018, **10**, 625–630.

20 B. P. Bandgar, V. S. Sadavarte and L. S. Uppalla, *Tetrahedron Lett.*, 2001, **42**, 951–953.

21 C. Li, S. Chen, J. Li, K. Han, M. Xu, B. Hu, Y. Yu and X. Jia, *Chem. Commun.*, 2011, **47**, 11294–11296.

22 Y. Liu, C. Chipot, X. Shao and W. Cai, *J. Phys. Chem. C*, 2016, **120**, 6287–6293.

23 T. Ogoshi, D. Kotera, S. Nishida, T. Kakuta, T. A. Yamagishi and A. M. Brouwer, *Chem. - A Eur. J.*, 2018, **24**, 6325–6329.

24 K. Yang, Z. Cai, A. Jaiswal, M. Tyagi, J. S. Moore and Y. Zhang, *Angew. Chemie - Int. Ed.*, 2016, **55**, 14090–14095.

25 H. Imahori, A. Fujimoto, S. Kang, H. Hotta, K. Yoshida, T. Umeyama, Y. Matano and S. Isoda, *Tetrahedron*, 2006, **62**, 1955–1966.

26 P. Tongkate, D. Phromyothin and J. Sumranjit, *Tetrahedron*, 2012, **68**, 3329–3335.

27 H. Meier, D. Ickenroth, U. Stalmach, K. Koynov, A. Bahtiar and C. Bubeck, *European J. Org. Chem.*, 2001, 4431–4443.

28 S. Maruyama and Y. Kawanishi, *J. Mater. Chem.*, 2002, **12**, 2245–2249.

29 T. Ogoshi, K. Kitajima, T. Aoki, S. Fujinami, T. A. Yamagishi and Y. Nakamoto, *J. Org. Chem.*, 2010, **75**, 3268–3273.

Chapter 3:

[2]Rotaxane Molecular Shuttles

3.1 Introduction

3.1.1 Pillar[5]arene based restricted molecular shuttles

The concepts of molecular shuttles and the translational motion of a macrocycle in rotaxanes have been outlined in **chapters 1** and **2**. A series of neutral two station [2]rotaxane shuttles using a pillar[5]arene as the macrocycle was studied by Ogoshi and co-workers (**Figure 3.1**).[1–3] The stations, which comprise of butyl chains connected to triazole groups at either end were linked together by a polyether or alkyl spacer of varying length. Axle formation progressed by sequential copper(I)-catalysed azide alkyne cycloaddition (CuAAC) reactions, where a pseudorotaxane was complexed using a diethoxypillar[5]arene (DEP5A) macrocycle to the axle which subsequently reacted in another CuAAC reaction to snap the stopper group onto the end of the axle and prevent dethreading. In DMSO they found the macrocycle to be situated at either station with shuttling between the stations occurring quickly, on a more rapid timescale than the NMR experiment used to study motion (**Figure 3.1**). This effect was attributed to the macrocycle shuttling rapidly over the central polyether spacer. Surprisingly, spacer length did not have a direct effect on rate of shuttling across the linker, however the substituents did as the oxygen atoms on the polyether spacers have a repulsive interaction with the electron rich pillararene cavities.

a)

b)

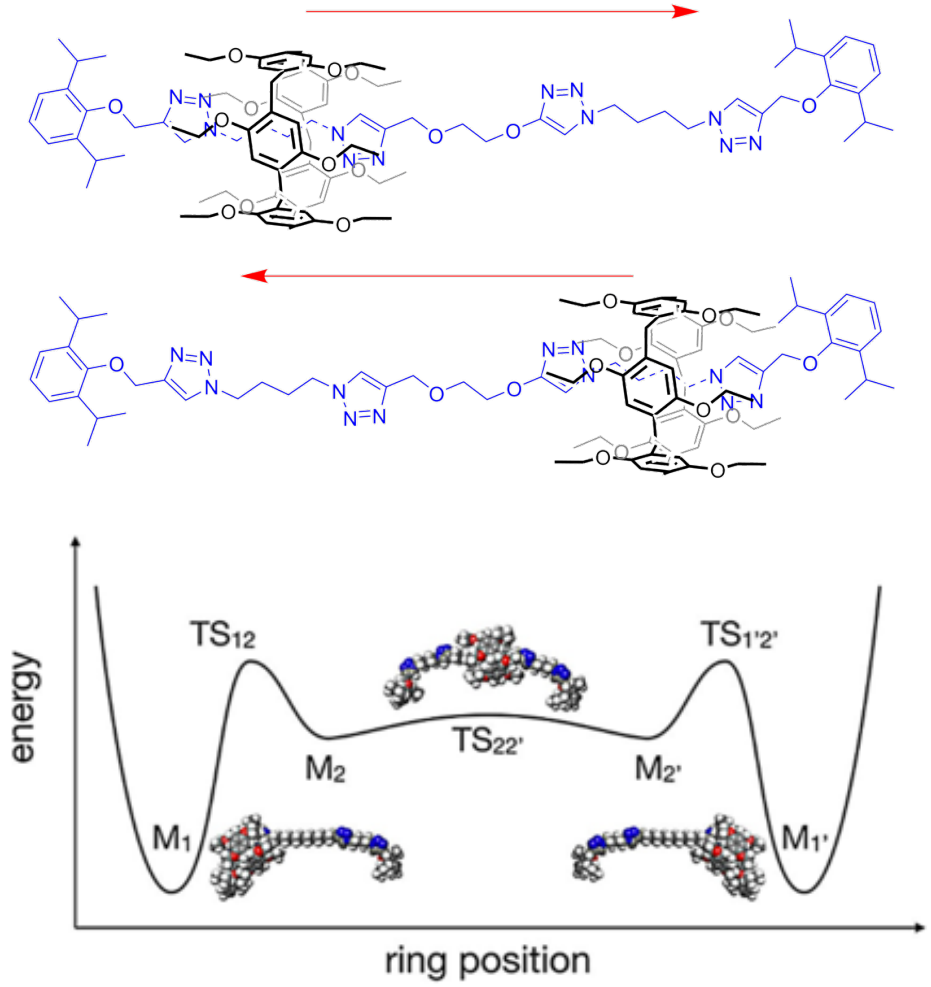

Figure 3.1. (a) the structure of Ogoshi's degenerate two station [2]rotaxane, showing favourable stations and direction of shuttling and (b) a schematic representation of the energy profile for shuttling within the [2]rotaxane that accounts for spacer-length-independent shuttling rates observed. Reprinted with permission from ref 1. Copyright 2018 Wiley-VCH Verlag GmbH & Co. KGaA.

The motion of a pillararene along an axle can be restricted such that the macrocycle is trapped onto a portion of the axle and this was the basis of the previous work done in the Champness group.[4] This consisted of restricting shuttling of dimethoxypillar[5]arene (DMP5A) along bis-imidazolium rods within [2]rotaxane systems (**Figure 3.2**). The rotaxanes were assembled by utilising DMP5A macrocycles to thread onto alkyl bis-imidazole rods of varying lengths, ranging from butyl to octyl.[5] The macrocycle was capped in place via S_N2 reactions between the mesityl stopper groups and the end imidazole groups of the rod. The reaction produces electron deficient imidazolium stations where the electron rich cavities of the pillararenes allow the macrocycles to be regularly situated.

The strength of the pillararene-imidazolium interaction can be disrupted by altering the solvent conditions. High polarity solvents interact more strongly with the imidazolium, confining the solvophobic pillar[5]arene between the imidazolium stations and onto the alkyl chain.[6] Similarly, coordinating metals such as Ag(I) and Pd(II) to the exposed N-heterocyclic carbene (NHC) on the imidazolium can sterically block DMP5A from residing over the imidazolium, and as there are two NHCs per axle, the pillar[5]arene is confined between these stations. To activate the NHC for metal coordination, the α proton had to be deprotonated. This was achieved by the reaction of the free rotaxane with Ag_2O, which acted as both a base to remove the α proton and a source of Ag(I) that could coordinate the NHC. The addition of Ag(I) complexes, as AgBr(NHC) groups, provided enough steric bulk to force the macrocycles onto the alkyl chains, however the silver complexes were not particularly stable to light, and thus were transmetallated to the corresponding Pd(II) complex. Interestingly, the smallest rotaxane with a butyl chain transmetallated asymmetrically, with one imidazolium station converting to the Pd(II) complex, whereas the other Ag(I)-blocked station was cleaved, allowing the macrocycle to reside over a newly reformed imidazolium station.

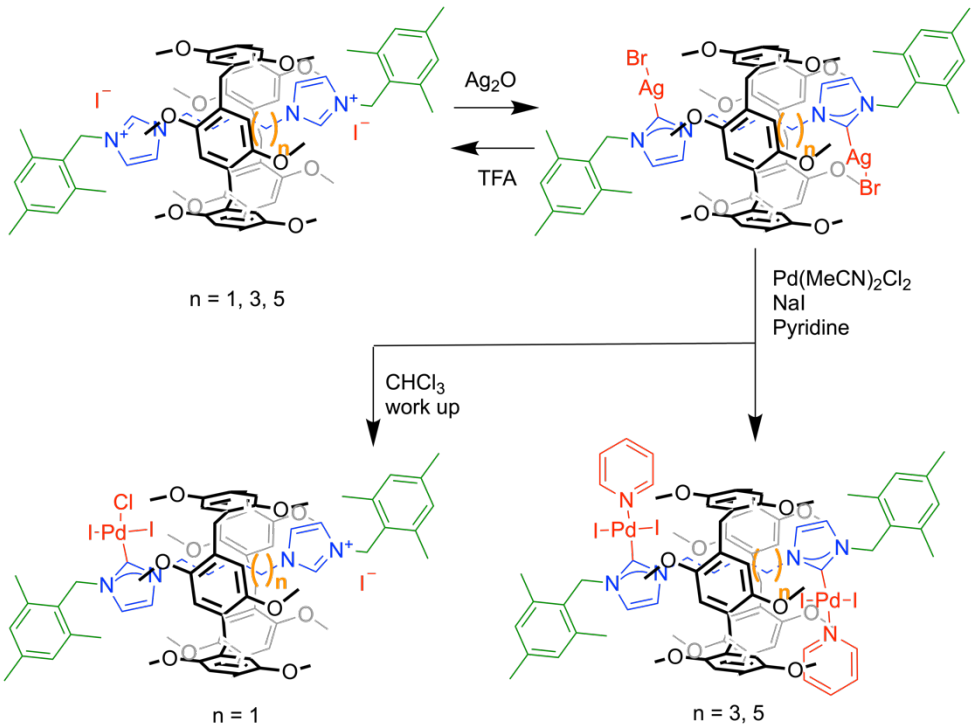

Figure 3.2. Champness' [2]rotaxane series where the macrocycle can be confined in between the imidazolium stations using Ag(I) and Pd(II) metal centres.[4]

3.1.2 Advanced molecular shuttling within energy ratchets

More advanced molecular machines can be fabricated by exploiting the translational motion of a macrocycle. A two-station [2]rotaxane[7] was the basis of an energy ratchet, developed by Leigh and co-workers, where the macrocycle is distributed against a concentration gradient whilst maintaining the dumbbell's structure (**Figure 3.3**).[8] The axle contains fumaramide and succinimide stations which are separated by a silyl ether steric barrier. The macrocycle is snapped (end capped, but on only one side of the axle) onto the side with the fumaramide station and as such is unable to shuttle over to the succinimide station. The mode of action initially requires desilylation, where the steric barricade is removed and the macrocycle is free to equilibrate over the succinimide station. This initial step only allows a small portion of the macrocycle to populate the succinimide station which is around 15%. The next step is photoisomerisation which converts the fumaramide station into its geometrical isomer maleamide. This once again changes the distribution of the macrocycle along the axle in slight favour of the succinimide station at 56% via the removal of H-bonding sites for the macrocycle. Resilylation locks this distribution into place and upon Z to E olefin isomerisation of the maleamide station into fumaramide, the axle can maintain a non-equilibrated distribution of macrocycle. The system can then be reset to its most favourable configuration by an "escapement" mechanism via desilylation, thus allowing the process to be repeated.[9]

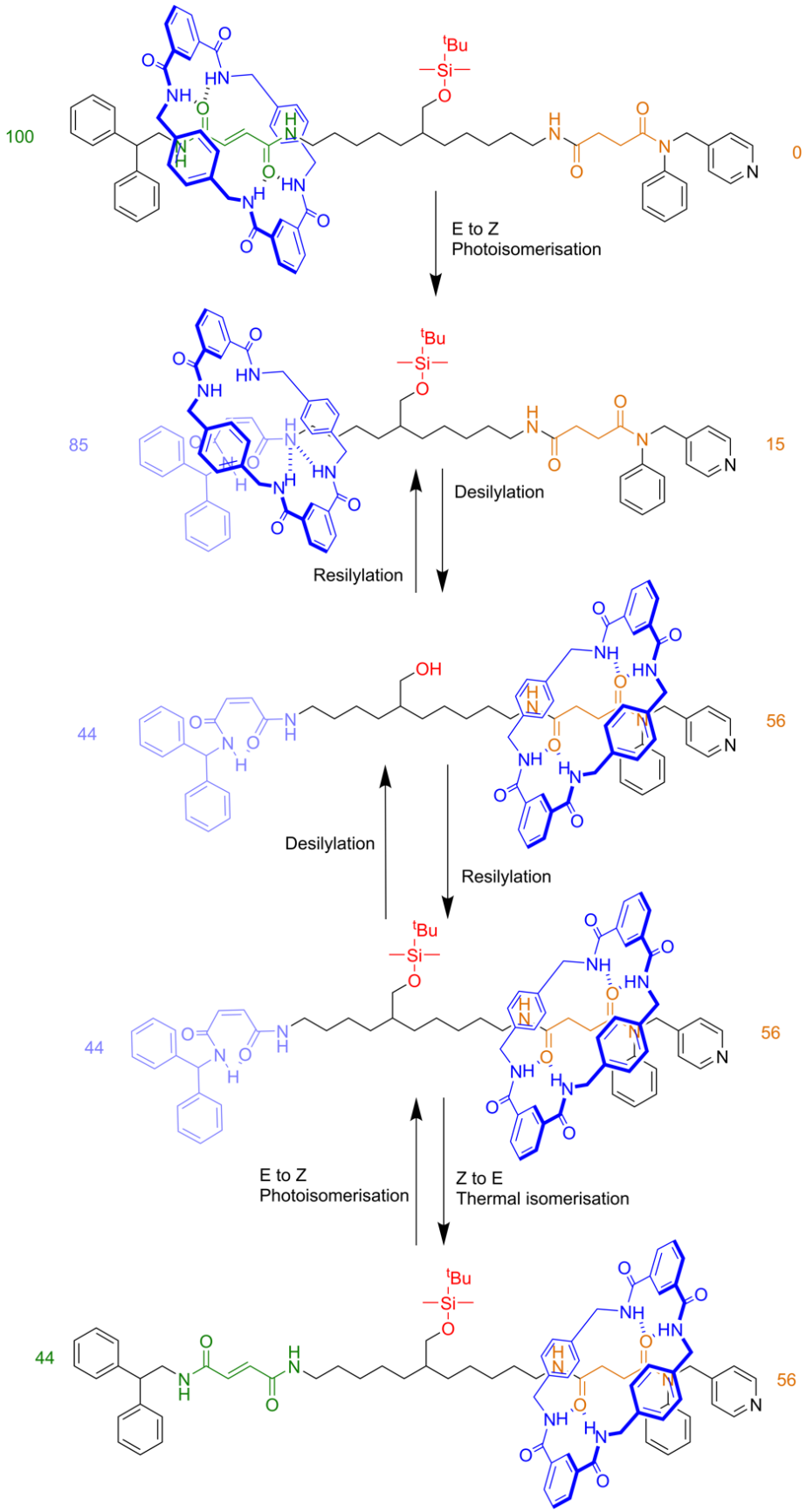

Figure 3.3. Schematic representation of Leigh's energy ratchet. The numbers on each side of the dumbbell denote the percentage of macrocycle residing at each station during the ratchetting process, where colours green, lilac and orange correspond to fumaramide, maleamide and succinimide stations respectively.[8]

The principles outlined here have been utilised by Leigh and co-workers to produce more advanced molecular information ratchets.[10–12]

Similar concepts have been utilised by other groups, such as the energy ratchet reported by Stoddart and co-workers. This [2]pseuodorotaxane system expresses unidirectional translational motion of the macrocycle (**Figure 3.4**) where the π-accepting $CBPQT^{4+}$ macrocycle threads onto the central π-donating naphthalene unit of an asymmetric dumbbell molecule.[13] To one side of the naphthalene unit was a positively charged 3,5-dimethylpyridinium unit acting as a coulombic barrier and to the other was a neutral 2-isopropylphenyl group acting as a steric barrier. Reduction of $CBPQT^{4+}$ decreases the coulombic repulsion between the macrocycle and the 3,5-dimethylpyridinium moiety and also reduces the favourable π-interactions between the naphthalene unit and the macrocycle, allowing $CBPQT^{4+}$ to dethread over the coulombic barrier. Subsequent oxidation to its initial state allows the macrocycle to once again thread through the axle, however it has to pass over the neutral 2-isopropylphenyl unit as the coulombic barrier prevents threading from the other side. The energy ratchet mechanism was tested against symmetrical axles, where both sides were either 3,5-dimethylpyridinium or 2-isopropylphenyl ends (two coulombic barriers and two steric barriers, respectively), where the former would not thread under normal conditions whereas threading occurred quickly in the latter. The pseudorotaxane utilising the bis-3,5-dimethylpyridinium ended axle required pseudorotaxane complexation of the naphthalene unit and $CBPQT^{4+}$ prior to the addition of the 3,5-dimethylpyridinium units via a Cu-AAC reaction. The macrocycles on this axle could not dethread under ambient conditions due to a coulombic barrier over both ends of the axle and required reduction of the macrocycle.

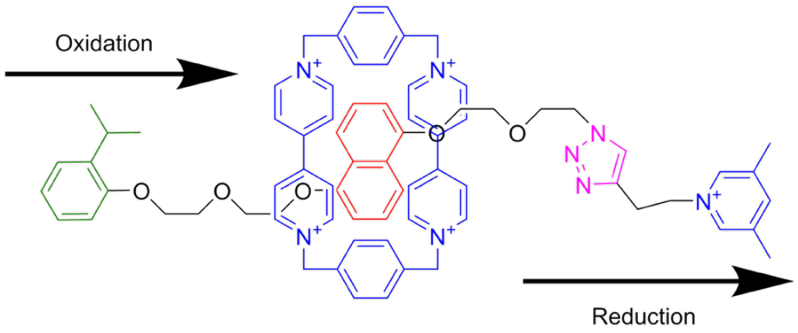

Figure 3.4. Stoddart's energy ratchet composed of a [2]pseudorotaxane. $CBPQT^{4+}$ initially threads via the steric barrier (green) and dethreads via the coulombic barrier (blue) upon reduction. Hexafluorophosphate counterions have been omitted for clarity.[13]

The principles outlined by the energy ratchet were utilised in a molecular pump by Stoddart and co-workers (**Figure 3.5**). The naphthalene recognition sites were replaced in favour of a 4,4-bipyridinium group (4,4-bipy), in addition to extending the length of the axle to incorporate an alkyl chain. The alkyl chain was stoppered by 2,6-diisopropylphenyl and connected to the neutral 2-isopropylphenyl "steric speed bump" on the other side.[14] The $CBPQT^{4+}$ macrocycle cannot form a host-guest inclusion complex with doubly charged 4,4-bipy under ambient conditions, so it must be reduced to allow $CBPQT^{4+}$ to pass through the columbic barrier and form the pseudorotaxane with the recognition site. Upon oxidation, the macrocycle cannot dethread via the columbic barrier and so is forced onto the steric speed bump, where upon heating can finally shuttle over it onto the alkyl chain. This cycle can be repeated up to once more to allow two macrocycles to be pumped into close proximity to each other along the alkyl chain, where dethreading of the rings on the [3]rotaxane does not occur due to the presence of a sufficiently long alkyl chain.

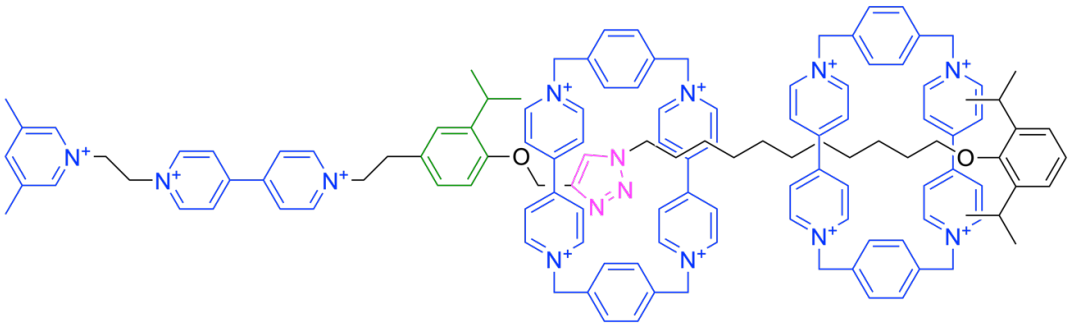

Figure 3.5. Stoddart's artificial molecular pump, consisting of a [3]rotaxane species where two $CBPQT^{4+}$ macrocycles have been pumped over the steric barrier onto the same section of the axle. Hexafluorophosphate counterions have been omitted for clarity.[14]

3.2 Results and Discussion

The synthesis and characterisation of a series of pillar[5]arene based [2]rotaxanes, utilising different length alkyl chains along the rim of each pillararene is reported in this chapter. The rotaxanes have been characterised via ^{1}H and 2D NMR spectroscopy, with shuttling behaviour being analysed under different solvent conditions and temperatures.

3.2.1 Synthesis and characterisation of [2]rotaxanes

Detailed synthetic procedures for precursor molecules (**2.1 – 2.10**) and [3]rotaxanes (**2.11-2.14**) along with the dumbbell molecule (**2.15**) can be found in **chapter 2**. As a result of the [3]rotaxane reactions described in **chapter 2**, [2]rotaxane by-products were formed (**Scheme 3.1**).

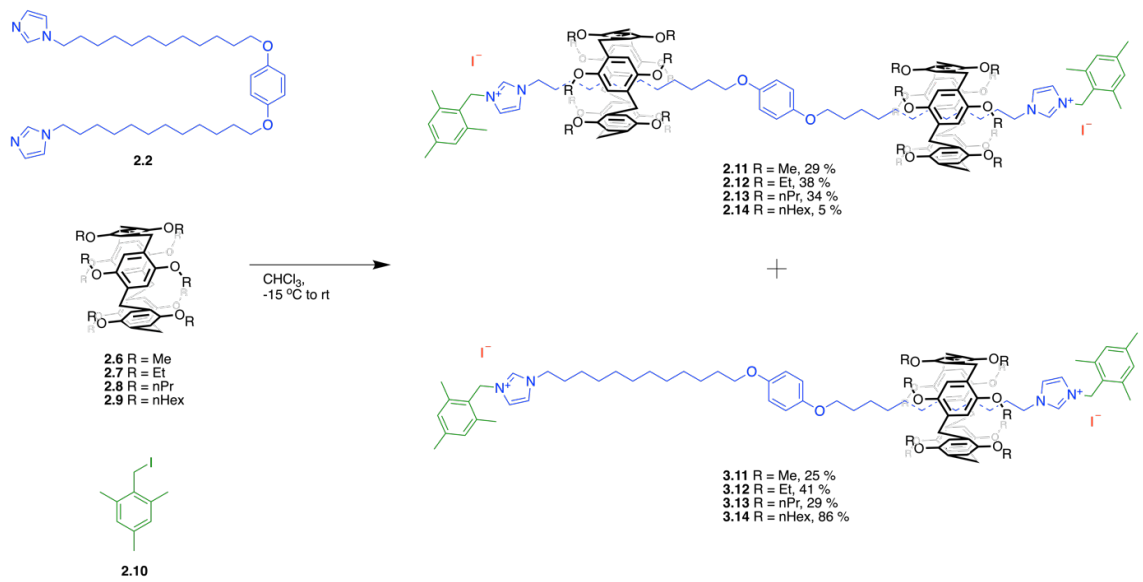

*Scheme 3.1. Toolkit of components required to assembled [2] and [3]rotaxanes. [3]Rotaxanes were explored in **chapter 2**.*

[2]Rotaxanes **3.12-3.14** were separated from their [3]rotaxane counterparts via flash column chromatography. [2]Rotaxane **3.11** had to be synthesised at a higher dilution using only 1 equivalent of DMP5A with respect to axle **2.2**, as only trace amounts of the [2]rotaxane were present when the [3]rotaxane was synthesised.

Of the [2]rotaxanes that were separated from their [3]rotaxane counterparts (**3.12, 3.13** and **2.12, 2.13** respectively), the yields of both products were quite similar, with [2]rotaxane **3.12** being the major product by 3%, and [3]rotaxane **2.13** being the major

product by 5%. Although there was some preference in which rotaxane was formed using different pillararenes, the yields of both products were relatively high, suggesting the difference in selectivity was negligible.

When the potential area encapsulated by the pillararene is longer than that of half of the axle, the major product is the [2]rotaxane with 86% yield, compared to a measly 5% yield of the corresponding [3]rotaxane, as illustrated by [2]rotaxane **3.14** where the pillar[5]arene macrocycle is functionalised with hexyl groups. It is proposed that this is due to a steric clash between dihexyloypillar[5]arene (DHP5A) macrocycles along the axle in the [3]rotaxane, as the 1,4-dialkoxybenzene barrier cannot prevent the macrocycles from interacting with each other. In chloroform, shuttling occurs in all [2]rotaxanes with shifts observed from peaks H_b to H_q on a single side of the axle (for numbering of environments see **Figure 3.6**). This is a consequence of the single pillar[5]arene macrocycle being barricaded onto one side of the axle by the 1,4-dialkoxybenzene unit. This leads to a dumbbell-like region across the axle (labelled $H_{b'-q'}$) and a rotaxane-like region (labelled H_{b-q}).

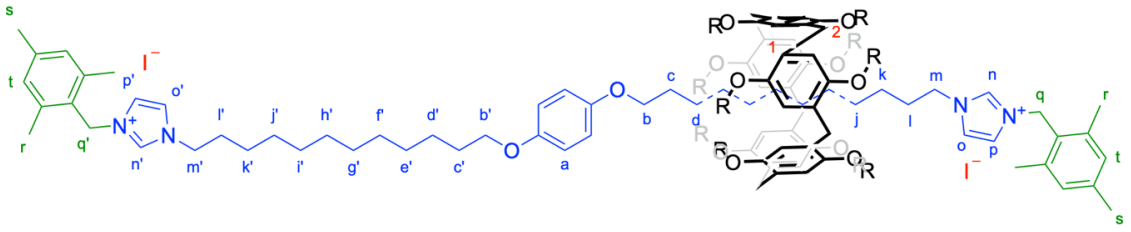

*Figure 3.6. General structure of [2]rotaxanes **3.11**-**3.14** in $CDCl_3$ where the protons are labelled for clarity.*

Comparison of the ^{1}H NMR spectra observed for the dumbbell, [2]rotaxane and [3]rotaxane helped identify peaks which had not shifted with respect to the dumbbell and identified key dumbbell-like peaks on the [2]rotaxane. All other peaks were confirmed using 2D NMR spectroscopies ^{1}H-^{1}H COSY and ^{1}H-^{1}H NOESY.

Shielding factors (**Formula 2.1, chapter 2**) were calculated for the [2]rotaxane systems and plotted against the location of the proton on the axle. In chloroform, the plots do not contain a mirror plane as the macrocycle is barricaded onto one side of the axle. In DMSO,

a partial mirror plane is observed as the pillararenes are able to slip over the 1,4-dialkoxybenzene barricade due to the stabilisation of the (DMSO-imidazolium) solvent-ion pair. However, as shuttling occurs over a larger area, the imidazolium regions are desymmetrised.

3.2.2 Shuttling of macrocycles in $CDCl_3$

For the series of [2]rotaxanes (**3.11-3.14**) in chloroform solution, one section of the axle remains unshifted with respect to the dumbbell molecule, whilst the other section is observed to have characteristic shielding relating to the macrocycle being threaded onto the axle. This reveals the pillararenes are barricaded onto one side of the axle from the 1,4-dialkoxybenzene moiety.

a)

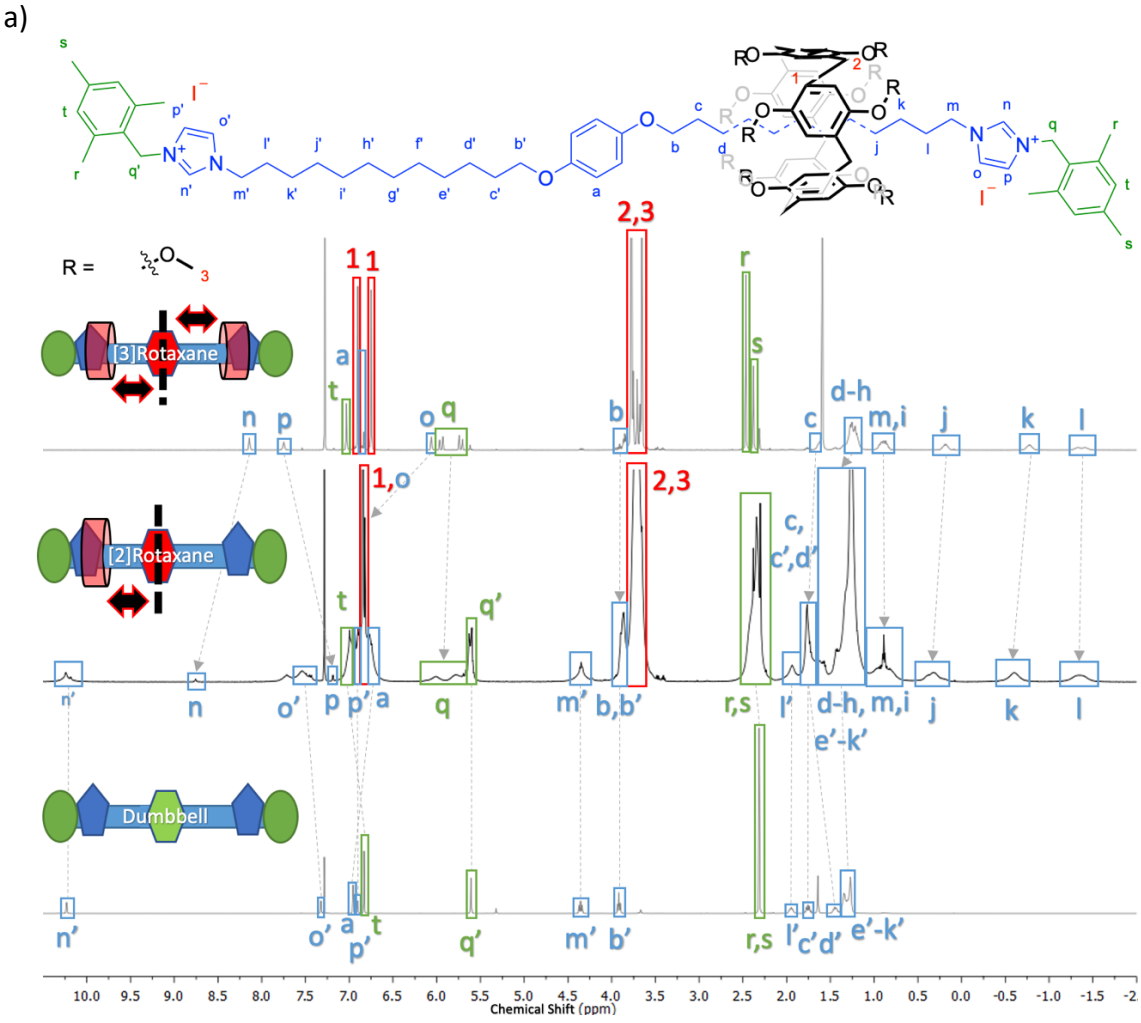

b)

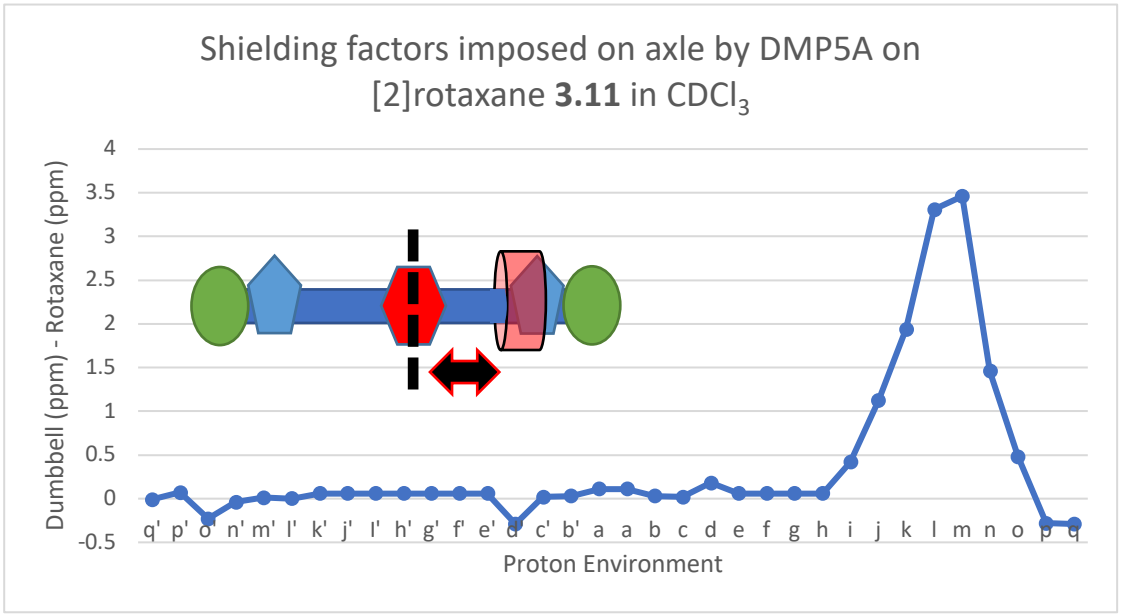

*Figure 3.7. (a) ^{1}H NMR stack of [3]rotaxane (**2.11**), [2]rotaxane (**3.11**) and dumbbell molecule (**2.15**) in descending order in $CDCl_3$ and (b) plot of shielding factors for [2]rotaxane **3.11**.*

From the calculated shielding factors of [2]rotaxane **3.11** (**Figure 3.7**), we see peaks $H_{q'}$ to $H_{b'}$ have little to no deviation from the origin, as these are dumbbell-like peaks which are not affected by shielding from the pillararene. Along the rotaxane-like peaks there is a global maximum over H_m in the imidazolium region. DMP5A most likely resides close to the imidazolium group and neighbouring carbons along the alkyl chain. Environments H_p and H_q have downfield shifts resulting in negative shielding factor values suggesting a steric clash between the pillararene macrocycle and the mesityl stopper group in addition to being deshielded by the oxygen atoms along the rim of the pillararene, like that of its counterpart [3]rotaxane **2.11**.

There is also a smaller maximum about peak H_d, similar to that observed for the [3]rotaxane counterpart **2.11**. This may suggest that the pillararene is able to shuttle towards the 1,4-dialkoxybenzene barricade, however due to the low value of the shielding constant, shuttling could be slow or even non-existent. This suggests, as with the [3]rotaxane counterpart **2.11**, DMP5A on [2]rotaxane **3.11** is simply pirouetting close to the imidazolium moiety.

Pillararene peak H_1 on **3.11** behaves similar to an unthreaded pillararene as only a single DMP5A moiety is threaded through the axle. Peaks H_2 and H_3 are however merged into one section as observed for its [3]rotaxane counterpart.

a)

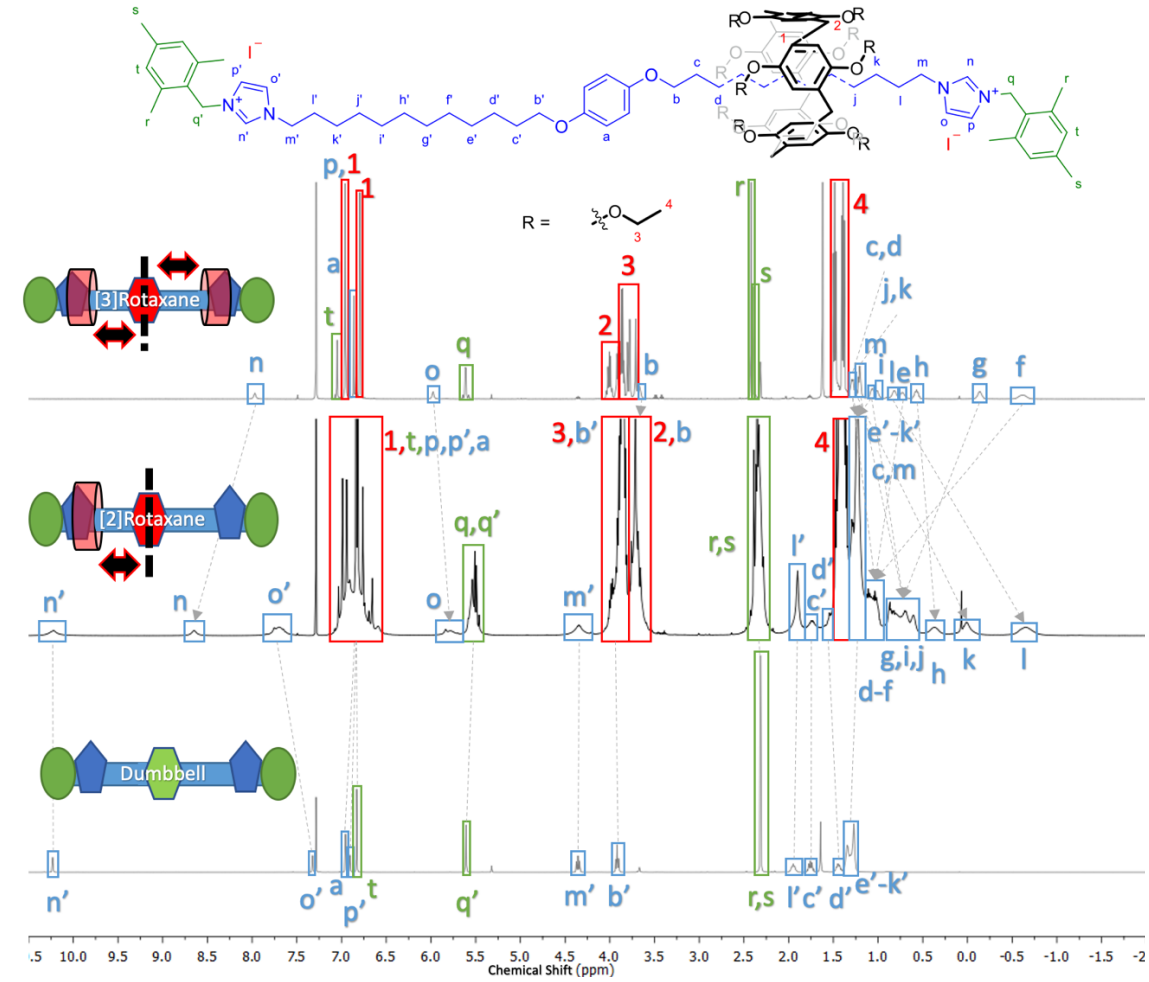

b)

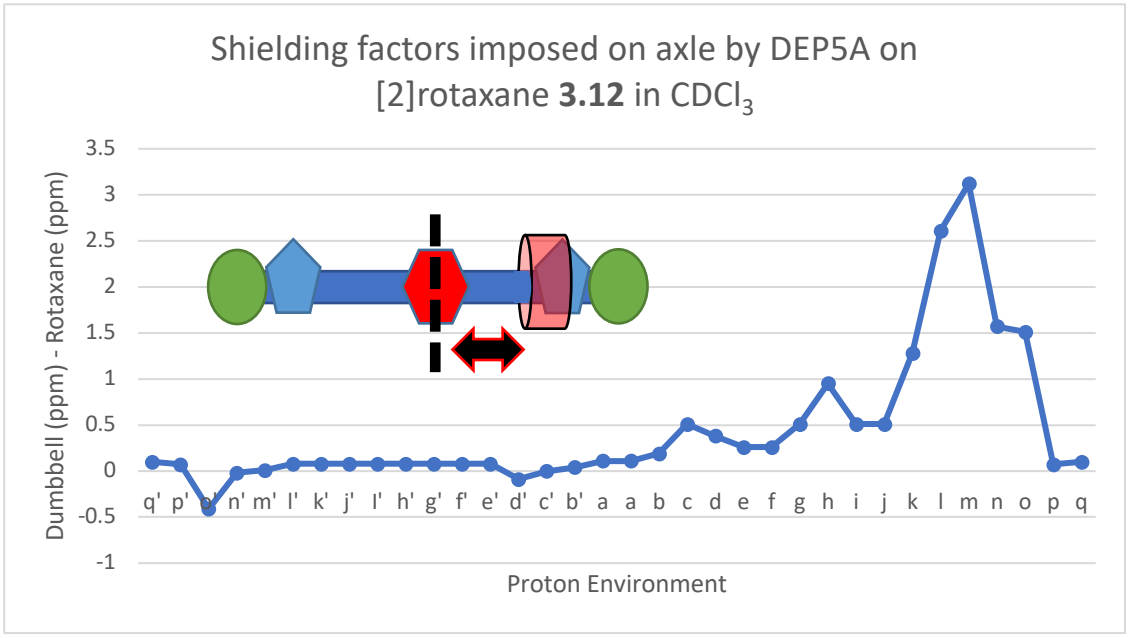

*Figure 3.8. (a) ^{1}H NMR stack of [3]rotaxane (**2.12**), [2]rotaxane (**3.12**) and dumbbell molecule (**2.15**) in descending order in $CDCl_3$ and (b) plot of shielding factors for [2]rotaxane **3.12**.*

Similarly, shuttling of DEP5A in [2]rotaxane **3.12** occurs on one side of the axle (**Figure 3.8**). There is a large maximum located around H_m resulting from the pillararene-imidazolium interaction. Environments H_q and H_p are somewhat unchanged as the stopper group blocks off this section, however they are not negative values like that of [2]rotaxane **3.11** as the ethoxy chains inhibit a steric clash between the macrocyclic core and the mesityl stopper groups. There is a stepwise decrease in shielding constants from H_m to H_o, due to the longer ethoxy chains interacting with the stopper group.

Two smaller maxima are observed, similar to the [3]rotaxane counterpart **2.12**, around environments H_c and H_h suggesting that the DEP5A macrocycle is shuttling along the axle towards the barricade. The magnitude of the maxima drop as they arrive closer to H_a, corresponding to the 1,4-dialkoxybenzene unit, as shuttling reaches its limit closest to the barricade. Environment H_h is approximately half way between the barricade and the stopper group, and may be a relatively stable environment for DEP5A to reside over.

When comparing [2]rotaxane **3.12** to that of **3.11**, shuttling does occur, rather than stationary pirouetting of the macrocycle around a central point. Shielding factors of [2]rotaxane **3.12** in relation to the [3]rotaxane **2.12** seems subdued. Other than the maximum of H_m over the imidazolium, all other maxima have lost magnitude in the case of the [2]rotaxane in comparison to the [3]rotaxane, suggesting that the DE5PA macrocycle is primarily located in a single position (H_m). This may be due to the absence of the second macrocycle in the [3]rotaxane acting as a second steric barrier once DEP5A is close enough to reach the 1,4-dialkoxybenzene unit. Additionally, protons on the dodecyl chain of the [3]rotaxane are not at the same shift as the [2]rotaxane.

Similar to [2]rotaxane **3.11**, H_1 on **3.12** is observed as a single peak as only one macrocycle is threaded through the axle. Interestingly, peaks H_2 and H_3 on DEP5A which had swapped positions from [3]rotaxane **2.12** to [2]rotaxane **3.12**, resembling their arrangement as a free macrocycle.

a)

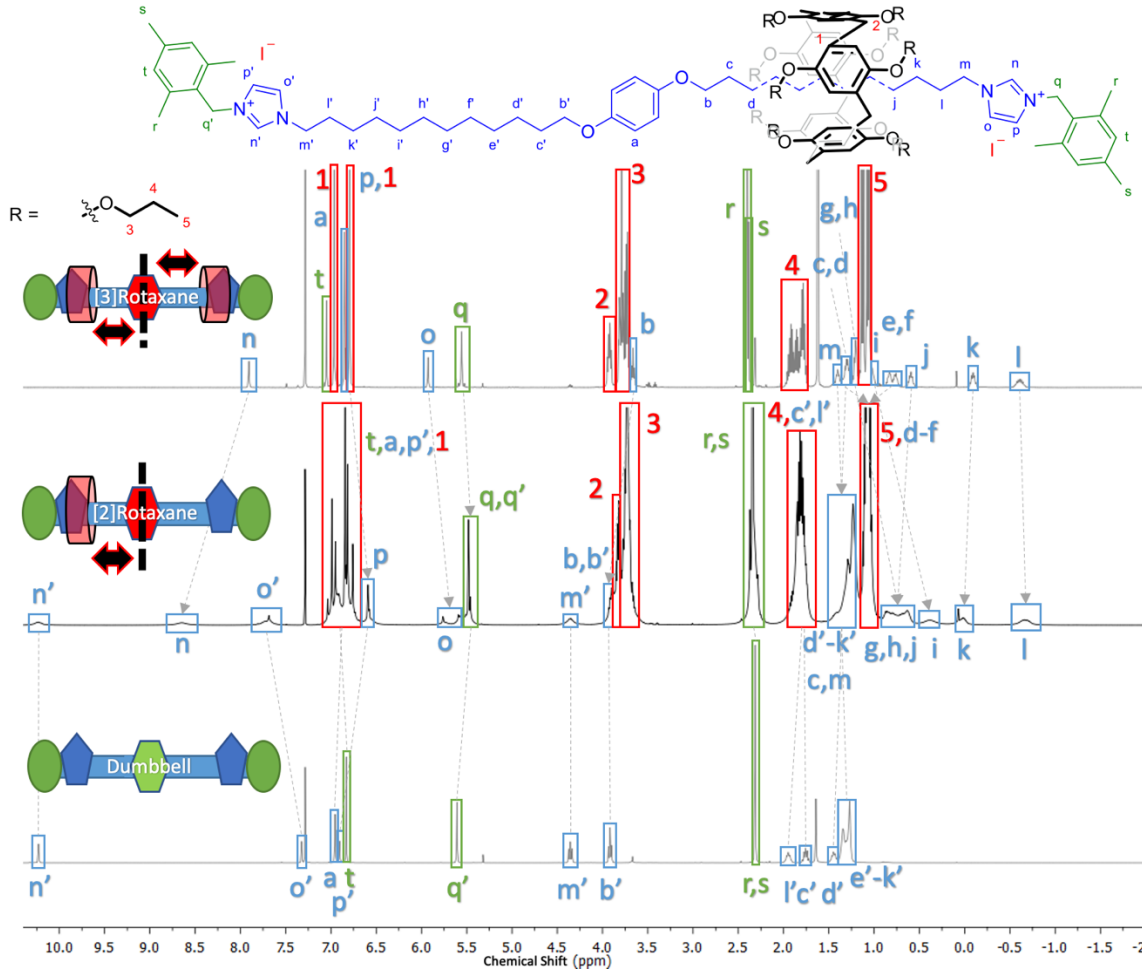

b)

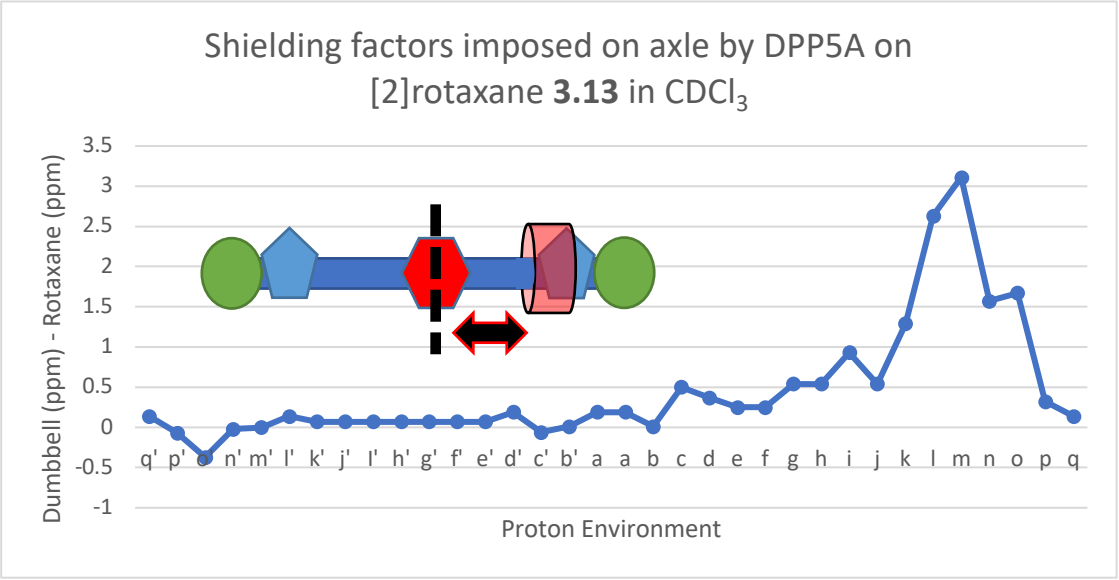

*Figure 3.9. (a) ^{1}H NMR stack of [3]rotaxane (**2.13**), [2]rotaxane (**3.13**) and dumbbell molecule (**2.15**) in descending order in $CDCl_3$ and (b) plot of shielding factors for [2]rotaxane **3.13**.*

Shuttling of the DPP5A macrocycle in **3.13** (**Figure 3.9**) is similar to that of **3.12**. The pillararene is trapped on one side of the barricade where dumbbell-like peaks $H_{b'-q'}$ are not shielded by the macrocycle. Conversely, maxima about peaks H_c, H_i and H_m are subject to shielding. The height of the maxima reduce as they approach the central 1,4-dialkoxybenzene unit (H_a), H_m exhibiting the largest shielding factor due to pillar[5]arene-imidazolium interaction. H_c is closest to the barricade and shows the smallest maximum shielding factor, with H_i half way between the extremes. H_b shows no shift from the origin resulting in a negligible shielding factor, which could be attributed to the lengthened propoxy chains on the rim of the pillararene. Additionally, the shielding factor of H_o is larger than that of H_n, which could similarly be attributed to the longer propoxy chains. The slight deshielding of H_n may be attributed to interactions with the oxygen atoms of the DPP5A.

In direct contrast to [3]rotaxane **2.13**, the DPP5A molecule on **3.13** is situated closer to the imidazolium, with shielding factors of greater than 0.5 from H_i to H_o. Within the region of H_b to H_i there are less troughs observed for [2]rotaxane **3.13** than for [3]rotaxane **2.13** which confirms shuttling ability is directly affected by the presence of a second macrocycle in the [3]rotaxane.

a)

b)

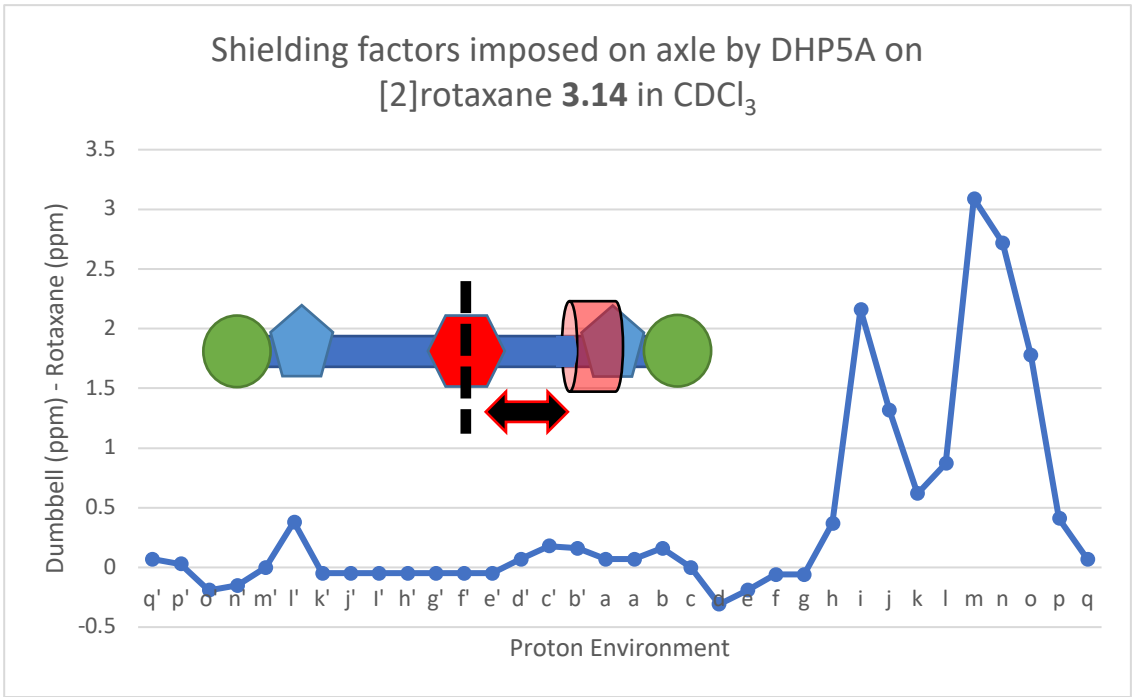

*Figure 3.10. (a) ^{1}H NMR stack of [3]rotaxane (**2.14**), [2]rotaxane (**3.14**) and dumbbell molecule (**2.15**) in descending order in $CDCl_3$ and (b) plot of shielding factors for [2]rotaxane **3.14**.*

As observed for its analogues, shuttling of DHP5A on [2]rotaxane **3.14** occurs on one side of the axle (**Figure 3.10**). The largest shielding factor value is observed for H_m, near the imidazolium station, however another large maximum is observed at H_i, which is an interim position between the favourable imidazolium station and the 1,4-dialkoxybenzene barricade. Shuttling seemingly does not occur beyond H_g, perhaps as a result of the absence of a second macrocycle on the axle or due to the enhanced sterics of the terminal hexyl chains of DHP5A clashing with the steric barricade. This confinement behaviour, in addition to shifts along the dumbbell-like region, could suggest that the unencapsulated section is affected by folding or other conformational effects.

Additionally, the second largest shielding factor value for [3]rotaxane **2.14** was found at H_g, with shuttling occurring up to the barricade. This could imply that there is short range communication between two macrocycles of the [3]rotaxane, through either steric repulsion or favourable van der Waals interactions or a mixture of both.

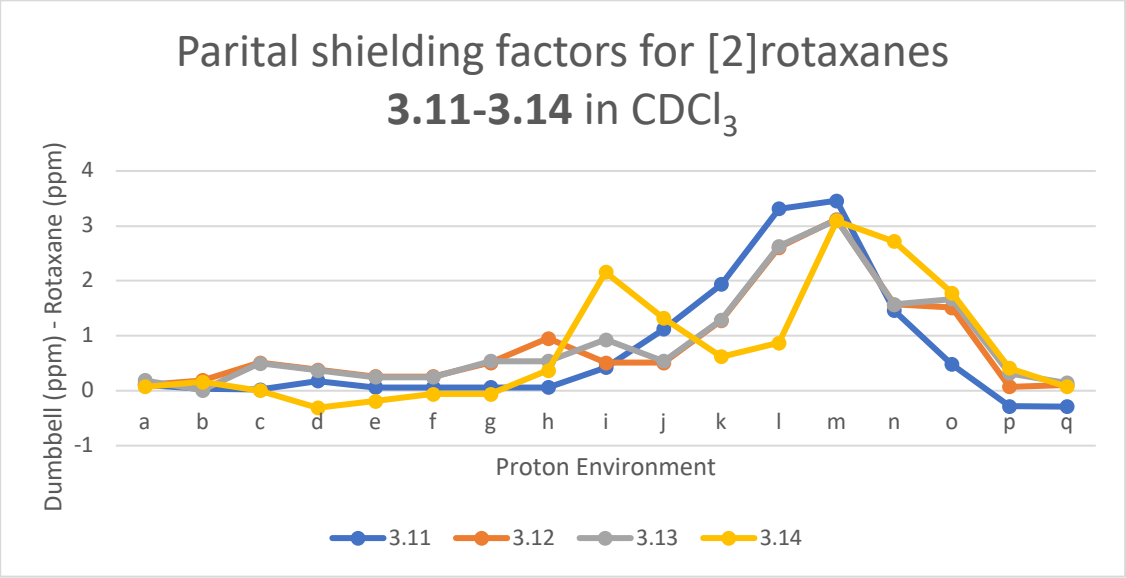

*Figure 3.11. Plot of partial shielding factors of the encapsulated rotaxane region of [2]rotaxanes **3.11-3.14** in $CDCl_3$.*

A set of trends can be observed when the shielding factors of the [2]rotaxane series **3.11-3.14** are overlaid (**Figure 3.11**). Only the rotaxane region, not the dumbbell portion of the [2]rotaxane, is presented for clarity. All of the [2]rotaxanes have a global maximum at H_m, suggesting that the steric contribution of the pillararenes interacting with the stopper group is overcome by the favourable interaction with the imidazolium.

A steric contribution of the terminal alkoxy chains is observed when comparing the pillararenes over the dodecyl region. Shuttling of **3.11** is highly localised over the imidazolium stations and is thus somewhat of an outlier. On **3.12**, the largest shielding factor outside of the imidazolium region is found at H_h, whereas for **3.13** and **3.14** it is H_i. This suggests that there is some steric contribution in relation to shielding factors as the propoxy chains are shifted slightly further away from the 1,4-dialkoxybenzene barricade than the ethoxy chains. The steric contribution does not affect chains of longer lengths than propoxy as they lack rigidity.

3.2.3 Shuttling of macrocycles in DMSO-d_6 and high temperature ^{1}H NMR studies

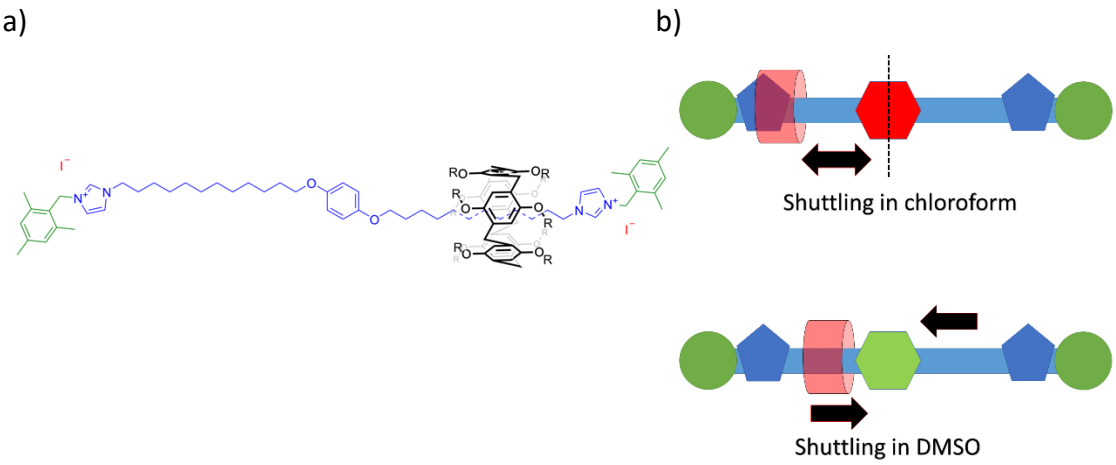

Figure 3.12. (a) the general structure of the [2]rotaxane series and (b) cartoon model of shuttling within the [2]rotaxane systems, either at low polarity when in $CDCl_3$ or high polarity when in DMSO-d_6.

When the [2]rotaxanes are dissolved in DMSO-d_6, the solvent-ion pair is stabilised, such that it becomes unfavourable for the macrocycles to reside close to the imidazolium moiety (**Figure 3.12**).[6] As a result, the macrocycles are pushed onto the dodecyl chains, with the stopper groups proving adequate enough to prevent dethreading at ambient temperatures. This results in the pillararene macrocycles slipping over the 1,4-dialkoxybenzene steric barrier as they shuttle near the centre of the axle.

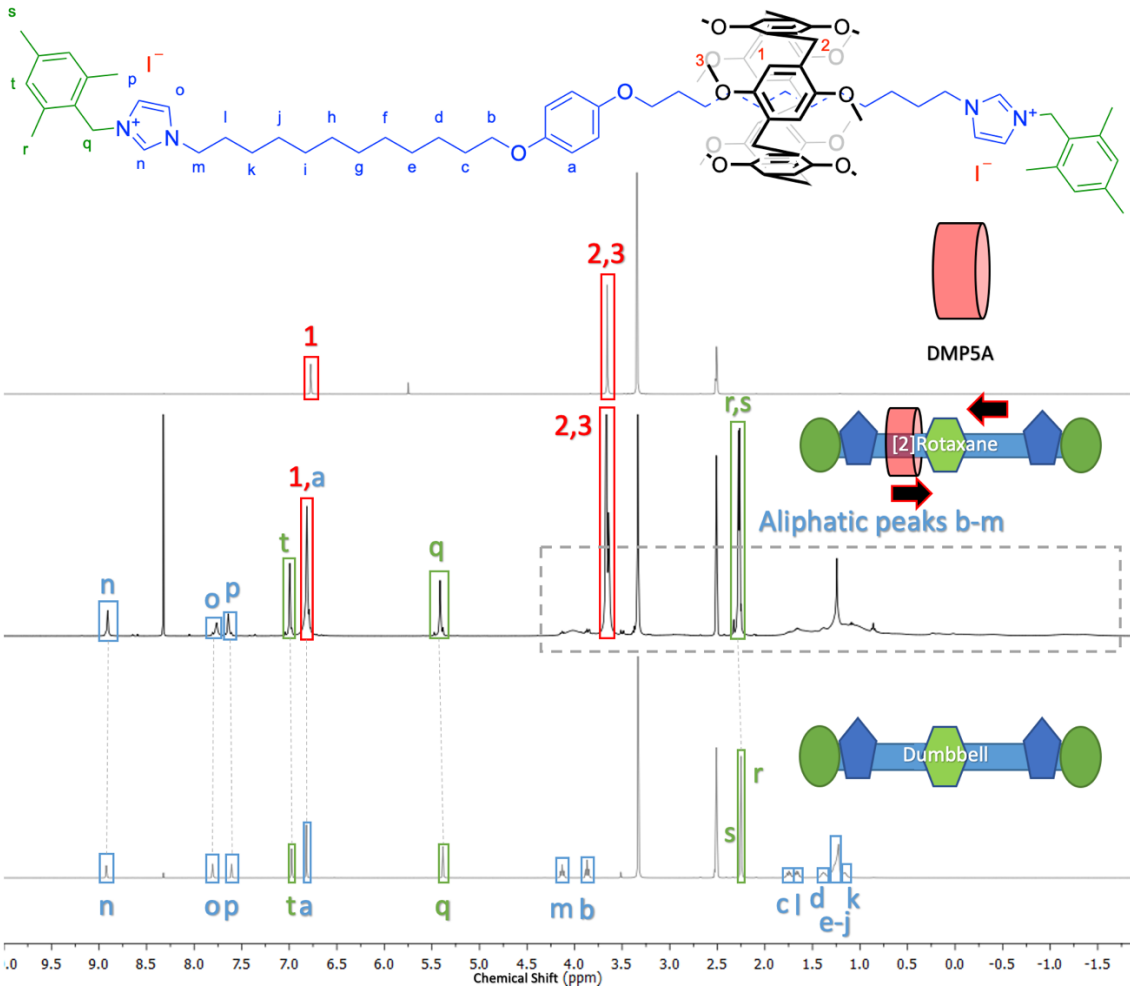

*Figure 3.13. ^{1}H NMR stack of DMP5A (**2.6**), [2]rotaxane (**3.11**) and the dumbbell molecule (**2.15**) in descending order in DMSO-d_6. Aliphatic peaks on the [2]rotaxane cannot be defined.*

In DMSO, protons $H_{n\text{-}q}$ are unshifted with respect to the dumbbell **2.15** on [2]rotaxane **3.11** at room temperature, because DMP5A shifted away from the imidazolium stations (**Figure 3.13**). However, aliphatic protons $H_{b\text{-}m}$ along the dodecyl chains cannot be assigned, because the peaks in the aliphatic region had coalesced and broadened. Additionally, the imidazolium region is not desymmetrised as demonstrated by the absence of distinct peaks $H_{n+\text{-}q+}$ indicating minimal shuttling across the length of the axle.

a)

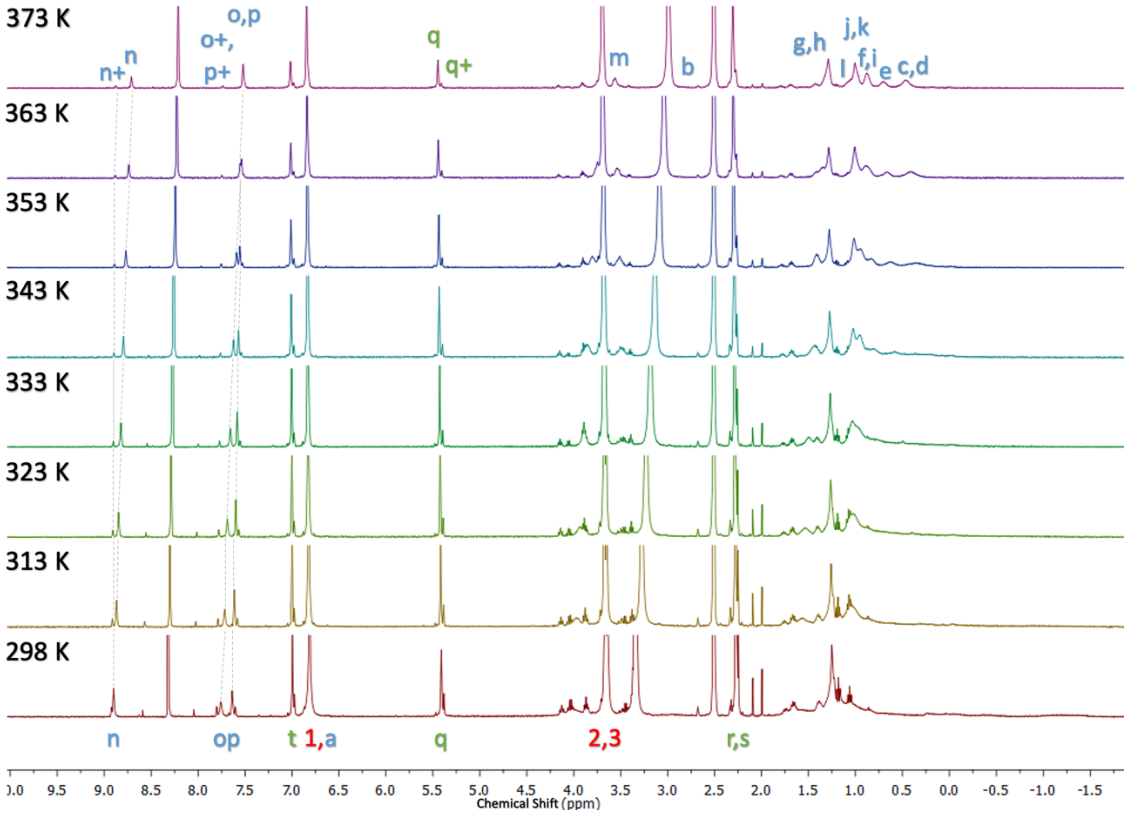

b)

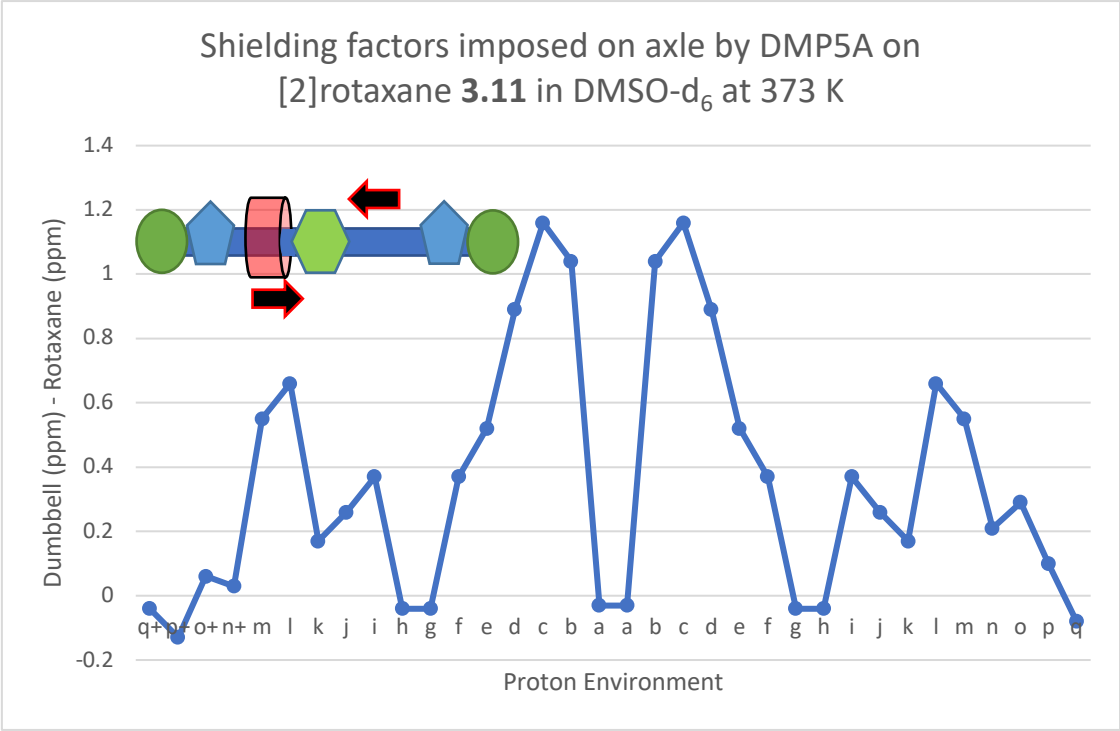

*Figure 3.14. (a) variable temperature ^{1}H NMR stack of [2]rotaxane **3.11** in DMSO-d_6 at 600 MHz, revealing positions of aliphatic protons $H_{b\text{-}m}$ at elevated temperatures and (b) plot of shielding factors of [2]rotaxane **3.11** in DMSO-d_6 at 373 K.*

High temperature ^{1}H NMR studies were used to assess the shuttling of **3.11**. Through incremental increase in temperature from 298 K to 373 K, the rate of shuttling increased, where protons along the axle were assignable, aiding confirmation that the DMP5A macrocycle shuttles over the 1,4-dialkoxybenzene spacer (**Figure 3.14**). Protons $H_{b\text{-}f}$ are the most affected by the macrocycle from their large chemical shifts, with a maximum at H_c. These protons are symmetrical from mirror plane H_a to H_m suggesting rapid shuttling over the barricade. Peak H_a shows no change in chemical shift as the 1,4-dialkoxybenzene is too large for the DMP5A macrocycle to reside over, thus slipping over it quickly.

The enhanced thermal energy of the system at 373 K allows DMP5A to reside over the imidazolium stations for a significant period, suggesting that the additional thermal energy weakens the solvent-ion pair interaction. This is shown by the increase in shielding factors calculated for protons $H_{l\text{-}p}$, although the larger shielding factors near the centre of the axle suggests that the DMP5A preferentially resides close to the global maximum of H_c.

As the axle is long, protons $H_{n\text{-}q}$ are desymmetrised, where peaks $H_{n+\text{-}q+}$ are produced at high temperatures, because the macrocycle cannot be present over both imidazolium groups on the timescale of the ^{1}H NMR experiment.

DEP5A, DPP5A and DHP5A were insoluble in DMSO, thus full ^{1}H NMR stacked spectra could not be achieved. However, relative shifts could still be seen and therefore shielding factors calculated as solubility of the rotaxanes (**3.12-3.14**) and the dumbbell molecule (**2.15**) in DMSO was favourable.

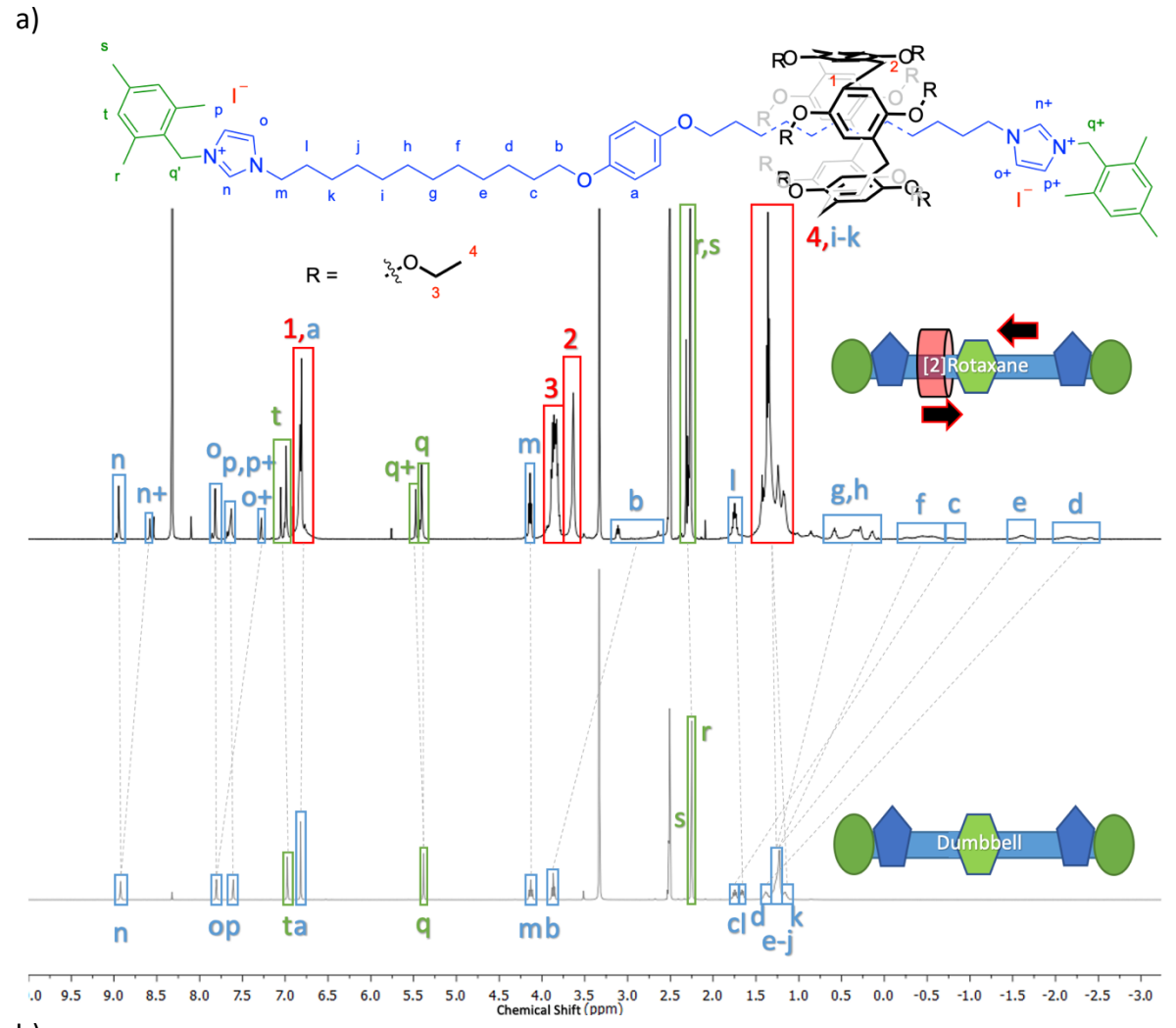

*Figure 3.15. (a) ^{1}H NMR stack of [2]rotaxane (**3.12**) and dumbbell molecule (**2.15**) in DMSO-d_6 at room temperature and (b) plot of shielding factors for [2]rotaxane **3.12** in DMSO-d_6 (orange) and $CDCl_3$ (blue).*

For [2]rotaxane **3.12**, shielding factors are largest about maxima $H_{d,d'}$ as DEP5A is displaced towards the centre of the axle (**Figure 3.15**). The plotted shielding factor is symmetrised as the macrocycle is now able to slip over the 1,4-dialkoxybenzene barricade. Proton H_a shows no change in shift, as the macrocycle cannot reside over this moiety.

At first it would seem that the DEP5A macrocycles on [2]rotaxane **3.12** are prevented from accessing the imidazolium and surrounding area as seen from peaks $H_{i\text{-}q}$ which show no change in shift with respect to the dumbbell molecule. However, the imidazolium regions are desymmetrised as subtle shifts in peaks $H_{m'\text{-}o'}$ are observed, suggesting that the pillararene can interact close to the imidazolium station, but this is not a strongly favoured position in this case. Since there is only one macrocycle on the axle, it cannot be in two places at once, nor can it shuttle over the barricade quickly enough to symmetrise the imidazolium stations.

When comparing shuttling to the [3]rotaxane counterpart **2.12**, [2]rotaxane **3.12** is interesting due to its ability to overcome the stabilisation of the solvent-ion pair at room temperature, even for a small population of DEP5A across the axle.

a)

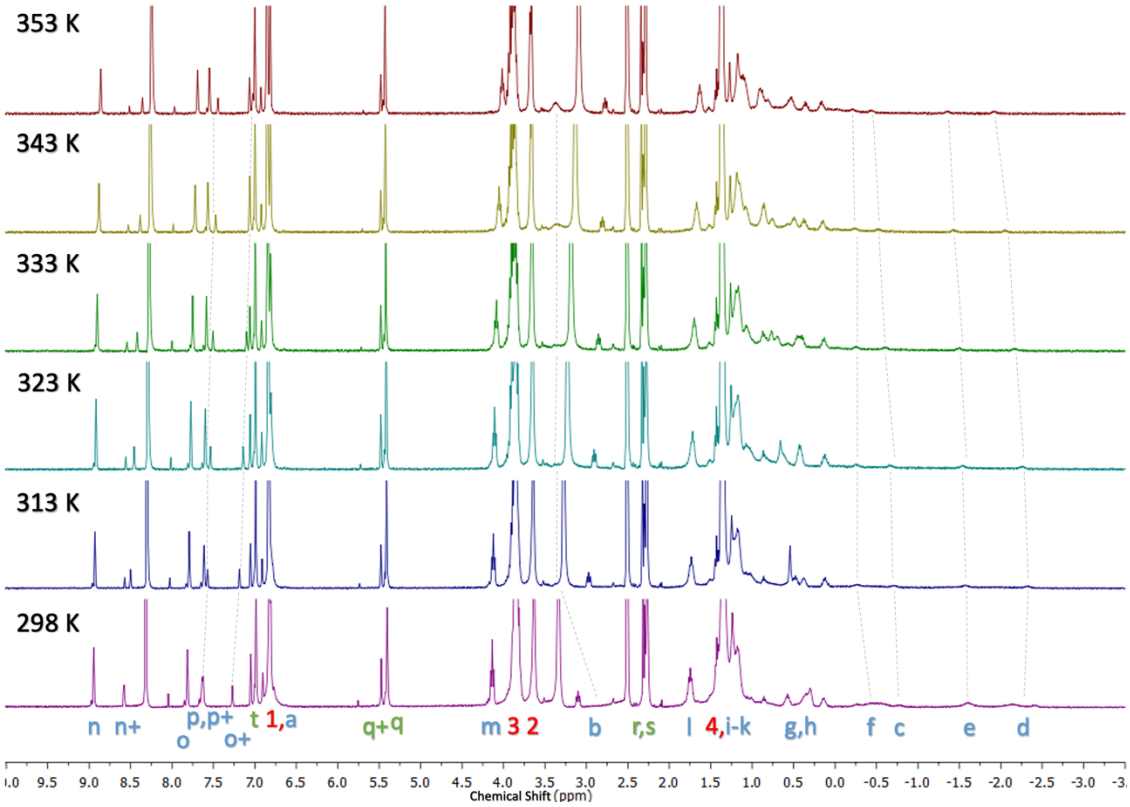

b)

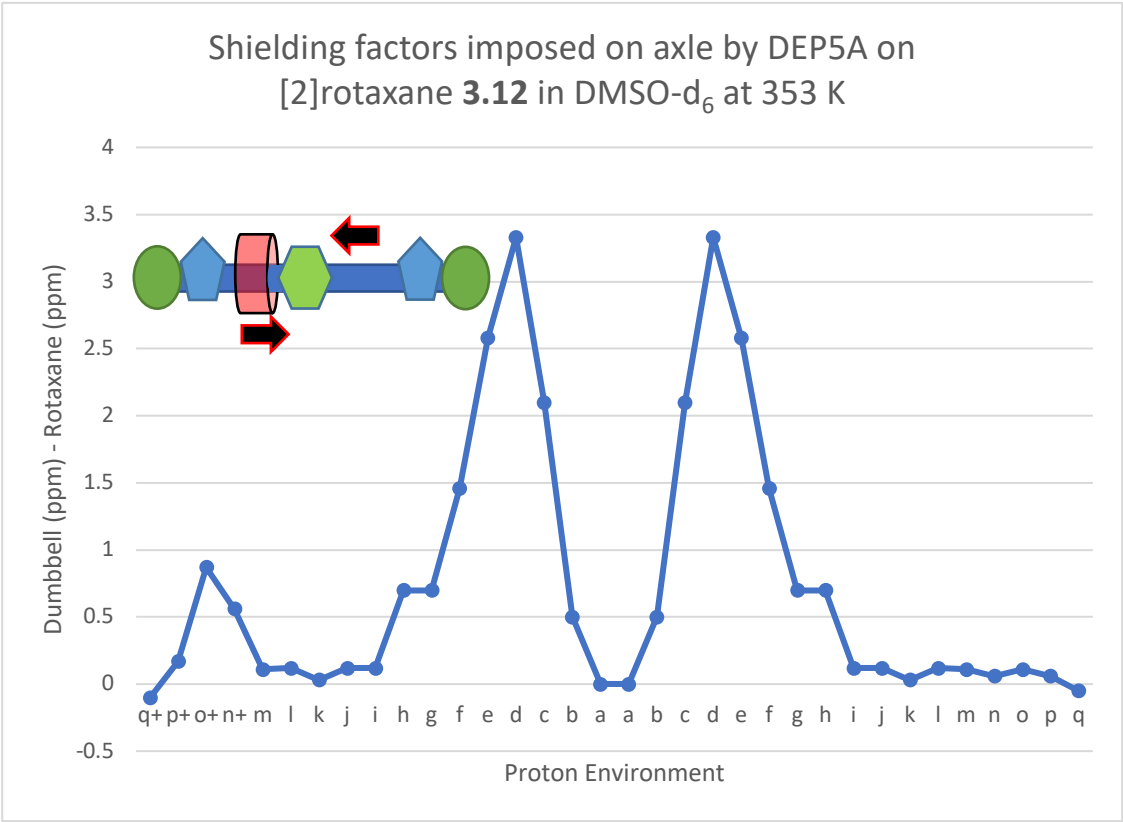

*Figure 3.16. (a) variable temperature ^{1}H NMR stack of [2]rotaxane **3.12** in DMSO-d_6 at 400 MHz and (b) plot of shielding factors of [2]rotaxane **3.12** in DMSO-d_6.*

When the temperature of [2]rotaxane **3.12** is increased to 353 K in DMSO (**Figure 3.16**), shielding occurs over the same region of the axle as observed at room temperature. The increase in thermal energy weakens the imidazolium-solvent interactions, with larger shielding factors being observed for protons $H_{i\text{-}p}$ at room temperature. Additionally, the shielding factor for imidazolium proton H_{o+} is larger than at 353 K than at room temperature. The drop in population of DEP5A is significant as it approaches the 1,4-dioxybenzene barricade, visualised by the drop in shielding factor of H_b by about a half to that at room temperature, implying that DEP5A resides further away from the barricade after slipping over it.

a)

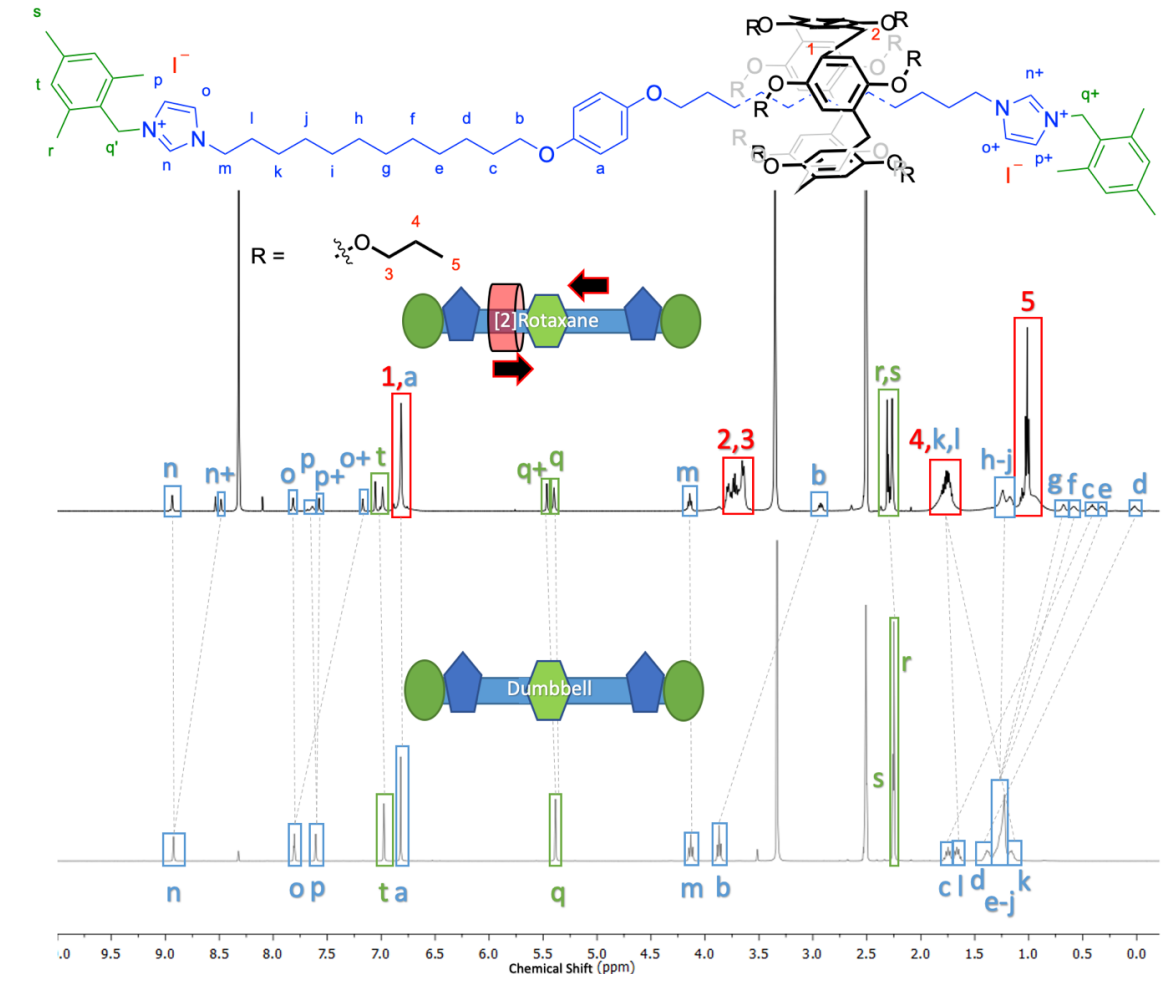

b)

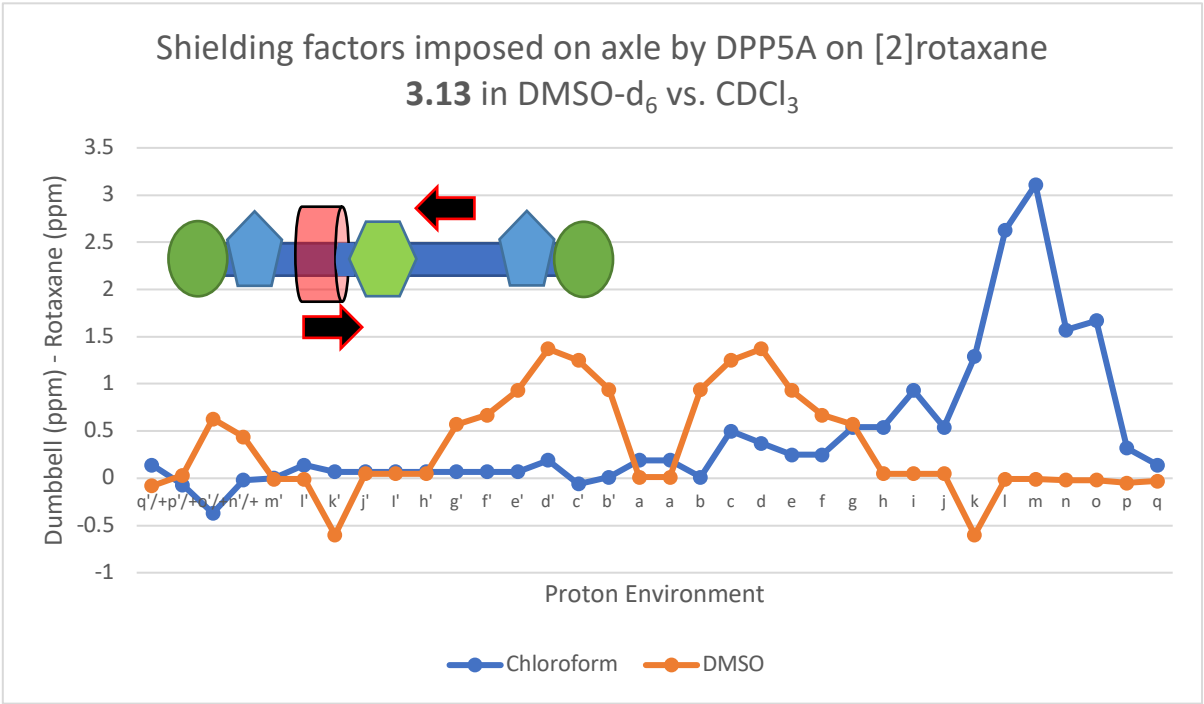

*Figure 3.17. (a) ^{1}H NMR stack of [2]rotaxane (**3.13**) and dumbbell molecule (**2.15**) in DMSO-d_6 at room temperature and (b) plot of shielding factors for [2]rotaxane **3.13** in DMSO-d_6 (orange) and $CDCl_3$ (blue).*

Shuttling in [2]rotaxane **3.13** in DMSO is similar to that of **3.12** (**Figure 3.17**). The DPP5A macrocycle is shifted onto the dodecyl chains and can shuttle over the 1,4-dialkoxybenzene barricade, as shown in the upfield shift of protons $H_{b\text{-}g}$. The imidazolium stations are also desymmetrised, as the macrocycle cannot shuttle over the barricade fast enough to reside on both imidazolium stations in the time frame of a ^{1}H NMR measurement.

In contrast to **3.12**, peak height of the maxima of shielding factors about environment H_d is lower. The area encapsulated by DPP5A ($H_{b\text{-}h}$) is confined with respect to DEP5A, which extended from $H_{b\text{-}i}$.

Proton environment H_k expresses a downfield shift in relation to the dumbbell molecule which could be attributed to the oxygen atoms along either rim of the DPP5A macrocycle deshielding this environment.

a)

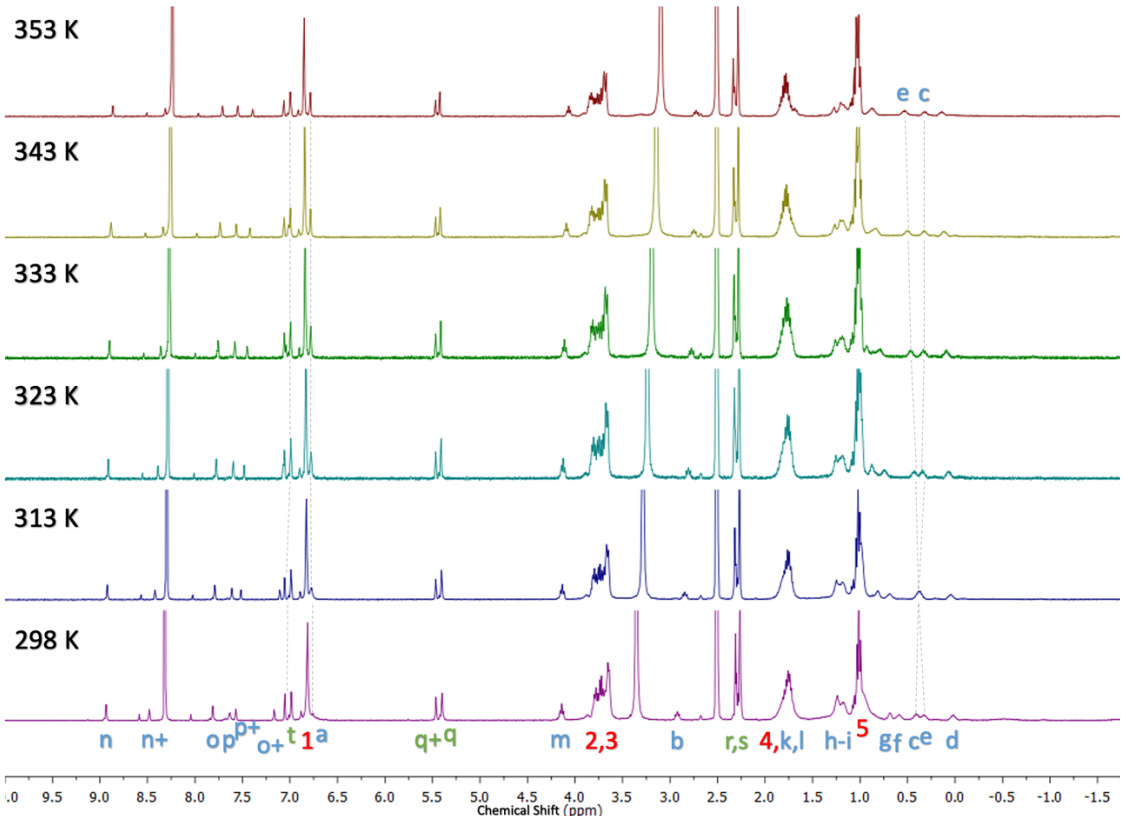

b)

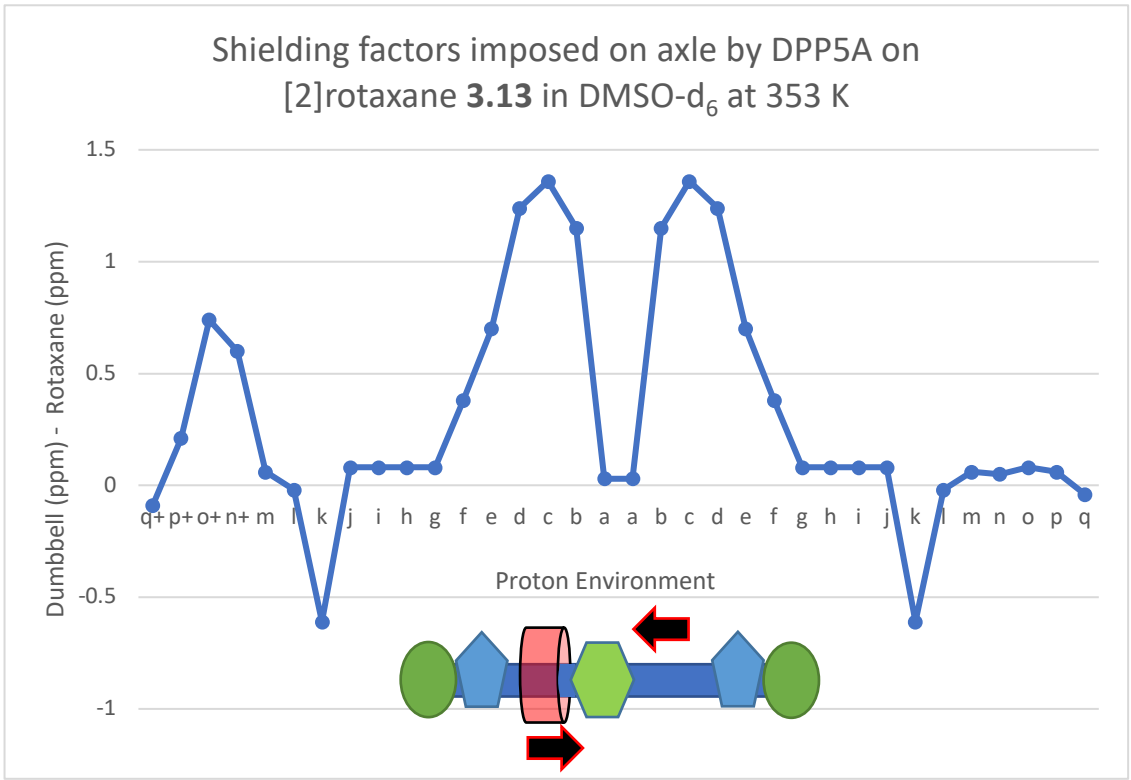

*Figure 3.18. (a) variable temperature ^{1}H NMR stack of [2]rotaxane **3.13** in DMSO-d_6 at 400 MHz and (b) plot of shielding factors of [2]rotaxane **3.13** in DMSO-d_6.*

When increasing the temperature of [2]rotaxane **3.13** in DMSO (**Figure 3.18**), shuttling of DPP5A is affected in a similar manner to that of **3.12**, where thermal energy weakens the imidazolium-solvent interactions, and environments $H_{l\text{-}p}$ express larger shielding factors than at room temperature. Areas along the axle that were highly populated with DPP5A at room temperature remain similar at high temperatures, suggesting that overall shuttling ability is not affected by temperature.

At 353 K, peaks H_c and H_e swap places where H_e is additionally shielded and H_c is deshielded (they merge at 313 K), changing global maximum to H_c from H_d. This implies that any additional steric interactions between the propoxy chains and the 1,4-dioxybenzene unit are overcome by the increase in thermal energy. Additionally, the area of the axle encapsulated is more confined at 353 K, where peaks $H_{b\text{-}g}$ are affected by DPP5A, than $H_{b\text{-}h}$ at 298 K. This is possibly due to an increased rate of shuttling along the axle of DPP5A at elevated temperatures.

a)

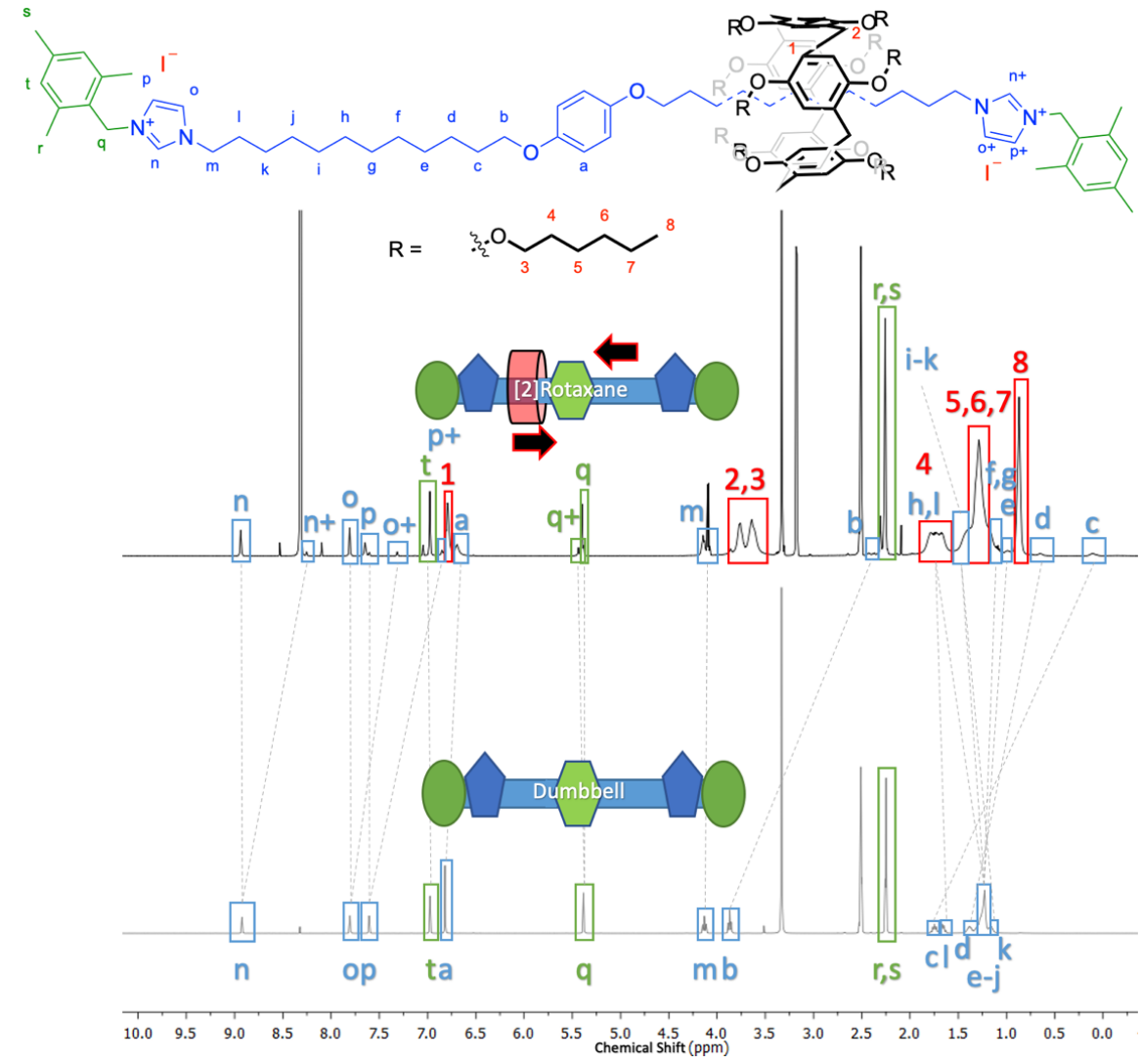

b)

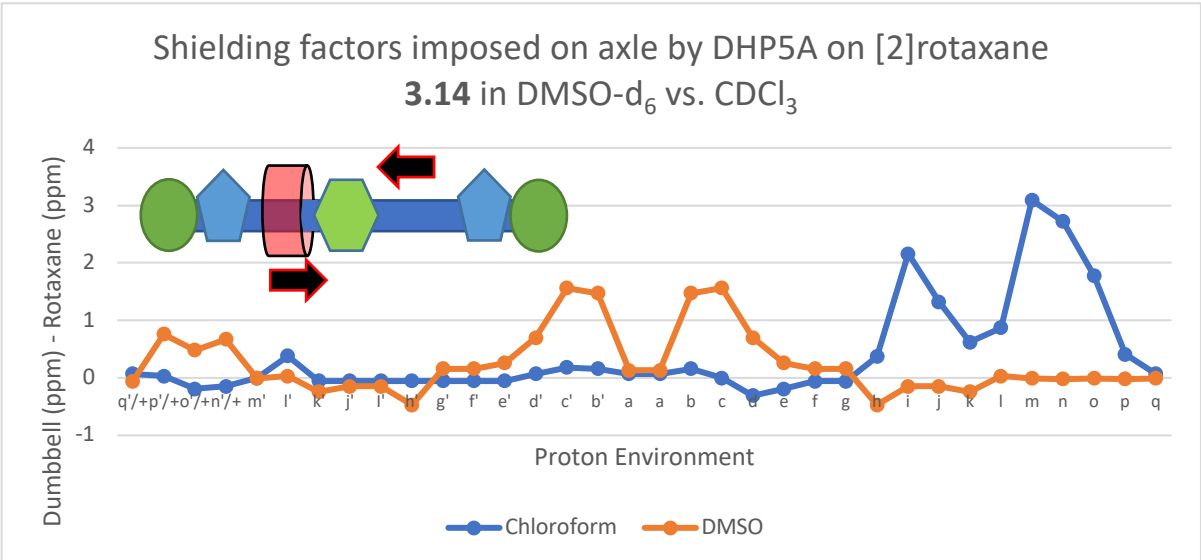

*Figure 3.19. (a) ^{1}H NMR stack of [2]rotaxane (**3.14**) and dumbbell molecule (**2.15**) in DMSO-d_6 at room temperature and (b) plot of shielding factors for [2]rotaxane **3.14** in DMSO-d_6 (orange) and $CDCl_3$ (blue).*

[2]Rotaxane **3.14** behaves in a similar manner to the other [2]rotaxanes in the series in DMSO (**Figure 3.19**). The dodecyl region is symmetrised as a result of the solvent-ion pair interactions displacing the DHP5A macrocycle onto the dodecyl chain and allowing it to slip over the 1,4-dialkoxybenzene barricade, as with the other [2]rotaxanes. Environment H_a shows virtually no change in shift relative to **3.14** dissolved in chloroform. The imidazolium region is desymmetrised, due to presence of only one macrocycle across the axle and the relatively slow shuttling rate across the length of the axle.

Global maxima are found about environments $H_{c,c'}$, closer to the central peak H_a than that of [2]rotaxane **3.13**.

a)

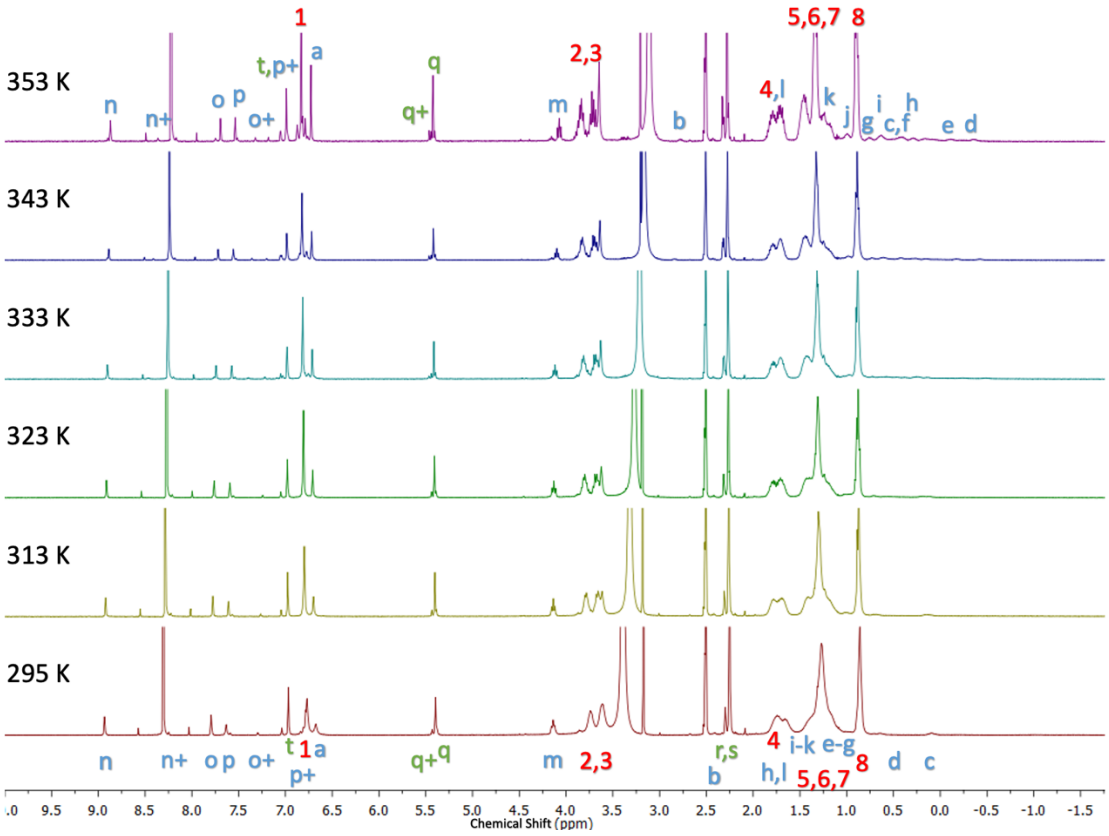

b)

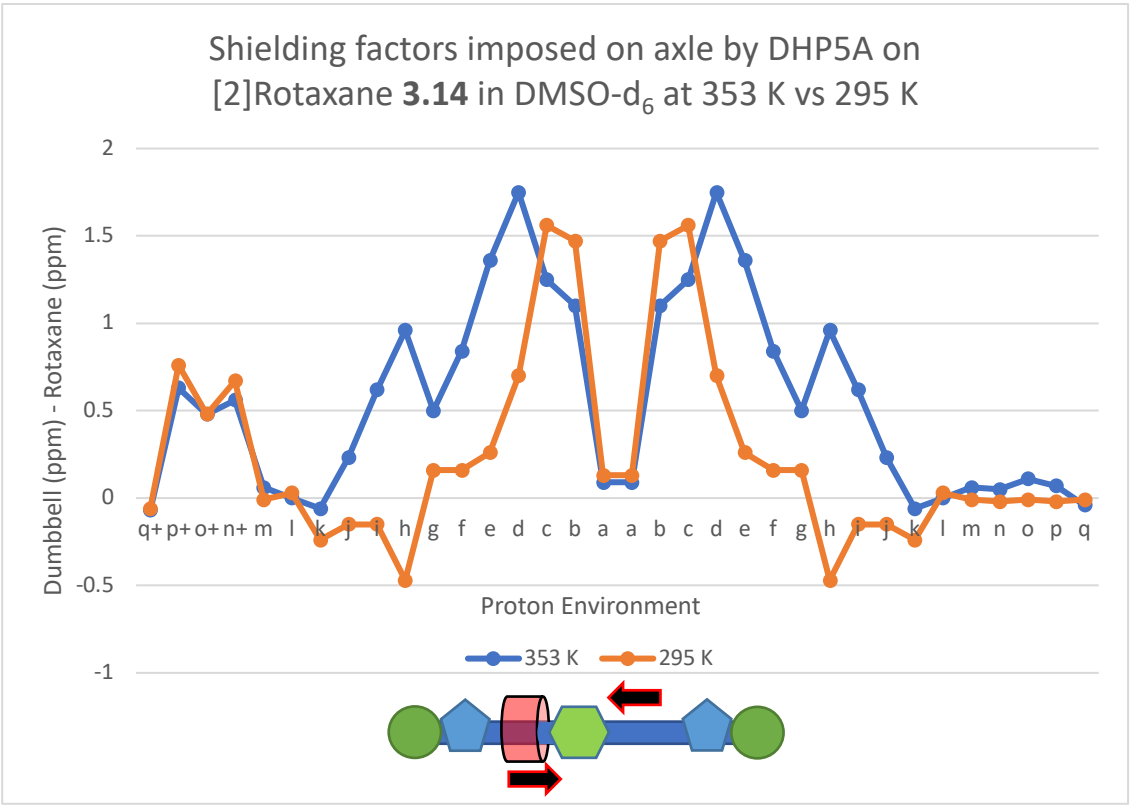

*Figure 3.20. (a) variable temperature ^{1}H NMR stack of [2]rotaxane **3.14** in DMSO-d_6 at 400 MHz and (b) plot of shielding factors comparing [2]rotaxane **3.14** in DMSO-d_6 at 295 K (orange) and 353 K (blue).*

When ^{1}H NMR spectra of **3.14** in DMSO are recorded at 353 K (**Figure 3.20**), protons along the dodecyl chains are all shifted, indicating that the pillararene shuttles along the length of the alkyl chain. At 295 K, only $H_{b\text{-}g}$ are shielded, but at 353 K, environments $H_{b\text{-}k}$ are affected. Similarly, the global maximum is shifted away from H_c to H_d suggesting that the hexyl chains of DHP5A interact along the axle. Population of DHP5A around the imidazolium region is relatively unchanged at 353 K, which is different to the corresponding [3]rotaxane **2.14**, which shows more DHP5A/imidazolium interaction possibly as a result of more inter-DH5PA interactions in the [3]-component rotaxane.

3.3 Conclusions and future work

In conclusion, a series of [2]rotaxanes have been assembled from their components, utilising pillar[5]arenes with different terminal chain lengths. Shuttling studies of the macrocycles along the axle have been conducted in different solvents; $CDCl_3$ and DMSO-d_6, with high temperature studies being conducted in the latter.

In $CDCl_3$, a dumbbell-like region and a rotaxane-like region exist along the axle on either side of the 1,4-dialkoxybenzene unit which acts as a barricade or steric barrier, preventing the pillar[5]arene macrocycles from shuttling the full length of the axle. Shielding factors for the encapsulated regions are similar to those observed for the [3]rotaxane counterparts, where large maxima are found around the imidazolium regions due to imidazolium-pillar[5]arene interactions. Smaller shielding factors are seen along the dodecyl chains up to the barricade for DEP5A, DPP5A and DHP5A. As in the [3]rotaxanes examples, DMP5A is once again the outlier, where little to no shift in shielding factors is observed along the dodecyl chains, indicating that the macrocycle pirouettes close to the imidazolium station.

When the solvent the [2]rotaxanes are dissolved in is changed to DMSO-d_6, the pillar[5]arenes are forced away from the imidazolium stations due to the solvent-ion pair interactions being greater than that of the pillar[5]arene-imidazolium interactions. As a result, the displacement of the macrocycles onto the dodecyl chains allows them to slip over the 1,4-dialkoxybenzene barricade, symmetrising the dodecyl region of the axle. The imidazolium stations, however, remain asymmetric as the pillararenes are observed to overcome the solvent-ion pair interactions, but only on one side of the axle. We propose that this effect is observed due to the presence of a single pillararene being present along a long axle. High temperature ^{1}H NMR studies aided assignments, especially in the case of [2]rotaxane **3.11**, whose DMP5A macrocycle did not shuttle at room temperature and an increase in thermal energy initiated shuttling.

To further enhance the studies conducted here, a series of asymmetric [2]rotaxanes would need to be synthesised in order to better understand how the pillar[5]arene

macrocycles shuttle (**Figure 3.21**). These hypothetical asymmetric rotaxanes **3.W-3.Y** would only incorporate one imidazolium station close to a stopper group. **3.V** would also need to be synthesised as a baseline to understand shuttling on a shorter chain, symmetrical [2]rotaxane system. **3.W** would be used to understand how shuttling is affected by only having one imidazolium station, whilst **3.X** is necessary to test the system's ability to dethread. Finally, **3.Y** would be a culmination of these smaller aspects of shuttling, providing shuttling information across a neutral zone.

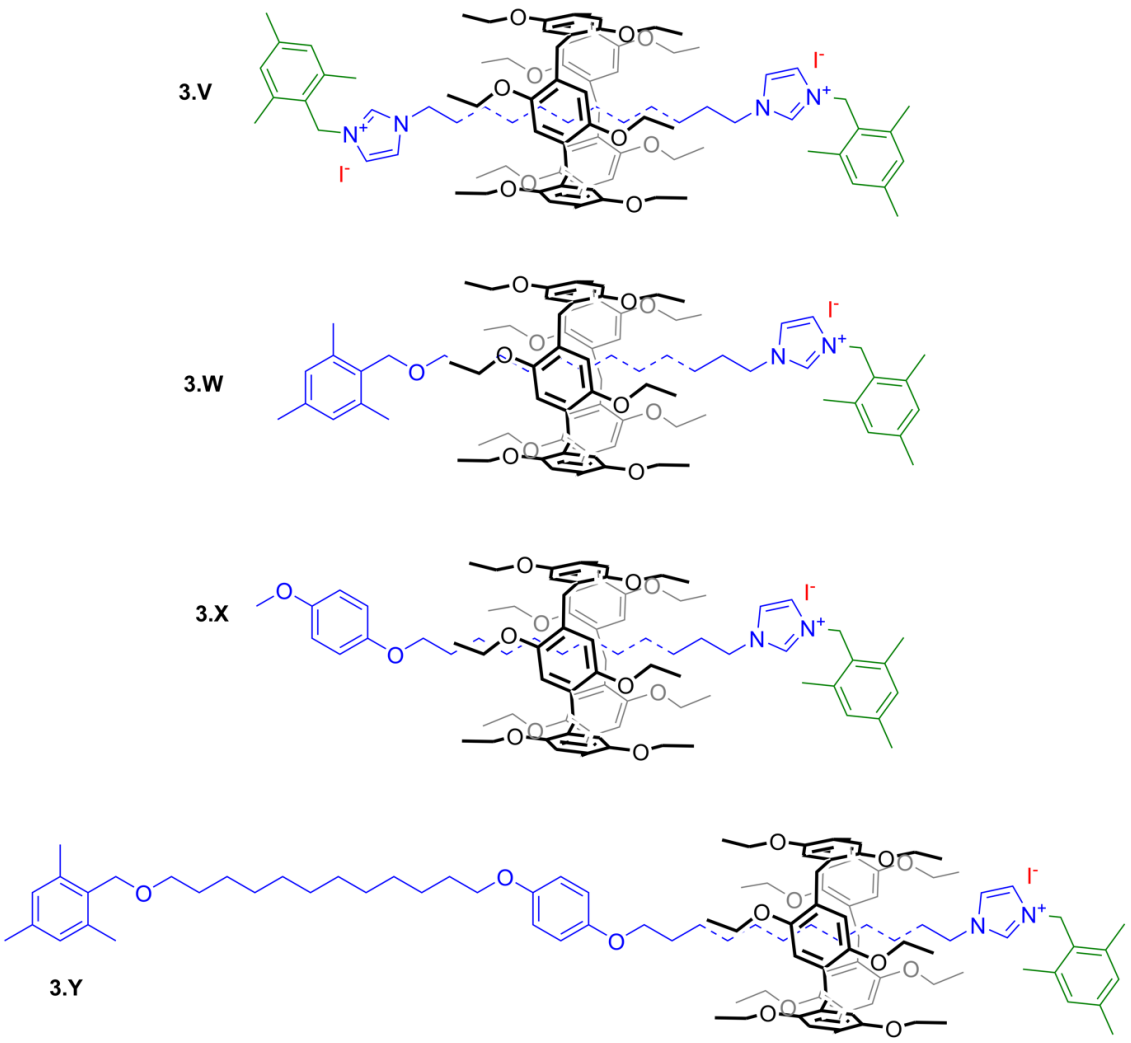

*Figure 3.21. Proposed [2]rotaxanes **3.V-3.Y** to enhance the shuttling studies conducted on this chapter.*

Finally, using the imidazolium moieties on the [2]rotaxanes that have been synthesised in this chapter, a silver based-NHC complex would be an interesting molecule to study (**Figure 3.22**). It could be synthesised via a dimerization of two [2]rotaxane species in order to form [3]catenane **3.Z**. A [2]rotaxane (such as **3.12**) would firstly need to undergo an ion

exchange reaction to replace the iodide ions in favour of non-binding counterions, such as hexafluorophosphate. This could be reacted with a source of silver, such as Ag_2O, in order to both deprotonate the imidazolium and coordinate to it, forming a large macrocycle by dimerising two [2]rotaxanes.[15]

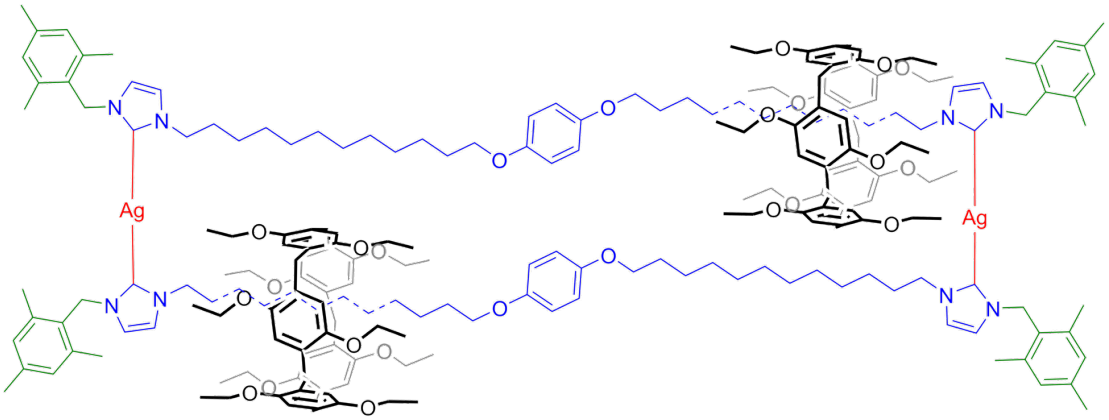

3.Z

*Figure 3.22. A proposed [3]catenane **3.Z** based off existing [2]rotaxane **3.12**.*

3.4 Materials and methods

All chemicals were obtained from commercial sources and used without further purification (see **Chapter 6**). ^{1}H and ^{13}C NMR spectra were recorded using a Bruker AV(III)400HD, Bruker AV(III)400, Bruker AV400 and Bruker AV(III)500 machines at room temperature. High temperature ^{1}H NMR spectra were recorded using a Bruker AV(III)400, Bruker AV(III)400HD, or a Bruker AV(III)600. Deuterated solvents were used as specified. Chemical shifts were recorded referenced to solvent residue. ESI-MS spectra were taken using a Bruker microTOF II mass spectrometer.

3.4.1 Synthesis

Synthesis of [2]rotaxane [**3.11**]

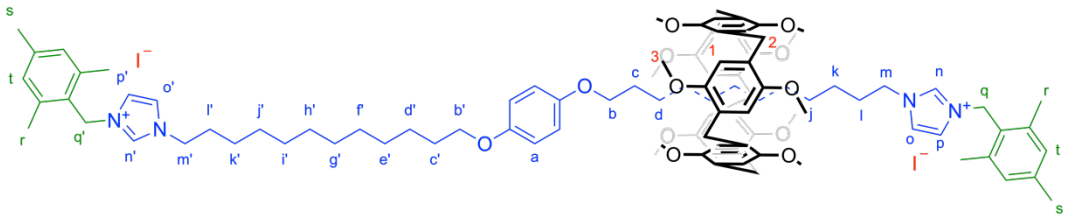

1,4-Bis((12-(1*H*-imidazol-1-yl)dodecyl)oxy)benzene (75.0 mg, 129 μmol) and dimethoxypillar[5]arene (97.0 mg, 129 μmol), were dissolved in chloroform (12.5 mL) and sonicated for 30 mins. The solution was cooled to -15 °C and, under the exclusion of light, 2-(iodomethyl)-1,3,5-trimethylbenzene (78.0 mg, 300 μmol) was added. The mixture was left to warm to room temperature and stirred for 3 days. The crude residue was purified by column chromatography [silica, dichloromethane: methanol (193:7)] to yield a yellow gel (61 mg, 33.0 μmol, 25 %). ^{1}H NMR (500 MHz, Chloroform-*d*) δ 10.27 (s, 1H, $H_{n'}$), 8.77 (s, 1H, H_{n}), 7.87 – 7.39 (m, 1H, $H_{o'}$), 7.24 – 7.14 (m, 1H, H_{p}), 7.13 – 6.63 (m, 20H, $H_{1,a,o,p',t}$), 5.90 (d, *J* = 110.4 Hz, 2H, H_{q}), 5.76 – 5.53 (m, 2H, $H_{q'}$), 4.56 – 4.18 (m, 2H, H_{m}), 3.89 (dd, *J* = 15.3, 7.9 Hz, 4H, $H_{b,b'}$), 3.83 – 3.44 (m, 40H, $H_{2,3}$), 2.58 – 2.15 (m, 18H, $H_{r,s}$), 2.09 – 1.85 (m, 2H, $H_{l'}$), 1.73 (t, *J* = 8.3 Hz, 6H, $H_{c,c',d'}$), 1.68 – 1.09 (m, 24H, $H_{d-h,e'-k'}$), 1.08 – 0.68 (m, 4H, $H_{i,m}$), 0.20 (d, *J* = 113.4 Hz, 2H, H_{j}), -0.62 (s, 2H, H_{k}), -1.36 (s, 2H, H_{l}) ppm. ^{13}C NMR (126 MHz, Chloroform-*d*) δ 153.19, 150.90 (d, *J* = 24.7 Hz), 140.01, 138.09, 136.35, 132.47, 130.01, 129.41, 125.34, 122.65 – 120.29, 116.71 – 112.80, 68.61, 63.06, 58.15, 57.17, 55.65, 50.43, 48.97 – 47.03, 32.82, 31.93, 31.32 – 28.38, 26.78 – 25.47, 22.70, 21.14,

20.05, 14.14 ppm. ESI-MS (positive mode) m/z calc'd. for $C_{101}H_{134}N_4O_{12}$ $[M]^{2+}$: 798.0010, found: 798.0040.

Synthesis of [2]rotaxane [**3.12**]

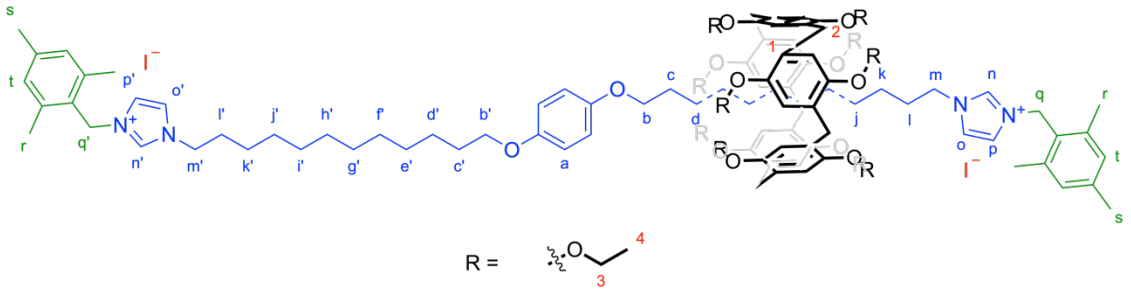

1,4-Bis((12-(1*H*-imidazol-1-yl)dodecyl)oxy)benzene (100 mg, 173 μmol) and diethoxypillar[5]arene (385 mg, 432 μmol), were dissolved in chloroform (1.6 mL) and sonicated for 30 mins. The solution was cooled to -15 °C and, under the exclusion of light, 2-(iodomethyl)-1,3,5-trimethylbenzene (158 mg, 607 μmol) was added. The mixture was left to warm to room temperature and stirred for 3 days. The crude residue was purified by column chromatography [silica, dichloromethane: methanol (193:7)] to yield an orange gel (141 mg, 70.8 μmol, 41 %). ^{1}H NMR (500 MHz, Chloroform-*d*) δ 10.25 (s, 1H, $H_{n'}$), 8.66 (s, 1H, H_n), 7.73 (d, *J* = 33.9 Hz, 1H, $H_{o'}$), 7.17 – 6.46 (m, 20H, $H_{1,a,p,p',t}$), 5.81 (d, *J* = 33.9 Hz, 1H, H_o), 5.51 (dt, *J* = 23.2, 12.3 Hz, 4H, $H_{q,q'}$), 4.55 – 4.20 (m, 2H, $H_{m'}$), 3.88 (dddd, *J* = 21.3, 17.2, 13.3, 8.7 Hz, 22H, $H_{3,b'}$), 3.73 (q, *J* = 13.0, 12.3 Hz, 12H, $H_{2,b}$), 2.58 – 2.16 (m, 18H, $H_{r,s}$), 1.87 (s, 2H, $H_{l'}$), 1.75 (dt, *J* = 16.3, 6.6 Hz, 2H, $H_{c'}$), 1.65 – 1.49 (m, 2H, $H_{d'}$), 1.49 – 1.32 (m, 30H, H_4), 1.32 – 1.16 (m, 18H, $H_{c,m,e'-k'}$), 1.16 – 0.93 (m, 6H, H_{d-f}), 0.91 – 0.55 (m, 6H, $H_{g,i,j}$), 0.37 (s, 2H, H_h), 0.04 (d, *J* = 33.2 Hz, 2H, H_k), -0.66 (s, 2H, H_l) ppm. ^{13}C NMR (126 MHz, Chloroform-*d*) δ 153.18, 150.58, 150.06, 149.29, 140.17, 137.95, 137.88, 136.08, 134.19, 130.20, 130.06, 130.02, 129.95, 125.29, 125.25, 122.80, 122.35, 119.70, 117.03, 116.80, 116.33, 115.24, 115.04, 114.59, 114.53, 68.62, 66.07, 65.43, 63.71, 48.62, 47.79, 47.54, 30.97, 30.44, 30.34, 29.79, 29.68, 29.53, 29.39, 29.28, 29.21, 28.69, 26.41, 26.32, 21.11, 19.94, 19.89, 15.66, 15.60, 15.56, 15.52, 15.45 ppm. ESI-MS (positive mode) m/z calc'd. for $C_{111}H_{154}N_4O_{12}$ $[M]^{2+}$: 868.0793, found: 868.0805.

Synthesis of [2]rotaxane [**3.13**]

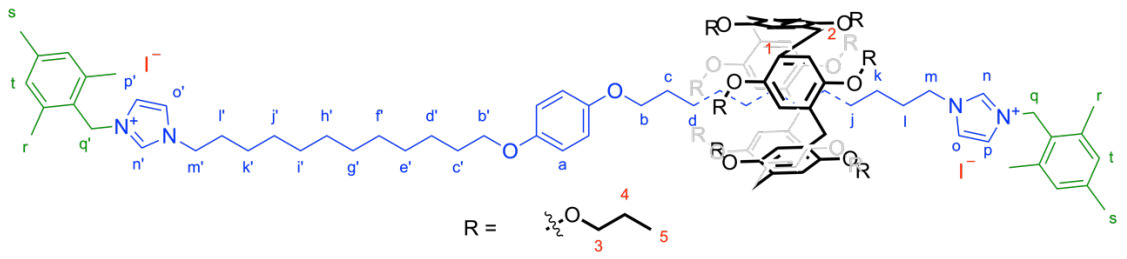

1,4-Bis((12-(1*H*-imidazol-1-yl)dodecyl)oxy)benzene (100 mg, 173 μmol) and dipropoxypillar[5]arene (445 mg, 432 μmol), were dissolved in chloroform (1.6 mL) and sonicated for 30 mins. The solution was cooled to -15 °C and, under the exclusion of light, 2-(iodomethyl)-1,3,5-trimethylbenzene (158 mg, 607 μmol) was added. The mixture was left to warm to room temperature and stirred for 3 days. The crude residue was purified by column chromatography [silica, dichloromethane: methanol (193:7)] to yield a yellow gel (107 mg, 50.2 μmol, 29 %). ^{1}H NMR (500 MHz, Chloroform-*d*) δ 10.25 (s, 1H, $H_{n'}$), 8.66 (s, 1H, H_{n}), 7.69 (s, 1H, $H_{o'}$), 6.98 (q, *J* = 16.2, 9.1 Hz, 5H, $H_{t,p'}$), 6.83 (d, *J* = 13.2 Hz, 10H, H_{1}), 6.76 (s, 4H, H_{a}), 6.59 (s, 1H, H_{p}), 5.86 – 5.56 (m, 1H, H_{o}), 5.47 (d, *J* = 9.0 Hz, 4H, $H_{q,q'}$), 4.53 – 4.20 (m, 2H, $H_{m'}$), 4.05 – 3.86 (m, 4H, $H_{b,b'}$), 3.81 (ddt, *J* = 18.7, 15.4, 4.7 Hz, 10H, H_{2}), 3.75 – 3.61 (m, 20H, H_{3}), 2.51 – 2.19 (m, 18H, $H_{r,s}$), 1.81 (dh, *J* = 21.0, 7.9, 6.9 Hz, 24H, $H_{4,c',l'}$), 1.48 – 1.16 (m, 20H, $H_{c,m,d'-k'}$), 1.07 (dt, *J* = 14.8, 7.3 Hz, 36H, $H_{5,d-f}$), 0.94 – 0.54 (m, 6H, $H_{g,h,j}$), 0.39 (s, 2H, H_{l}), 0.15 – -0.08 (m, 2H, H_{k}), -0.50 – -0.81 (m, 2H, H_{l}) ppm. ^{13}C NMR (126 MHz, Chloroform-*d*) δ 153.19, 150.77, 150.28, 149.50, 140.20, 139.90, 137.86, 136.06, 134.21, 130.27, 130.19, 130.07, 130.01, 129.01, 125.18, 122.87, 122.12, 120.84, 119.56, 119.38, 117.19, 116.45, 115.27, 114.78, 114.71, 72.56, 71.84, 70.13, 68.64, 50.33, 48.62, 47.77, 47.50, 30.80, 30.72, 30.62, 29.56, 29.46, 29.41, 29.29, 29.15, 28.81, 26.52, 26.39, 23.21, 21.11, 19.97, 19.91, 10.81, 10.76, 10.69 ppm. ESI-MS (positive mode) m/z calc'd. for $C_{121}H_{174}N_4O_{12}$ $[M]^{2+}$: 938.1575, found: 938.1571.

Synthesis of [2]rotaxane [**3.14**]

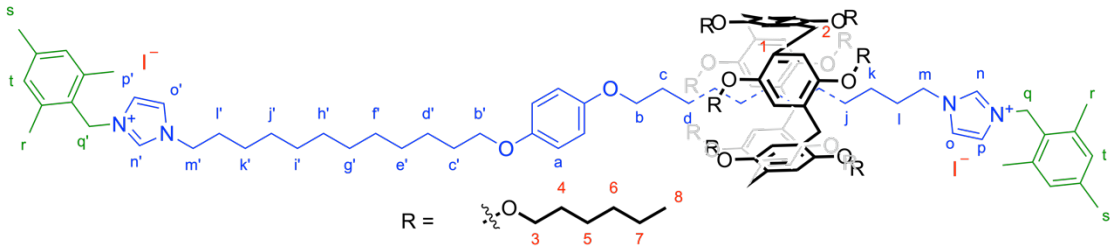

1,4-Bis((12-(1*H*-imidazol-1-yl)dodecyl)oxy)benzene (79.0 mg, 136 μmol) and dihexyloxypillar[5]arene (500 mg, 344 μmol), were dissolved in chloroform (1.7 mL) and sonicated for 30 mins. The solution was cooled to -15 °C and, under the exclusion of light, 2-(iodomethyl)-1,3,5-trimethylbenzene (134 mg, 516 μmol) was added. The mixture was left to warm to room temperature and stirred for 3 days. The crude residue was purified by column chromatography [silica, dichloromethane: methanol (193:7)] to yield a pale yellow gel (300 mg, 118 μmol, 86 %). ^{1}H NMR (500 MHz, Chloroform-*d*) δ 10.65 – 10.24 (m, 1H, $H_{n'}$), 7.81 – 7.37 (m, 2H, $H_{n,o'}$), 7.14 – 6.66 (m, 19H, $H_{1,a,p',t}$), 6.58 – 6.39 (m, 1H, H_{p}), 5.67 – 5.35 (m, 5H, $H_{o,q,q'}$), 4.36 (t, *J* = 7.5 Hz, 2H, $H_{m'}$), 4.08 – 3.84 (m, 10H, H_{2}), 3.83 – 3.65 (m, 24H, $H_{3,b,b'}$), 2.52 – 2.17 (m, 18H, $H_{r,s}$), 2.09 – 1.63 (m, 28H, $H_{4,5,c,c',d,e,l'}$), 1.62 – 1.45 (m, 22H, $H_{4,5,c,c',d,e,l'}$), 1.38 (dtt, *J* = 14.3, 7.1, 3.5 Hz, 62H, $H_{6,7,g,f,m,d'-k'}$), 1.12 – 1.04 (m, 2H, H_{l}), 1.00 – 0.87 (m, 32H, $H_{8,h}$), 0.77 – 0.60 (m, 2H, H_{k}), 0.16 – -0.13 (m, 2H, H_{j}), -0.84 (dt, *J* = 24.5, 8.7 Hz, 2H, H_{i}) ppm. ^{13}C NMR (126 MHz, Chloroform-*d*) δ 153.21, 150.84, 150.33, 149.50, 140.50, 138.17, 137.89, 137.69, 136.43, 133.13, 130.41, 130.22, 130.08, 129.98, 129.04, 125.12, 121.92, 120.77, 119.04, 117.35, 116.47, 115.39, 115.26, 115.06, 114.66, 71.25, 70.41, 68.70, 68.58, 50.40, 48.09, 47.59, 47.50, 47.43, 31.92, 31.81, 31.73, 31.62, 31.07, 31.02, 30.90, 30.35, 30.29, 30.11, 30.05, 29.99, 29.85, 29.64, 29.58, 29.51, 29.46, 29.42, 29.37, 29.20, 27.52, 26.67, 26.60, 26.19, 26.05, 25.91, 25.82, 22.71, 22.68, 21.17, 21.11, 21.07, 20.05, 19.98, 19.93, 14.09 ppm. ESI-MS (positive mode) m/z calc'd. for $C_{151}H_{234}N_4O_{12}$ $[M]^{2+}$: 1148.3923, found: 1148.3906.

3.5 References

1 T. Ogoshi, D. Kotera, S. Nishida, T. Kakuta, T. A. Yamagishi and A. M. Brouwer, *Chem. - A Eur. J.*, 2018, **24**, 6325–6329.

2 T. Ogoshi, R. Iizuka, D. Kotera and T. A. Yamagishi, *Org. Lett.*, 2015, **17**, 350–353.

3 S. Wang, X. Shao and W. Cai, *J. Phys. Chem. C*, 2017, **121**, 25547–25553.

4 P. Langer, L. Yang, C. R. Pfeiffer, W. Lewis and N. R. Champness, *Dalt. Trans.*, 2019, **48**, 58–64.

5 C. Li, S. Chen, J. Li, K. Han, M. Xu, B. Hu, Y. Yu and X. Jia, *Chem. Commun.*, 2011, **47**, 11294–11296.

6 S. Dong, J. Yuan and F. Huang, *Chem. Sci.*, 2014, **5**, 247–252.

7 A. Altieri, G. Bottari, F. Dehez, D. A. Leigh, J. K. Y. Wong and F. Zerbetto, *Angew. Chemie - Int. Ed.*, 2003, **42**, 2296–2300.

8 M. N. Chatterjee, E. R. Kay and D. A. Leigh, *J. Am. Chem. Soc.*, 2006, **128**, 4058–4073.

9 S. Kassem, T. Van Leeuwen, A. S. Lubbe, M. R. Wilson, B. L. Feringa and D. A. Leigh, *Chem. Soc. Rev.*, 2017, **46**, 2592–2621.

10 V. Serreli, C. F. Lee, E. R. Kay and D. A. Leigh, *Nature*, 2007, **445**, 523–527.

11 M. Alvarez-Pérez, S. M. Goldup, D. A. Leigh and A. M. Z. Slawin, *J. Am. Chem. Soc.*, 2008, **130**, 1836–1838.

12 A. Carlone, S. M. Goldup, N. Lebrasseur, D. A. Leigh and A. Wilson, *J. Am. Chem. Soc.*, 2012, **134**, 8321–8323.

13 H. Li, C. Cheng, P. R. McGonigal, A. C. Fahrenbach, M. Frasconi, W. G. Liu, Z. Zhu, Y. Zhao, C. Ke, J. Lei, R. M. Young, S. M. Dyar, D. T. Co, Y. W. Yang, Y. Y. Botros, W. A. Goddard, M. R. Wasielewski, R. D. Astumian and J. F. Stoddart, *J. Am. Chem. Soc.*, 2013, **135**, 18609–18620.

14 C. Cheng, P. R. McGonigal, S. T. Schneebeli, H. Li, N. A. Vermeulen, C. Ke and J. F. Stoddart, *Nat. Nanotechnol.*, 2015, **10**, 547–553.

15 C. Hemmert, A. Fabié, A. Fabre, F. Benoit-Vical and H. Gornitzka, *Eur. J. Med. Chem.*, 2013, **60**, 64–75.

Chapter 4:

Anthracene Stoppered [2]rotaxanes

4.1 Introduction

4.1.1 Anthracene

Anthracene is a polycyclic aromatic hydrocarbon consisting of three linearly-fused benzene rings. Two molecules of anthracene can undergo a [4 + 4] photocycloaddition reaction via irradiation of light of higher wavelength than 350 nm and this process is reversible upon heating or higher energy irradiation (300 nm), decomposing the cycloadduct into the starting components (**Scheme 4.1**).[1] Anthracene molecules only produce one isomer as a result of photodimerisation, where four benzene rings are left intact and only the central benzene moieties lose their aromaticity. It has been shown that this can occur in both the solid state[2] and in solution with a variety of substituents.[3]

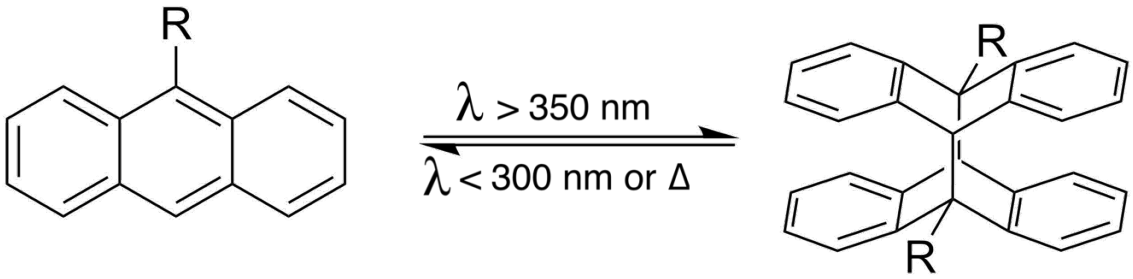

Scheme 4.1. Conversion between anthracene and its dimer.

4.1.2 Anthracene containing rotaxanes

Anthracene molecules are large aromatic moieties and as such, they can be used as stopper groups to prevent macrocycles from dethreading from an axle. The first example of anthracene stoppered [2]rotaxanes were synthesised by Harriman and co-workers, where they used a templating method to clip a $CBPQT^{4+}$ macrocycle around a series of pre-synthesised axles (**Figure 4.1**).[4] The axle contained either one or two 1,4-dioxybenzene units which were separated by glycol chains and terminated with anthracene stopper groups. The 1,4-dioxybenzene unit was used as a recognition site to allow the macrocycle to be templated by the axle and once clipped, acted as a station. For the axle which had two recognition sites, the axle was used in excess to prevent formation of the corresponding [3]rotaxane.

The single-station anthracene stoppered [2]rotaxane favoured a “closed” conformation where the anthracene stoppers weakly π-π stacked over the macrocycle, however the macrocycle had the capacity to shuttle across the axle which allowed the rotaxane to exhibit an “open” conformation where the anthracene moieties are far away from each other. Interpretation of the structural information for the two-station [2]rotaxane is more complex since shuttling between the two stations was observed at room temperature. This slowed as the temperature decreased, allowing π-interactions to occur between the macrocycle and stopper. This could also mean that there were additional aromatic interactions between the macrocycle and the free station. As these processes occurred simultaneously it was concluded that a combination of the above processes were occurring at any given time.

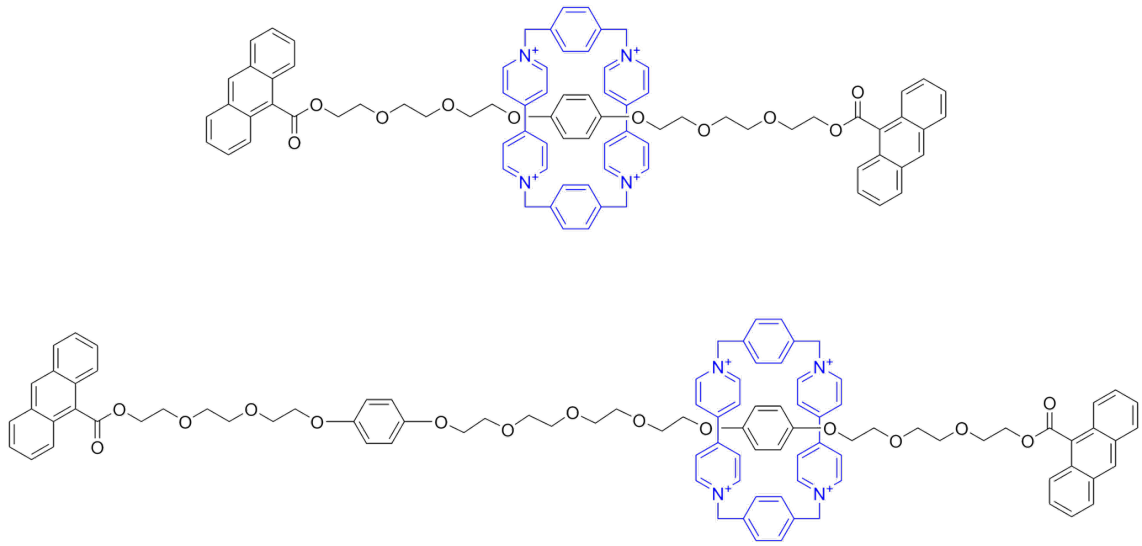

Figure 4.1. Harriman's anthracene stoppered [2]rotaxanes utilising 1,4-dioxybenzene stations. Hexafluorophosphate counterions have been omitted for clarity.[4]

Anthracene groups can also serve other purposes within the construction of rotaxanes such as when Stoddart and co-workers utilised anthracene moieties as the central component of the axle.[5] The orientation of the anthracene can play a large role in shuttling and construction of the system, as the 9,10-anthracene orientation prevents shuttling of the $CBPQT^{4+}$ macrocycle and facilitated the formation of a [3]rotaxane, whereas the 2,6-anthracene orientation allows the macrocycle to reside over it exclusively, allowing only a [2]rotaxane to assemble. More recently they have gone on to assemble hetero[4]rotaxanes using cooperative hydrogen bonding between cyclodextrins

and cucurbiturils and employing anthracene stopper groups to cap the macrocycles in place.[6]

4.1.3 Anthracene containing poly[n]rotaxanes

Poly[n]rotaxanes can be fabricated when anthracene molecules are used as stopper groups and subsequently using a [4 + 4] photocycloaddition reaction between two molecules of anthracene. Using an anthracene stoppered [3]rotaxane as a building block, Huang and co-workers synthesised a poly[3]rotaxane (**Figure 4.2**).[7] The [3]rotaxane comprised of two axles capped asymmetrically with one anthracene and one phenyl group. The rotaxane was dynamically polymerised via irradiation at $\lambda > 360$ nm using a 500 W Xe lamp producing a poly[3]rotaxane with up to 25 repeat units. Due to the reversible nature of the cycloadduct, the [3]rotaxane could be reformed, if necessary, by heating the sample.

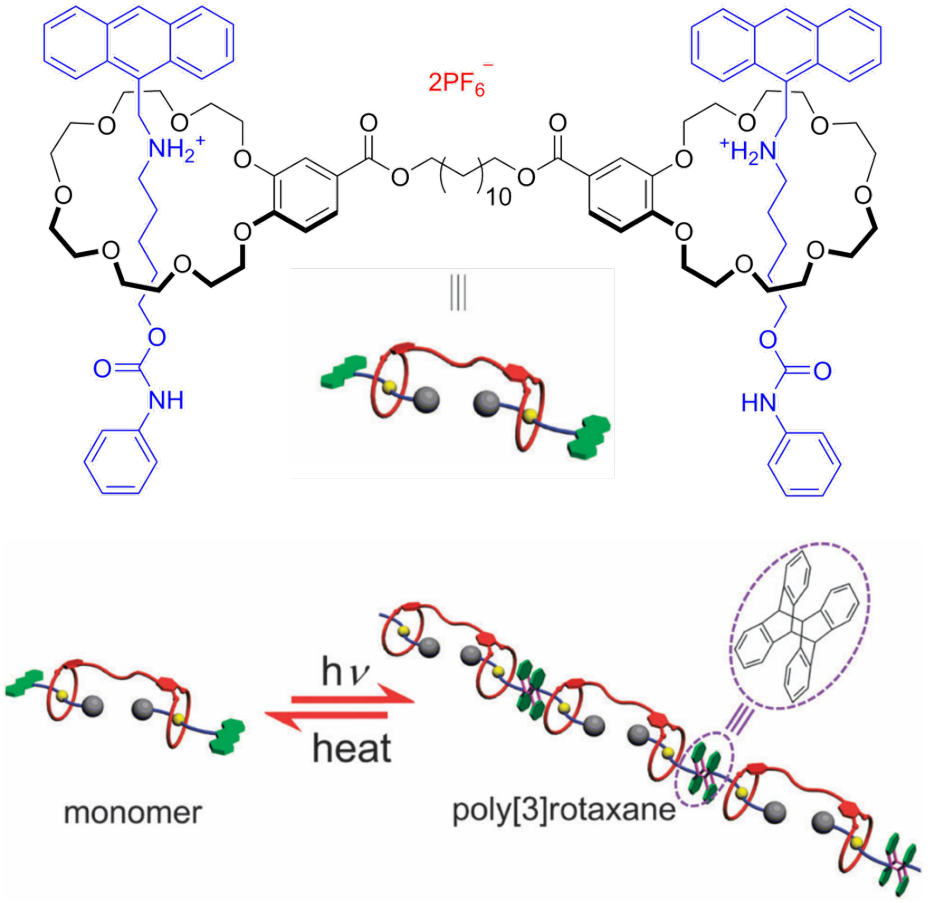

Figure 4.2. Huang's anthracene stoppered [3]rotaxane and a cartoon representation of the reversible formation of the poly[3]rotaxane. Adapted with permission from ref 7. Copyright 2014 The Royal Society of Chemistry.

4.1.4 Anthracene containing pillar[5]arene molecules

The versatility of the [4 + 4] photocycloaddition reaction has allowed pillar[5]arene molecules to be dynamically dimerised. This was the basis of Yang and co-workers' doubly-dynamic polymer (**Figure 4.3**).[8] The basis of this was a co-pillar[5]arene where one of the methoxy units was replaced with a decyl chain terminating with an anthracene moiety. These polymers are doubly-dynamic, because the anthracene [4 + 4] cycloaddition is one part of the polymerisation process which forms pillar[5]arene dimers, and these dimers were assembled into a supramolecular polymer via pseudorotaxane formation by the pillararene moiety and a bis-imidazole dodecyl rod.[9] The polymer can be converted back to the monomer units by heating, as this dethreads the polypseuodrotaxane in addition to cleaving the anthracene dimer. Upon cooling the pseudorotaxane is reformed and can be polymerised via photo irradiation and the process can be repeated as necessary.

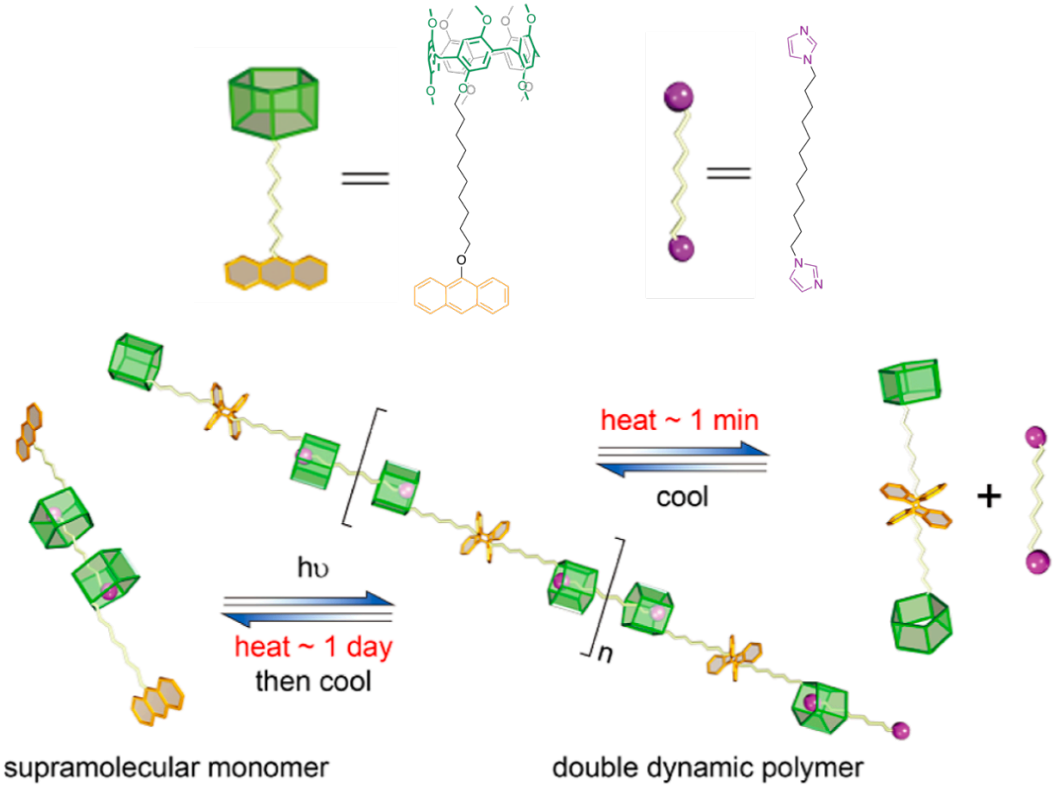

Figure 4.3. Yang's doubly dynamic polymer where bis-imidazole rods threaded through pillar[5]arene dimers made polypseudorotaxanes. Components: pillar[5]arene – green, imidazole – purple, anthracene – orange and alkyl chain – beige. Adapted with permission from ref 8. Copyright 2013 American Chemical Society.

Other supramolecular polymers have also been prepared using pillar[5]arene dimers which contain a central anthracene moiety.[10,11]

A similar pillar[5]arene moiety was utilised by Yang and co-workers to make a [c2]daisy chain fluorescence enhanced material (**Figure 4.4**).[12] A [c2]daisy chain is a macrocyclic dimer in which both host and guest components are covalently attached which can be subsequently dimerised through host/guest complexation. To construct this daisy chain, a ditopic co-pillar[5]arene was used where one of the units had a long chain alkane terminated with a dimethylammonium hexafluorophosphate group. To the other side of a linking 1,4-dialkoxybenzene group, a triazole was used to connect an anthracene moiety. The pillararene is ditopic, because the dimethylammonium terminating end can be used as a guest and the pillar[5]arene ring can be used a host, facilitating the formation of pseudorotaxanes.

Anthracene molecules have a tendency to interact via π-π stacking which in turn leads to quenching of fluorescence, however by appropriate tuning of these π-π stacks, fluorescence can occur. As a [c2]daisy chain, fluorescence is observed as the supramolecular complex restricts rotation of the anthracene moiety due to close proximity to the pillar[5]arene moiety. The fluorescence properties can be reversibly turned “on” or “off” via selective dethreading of the daisy chain to the corresponding monomer units. Quenching is accomplished by heating the solution, which produces the pillar[5]arene monomer and cooling reverses the process which complexes the [c2]daisy chain. The second way quenching can occur is by charge neutralisation via addition of 1,8-diazabicyclo[5.4.0]undec-7-ene, converting the dimethylammonium cation into a tertiary amine. Addition of trifluoroacetic acid reforms the dimethylammonium cation restoring fluorescence. The third method that quenching can be accomplished is by counterion exchange from hexafluorophosphate anions to chloride anions. The chloride anion forms a close-contact ion pair with the dimethylammonium cation which leads to fluorescence quenching.

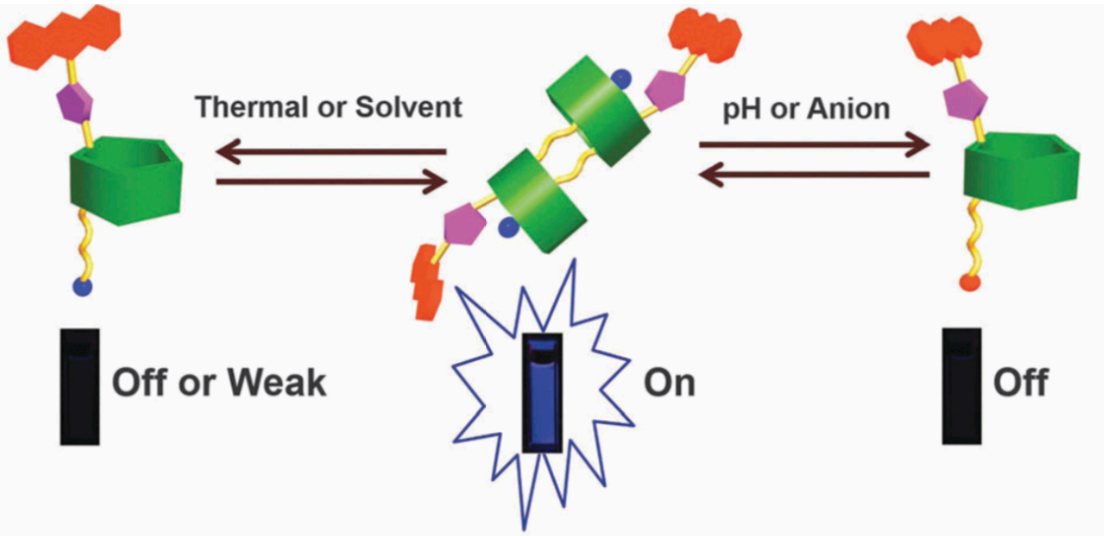

Figure 4.4. Yang's switchable fluorescent [c2]daisy chain. Components: pillar[5]arene - green, imidazolium - purple, anthracene – red, dimethylammonium hexafluorophosphate – blue, ammonium chloride – orange and alkyl chain - yellow. Reprinted with permission from ref 12. Copyright 2014 The Royal Society of Chemistry.

Anthracene containing co-pillar[5]arenes were further studied by Li and co-workers. A symmetrical pillar[5]arene functionalised with anthracene moieties on opposing rims was synthesised (**Figure 4.5**).[13] This pillar[5]arene was used as a temperature-controlled molecular switch when it came into contact with a self-assembled monolayer (SAM) of an imidazolium bromide ionic liquid attached to a gold surface. Similar to Yang's system described above, an increase in fluorescence was observed when the pillar[5]arene complexed to the SAM leading to restricted rotation of the anthracene moiety. Upon increasing the temperature, fluorescence was quenched and the pillar[5]arene unit dethreaded.

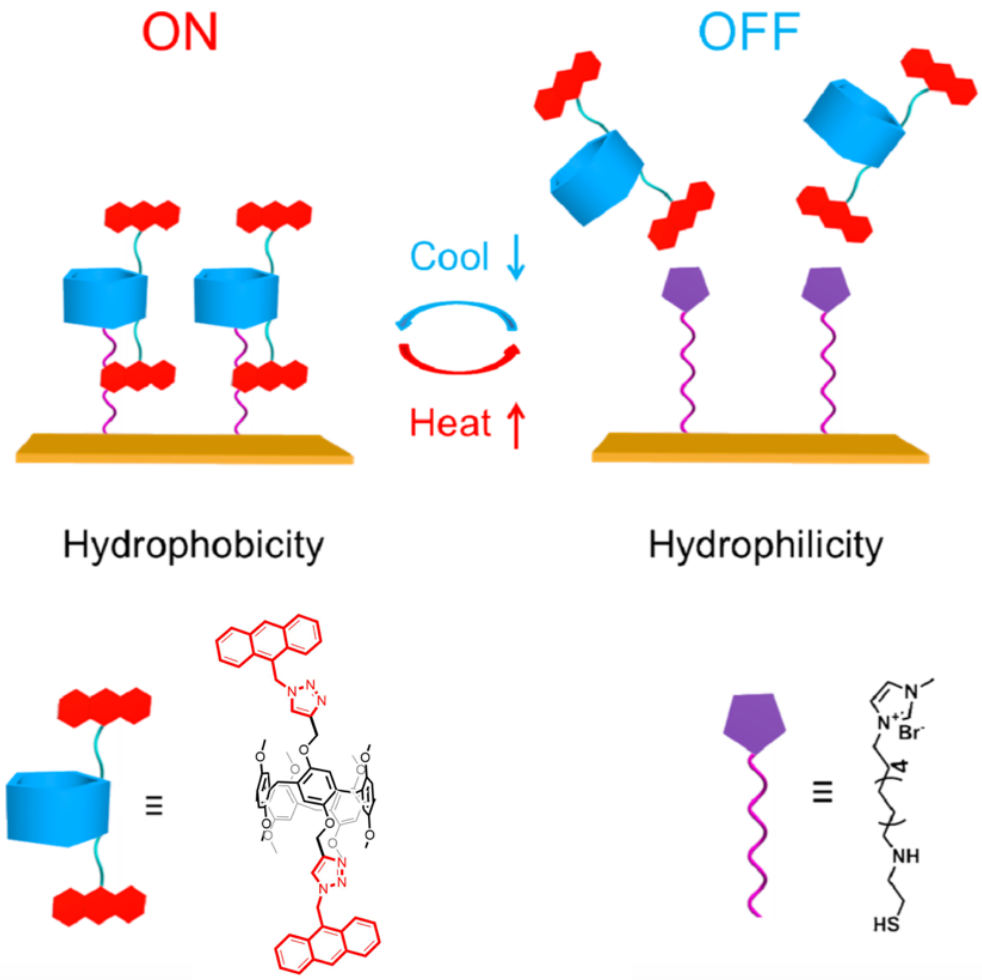

Figure 4.5. Li's molecular switch on a self-assembled monolayer of ionic liquid. Adapted with permission from ref 13. Copyright 2016 American Chemical Society.

Further modifications of pillar[5]arenes have been reported where more than one face of the pillar[5]arene has been substituted with anthracene moieties. Huang reported the synthesis of a pillar[5]arene where two faces have terminal anthracene moieties.[14] The use of copper(I)-catalysed azide alkyne cycloaddition (CuAAC) reactions to functionalise pillar[5]arenes has been adopted by Nierengarten and co-workers in which they prepared functionalised pillar[5]arenes in which all terminal groups have been substituted by other functional groups such as ferrocenes,[15] porphyrins[16] and other aryl moieties.[17,18]

4.2 Results and discussion

This chapter discusses the synthesis and characterisation of a series of [2]rotaxanes stoppered by anthracene moieties along with a model rotaxane system, akin to that previously studied in the Champness group.[19] Cyclic voltammetry and fluorescence data has been measured and compared across the series. In addition, crystallography data was acquired for some of the rotaxanes.

4.2.1 Expanded toolkit for construction of [2]rotaxanes

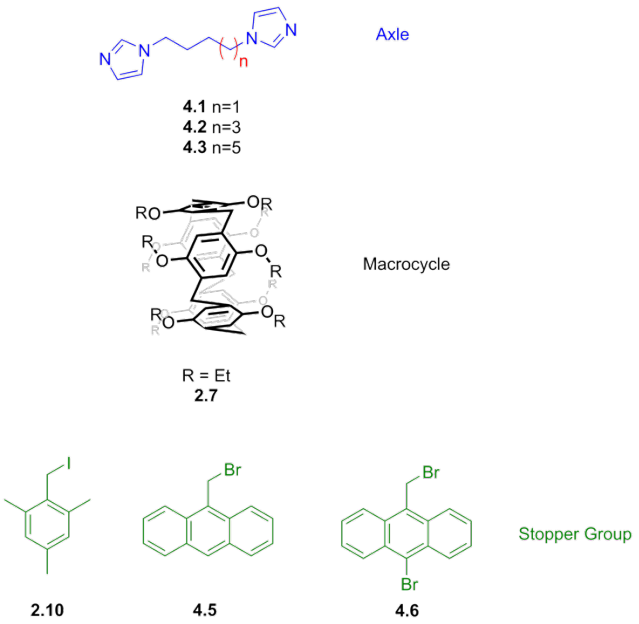

Figure 4.6. Toolkit of components used to construct rotaxanes. Blue represents the axle, black represents the DEP5A macrocycle and green represents the stopper groups.

The toolkit of components used to assemble rotaxanes in this chapter was expanded to include anthracene stopper groups (**Figure 4.6**). As before, bis-imidazole rods (**4.1**-**4.3**) were used as axles, however short chain dibromoalkanes were used to construct the axles in order to allow a 1:1 pseudorotaxane-complex formation with a macrocycle which could then be end-capped by stopper groups. DEP5A **2.7** was chosen as the only macrocycle to construct the [2]rotaxanes due to the relative ease of synthesis and high yield. Similarly, the mesityl stopper group **2.10** was used to construct a model rotaxane. Anthracene stopper groups (**4.5** and **4.6**) were used for comparison, with compound **4.6** of interest due to the potential for post synthetic modification of an assembled rotaxane.

Characterisation of the [2]rotaxanes was completed using ^{1}H, ^{13}C, ^{1}H-^{1}H COSY, ^{1}H-^{1}H NOESY NMR spectroscopies and electron spray ionisation mass spectrometry. Calculation of shielding factors (where appropriate) were made with respect to the corresponding dumbbell molecule in the corresponding deuterated solvent (**Formula 2.1**).

4.2.2 Anthracene stoppered [2]rotaxanes

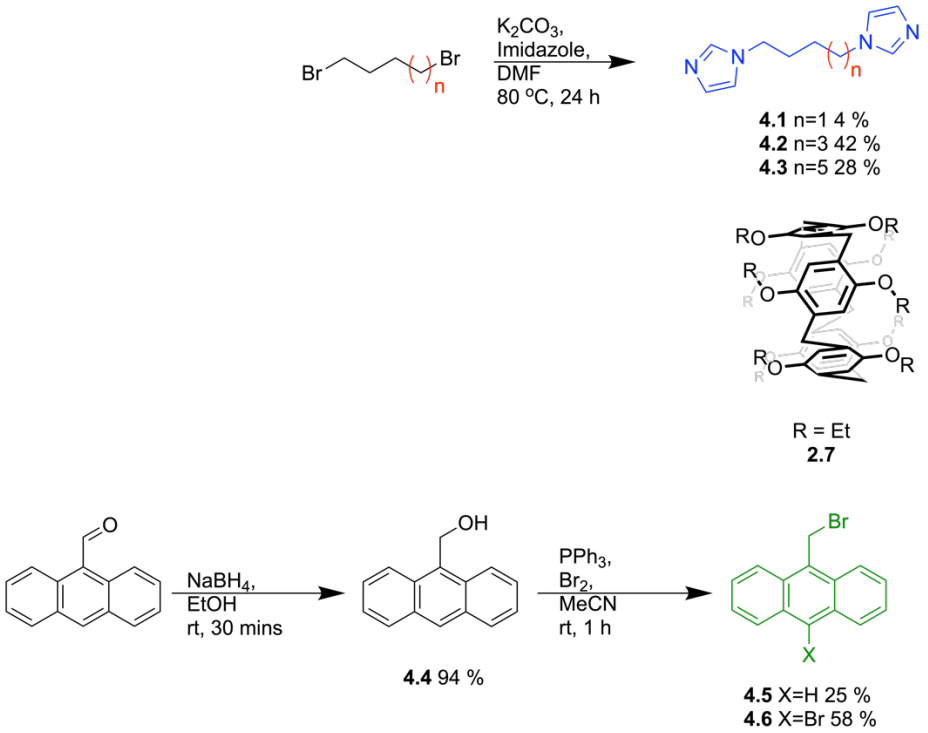

Scheme 4.2. Reaction scheme for components used to assemble the anthracene stoppered [2]rotaxanes.

By using a toolkit approach to rotaxane synthesis (**Scheme 4.2**), bis-imidazole axles (**4.1** - **4.3**) were synthesised from their corresponding dibromoalkane. Whereas the butyl rod **4.1** was low yielding, the larger chains gave moderate yields. To make the anthracene stopper groups, the corresponding alcohol **4.4** was synthesised in high yield via the reduction of the corresponding aldehyde. The alcohol was converted to stopper group **4.5** in low yield following a literature procedure.[20] When Br_2 was added in excess, stopper group **4.6** was synthesised in moderate yield. The synthesis of diethoxypillar[5]arene (DEP5A) **2.7** is reported in **chapter 2**.

The [2]rotaxanes were assembled using the end capping method (**Scheme 4.3**) where the axle component and DEP5A were initially dissolved in a minimum amount of chloroform, and then the stopper groups added to the mixture in absence of light.

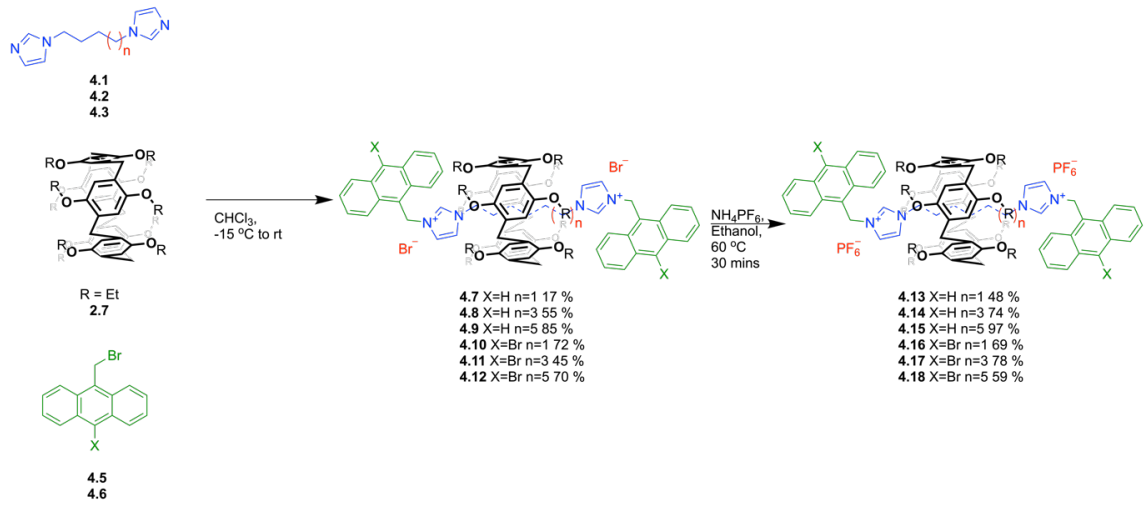

Scheme 4.3. Reaction scheme used to assemble the anthracene stoppered [2]rotaxanes.

A trend is observed when stopper group **4.5** is used to construct [2]rotaxanes, with longer chain bis-imidazole rods resulting in higher yields. This same trend was not observed when using **4.6** as the stopper, as the shortest and longest axles were high yielding, and when using rod **4.2** the corresponding [2]rotaxane gave only a moderate yield. Ion exchange to afford the corresponding PF_6^- salts were moderate to high yielding, facile reactions and were necessary for subsequent electrochemical measurements, removing contributions from bromide anions to the cyclic voltammograms.

No dumbbell molecules, anthracenyl-functionalised bis-imidazoliums, were formed for either series during the rotaxane synthesis. However, a partially reacted substrate was observed in MS spectra for all of these [2]rotaxanes from the stopper group reacting with only one end of any given bis-imidazole rod. When refluxing the axles with stopper groups **4.5** and **4.6** in chloroform in the absence of pillar[5]arene, no dumbbell was produced either. This may suggest that the pillar[5]arene is behaving as a phase transfer catalyst which is incorporated in the final product.

The dumbbell molecules were synthesised by refluxing the reactants in acetonitrile. The formation of dumbbells was shown by their corresponding MS spectra (**Figure 7.173**). However, no NMR data could be recorded as the products were insoluble in the solvents used for comparative shielding studies and therefore the corresponding shielding factors could not be calculated.

4.2.3 Comparison to a mesityl-stoppered [2]rotaxane

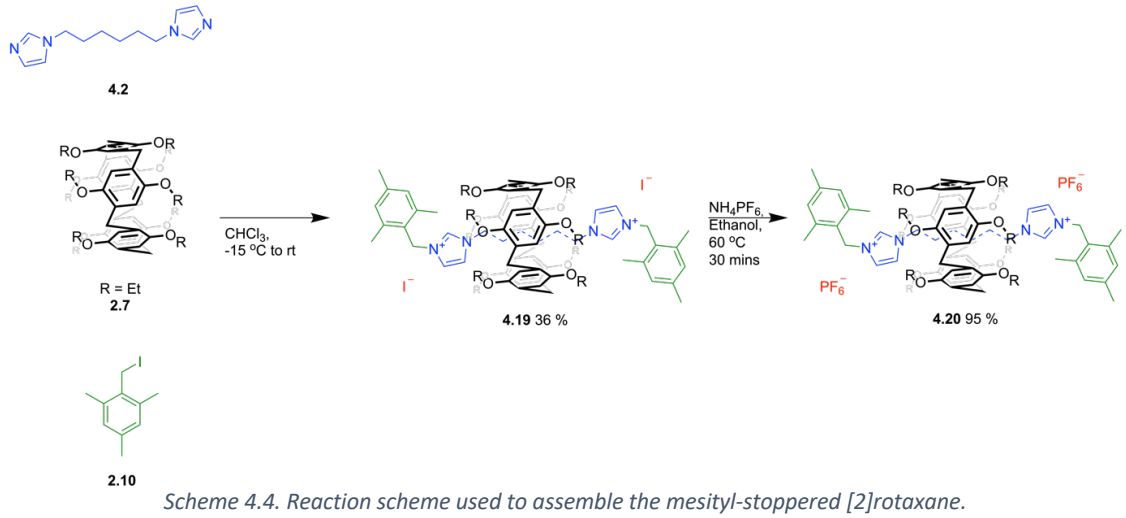

Scheme 4.4. Reaction scheme used to assemble the mesityl-stoppered [2]rotaxane.

As no ^{1}H NMR stacks could be recorded for the anthracene-stoppered series, a rotaxane was required for comparison in order to understand the shuttling behaviour. By using the components available, the anthracene stoppers groups were replaced by a mesityl stopper (**Scheme 4.4**).

Axle **4.2**, DEP5A and the mesityl stopper group **2.10** were used to construct [2]rotaxane **4.19** in relatively low yield. Conversion to the hexafluorophosphate salt (**4.20**) was a high yielding, facile reaction. The corresponding dumbbell **4.21** was synthesised in moderate yield and was also converted to the corresponding hexafluorophosphate salt (**4.22**) in high yield. Dumbbell **4.22** was not soluble in chloroform, thus shuttling parameters could not be verified for corresponding rotaxane **4.20** in chloroform.

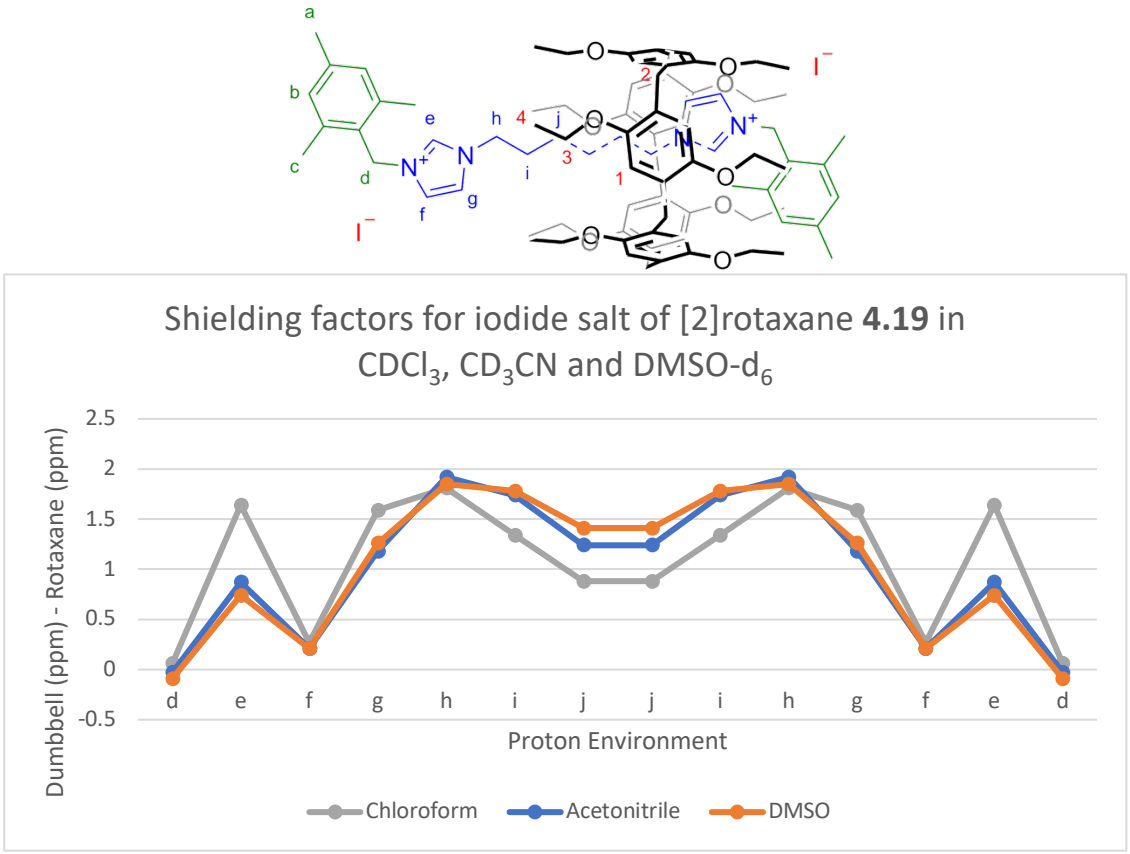

*Figure 4.7. Plot of shielding factors for [2]rotaxane **4.19** in $CDCl_3$, CD_3CN and DMSO-d_6.*

Shielding factors were calculated for [2]rotaxane **4.19** in chloroform, acetonitrile and DMSO with respect to dumbbell **4.21** to assess the difference in shuttling of DEP5A along a mesityl stoppered axle (**Figure 4.7**).

In chloroform the DEP5A macrocycle has a high population nearest to the imidazolium stations $H_{e,g}$, however due to the close proximity to the stopper group environments $H_{d,f}$ do not experience significant shielding. Due to the large size of the macrocycle with respect to the short axle, it is not surprising that the global maximum is around environment H_h, as this is along the hexyl chain but very close to the imidazolium station. From H_h to H_j there is a linear decline in population of macrocycle and yet the shielding factors are still relatively high due to the short distance between imidazolium charges. As such, shuttling is observed to be symmetrical.

When in a polar solvent such as acetonitrile, the population of DEP5A around environment H_e dramatically decreases due to the solvophilic interactions with the

imidazolium axle and the solvophobic interactions with DEP5A. This in turn causes the population of environments H_i and H_j to increase. This effect is subtly larger in DMSO as the population of macrocycle around environment H_j only slightly increases and the population around H_e slightly decreases, in comparison to acetonitrile.

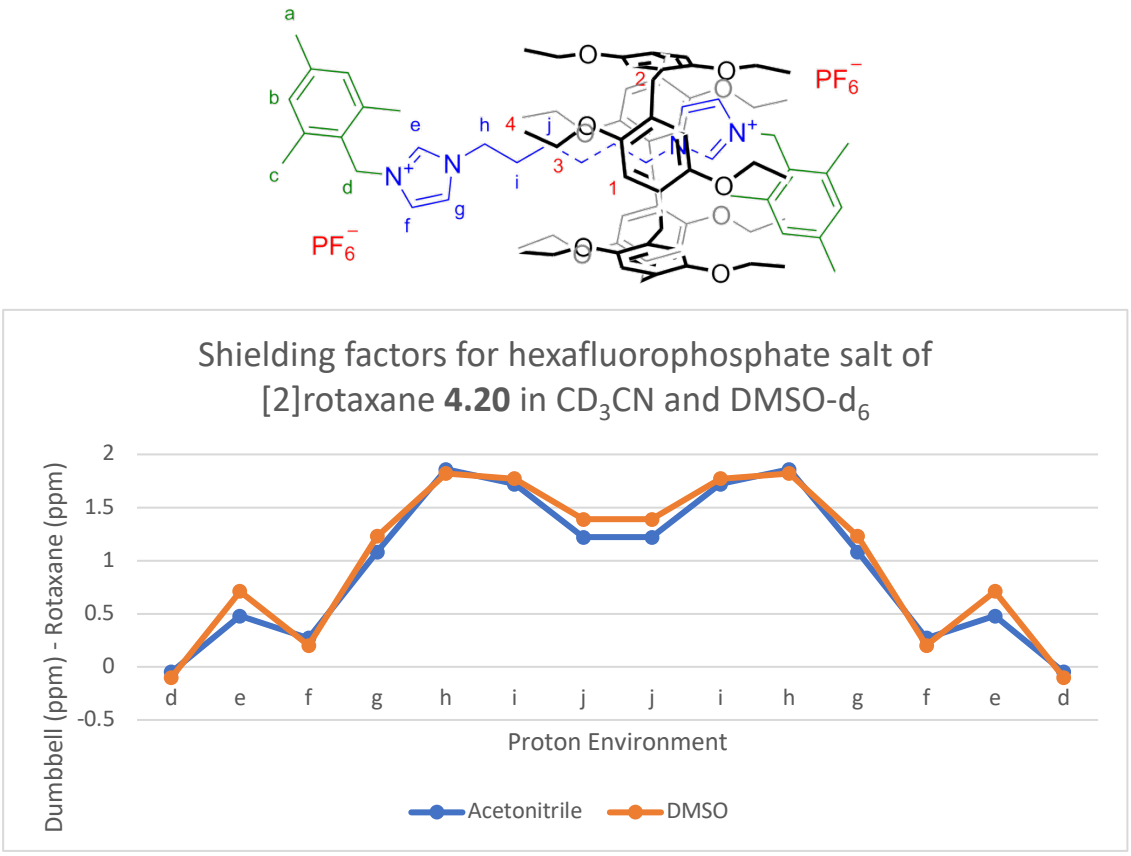

*Figure 4.8. Plot of shielding factors for [2]rotaxane **4.20** in CD_3CN and DMSO-d_6.*

Although shielding factors could not be calculated for **4.20** in chloroform, its corresponding ^{1}H NMR data would suggest that shuttling would be similar to that of its iodide salt counterpart **4.19**.

Shuttling of the hexafluorophosphate salt of rotaxane **4.20** in DMSO is similar to that of its iodide counterpart **4.19** (**Figure 4.8**), however in acetonitrile there is a greater drop in population around environment H_e with respect to the iodide salt, perhaps due to increased stabilisation of the solvent-ion pair.

The shuttling behaviour observed for rotaxanes **4.19** and **4.20** is identical to those studied previously in the group which use the same axles and DMP5A.[19] This would suggest that the shuttling behaviour of butyl or octyl linked variants would be analogous to what has been previously reported. Similarly, exchanging stopper groups to slightly larger anthracene moieties should have a minimal effect on shuttling.

4.2.4 Electrochemistry of the [2]rotaxanes

The electrochemistry of pillar[5]quinone and pillar[n]arene[5-n]quinone, where n is the number of repeat units has been reported, however electrochemistry data for pillar[5]arenes are scarce.[21,22]

The anthracene stoppered [2]rotaxanes **4.13** – **4.18** were studied using cyclic voltammetry (**Figure 4.9**). Each process was studied in detail at five different potential sweep rates: 300, 200, 100, 50 and 20 mVs^{-1}. Both the overall shape of the voltammogram as well as the peak anodic and cathodic currents were found to be independent of the scan rate, signifying that each process was reversible. The rotaxanes were not stable to multiple scans, so studies were not pursued further with other electrochemical techniques.

A one electron reversible oxidation was observed for **4.13**, **4.15**, **4.16** and **4.18**,[23] however a two electron reversible oxidation process was observed for the mid-length hexyl chain [2]rotaxanes **4.14** and **4.17**. Although visible, the resolution of the voltammograms were low, so the oxidation processes were probed further using a square wave oxidation.

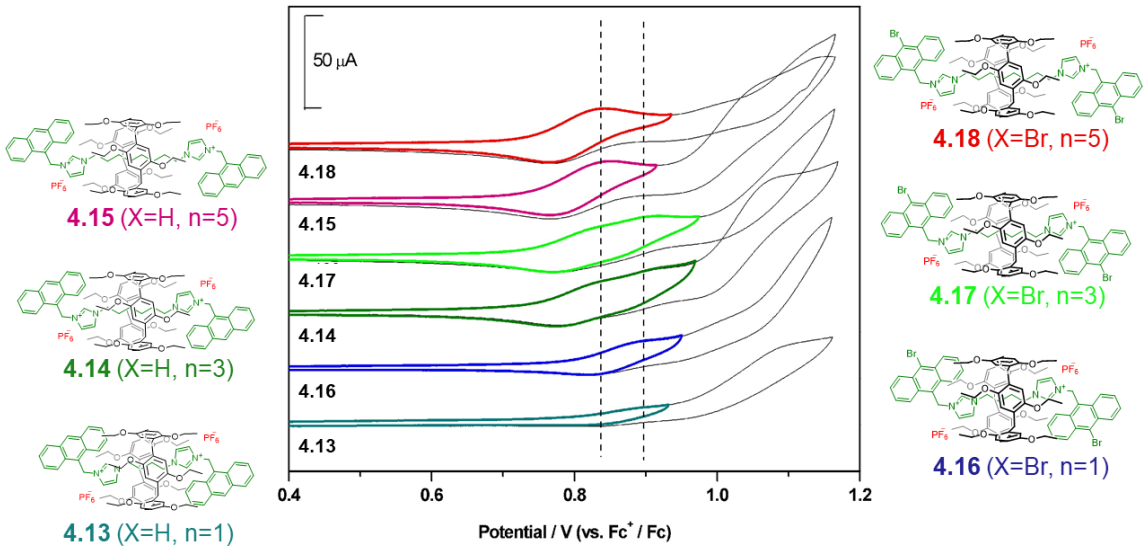

*Figure 4.9. Stacked cyclic voltammograms of the oxidation processes of the anthracene stoppered [2]rotaxanes **4.13** - **4.18** in ascending order, recorded in DCM containing $[Bu_4N][BF_4]$ (0.4 M).*

The processes observed are all pillar[5]arene based oxidation processes, as the anthracene processes occur at approximately 0.9 V across the series. Using square wave voltammetry to resolve [2]rotaxanes **4.13** – **4.15** further (**Figure 4.10**), the oxidation for the butyl chain [2]rotaxane **4.13** is shifted to a more positive potential of 0.86 V, whereas the oxidation process for longest octyl chain [2]rotaxane **4.15** is at a slightly lower potential, 0.81 V. The mid-length hexyl chain [2]rotaxane **4.14** exhibits an interesting property where two one electron oxidation processes are observed, with one corresponding to the lower potential of **4.15** at 0.81 V and the other corresponding to the higher potential of **4.13** at 0.89 V.

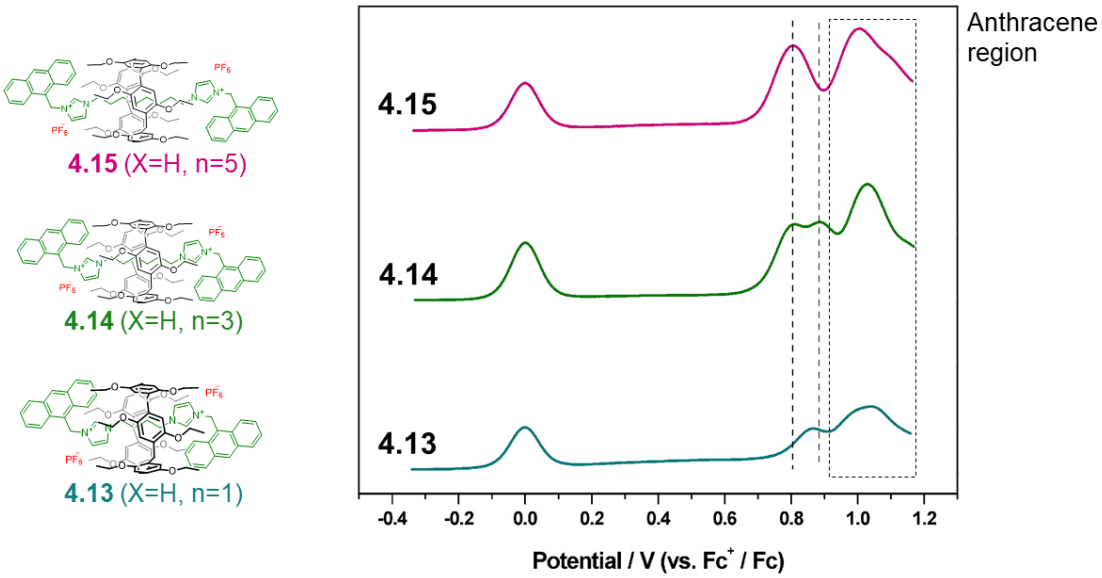

*Figure 4.10. Stacked square wave voltammograms of the oxidation processes of [2]rotaxanes **4.13** - **4.15** in ascending order, recorded in DCM containing $[Bu_4N][BF_4]$ (0.4 M). Anthracene processes occur within the boxed region.*

To confirm these processes were specifically related to the length of the axle and the DEP5A macrocycle, square wave oxidations were also recorded for [2]rotaxanes **4.16** – **4.18** (**Figure 4.11**). As before, the longest rotaxane **4.18** exhibited an oxidation at 0.8 V, the shortest **4.16** had the highest potential at 0.86 V, and both oxidation processes were observed for **4.17** at 0.81 V and 0.87 V.

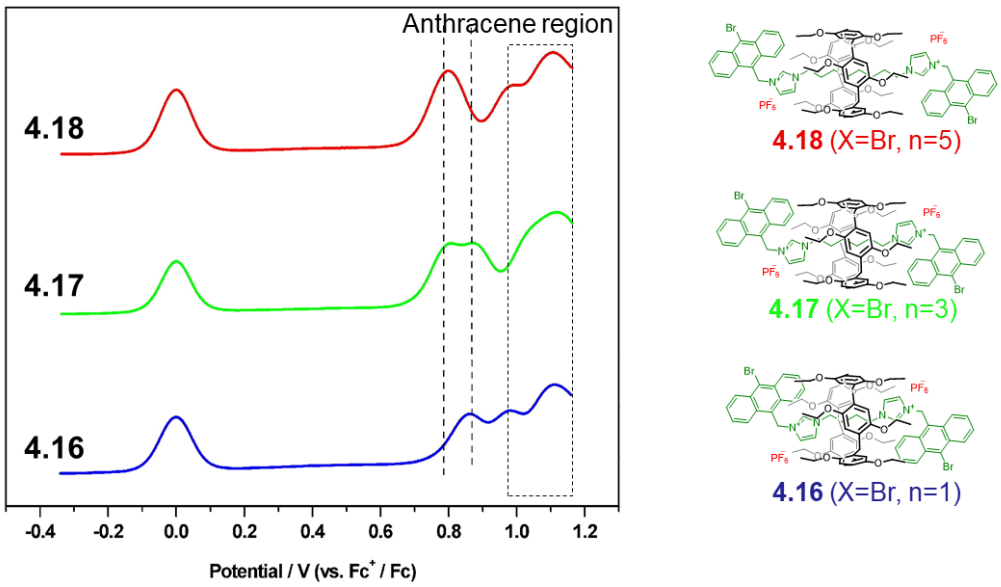

*Figure 4.11. Stacked square wave voltammograms of the oxidation processes of [2]rotaxanes **4.16** - **4.18** in ascending order, recorded in DCM containing $[Bu_4N][BF_4]$ (0.4 M). Anthracene processes occur within the boxed region.*

In order to confirm no communication was occurring from the stopper groups and the pillar[5]arene or the stopper groups with themselves through the pillar[5]arene, the mesityl stoppered [2]rotaxane **4.20** was also studied using cyclic voltammetry (**Figure 4.12**). Two reversible oxidation processes were observed, however once again resolution was poor and square wave voltammetry was used to identify the oxidation processes.

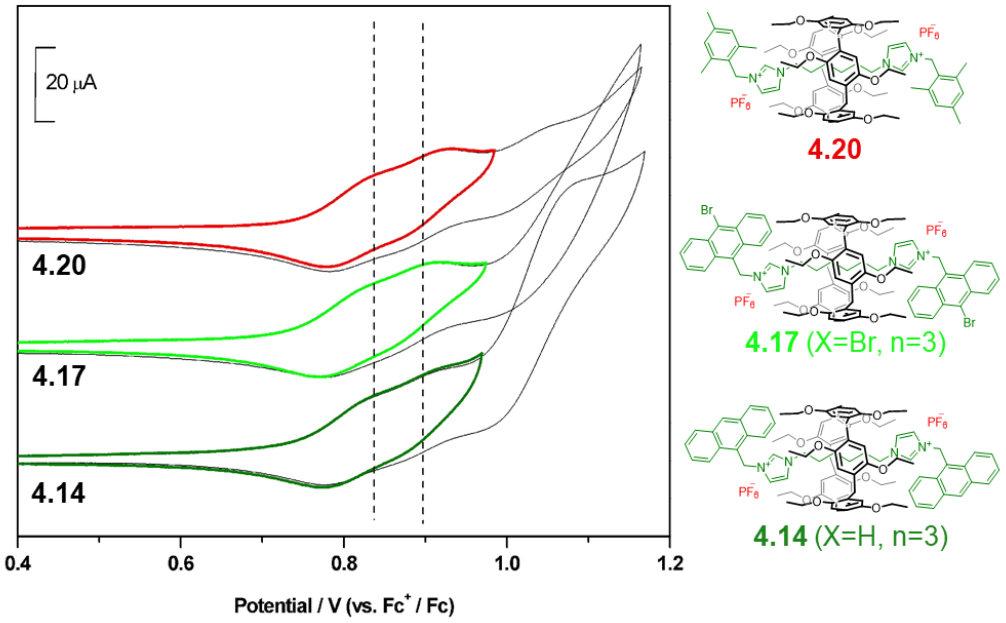

*Figure 4.12. Stacked cyclic voltammograms of the oxidation processes of [2]rotaxanes **4.14**, **4.17** and **4.20** in ascending order, recorded in DCM containing $[Bu_4N][BF_4]$ (0.4 M).*

The square wave voltammogram of [2]rotaxane **4.20** confirms the two oxidation process is stopper group independent (**Figure 4.13**) and only relates to the pillar[5]arene and the length of the axle. The oxidation processes are observed at similar potentials to **4.14** and **4.17** at 0.81 V and 0.89 V. DEP5A showed a four electron oxidation process at 0.57 V, 0.72V, 0.8 V and 0.94 V. In all cases these are tuned to either one or two oxidation processes. This means that confinement of the pillar[5]arene species prevents all possible oxidations from occurring.

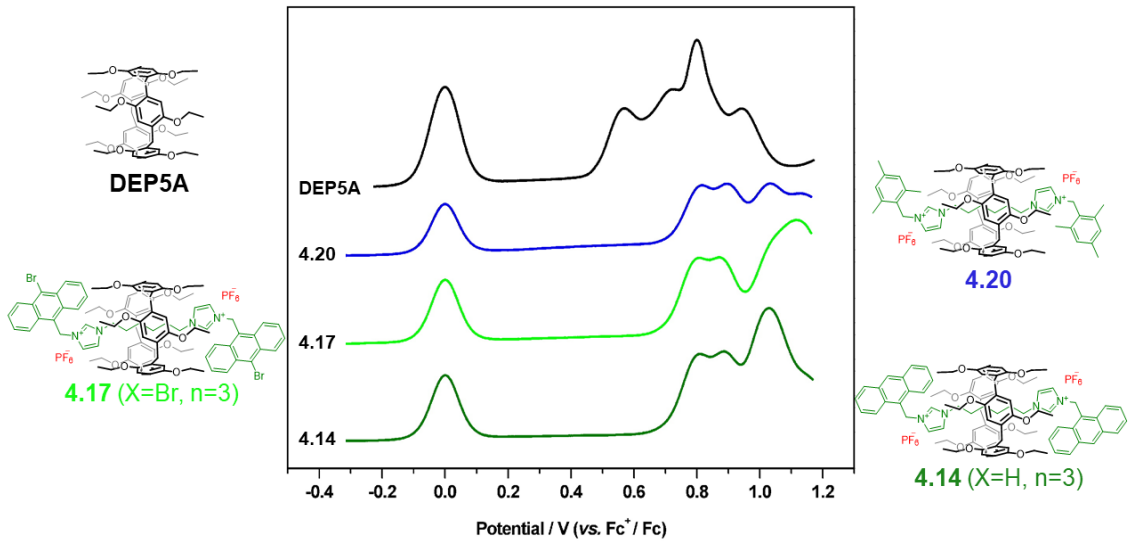

*Figure 4.13. Stacked square wave voltammograms of the oxidation processes of [2]rotaxanes **4.14**, **4.17**, **4.20** and DEP5A in ascending order, recorded in DCM containing $[Bu_4N][BF_4]$ (0.4 M).*

If confinement was the only cause of these oxidations, then the large octyl variants **4.15** and **4.18** should have shown the most oxidations and the shortest butyl variants **4.13** and **4.16** would have had the least. This is not the case as the mid length hexyl variants have the most pillar[5]arene oxidations. This suggests that some other factor is involved which may be shuttling.

A high potential is observed with the octyl variants due to the enhanced length of the spacer between the charged imidazolium groups. The oxidation of the pillar[5]arene could be forcing it onto the alkyl chain as a result of the repulsive charges of each positively charged component. Due to the high level of confinement observed for the butyl-linked variants, the pillar[5]arene cannot move onto the alkyl chain without also encountering a repelling imidazolium group and thus one oxidation is observed at a higher potential. The mid length hexyl variants show both of these oxidations as the pillar[5]arene can sit on the alkyl chain leading to an oxidation at the lower potential, however the axle is still relatively short, leading to oxidations at the higher potential whenever an imidazolium moiety is encountered as a result of steric interactions with the stopper groups.

4.2.5 Fluorescence measurements of the [2]rotaxanes

Absorbance and emission spectra were recorded for the anthracene stoppered [2]rotaxanes **4.13** – **4.18** (**Figure 4.14**). Emission across the series are mirror images of the absorbance spectra with relatively low Stokes shifts, from the bands closest to each other. Where symmetry breaking in emission is observed this was possibly due to dimerisation of anthracene moieties from the excitation at 370 nm. However we note that the effective yield of this process may have been low.

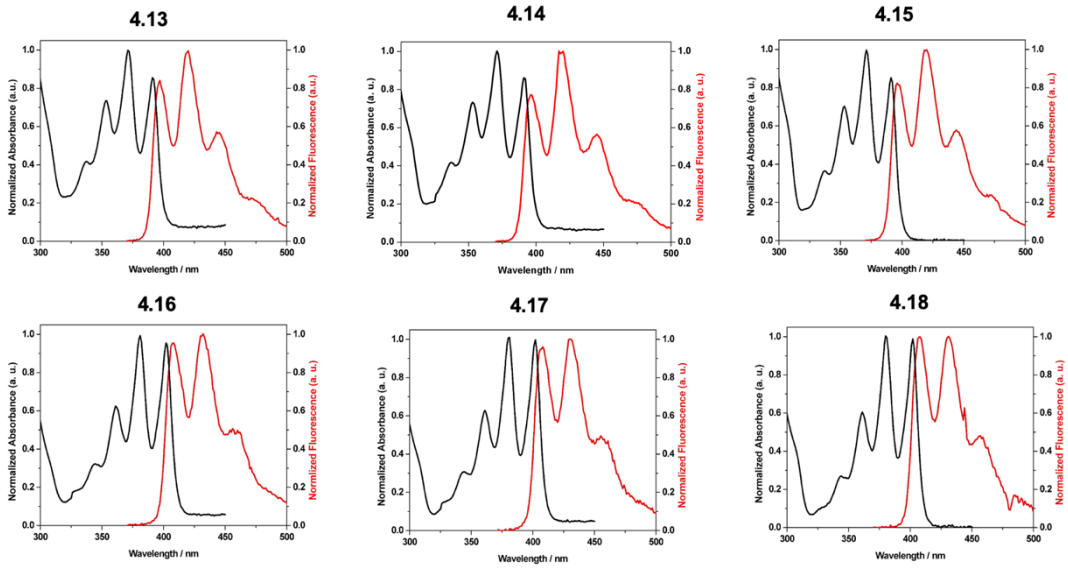

*Figure 4.14. Absorbance (black) and emission (red) spectra of anthracene stoppered [2]rotaxanes **4.13** - **4.18** in DCM (excitation at 370 nm).*

Rotaxane **4.14** had a Stokes shift of 5 nm, **4.17** had a Stokes shift of 7 nm and the rest (**4.13**, **4.15**, **4.16** and **4.18**) had a Stokes shift of 6 nm (**Table 4.1**). Quantum yields were calculated in relation to the quinine sulfate standard which was dissolved in sulfuric acid (0.5 M). All of the anthracene stoppered [2]rotaxanes fluoresced, however the addition of the bromo-group, on the 10-position of the anthracene stopper, resulted in significant quenching when compared to the non-brominated variants. Similarly, the fluorescence of the hexyl chain analogue were the lowest when comparing chain length as a result of quenching from the pillar[5]arene. The increase in fluorescence for the shorter butyl variants is attributed to the enhanced rigidity of the species overcoming quenching from the pillar[5]arene. The octyl variants fluoresced the most as the pillar[5]arene quenched

fluorescence less efficiently due to the additional length of the axle, and enhanced separation of the anthracene groups.

*Table 4.1. Stokes shifts and quantum yields of [2]rotaxanes **4.13** - **4.18**.*

Compound	Stokes Shift (nm)	Quantum Yield
4.13	6	0.043
4.14	5	0.034
4.15	6	0.045

Compound	Stokes Shift (nm)	Quantum Yield
4.16	6	0.014
4.17	7	0.011
4.18	6	0.016

4.2.6 X-Ray crystallography of [2]rotaxanes

Crystals were grown for **4.8** – **4.11** by vapour diffusion of hexane into chloroform solutions of the compounds and crystal structures were obtained for these rotaxanes. X-ray diffraction was run at Diamond Light Source by Rosemary Young and the crystal structures were solved by Dr Stephen Argent.

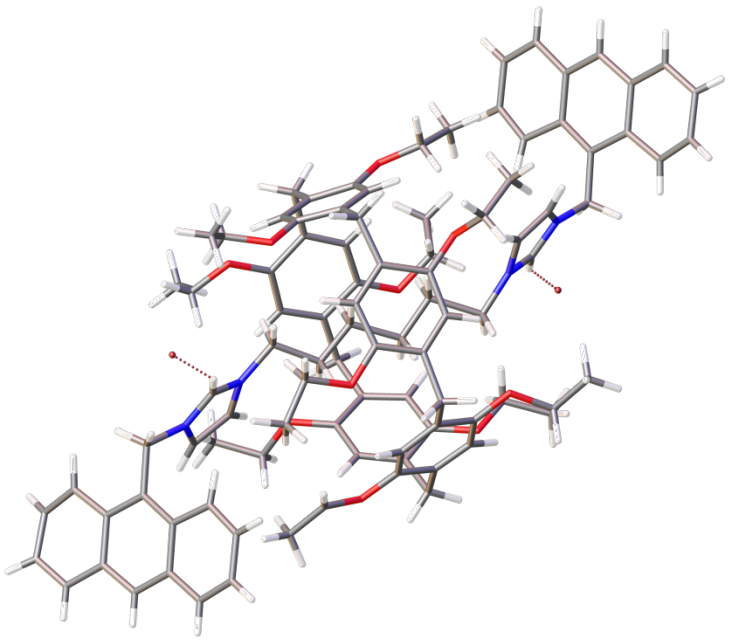

*Figure 4.15. X-ray crystal structure of [2]rotaxane **4.8** where solvent molecules have been omitted for clarity. Atoms C – grey, H – white, O – red, N – blue, Br – burgundy. Dotted lines represent hydrogen-bonding interactions.*

4.8 crystallises into the triclinic space group $P\bar{1}$ (**Figure 4.15**) and the crystal structure shows interaction of the bromide counterions with the imidazolium moieties via a C-H···Br hydrogen bond. The imidazolium moieties are twisted away from each other into a trans arrangement. The pillar[5]arene moiety is situated in the centre of the axle, away from

the favourable imidazolium stations which is the least favourable position in non-polar solvents. Arrangements in the solid-state are governed by intermolecular interactions and favourable packing configurations.

a)

b)

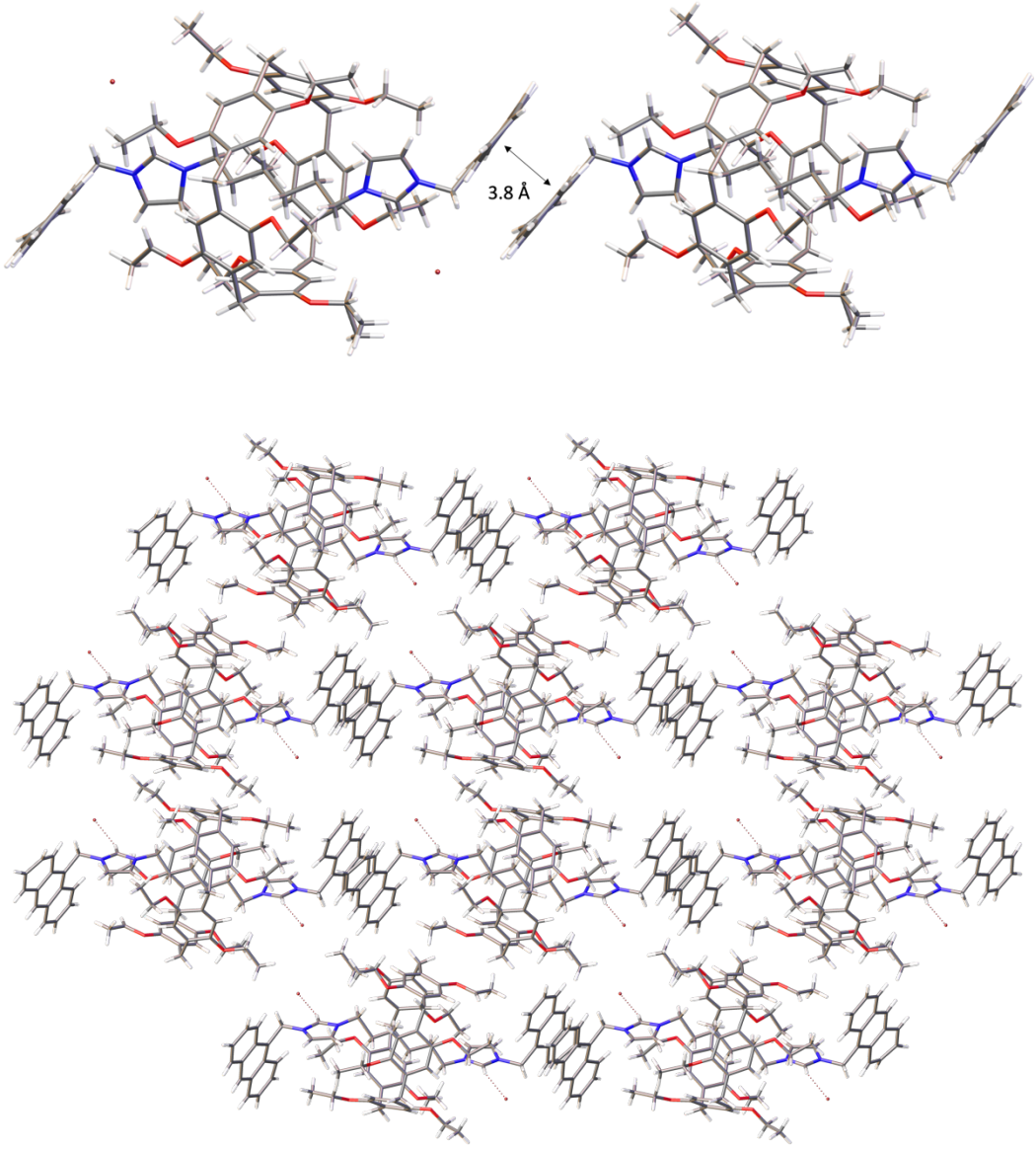

*Figure 4.16. (a) two molecules of **4.8** showing π-π stacks between the anthracene stoppers and (b) π-π stacks between many rotaxanes within a single crystal where solvent molecules have been omitted for clarity. Atoms C – grey, H – white, O – red, N – blue, Br – burgundy.*

When more than one molecule of the rotaxane is considered, interactions between anthracene stopper groups can be observed (**Figure 4.16**). Between two molecules, the anthracene stopper groups have plane centroid – plane centroid distance of 3.8 Å and in addition they are offset slightly. When looking at more than two molecules, anthracene

moieties on both sides of any given rotaxane molecule within the crystal structure have symmetrical stacking with adjacent rotaxane molecules leading to the formation of chains of interacting rotaxanes.

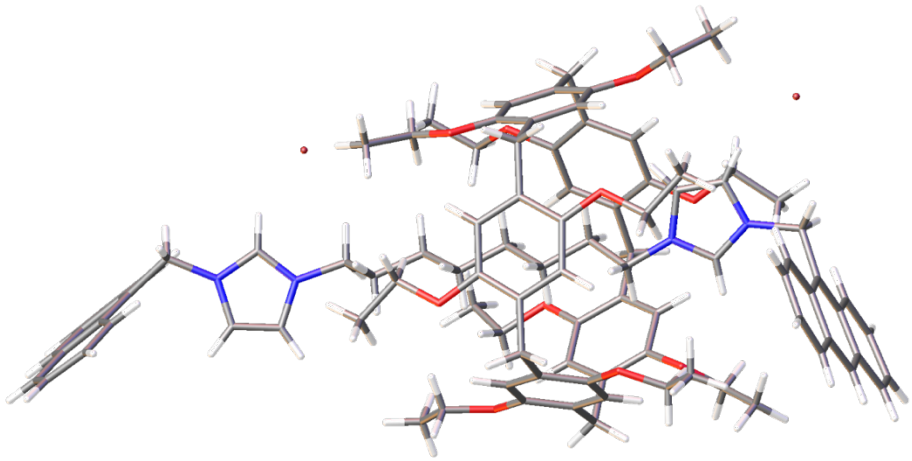

*Figure 4.17. X-ray crystal structure of [2]rotaxane **4.9** where solvent molecules have been omitted for clarity. Atoms C – grey, H – white, O – red, N – blue, Br – burgundy.*

4.9 crystallises into the triclinic space group $P\bar{1}$. Dissimilarly, the pillar[5]arene moiety on [2]rotaxane **4.9** shows the macrocycle favouring one side of the molecule over the other, although it resides on the alkyl chain rather than over an imidazolium moiety (**Figure 4.17**). The imidazoliums also adopt a trans orientation in relation to each other.

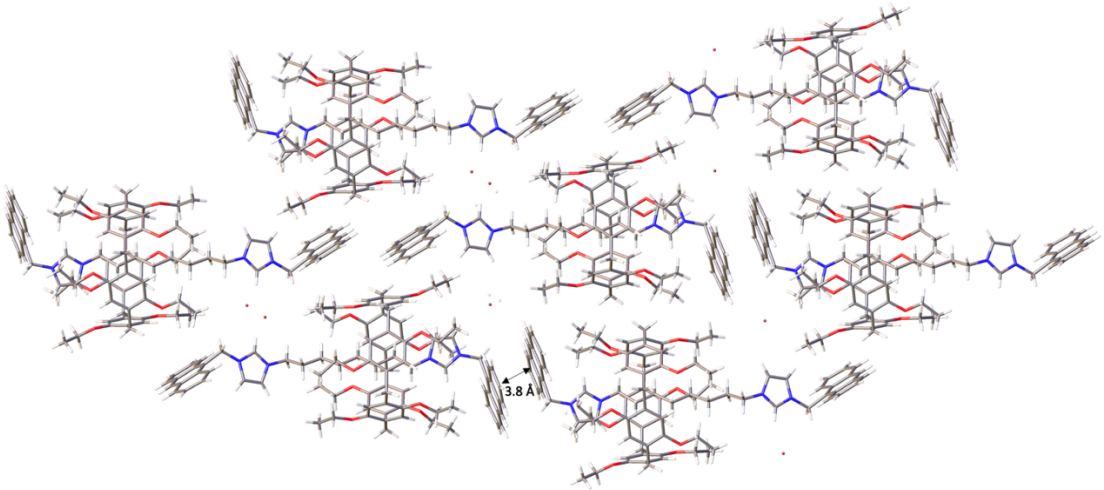

*Figure 4.18. Packing of **4.9** shown within a single crystal where the solvent molecules have been omitted for clarity. Atoms C – grey, H – white, O – red, N – blue, Br – burgundy.*

The π-π stacking between the anthracene stopper groups is distinct from that observed for the structure of **4.8** (**Figure 4.18**). The ends capped closest to the pillar[5]arene show well aligned face to face interactions of distance 3.8 Å. The other side is significantly offset with no face to face interactions between neighbouring molecules.

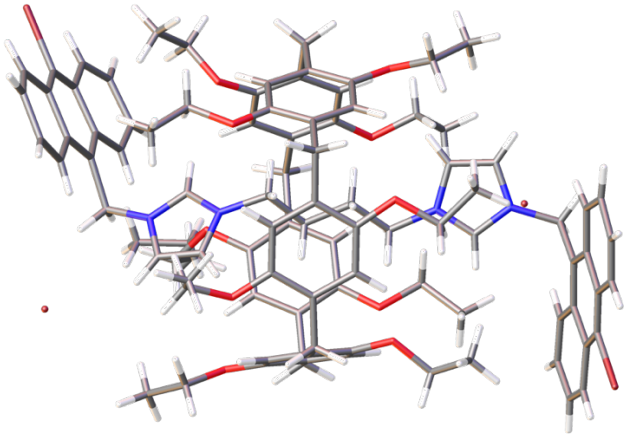

*Figure 4.19. X-ray crystal structure of [2]rotaxane **4.10** where solvent molecules have been omitted for clarity. Atoms C – grey, H – white, O – red, N – blue, Br – burgundy.*

4.10 crystallises into the monoclinic space group P2/n. The imidazolium groups and the anthracene stopper groups of **4.10** are twisted away from each other in a trans-like arrangement (**Figure 4.19**). The pillar[5]arene is positioned in the centre of the axle.

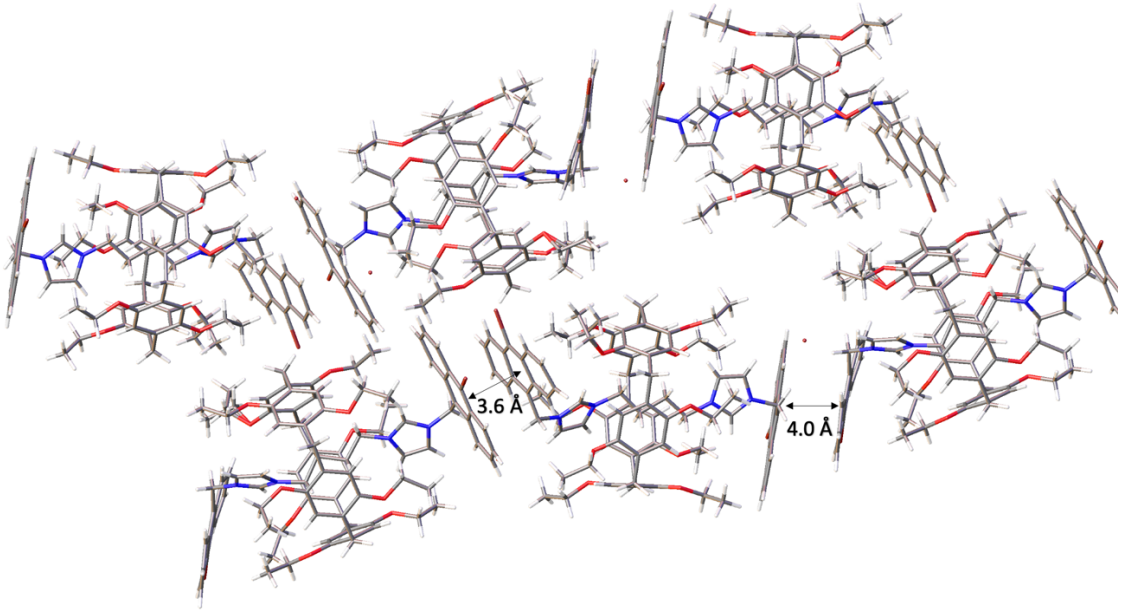

*Figure 4.20. Packing observed for **4.10** shown within a single crystal where the solvent molecules have been omitted for clarity. Atoms C – grey, H – white, O – red, N – blue, Br – burgundy.*

As a consequence of the pendant bromo-group, the anthracene moieties are not fully planar. This has implications for the face to face aromatic interactions between anthracene moieties on adjacent molecules of **4.10**, pairs of anthracenes are offset and twisted with respect to each other (**Figure 4.20**). Anthracene-anthracene stacking at either end of rotaxanes is asymmetric, with distances of 3.6 Å and 4.0 Å between stopper groups.

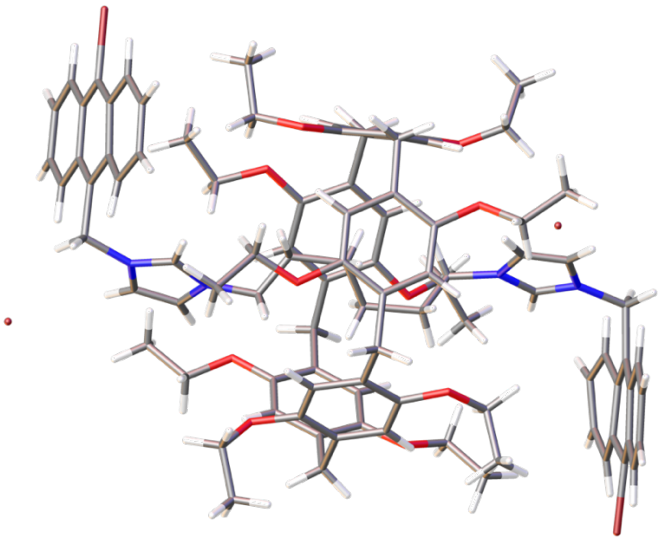

*Figure 4.21. X-ray crystal structure of [2]rotaxane **4.11** where solvent molecules have been omitted for clarity. Atoms C – grey, H – white, O – red, N – blue, Br – burgundy.*

4.11 crystallises into the triclinic space group $P\bar{1}$. The crystal structure of [2]rotaxane **4.11** reveals the pillar[5]arene moiety positioned in the centre of the axle (**Figure 4.21**). The addition of the bromo-group on the anthracenyl 10-position induces strain onto the anthracene's aromatic rings, reducing planarity. Like the others, the imidazolium moieties adopt a trans arrangement (**Figure 4.22**).

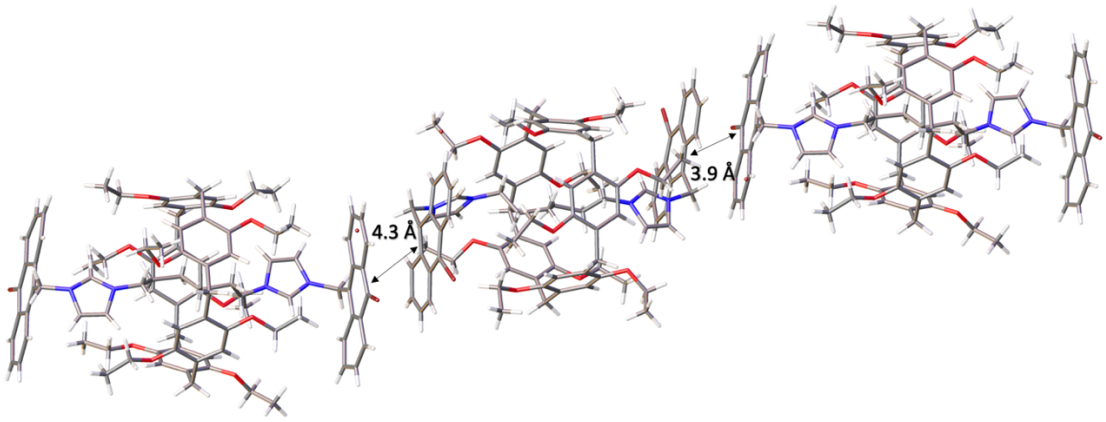

*Figure 4.22. X-ray crystal structure of **4.11** showing offset and twisted face to face interactions between adjacent anthracene stopper groups where solvent molecules have been omitted for clarity. Atoms C – grey, H – white, O – red, N – blue, Br – burgundy.*

The face to face interactions in **4.11** between the stopper groups are offset and twisted, with non-equivalent distances of 4.3 Å and 3.9 Å between adjacent molecules.

4.2.7 Photoirradiation of [2]rotaxanes

[2]Rotaxane **4.9** was chosen to trial photoirradiation experiments due to high solubility in chloroform and its well aligned π-π stacks on one side of the rotaxane, which has been shown in the solid state. This would suggest that the rotaxane should dimerise, rather than making a polyrotaxane. As such, the rotaxane was irradiated at 365 nm in the solid state and was monitored via ^{1}H NMR at one hour intervals. At each interval, the analyte was dissolved in deuterated chloroform, the ^{1}H NMR was recorded and the deuterated solvent was removed to allow further irradiation in the solid state.

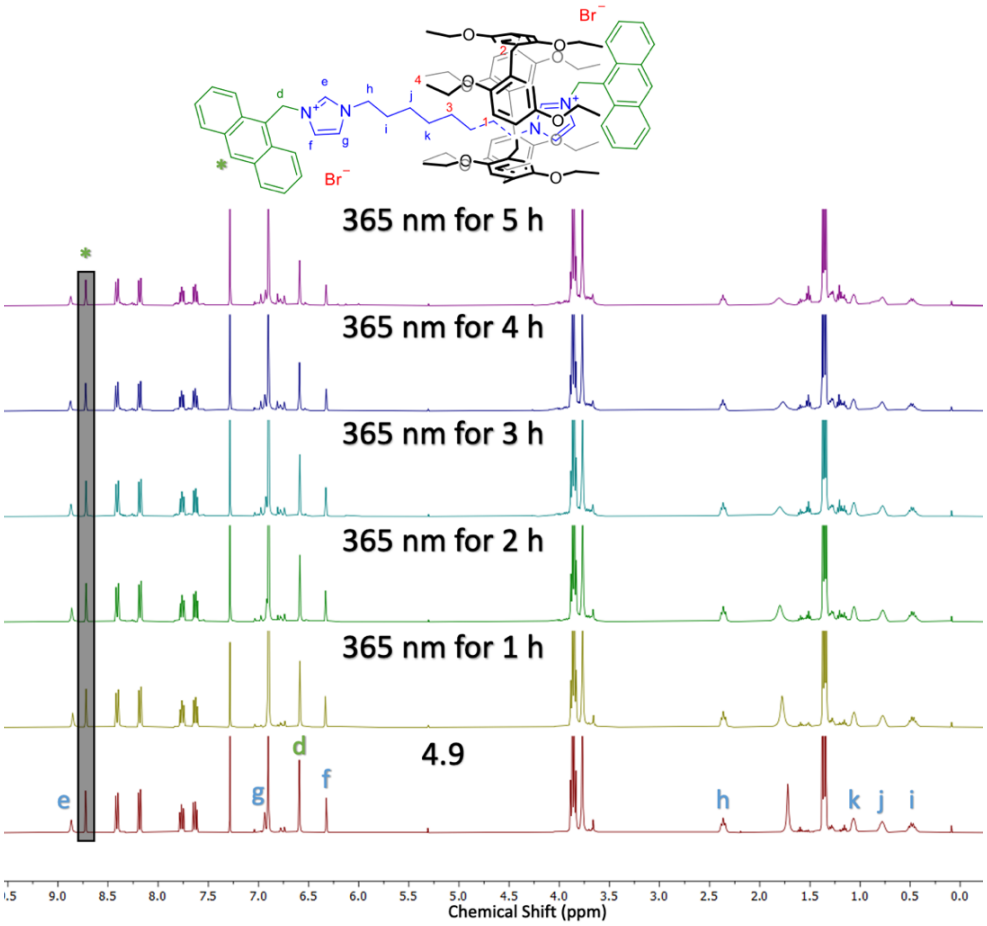

*Figure 4.23. ^{1}H NMR stack of [2]rotaxane **4.9** before and after irradiation at 365 nm in one hour intervals in ascending order.*

The intensity of the signal for proton H* would be expected to diminish if a photoreaction occurred, however this was not the case (**Figure 4.23**). After five hours, no such change was observed, suggesting that no polyrotaxane species was present. Further experiments would be required to establish the optimum conditions for the photoirridiation process.

4.3 Conclusions and future work

By expanding the toolkit used, a series of pillar[5]arene based [2]rotaxanes using anthracene moieties as their stopper groups have been synthesised and characterised by NMR spectroscopies. For some examples single crystal X-ray diffraction studies allows characterisation in the solid-state. Although shuttling information could not be gathered due to the insolubility of the corresponding dumbbell molecules in the relevant solvents.

The electrochemical behaviour of the rotaxanes was probed using cyclic voltammetry. Rotaxanes with different axle lengths exhibited differing behaviour in response to electrochemical oxidation. This was compared to a mesityl stoppered rotaxane in order to confirm the processes observed were not due to anthracene oxidations but rather were confined to pillar[5]arene oxidations.

Absorbance and emission spectroscopies have also been used to probe fluorescence of the anthracene rotaxanes. All the compounds that were tested exhibited fluorescence to varying degrees due to quenching from the pillar[5]arene and other factors.

Crystal structures were obtained for some of the anthracene rotaxanes and their structures determined in the solid state. By using the information provided, a light initiated [4 + 4] cycloaddition reaction was attempted. Dimerisation of anthracene groups was not conclusive and thus further experiments are required. Similarly, other rotaxanes in the series with well aligned π-π stacks could be studied to investigate polymerisation of the rotaxanes. Using a more powerful light source of may also be required to effect the dimerisation process.

Additional future work would involve post synthetic modification of the bromo-variants of the anthracene stoppered rotaxanes **4.15**, **4.16** and **4.18** using palladium catalysed cross coupling reactions.

4.4 Materials and methods

All chemicals were obtained from commercial sources and used without further purification (see **Chapter 6**). ^{1}H and ^{13}C NMR spectra were recorded using a Bruker AV(III)400HD, Bruker AV(III)400, Bruker AV400 and Bruker AV(III)500 machines at room temperature. Deuterated solvents were used as specified. Chemical shifts were recorded referenced to solvent residue. ESI-MS spectra were taken using a Bruker microTOF II mass spectrometer.

4.4.1 Synthesis

Synthesis of 1,4-di(1*H*-imidazol-1-yl)butane [**4.1**][19]

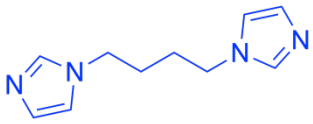

To a solution of potassium carbonate (11.6 g, 83.7 mmol) dissolved in DMF (60 mL), 1,4-dibromobutane (2.00 mL, 16.7 mmol) and imidazole (5.77 g, 84.8 mmol) were added and heated at 80 °C with vigorous stirring overnight. The solution was allowed to cool to room temperature and the solvent was removed under reduced pressure. The residue was subsequently redissolved in dichloromethane (10 mL) and washed with water (3 x 10 mL) and then brine (10 mL). The organic fraction was dried over $MgSO_4$, filtered and the solvent was removed under reduced pressure to yield a yellow oil (120 mg, 631 μmol, 4 %). ^{1}H NMR (400 MHz, Chloroform-*d*) δ 7.46 (t, *J* = 1.2 Hz, 2H), 7.09 (t, *J* = 1.1 Hz, 2H), 6.88 (t, *J* = 1.3 Hz, 2H), 4.03 – 3.88 (m, 4H), 1.80 – 1.74 (m, 4H) ppm. ^{13}C NMR (101 MHz, Chloroform-*d*) δ 137.04, 129.93, 118.60, 46.38, 28.15 ppm. ESI-MS (positive mode) m/z calc'd. for $C_{10}H_{15}N_4$ $[M + H]^+$: 191.1291, found: 191.1293.

Synthesis of 1,6-di(1*H*-imidazol-1-yl)hexane [**4.2**][19]

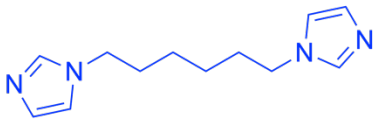

To a solution of potassium carbonate (5.37 g, 38.9 mmol) dissolved in DMF (30 mL), 1,6-dibromohexane (1.00 mL, 6.50 mmol) and imidazole (2.71 g, 39.8 mmol) were added and heated at 80 °C with vigorous stirring overnight. The solution was allowed to cool to room temperature and the solvent was removed under reduced pressure. The white solid was subsequently redissolved in dichloromethane (10 mL) and washed with water (3 x 10 mL) and then brine (10 mL). The organic fraction was dried over $MgSO_4$, filtered and the solvent was removed under reduced pressure to yield a yellow solid (603 mg, 2.76 mmol, 42 %). ^{1}H NMR (400 MHz, Chloroform-*d*) δ 7.44 (s, 2H), 7.06 (t, *J* = 1.1 Hz, 2H), 6.88 (t, *J* = 1.3 Hz, 2H), 3.91 (t, *J* = 7.0 Hz, 4H), 1.85 – 1.68 (m, 4H), 1.43 – 1.17 (m, 4H) ppm. ^{13}C NMR (101 MHz, Chloroform-*d*) δ 137.05, 129.55, 118.69, 46.79, 30.86, 26.06 ppm. ESI-MS (positive mode) m/z calc'd. for $C_{12}H_{19}N_4$ $[M + H]^+$: 219.1604, found: 219.1612.

Synthesis of 1,8-di(1*H*-imidazol-1-yl)octane [**4.3**][19]

To a solution of potassium carbonate (7.50 g, 54.3 mmol) dissolved in DMF (50 mL), 1,8-dibromooctane (2.00 mL, 10.9 mmol) and imidazole (3.40 g, 49.9 mmol) were added and heated at 80 °C with vigorous stirring overnight. The solution was allowed to cool to room temperature and the solvent was removed under reduced pressure. The residue was subsequently redissolved in dichloromethane (10 mL) and washed with water (3 x 10 mL) and then brine (10 mL). The organic fraction was dried over $MgSO_4$, filtered and the solvent was removed under reduced pressure to yield a yellow oil (750 mg, 3.04 mmol, 28 %).^{1}H NMR (400 MHz, Chloroform-*d*) δ 7.47 (d, *J* = 1.2 Hz, 2H), 7.08 (t, *J* = 1.1 Hz, 2H), 6.91 (t, *J* = 1.3 Hz, 2H), 3.94 (t, *J* = 7.1 Hz, 4H), 1.79 (q, *J* = 7.1 Hz, 4H), 1.31 (s, 8H) ppm. ^{13}C NMR (101 MHz, Chloroform-*d*) δ 137.08, 129.46, 118.74, 46.97, 31.01, 28.91, 26.43 ppm. ESI-MS (positive mode) m/z calc'd. for $C_{14}H_{23}N_4$ $[M + H]^+$: 247.1917, found: 247.1920.

Synthesis of anthracen-9-ylmethanol [**4.4**][24]

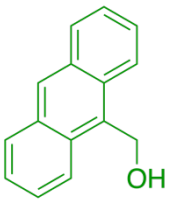

9-Anthracene carboxaldehyde (2.00 g, 9.70 mmol) and sodium borohydride (380 mg, 10.0 mmol) were dissolved in ethanol (30 mL) and stirred at 30 minutes at room temperature. The reaction was quenched with water and washed with diethyl ether (3 x 30 mL). The organic fractions were combined, dried with $MgSO_4$, filtered and the solvent was removed under reduced pressure which yielded a golden-yellow solid (1.89 g, 9.08 mmol, 94 %). ^{1}H NMR (400 MHz, Chloroform-*d*) δ 8.49 (s, 1H), 8.43 (dq, *J* = 8.9, 1.0 Hz, 2H), 8.08 – 8.00 (m, 2H), 7.59 (ddd, *J* = 8.9, 6.5, 1.4 Hz, 2H), 7.51 (ddd, *J* = 7.9, 6.5, 1.1 Hz, 2H), 5.68 (d, *J* = 4.2 Hz, 2H) ppm. ^{13}C NMR (101 MHz, Chloroform-*d*) δ 131.56, 131.02, 130.26, 129.16, 128.40, 126.47, 125.12, 123.90, 57.41 ppm. ESI-MS (positive mode) m/z calc'd. for $C_{15}H_{12}ONa$ [M + Na]$^+$: 231.0780, found: 231.0776.

Synthesis of 9-(bromomethyl)anthracene [**4.5**][20]

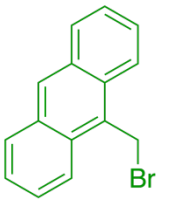

To a flame dried flask, triphenylphosphine (2.30 g, 8.77 mmol) in dry acetonitrile (20 mL) was purged under N_2 for 10 mins. Bromine (0.44 mL, 8.59 mmol) was added to the mixture slowly. Anthracen-9-ylmethanol (2.00 g, 9.60 mmol) was added to the mixture in the absence of light and was reacted until it was homogeneous (about 1 hour). The mixture was refrigerated overnight, cooled to 0 °C for 30 mins and was filtered and washed with cold acetonitrile. The solid was recrystallized in cold chloroform yielding yellow needles (588 mg, 2.17 mmol, 25 %). ^{1}H NMR (400 MHz, Chloroform-*d*) δ 8.53 (s, 1H), 8.33 (dd, *J* = 8.9, 1.1 Hz, 2H), 8.07 (dd, *J* = 8.3, 1.2 Hz, 2H), 7.67 (ddd, *J* = 8.9, 6.5, 1.3 Hz, 2H), 7.53 (ddd,

J = 7.8, 6.5, 1.0 Hz, 2H), 5.58 (s, 2H) ppm. ^{13}C NMR (101 MHz, Chloroform-*d*) δ 131.61, 129.74, 129.29, 129.20, 127.88, 126.81, 125.39, 123.53, 26.96 ppm.

Synthesis of 9-bromo-10(bromomethyl)anthracene [**4.6**][25]

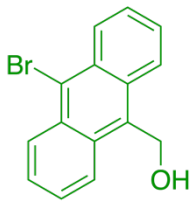

To a flame dried flask, triphenylphosphine (1.49 g, 5.68 mmol) in dry acetonitrile (10 mL) was purged under N_2 for 10 mins. Bromine (0.77 mL, 15.0 mmol) was added to the mixture slowly. Anthracen-9-ylmethanol (1.18 g, 5.68 mmol) was added to the mixture in the absence of light and was reacted until it was homogeneous (about 1 hour). The mixture was refrigerated overnight, cooled to 0 °C for 30 mins and was filtered and washed with cold acetonitrile. The solid was recrystallized in cold chloroform yielding yellow needles (1.01 g, 3.89 mmol, 58 %). ^{1}H NMR (400 MHz, Chloroform-*d*) δ 8.73 – 8.55 (m, 2H), 8.33 (dt, *J* = 9.0, 0.9 Hz, 2H), 7.77 – 7.58 (m, 4H), 5.51 (s, 2H) ppm. ^{13}C NMR (101 MHz, Chloroform-*d*) δ 130.60, 130.25, 128.88, 128.56, 127.20, 127.04, 125.78, 123.89, 26.66 ppm.

Synthesis of [2]rotaxane.2Br [**4.7**]

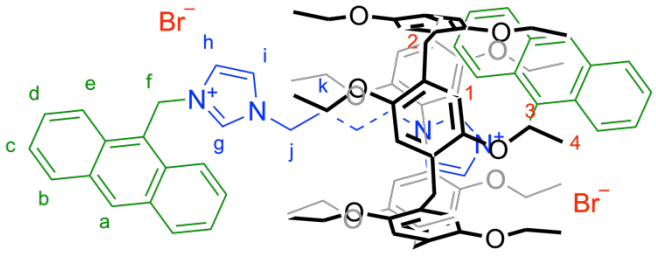

Diethoxypillar[5]arene (356 mg, 400 μmol) and 1,4-di(1*H*-imidazol-1-yl)butane (36.0 mg, 189 μmol) was dissolved in chloroform (0.7 mL). The solution was cooled to -15 °C and under the exclusion of light, 9-(bromomethyl)anthracene (120 mg, 442 μmol) was added. The mixture was left to warm to room temperature and stirred for 3 days. The crude residue was purified by column chromatography [silica, dichloromethane: methanol

(95:5)] to yield a yellow solid (53.0 mg, 32.6 μmol, 17 %). ^{1}H NMR (400 MHz, Chloroform-*d*) δ 9.05 (s, 2H, H_g), 8.71 (s, 2H, H_a), 8.63 – 8.55 (m, 4H, H_b), 8.20 – 8.15 (m, 4H, H_e), 7.77 (ddd, *J* = 8.9, 6.5, 1.3 Hz, 4H, H_c), 7.65 – 7.59 (m, 4H, H_d), 7.56 (d, *J* = 1.7 Hz, 2H, H_l), 7.10 – 6.86 (m, 4H, H_f), 6.82 (s, 10H, H_1), 6.60 (t, *J* = 1.8 Hz, 2H, H_h), 3.72 (qd, *J* = 6.7, 2.2 Hz, 20H, H_3), 3.67 (s, 10H, H_2), 1.93 (d, *J* = 8.6 Hz, 4H, H_j), 1.16 (t, *J* = 6.9 Hz, 30H, H_4), -1.10 (d, *J* = 8.3 Hz, 4H, H_k) ppm. ^{13}C NMR (101 MHz, Chloroform-*d*) δ 149.98, 134.61, 131.52, 131.27, 130.82, 130.66, 129.81, 128.37, 125.80, 123.06, 122.43, 122.29, 120.50, 117.05, 66.20, 47.23, 46.39, 29.72, 29.40, 22.71, 15.28 ppm. ESI-MS (positive mode) m/z calc'd. for $C_{95}H_{106}O_{10}N_4$ $[M]^{2+}$: 731.8966, found: 731.8989.

Synthesis of [2]rotaxane.2Br [**4.8**]

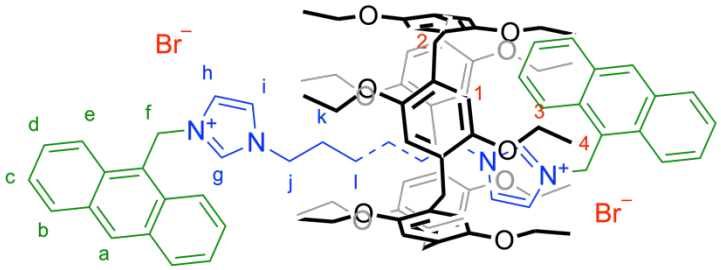

Diethoxypillar[5]arene (131 mg, 148 μmol) and 1,6-di(1*H*-imidazol-1-yl)hexane (16.0 mg, 73.3 μmol) was dissolved in chloroform (0.5 mL). The solution was cooled to -15 °C and under the exclusion of light, 9-(bromomethyl)anthracene (70.0 mg, 258 μmol) was added. The mixture was left to warm to room temperature and stirred for 3 days. The crude residue was purified by column chromatography [silica, dichloromethane: methanol (95:5)] to yield a pale yellow solid (66.0 mg, 40.0 μmol, 55 %). ^{1}H NMR (400 MHz, Chloroform-*d*) δ 9.30 (s, 2H, H_g), 8.71 (s, 2H, H_a), 8.50 (dd, *J* = 9.0, 1.0 Hz, 4H, H_b), 8.26 – 8.08 (m, 4H, H_c), 7.78 (ddd, *J* = 8.9, 6.5, 1.3 Hz, 4H, H_d), 7.63 (ddd, *J* = 8.4, 6.6, 0.9 Hz, 4H, H_e), 6.88 (s, 12H, $H_{1,h}$), 6.74 (s, 2H, H_i), 6.72 (d, *J* = 1.8 Hz, 4H, H_f), 3.93 – 3.79 (m, 20H, H_3), 3.73 (s, 10H, H_2), 2.80 – 2.42 (m, 4H, H_j), 1.30 (t, *J* = 7.0 Hz, 30H, H_4), 0.33 (d, *J* = 9.7 Hz, 4H, H_k), -0.08 (d, *J* = 6.7 Hz, 4H, H_l) ppm. ^{13}C NMR (101 MHz, Chloroform-*d*) δ 150.17, 134.92, 131.50, 131.19, 130.84, 130.30, 129.81, 128.33, 125.73, 122.93, 122.25, 122.05, 120.48, 116.90, 70.56, 66.04, 48.57, 45.52, 29.39, 29.05, 24.91, 15.52 ppm. ESI-MS (positive mode) m/z calc'd. for $C_{97}H_{110}O_{10}N_4$ $[M]^{2+}$: 745.9122, found: 745.9156.

Synthesis of [2]rotaxane.2Br [**4.9**]

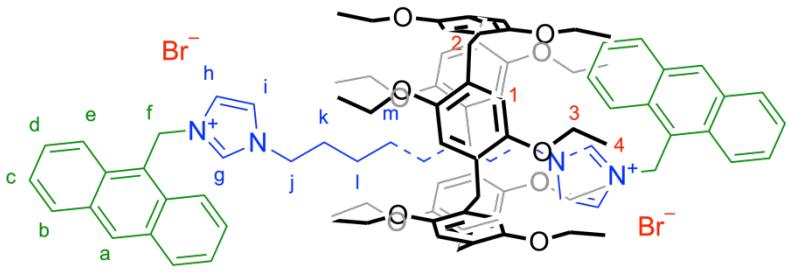

Diethoxypillar[5]arene (263 mg, 295 μmol) and 1,8-di(1*H*-imidazol-1-yl)octane (36.0 mg, 146 μmol) was dissolved in chloroform (0.8 mL). The solution was cooled to -15 °C and under the exclusion of light, 9-(bromomethyl)anthracene (100 mg, 369 μmol) was added. The mixture was left to warm to room temperature and stirred for 3 days. The crude residue was purified by column chromatography [silica, dichloromethane: methanol (95:5)] to yield a beige solid (209 mg, 124 μmol, 85 %). ^{1}H NMR (400 MHz, Chloroform-*d*) δ 8.88 (s, 2H, H_g), 8.73 (s, 2H, H_a), 8.47 – 8.38 (m, 4H, H_b), 8.19 (d, *J* = 8.4 Hz, 4H, H_e), 7.77 (ddd, *J* = 8.8, 6.5, 1.3 Hz, 4H, H_c), 7.68 – 7.59 (m, 4H, H_d), 6.96 (s, 2H, H_i), 6.91 (s, 10H, H_1), 6.60 (s, 4H, H_f), 6.32 (t, *J* = 1.8 Hz, 2H, H_h), 3.87 (q, *J* = 7.0 Hz, 20H, H_3), 3.78 (s, 10H, H_2), 2.38 (t, *J* = 8.6 Hz, 4H, H_j), 1.36 (t, *J* = 6.9 Hz, 30H, H_4), 1.06 (d, *J* = 7.3 Hz, 4H, H_m), 0.79 (s, 4H, H_l), 0.50 (q, *J* = 8.4 Hz, 4H, H_k) ppm. ^{13}C NMR (101 MHz, Chloroform-*d*) δ 150.18, 134.59, 131.50, 131.21, 130.97, 130.19, 129.86, 128.33, 125.74, 123.15, 122.74, 121.55, 119.35, 116.58, 65.81, 48.54, 45.10, 30.02, 29.36, 29.19, 26.91, 15.55 ppm. ESI-MS (positive mode) m/z calc'd. for $C_{99}H_{114}O_{10}N_4$ $[M]^{2+}$: 759.9279, found: 759.9094.

Synthesis of [2]rotaxane.2Br [**4.10**]

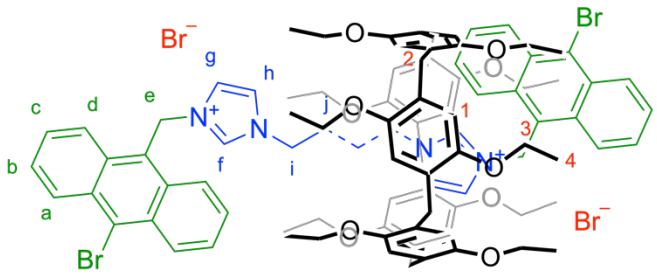

Diethoxypillar[5]arene (356 mg, 400 μmol) and 1,4-di(1*H*-imidazol-1-yl)butane (37.0 mg, 194 μmol) was dissolved in chloroform (0.6 mL). The solution was cooled to -15 °C and

under the exclusion of light, 9-bromo-10(bromomethyl)anthracene (150 mg, 428 μmol) was added. The mixture was left to warm to room temperature and stirred for 3 days. The crude residue was purified by column chromatography [silica, dichloromethane: methanol (95:5)] to yield a yellow solid (250 mg, 140 μmol, 72 %). ^{1}H NMR (400 MHz, Chloroform-*d*) δ 9.02 (t, *J* = 1.7 Hz, 2H, H_f), 8.71 (ddd, *J* = 9.9, 8.8, 1.0 Hz, 8H, $H_{a,d}$), 7.81 (ddd, *J* = 8.8, 6.6, 1.3 Hz, 4H, H_b), 7.73 (ddd, *J* = 8.8, 6.5, 1.0 Hz, 4H, H_c), 7.68 (t, *J* = 1.7 Hz, 2H, H_g), 7.16 – 6.95 (m, 4H, H_e), 6.80 (s, 10H, H_1), 6.61 (t, *J* = 1.8 Hz, 2H, H_h), 3.71 (qd, *J* = 6.9, 2.0 Hz, 20H, H_3), 3.65 (s, 10H, H_2), 1.93 (dt, *J* = 10.5, 4.9 Hz, 4H, H_i), 1.16 (t, *J* = 6.9 Hz, 30H, H_4), -1.16 (t, *J* = 7.3 Hz, 4H, H_j) ppm. ^{13}C NMR (101 MHz, Chloroform-*d*) δ 149.98, 134.43, 131.76, 130.71, 130.51, 129.38, 128.62, 127.60, 123.78, 123.26, 122.45, 120.51, 117.15, 115.16, 77.26, 66.30, 47.27, 46.62, 29.39, 23.14, 15.33 ppm. ESI-MS (positive mode) m/z calc'd. for $C_{95}H_{106}O_{10}N_4Br_2$ $[M]^{2+}$: 810.3044, found: 810.3079.

Synthesis of [2]rotaxane.2Br [**4.11**]

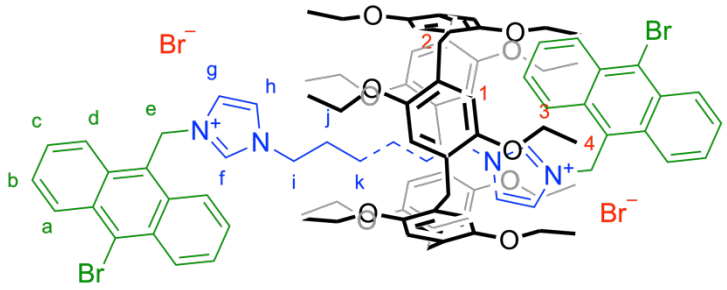

Diethoxypillar[5]arene (131 mg, 148 μmol) and 1,6-di(1*H*-imidazol-1-yl)hexane (16.0 mg, 73.3 μmol) was dissolved in chloroform (0.8 mL). The solution was cooled to -15 °C and under the exclusion of light, 9-bromo-10(bromomethyl)anthracene (60.0 mg, 171 μmol) was added. The mixture was left to warm to room temperature and stirred for 3 days. The crude residue was purified by column chromatography [silica, dichloromethane: methanol (95:5)] to yield a yellow solid (60.0 mg, 33.2 μmol, 45 %). ^{1}H NMR (500 MHz, Chloroform-*d*) δ 9.37 (s, 2H, H_f), 8.80 – 8.73 (m, 4H, H_a), 8.56 (d, *J* = 8.8 Hz, 4H, H_d), 7.82 (ddd, *J* = 8.8, 6.6, 1.3 Hz, 4H, H_c), 7.76 (ddd, *J* = 8.7, 6.6, 1.0 Hz, 4H, H_b), 6.98 (t, *J* = 1.7 Hz, 2H, H_h), 6.87 (s, 10H, H_1), 6.79 (d, *J* = 8.8 Hz, 4H, H_e), 6.75 (t, *J* = 1.9 Hz, 2H, H_g), 3.92 – 3.79 (m, 20H, H_3), 3.72 (s, 10H, H_2), 2.64 (dd, *J* = 11.0, 6.7 Hz, 4H, H_i), 1.29 (t, *J* = 7.0 Hz, 30H, H_4), 0.28 (s, 4H, H_j), -0.25 (s, 4H, H_k) ppm. ^{13}C NMR (126 MHz, Chloroform-*d*) δ 150.16,

135.11, 131.74, 130.58, 130.34, 129.48, 128.60, 127.72, 127.54, 123.46, 122.79, 122.24, 120.47, 116.93, 66.09, 48.66, 45.61, 29.40, 28.95, 24.69, 15.52 ppm. ESI-MS (positive mode) m/z calc'd. for $C_{97}H_{110}O_{10}N_4Br_2$ $[M]^{2+}$: 824.8217, found: 824.3210.

Synthesis of [2]rotaxane.2Br [**4.12**]

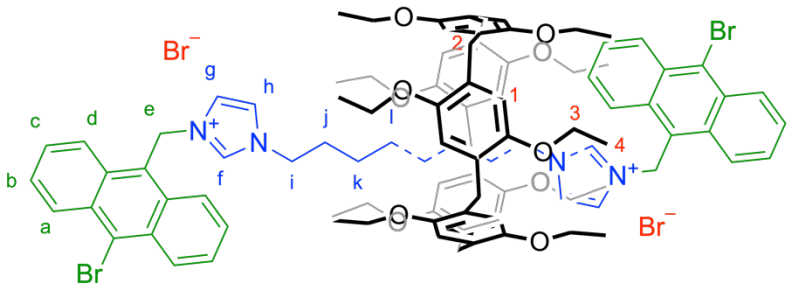

Diethoxypillar[5]arene (356 mg, 400 μmol) and 1,8-di(1*H*-imidazol-1-yl)octane (49.0 mg, 199 μmol) was dissolved in chloroform (2 mL). The solution was cooled to -15 °C and under the exclusion of light, 9-bromo-10(bromomethyl)anthracene (130 mg, 371 μmol) was added. The mixture was left to warm to room temperature and stirred for 3 days. The crude residue was purified by column chromatography [silica, dichloromethane: methanol (95:5)] to yield a yellow solid (255 mg, 139 μmol, 70 %). ^{1}H NMR (500 MHz, Chloroform-*d*) δ 8.83 (s, 2H, H_f), 8.81 – 8.74 (m, 4H, H_a), 8.49 – 8.44 (m, 4H, H_d), 7.82 (ddd, *J* = 8.8, 6.5, 1.3 Hz, 4H, H_c), 7.77 (ddd, *J* = 8.8, 6.5, 1.1 Hz, 4H, H_b), 7.07 (d, *J* = 3.1 Hz, 2H, H_h), 6.91 (s, 10H, H_1), 6.65 (s, 4H, H_e), 6.32 (t, *J* = 1.8 Hz, 2H, H_g), 3.88 (qd, *J* = 6.8, 2.7 Hz, 20H, H_3), 3.78 (s, 10H, H_2), 2.38 (s, 4H, H_i), 1.37 (t, *J* = 7.0 Hz, 30H, H_4), 1.06 (d, *J* = 7.0 Hz, 4H, H_l), 0.78 (s, 4H, H_k), 0.50 (s, 4H, H_j) ppm. ^{13}C NMR (126 MHz, Chloroform-*d*) δ 150.18, 134.61, 131.78, 130.62, 130.26, 129.55, 128.59, 127.88, 127.54, 123.31, 123.27, 122.21, 119.24, 116.63, 65.89, 48.60, 45.19, 30.00, 29.38, 29.13, 26.90, 15.58 ppm. ESI-MS (positive mode) m/z calc'd. for $C_{99}H_{114}O_{10}N_4Br_2$ $[M]^{2+}$: 838.3357, found: 838.3388.

Synthesis of [2]rotaxane.2PF_6 [**4.13**]

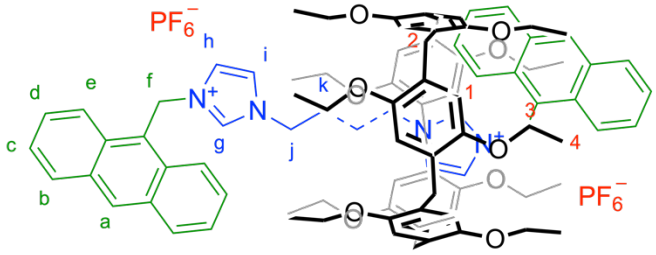

[2]Rotaxane [**4.7**] (40.0 mg, 24.6 μmol) was suspended in ethanol (35 mL) and heated to 60 °C until it dissolved. A saturated solution of ammonium hexafluorophosphate (1.00 g, 6.13 mmol) in ethanol (15 mL) was slowly pipetted into the hot ethanolic solution and heated for 30 mins. It was left to cool, the white solid was collected by vacuum filtration and then subjected to a silica plug [silica, dichloromethane: methanol (93:7)] to yield a beige solid (21.0 mg, 12.0 μmol, 48 %). ^{1}H NMR (400 MHz, DMSO-d_6) δ 9.00 (s, 2H, H_a), 8.50 (d, J = 8.9 Hz, 4H, H_b), 8.34 (d, J = 8.4 Hz, 4H, H_e), 8.20 (t, J = 1.7 Hz, 2H, H_g), 7.85 (ddd, J = 8.7, 6.6, 1.3 Hz, 4H, H_c), 7.73 (dd, J = 8.5, 6.5 Hz, 4H, H_d), 7.52 (t, J = 1.8 Hz, 2H, H_h), 6.82 (s, 10H, H_1), 6.69 (s, 4H, H_f), 6.46 (d, J = 2.0 Hz, 2H, H_i), 3.81 – 3.59 (m, 30H, $H_{2,3}$), 1.68 (d, J = 8.0 Hz, 4H, H_j), 1.11 (t, J = 6.9 Hz, 30H, H_4), -0.96 (d, J = 8.4 Hz, 4H, H_k) ppm. ^{19}F NMR (376 MHz, DMSO-d_6) δ -69.20, -71.09 ppm. ^{31}P NMR (162 MHz, DMSO-d_6) δ -131.01, -135.40, -139.80, -144.19, -148.58, -152.97, -157.36 ppm. ^{13}C NMR (101 MHz, DMSO-d_6) δ 149.95, 133.70, 131.69, 131.31, 131.17, 130.35, 130.29, 128.63, 126.34, 123.60, 123.24, 122.92, 120.77, 116.75, 65.77, 46.91, 45.92, 29.35, 23.67, 15.31 ppm. ESI-MS (positive mode) m/z calc'd. for $C_{95}H_{106}O_{10}N_4$ $[M]^{2+}$: 731.8966, found: 731.8959.

Synthesis of [2]rotaxane.2PF_6 [**4.14**]

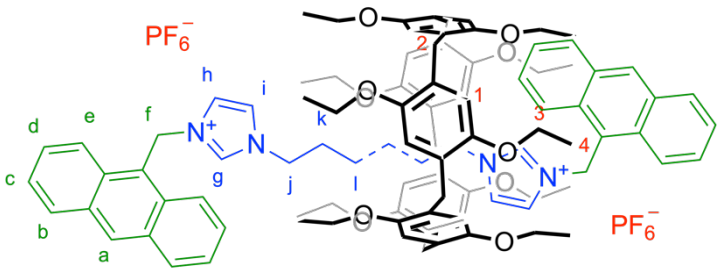

[2]Rotaxane [**4.8**] (86.0 mg, 52.1 μmol) was suspended in ethanol (35 mL) and heated to 70 °C until it dissolved. A saturated solution of ammonium hexafluorophosphate (1.00 g,

6.13 mmol) in ethanol (15 mL) was slowly pipetted into the hot ethanolic solution and heated for 30 mins. It was left to cool, the white solid was collected by vacuum filtration and then subjected to a silica plug [silica, dichloromethane: methanol (93:7)] to yield a beige solid (69.0 mg, 38.7 µmol, 74 %). ^{1}H NMR (400 MHz, DMSO-d_6) δ 8.97 (s, 2H, H_a), 8.47 (d, J = 8.9 Hz, 4H, H_b), 8.36 – 8.29 (m, 4H, H_e), 8.15 (d, J = 1.7 Hz, 2H, H_g), 7.82 (ddd, J = 8.7, 6.6, 1.3 Hz, 4H, H_c), 7.71 (dd, J = 8.5, 6.5 Hz, 4H, H_d), 7.45 (t, J = 1.8 Hz, 2H, H_h), 6.79 (s, 10H, H_1), 6.67 (t, J = 1.8 Hz, 2H, H_i), 6.60 (s, 4H, H_f), 3.89 – 3.54 (m, 30H, $H_{2,3}$), 2.23 (dd, J = 10.9, 6.2 Hz, 4H, H_j), 1.16 (t, J = 6.9 Hz, 30H, H_4), -0.17 (s, 4H, H_k), -0.35 (s, 4H, H_l) ppm. ^{19}F NMR (376 MHz, DMSO-d_6) δ -69.20, -71.09 ppm. ^{31}P NMR (162 MHz, DMSO-d_6) δ -131.02, -135.41, -139.80, -144.19, -148.59, -152.98, -157.37 ppm. ^{13}C NMR (101 MHz, DMSO-d_6) δ 149.84, 133.97, 131.68, 131.17, 131.13, 130.25, 129.58, 128.52, 126.29, 123.39, 123.09, 122.89, 121.82, 115.99, 65.14, 48.09, 45.63, 29.28, 28.66, 25.17, 15.39 ppm. ESI-MS (positive mode) m/z calc'd. for $C_{97}H_{110}O_{10}N_4$ $[M]^{2+}$: 745.9122, found: 745.9112.

Synthesis of [2]rotaxane.2PF_6 [**4.15**]

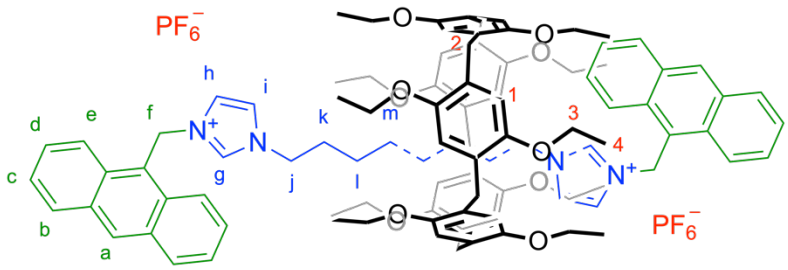

[2]Rotaxane [**4.9**] (151 mg, 89.9 µmol) was dissolved in ethanol (35 mL). A saturated solution of ammonium hexafluorophosphate (1.00 g, 6.13 mmol) in ethanol (15 mL) was slowly pipetted into the mixture and heated for 30 mins at 40 °C. It was left to cool, the beige solid was collected by vacuum filtration and then subjected to a silica plug [silica, dichloromethane: methanol (93:7)] to yield a pale yellow solid (158 mg, 87.3 µmol, 97 %). ^{1}H NMR (400 MHz, DMSO-d_6) δ 8.96 (s, 2H, H_a), 8.50 – 8.43 (m, 4H, H_b), 8.31 (dd, J = 8.5, 1.3 Hz, 4H, H_e), 8.19 (d, J = 1.7 Hz, 2H, H_g), 7.81 (ddd, J = 8.9, 6.5, 1.3 Hz, 4H, H_c), 7.76 – 7.65 (m, 4H, H_d), 7.54 (t, J = 1.8 Hz, 2H, H_h), 6.87 (t, J = 1.8 Hz, 2H, H_i), 6.78 (s, 10H, H_1), 6.58 (s, 4H, H_f), 3.86 – 3.55 (m, 30H, $H_{2,3}$), 2.45 – 2.27 (m, 4H, H_j), 1.18 (t, J = 6.9 Hz, 30H, H_4), 0.33 (s, 4H, H_m), -0.03 (s, 8H, $H_{k,l}$) ppm. ^{19}F NMR (376 MHz, DMSO-d_6) δ -69.20, -71.09

ppm. ^{31}P NMR (162 MHz, DMSO-d_6) δ -135.40, -139.80, -139.83, -144.19, -148.58, -152.97, -157.36 ppm. ^{13}C NMR (101 MHz, DMSO-d_6) δ 149.72, 134.18, 131.68, 131.17, 131.07, 130.20, 129.22, 128.48, 126.25, 123.45, 123.20, 122.73, 122.05, 115.47, 64.70, 48.45, 45.58, 31.76, 29.54, 29.23, 28.17, 26.31, 22.56, 15.41, 14.42 ppm. ESI-MS (positive mode) m/z calc'd. for $C_{99}H_{114}O_{10}N_4$ $[M]^{2+}$: 759.9279, found: 759.9300.

Synthesis of [2]rotaxane.2PF_6 [**4.16**]

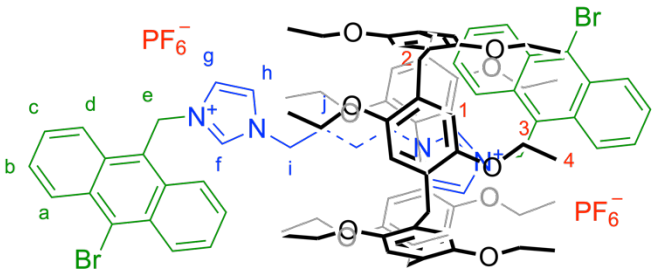

[2]Rotaxane [**4.10**] (184 mg, 103 μmol) was suspended in ethanol (35 mL) and heated to 100 °C until it dissolved. A saturated solution of ammonium hexafluorophosphate (1.00 g, 6.13 mmol) in ethanol (15 mL) was slowly pipetted into the hot ethanolic solution and refluxed for 30 mins. It was left to cool, the pale yellow solid was collected by vacuum filtration and then subjected to a silica plug [silica, dichloromethane: methanol (93:7)] to yield a pale yellow solid (136 mg, 71.1 μmol, 69 %). ^{1}H NMR (400 MHz, DMSO-d_6) δ 8.77 – 8.69 (m, 4H, H_a), 8.58 – 8.50 (m, 4H, H_d), 8.19 (d, J = 1.8 Hz, 2H, H_f), 7.98 – 7.88 (m, 8H, $H_{b,c}$), 7.55 (t, J = 1.8 Hz, 2H, H_g), 6.84 (s, 10H, H_1), 6.73 (s, 4H, H_e), 6.49 (t, J = 1.9 Hz, 2H, H_h), 3.81 – 3.59 (m, 30H, $H_{2,3}$), 1.69 (s, 4H, H_i), 1.12 (t, J = 6.9 Hz, 30H, H_4), -0.94 (s, 4H, H_j) ppm. ^{19}F NMR (376 MHz, DMSO-d_6) δ -69.21, -71.10 ppm. ^{31}P NMR (162 MHz, DMSO-d_6) δ -131.02, -135.41, -139.80, -144.19, -148.59, -152.98, -157.37 ppm. ^{13}C NMR (101 MHz, DMSO-d_6) δ 149.99, 133.82, 131.87, 130.49, 130.36, 129.18, 128.99, 128.80, 126.88, 124.17, 124.10, 123.72, 120.80, 116.86, 65.86, 55.38, 46.94, 45.99, 29.37, 23.75, 15.35 ppm. ESI-MS (positive mode) m/z calc'd. for $C_{95}H_{106}O_{10}N_4Br_2$ $[M]^{2+}$: 810.3044, found: 810.2996.

Synthesis of [2]rotaxane.2PF_6 [**4.17**]

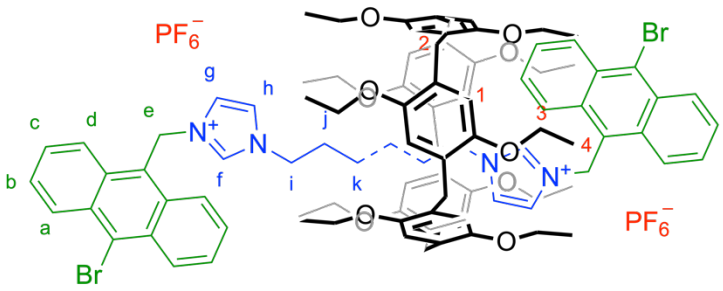

[2]Rotaxane [**4.11**] (157 mg, 86.8 μmol) was suspended in ethanol (35 mL) and heated to 70 °C until it dissolved. A saturated solution of ammonium hexafluorophosphate (1.00 g, 6.13 mmol) in ethanol (15 mL) was slowly pipetted into the hot ethanolic solution and heated for 30 mins. It was left to cool, the pale yellow solid was collected by vacuum filtration and then subjected to a silica plug [silica, dichloromethane: methanol (93:7)] to yield a yellow solid (132 mg, 68.1 μmol, 78 %). ^{1}H NMR (400 MHz, DMSO-d_6) δ 8.75 – 8.66 (m, 4H, H_a), 8.61 – 8.48 (m, 4H, H_d), 8.08 (d, J = 1.7 Hz, 2H, H_f), 7.97 – 7.86 (m, 8H, $H_{b,c}$), 7.51 (s, 2H, H_g), 6.80 (s, 10H, H_1), 6.73 (t, J = 1.9 Hz, 2H, H_h), 6.64 (s, 4H, H_e), 3.82 – 3.61 (m, 30H, $H_{2,3}$), 2.22 (dd, J = 10.9, 6.3 Hz, 4H, H_i), 1.17 (t, J = 6.9 Hz, 30H, H_4), -0.16 (s, 4H, H_j), -0.33 (d, J = 6.7 Hz, 4H, H_k) ppm. ^{19}F NMR (376 MHz, DMSO-d_6) δ -69.21, -71.10 ppm. ^{31}P NMR (162 MHz, DMSO-d_6) δ -131.02, -135.41, -139.80, -144.19, -148.59, -152.98, -157.37 ppm. ^{13}C NMR (101 MHz, DMSO-d_6) δ 149.87, 134.00, 131.88, 130.47, 129.64, 129.07, 128.89, 128.75, 126.70, 124.37, 124.27, 123.09, 121.85, 116.07, 65.22, 48.11, 45.72, 29.29, 28.67, 25.19, 15.41 ppm. ESI-MS (positive mode) m/z calc'd. for $C_{97}H_{110}O_{10}N_4Br_2$ $[M]^{2+}$: 824.8217, found: 824.3118.

Synthesis of [2]rotaxane.2PF_6 [**4.18**]

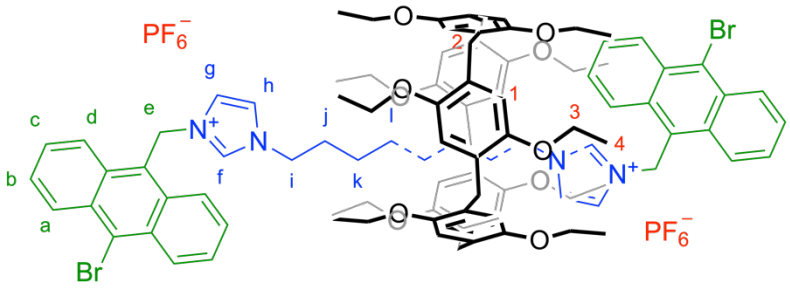

[2]Rotaxane [**4.12**] (255 mg, 139 μmol) was suspended in ethanol (35 mL) and heated to 80 °C until it dissolved. A saturated solution of ammonium hexafluorophosphate (1.00 g, 6.13 mmol) in ethanol (15 mL) was slowly pipetted into the hot ethanolic solution and heated for 30 mins. It was left to cool, the lime-yellow solid was collected by vacuum filtration and then subjected to a silica plug [silica, dichloromethane: methanol (93:7)] to yield a bright yellow solid (161 mg, 81.8 μmol, 59 %). ^{1}H NMR (400 MHz, DMSO-d_6) δ 8.76 – 8.66 (m, 4H, H_a), 8.57 – 8.46 (m, 4H, H_d), 8.11 (d, J = 1.7 Hz, 2H, H_f), 7.94 – 7.85 (m, 8H, $H_{b,c}$), 7.60 (t, J = 1.8 Hz, 2H, H_g), 6.92 (d, J = 1.8 Hz, 2H, H_h), 6.79 (s, 10H, H_1), 6.62 (s, 4H, H_e), 3.88 – 3.55 (m, 30H, $H_{2,3}$), 2.35 (d, J = 7.0 Hz, 4H, H_i), 1.18 (t, J = 6.9 Hz, 30H, H_4), 0.34 (s, 4H, H_l), -0.03 (s, 8H, $H_{j,k}$) ppm. ^{19}F NMR (376 MHz, DMSO-d_6) δ -69.21, -71.09 ppm. ^{31}P NMR (162 MHz, DMSO-d_6) δ -131.02, -135.41, -139.80, -144.19, -148.58, -152.97, -157.37 ppm. ^{13}C NMR (101 MHz, DMSO-d_6) δ 149.75, 134.22, 131.87, 130.47, 129.29, 129.03, 128.86, 128.71, 126.64, 124.49, 124.33, 122.93, 122.09, 115.56, 64.79, 48.48, 45.65, 29.52, 29.25, 28.19, 26.32, 15.42 ppm. ESI-MS (positive mode) m/z calc'd. for $C_{99}H_{114}O_{10}N_4Br_2$ $[M]^{2+}$: 838.3357, found: 838.3280.

Synthesis of [2]rotaxane.2I [**4.19**]

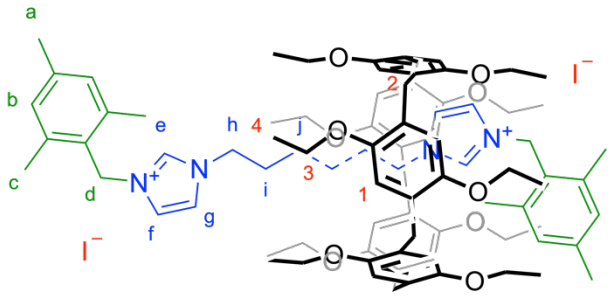

Diethoxypillar[5]arene (300 mg, 337 μmol) and 1,6-di(1*H*-imidazol-1-yl)hexane (32.0 mg, 147 μmol) was dissolved in chloroform (0.8 mL). The solution was cooled to -15 °C and under the exclusion of light, 2-(iodomethyl)-1,3,5-trimethylbenzene (114 mg, 440 μmol) was added. The mixture was left to warm to room temperature and stirred for 3 days. The crude residue was purified by column chromatography [silica, dichloromethane: methanol (98.5:1.5) to (96:4)] to yield a yellow solid (87.0 mg, 53.4 μmol, 36 %). ^{1}H NMR (400 MHz, Chloroform-*d*) δ 8.53 (s, 2H, H_e), 7.01 (s, 4H, H_b), 6.89 (s, 10H, H_1), 6.51 (t, *J* = 1.8 Hz, 2H, H_f), 6.28 (t, *J* = 1.8 Hz, 2H, H_g), 5.57 – 5.36 (m, 4H, H_d), 3.96 (ddq, *J* = 38.9, 9.6, 7.0 Hz, 20H, H_3), 3.73 (s, 10H, H_2), 2.76 – 2.60 (m, 4H, H_h), 2.40 (s, 12H, H_c), 2.37 (s, 6H, H_a), 1.45 (t, *J* = 6.9 Hz, 30H, H_4), 0.83 – 0.72 (m, 4H, H_i), 0.69 (t, *J* = 4.7 Hz, 4H, H_j) ppm. ^{13}C NMR (101 MHz, Chloroform-*d*) δ 150.31, 140.08, 138.06, 134.20, 130.28, 129.96, 125.46, 122.64, 119.73, 117.08, 66.19, 48.35, 47.40, 29.43, 29.32, 25.86, 21.11, 20.00, 15.74 ppm. ESI-MS (positive mode) m/z calc'd. for $C_{87}H_{114}O_{10}N_4$ $[M]^{2+}$: 686.4262, found: 687.4335.

Synthesis of [2]rotaxane.2PF_6 [**4.20**]

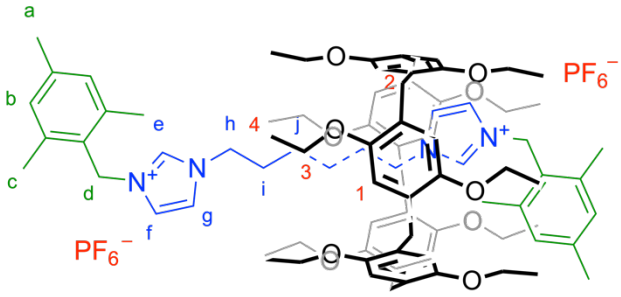

[2]Rotaxane [**4.19**] (69.0 mg, 42.0 μmol) was suspended in ethanol (35 mL) and heated to 70 °C until it dissolved. A saturated solution of ammonium hexafluorophosphate (1.00 g, 6.13 mmol) in ethanol (15 mL) was slowly pipetted into the hot ethanolic solution and

heated for 30 mins. It was then left to cool and the white solid was collected by vacuum filtration (67.0 mg, 40.2 μmol, 95 %). ^{1}H NMR (400 MHz, Chloroform-*d*) δ 7.55 (d, *J* = 2.0 Hz, 2H, H_e), 7.03 (s, 4H, H_b), 6.88 (s, 10H, H_1), 6.43 (t, *J* = 1.8 Hz, 2H, H_f), 5.82 (d, *J* = 1.9 Hz, 2H, H_g), 5.43 – 5.21 (m, 4H, H_d), 4.04 – 3.84 (m, 20H, H_3), 3.73 (s, 10H, H_2), 2.52 (t, *J* = 7.8 Hz, 4H, H_h), 2.38 (s, 18H, $H_{a,c}$), 1.43 (t, *J* = 6.9 Hz, 30H, H_4), 0.76 (s, 8H, $H_{i,j}$) ppm. ^{19}F NMR (376 MHz, Chloroform-*d*) δ -71.46, -73.35 ppm. ^{31}P NMR (162 MHz, Chloroform-*d*) δ -130.99, -135.39, -139.79, -144.19, -148.59, -152.99, -157.38 ppm. ^{13}C NMR (101 MHz, Chloroform-*d*) δ 150.33, 140.19, 138.09, 133.71, 130.29, 129.99, 125.19, 122.17, 119.79, 117.07, 66.04, 48.41, 47.12, 29.30, 29.14, 26.01, 21.09, 19.64, 15.34 ppm. ESI-MS (positive mode) m/z calc'd. for $C_{87}H_{114}O_{10}N_4$ $[M]^{2+}$: 686.4262, found: 687.4265.

Synthesis of dumbbell.2I [**4.21**]

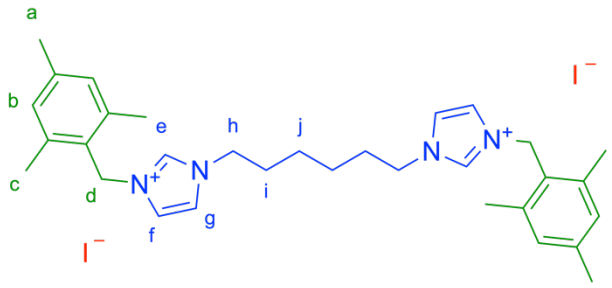

1,6-Di(1*H*-imidazol-1-yl)hexane (250 mg, 1.15 mmol) was dissolved in chloroform (10 mL) and 2-(iodomethyl)-1,3,5-trimethylbenzene (745 mg, 2.86 mmol) was refluxed overnight. It was left to cool and the solvent was removed under reduced pressure. The crude solid was recrystallised using hot ethanol and the off-white crystals were collected by vacuum filtration (469 mg, 635 μmol, 55 %). ^{1}H NMR (400 MHz, Chloroform-*d*) δ 10.19 (d, *J* = 1.7 Hz, 2H, H_e), 7.85 (t, *J* = 1.8 Hz, 2H, H_g), 6.95 (s, 4H, H_b), 6.78 (t, *J* = 1.8 Hz, 2H, H_f), 5.55 (s, 4H, H_d), 4.49 (dd, *J* = 8.2, 6.6 Hz, 4H, H_h), 2.31 (d, *J* = 3.3 Hz, 18H, $H_{a,c}$), 2.11 (p, *J* = 7.0 Hz, 4H, H_i), 1.65 – 1.50 (m, 4H, H_j) ppm. ^{13}C NMR (101 MHz, Chloroform-*d*) δ 140.02, 138.13, 136.08, 130.01, 125.18, 123.19, 120.38, 49.79, 48.09, 29.45, 24.67, 21.06, 20.13 ppm. ESI-MS (positive mode) m/z calc'd. for $C_{32}H_{44}N_4$ $[M]^{2+}$: 242.1778, found: 242.1791.

Synthesis of dumbbell.2PF_6 [**4.22**]

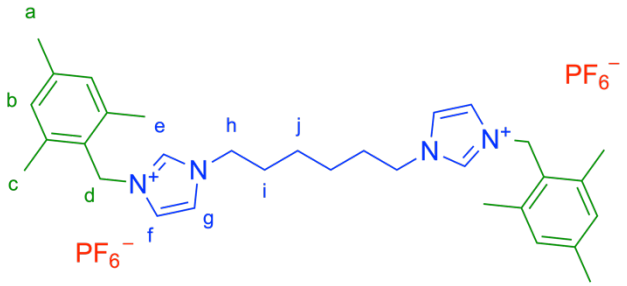

Dumbbell [**4.21**] (276 mg, 374 μmol) was suspended in ethanol (10 mL) and heated to 55 ^{o}C until it was dissolved and a saturated solution of ammonium hexafluorophosphate (1.00 g, 6.13 mmol) in ethanol (10 mL) was slowly pipetted into the hot ethanolic solution and heated for 30 mins. It was then left to cool and the white solid was collected by vacuum filtration (263 mg, 340 μmol, 91 %). ^{1}H NMR (400 MHz, Acetonitrile-d_3) δ 8.19 (d, J = 1.7 Hz, 2H, H_e), 7.39 (t, J = 1.8 Hz, 2H, H_g), 7.27 (t, J = 1.9 Hz, 2H, H_f), 7.04 (s, 4H, H_b), 5.34 (s, 4H, H_d), 4.12 – 3.98 (m, 4H, H_h), 2.28 (s, 12H, H_c), 2.17 (s, 6H, H_a), 1.85 – 1.73 (m, 4H, H_i), 1.29 (dq, J = 7.5, 3.6 Hz, 4H, H_j) ppm. ^{19}F NMR (376 MHz, Acetonitrile-d_3) δ -71.93, -73.81 ppm. ^{31}P NMR (162 MHz, Acetonitrile-d_3) δ -131.52, -135.89, -140.25, -144.62, -148.98, -153.34, -157.70 ppm. ^{13}C NMR (101 MHz, Acetonitrile-d_3) δ 139.84, 138.45, 134.70, 129.64, 125.87, 122.58, 122.23, 49.48, 47.58, 29.30, 25.04, 20.12, 18.71 ppm. ESI-MS (positive mode) m/z calc'd. for $C_{32}H_{44}N_4$ $[M]^{2+}$: 242.1778, found: 242.1802.

4.5 References

1 G. W. Breton and X. Vang, *J. Chem. Educ.*, 1998, **75**, 81–82.

2 I. Zouev, D.-K. Cao, T. V. Sreevidya, M. Telzhensky, M. Botoshansky and M. Kaftory, *CrystEngComm*, 2011, **13**, 4376.

3 H. Bouas-Laurent, A. Castellan, J. P. Desvergne and R. Lapouyade, *Chem. Soc. Rev.*, 2000, **29**, 43–55.

4 A. C. Benniston, A. Harriman and V. M. Lynch, *J. Am. Chem. Soc.*, 1995, **117**, 5275–5291.

5 R. Ballardini, V. Balzani, W. Dehaen, A. E. E. Dell'Erba, F. M. M. Raymo, J. F. Stoddart and M. Venturi, *European J. Org. Chem.*, 2000, **2000**, 591–602.

6 C. Ke, R. A. Smaldone, T. Kikuchi, H. Li, A. P. Davis and J. F. Stoddart, *Angew. Chemie - Int. Ed.*, 2013, **52**, 381–387.

7 P. Wei, X. Yan and F. Huang, *Chem. Commun.*, 2014, **50**, 14105–14108.

8 J. F. Xu, Y. Z. Chen, L. Z. Wu, C. H. Tung and Q. Z. Yang, *Org. Lett.*, 2013, **15**, 6148–6151.

9 C. Li, S. Chen, J. Li, K. Han, M. Xu, B. Hu, Y. Yu and X. Jia, *Chem. Commun.*, 2011, **47**, 11294–11296.

10 C. L. Sun, H. Q. Peng, L. Y. Niu, Y. Z. Chen, L. Z. Wu, C. H. Tung and Q. Z. Yang, *Chem. Commun.*, 2018, **54**, 1117–1120.

11 N. Song, D.-X. X. Chen, M.-C. C. Xia, X.-L. L. Qiu, K. Ma, B. Xu, W. Tian and Y.-W. W. Yang, *Chem. Commun. (Camb).*, 2014, **51**, 5526–5529.

12 K. Wang, C.-Y. Y. Wang, Y. Zhang, S. X.-A. A. Zhang, B. Yang and Y.-W. W. Yang, *Chem. Commun. (Camb).*, 2014, **50**, 9458–61.

13 J. Bi, X. Zeng, D. Tian and H. Li, *Org. Lett.*, 2016, **18**, 1092–1095.

14 P. Wei, D. Li, B. Shi, Q. Wang and F. Huang, *Chem. Commun.*, 2015, **51**, 15169–15172.

15 M. Steffenhagen, A. Latus, T. M. N. Trinh, I. Nierengarten, I. T. Lucas, S. Joiret, J. Landoulsi, B. Delavaux-Nicot, J. F. Nierengarten and E. Maisonhaute, *Chem. - A Eur. J.*, 2018, **24**, 1701–1708.

16 B. Delavaux-Nicot, H. Ben Aziza, I. Nierengarten, T. Minh Nguyet Trinh, E. Meichsner, M. Chessé, M. Holler, R. Abidi, E. Maisonhaute and J. F. Nierengarten,

Chem. - A Eur. J., 2018, **24**, 133–140.

17 I. Nierengarten, S. Guerra, H. Ben Aziza, M. Holler, R. Abidi, J. Barberá, R. Deschenaux and J. F. Nierengarten, *Chem. - A Eur. J.*, 2016, **22**, 6185–6189.

18 K. Buffet, I. Nierengarten, N. Galanos, E. Gillon, M. Holler, A. Imberty, S. E. Matthews, S. Vidal, S. P. Vincent and J. F. Nierengarten, *Chem. - A Eur. J.*, 2016, **22**, 2955–2963.

19 P. Langer, L. Yang, C. R. Pfeiffer, W. Lewis and N. R. Champness, *Dalt. Trans.*, 2019, **48**, 58–64.

20 D. E. Stack, A. L. Hill, C. B. Diffendaffer and N. M. Burns, *Org. Lett.*, 2002, **4**, 4487–4490.

21 B. Cheng and A. E. Kaifer, *J. Am. Chem. Soc.*, 2015, **137**, 9788–9791.

22 H. Saba, J. An, Y. Yang, M. Xue and Y. Liu, *Chinese J. Chem.*, 2016, **34**, 861–865.

23 N. Pearce, E. S. Davies and N. R. Champness, *Molecules*, 2020, **25**, 1627.

24 N. Mase, K. Takabe and F. Tanaka, *Tetrahedron Lett.*, 2013, **54**, 4306–4308.

25 M. Hosoyamada, N. Yanai, T. Ogawa and N. Kimizuka, *Chem. - A Eur. J.*, 2016, **22**, 2060–2067.

Chapter 5:

Conclusions

5.1 Conclusions

Over the past decade, research into pillararene chemistry has been rapidly developing, especially in the form of mechanically interlocked molecules and molecular machines, a field that had many decades to become establish and was recognised with a Nobel prize being awarded the same year as the research documented within this thesis was begun.

The research described herein used pillar[5]arenes as macrocycles for [n]rotaxanes utilising a toolkit approach where components could be exchanged to build a large library of rotaxanes. From the mechanical bonds present, translational motion of the rings was probed using NMR spectroscopies and studied under different polarities. For rotaxanes that could not be studied using this approach, electrochemical studies were used to probe information about redox activity within the molecule.

The rotaxanes described in chapters 2 and 3 were the result of attempting to make a target molecule like that of **3.Z**, where two [2]rotaxanes would be dimerised via the NHC moieties. This led to the design and synthesis of the [2]rotaxanes described in chapter 3, where a large unencapsulated region along the axle would be required to accommodate two macrocycles within a [3]catenane species. As a result of the statistical assembly of the [2]rotaxanes, [3]rotaxanes were also produced within the same reaction. Once separated, key findings of the [3]rotaxane species included:

- The hydroquinone moiety acted as a spacer, which kept two rings apart and facilitated the formation of the [3]rotaxane.
- Switch-like behaviour can be observed through change in solvent conditions where pillar[5]arenes can be displaced from the imidazolium stations such that they reside over the alkyl chain that links those imidazolium groups.
- An X-ray crystal structure was obtained for one of the [3]rotaxanes and revealed that the macrocycles reside over the alkyl chains between the imidazolium stations and the hydroquinone moiety. To our knowledge, this is the first example of a crystal structure for a pillar[5]arene based [3]rotaxane.

These findings for the [3]rotaxane series should enable more sophisticated molecular machines to be synthesised. The hydroquinone spacer could also be important when attempting to synthesise higher order rotaxanes incorporating pillar[5]arenes. The crystals of the [3]rotaxane that were formed contained both of the P[5]*R* and P[5]*S* diastereosiomers and crystallisation could be used as a method of separating the optically inactive diastereoisomers.

Additionally, the [2]rotaxane species that were described in chapter 3 provided an even greater insight into shuttling behaviour of pillar[5]arenes along the same axles. Key findings included:

- These individual rings are shown to be locked onto a single side of the axle. Shuttling over the hydroquinone spacer is only observed when the imidazolium stations are no longer accessible to the pillar[5]arenes.
- This shuttling process is specific to this system as the hydroquinone spacer behaves as a kinetic barrier, restricting the ring to a single side when the rotaxane is dissolved in chloroform, yet allowing the macrocycle to freely shuttle across the axle when dissolved in DMSO. Swapping the central spacer to a larger group would prevent this type of shuttling.

All of the [2]rotaxanes described in chapter 3 should be ideal candidates for a [3]catenane like **3.Z**. The axle specific shuttling behaviour could also be better understood via the synthesis and analysis of compounds **3.V** – **3.Y**. From our understanding of the reported [2]rotaxanes, the hydroquinone spacer could be used as a kinetic barrier component along an axle, rather than a steric blockade, to provide a ratchet-like environment for pillar[5]arenes.

Another aspect of this project was to expand the library of components that could be used to assemble rotaxanes where pillar[5]arenes were the macrocycles and bis(alkylimidazoles) were axles. By focussing on stopper groups, anthracene was chosen to be used due to its large aromatic core which would be suitable for preventing

macrocyclic dethreading, in addition to being a candidate for photoinduced [4 + 4] cycloaddition reactions to produced polyrotaxane spices. A summary of the results:

- Shuttling could not be studied in the same way for anthracene stoppered [2]rotaxanes since the analogous dumbbell molecules were not soluble in suitable solvents. Thus, the anthracene stoppered rotaxanes were probed electrochemically. Oxidations of the pillar[5]arene macrocycle were modified when threaded around a bis-imidazolium axle and by varying the alkyl chain length between the imidazolium groups these pillar[5]arene oxidation potentials were affected. Oxidations occurred at higher potentials when the pillar[5]arene resided over an imidazolium group. The same oxidation processes occurred at a lower potential when the length of the rod was sufficient for the pillar[5]arene macrocycle to be positioned on the alkyl chain.
- The X-ray crystal structures were determined for some of the anthracene stoppered [2]rotaxanes and the pillar[5]arene was shown to be positioned along the alkyl chain, in the centre of the axle. There was one case where the pillar[5]arene was shifted closer to an imidazolium station, which was attributed to π-π stacking of anthracene moieties to one side of the axle, but misaligned on the other end.
- Fluorescence was studied for all hexafluorophosphate salts of the anthracene stoppered rotaxanes, all of which exhibited fluorescence, but to varying degrees. The bromo-substituted variants had low quantum yield values in relation to their unsubstituted counterparts likely due to quenching from the bromo-anthracene stopper group. A trend was also observed between chain length of the axle and fluorescence quantum yields. The longest octyl chain variants had the highest quantum yields, with the shortest butyl-variants having slightly lower quantum yields as a result of some degree of pillar[5]arene based quenching. The mid-length hexyl-variants produced the least fluorescent rotaxanes which was attributed to quenching from the pillar[5]arenes in addition to unrestricted rotation of the anthracene moieties.

- A [4 + 4] photocycloaddition was trialled in the solid phase and no dimerised product was observed. Many other conditions should be explored before any assessment can be made on whether the confinement of a pillar[5]arene is preventing the reaction from occurring.

The toolkit was greatly expanded as not just one anthracene stopper successfully resulted in rotaxane synthesis, but a second bromo-substituted variant was also successful at preventing macrocyclic slippage. This can greatly increase the number of different combinations of components when building a library of rotaxanes. Likewise, as alternative conditions need to be trialled for the [4 + 4] photocycloaddition reactions, these bromo-variant rotaxanes could provide additional routes, such as cross coupling reactions, in order to form polyrotaxanes.

Overall, the toolkit deployed in this thesis for the fabrication of [n]rotaxane molecular shuttles can be widely adapted for any bis(alkylimidazole) axle and halomethyl aromatic stopper group to confine pillar[5]arenes. The results reported in this thesis should be used to develop more advanced molecular machinery using pillar[5]arenes as macrocycles, where the studied shuttling behaviour could be utilised in the form of ratchets, pumps and other technomimetics.

Chapter 6:

Materials and Methods

6.1 Reagents and purification

All chemicals and dry solvents were purchased from Alfa Aesar, Fischer Scientific, Fluorochem, Sigma-Aldrich and VWR International. Column chromatography was performed on silica gel 60 Å. Ferrocene was purchased from Aldrich and used as received. Reactions sensitive to air and moisture were performed using a standard Schlenk line, with dinitrogen as the inert atmosphere. Glassware was flame dried under vacuum and backfilled with dinitrogen.

6.2 General equipment

6.2.1 NMR spectroscopy

NMR spectra were recorded at room temperature using a Bruker DPX400, AV400, AV(III)400 or AV(III)500 instruments. Deuterated solvents were used as specified. Chemical shifts were reported referenced to solvent residue.

6.2.2 Mass spectrometry

Mass spectrometry was recorded using a Bruker microTOF II.

6.2.3 Absorbance / emission spectroscopy

Standard UV/vis spectra were collected on a Perkin Elmer Lambda 16 spectrophtometer using a 1 cm path length quartz cuvette. Fluorescence was recorded as solutions using a Jobin Yvon Horiba FlurorMax-3 spectrometer at ambient temperature in a 1 cm path length path length quartz cuvette. Quantum yields were measured using a standard method published by Williams, Winfield and Miller.[1]

6.2.4 Electrochemistry

All electrochemical studies were completed in conjunction with Dr. Stephen Davies.

6.2.4.1 Cyclic voltammetry

Cyclic and square wave voltammetry experiments were carried out using an Autolab PGSTA20 under a dinitrogen atmosphere using a three-electrode arrangement in a single

compartment cell. A glassy carbon electrode, a platinum wire secondary electrode and a saturated calomel reference electrode were used in the cell. The reference electrode was chemically isolated from the test solution using a bridge tube terminated with a Vycor frit and containing electrolyte solution. An analyte concentration of ca. 0.5 mM was used with [^{n}Bu$_4$N][BF$_4$] (0.4 M) as support electrolyte. Redox potentials are referenced to the ferrocenium/ferrocene couple used as the internal standard. No compensation was applied for internal resistance.

6.3 X-ray crystallography

6.3.1 Equipment and software

Single crystals were selected and mounted using fomblin film on a micromount. Data were collected with a SuperNova GV1000, Atlas S2 diffractometer where the crystals were kept at 120(2) K during data collection or the Diamond Light Source Beamline I19-1 diffractometer where the crystals were kept at 100(1) or 100(2) K during data collection, respectively. Using Olex 2,[2] the structures were solved by Dr. Stephen Argent using Shell XT[3] structure solution program using Intrinsic Phasing and refined with the ShellXL[4] refinement package using Least Squares minimisation.

6.3.2 Crystal data

2.13 $C_{188}H_{266}I_2N_4O_{22}Cl_6$ (*M* =3400.53 g/mol): monoclinic, space group C2/c (no. 15), *a* = 67.342(13) Å, *b* = 20.631(3) Å, *c* = 13.3292(18) Å, *β* = 92.710(14)°, *V* = 18498(5) Å^3, *Z* = 4, *T* = 120(2) K, μ(CuKα) = 3.964 mm^{-1}, *Dcalc* = 1.221 g/cm^3, 21438 reflections measured (7.846° ≤ 2Θ ≤ 61.834°), 2833 unique (R_{int} = 0.1372, R_{sigma} = 0.0777) which were used in all calculations. The final R_1 was 0.2147 (I > 2σ(I)) and wR_2 was 0.5383 (all data). GoF = 2.160.

Disordered solvent chloroform molecules could not be sensibly modelled and the structure was processed using PLATON SQUEEZE,[5] which gave an estimate of 456 e$^-$ per cell, corresponding to eight chloroform molecules. These molecules were included in the sum formula and calculation of derived parameters.

4.8 $C_{101}H_{112}Br_2Cl_{12}N_4O_{10}$ (*M* =2127.16 g/mol): triclinic, space group P-1 (no. 2), *a* = 12.5827(14) Å, *b* = 20.3273(17) Å, *c* = 23.3832(17) Å, *α* = 72.000(6)°, *β* = 76.248(7)°, *γ* = 88.980(8)°, *V* = 5515.0(8) Å^3, *Z* = 2, *T* = 100(1) K, μ(synchrotron) = 1.076 mm^{-1}, *Dcalc* = 1.281 g/cm^3, 12902 reflections measured (1.83° ≤ 2Θ ≤ 30.722°), 5205 unique (R_{int} = 0.2736, R_{sigma} = 0.2902) which were used in all calculations. The final R_1 was 0.2808 (I > 2σ(I)) and wR_2 was 0.5632 (all data). GoF = 1.586.

Disordered solvent chloroform molecules could not be sensibly modelled and the structure was processed using PLATON SQUEEZE,[5] which gave an estimate of 131 e$^-$ per cell, corresponding to two chloroform molecules. These molecules were included in the sum formula and calculation of derived parameters.

4.9 $C_{103.5}H_{118.5}Br_2Cl_{13.5}N_4O_{10}$ (*M* =2216.91 g/mol): triclinic, space group P-1 (no. 2), *a* = 18.1607(5) Å, *b* = 18.2261(5) Å, *c* = 18.6792(6) Å, *α* = 75.242(3)°, *β* = 78.406(3)°, *γ* = 72.635(2)°, *V* = 5653.8(3) Å^3, *Z* = 2,*T* = 100.0(10) K, μ(Synchrotron) = 1.028 mm^{-1}, *Dcalc* = 1.302 g/cm^3, 24913 reflections measured (2.206° ≤ 2Θ ≤ 38.3°), 10051 unique (R_{int} = 0.1645, R_{sigma} = 0.1863) which were used in all calculations. The final R_1 was 0.1245 (I > 2σ(I)) and wR_2 was 0.3459 (all data). GoF = 1.130.

4.10 $C_{96.5}H_{104.75}Br_4Cl_{4.5}N_4O_{14.69}$ (*M* =2034.79 g/mol): monoclinic, space group P2/n (no. 13), *a* = 30.4278(10) Å, *b* = 14.2645(4) Å, *c* = 48.1330(13) Å, *β* = 92.260(3)°, *V* = 20875.3(7) Å^3, *Z* = 8, *T* = 100(2) K, μ(synchrotron) = 1.585 mm^{-1}, *Dcalc* = 1.295 g/cm^3, 40190 reflections measured (1.564° ≤ 2Θ ≤ 33.36°), 12580 unique (R_{int} = 0.1626, R_{sigma} = 0.1569) which were used in all calculations. The final R_1 was 0.2185 (I > 2σ(I)) and wR_2 was 0.5213 (all data). GoF = 1.836.

4.11 $C_{99}H_{112}Br_4Cl_6N_4O_{10}$ (*M* =2050.26 g/mol): triclinic, space group P-1 (no. 2), *a* = 15.9885(3) Å, *b* = 23.9128(4) Å, *c* = 27.8839(7) Å, *α* = 66.497(2)°, *β* = 84.412(2)°, *γ* = 82.617(2)°, *V* = 9682.9(3) Å^3, *Z* = 4, *T* = 100(1) K, μ(synchrotron) = 1.746 mm^{-1}, *Dcalc* = 1.406 g/cm^3, 33575 reflections measured (1.808° ≤ 2Θ ≤ 34.856°), 13127 unique (R_{int} = 0.0715, R_{sigma} = 0.1088) which were used in all calculations. The final R_1 was 0.2275 (I > 2σ(I)) and wR_2 was 0.5552 (all data). GoF = 2.252.

Disordered solvent chloroform molecules could not be sensibly modelled and the structure was processed using PLATON SQUEEZE,[5] which gave an estimate of 131 e^- per cell, corresponding to two chloroform molecules. These molecules were included in the sum formula and calculation of derived parameters.

6.4 References

1 A. T. Rhys Williams, S. A. Winfield and J. N. Miller, *Analyst*, 1983, **108**, 1067–1071.

2 O. V. Dolomanov, L. J. Bourhis, R. J. Gildea, J. A. K. Howard and H. Puschmann, *J. Appl. Crystallogr.*, 2009, **42**, 339–341.

3 G. M. Sheldrick, *Acta Crystallogr. Sect. A Found. Crystallogr.*, 2015, **71**, 3–8.

4 G. M. Sheldrick, *Acta Crystallogr. Sect. C Struct. Chem.*, 2015, **71**, 3–8.

5 A. L. Spek, *Acta Crystallogr. Sect. D Biol. Crystallogr.*, 2009, **65**, 148–155.

Appendix

7.1 NMR spectroscopy

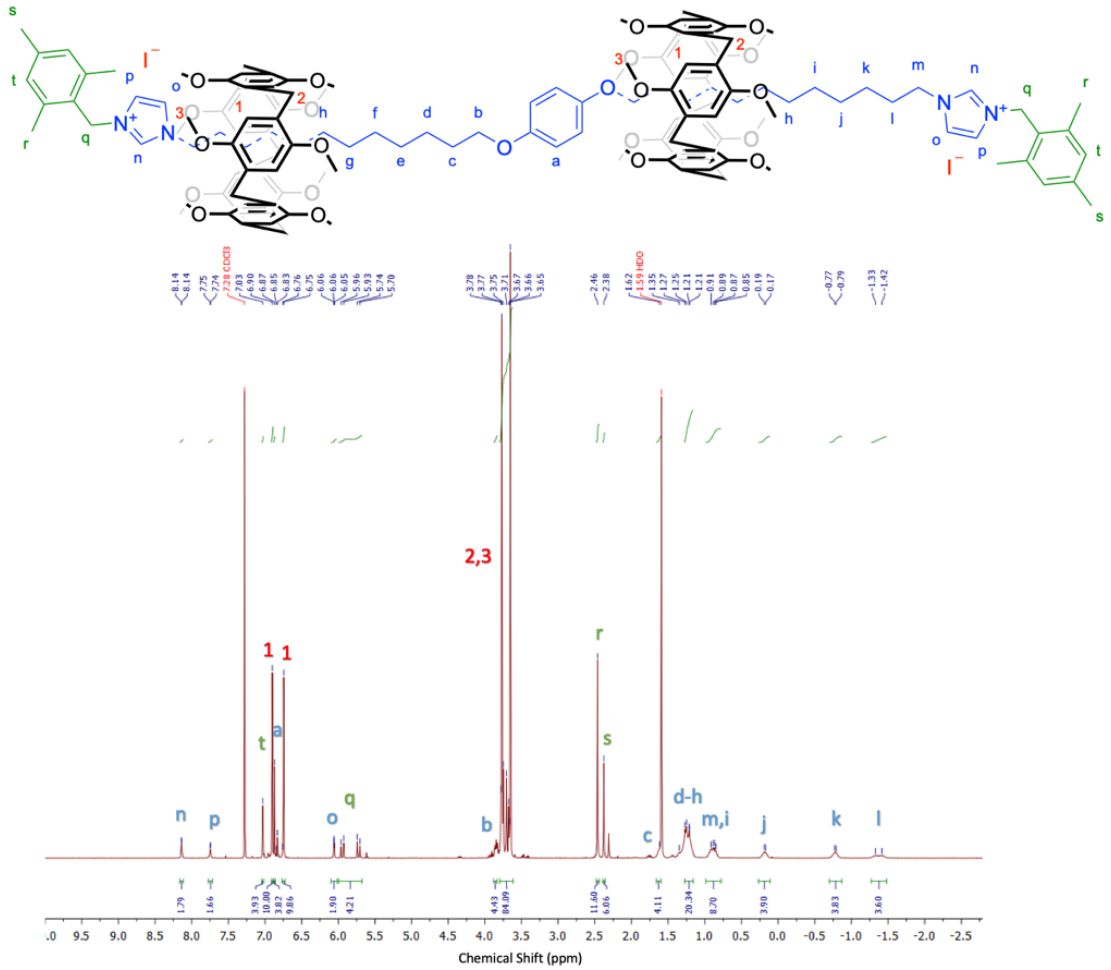

*Figure 7.1. ^{1}H NMR spectrum (400 MHz, $CDCl_3$, 298 K) of **2.11**.*

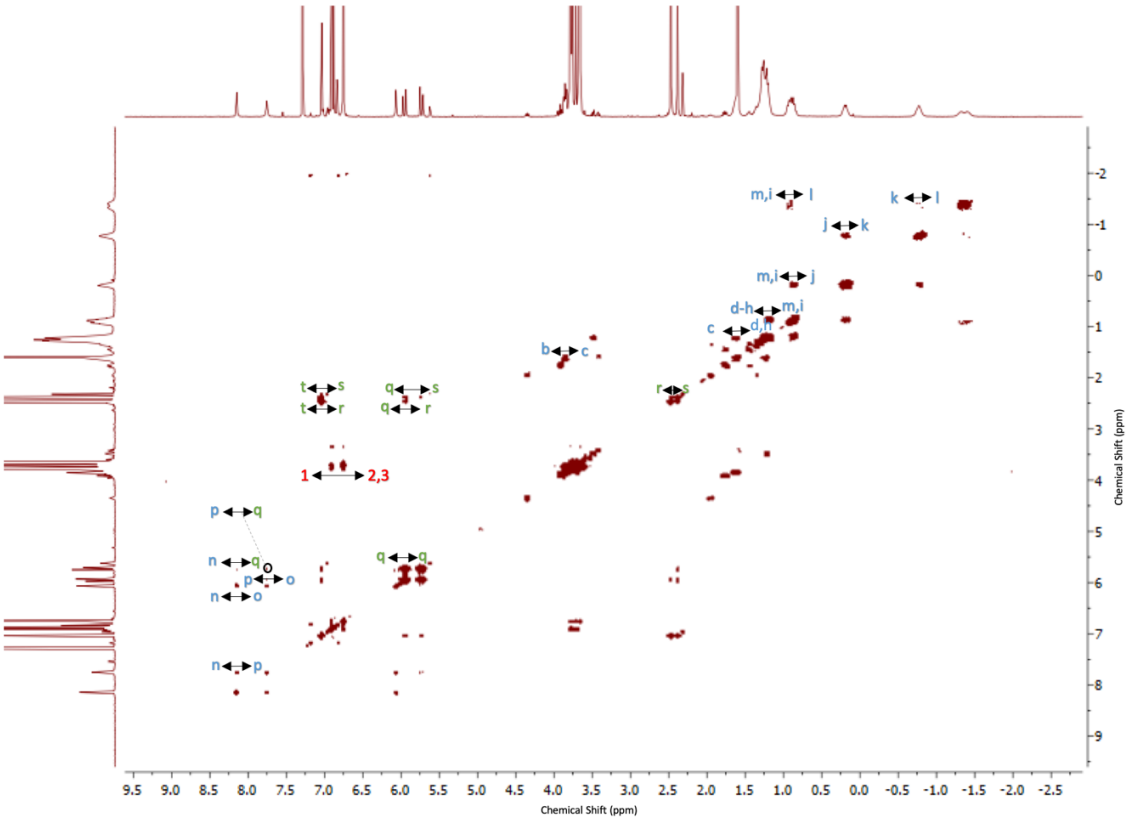

*Figure 7.2. 2D ^{1}H-^{1}H COSY NMR spectrum (400 MHz, $CDCl_3$, 298 K) of **2.11**.*

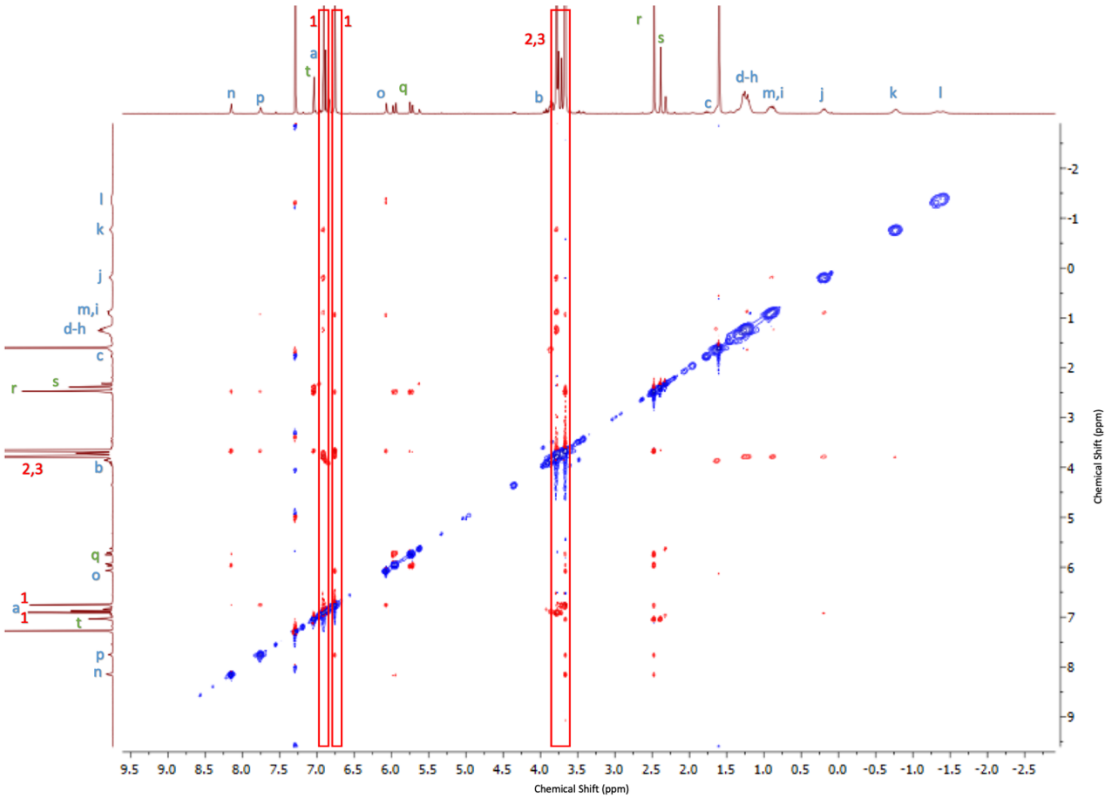

*Figure 7.3. 2D ^{1}H-^{1}H NOESY NMR spectrum (400 MHz, $CDCl_3$, 298 K) of **2.11**.*

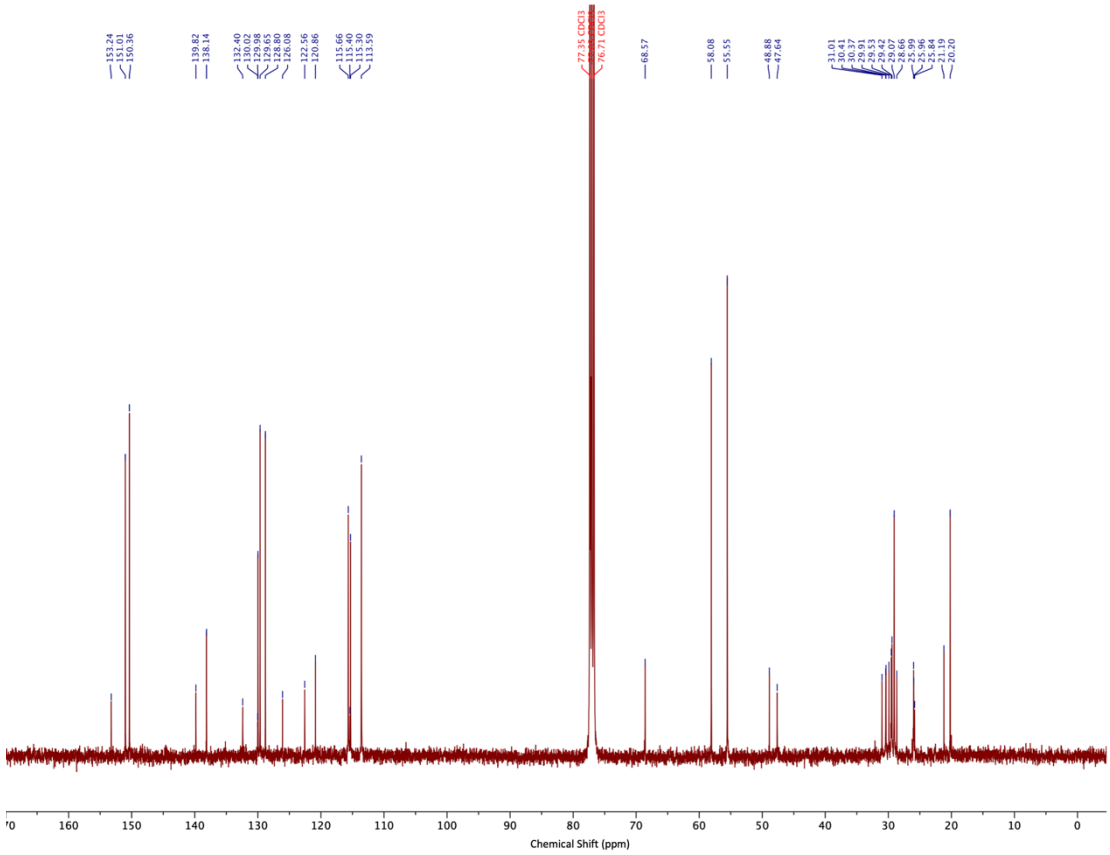

*Figure 7.4. ^{13}C NMR spectrum (101 MHz, $CDCl_3$, 298 K) of **2.11**.*

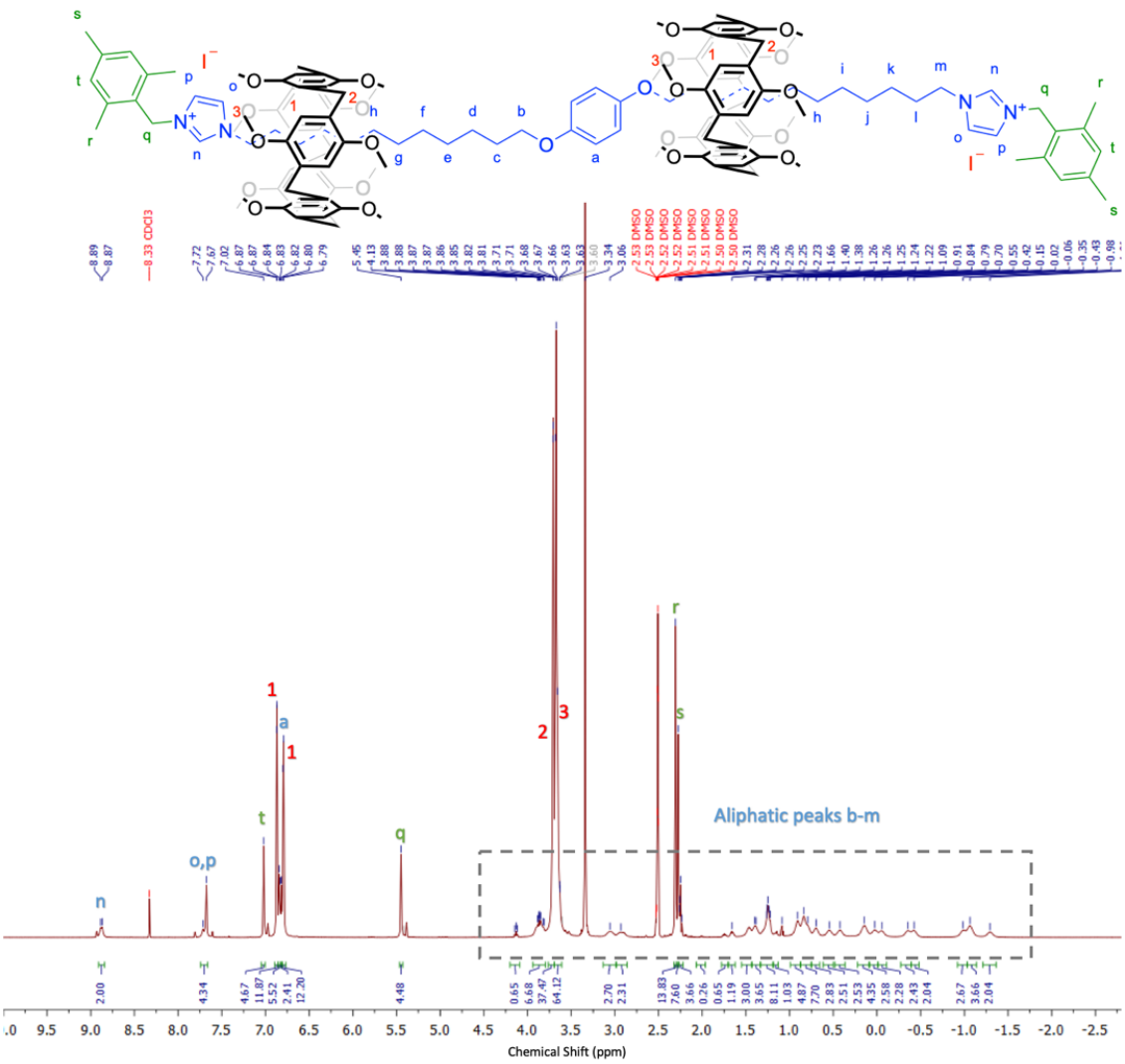

*Figure 7.5. ^{1}H NMR spectrum (500 MHz, DMSO-d_6, 298 K) of **2.11**.*

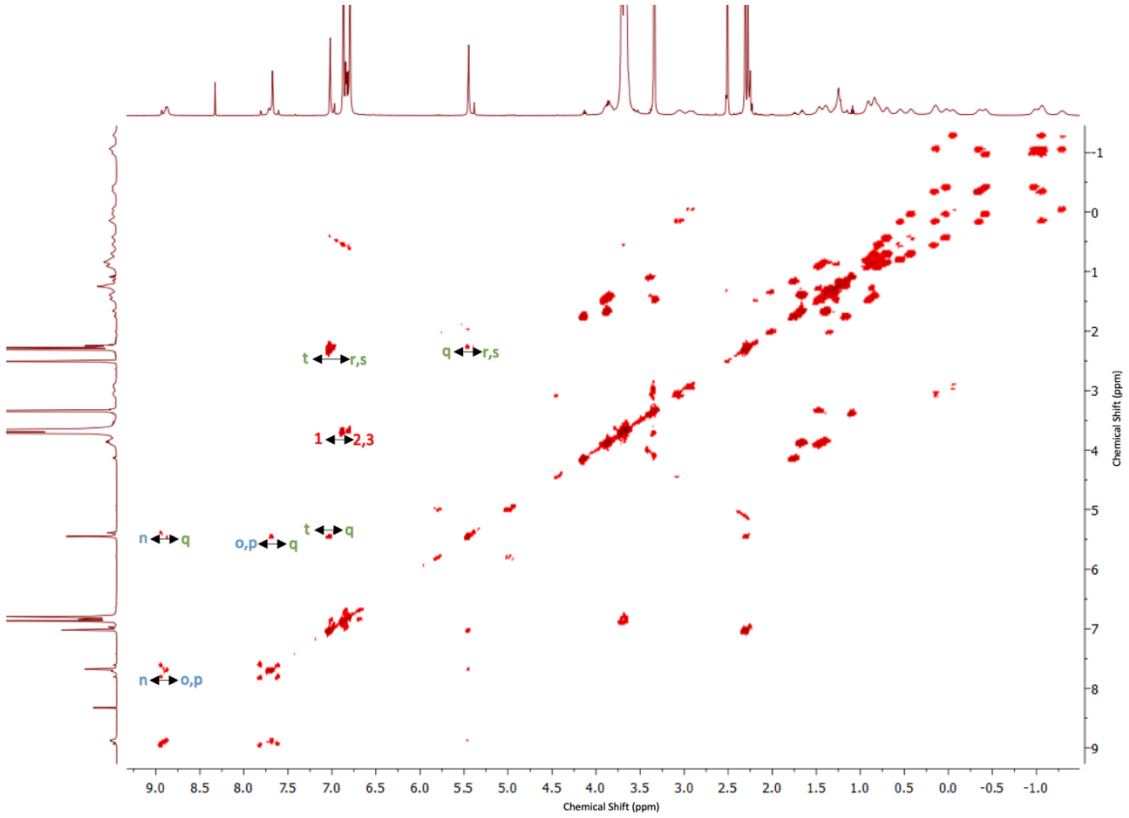

*Figure 7.6. 2D ^{1}H-^{1}H COSY NMR spectrum (500 MHz, DMSO-d_6, 298 K) of **2.11**.*

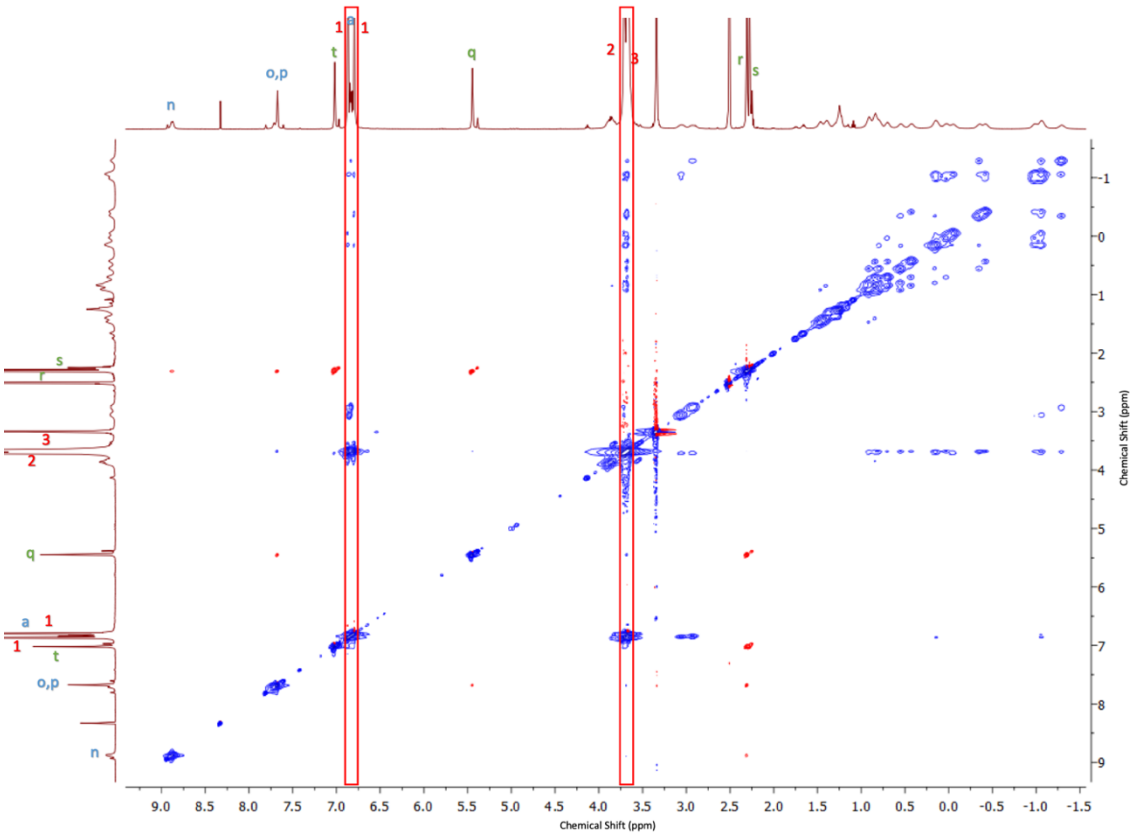

*Figure 7.7. 2D ^{1}H-^{1}H NOESY NMR spectrum (500 MHz, DMSO-d_6, 298 K) of **2.11**.*

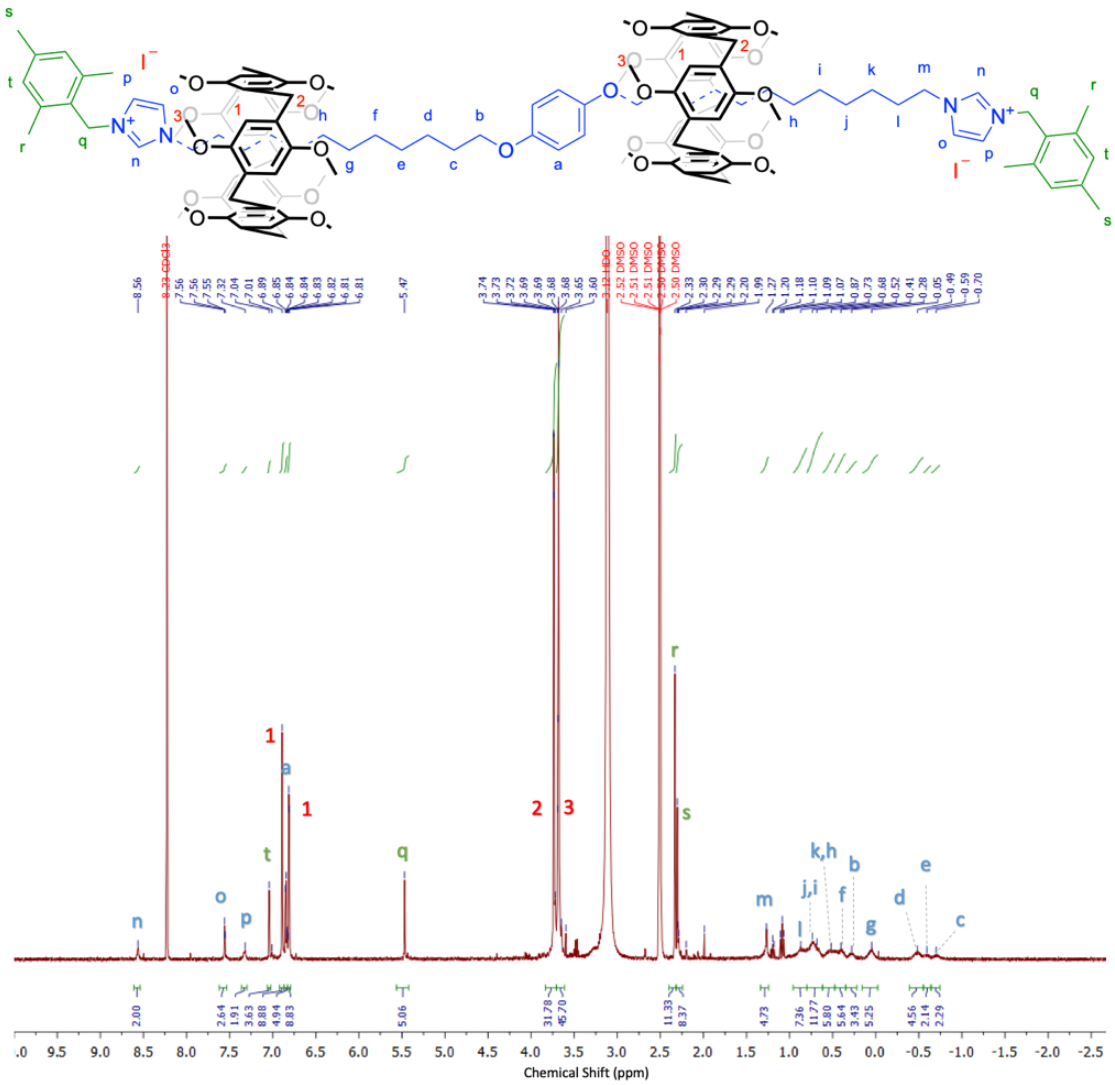

*Figure 7.8. ^{1}H NMR spectrum (600 MHz, DMSO-d_6, 373 K) of **2.11**.*

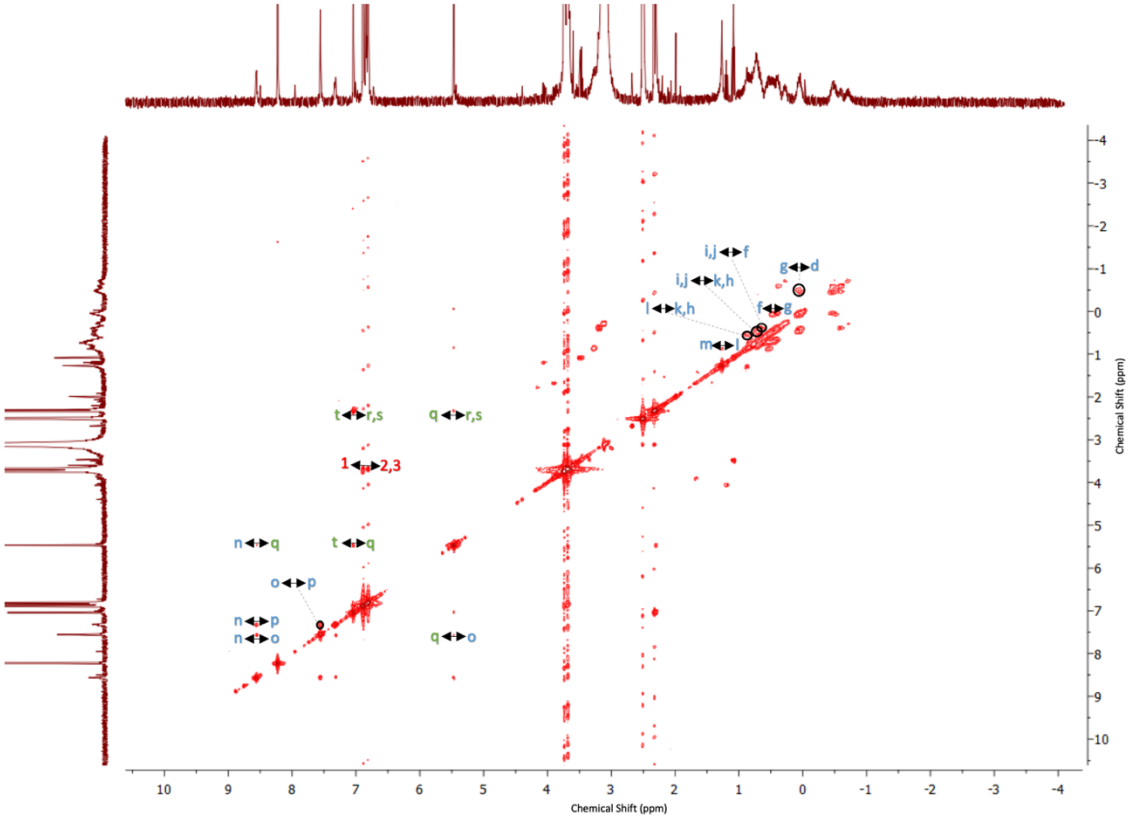

*Figure 7.9. 2D ^{1}H-^{1}H COSY NMR spectrum (600 MHz, DMSO-d_6, 373 K) of **2.11**.*

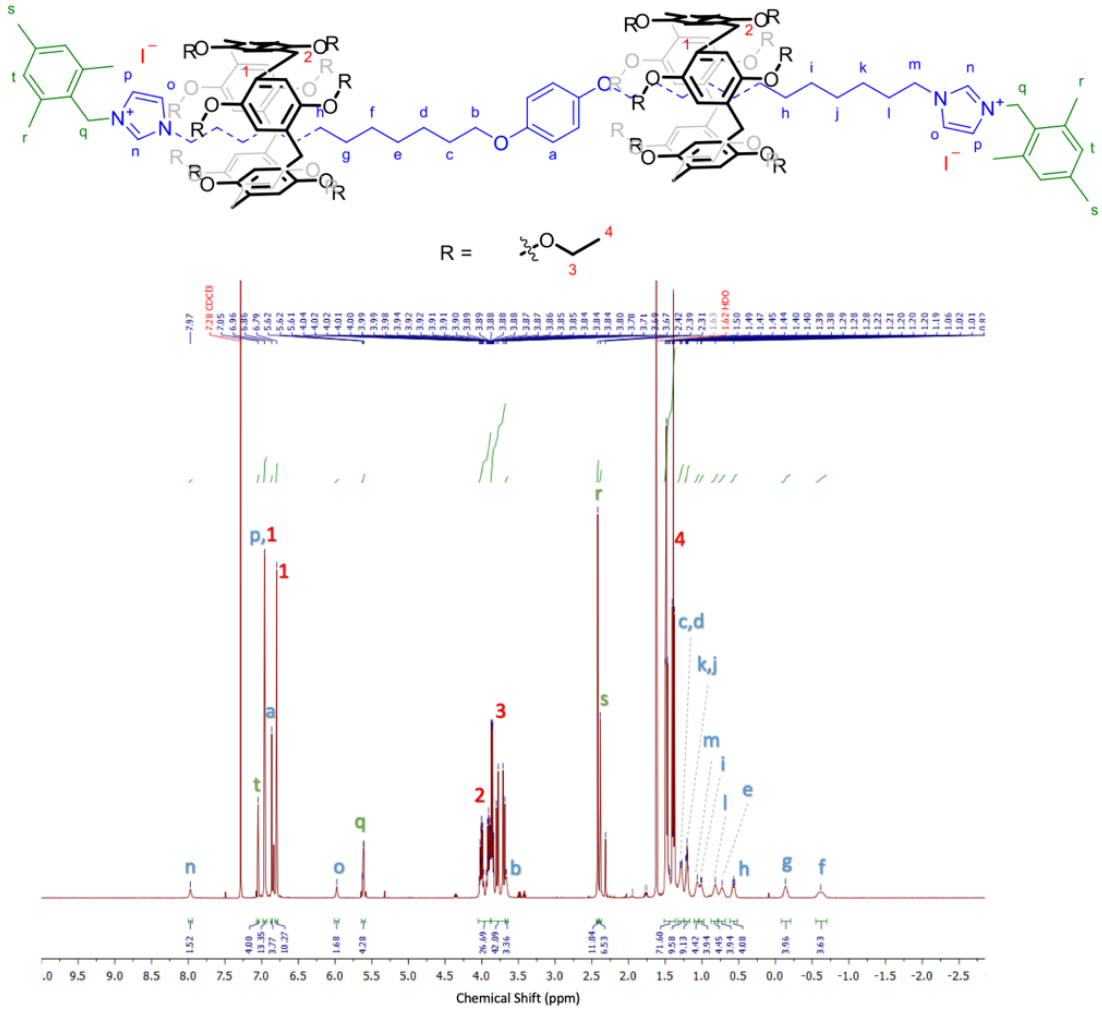

*Figure 7.10. ^{1}H NMR spectrum (500 MHz, $CDCl_3$, 298 K) of **2.12**.*

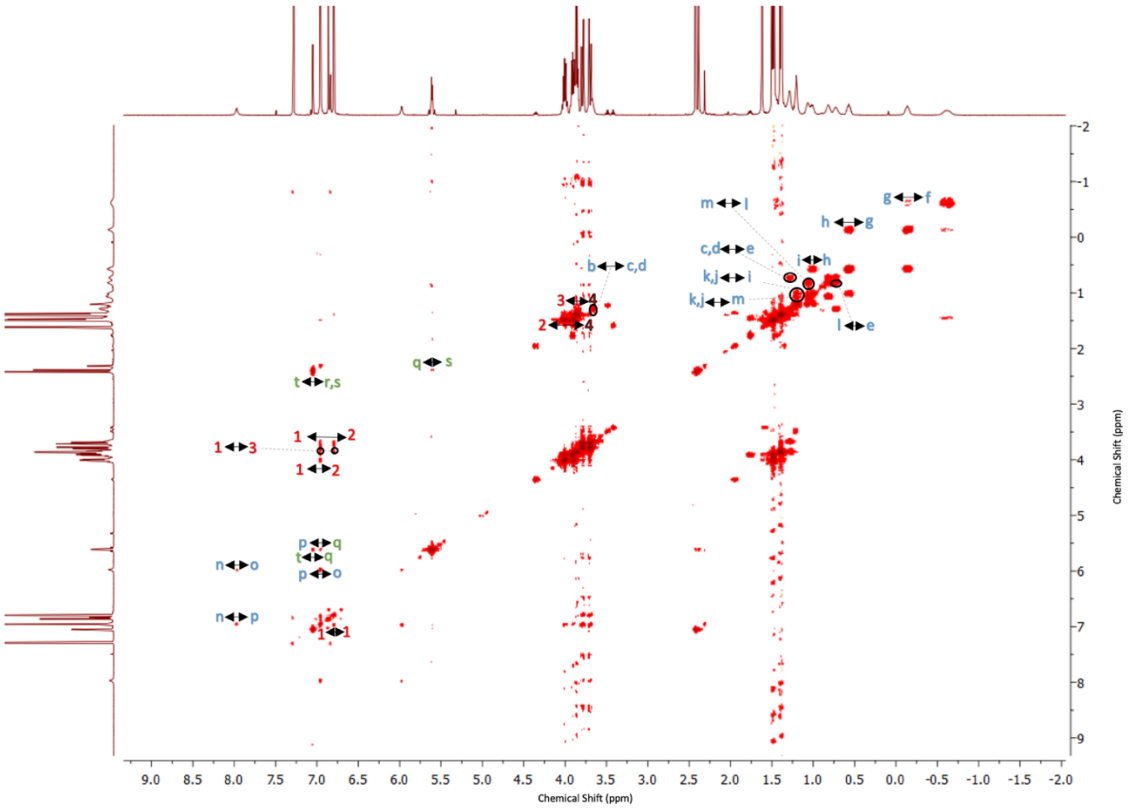

*Figure 7.11. 2D ^{1}H-^{1}H COSY NMR spectrum (500 MHz, $CDCl_3$, 298 K) of **2.12**.*

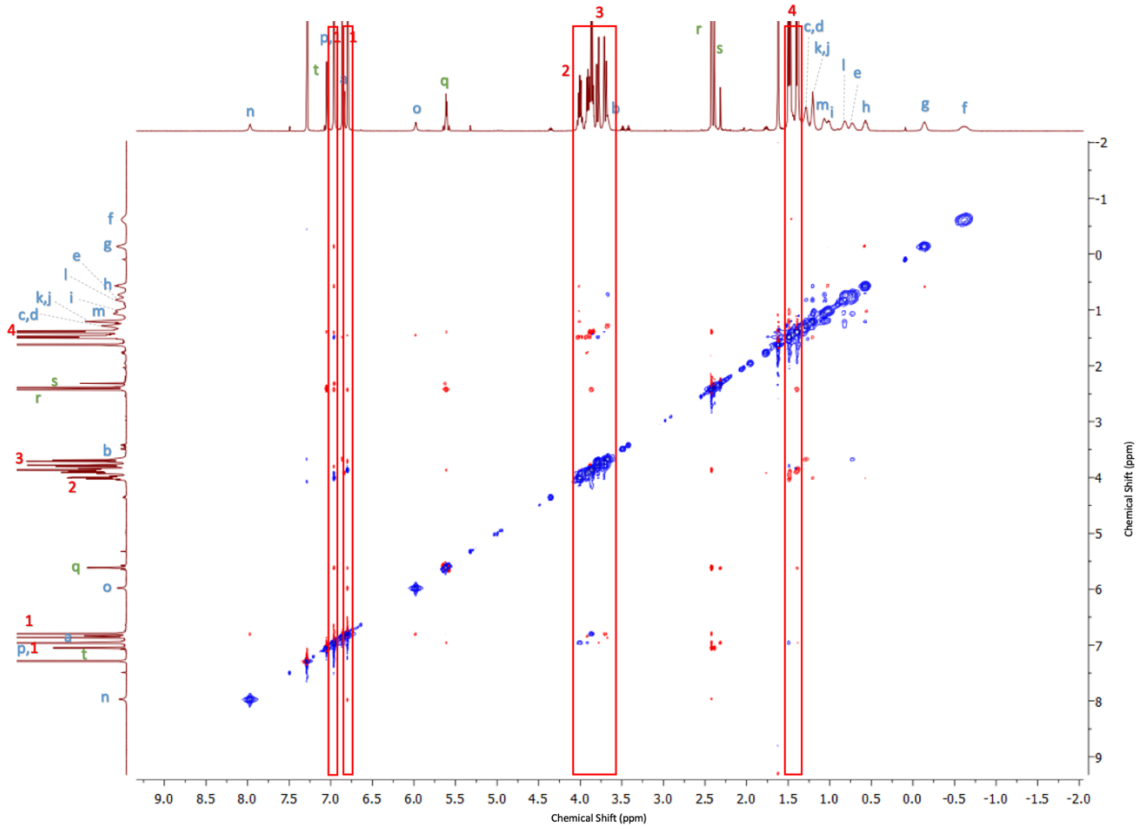

*Figure 7.12. 2D ^{1}H-^{1}H NOESY NMR spectrum (500 MHz, $CDCl_3$, 298 K) of **2.12**.*

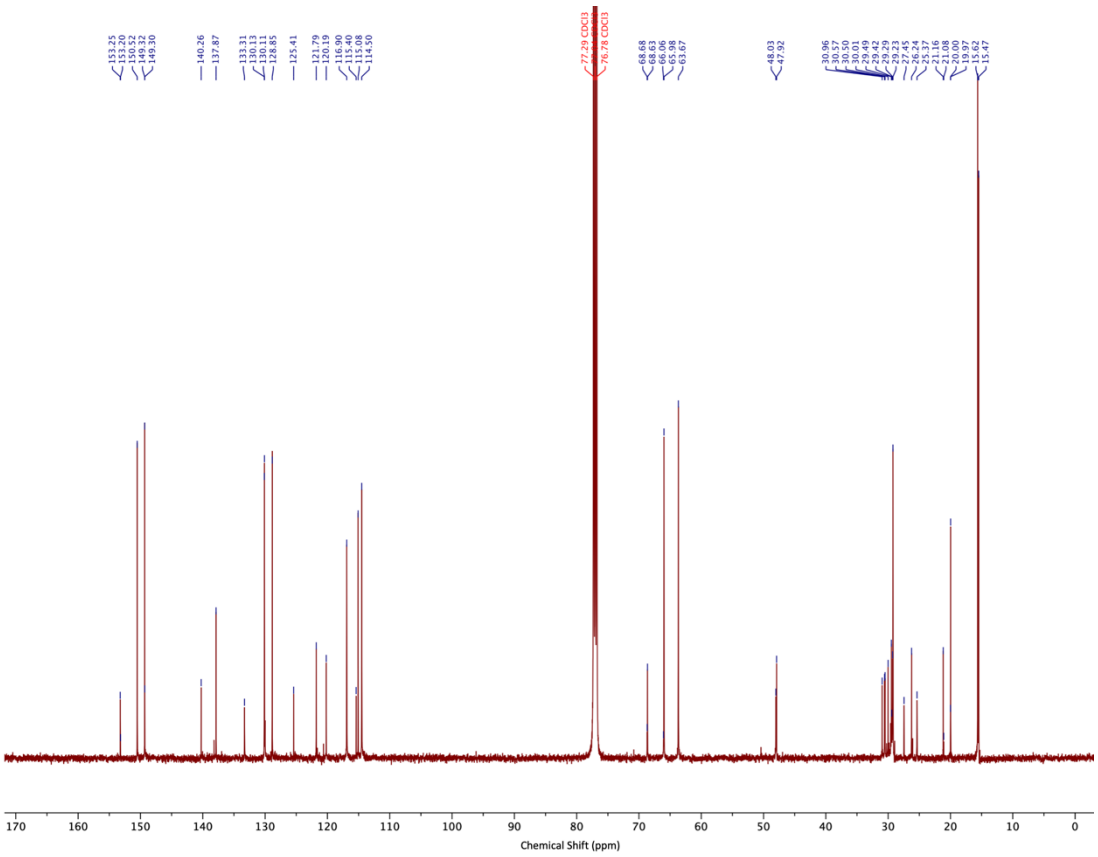

*Figure 7.13. ^{13}C NMR spectrum (126 MHz, $CDCl_3$, 298 K) of **2.12**.*

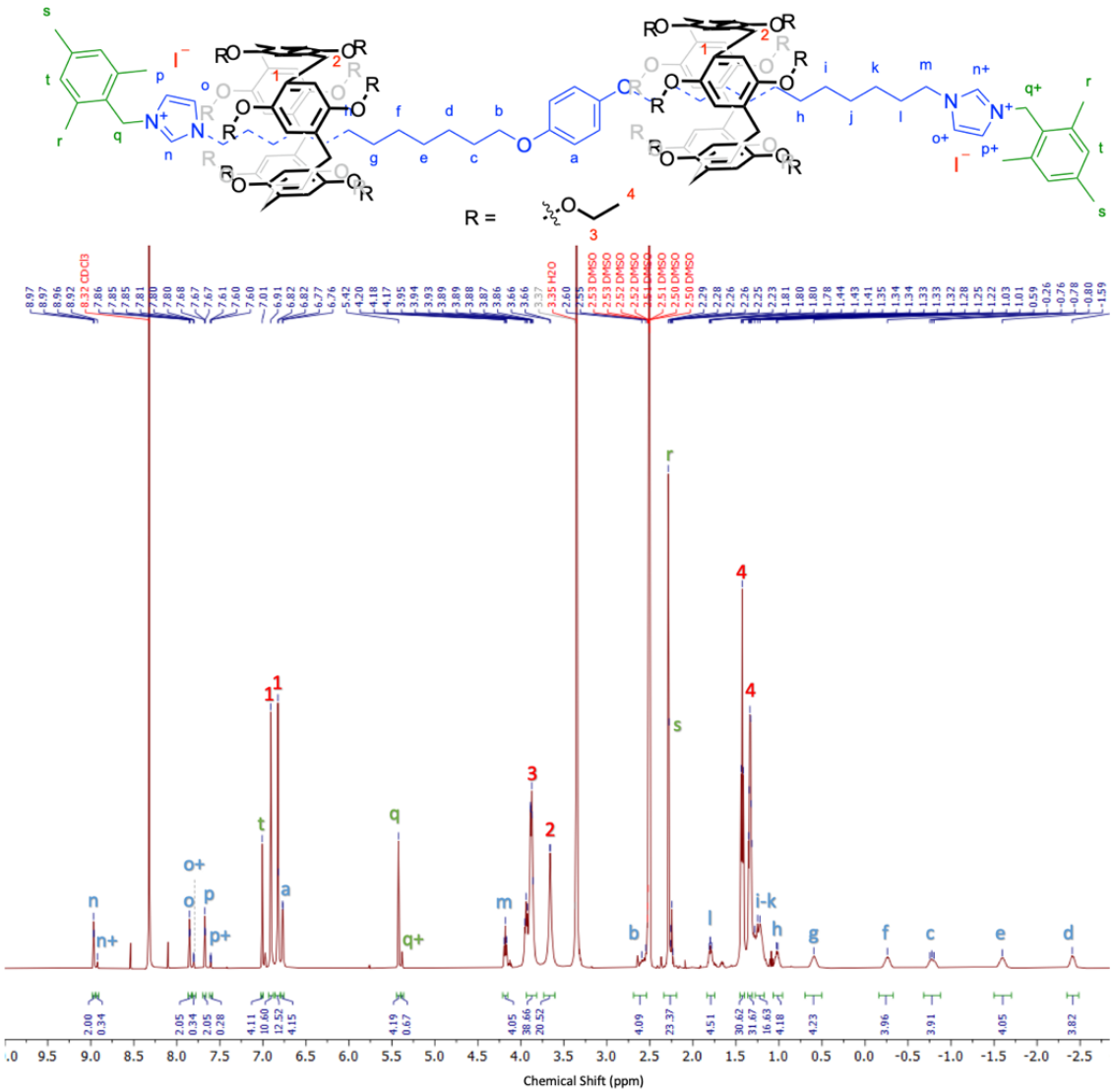

*Figure 7.14. ^{1}H NMR spectrum (500 MHz, DMSO-d_6, 298 K) of **2.12**.*

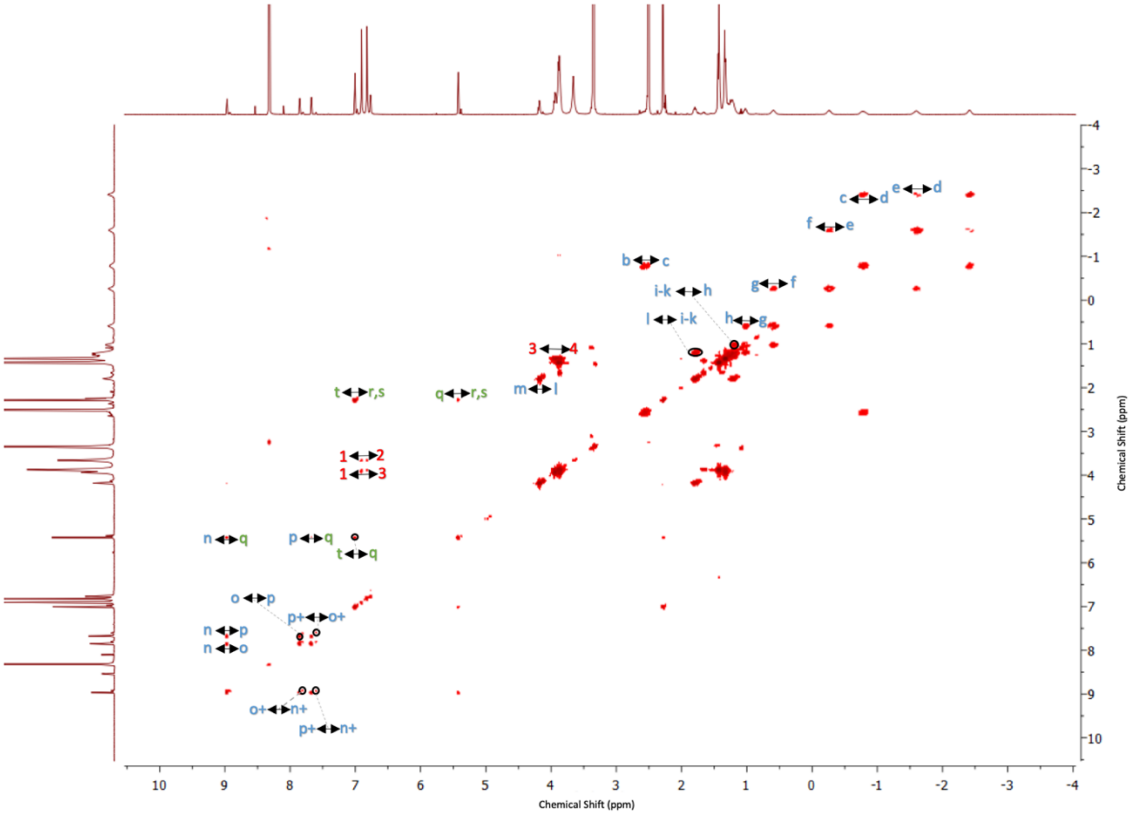

*Figure 7.15. 2D ^{1}H-^{1}H COSY NMR spectrum (500 MHz, DMSO-d_6, 298 K) of **2.12**.*

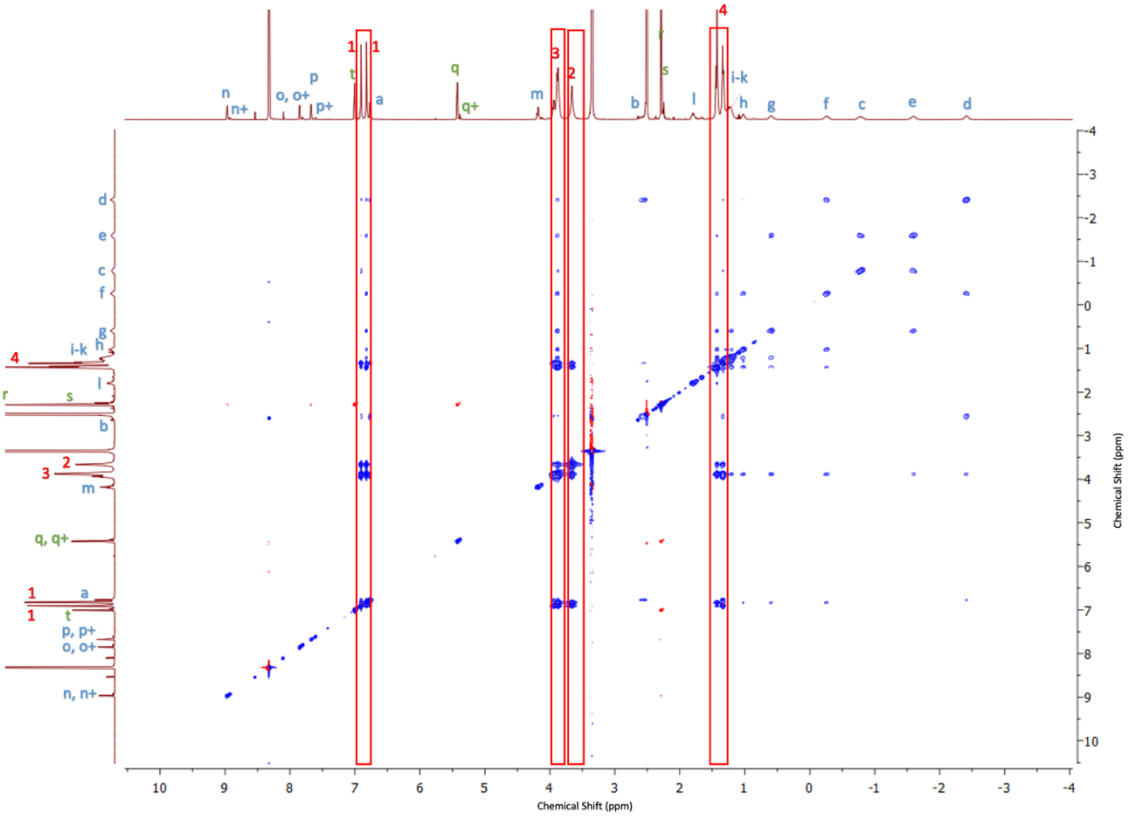

*Figure 7.16. 2D ^{1}H-^{1}H NOESY NMR spectrum (500 MHz, DMSO-d_6, 298 K) of **2.12**.*

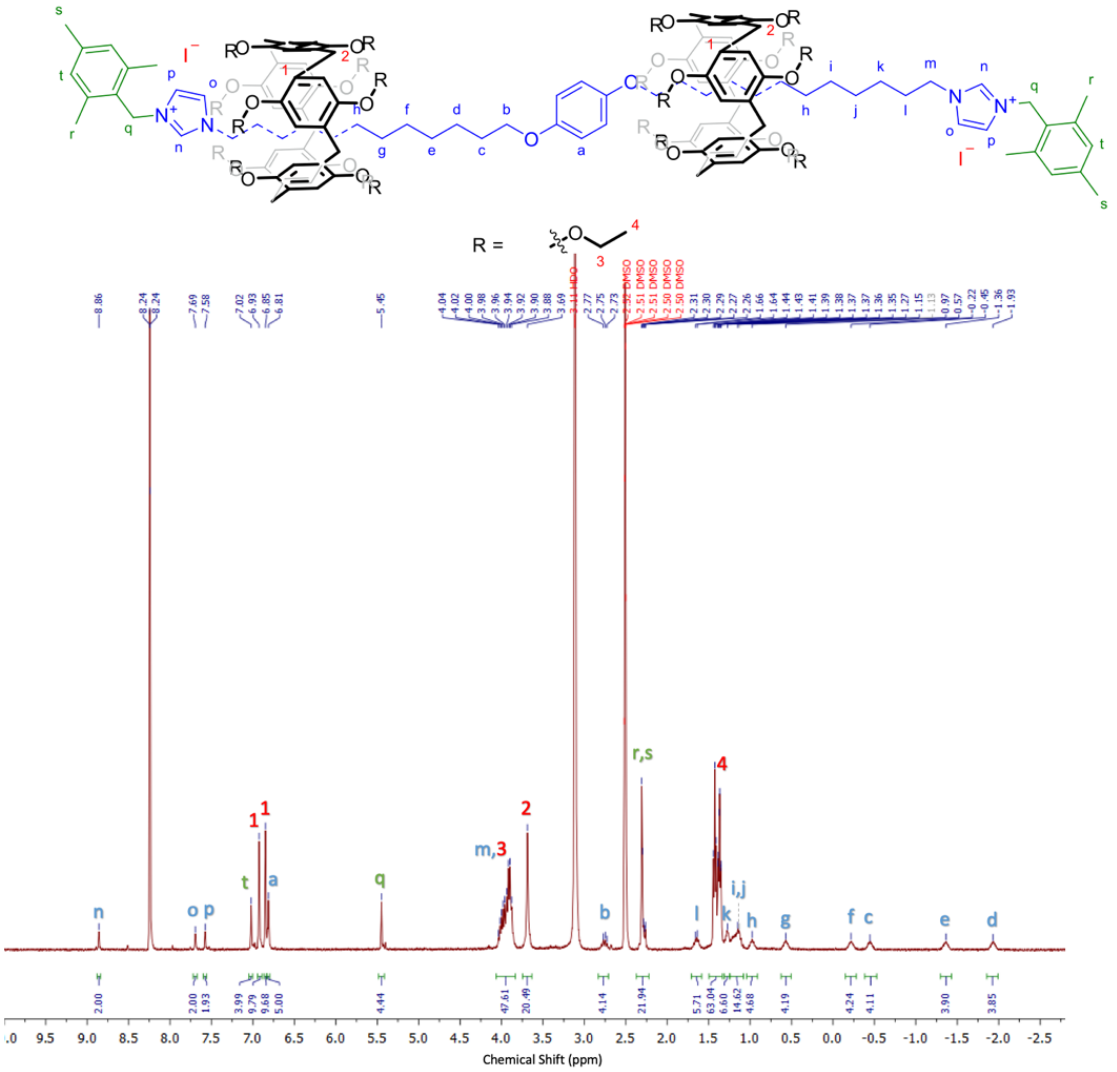

*Figure 7.17. ^{1}H NMR spectrum (400 MHz, DMSO-d_6, 353 K) of **2.12**.*

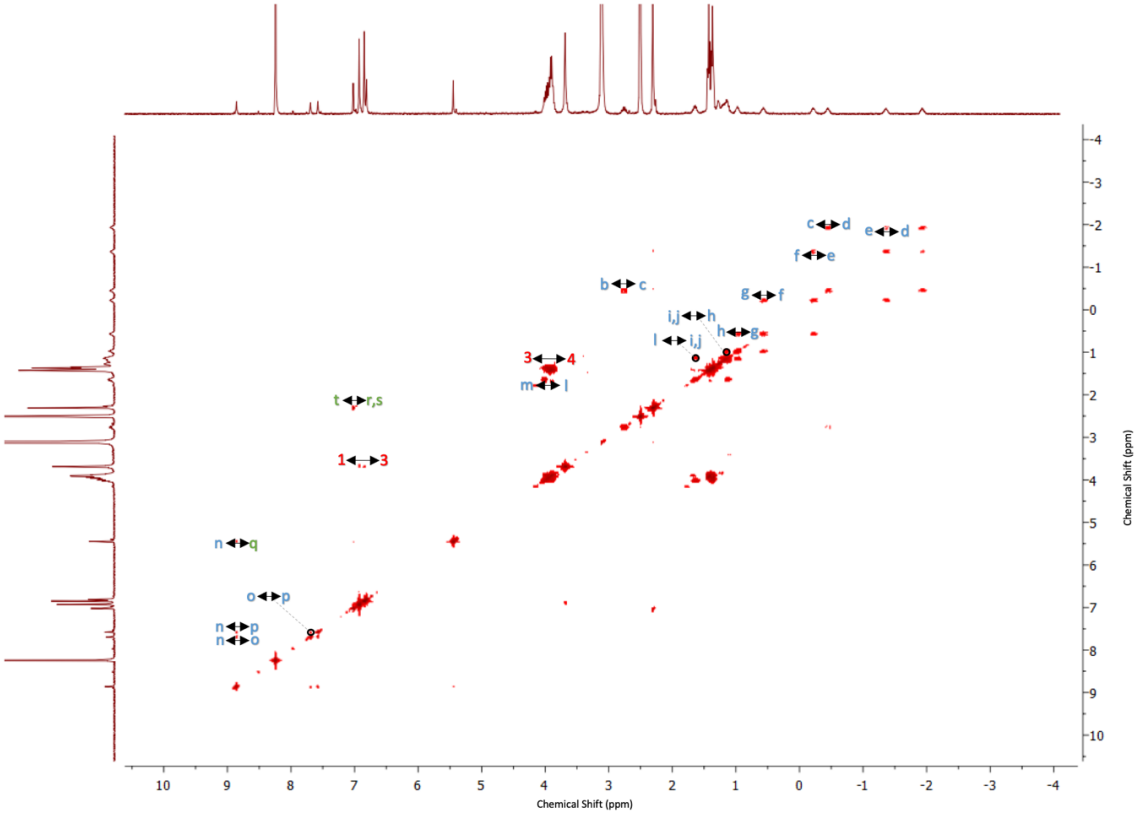

*Figure 7.18. 2D ^{1}H-^{1}H COSY NMR spectrum (400 MHz, DMSO-d_6, 353 K) of **2.12**.*

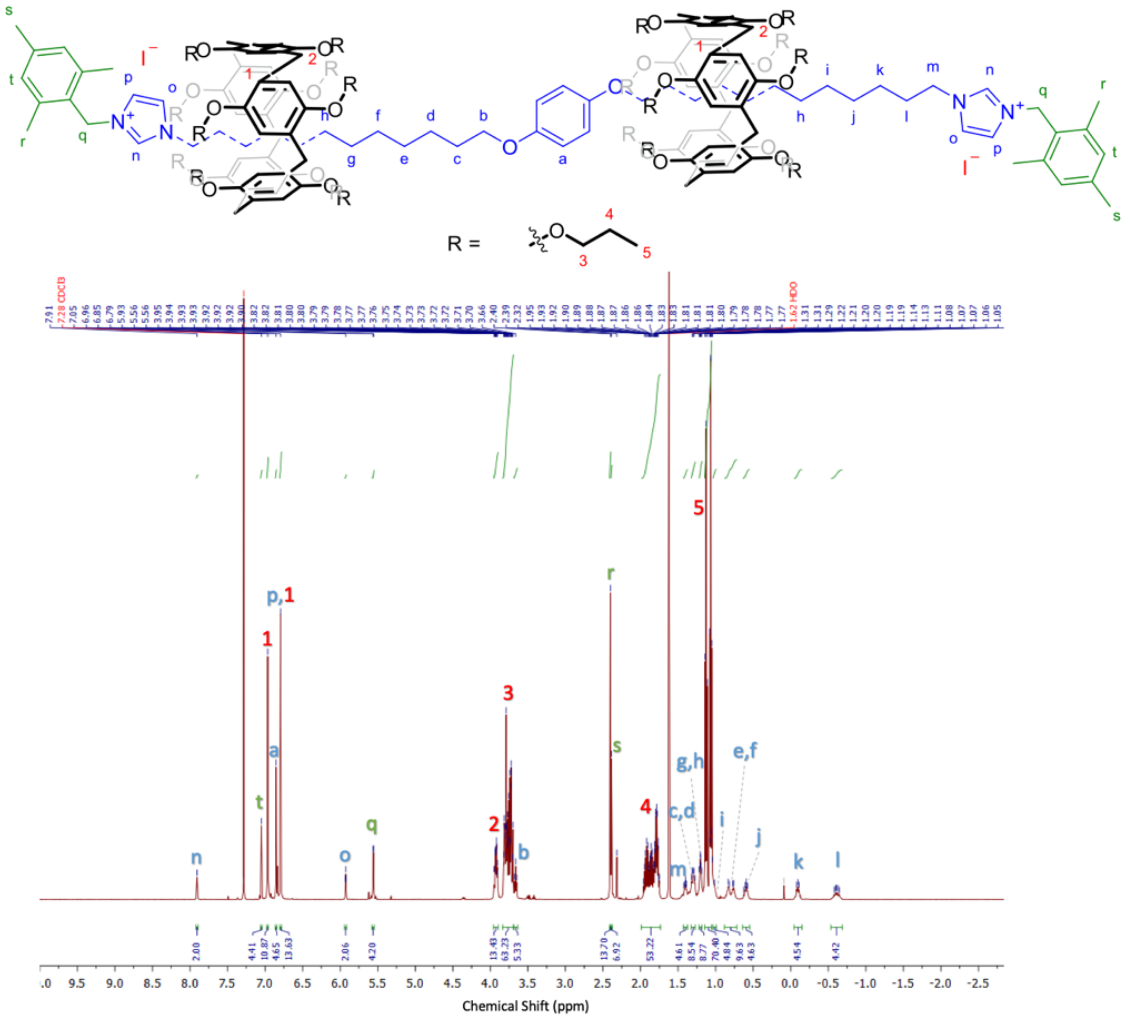

*Figure 7.19. ^{1}H NMR spectrum (500 MHz, $CDCl_3$, 298 K) of **2.13**.*

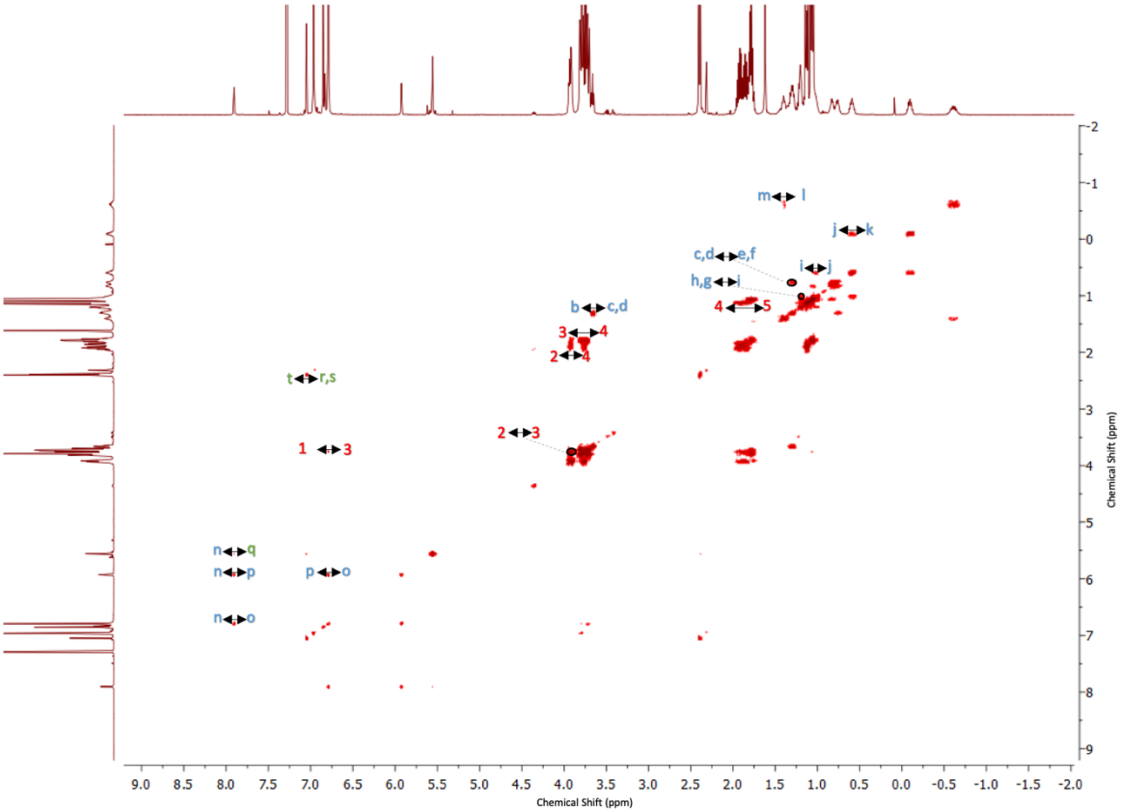

*Figure 7.20. 2D ^{1}H-^{1}H COSY NMR spectrum (500 MHz, $CDCl_3$, 298 K) of **2.13**.*

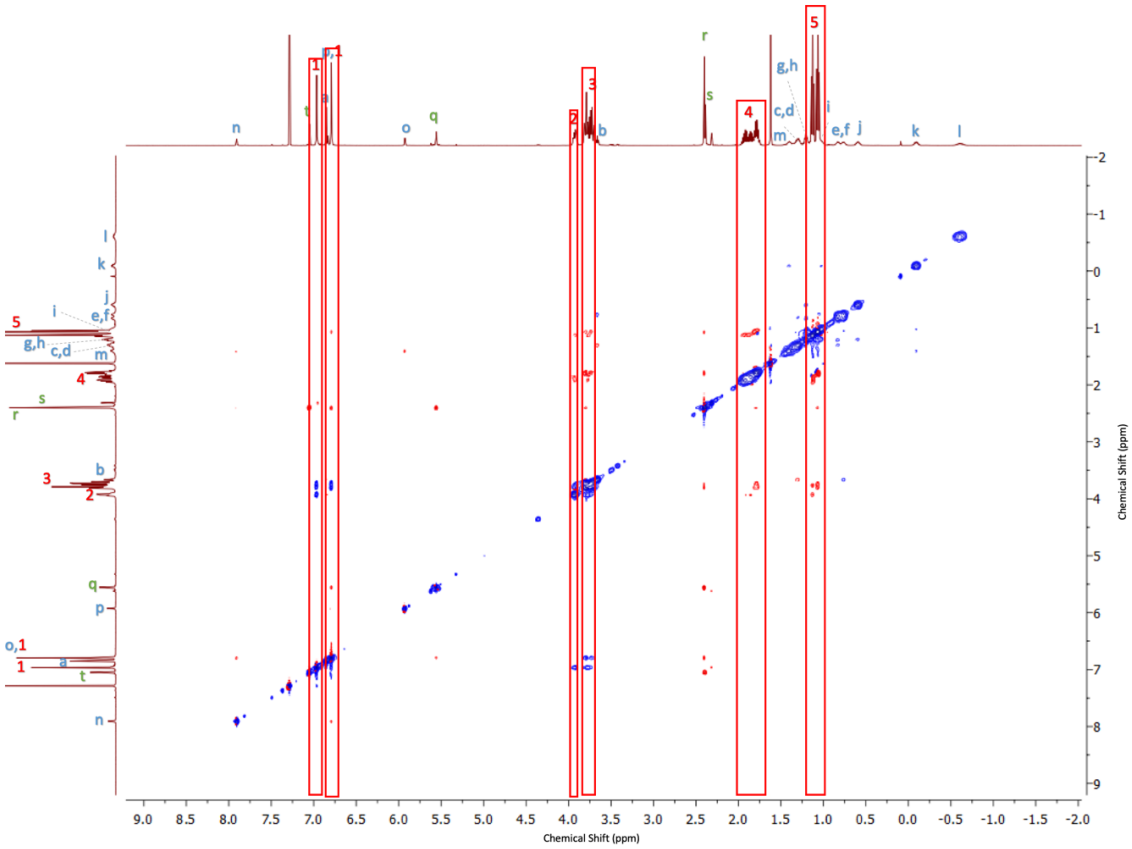

*Figure 7.21. 2D ^{1}H-^{1}H NOESY NMR spectrum (500 MHz, $CDCl_3$, 298 K) of **2.13**.*

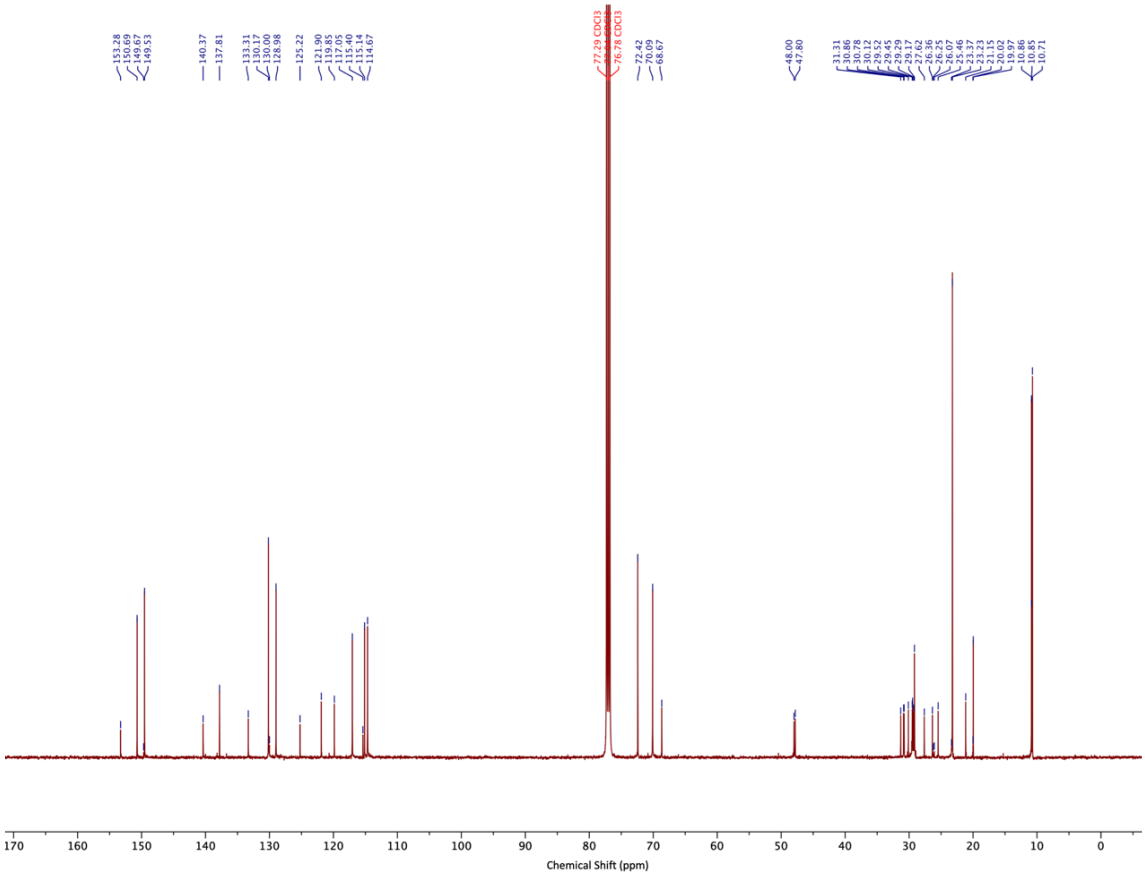

*Figure 7.22. ^{13}C NMR spectrum (126 MHz, $CDCl_3$, 298 K) of **2.13**.*

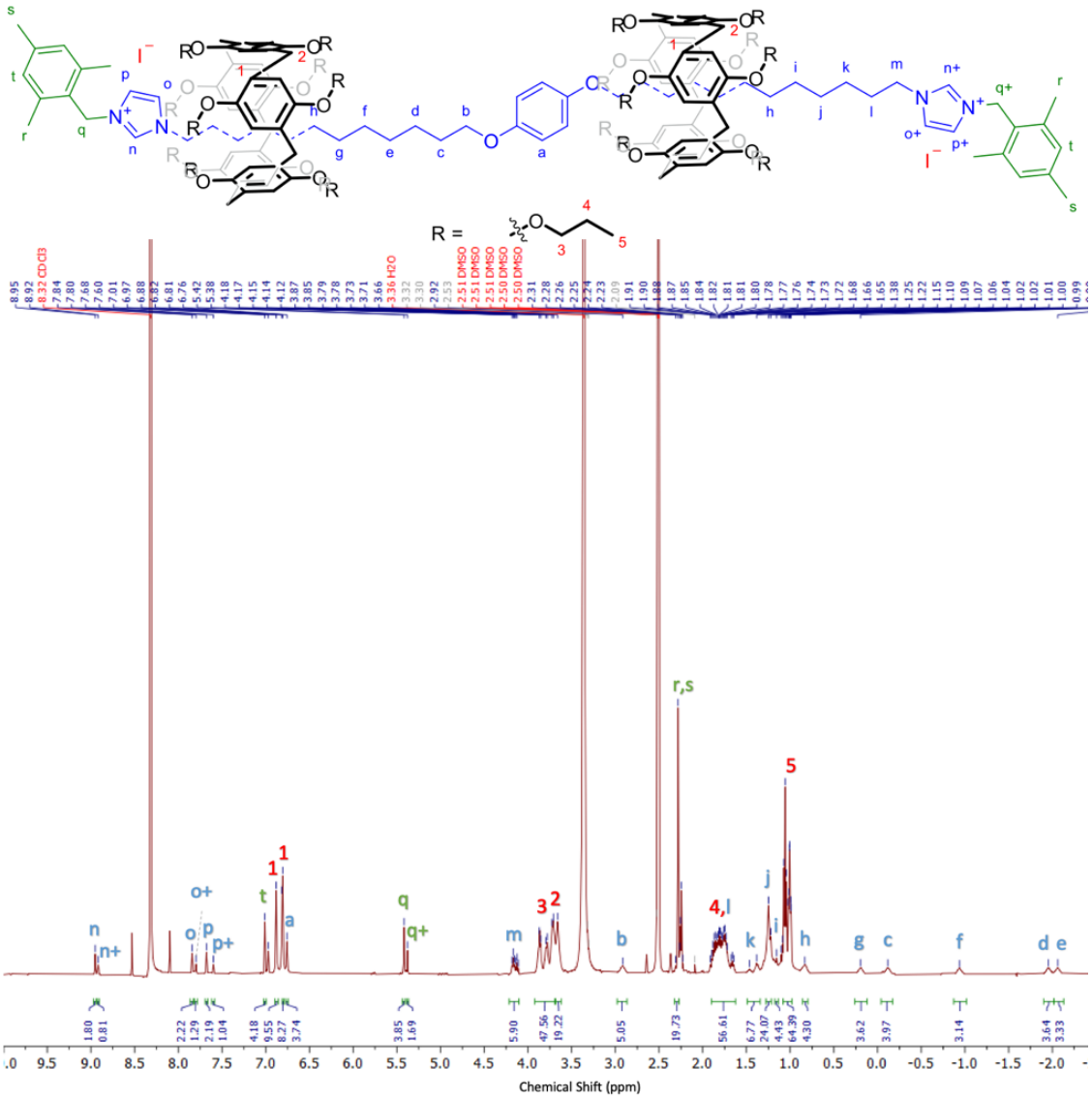

*Figure 7.23. ^{1}H NMR spectrum (500 MHz, DMSO-d_6, 298 K) of **2.13**.*

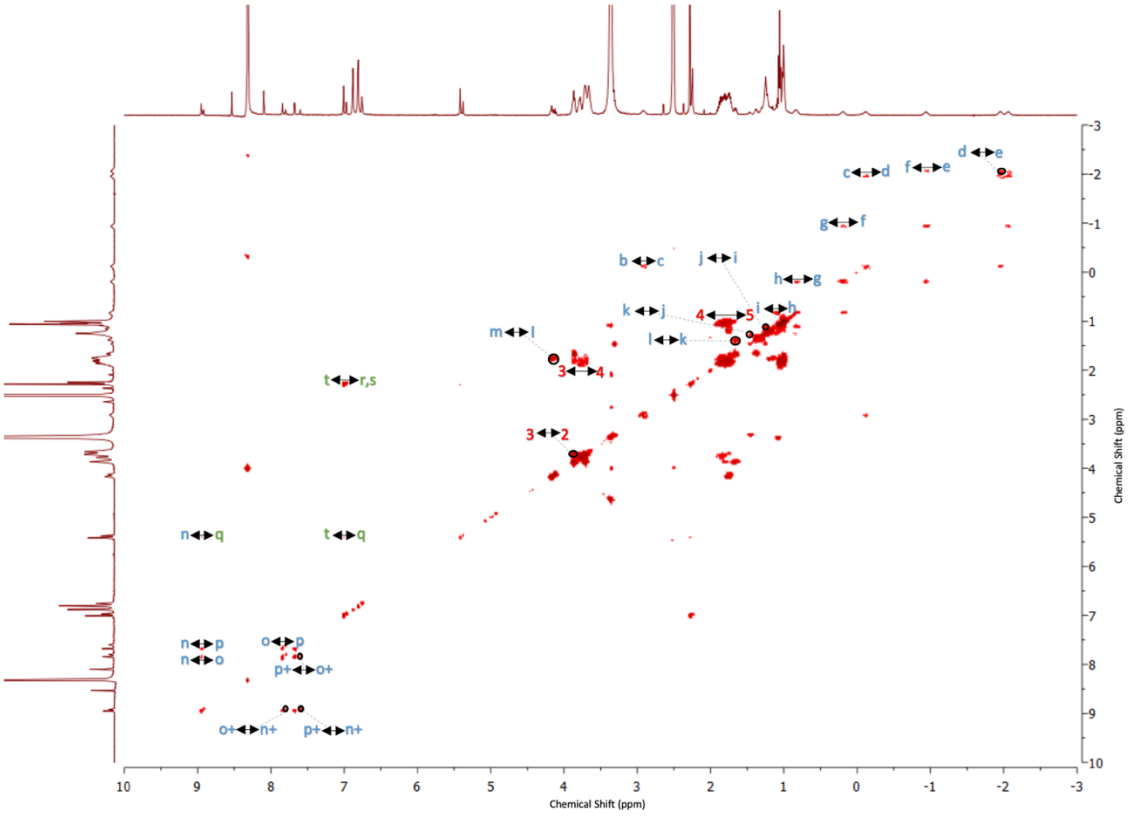

*Figure 7.24. 2D ^{1}H-^{1}H COSY NMR spectrum (500 MHz, DMSO-d_6, 298 K) of **2.13**.*

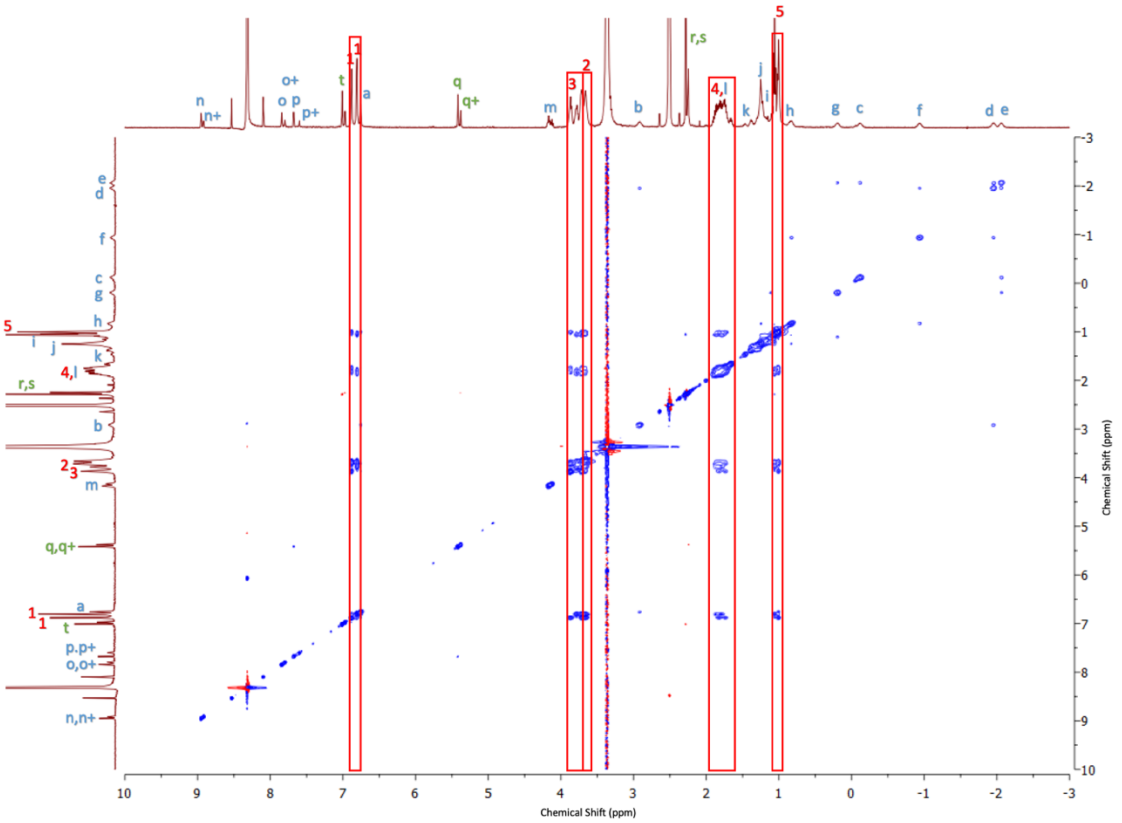

*Figure 7.25. 2D ^{1}H-^{1}H NOESY NMR spectrum (500 MHz, DMSO-d_6, 298 K) of **2.13**.*

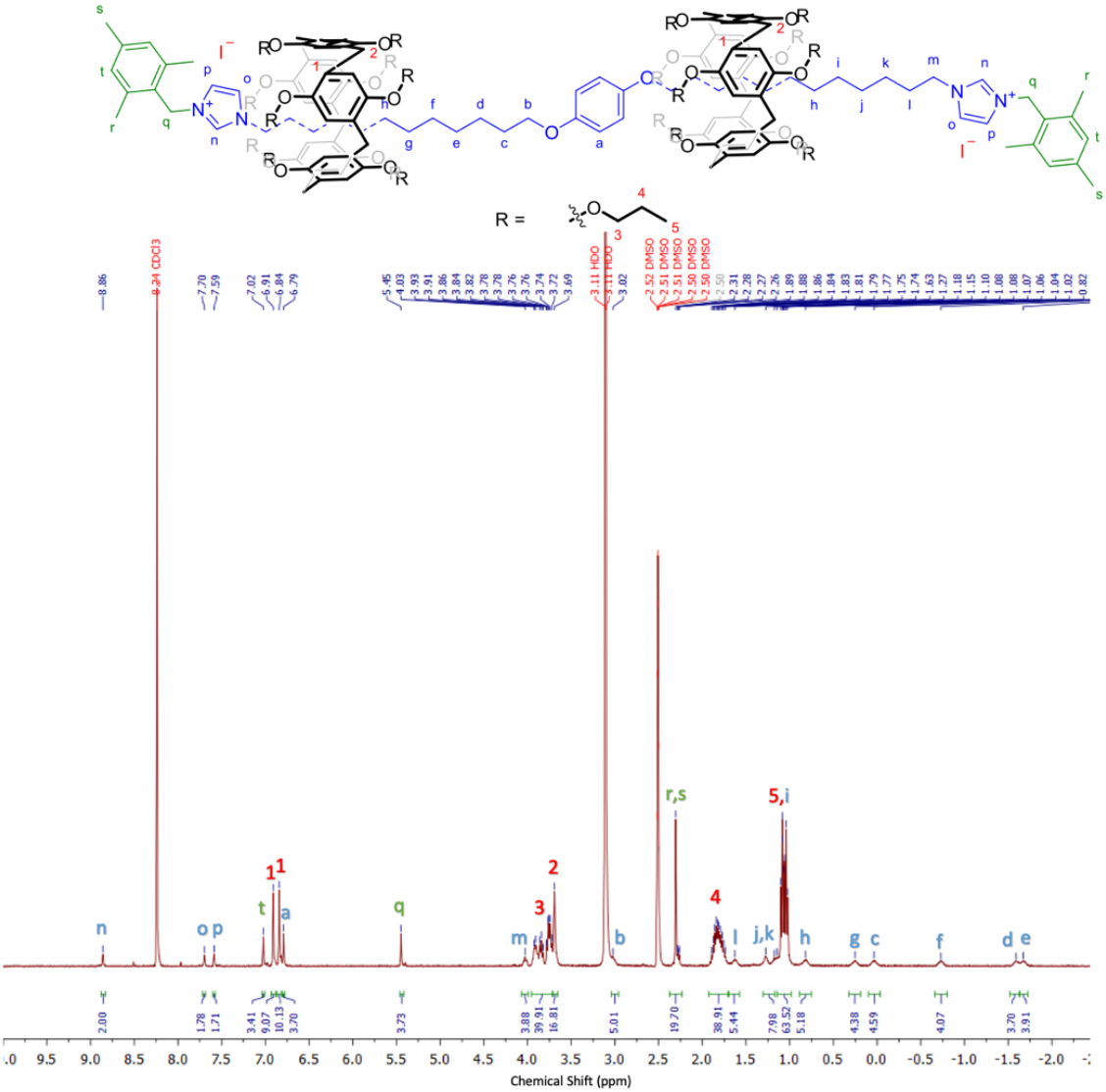

*Figure 7.26. ^{1}H NMR spectrum (400 MHz, DMSO-d_6, 353 K) of **2.13**.*

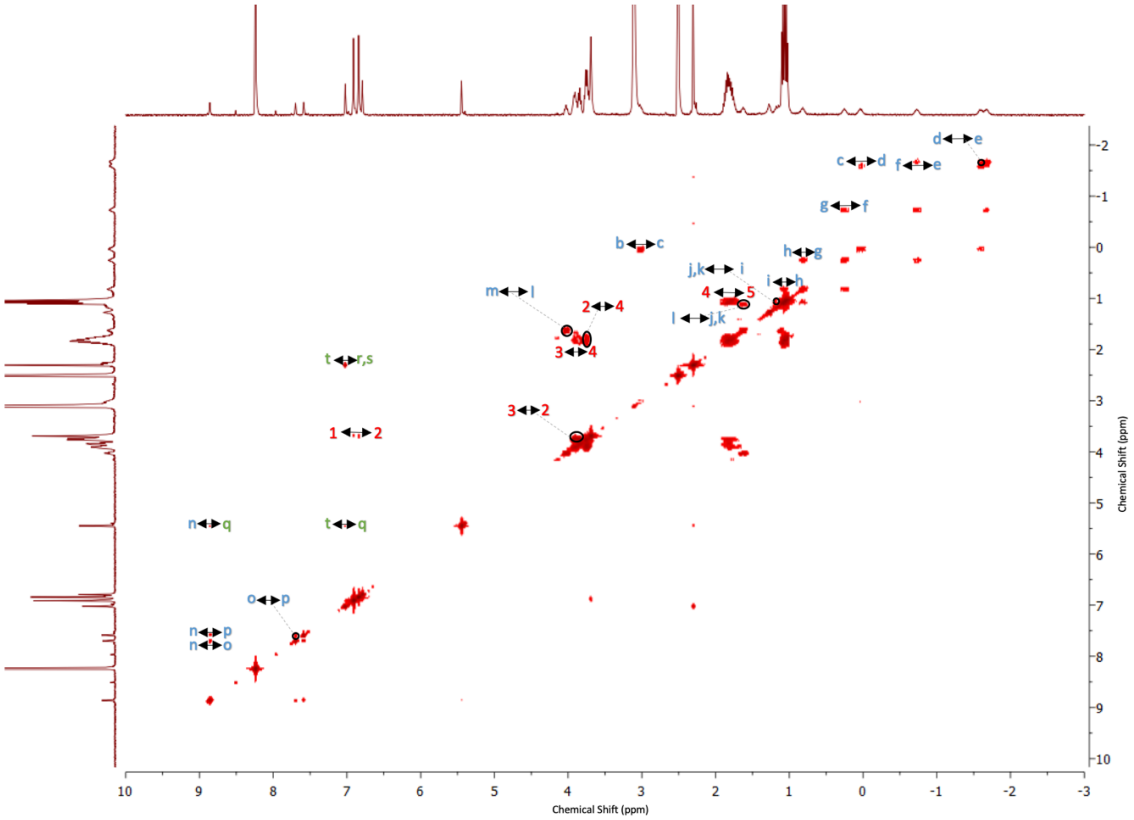

*Figure 7.27. 2D ^{1}H-^{1}H COSY NMR spectrum (400 MHz, DMSO-d_6, 353 K) of **2.13**.*

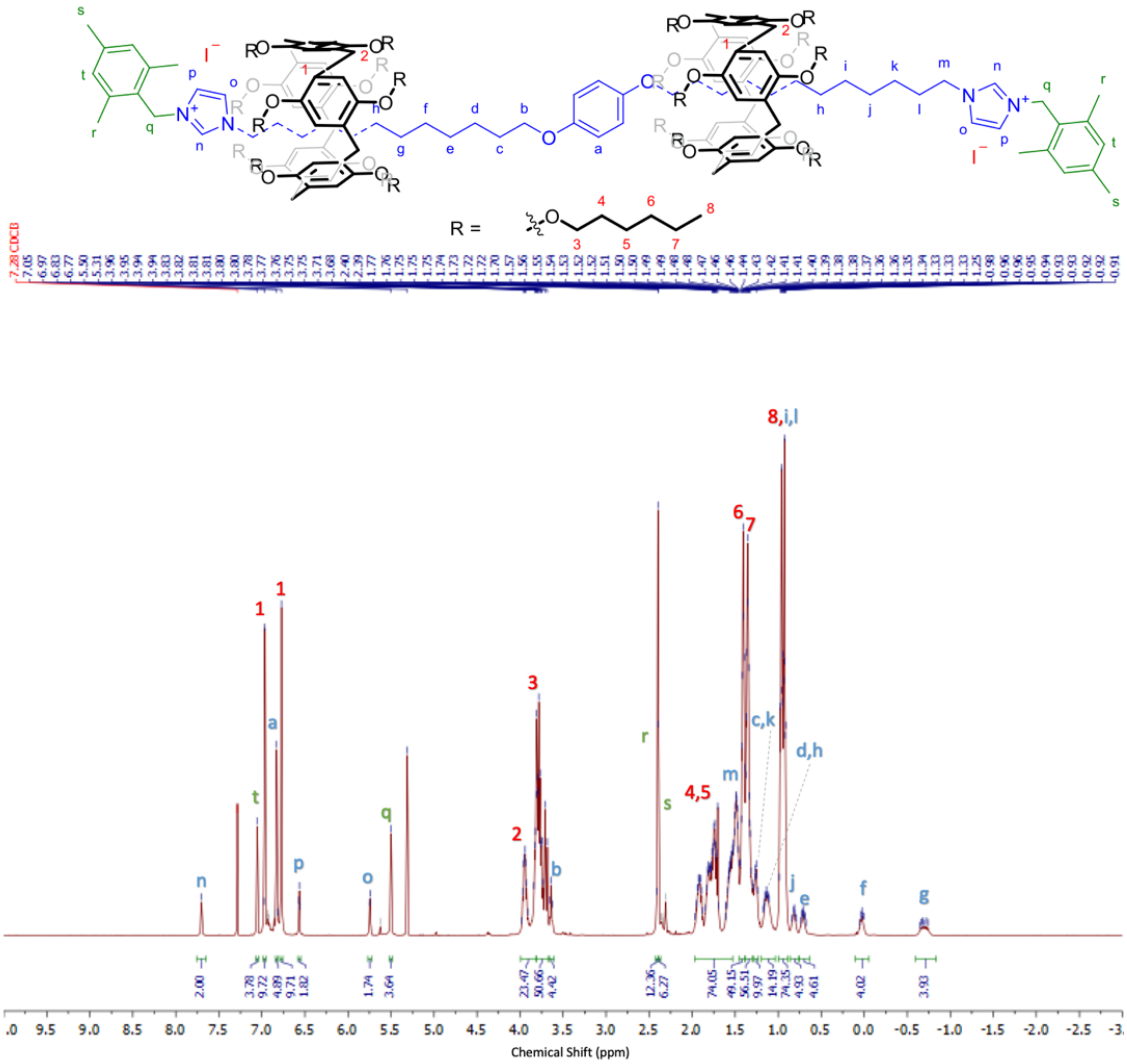

*Figure 7.28. ^{1}H NMR spectrum (500 MHz, $CDCl_3$, 298 K) of **2.14**.*

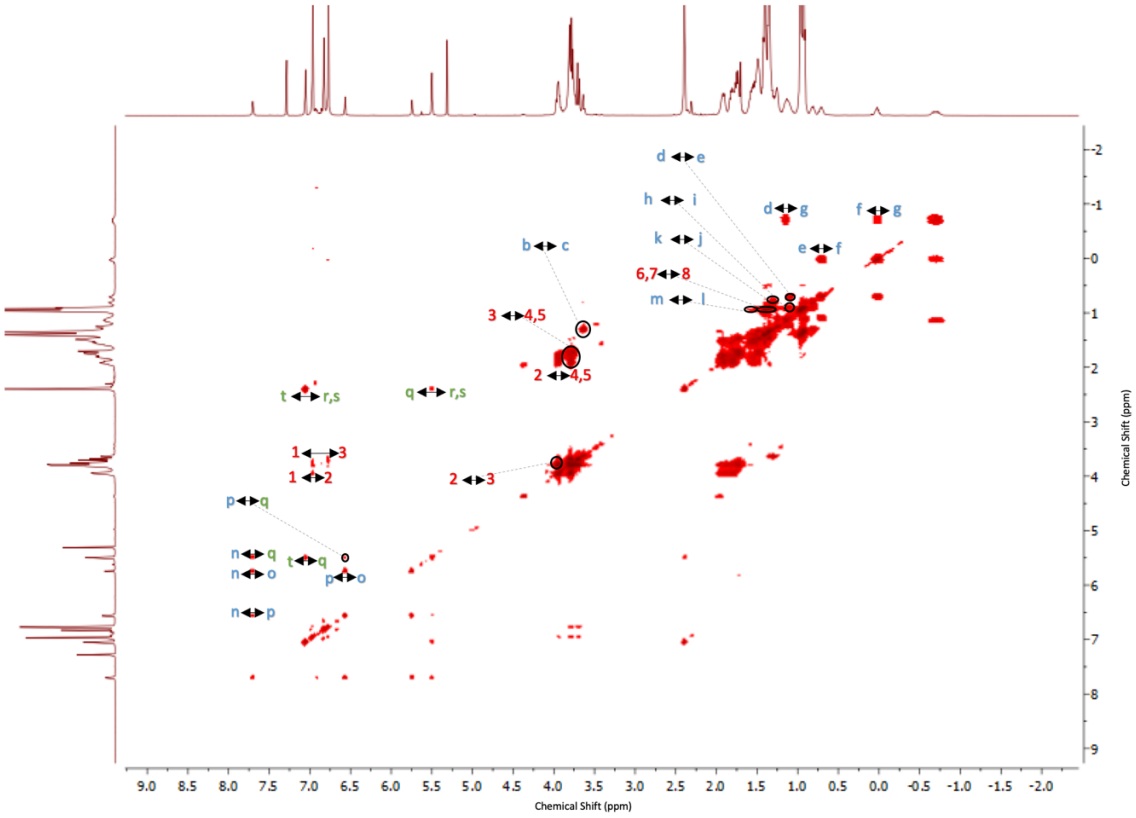

*Figure 7.29. 2D ^{1}H-^{1}H COSY NMR spectrum (500 MHz, $CDCl_3$, 298 K) of **2.14**.*

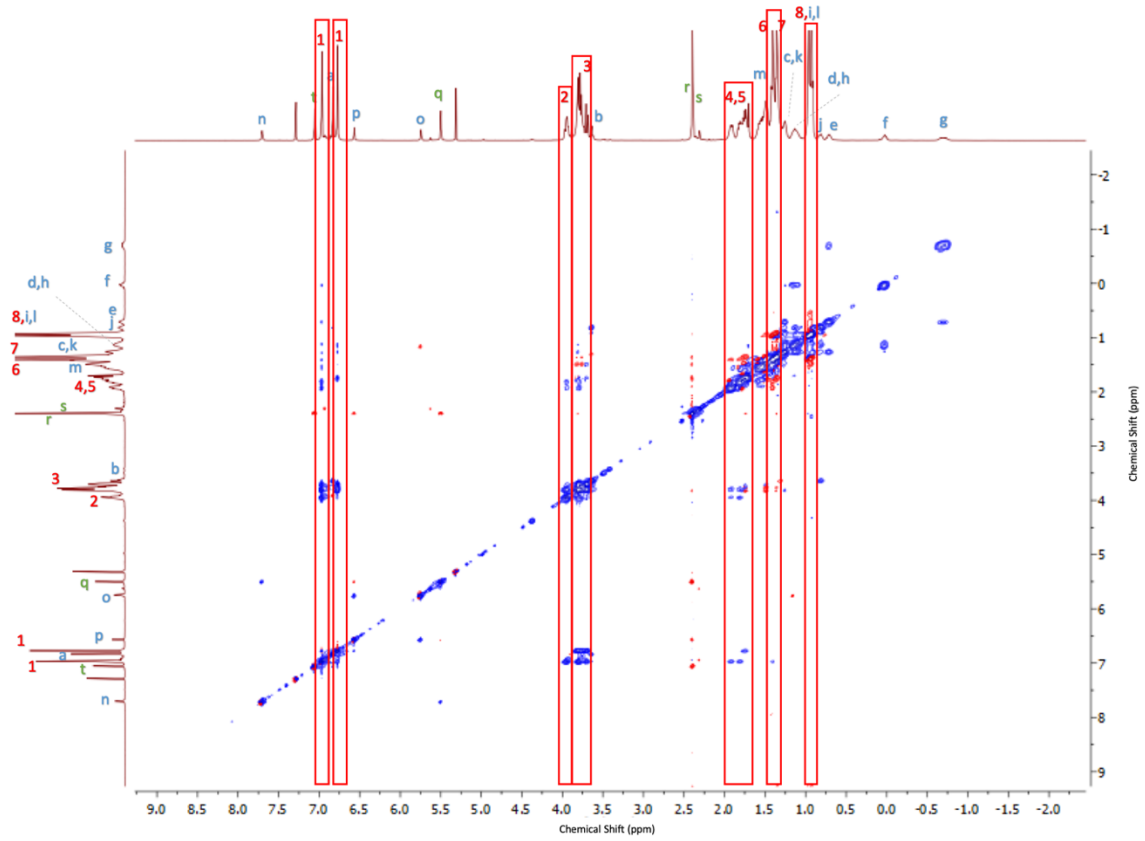

*Figure 7.30. 2D ^{1}H-^{1}H NOESY NMR spectrum (500 MHz, $CDCl_3$, 298 K) of **2.14**.*

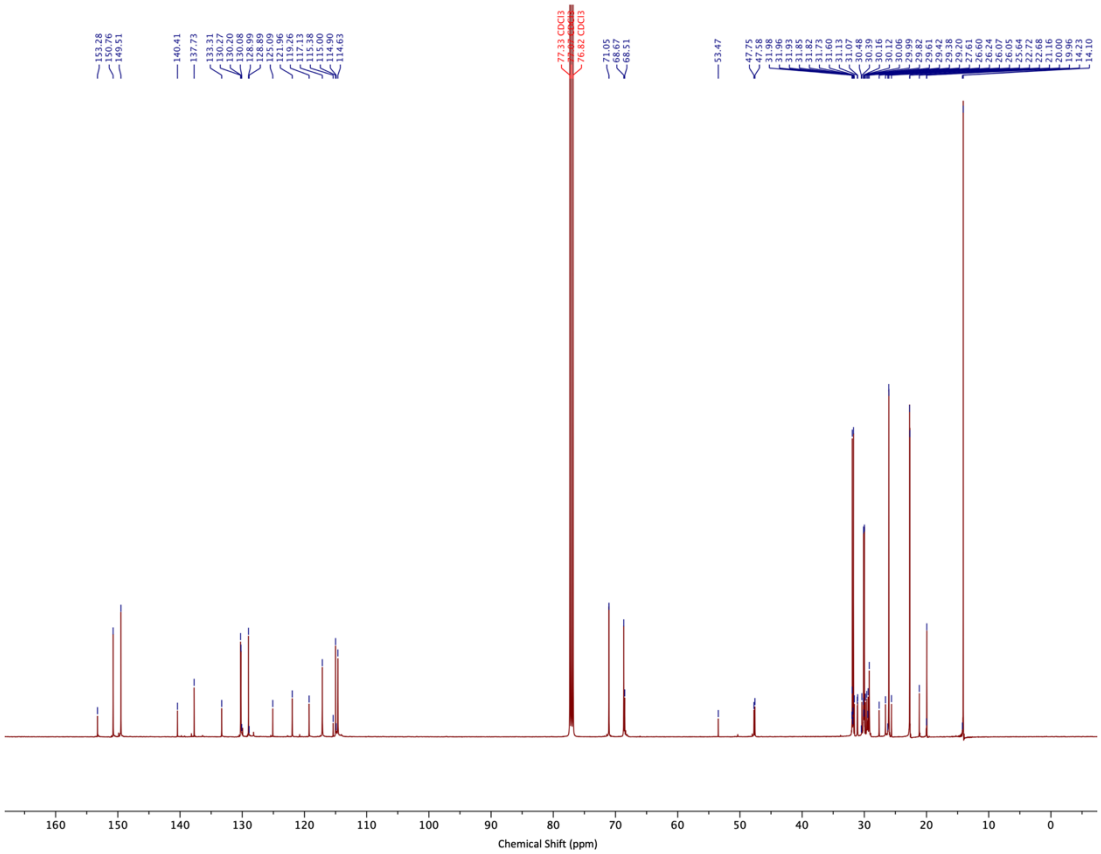

*Figure 7.31. ^{13}C NMR spectrum (126 MHz, $CDCl_3$, 298 K) of **2.14**.*

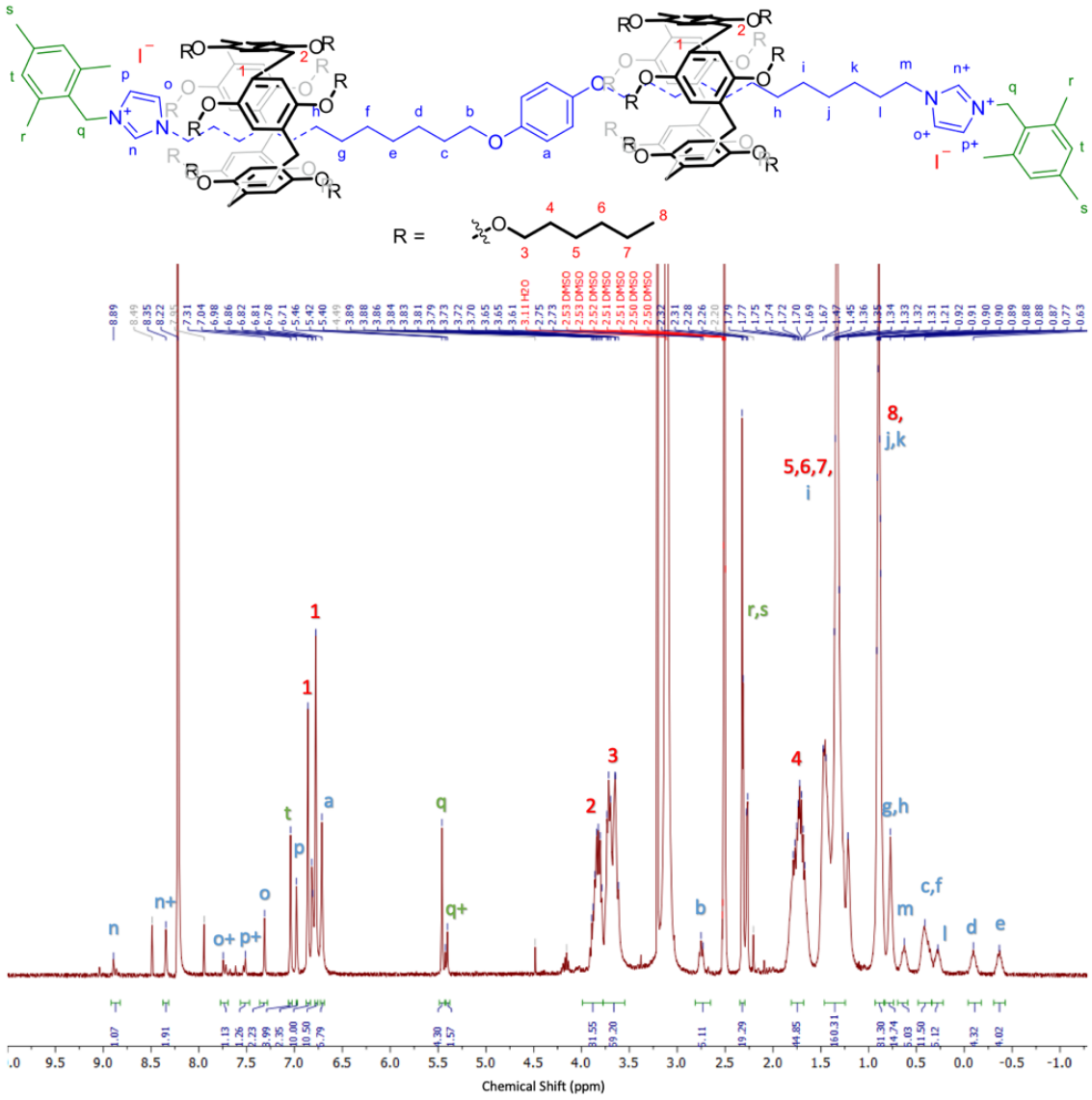

*Figure 7.32. ^{1}H NMR spectrum (400 MHz, DMSO-d_6, 353 K) of **2.14**.*

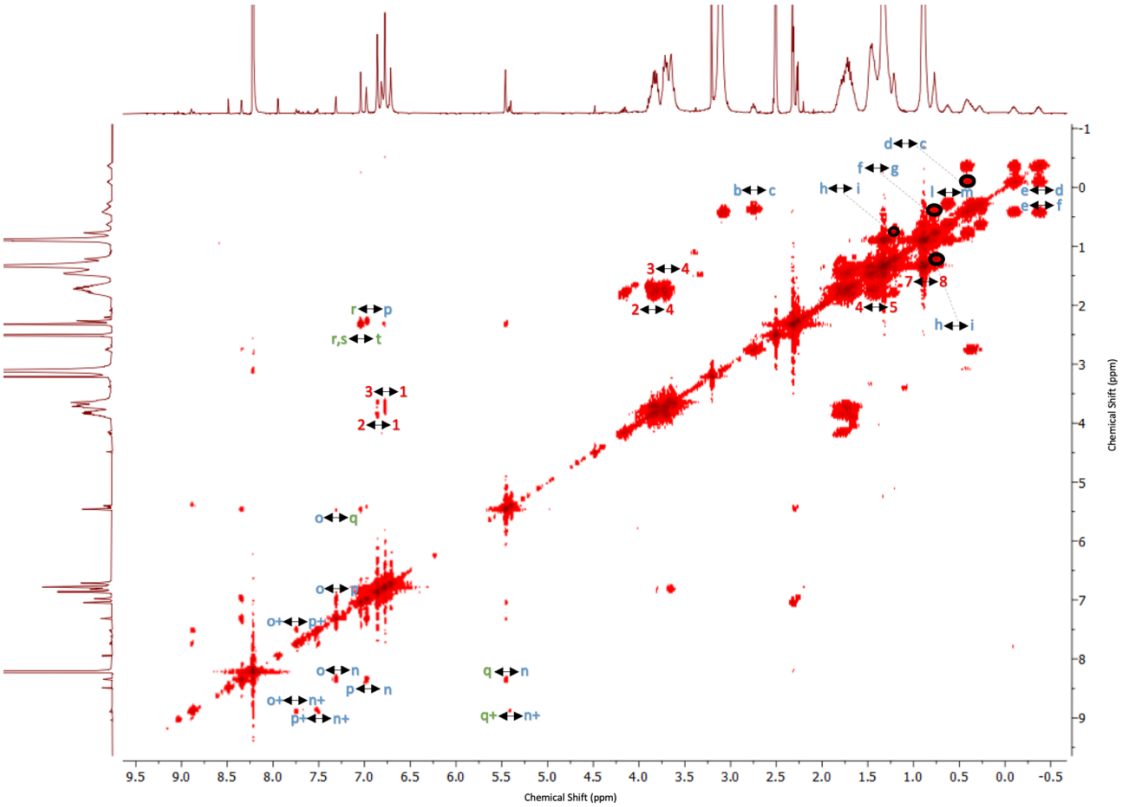

*Figure 7.33. 2D ^{1}H-^{1}H COSY NMR spectrum (400 MHz, DMSO-d_6, 353 K) of **2.14**.*

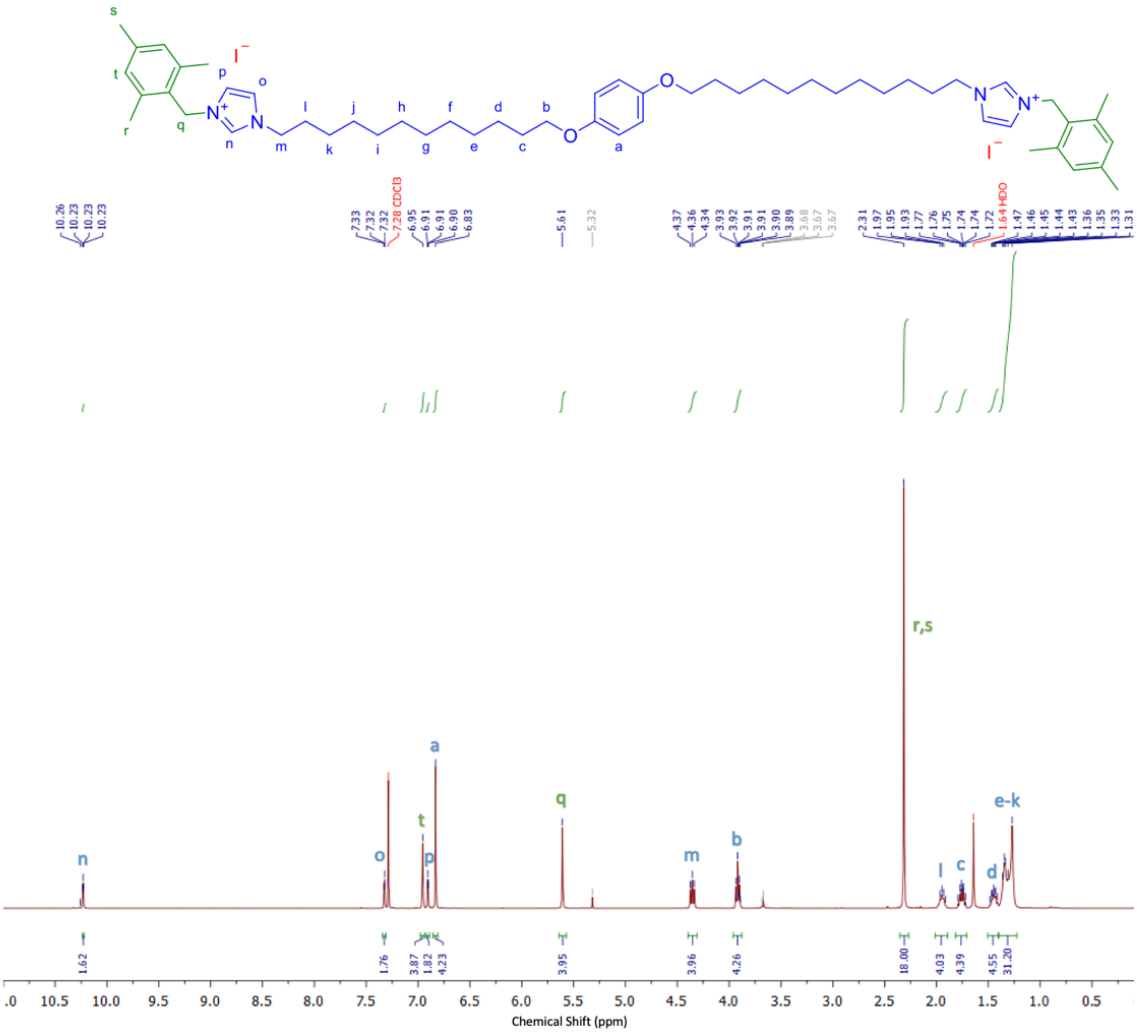

*Figure 7.34. ^{1}H NMR spectrum (400 MHz, $CDCl_3$, 298 K) of **2.15**.*

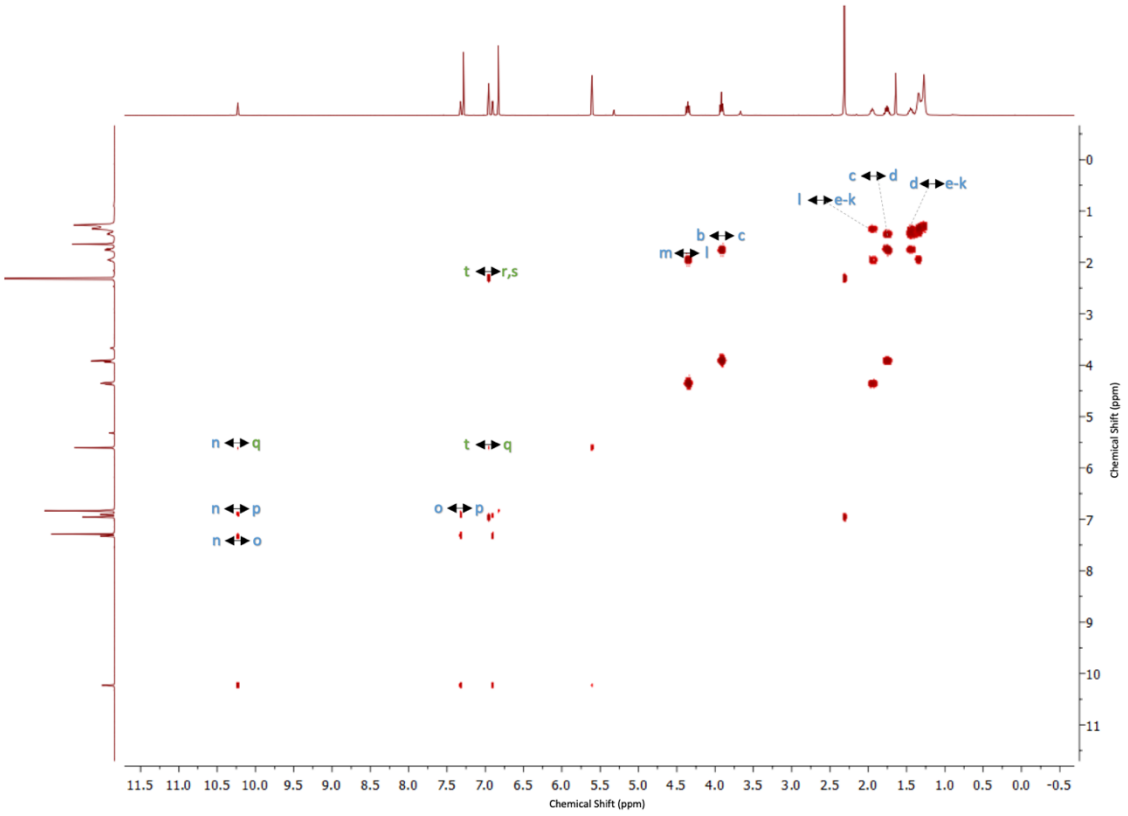

*Figure 7.35. 2D ^{1}H-^{1}H COSY NMR spectrum (400 MHz, $CDCl_3$, 298 K) of **2.15**.*

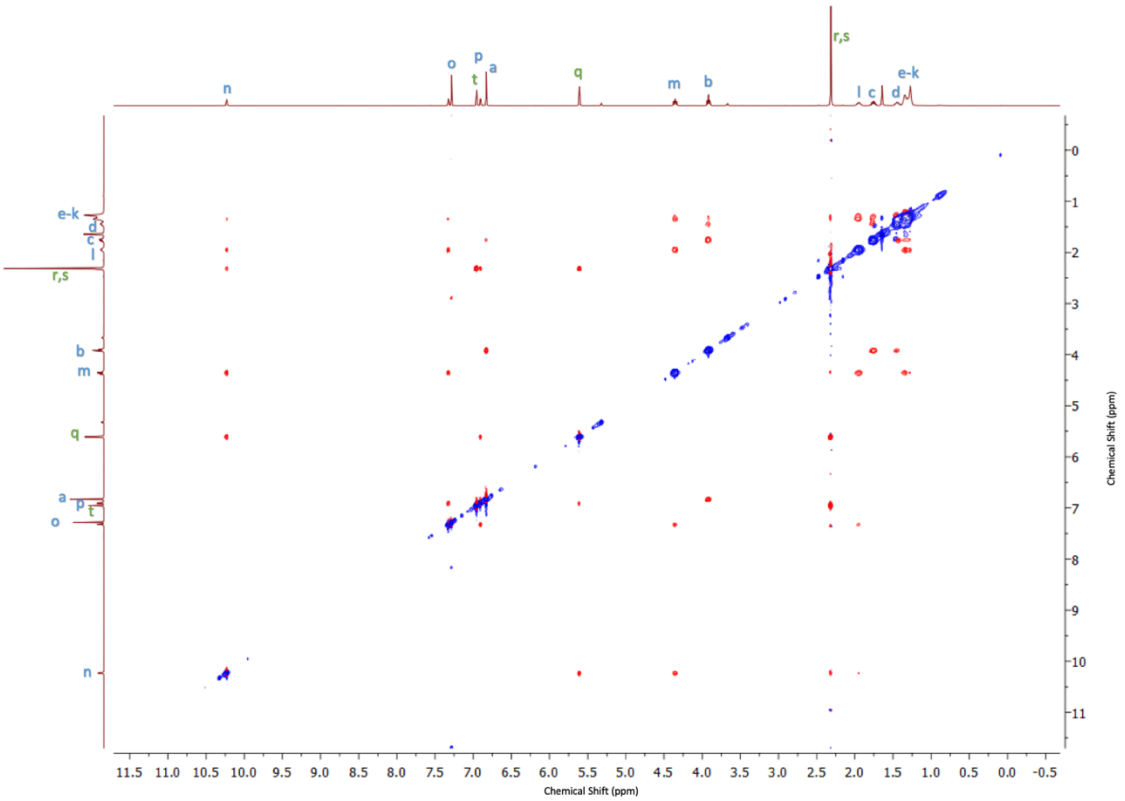

*Figure 7.36. 2D ^{1}H-^{1}H NOESY NMR spectrum (400 MHz, $CDCl_3$, 298 K) of **2.15**.*

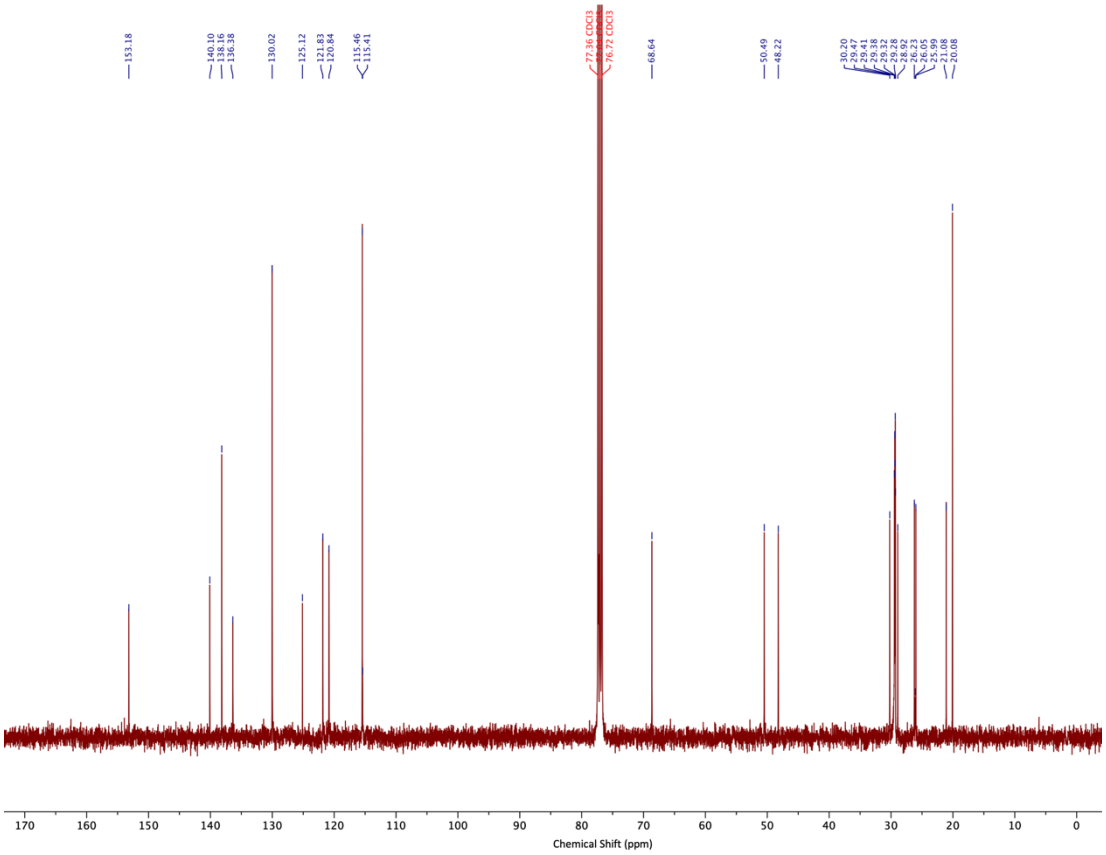

*Figure 7.37. ^{13}C NMR spectrum (101 MHz, $CDCl_3$, 298 K) of **2.15**.*

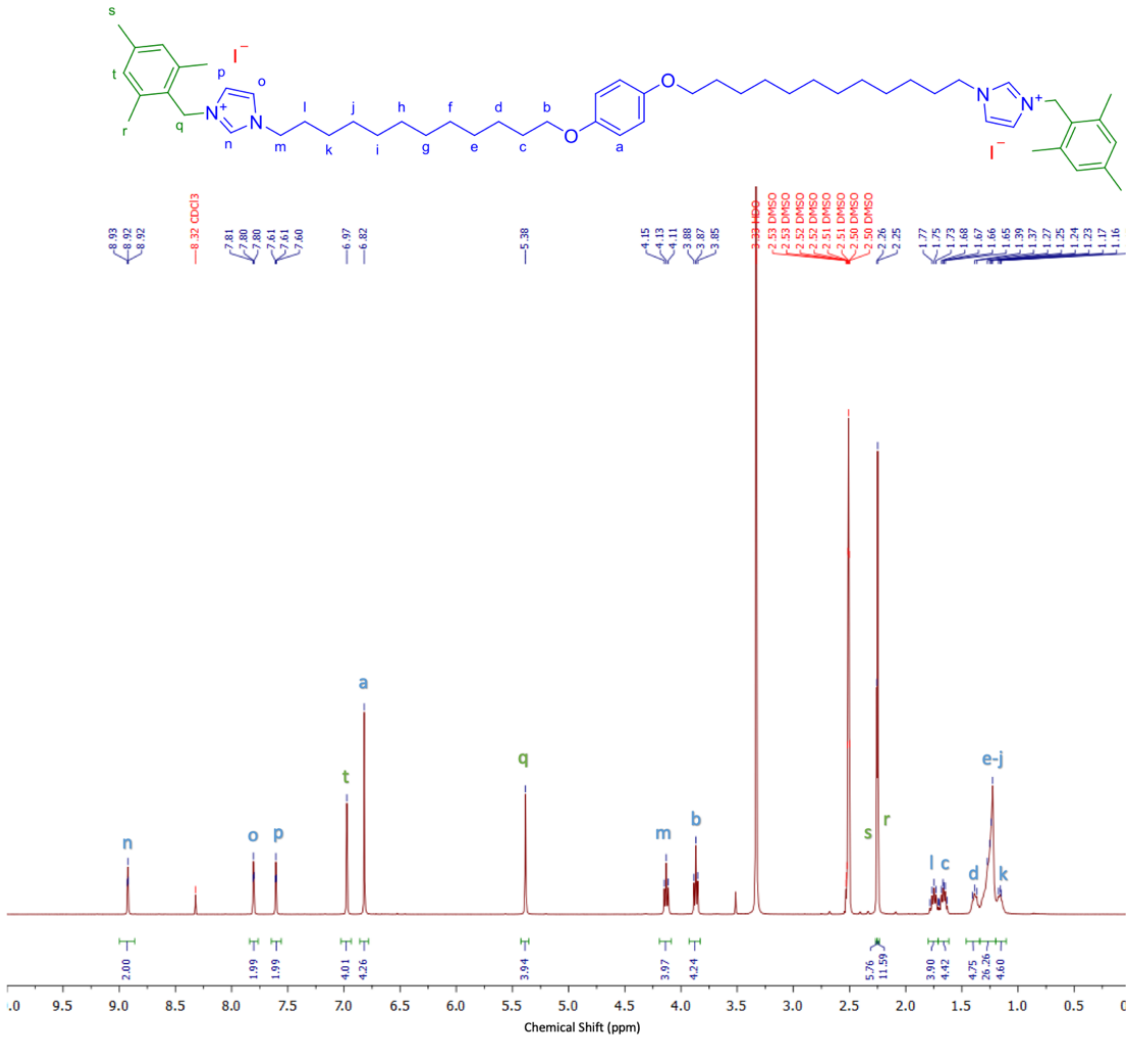

*Figure 7.38. ^{1}H NMR spectrum (400 MHz, DMSO-d_6, 298 K) of **2.15**.*

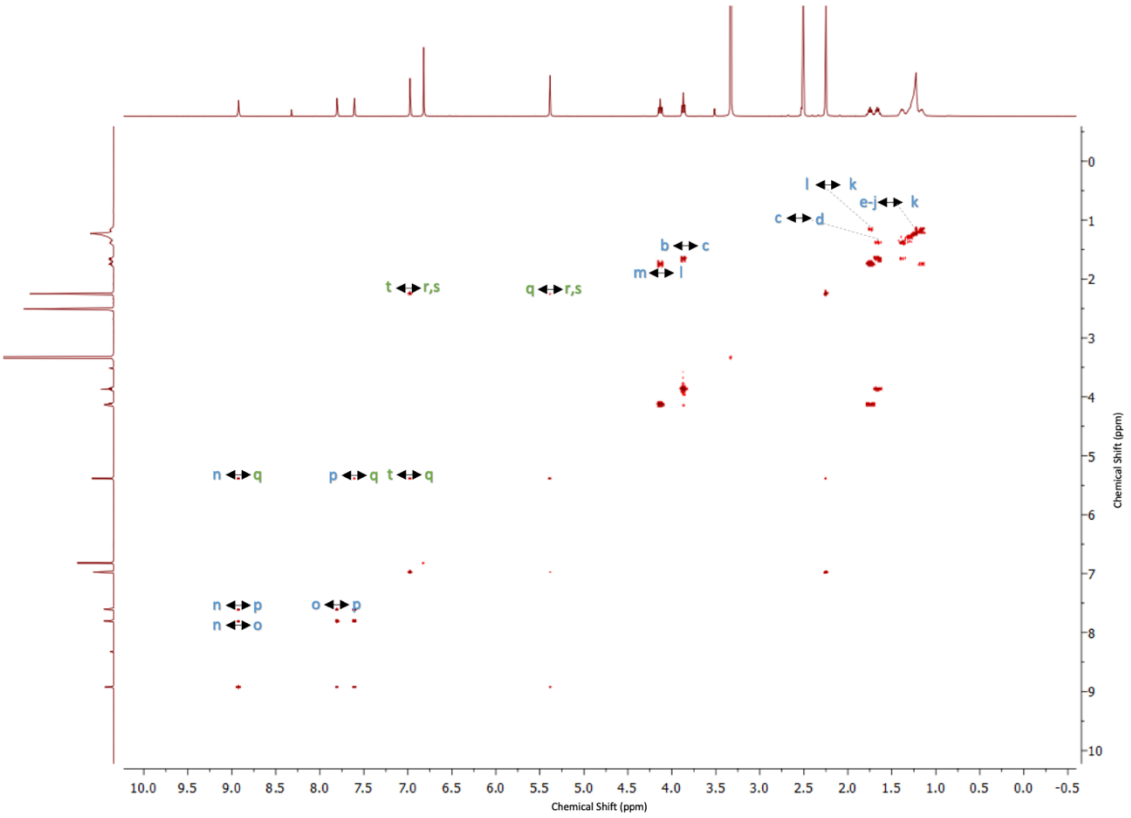

*Figure 7.39. 2D ^{1}H-^{1}H COSY NMR spectrum (400 MHz, DMSO-d_6, 298 K) of **2.15**.*

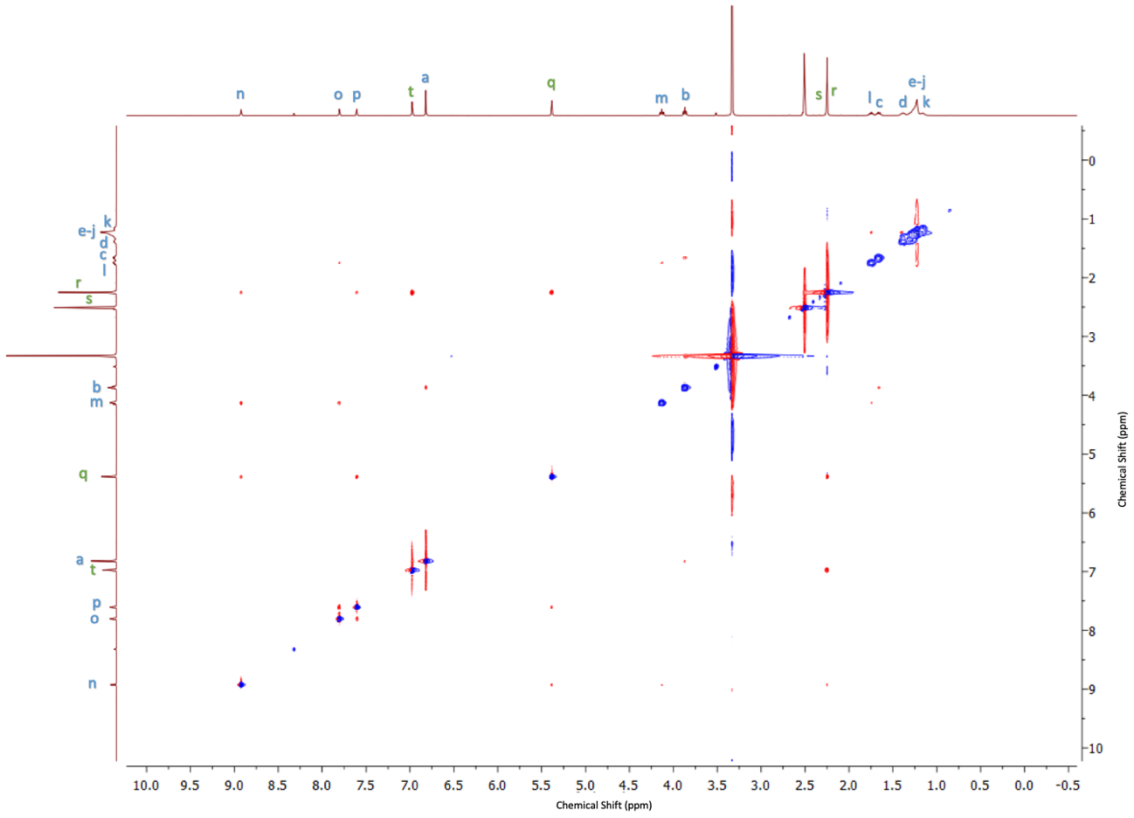

*Figure 7.40. 2D ^{1}H-^{1}H NOESY NMR spectrum (400 MHz, DMSO-d_6, 298 K) of **2.15**.*

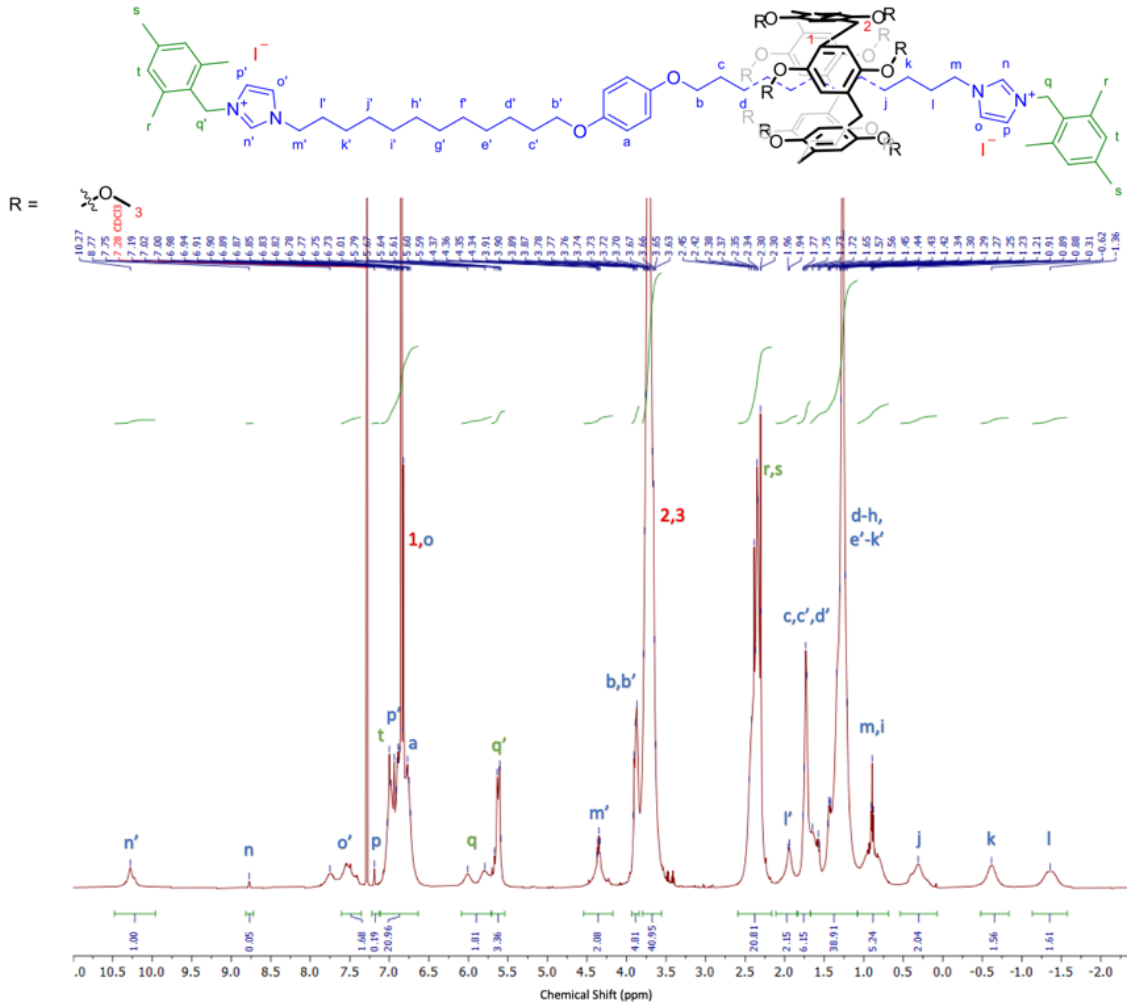

*Figure 7.41. ^{1}H NMR spectrum (500 MHz, $CDCl_3$, 298 K) of **3.11**.*

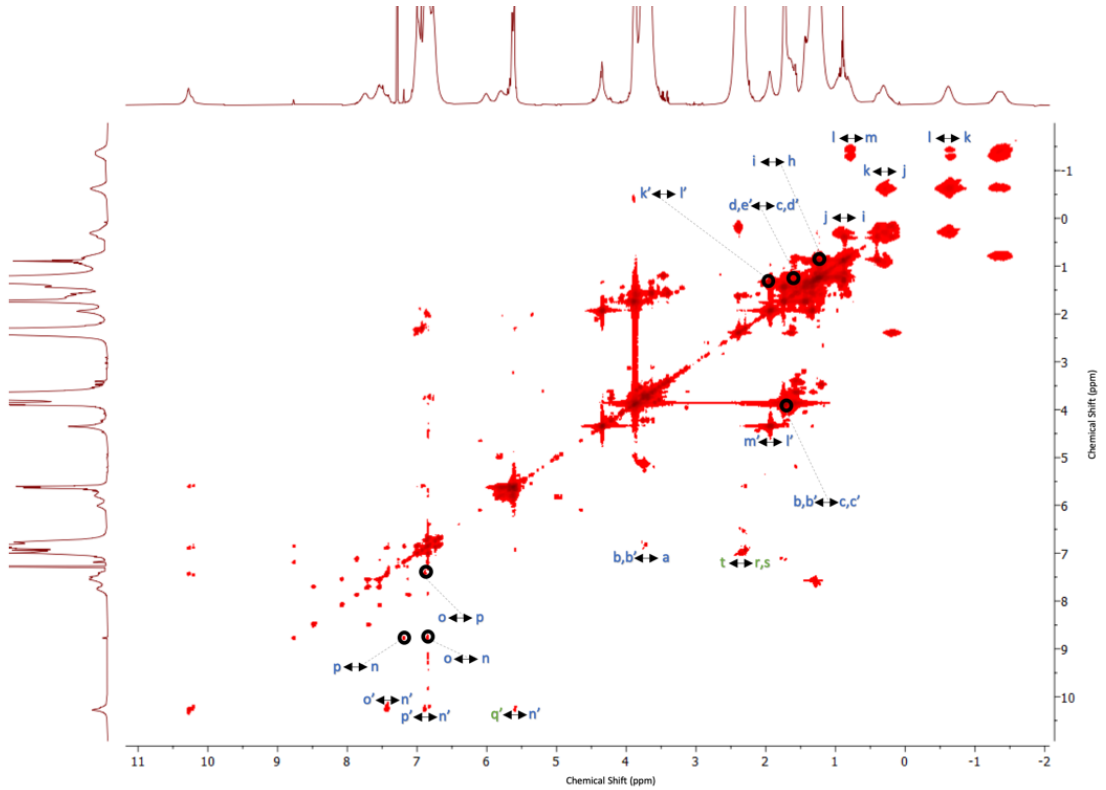

*Figure 7.42. 2D ^{1}H-^{1}H COSY NMR spectrum (500 MHz, $CDCl_3$, 298 K) of **3.11**.*

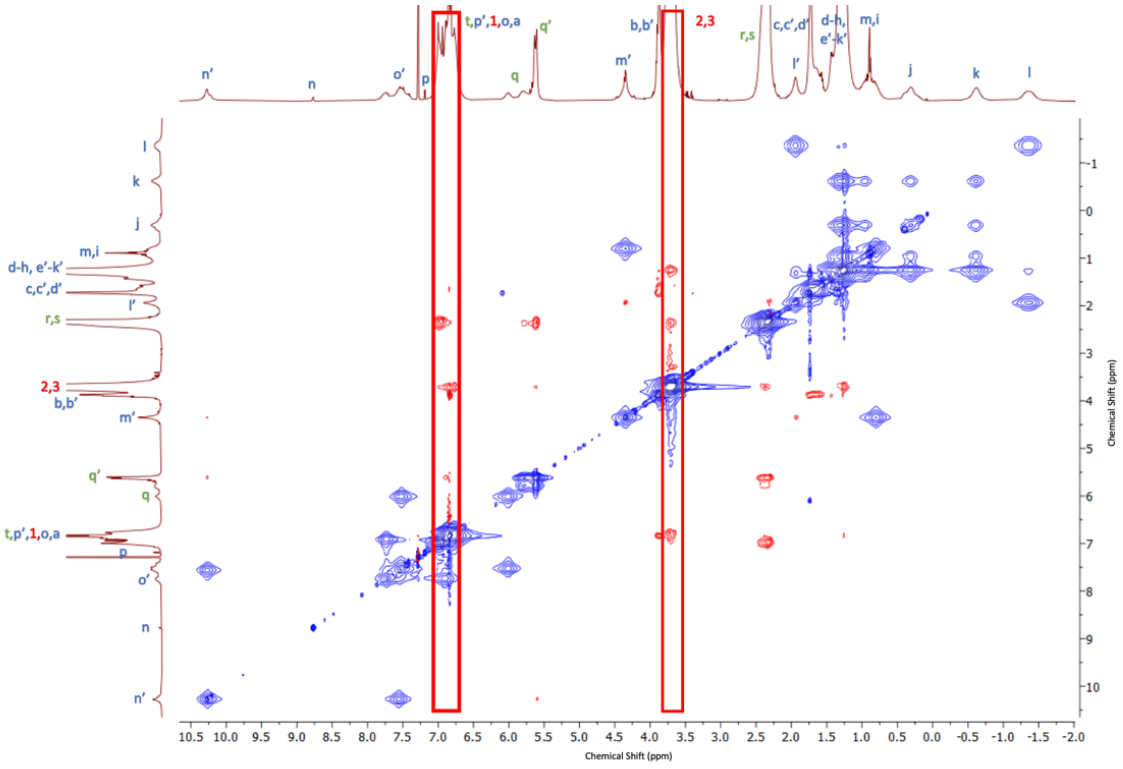

*Figure 7.43. 2D ^{1}H-^{1}H NOESY NMR spectrum (500 MHz, $CDCl_3$, 298 K) of **3.11**.*

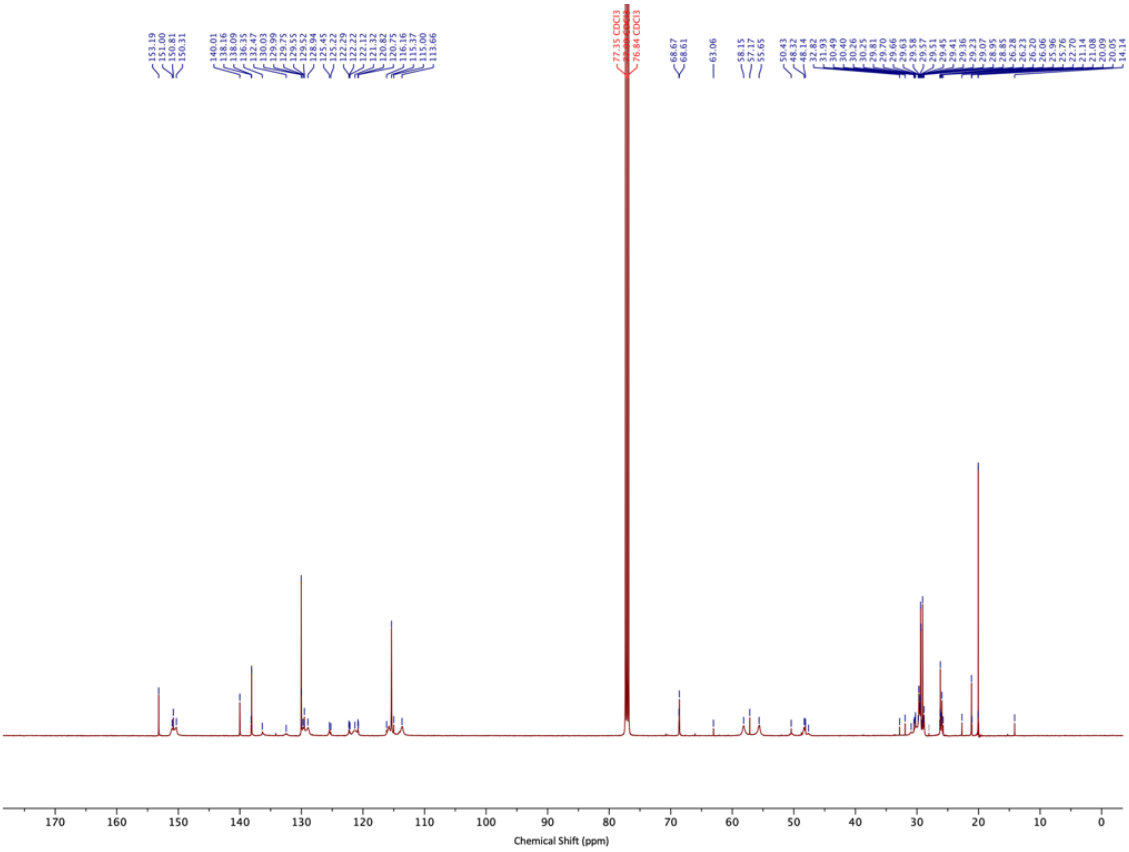

*Figure 7.44. ^{13}C NMR spectrum (126 MHz, $CDCl_3$, 298 K) of **3.11**.*

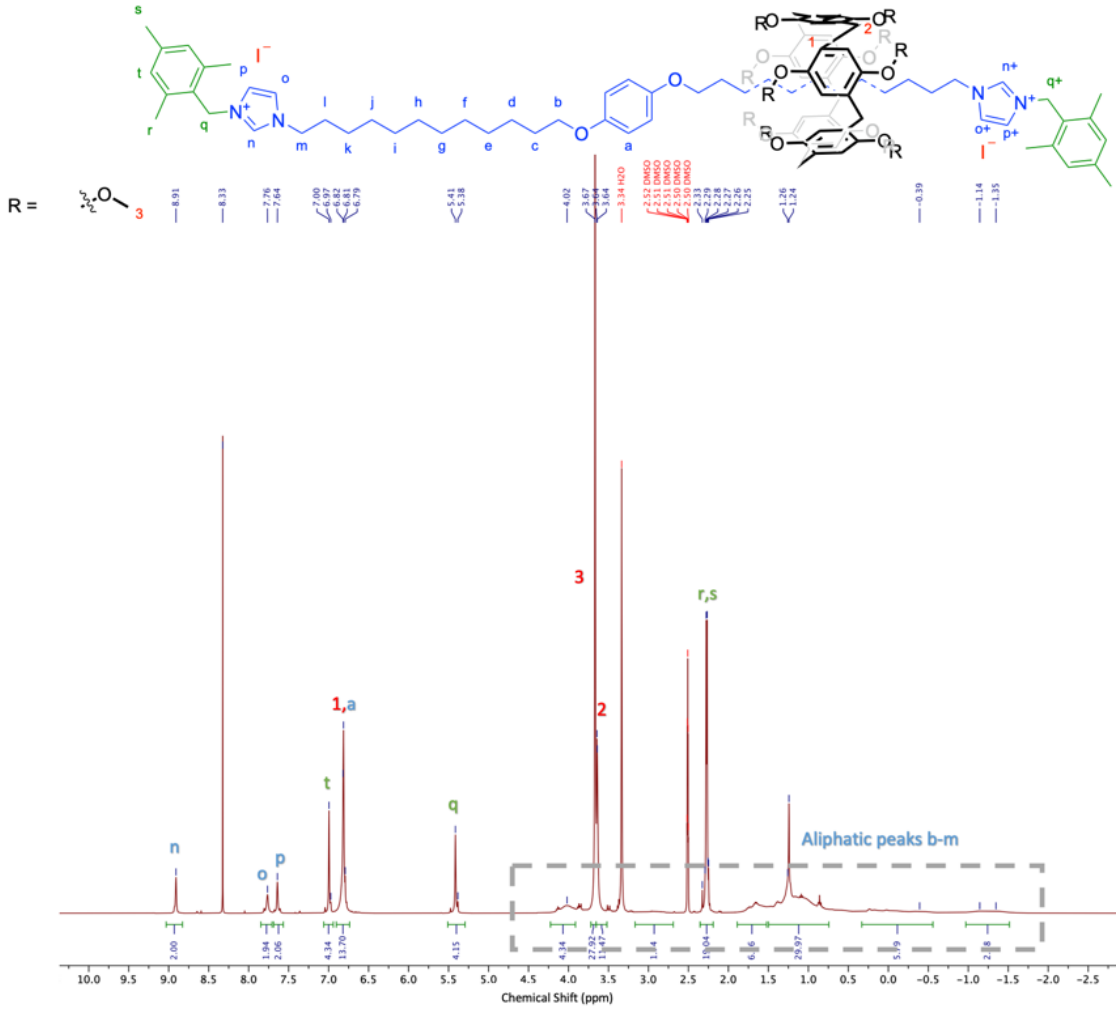

*Figure 7.45. ^{1}H NMR spectrum (500 MHz, DMSO-d_6, 298 K) of **3.11**.*

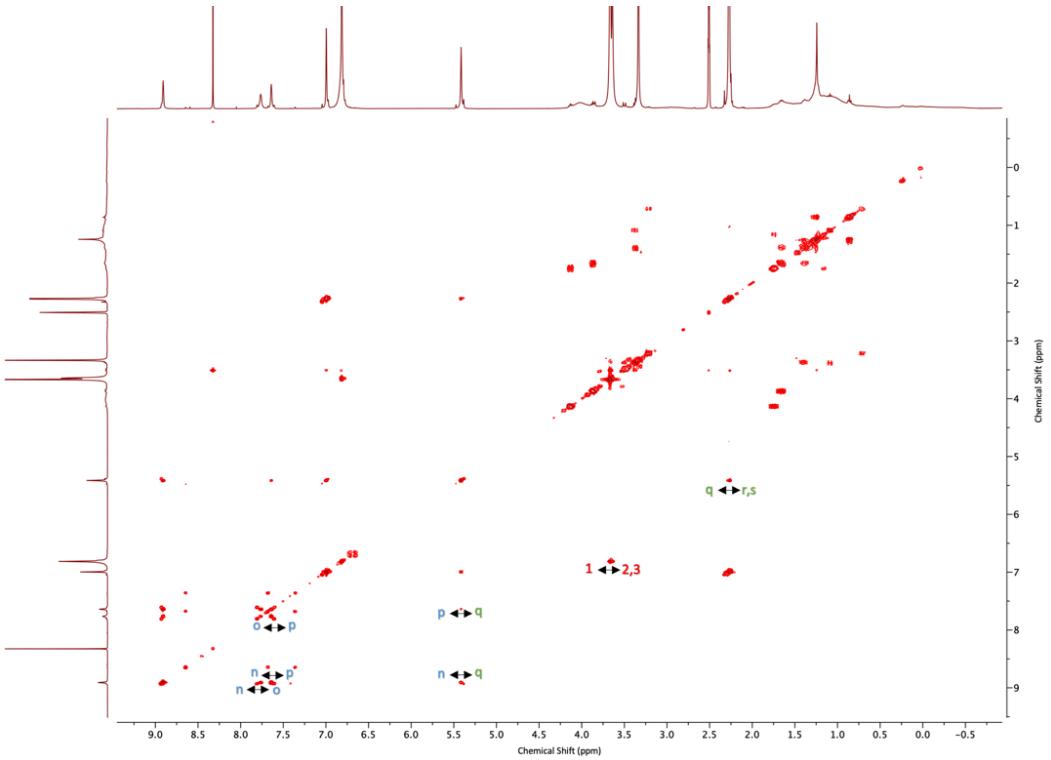

*Figure 7.46. 2D ^{1}H-^{1}H COSY NMR spectrum (500 MHz, DMSO-d_6, 298 K) of **3.11**.*

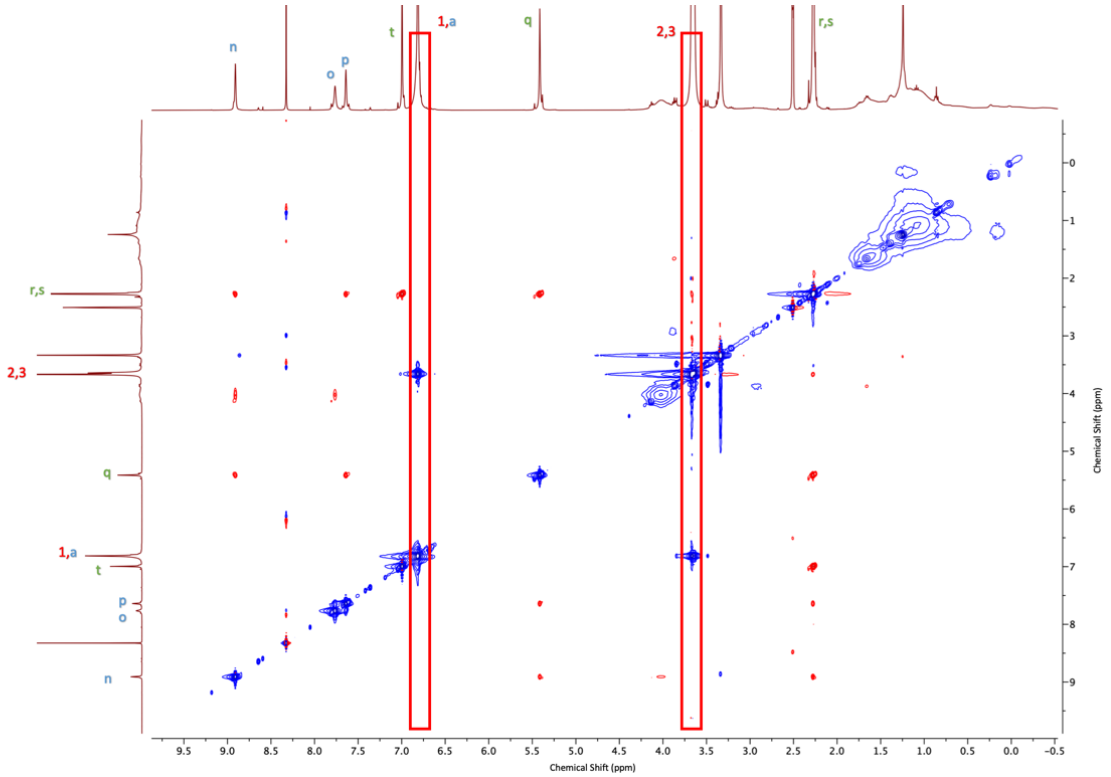

*Figure 7.47. 2D ^{1}H-^{1}H NOESY NMR spectrum (500 MHz, DMSO-d_6, 298 K) of **3.11**.*

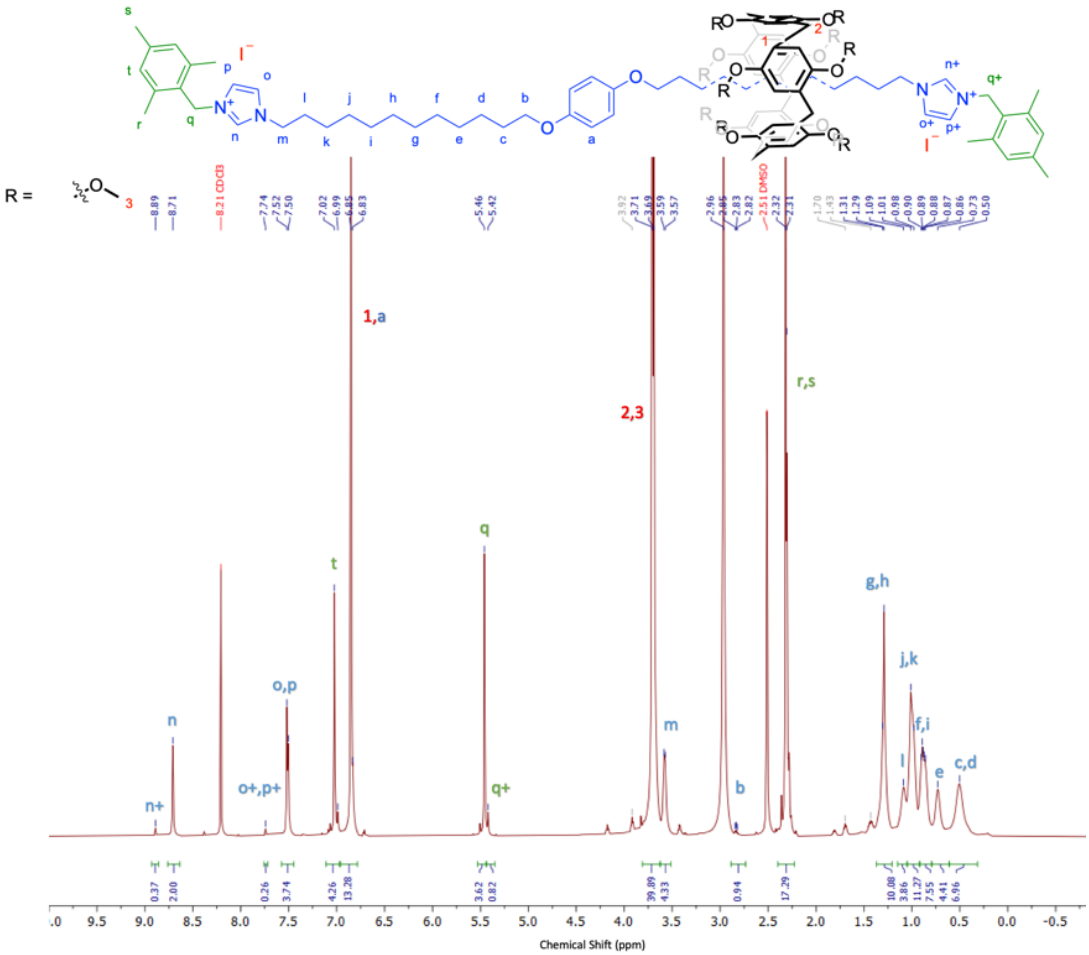

*Figure 7 48. ^{1}H NMR spectrum (600 MHz, DMSO-d_6, 373 K) of **3.11**.*

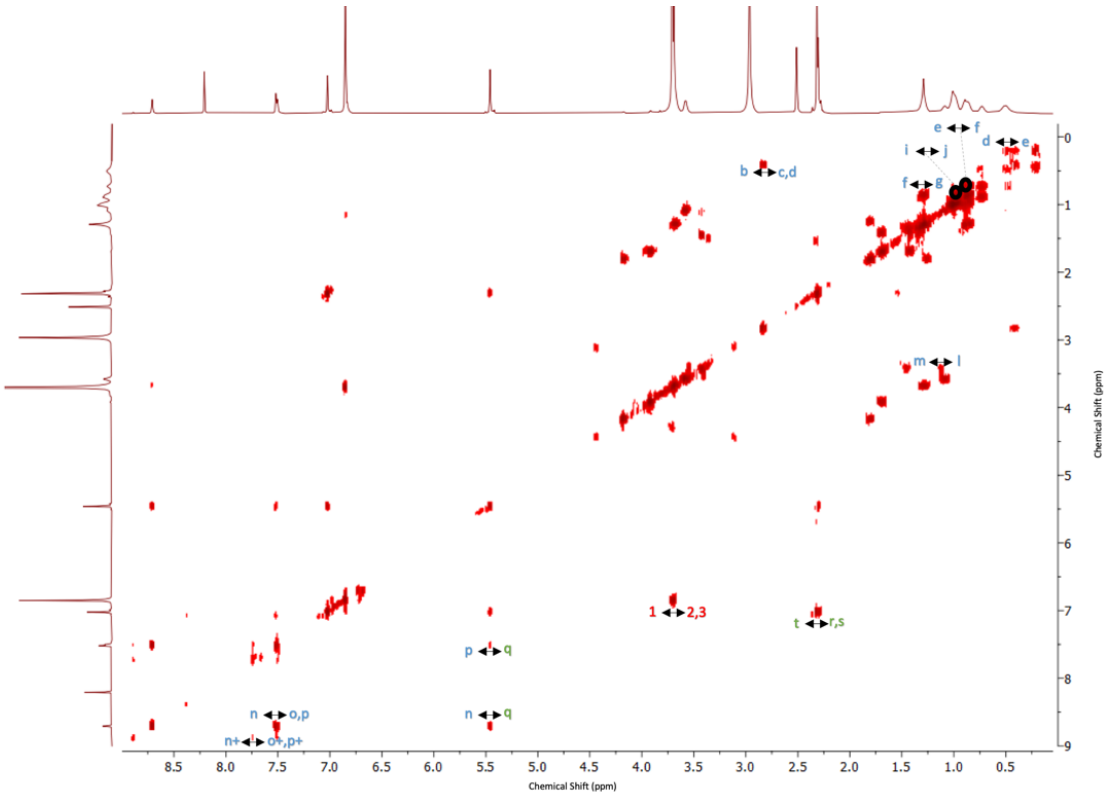

*Figure 7.49. 2D ^{1}H-^{1}H COSY NMR spectrum (600 MHz, DMSO-d_6, 373 K) of **3.11**.*

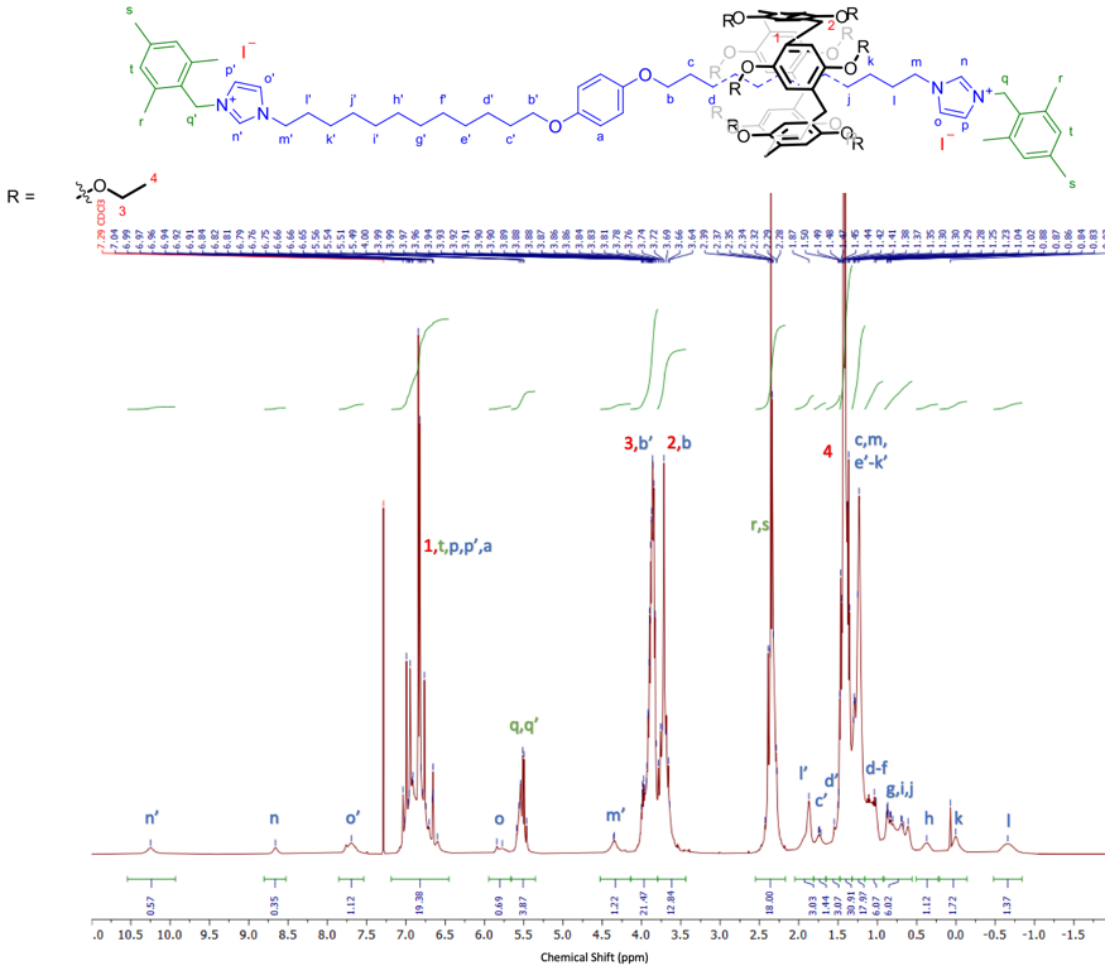

*Figure 7.50. ^{1}H NMR spectrum (500 MHz, $CDCl_3$, 298 K) of **3.12**.*

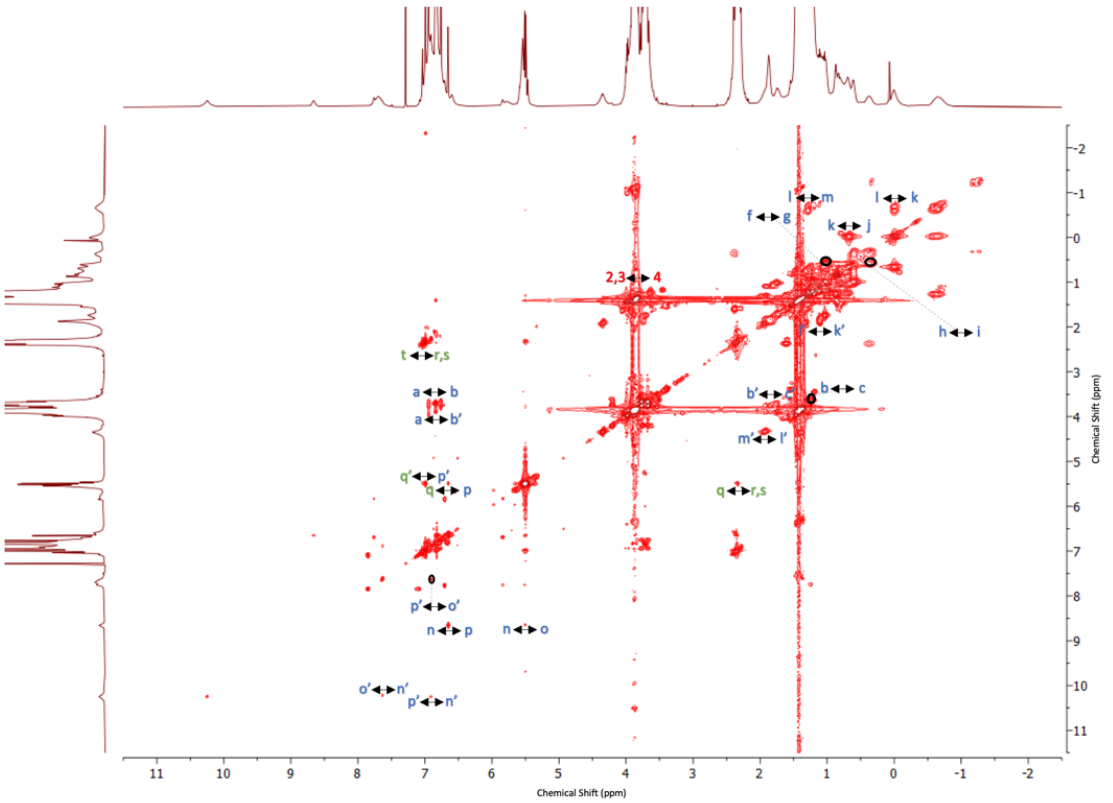

*Figure 7.51. 2D ^{1}H-^{1}H COSY NMR spectrum (500 MHz, $CDCl_3$, 298 K) of **3.12**.*

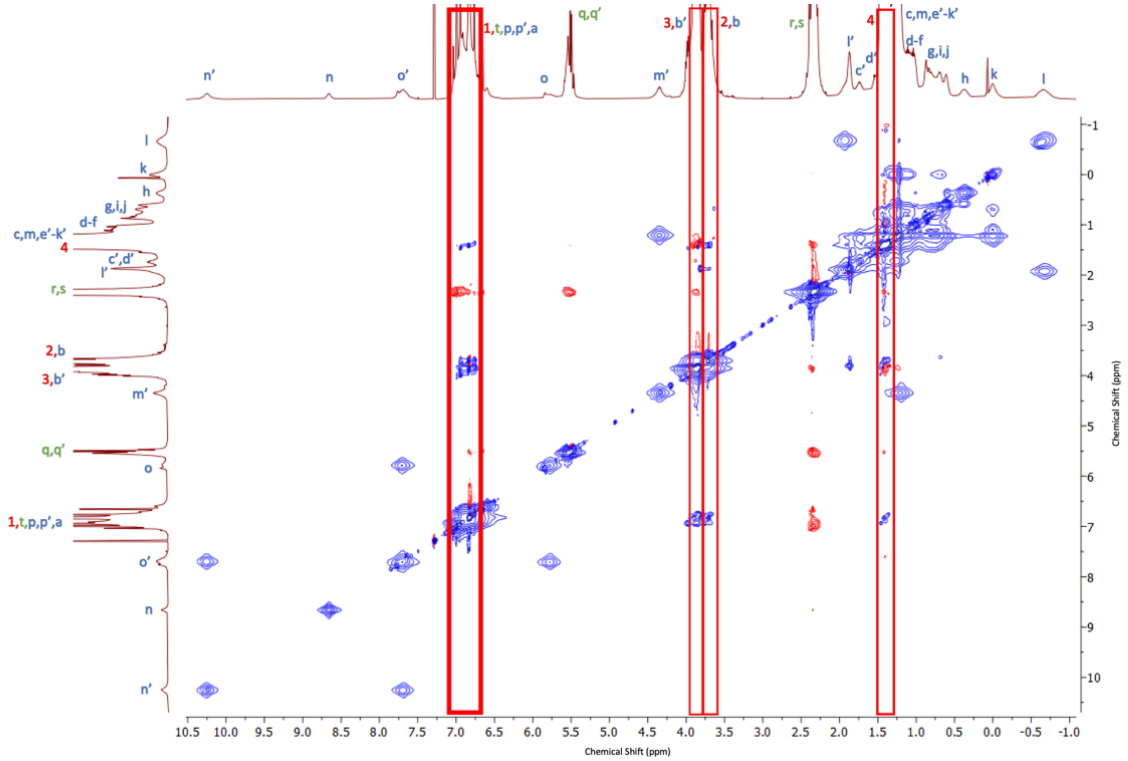

*Figure 7.52. 2D ^{1}H-^{1}H NOESY NMR spectrum (500 MHz, $CDCl_3$, 298 K) of **3.12**.*

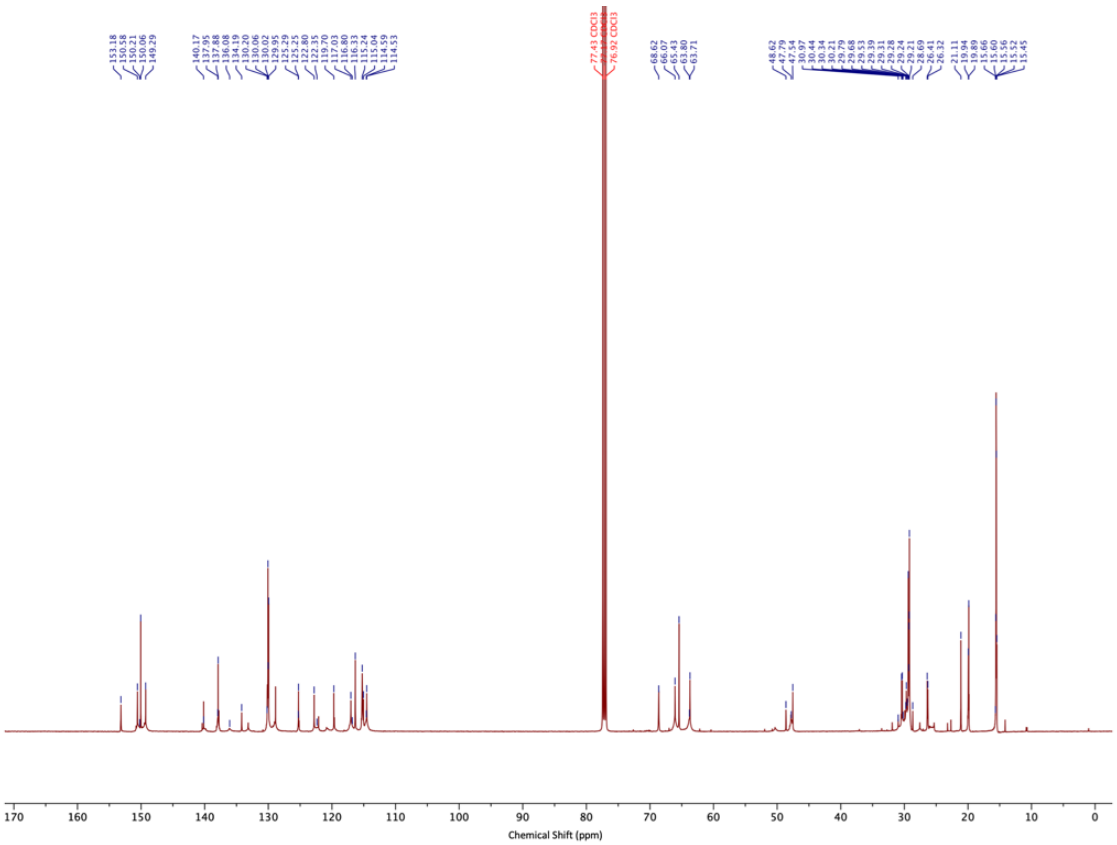

*Figure 7.53. ^{13}C NMR spectrum (126 MHz, $CDCl_3$, 298 K) of **3.12**.*

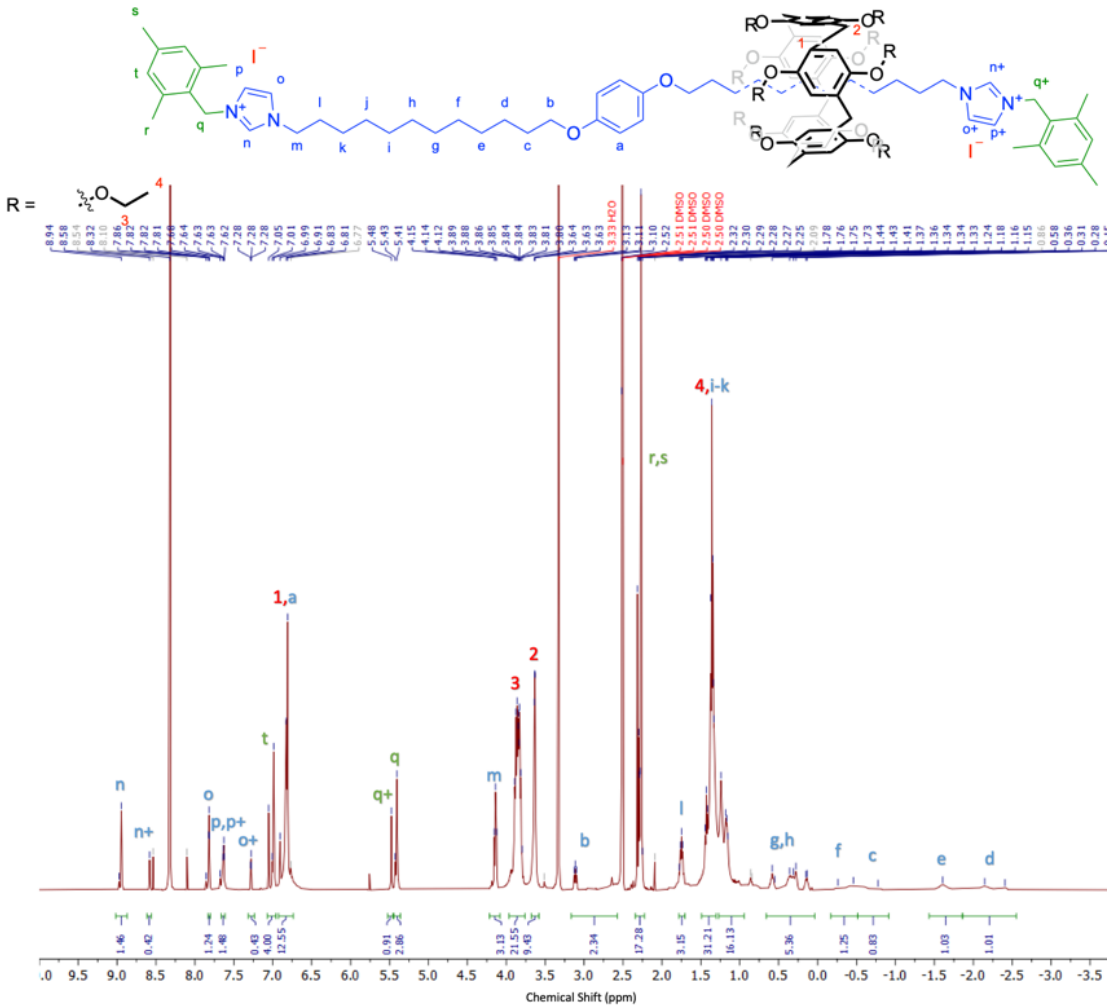

*Figure 7.54. ^{1}H NMR spectrum (500 MHz, DMSO-d_6, 298 K) of **3.12**.*

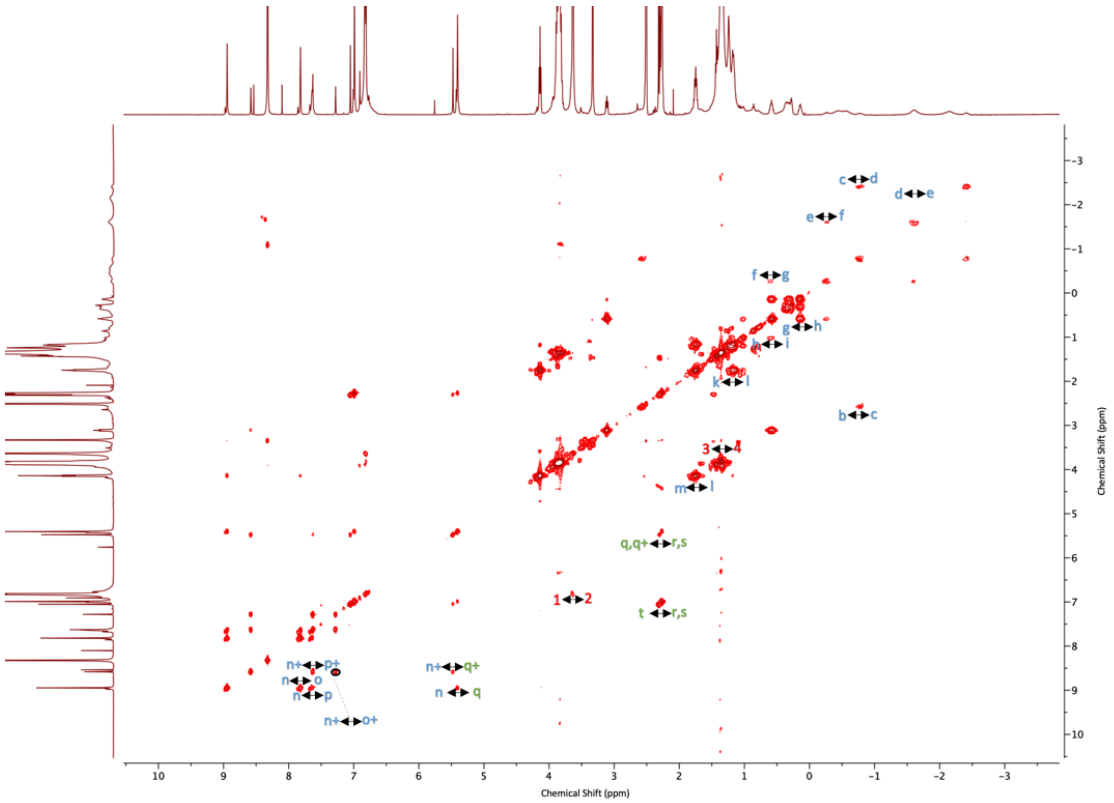

*Figure 7.55. 2D ^{1}H-^{1}H COSY NMR spectrum (500 MHz, DMSO-d_6, 298 K) of **3.12**.*

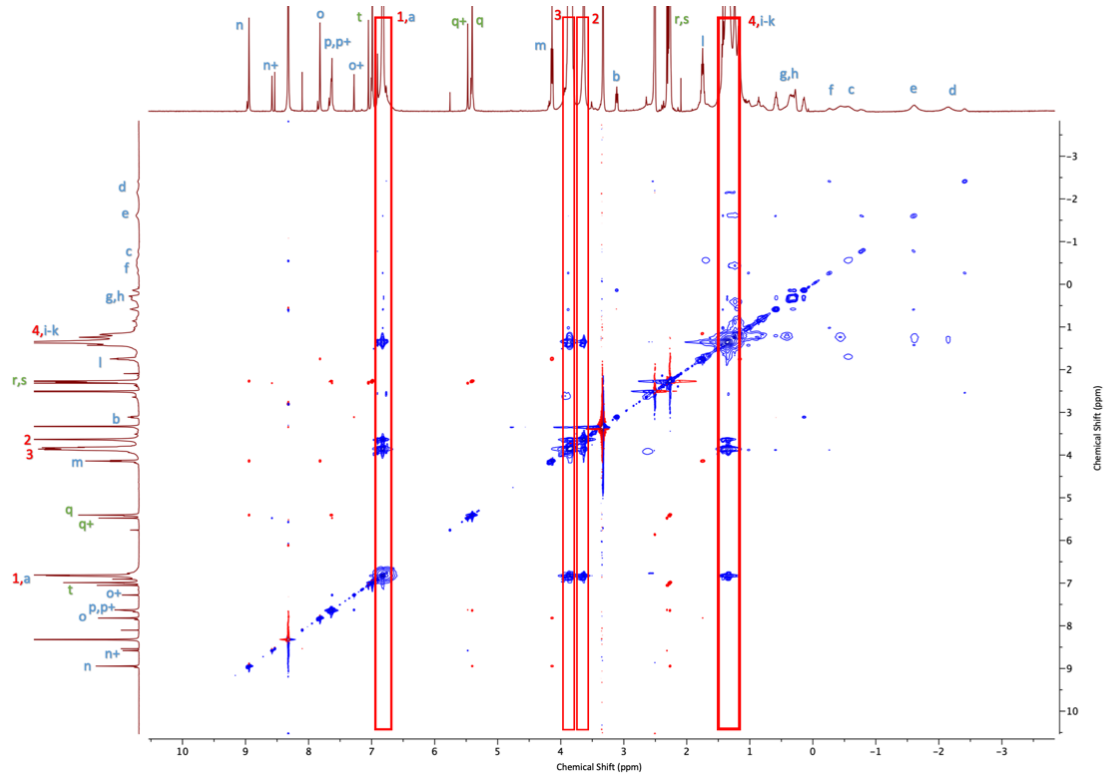

*Figure 7.56. 2D ^{1}H-^{1}H NOESY NMR spectrum (500 MHz, DMSO-d_6, 298 K) of **3.12**.*

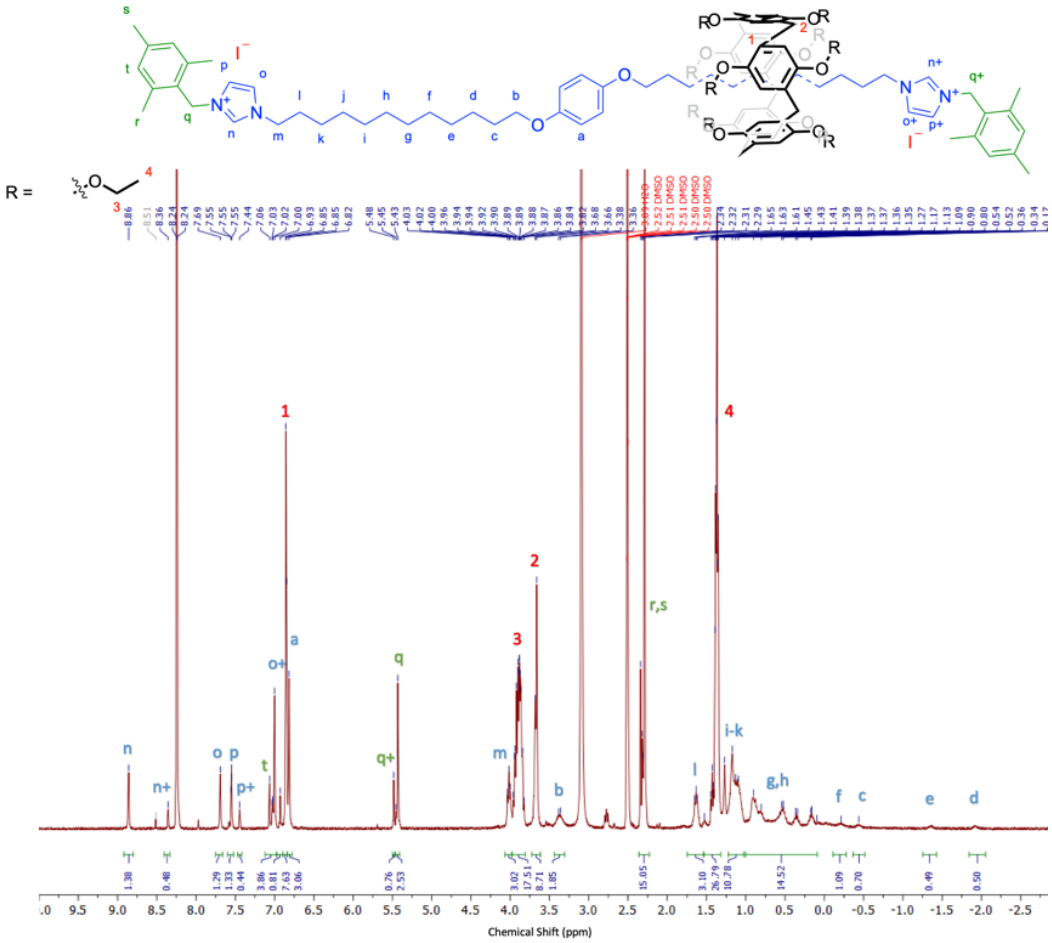

*Figure 7.57. ^{1}H NMR spectrum (400 MHz, DMSO-d_6, 353 K) of **3.12**.*

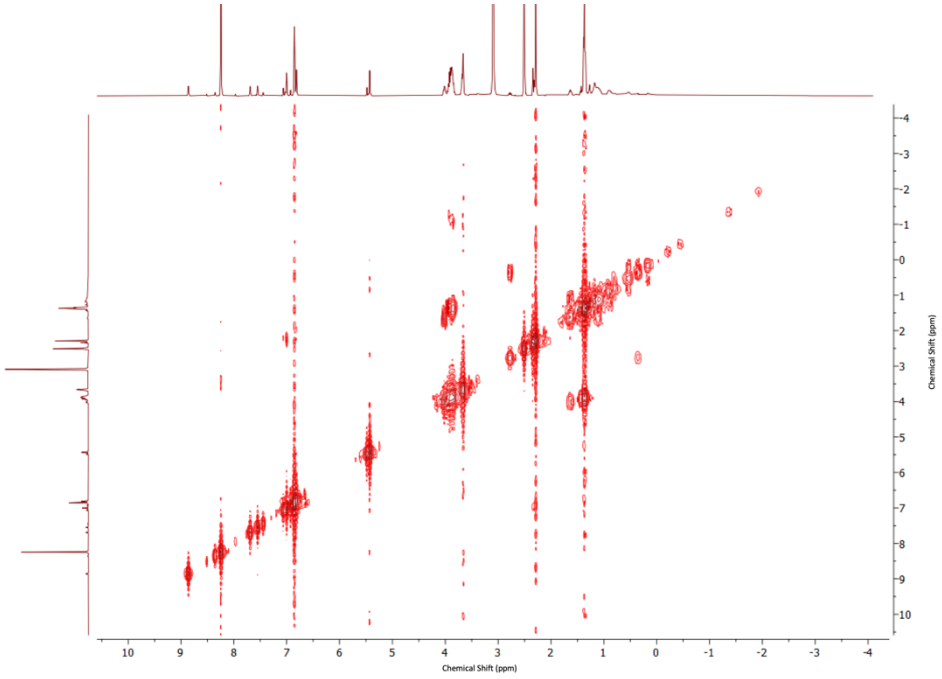

*Figure 7.58. 2D ^{1}H-^{1}H COSY NMR spectrum (400 MHz, DMSO-d_6, 353 K) of **3.12**.*

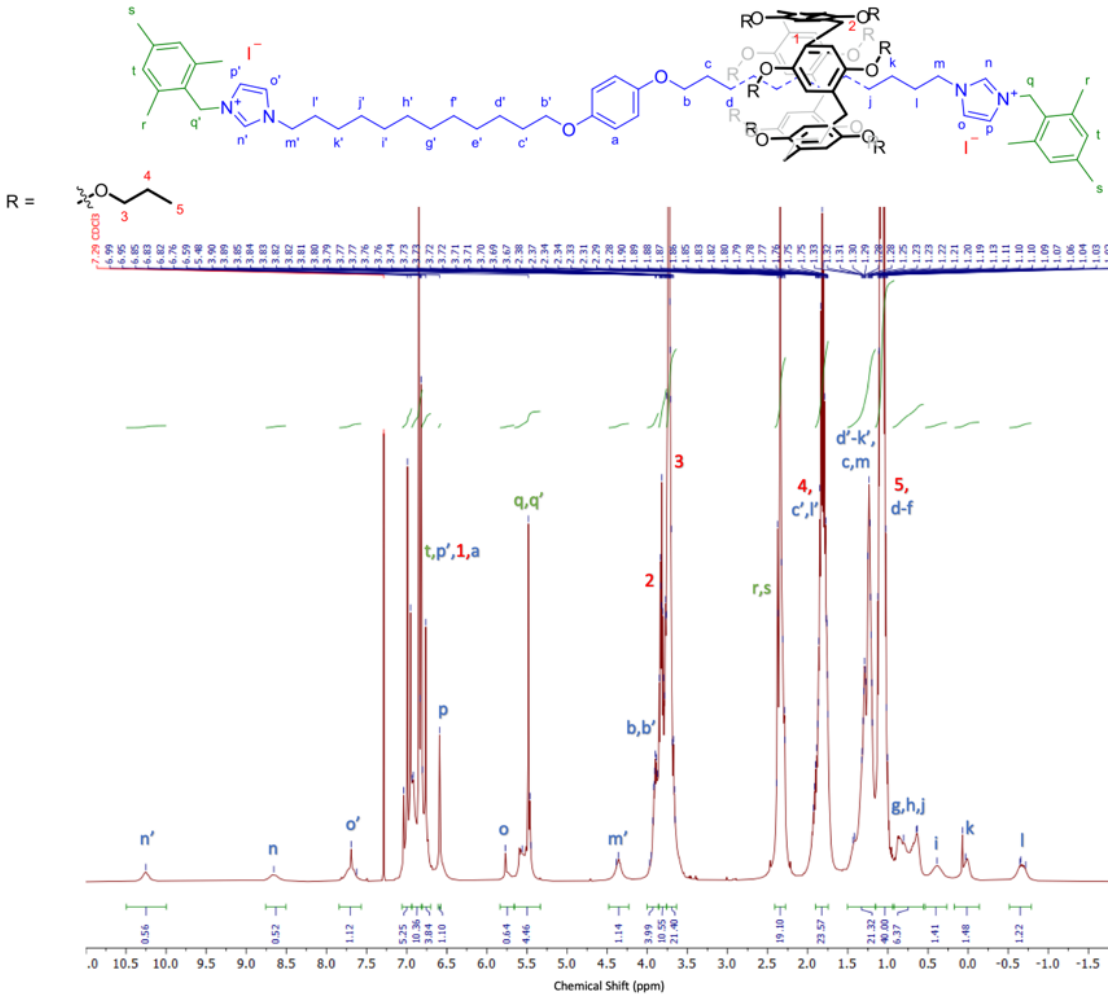

*Figure 7.59. ^{1}H NMR spectrum (500 MHz, $CDCl_3$, 298 K) of **3.13**.*

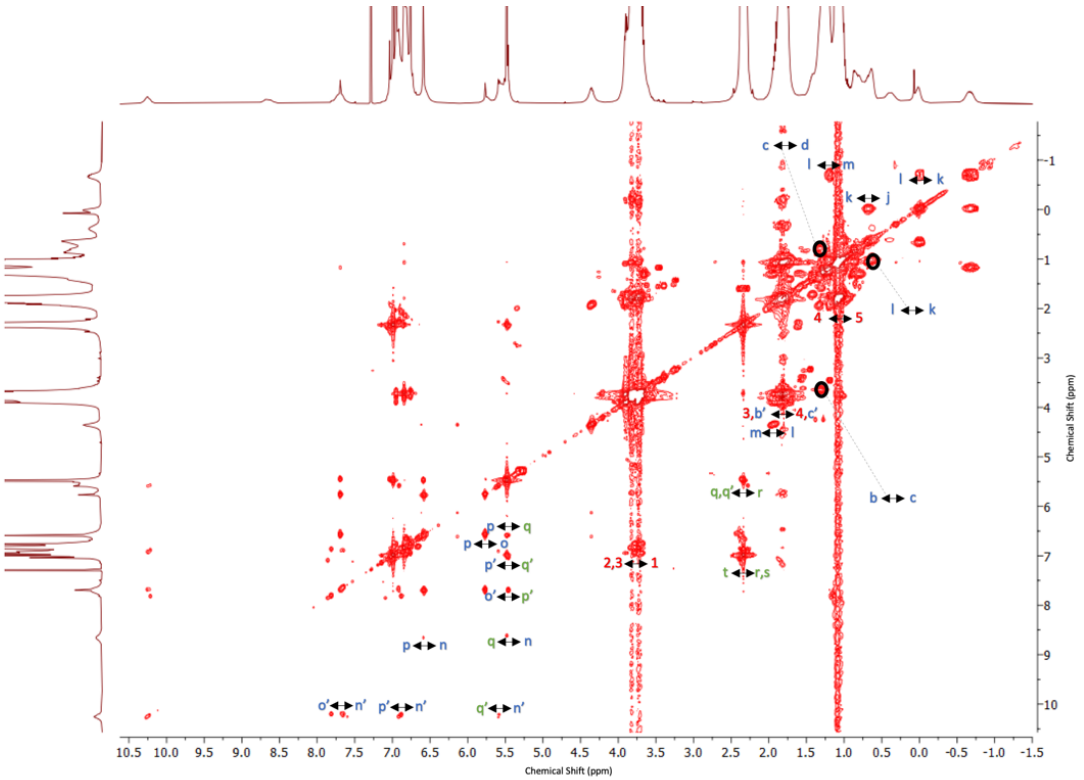

*Figure 7.60. 2D ^{1}H-^{1}H COSY NMR spectrum (500 MHz, $CDCl_3$, 298 K) of **3.13**.*

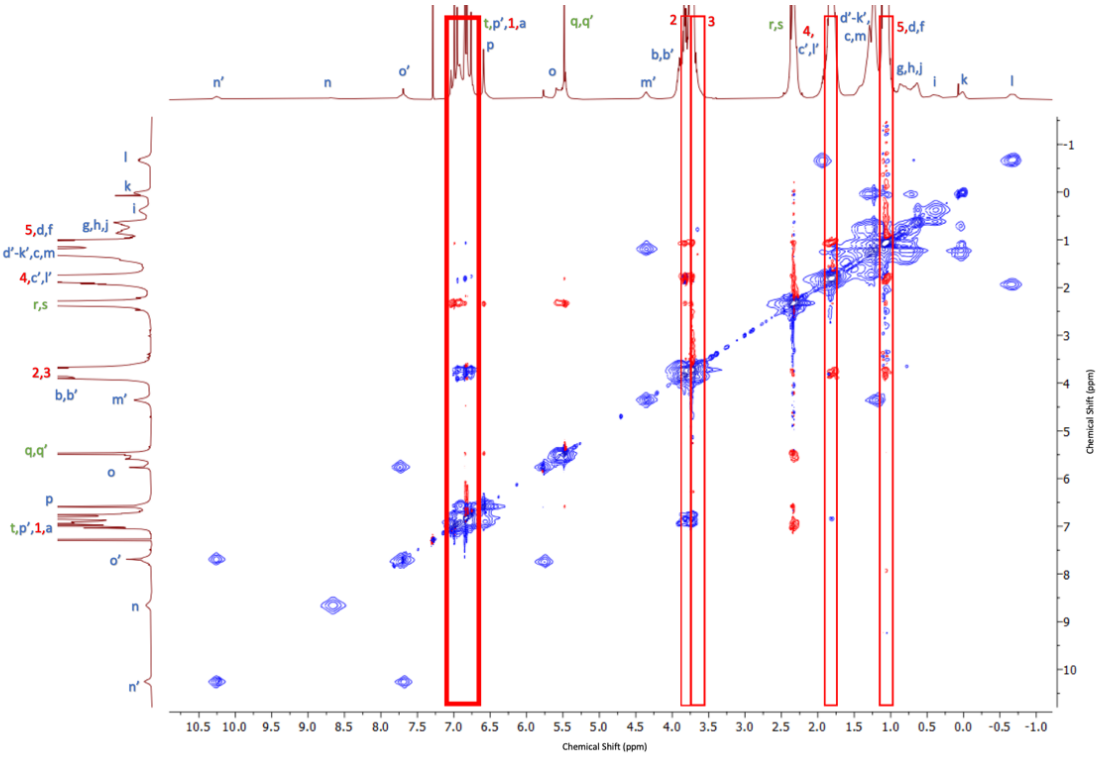

*Figure 7.61. 2D ^{1}H-^{1}H NOESY NMR spectrum (500 MHz, $CDCl_3$, 298 K) of **3.13**.*

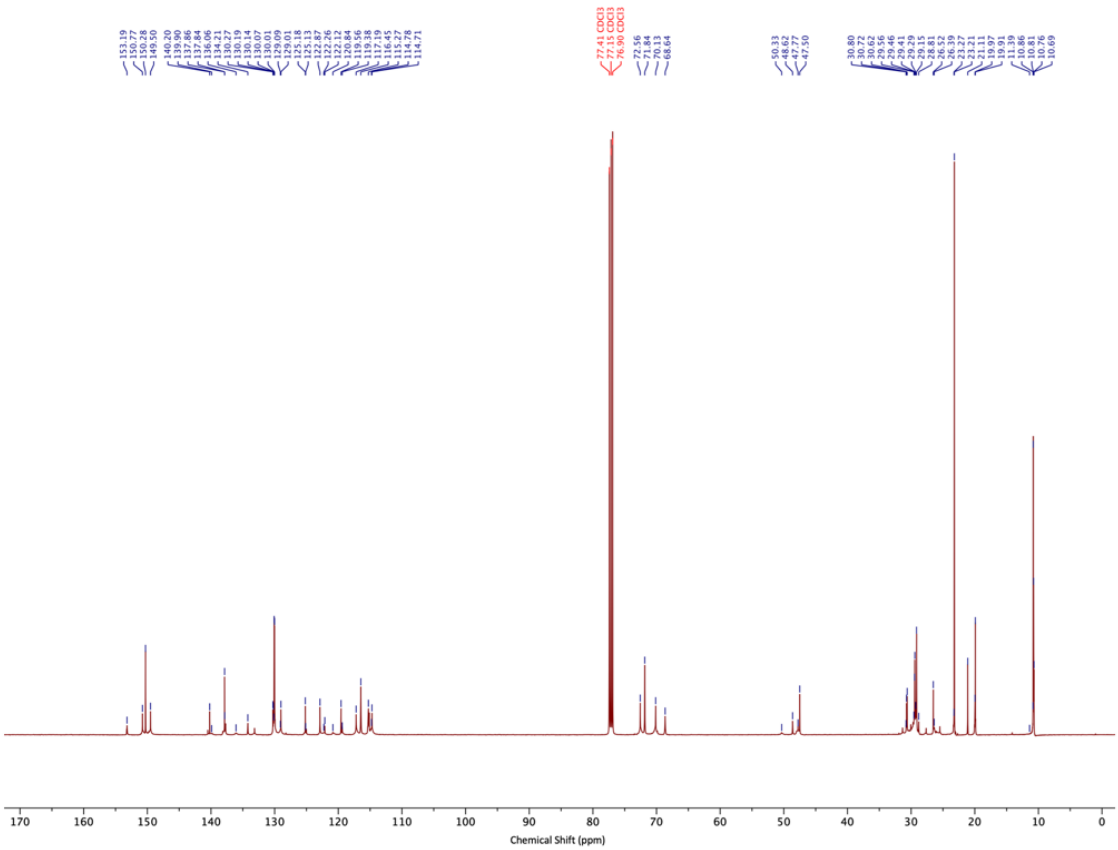

*Figure 7.62. ^{13}C NMR spectrum (126 MHz, $CDCl_3$, 298 K) of **3.13**.*

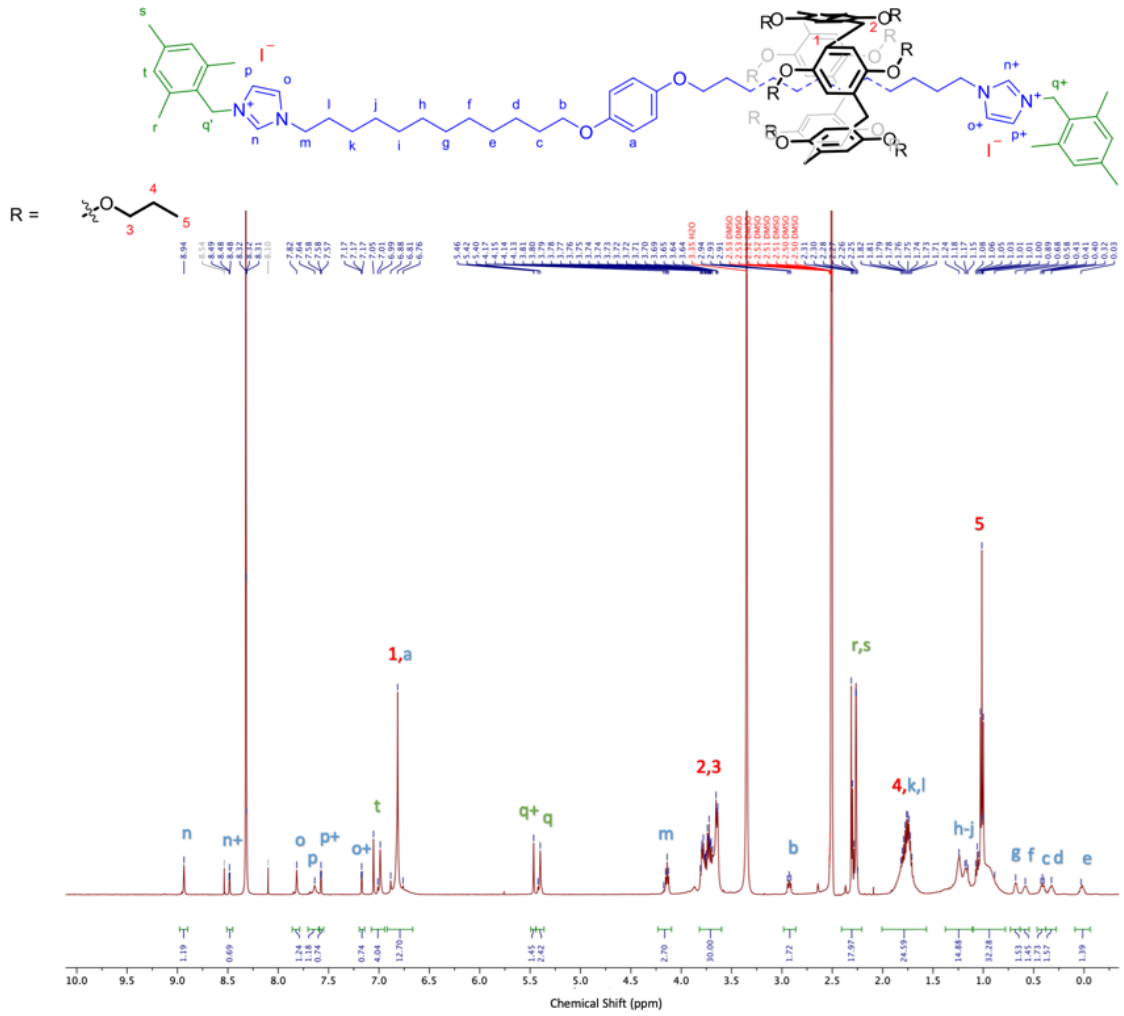

*Figure 7.63. ^{1}H NMR spectrum (500 MHz, DMSO-d_6, 298 K) of **3.13**.*

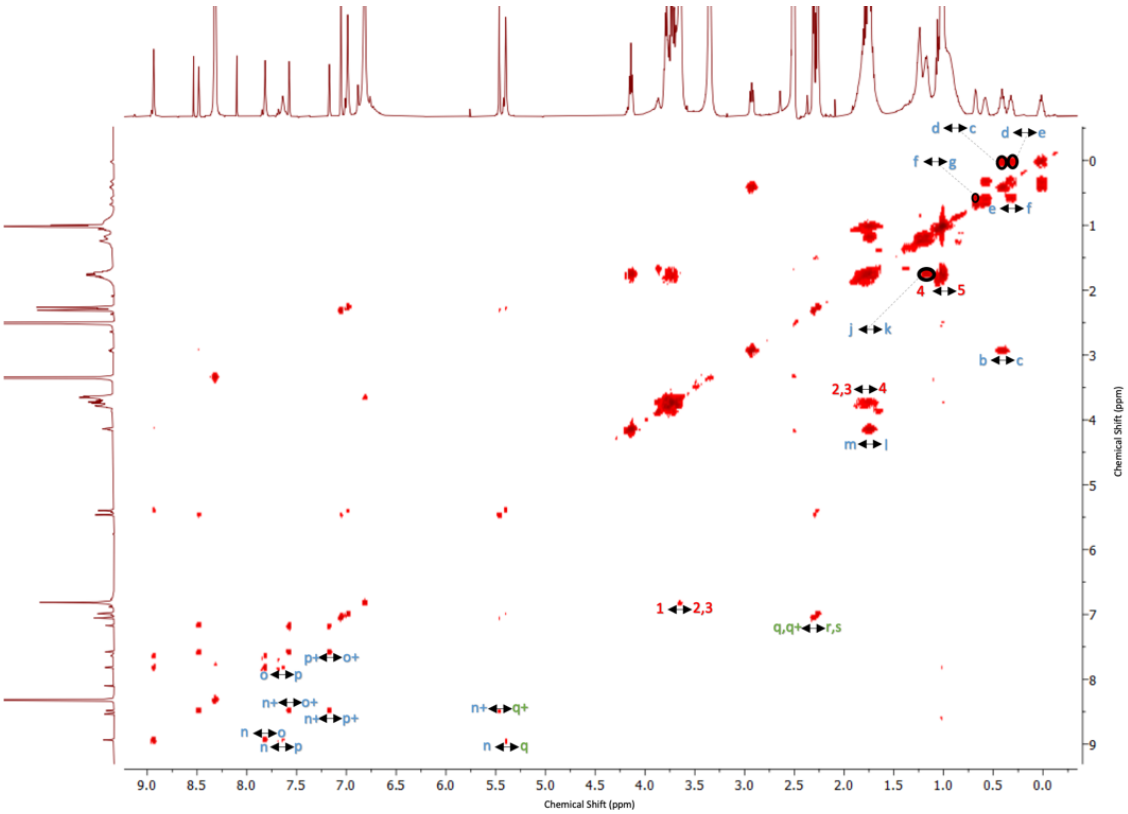

*Figure 7.64. 2D ^{1}H-^{1}H COSY NMR spectrum (500 MHz, DMSO-d_6, 298 K) of **3.13**.*

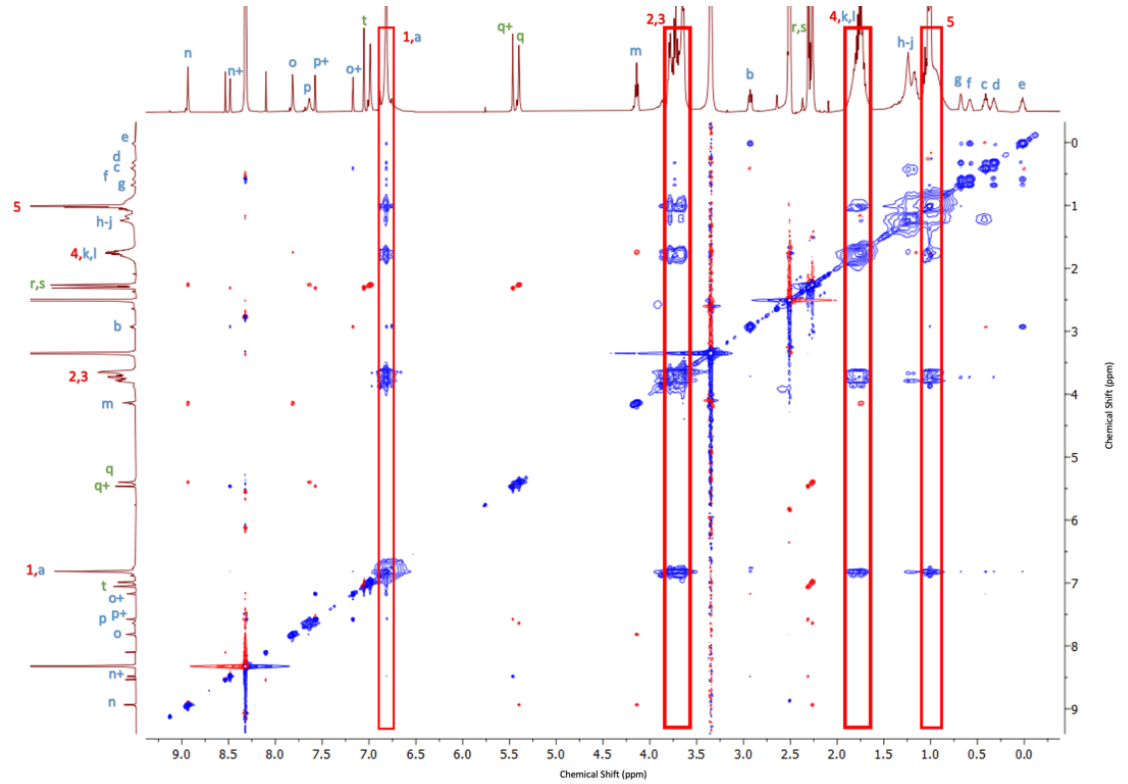

*Figure 7.65. 2D ^{1}H-^{1}H NOESY NMR spectrum (500 MHz, DMSO-d_6, 298 K) of **3.13**.*

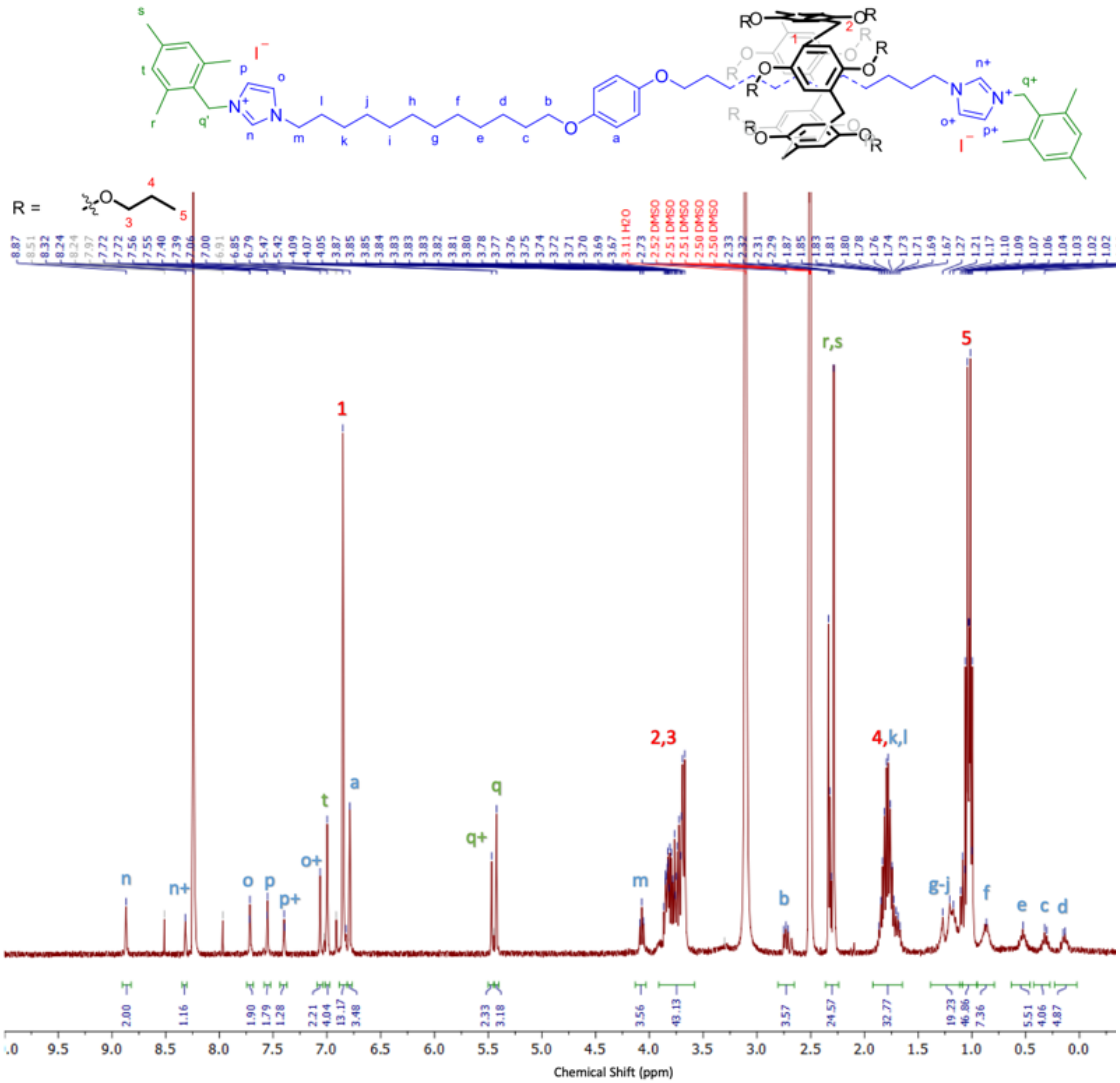

*Figure 7.66. ^{1}H NMR spectrum (400 MHz, DMSO-d_6, 353 K) of **3.13**.*

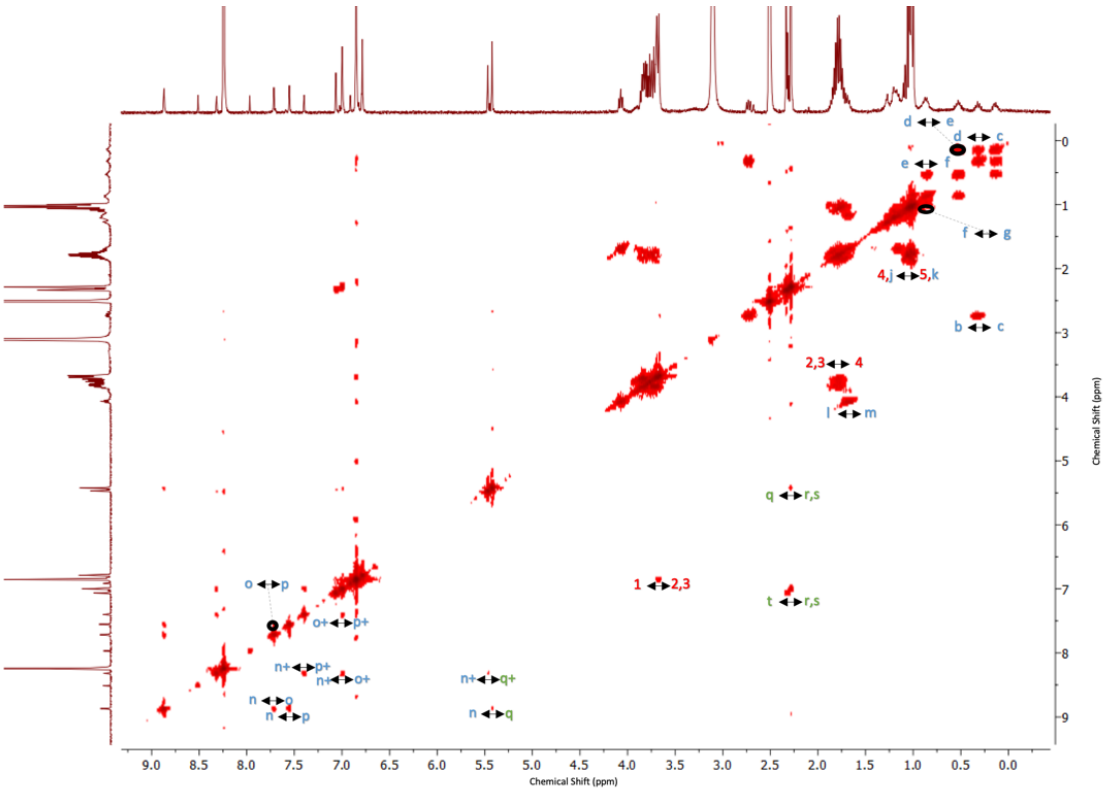

*Figure 7.67. 2D ^{1}H-^{1}H COSY NMR spectrum (400 MHz, DMSO-d_6, 353 K) of **3.13**.*

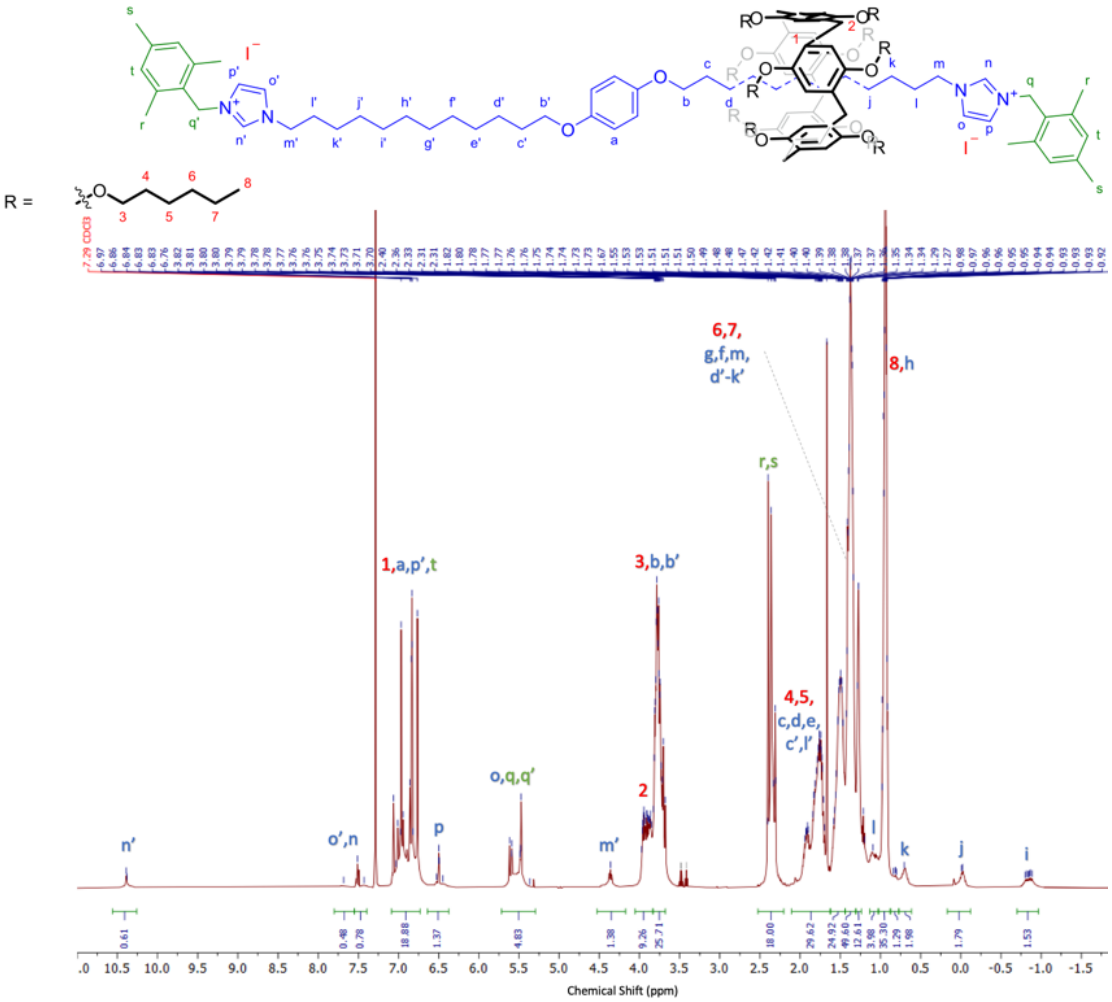

*Figure 7.68. ^{1}H NMR spectrum (500 MHz, $CDCl_3$, 298 K) of **3.14**.*

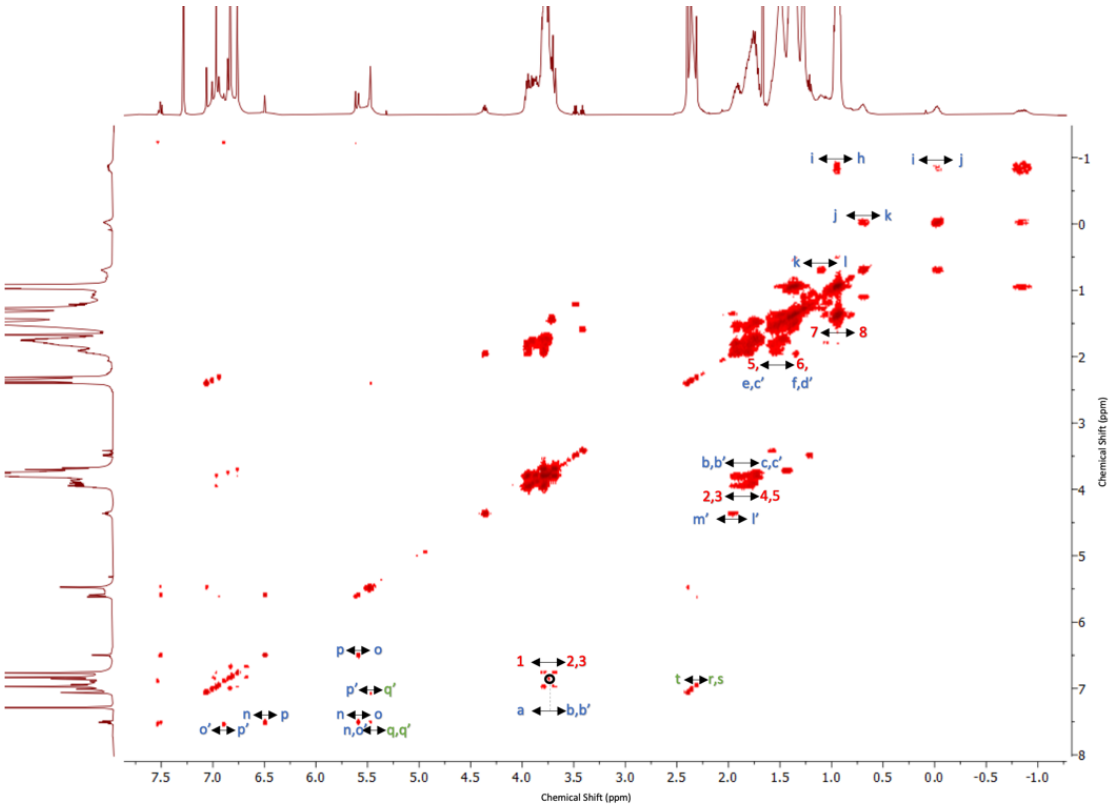

*Figure 7.69. 2D ^{1}H-^{1}H COSY NMR spectrum (500 MHz, $CDCl_3$, 298 K) of **3.14**.*

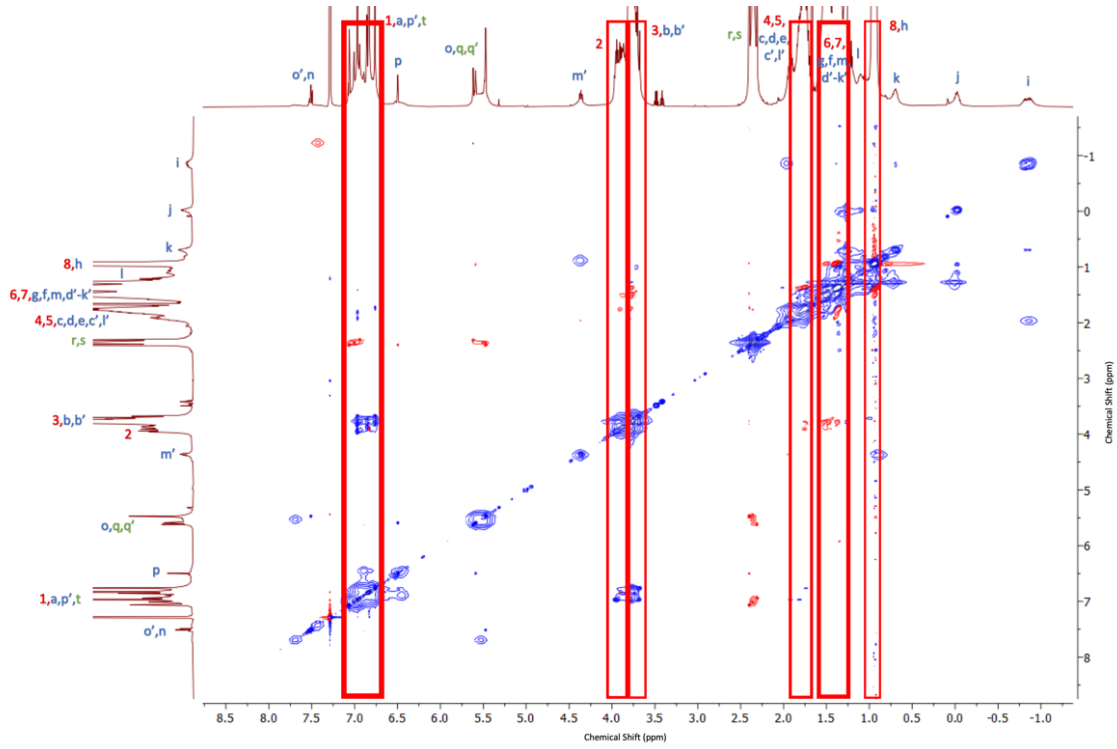

*Figure 7.70. 2D ^{1}H-^{1}H NOESY NMR spectrum (500 MHz, $CDCl_3$, 298 K) of **3.14**.*

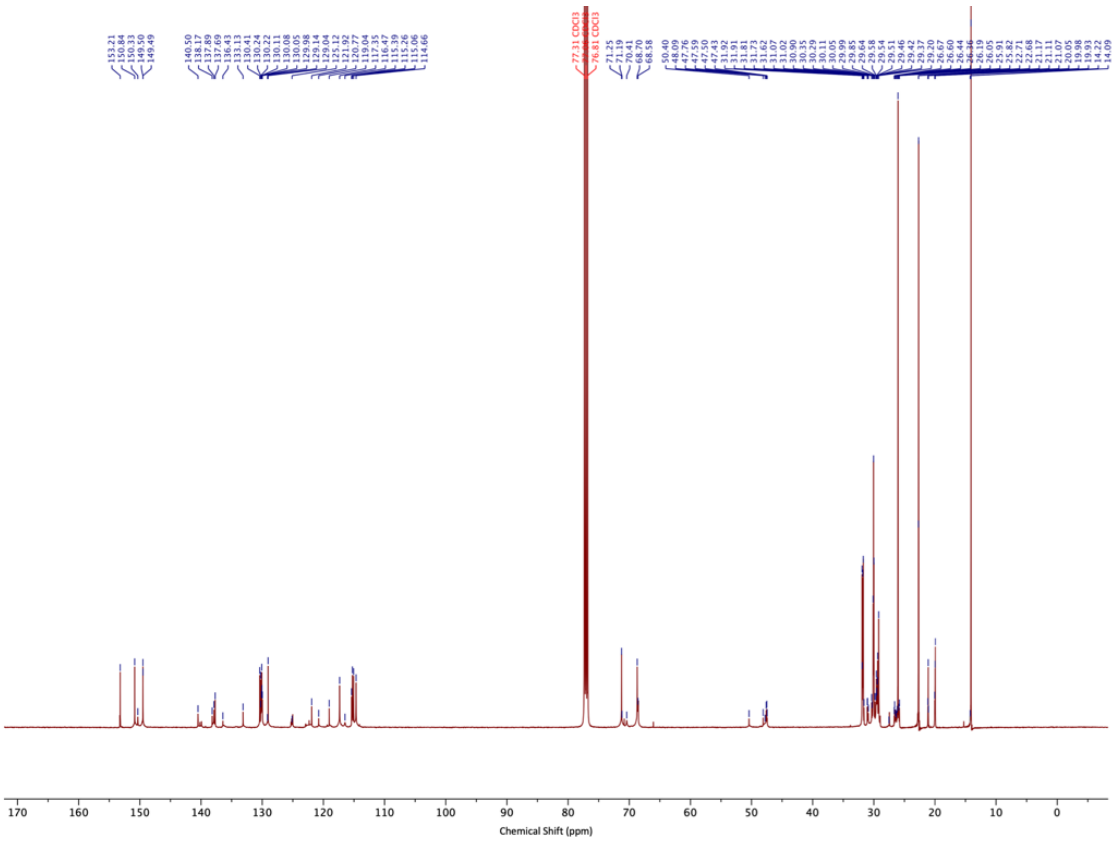

*Figure 7.71. ^{13}C NMR spectrum (126 MHz, $CDCl_3$, 298 K) of **3.14**.*

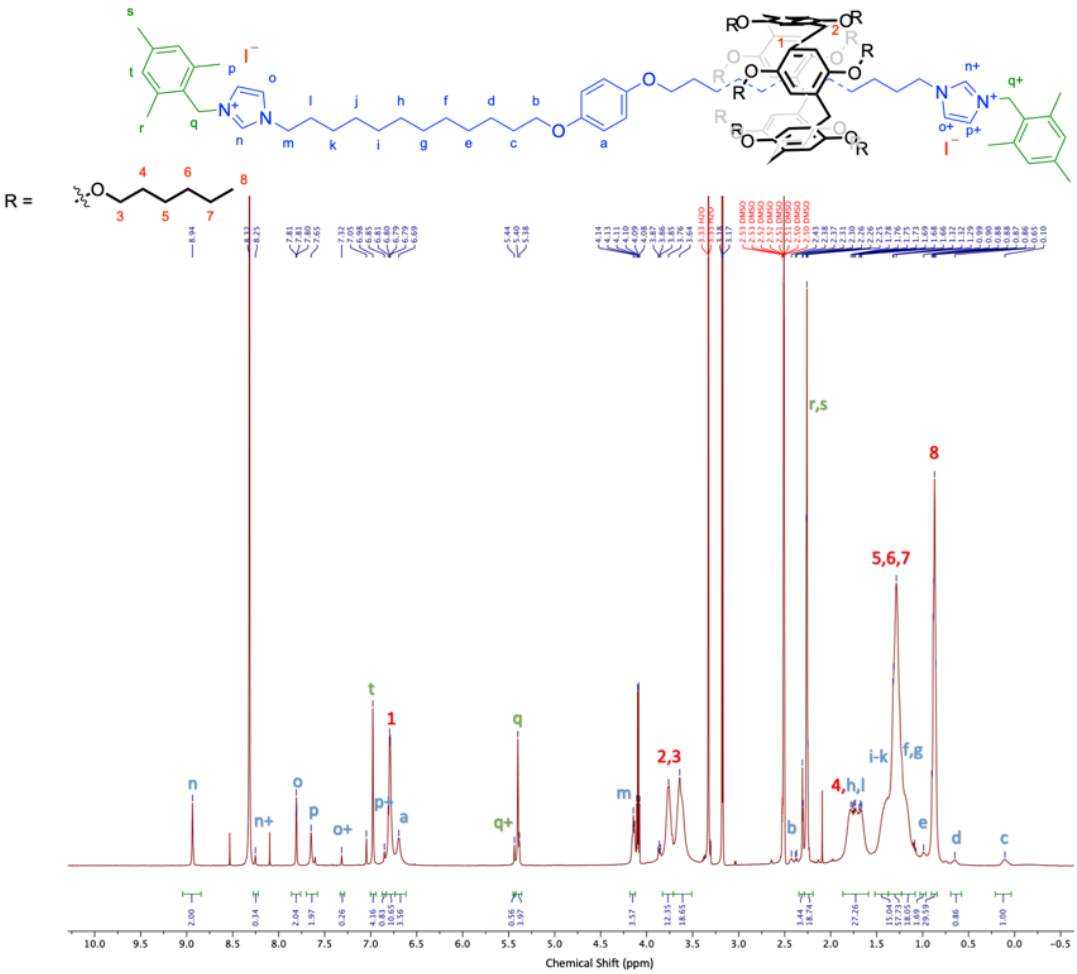

*Figure 7.72. ^{1}H NMR spectrum (500 MHz, DMSO-d_6, 298 K) of **3.14**.*

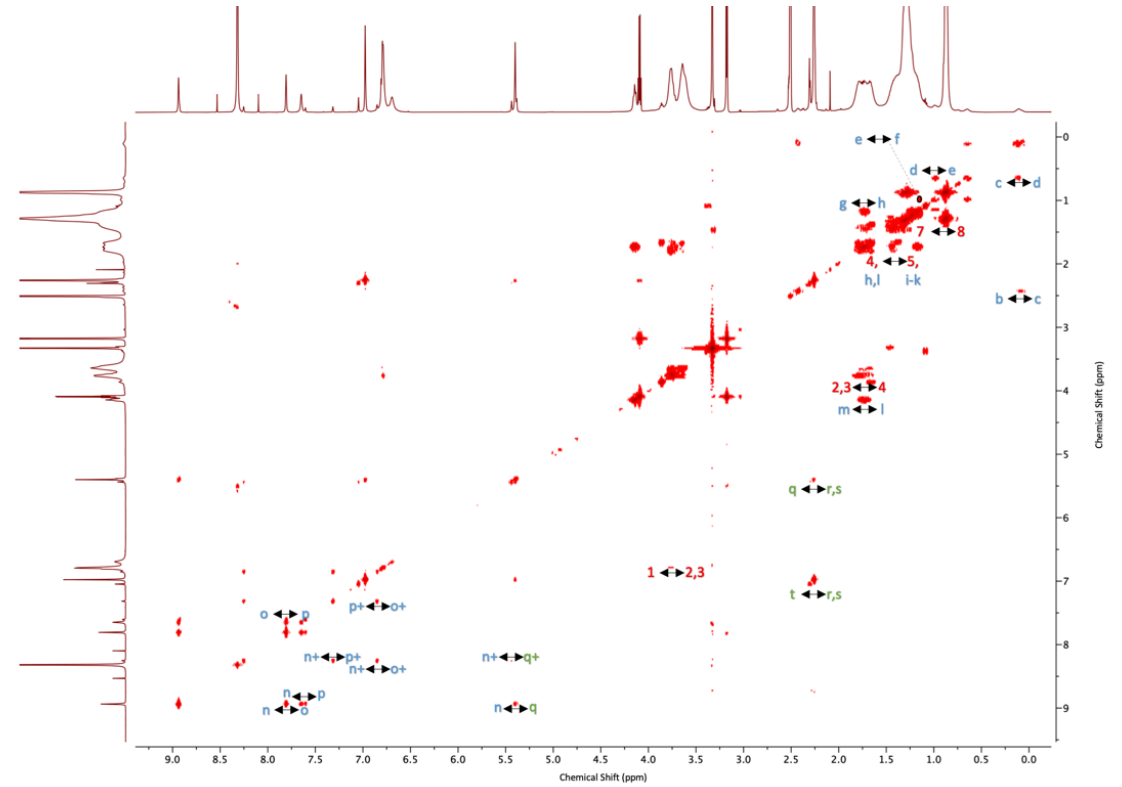

*Figure 7.73. 2D ^{1}H-^{1}H COSY NMR spectrum (500 MHz, DMSO-d_6, 298 K) of **3.14**.*

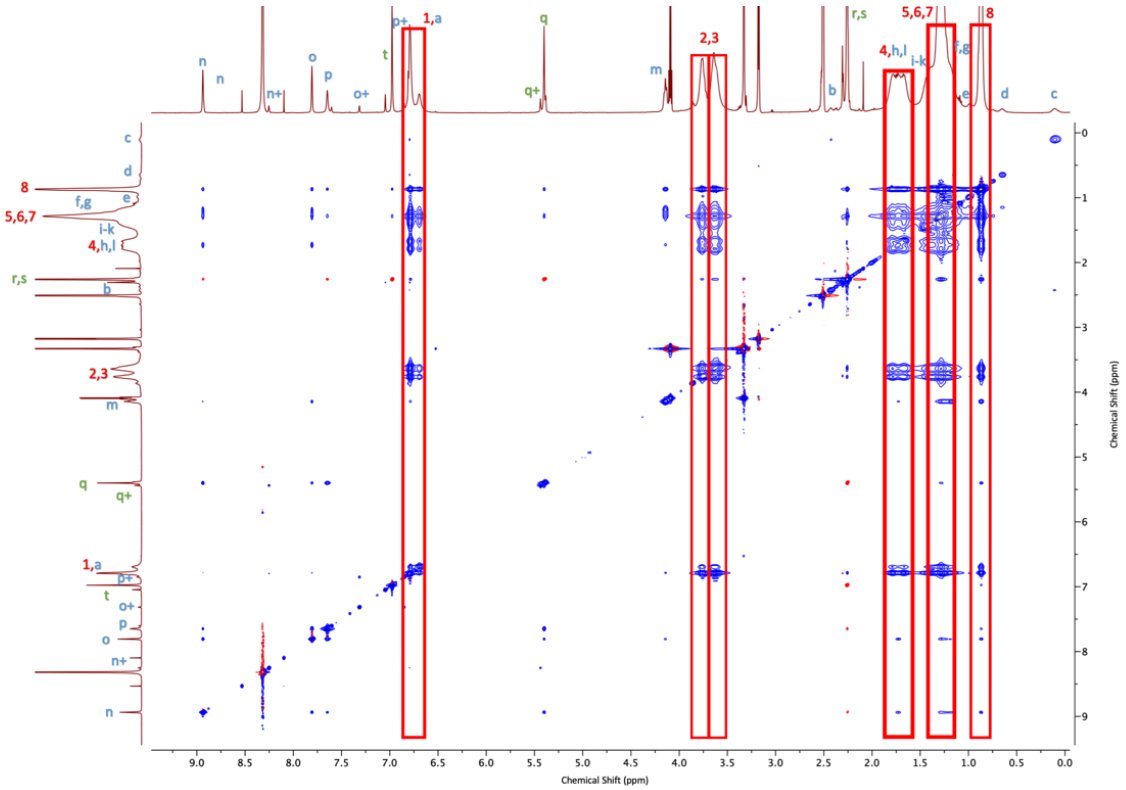

*Figure 7.74. 2D ^{1}H-^{1}H NOESY NMR spectrum (500 MHz, DMSO-d_6, 298 K) of **3.14**.*

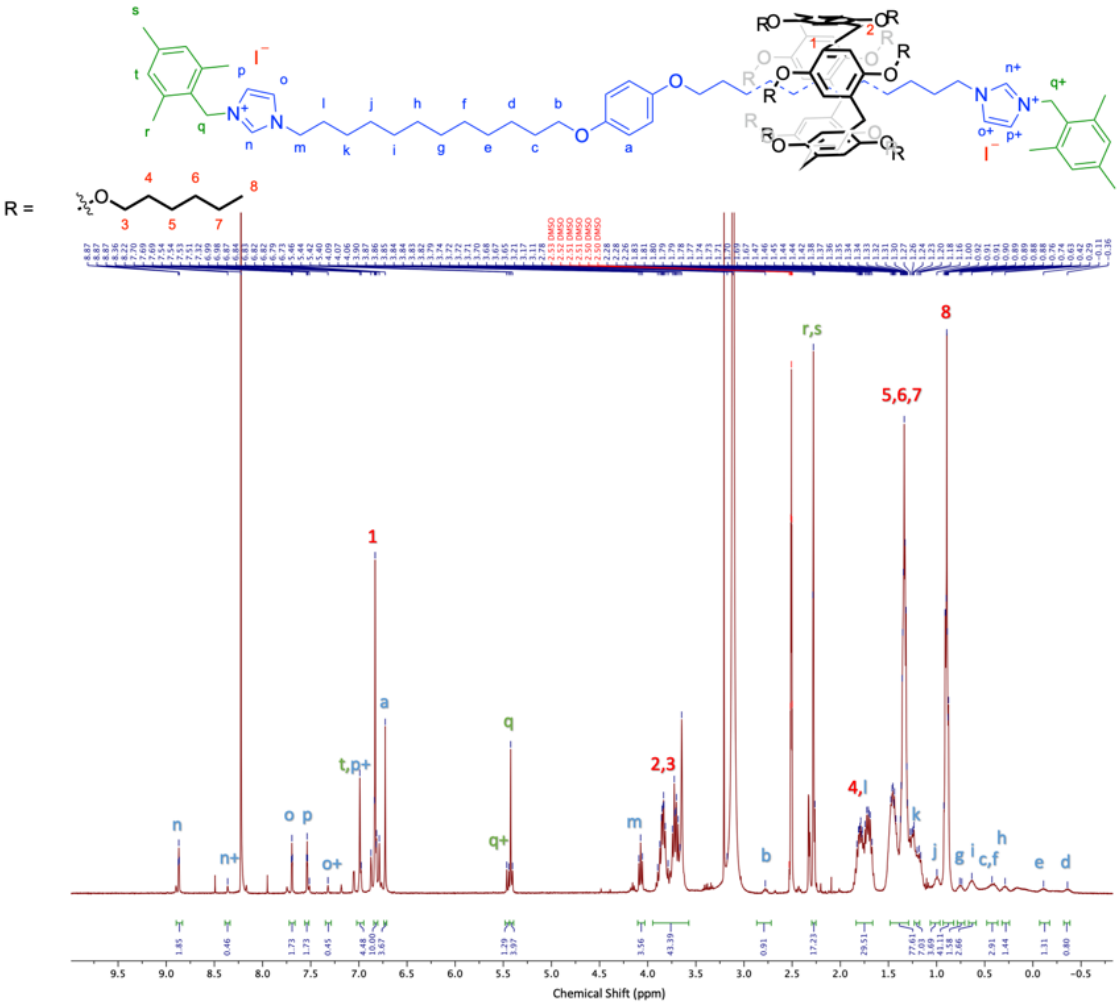

*Figure 7.75. ^{1}H NMR spectrum (400 MHz, DMSO-d_6, 353 K) of **3.14**.*

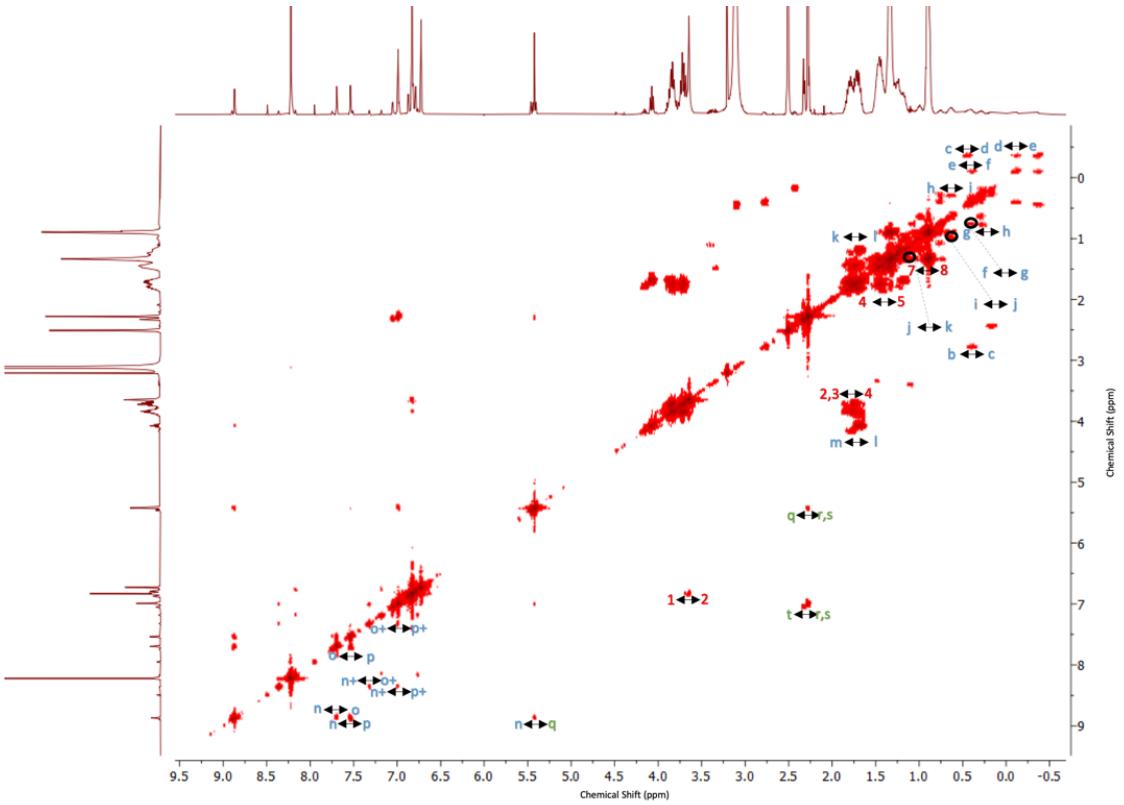

*Figure 7.76. 2D ^{1}H-^{1}H COSY NMR spectrum (400 MHz, DMSO-d_6, 353 K) of **3.14**.*

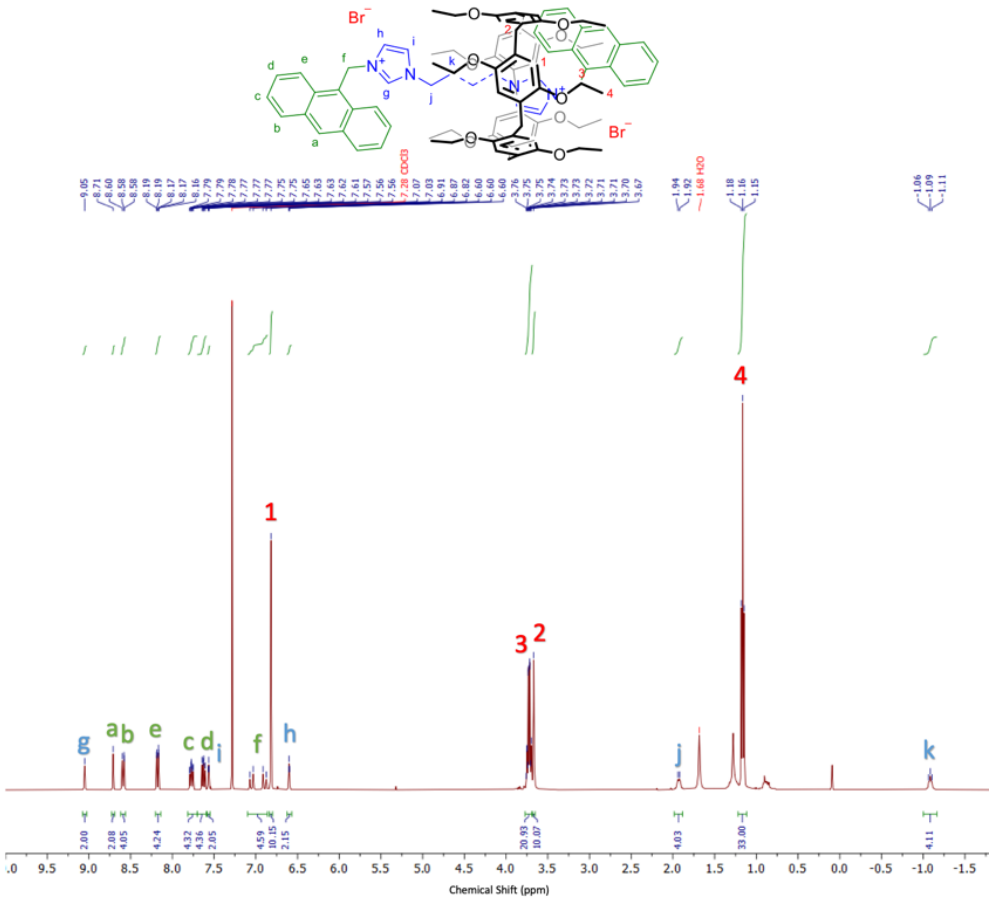

*Figure 7.77. ^{1}H NMR spectrum (400 MHz, $CDCl_3$, 298 K) of **4.7**.*

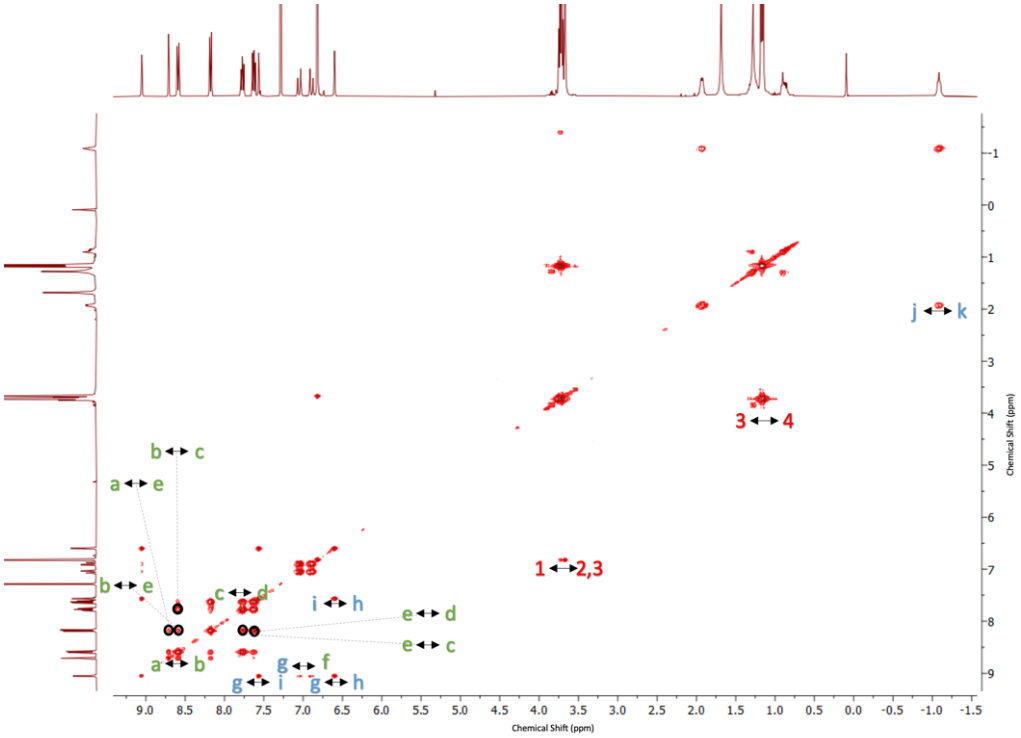

*Figure 7.78. 2D ^{1}H-^{1}H COSY NMR spectrum (400 MHz, $CDCl_3$, 298 K) of **4.7**.*

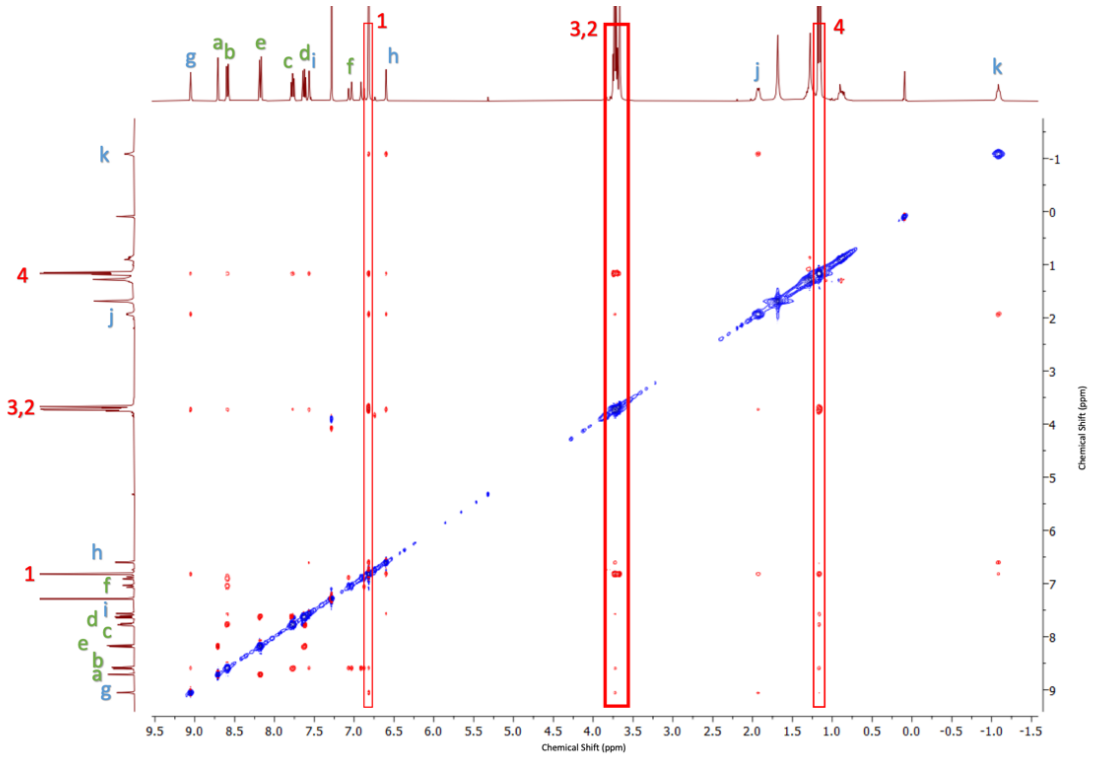

*Figure 7.79. 2D ^{1}H-^{1}H NOESY NMR spectrum (400 MHz, $CDCl_3$, 298 K) of **4.7**.*

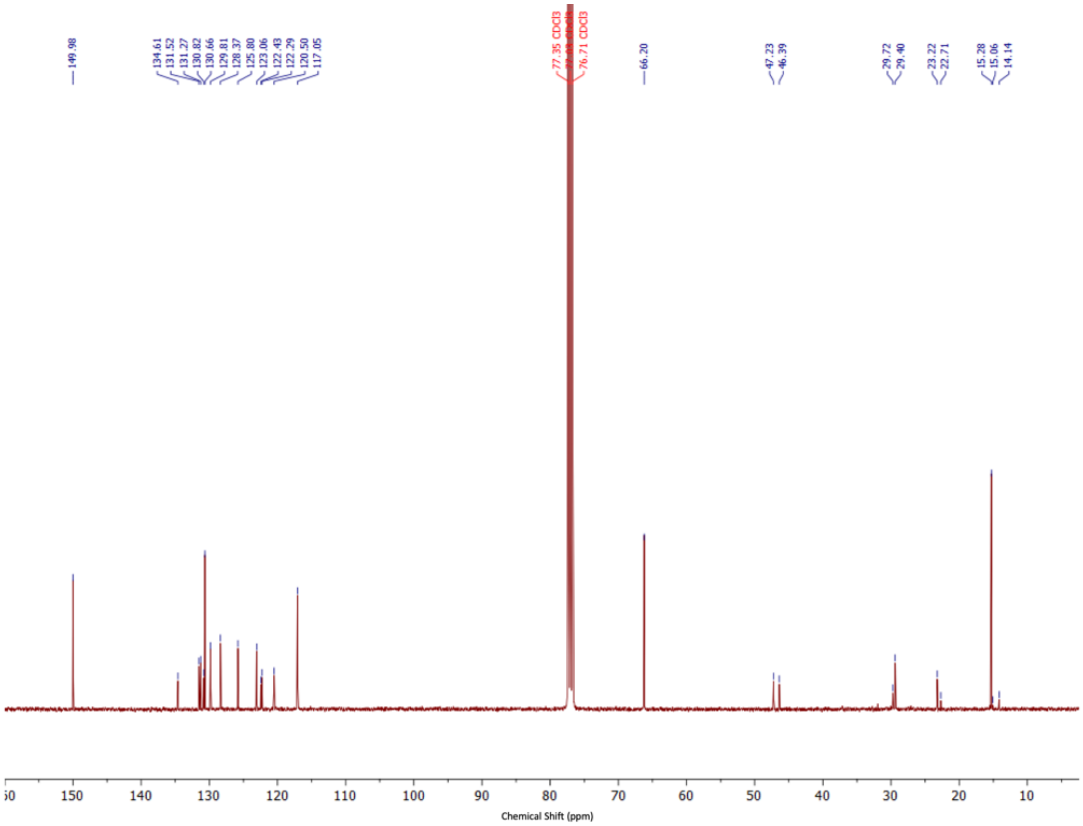

*Figure 7.80. ^{13}C NMR spectrum (101 MHz, $CDCl_3$, 298 K) of **4.7**.*

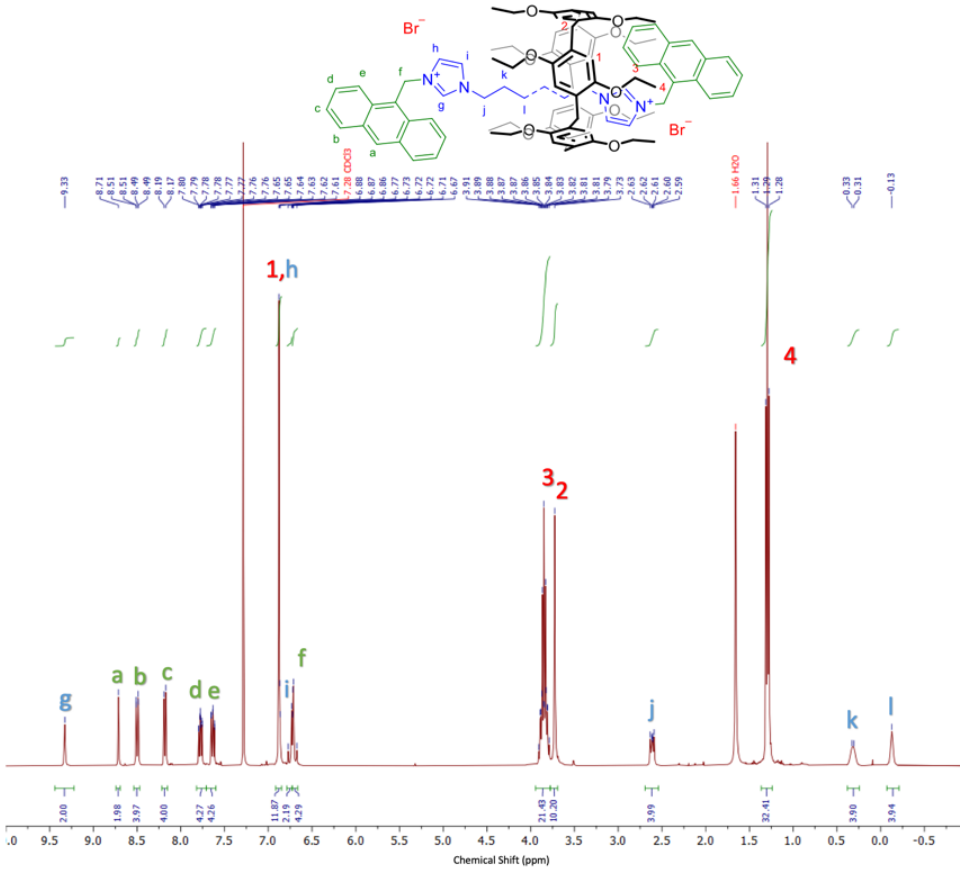

*Figure 7.81. ^{1}H NMR spectrum (400 MHz, $CDCl_3$, 298 K) of **4.8**.*

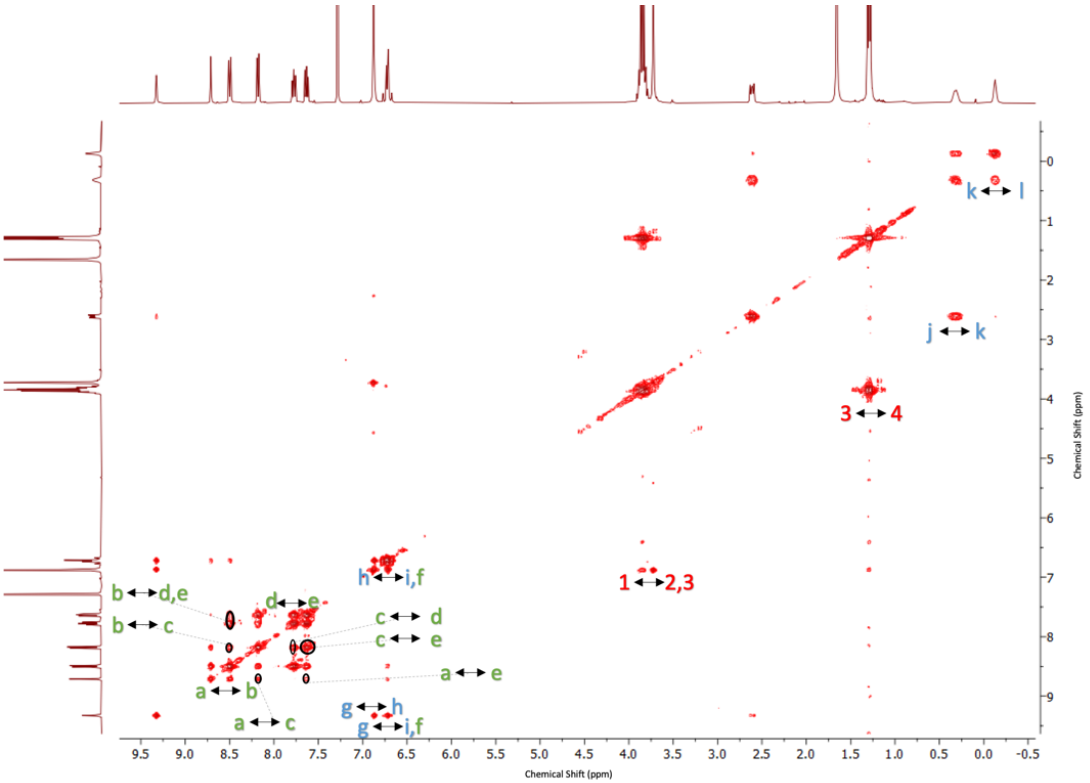

*Figure 7.82. 2D ^{1}H-^{1}H COSY NMR spectrum (400 MHz, $CDCl_3$, 298 K) of **4.8**.*

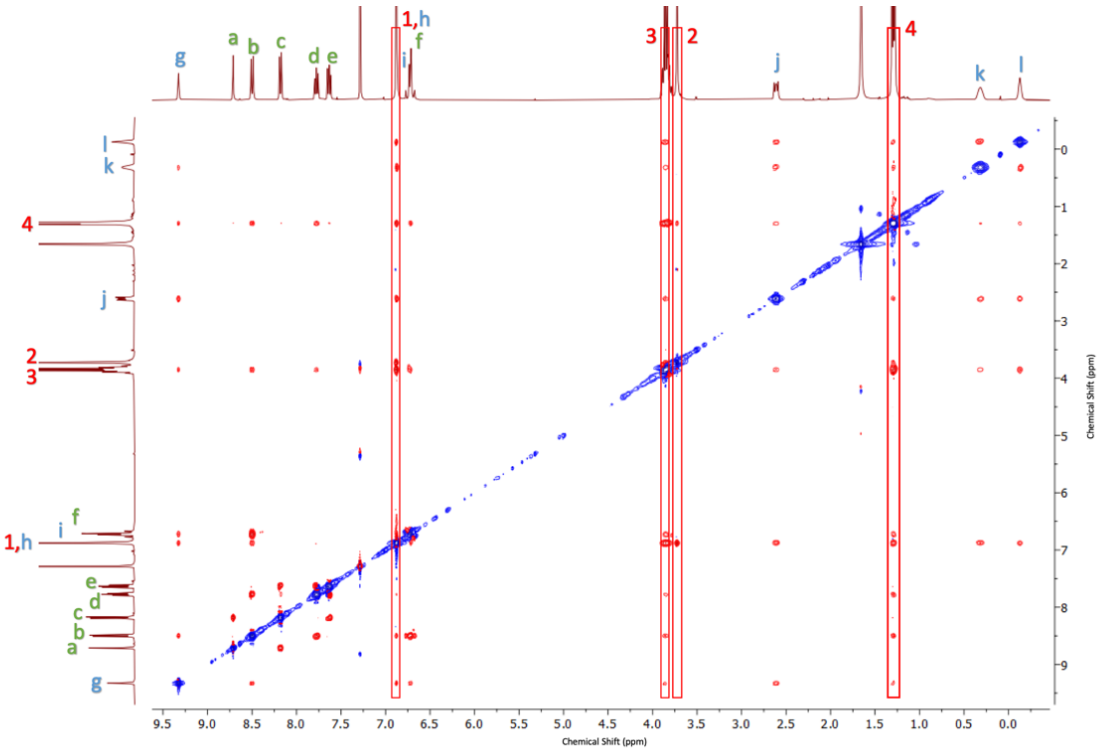

*Figure 7.83. 2D ^{1}H-^{1}H NOESY NMR spectrum (400 MHz, $CDCl_3$, 298 K) of **4.8**.*

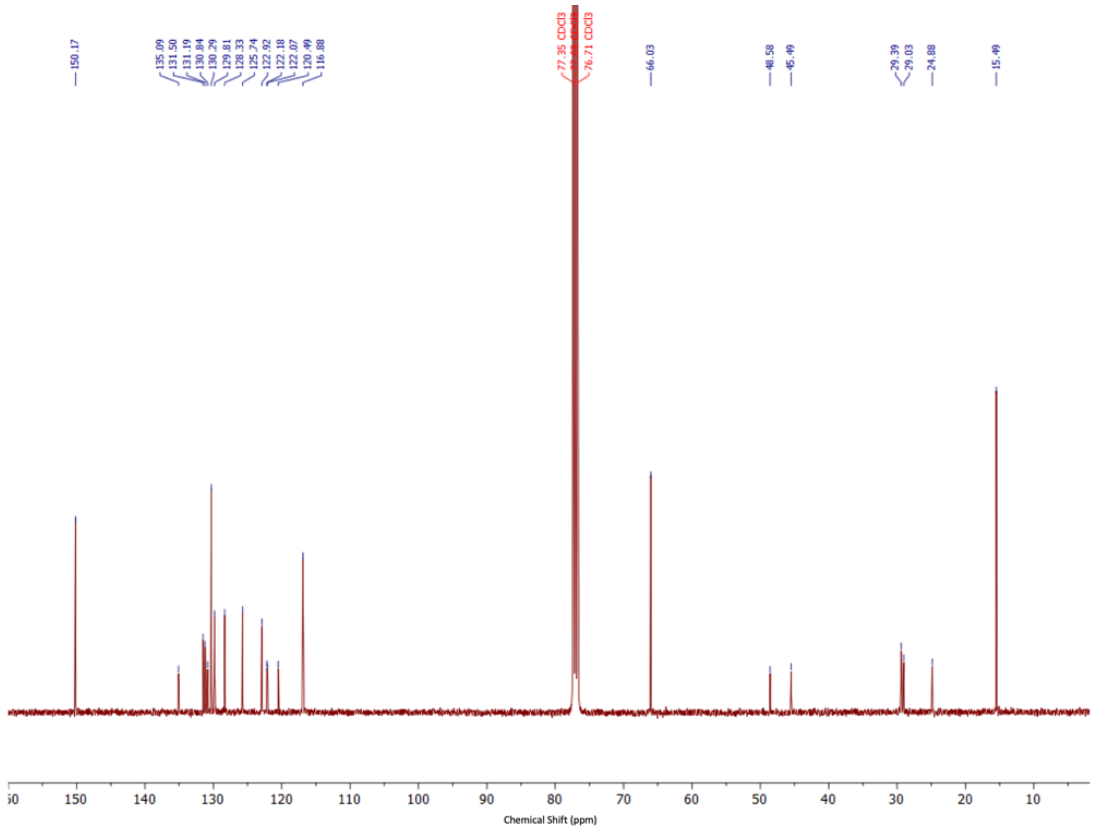

*Figure 7.84. ^{13}C NMR spectrum (101 MHz, $CDCl_3$, 298 K) of **4.8**.*

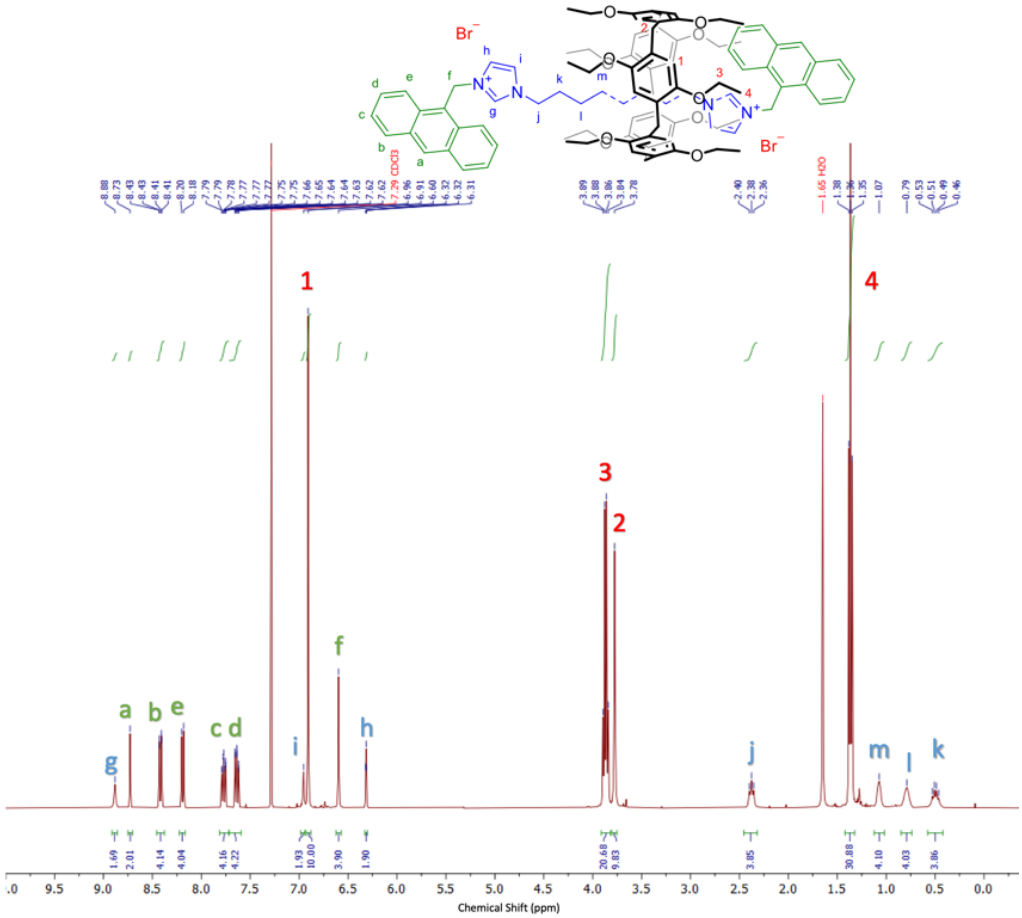

*Figure 7.85. ^{1}H NMR spectrum (400 MHz, $CDCl_3$, 298 K) of **4.9**.*

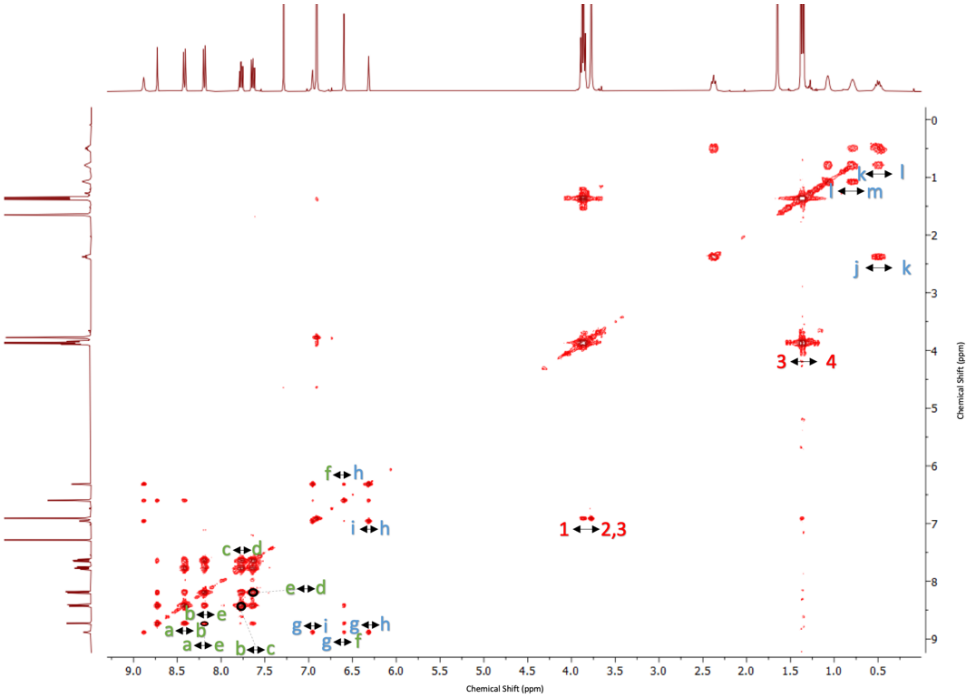

*Figure 7.86. 2D ^{1}H-^{1}H COSY NMR spectrum (400 MHz, $CDCl_3$, 298 K) of **4.9**.*

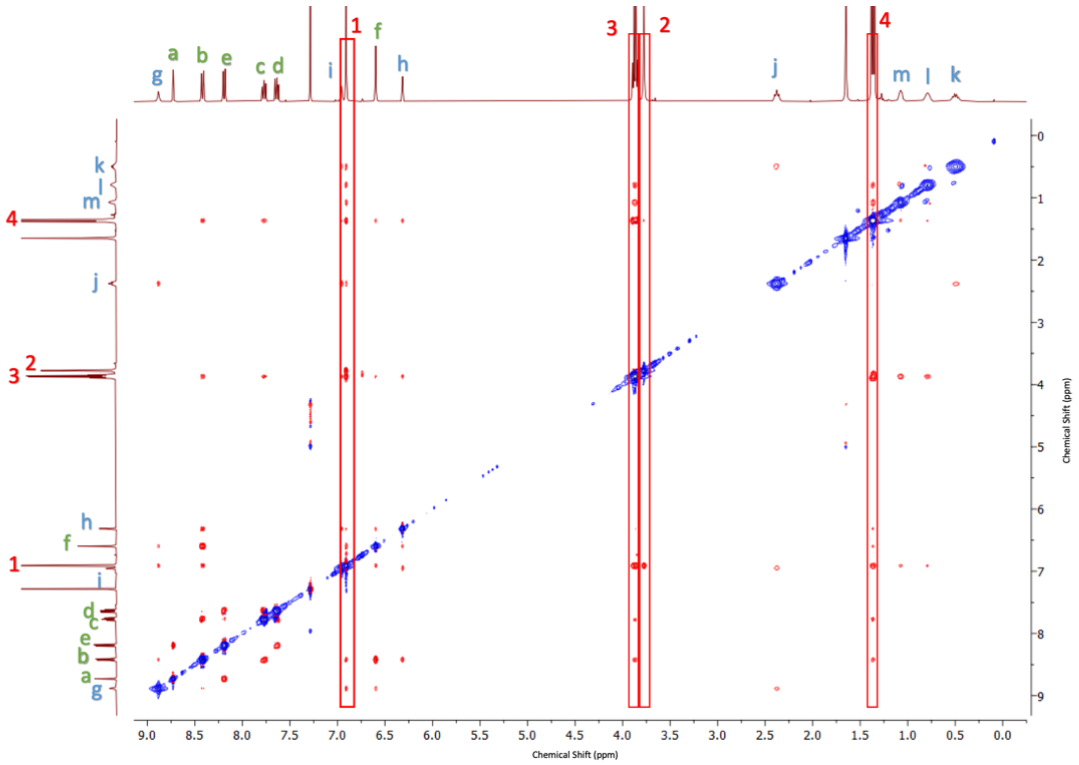

*Figure 7.87. 2D ^{1}H-^{1}H NOESY NMR spectrum (400 MHz, $CDCl_3$, 298 K) of **4.9**.*

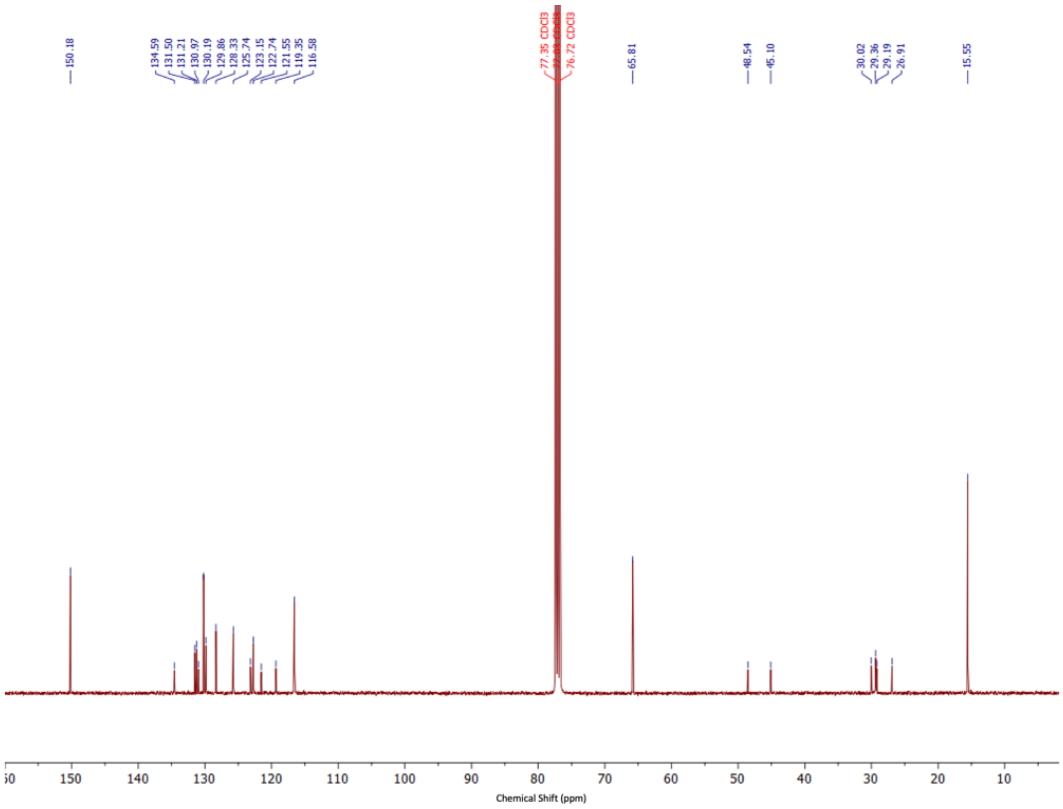

*Figure 7.88. ^{13}C NMR spectrum (101 MHz, $CDCl_3$, 298 K) of **4.9**.*

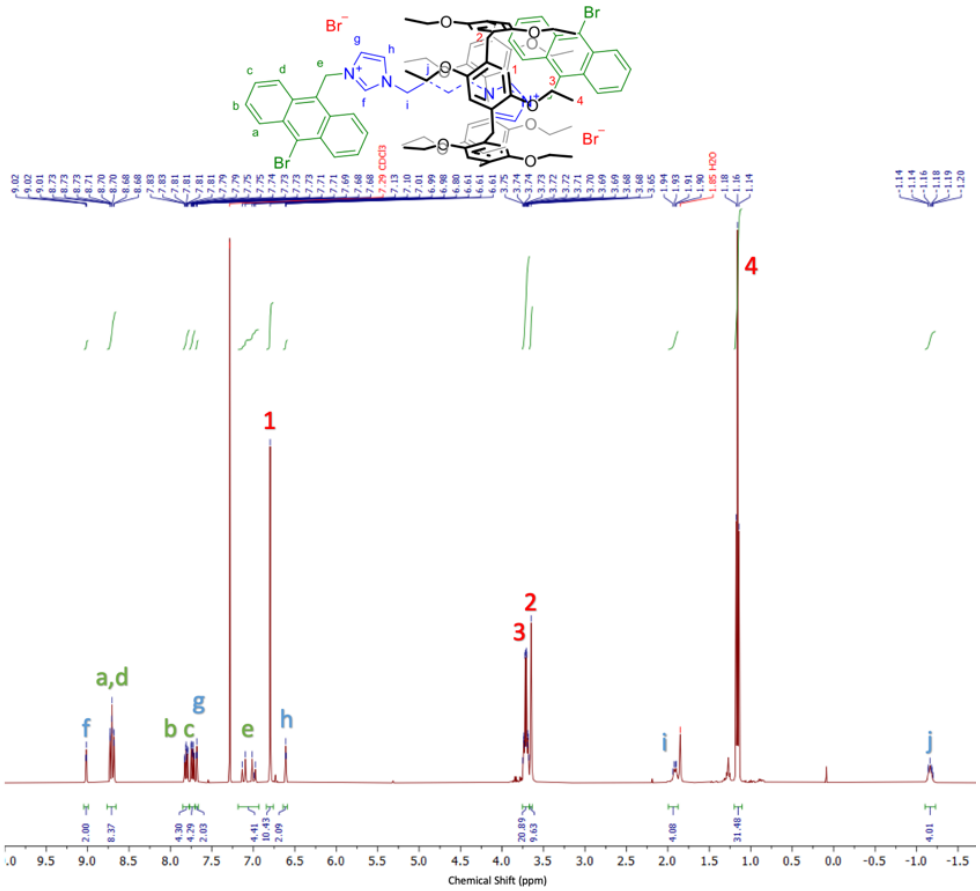

*Figure 7.89. ^{1}H NMR spectrum (400 MHz, $CDCl_3$, 298 K) of **4.10**.*

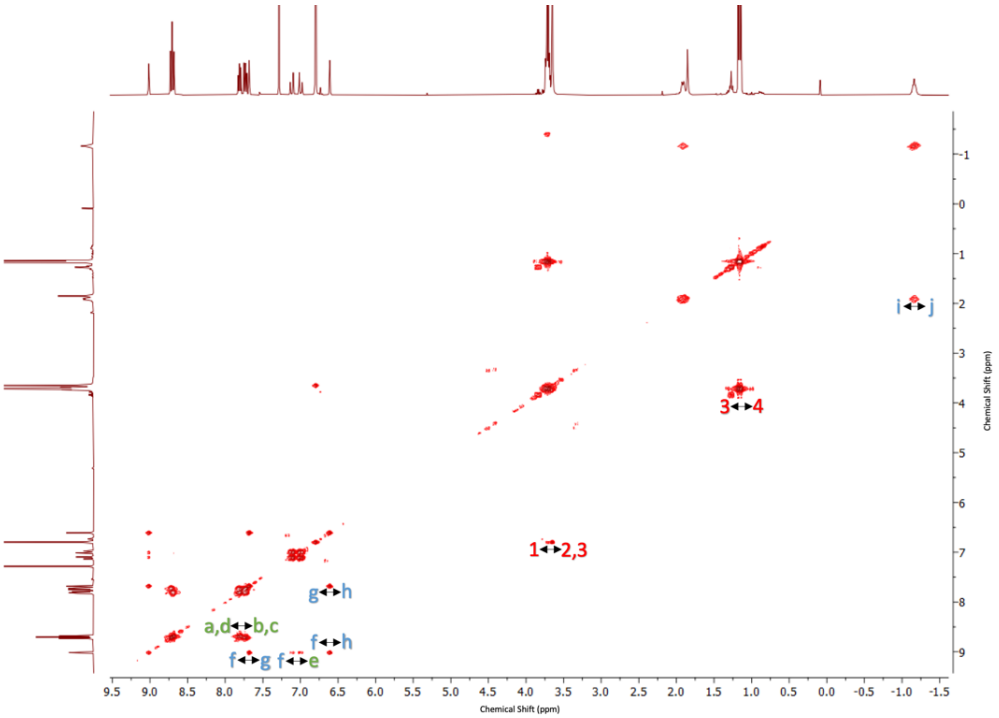

*Figure 7.90. 2D ^{1}H-^{1}H COSY NMR spectrum (400 MHz, $CDCl_3$, 298 K) of **4.10**.*

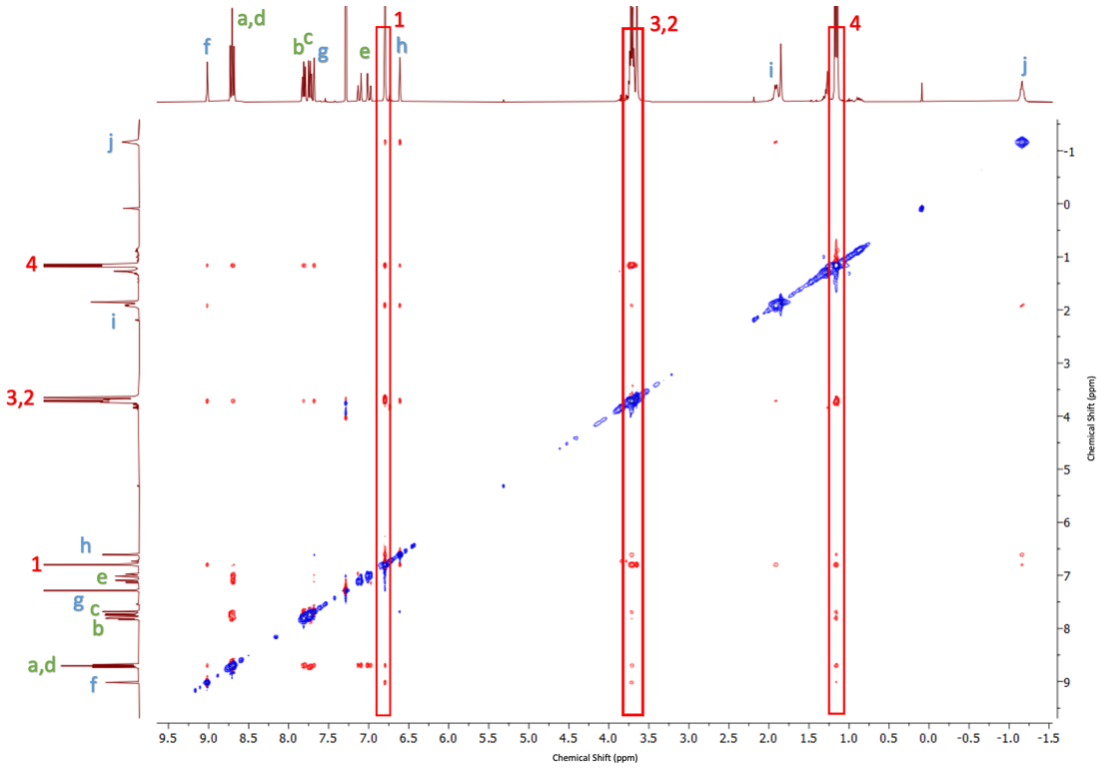

*Figure 7.91. 2D ^{1}H-^{1}H NOESY NMR spectrum (400 MHz, $CDCl_3$, 298 K) of **4.10**.*

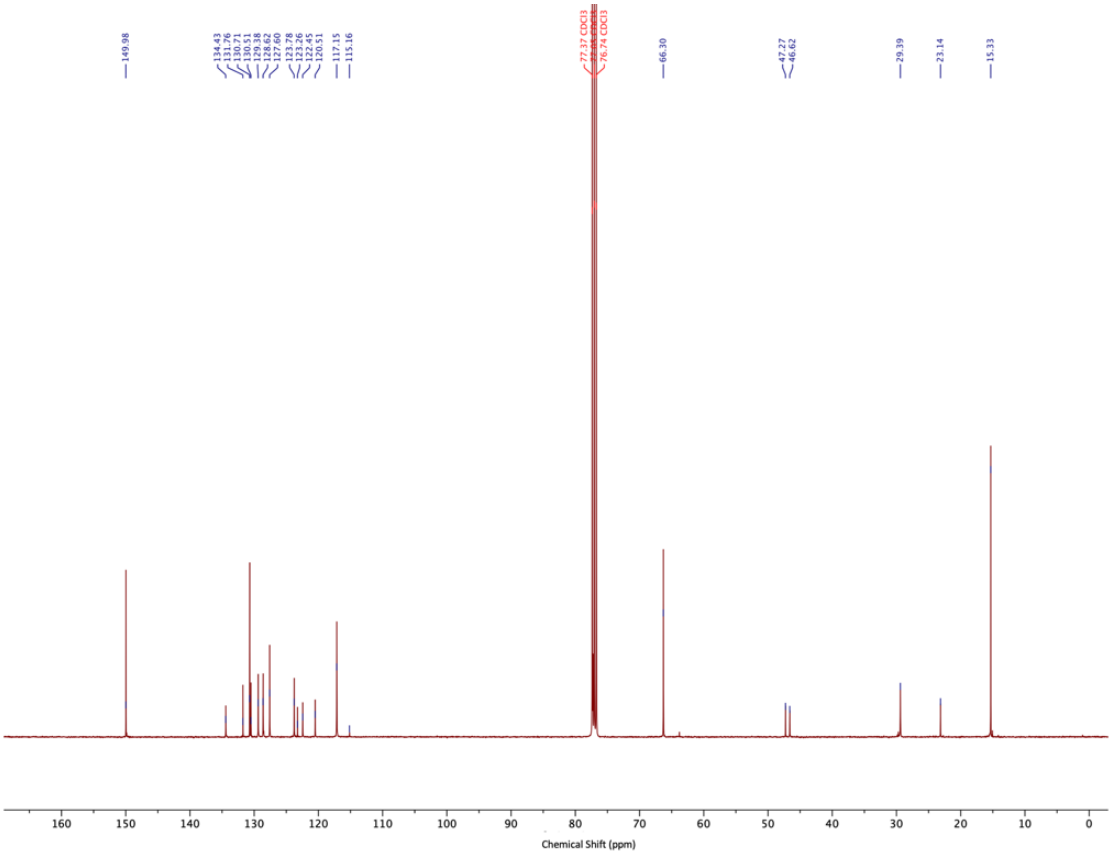

*Figure 7.92. ^{13}C NMR spectrum (101 MHz, $CDCl_3$, 298 K) of **4.10**.*

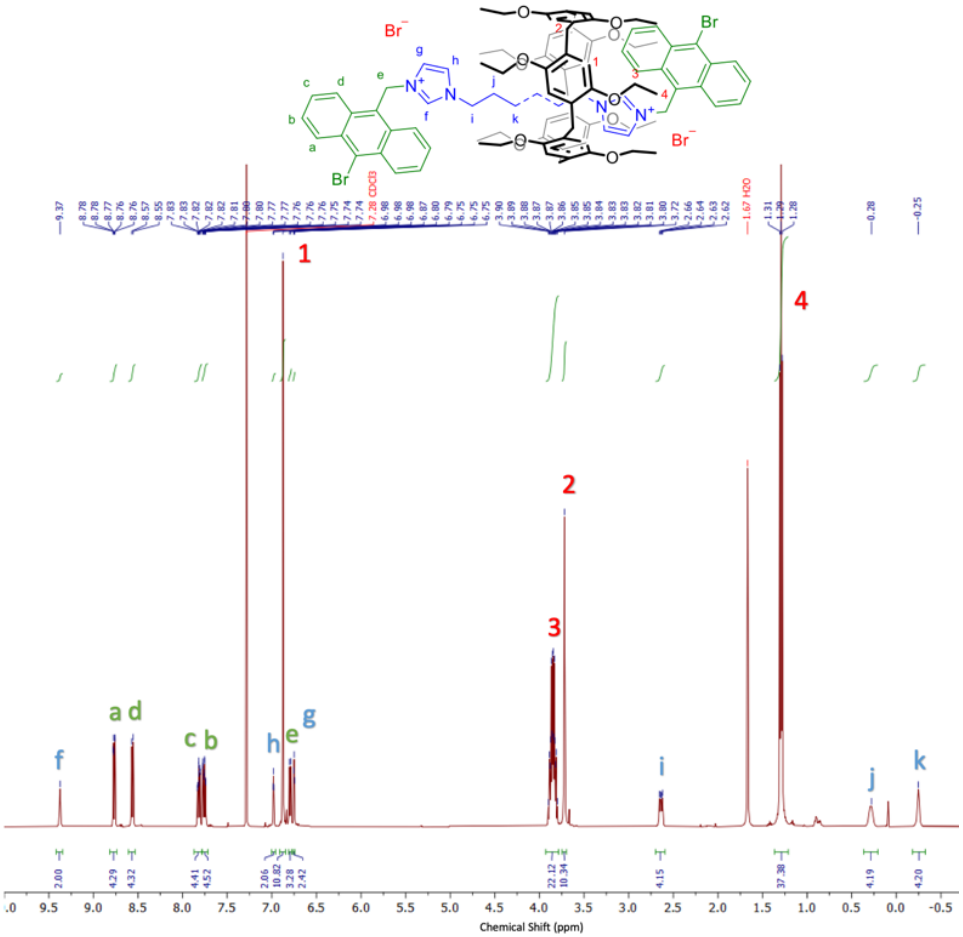

*Figure 7.93. ^{1}H NMR spectrum (500 MHz, $CDCl_3$, 298 K) of **4.11**.*

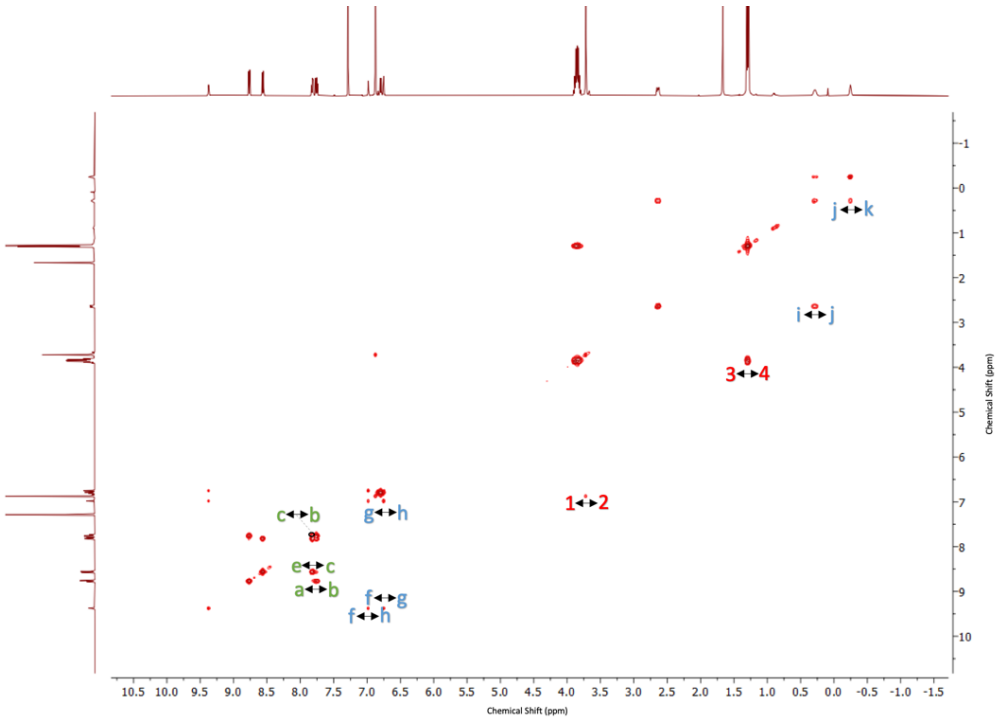

*Figure 7.94. 2D ^{1}H-^{1}H COSY NMR spectrum (500 MHz, $CDCl_3$, 298 K) of **4.11**.*

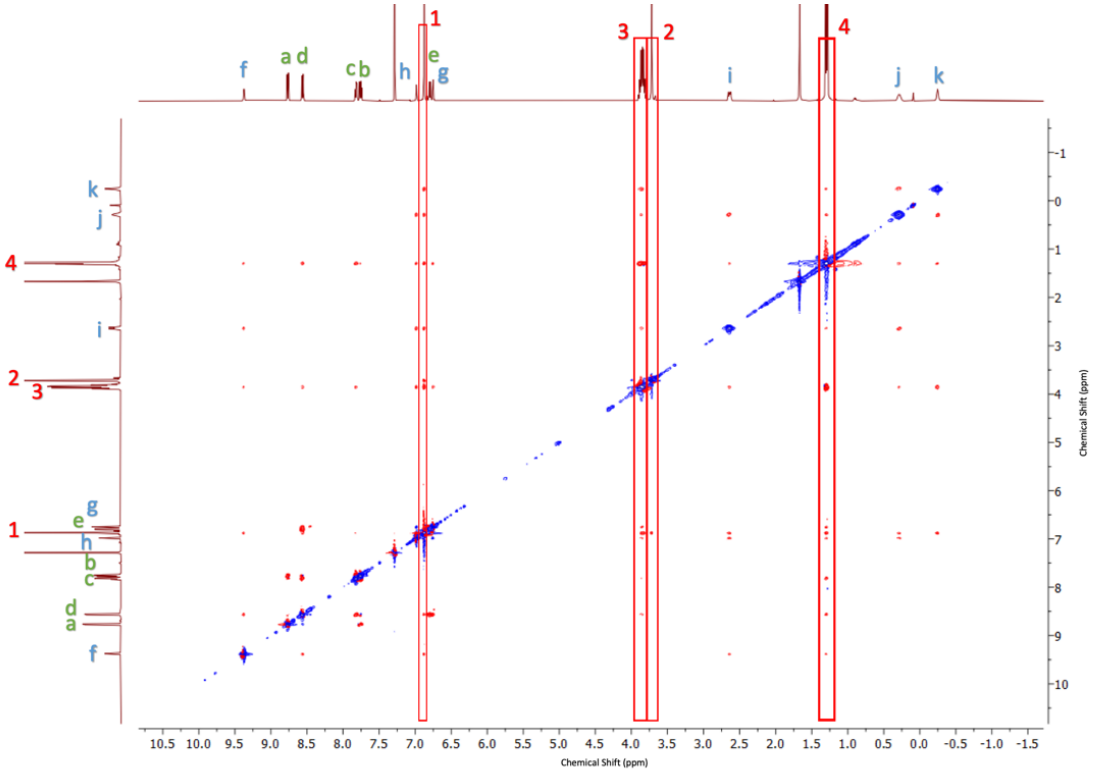

*Figure 7.95. 2D ^{1}H-^{1}H NOESY NMR spectrum (500 MHz, $CDCl_3$, 298 K) of **4.11**.*

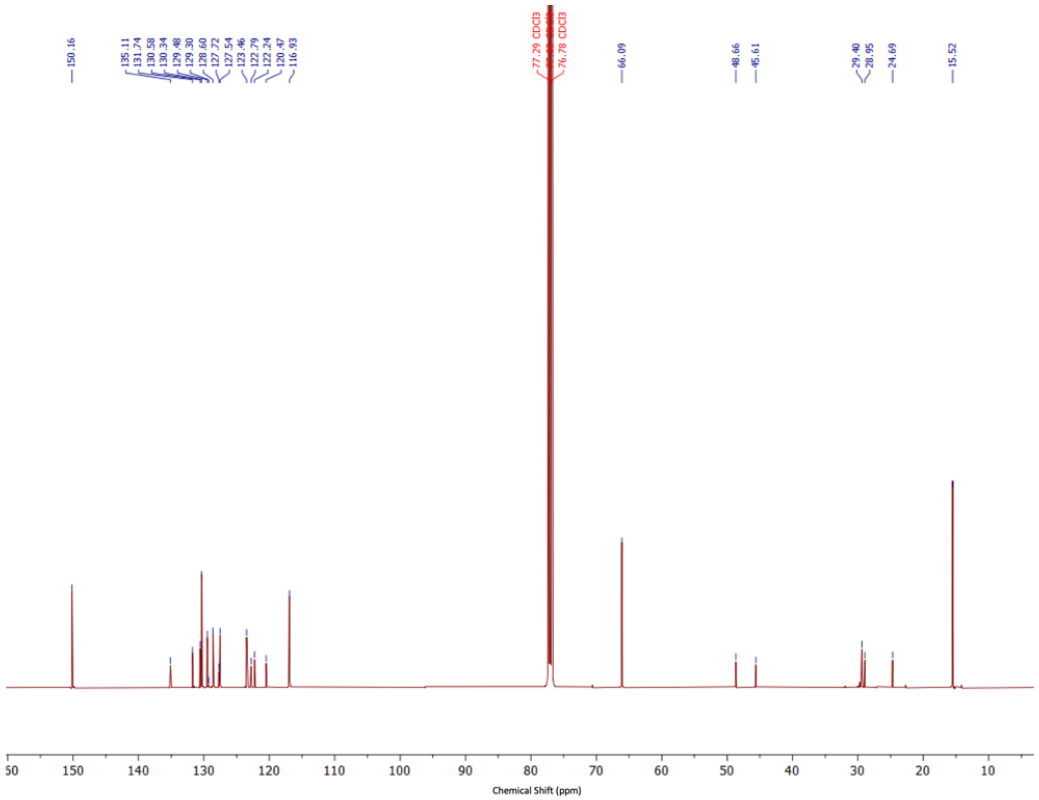

*Figure 7.96. ^{13}C NMR spectrum (126 MHz, $CDCl_3$, 298 K) of **4.11**.*

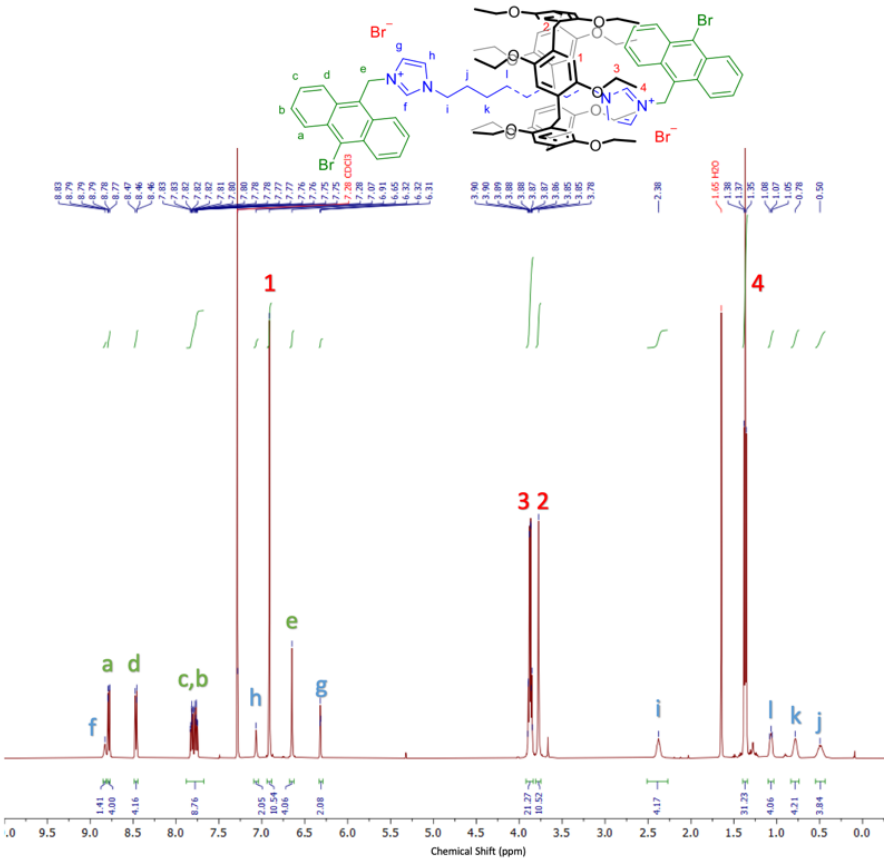

*Figure 7.97. ^{1}H NMR spectrum (500 MHz, $CDCl_3$, 298 K) of **4.12**.*

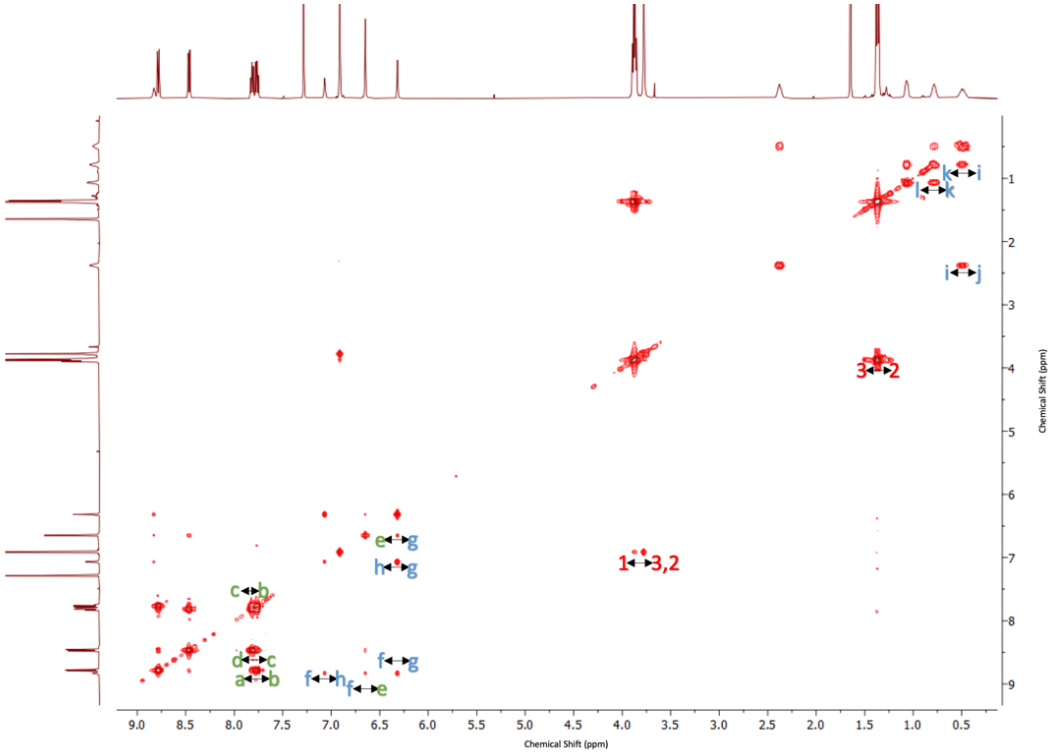

*Figure 7.98. 2D ^{1}H-^{1}H COSY NMR spectrum (500 MHz, $CDCl_3$, 298 K) of **4.12**.*

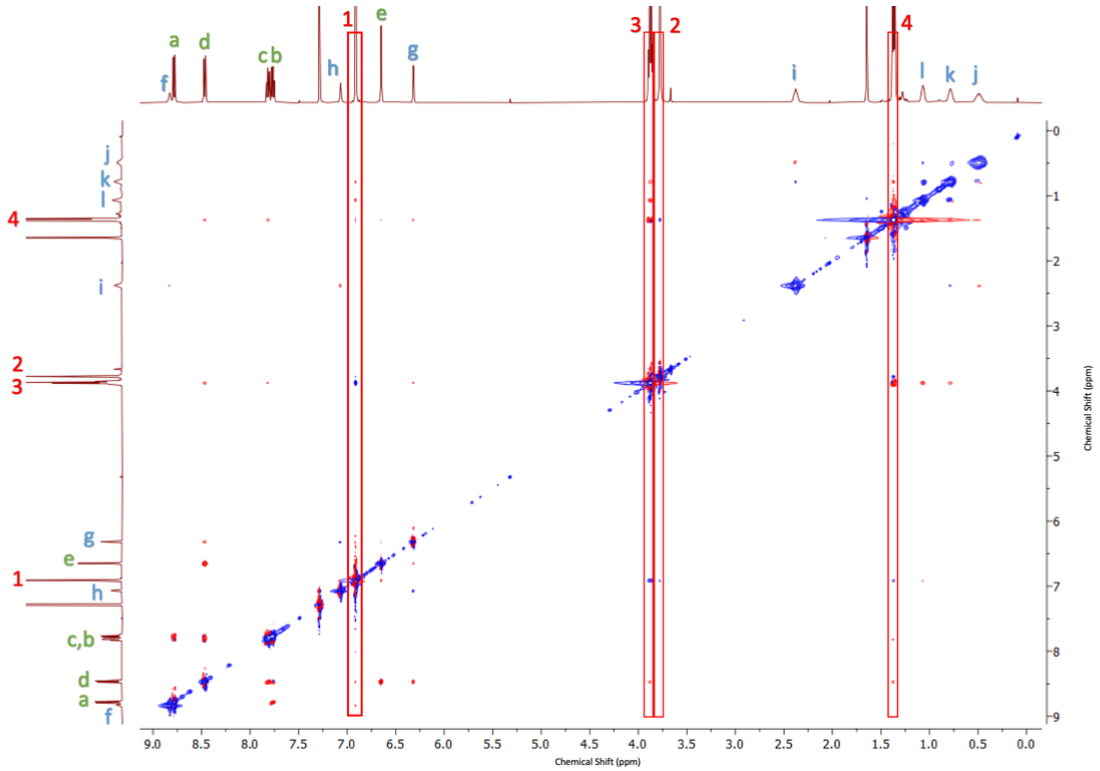

*Figure 7.99. 2D ^{1}H-^{1}H NOESY NMR spectrum (500 MHz, $CDCl_3$, 298 K) of **4.12**.*

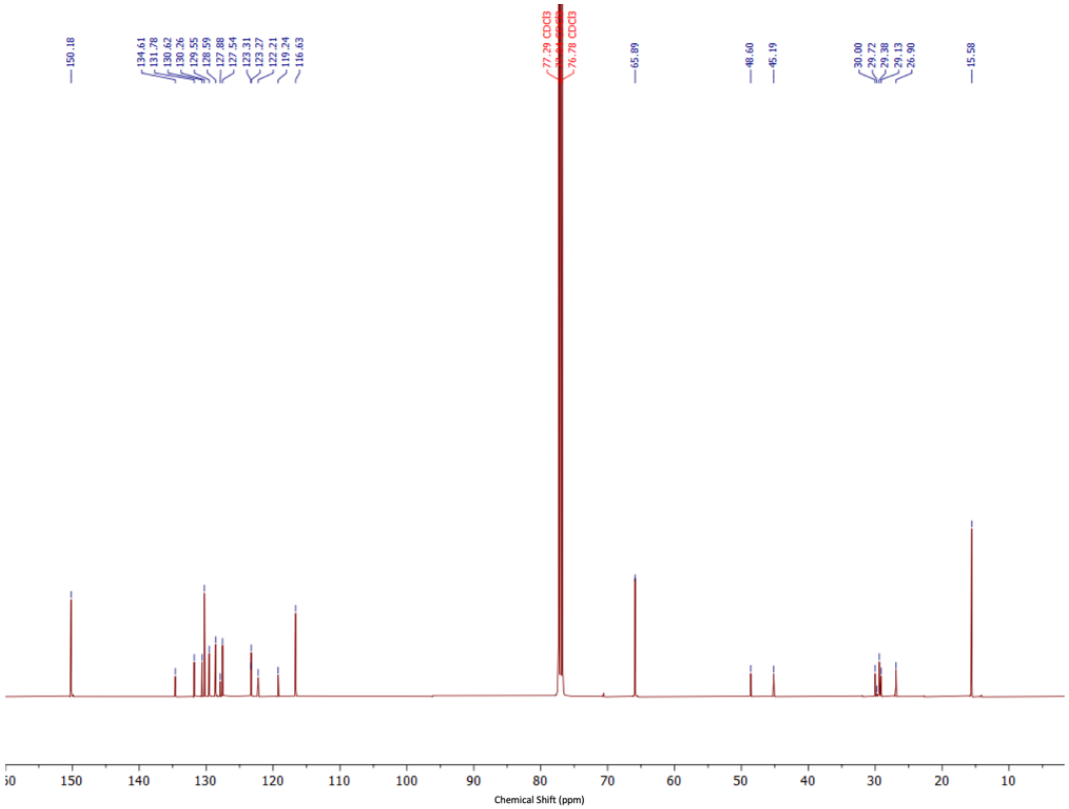

*Figure 7.100. ^{13}C NMR spectrum (126 MHz, $CDCl_3$, 298 K) of **4.12**.*

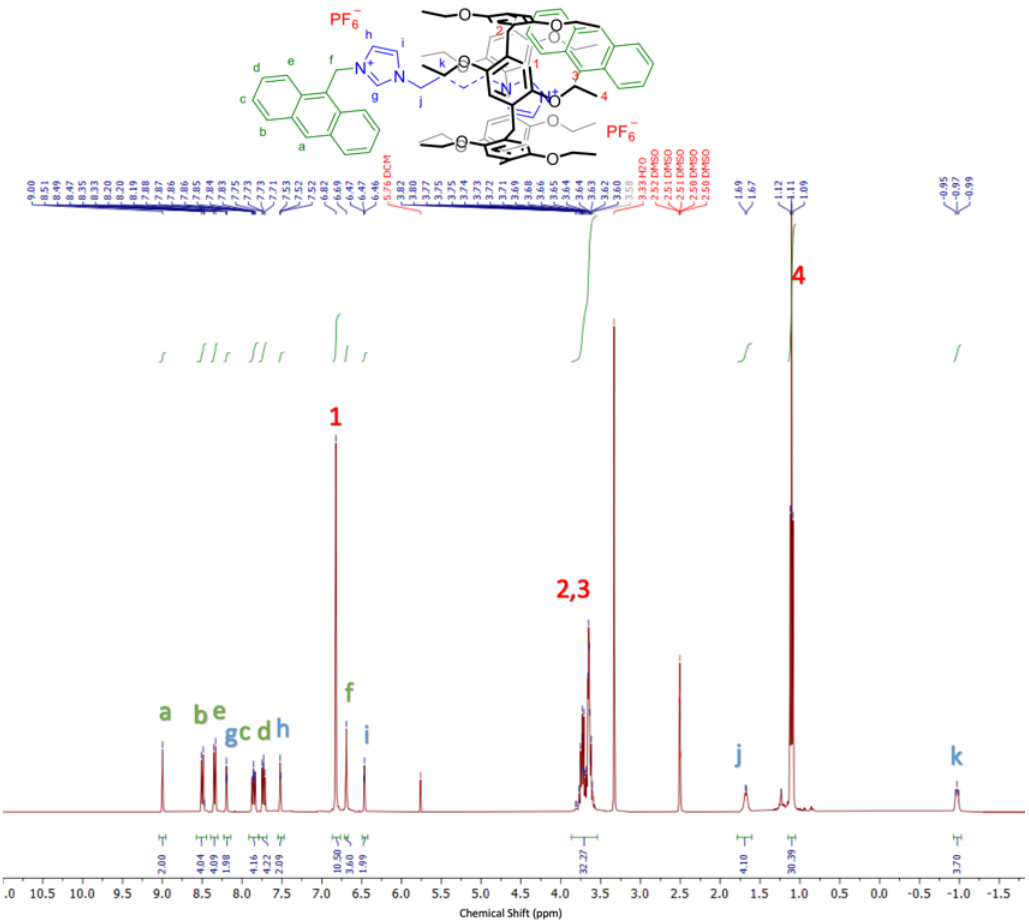

*Figure 7.101. ^{1}H NMR spectrum (400 MHz, DMSO-d_6, 298 K) of **4.13**.*

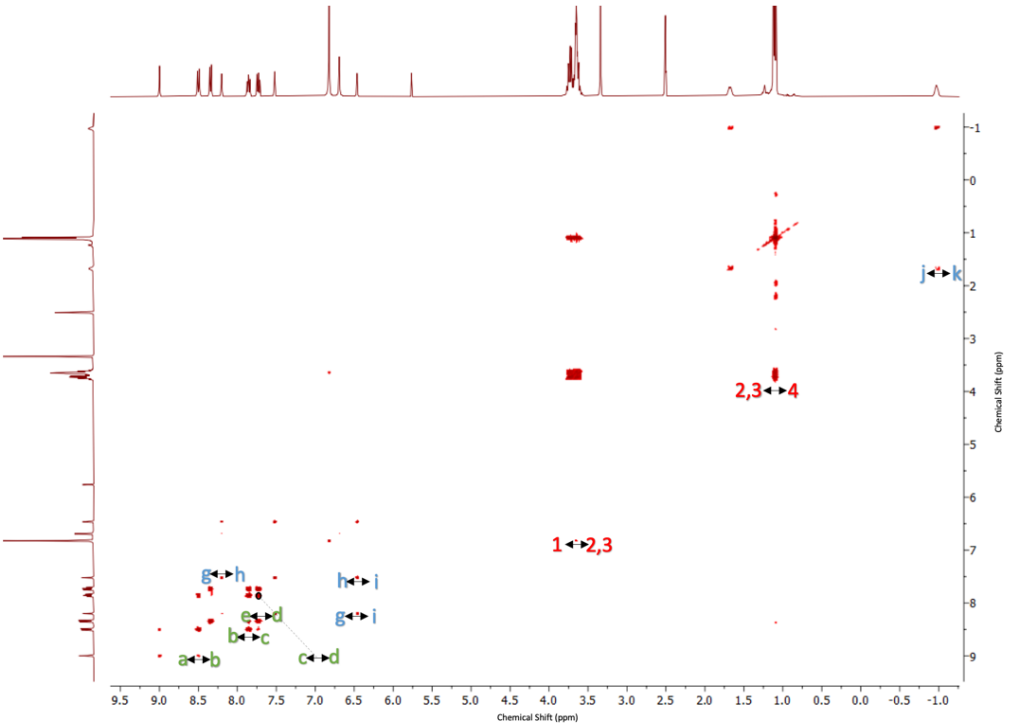

*Figure 7.102. 2D ^{1}H-^{1}H COSY NMR spectrum (400 MHz, DMSO-d_6, 298 K) of **4.13**.*

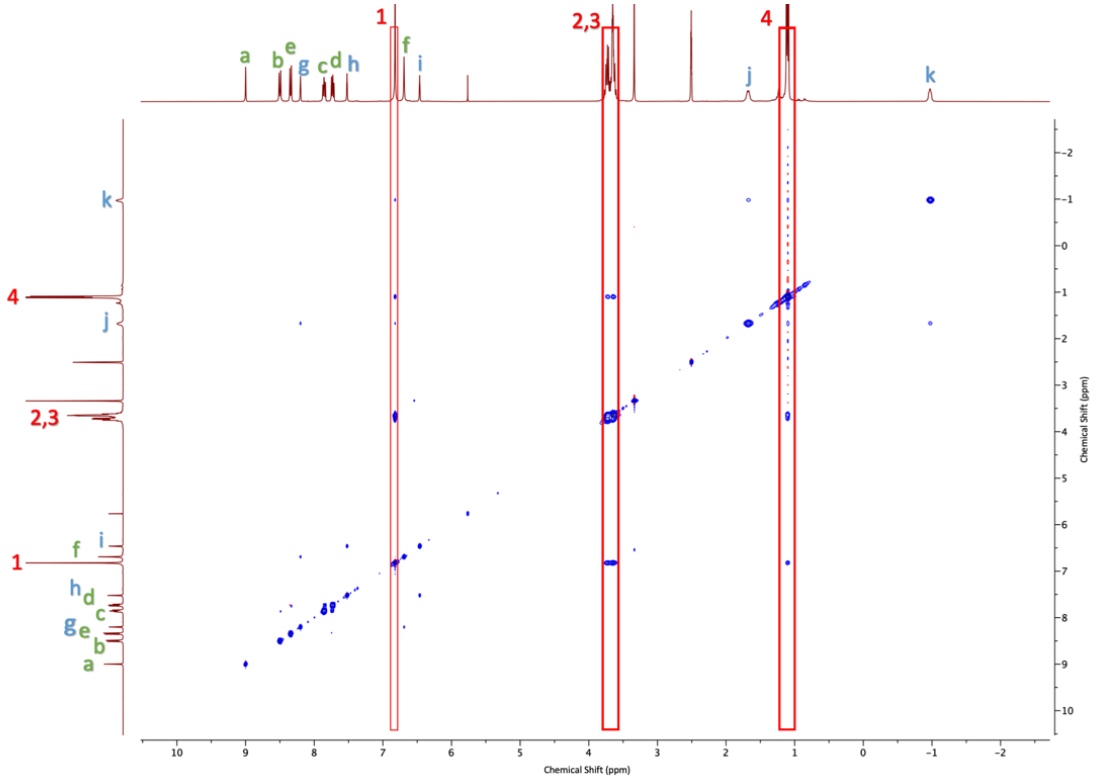

*Figure 7.103. 2D ^{1}H-^{1}H NOESY NMR spectrum (400 MHz, DMSO-d_6, 298 K) of **4.13**.*

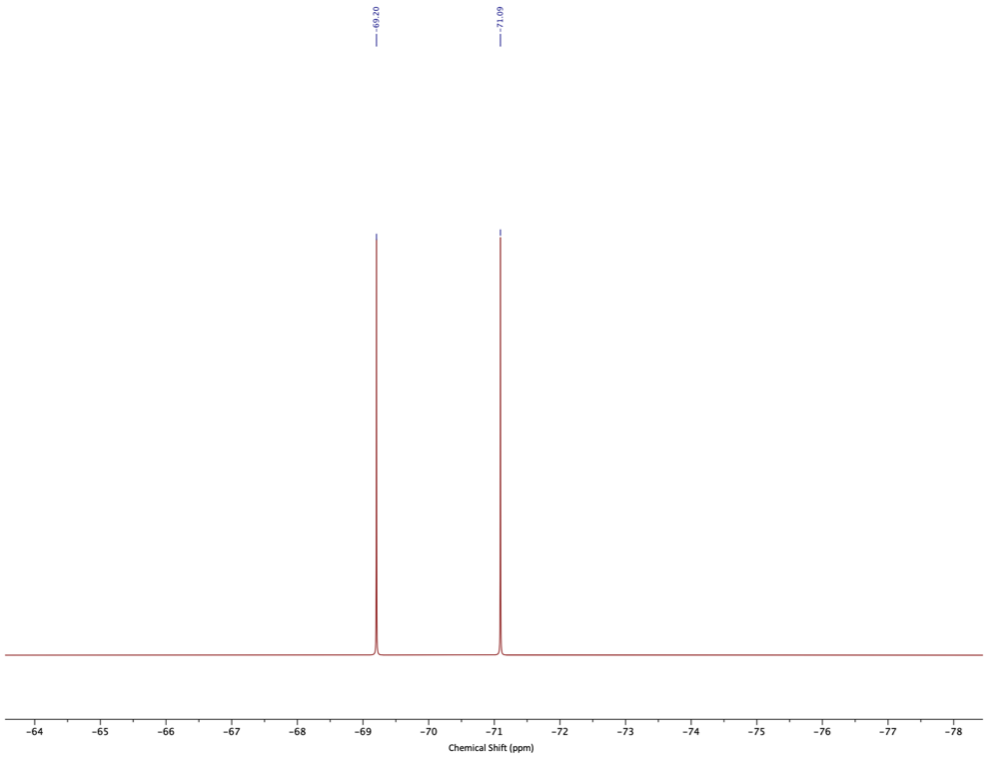

*Figure 7.104. ^{19}F NMR spectrum (376 MHz, DMSO-d_6, 298 K) of **4.13**.*

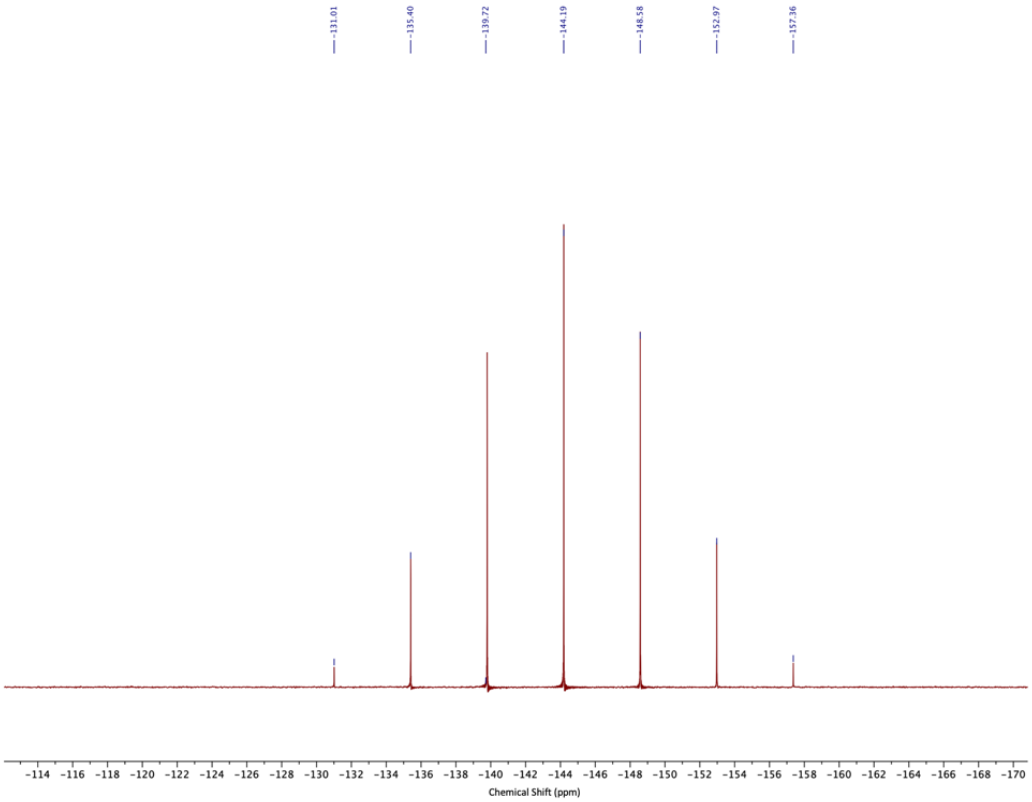

*Figure 7.105. ^{31}P NMR spectrum (162 MHz, DMSO-d_6, 298 K) of **4.13**.*

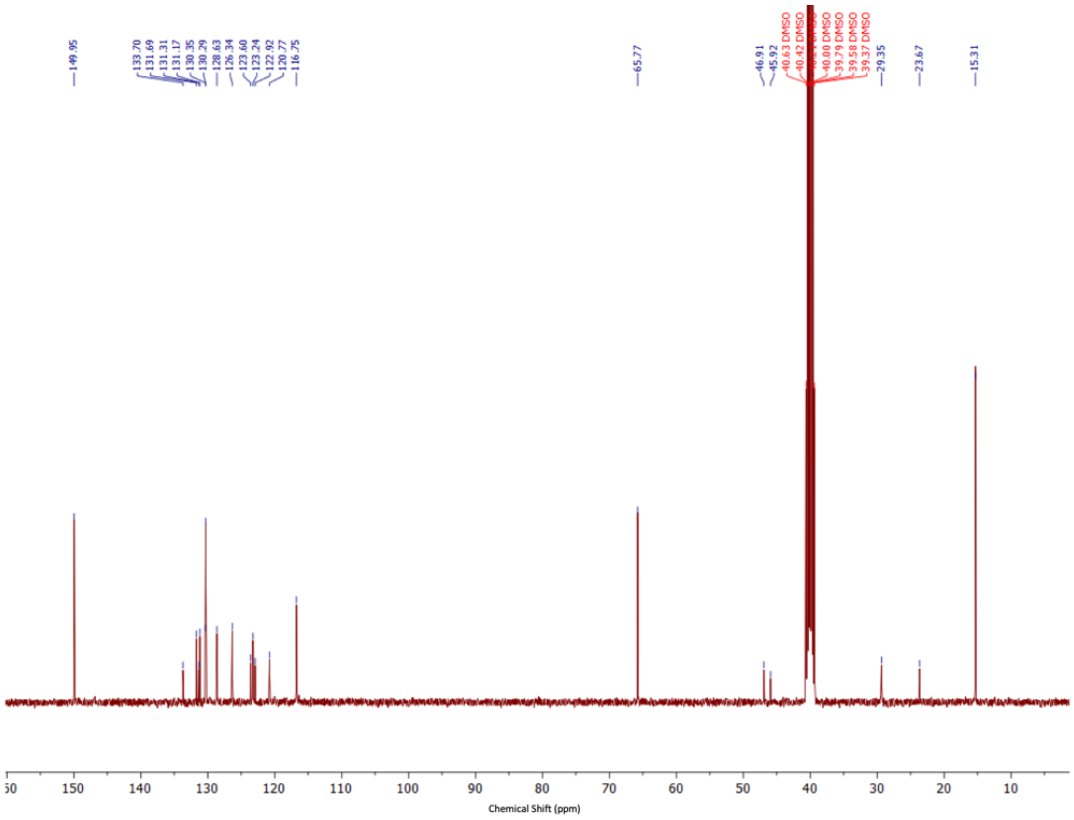

*Figure 7.106. ^{13}C NMR spectrum (101 MHz, DMSO-d_6, 298 K) of **4.13**.*

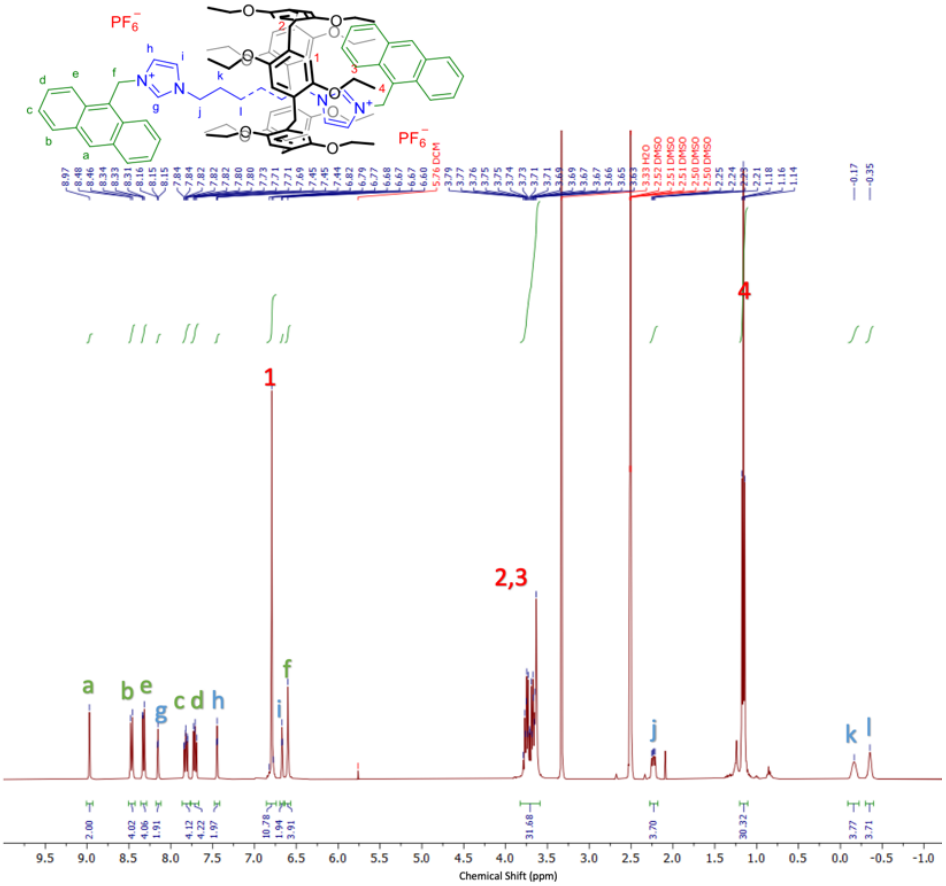

*Figure 7.107. ^{1}H NMR spectrum (400 MHz, DMSO-d_6, 298 K) of **4.14**.*

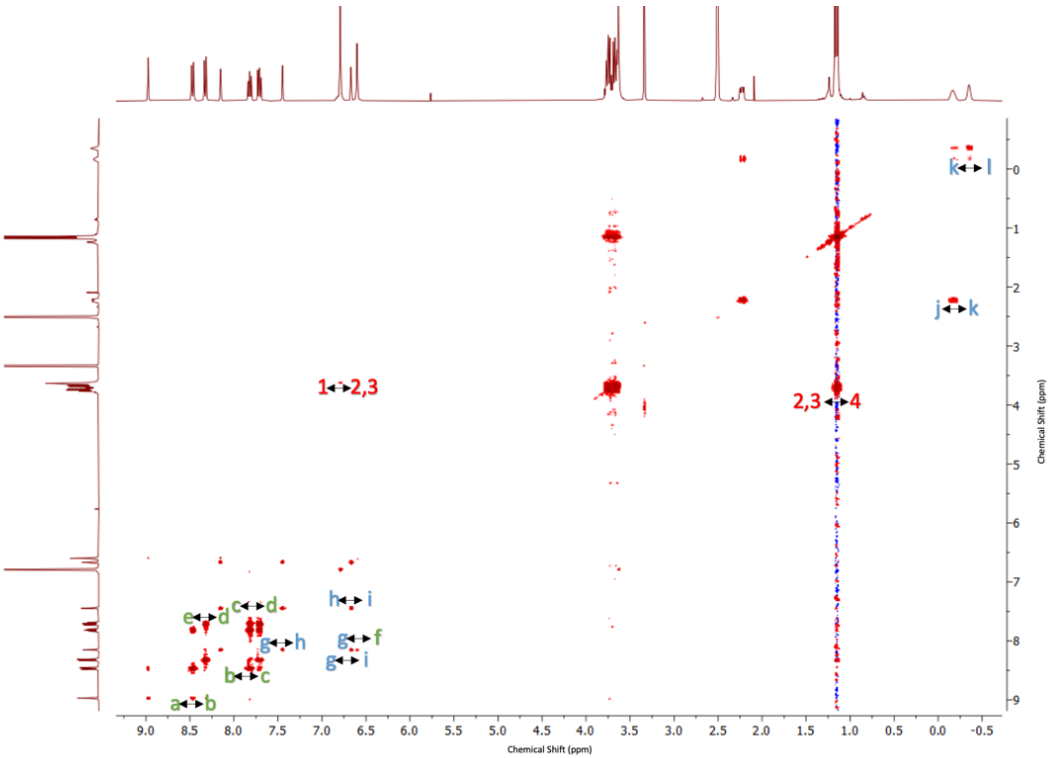

*Figure 7.108. 2D ^{1}H-^{1}H COSY NMR spectrum (400 MHz, DMSO-d_6, 298 K) of **4.14**.*

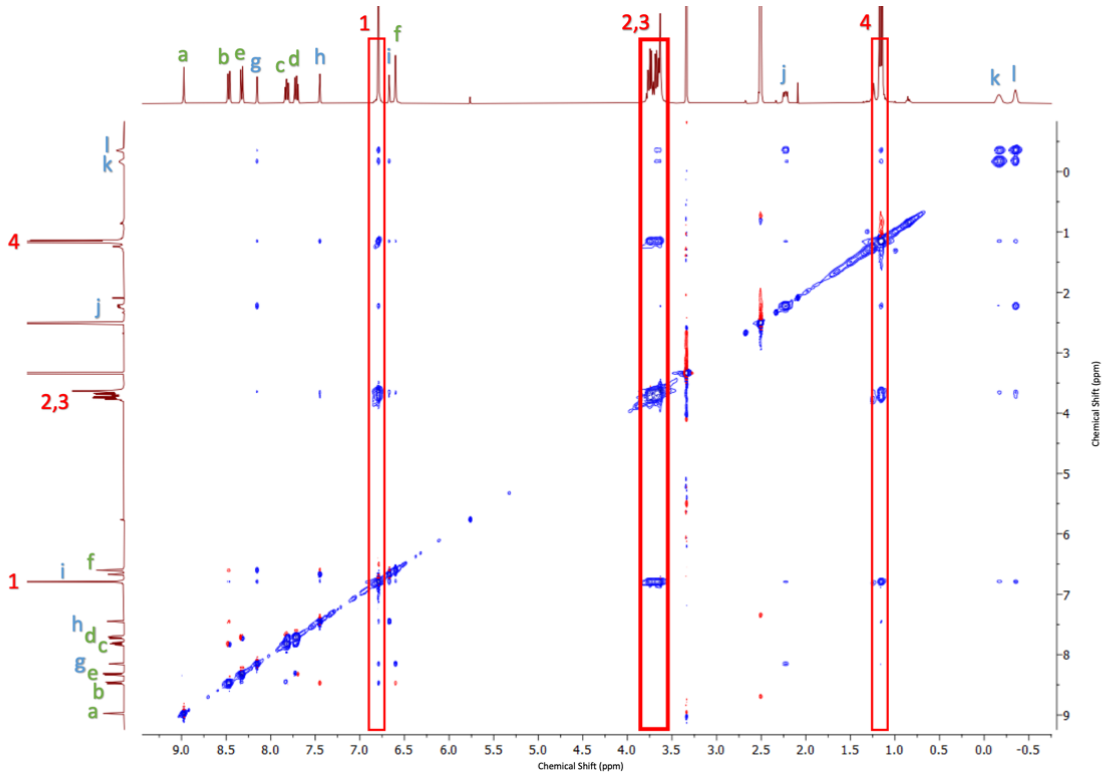

*Figure 7.109. 2D ^{1}H-^{1}H NOESY NMR spectrum (400 MHz, DMSO-d_6, 298 K) of **4.14**.*

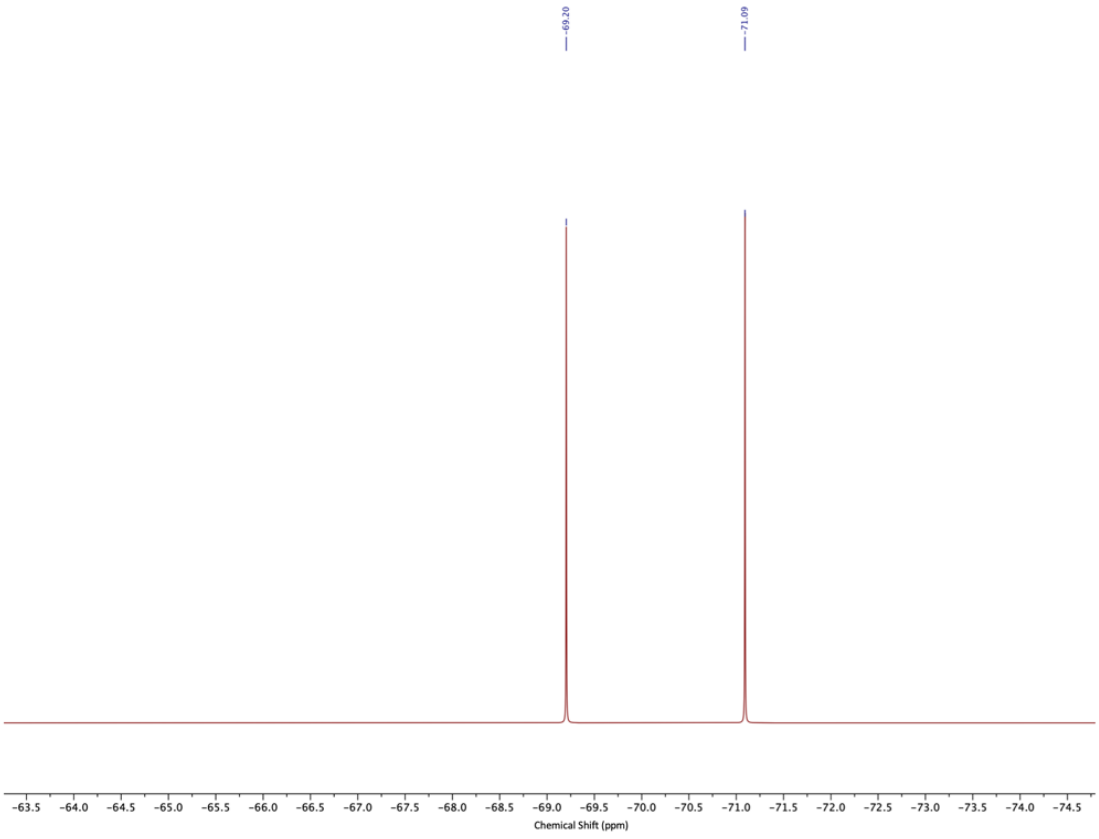

*Figure 7.110. ^{19}F NMR spectrum (376 MHz, DMSO-d_6, 298 K) of **4.14**.*

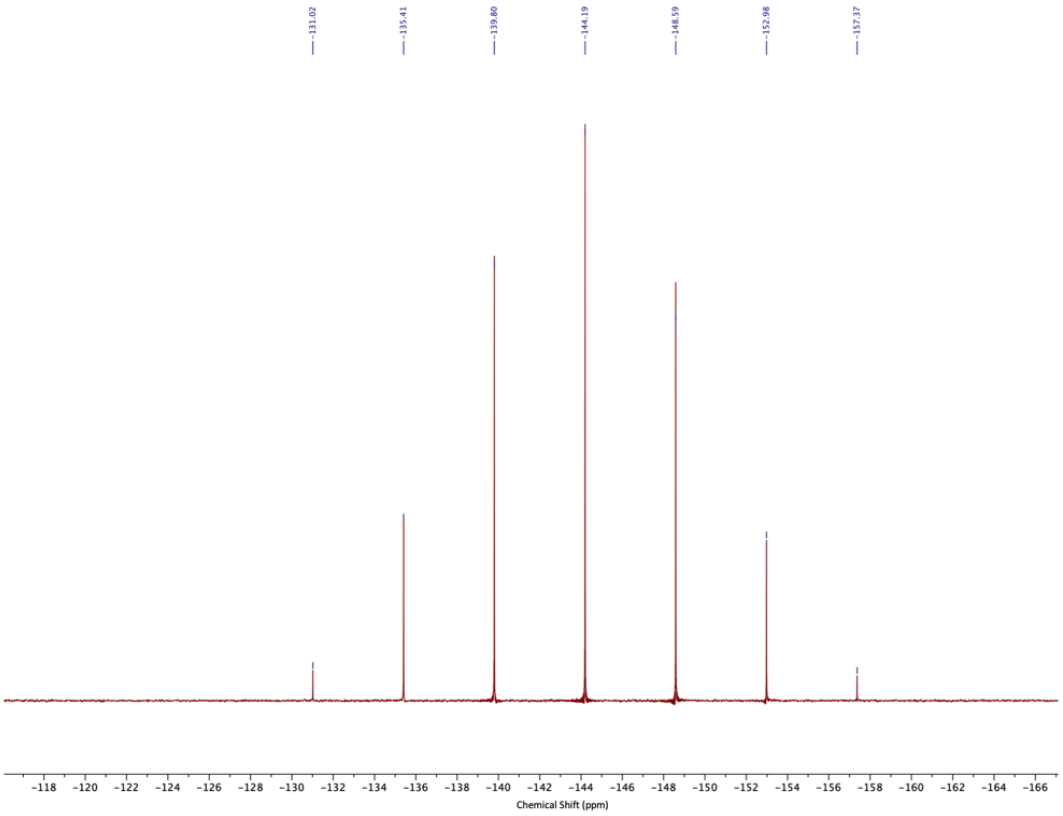

*Figure 7.111. ^{31}P NMR spectrum (162 MHz, DMSO-d_6, 298 K) of **4.14**.*

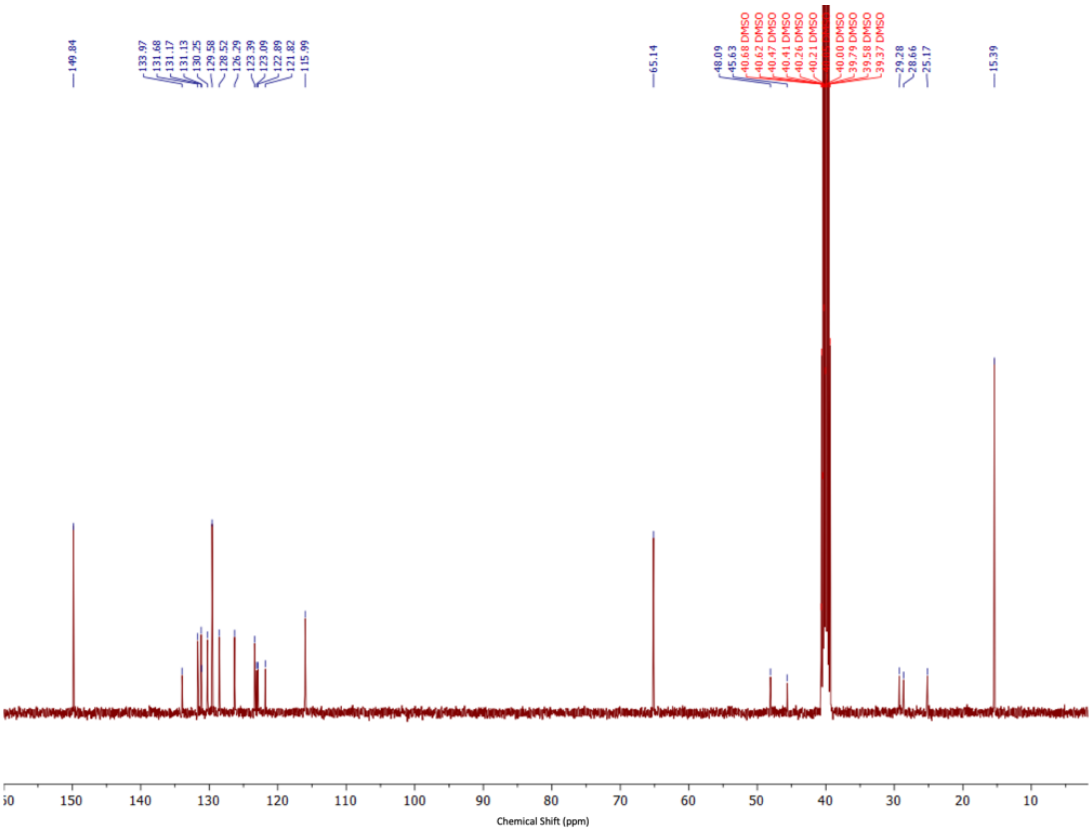

*Figure 7.112. ^{13}C NMR spectrum (101 MHz, DMSO-d_6, 298 K) of **4.14**.*

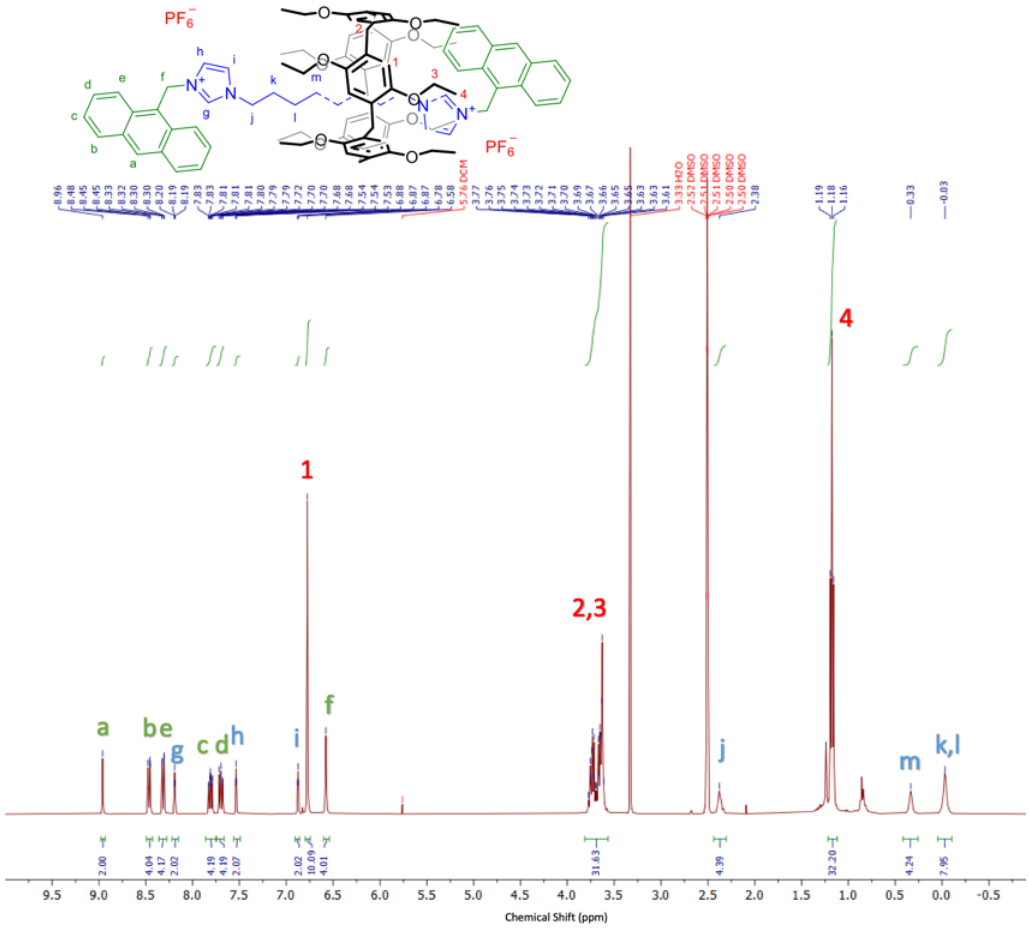

*Figure 7.113. ^{1}H NMR spectrum (400 MHz, DMSO-d_6, 298 K) of **4.15**.*

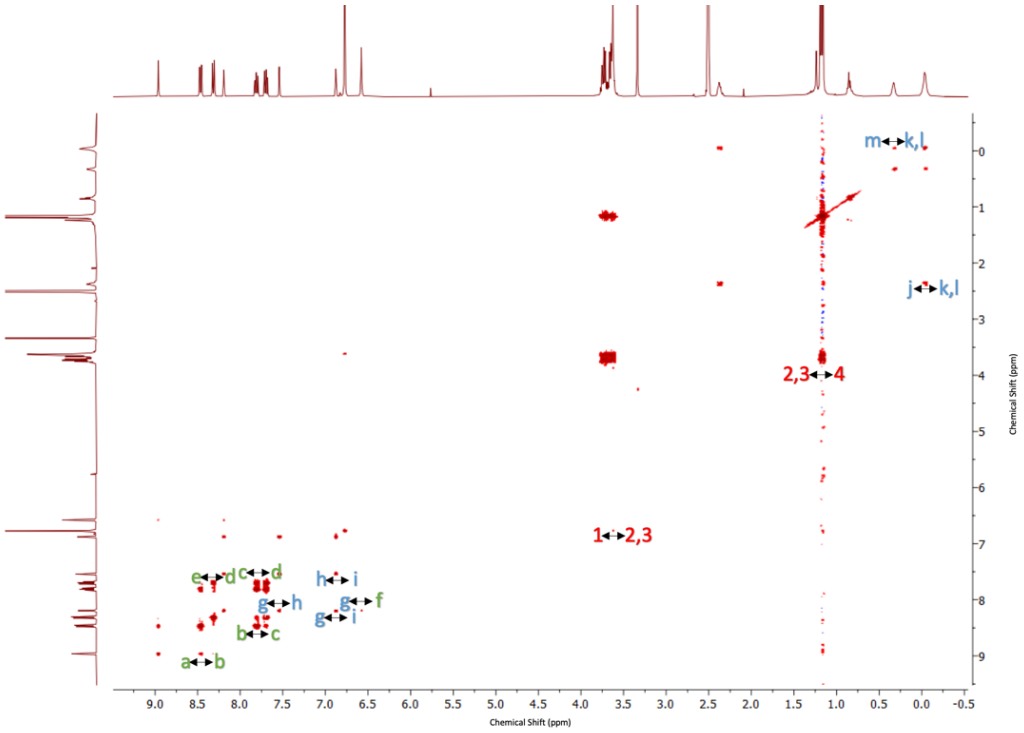

*Figure 7.114. 2D ^{1}H-^{1}H COSY NMR spectrum (400 MHz, DMSO-d_6, 298 K) of **4.15**.*

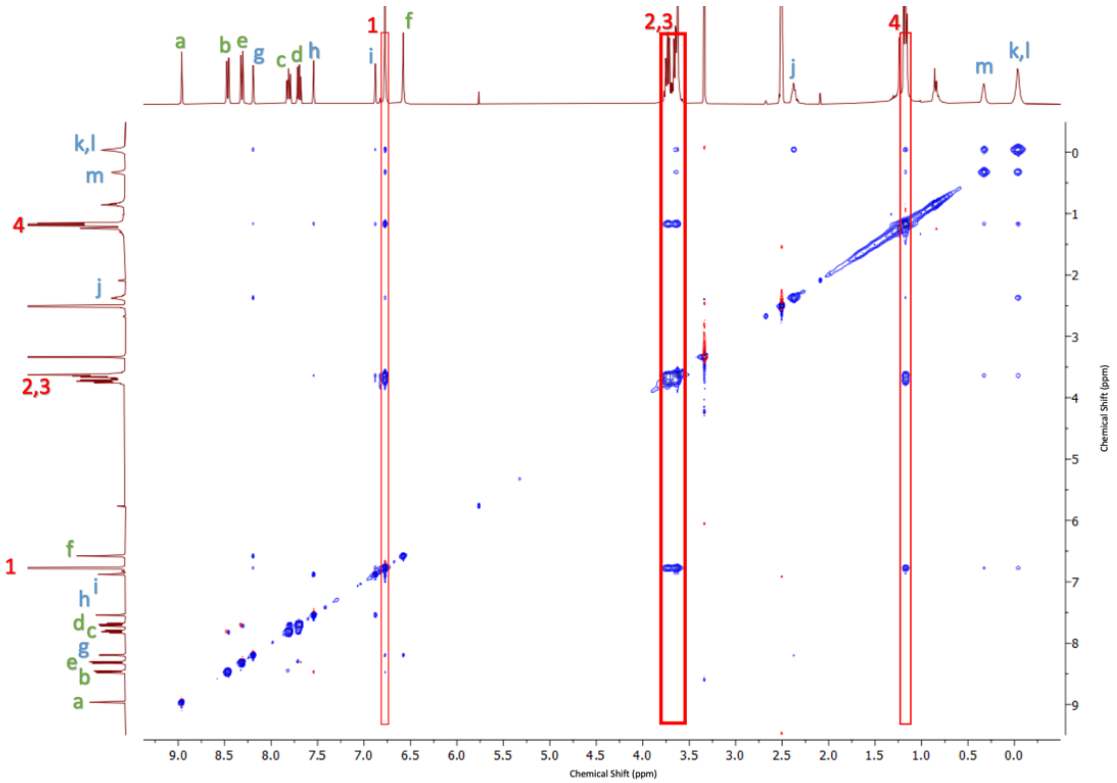

*Figure 7.115. 2D ^{1}H-^{1}H NOESY NMR spectrum (400 MHz, DMSO-d_6, 298 K) of **4.15**.*

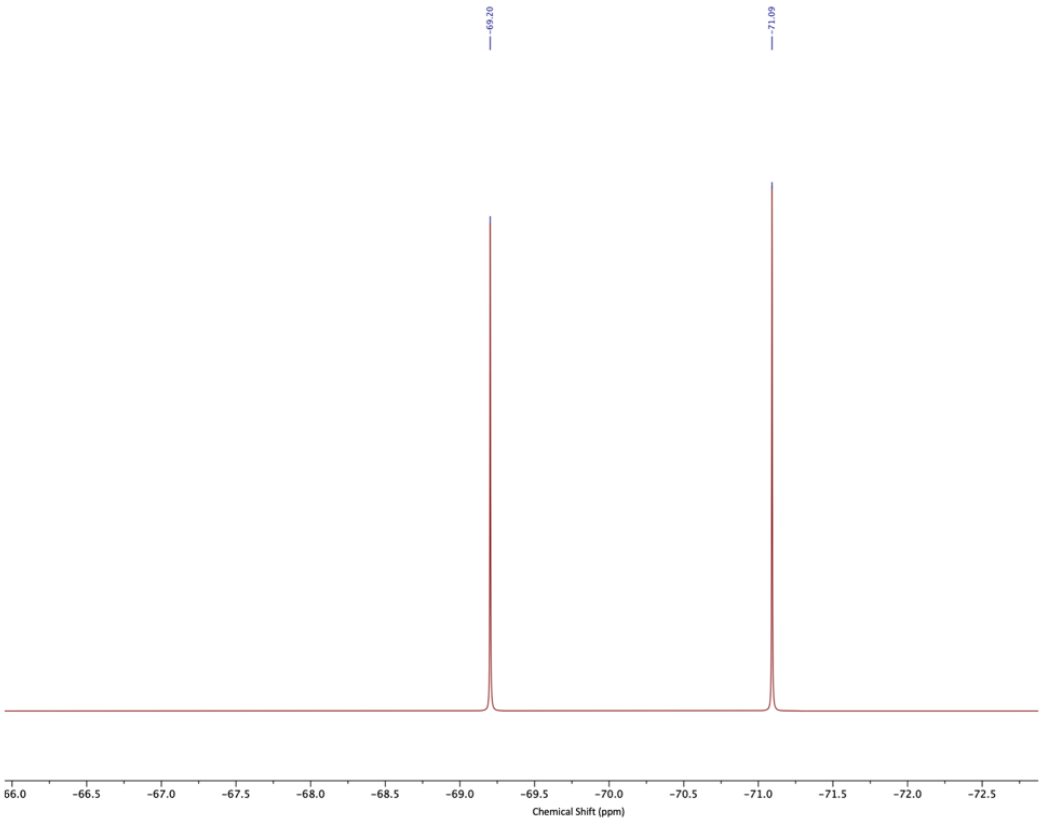

*Figure 7.116. ^{19}F NMR spectrum (376 MHz, DMSO-d_6, 298 K) of **4.15**.*

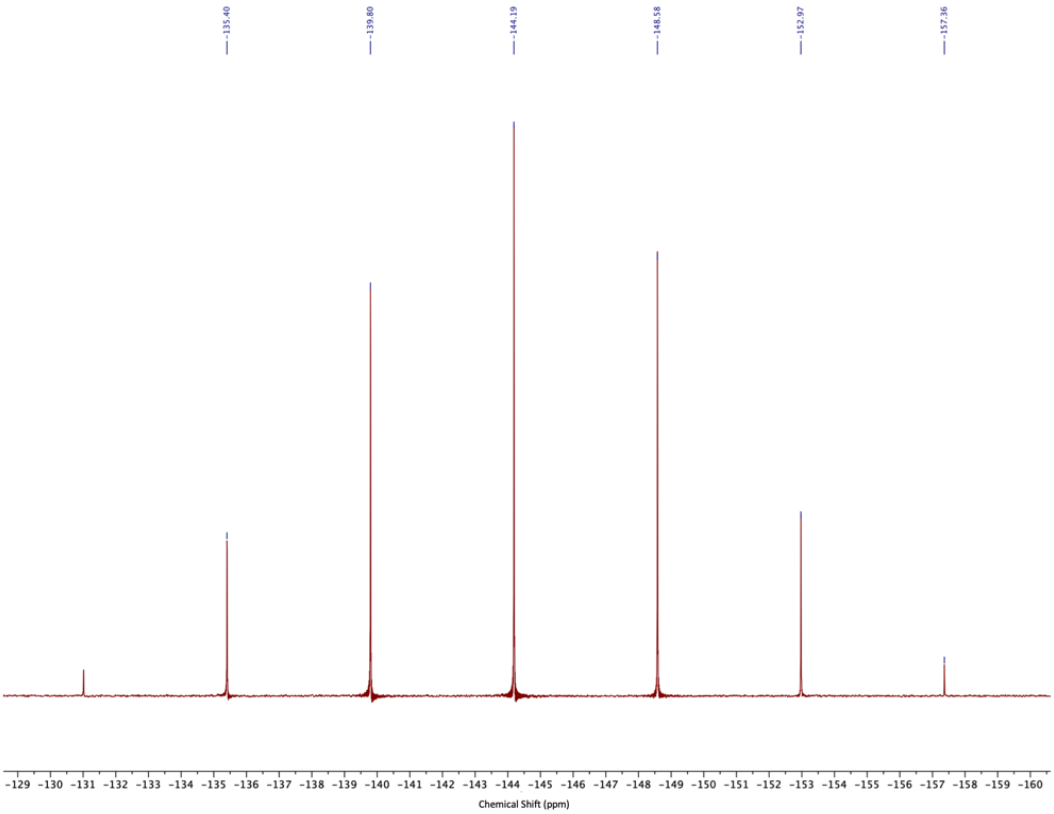

*Figure 7.117. ^{31}P NMR spectrum (162 MHz, DMSO-d_6, 298 K) of **4.15**.*

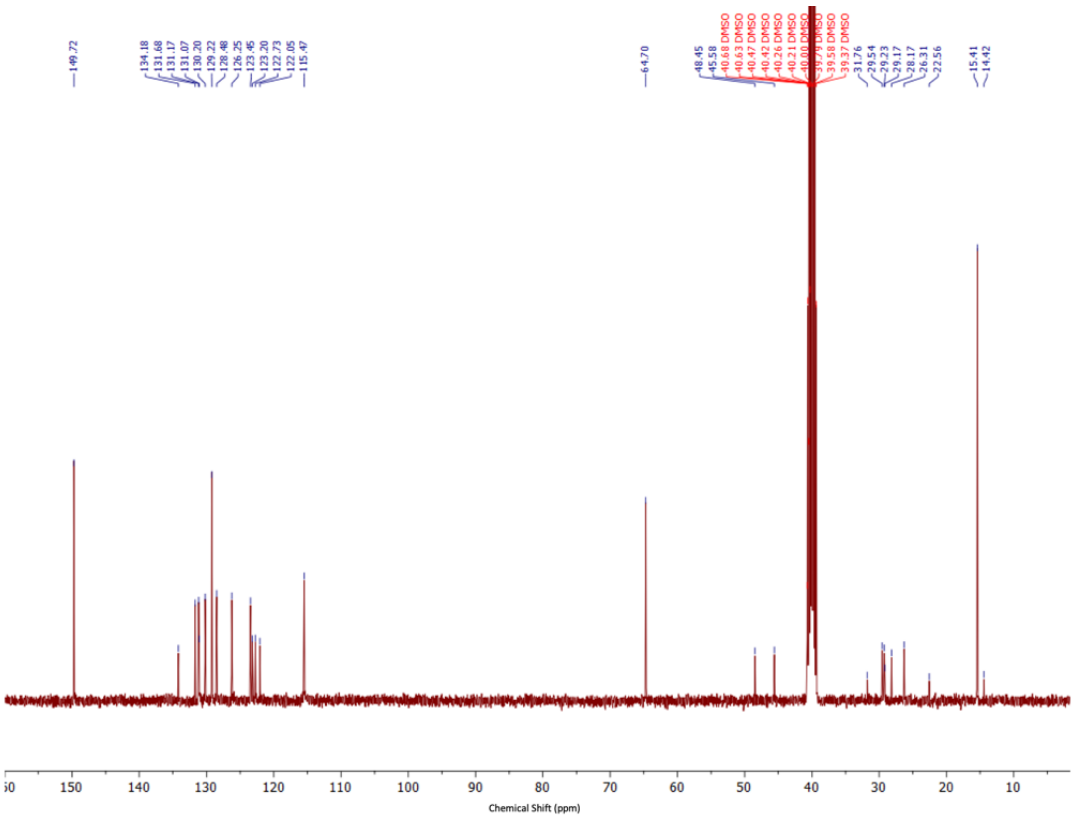

*Figure 7.118. ^{13}C NMR spectrum (101 MHz, DMSO-d_6, 298 K) of **4.15**.*

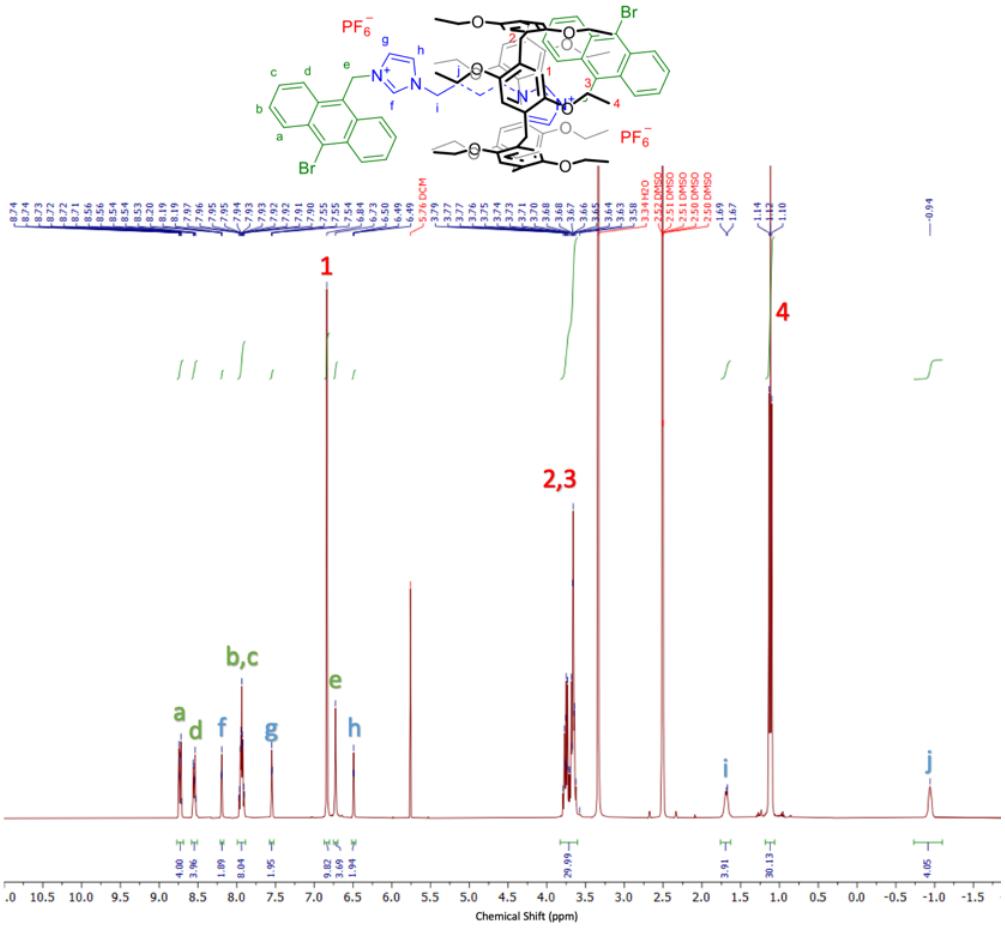

*Figure 7.119. ^{1}H NMR spectrum (400 MHz, DMSO-d_6, 298 K) of **4.16**.*

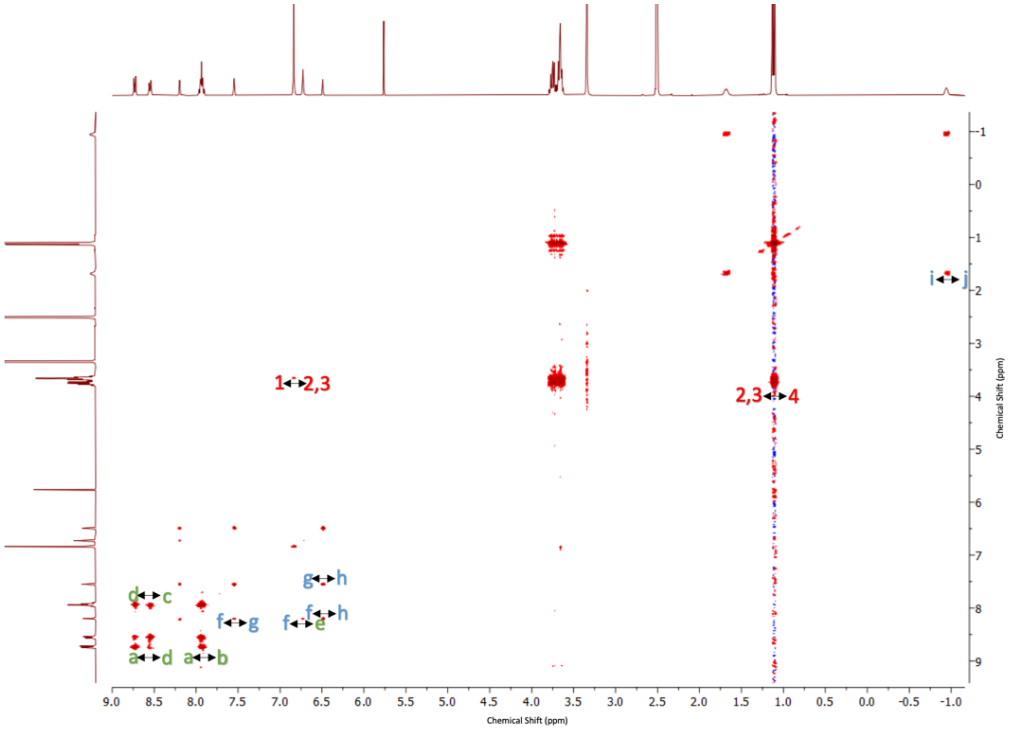

*Figure 7.120. 2D ^{1}H-^{1}H COSY NMR spectrum (400 MHz, DMSO-d_6, 298 K) of **4.16**.*

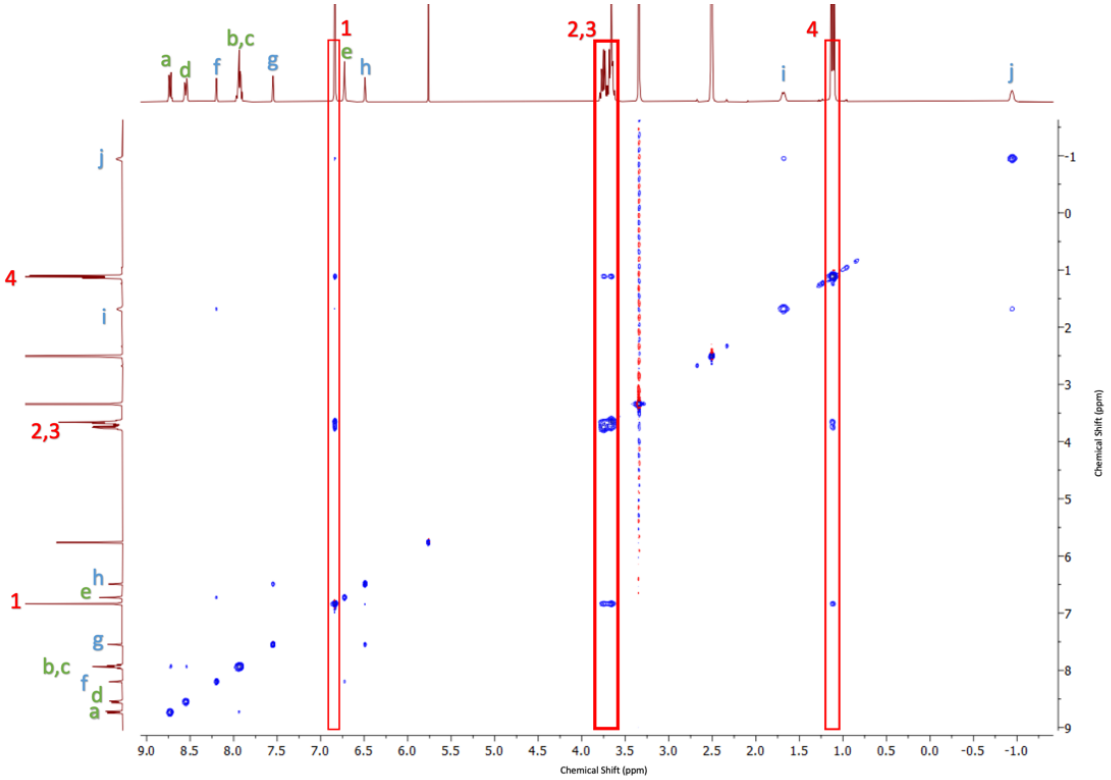

*Figure 7.121. 2D ^{1}H-^{1}H NOESY NMR spectrum (400 MHz, DMSO-d_6, 298 K) of **4.16**.*

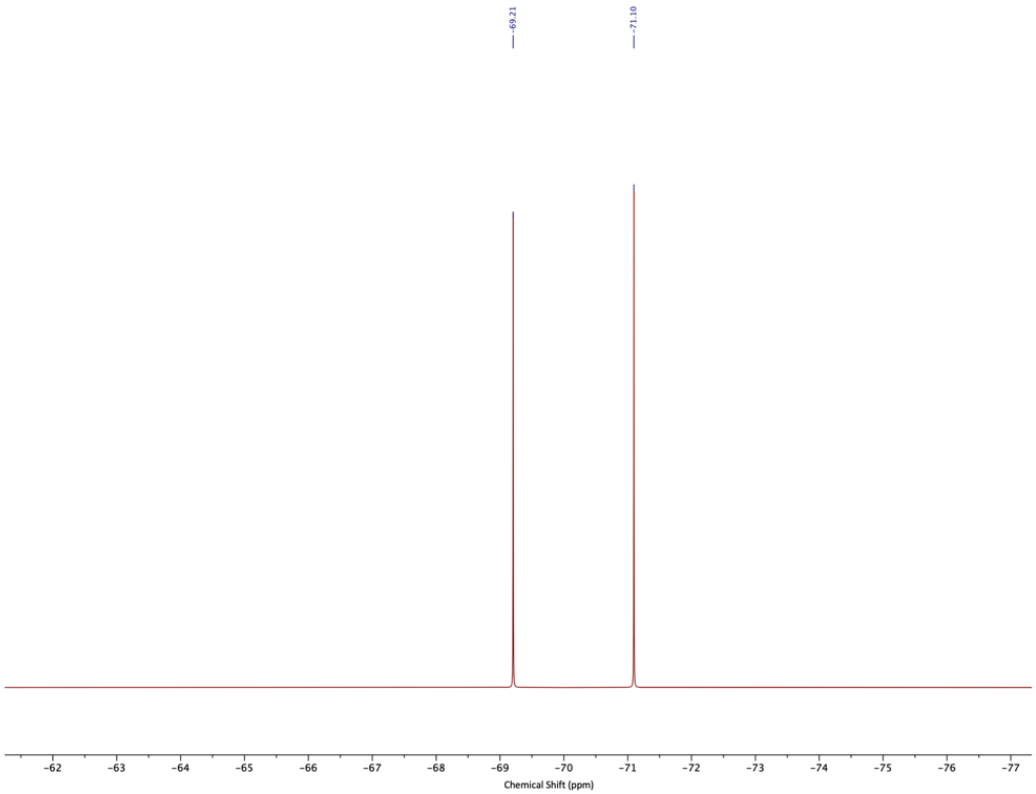

*Figure 7. 122. ^{19}F NMR spectrum (376 MHz, DMSO-d_6, 298 K) of **4.16**.*

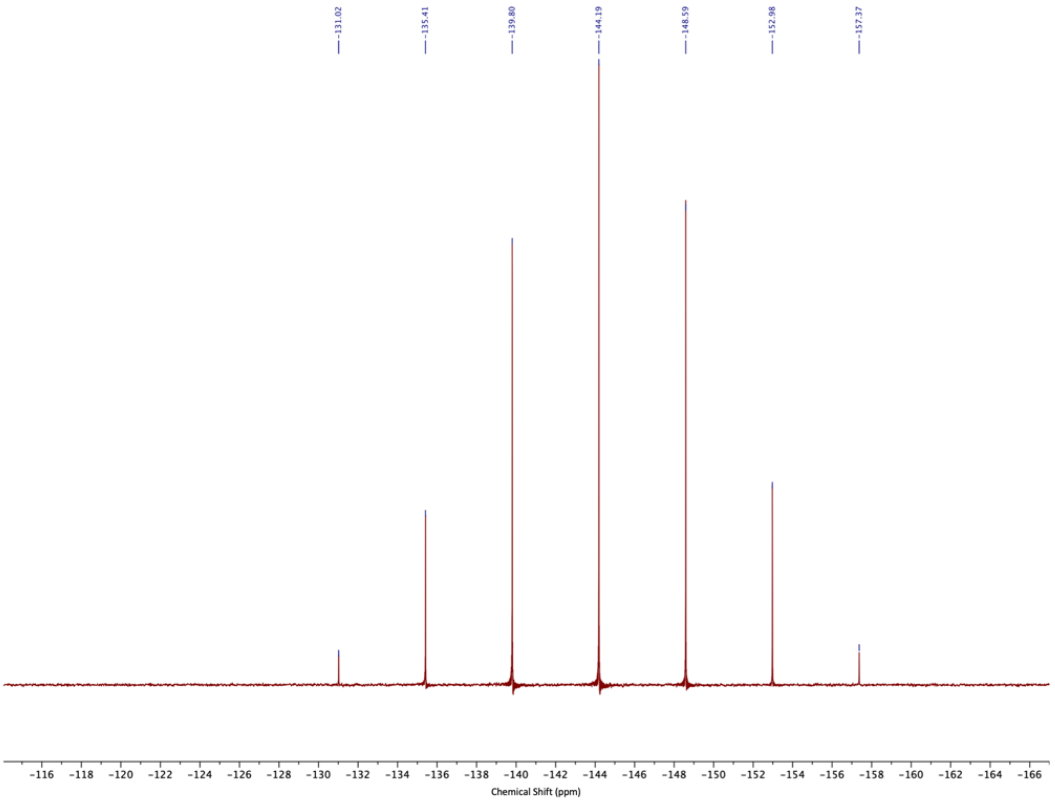

*Figure 7.123. ^{31}P NMR spectrum (162 MHz, DMSO-d_6, 298 K) of **4.16**.*

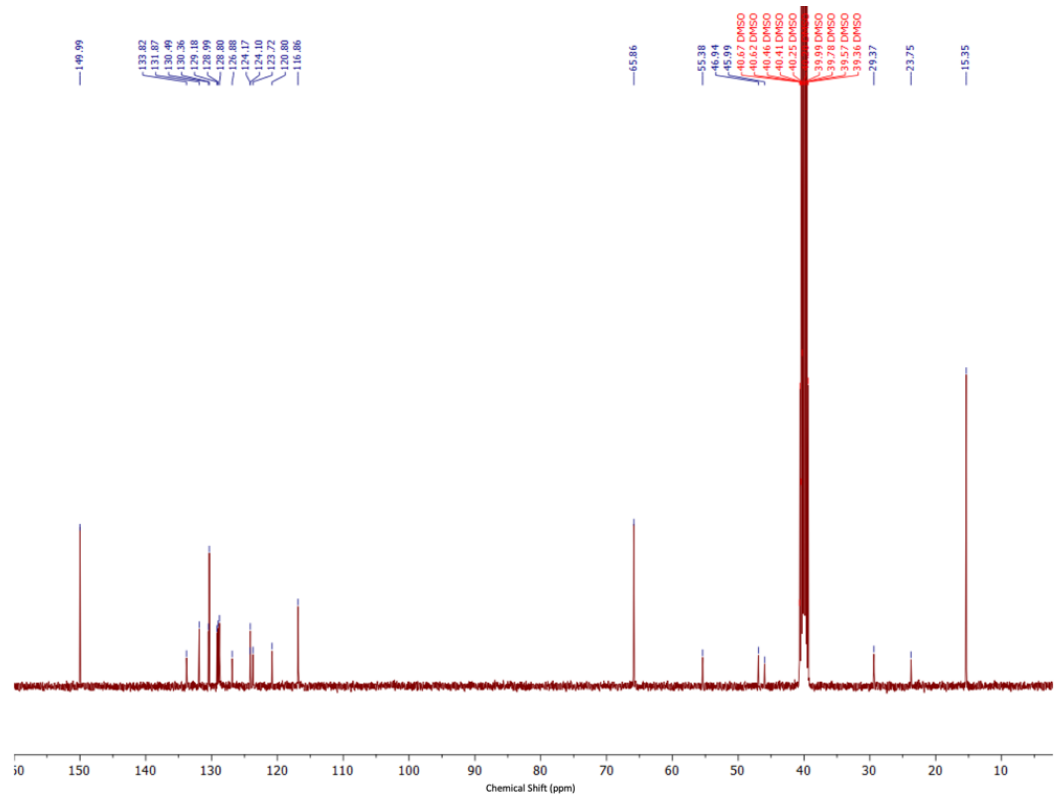

*Figure 7.124. ^{13}C NMR spectrum (101 MHz, DMSO-d_6, 298 K) of **4.16**.*

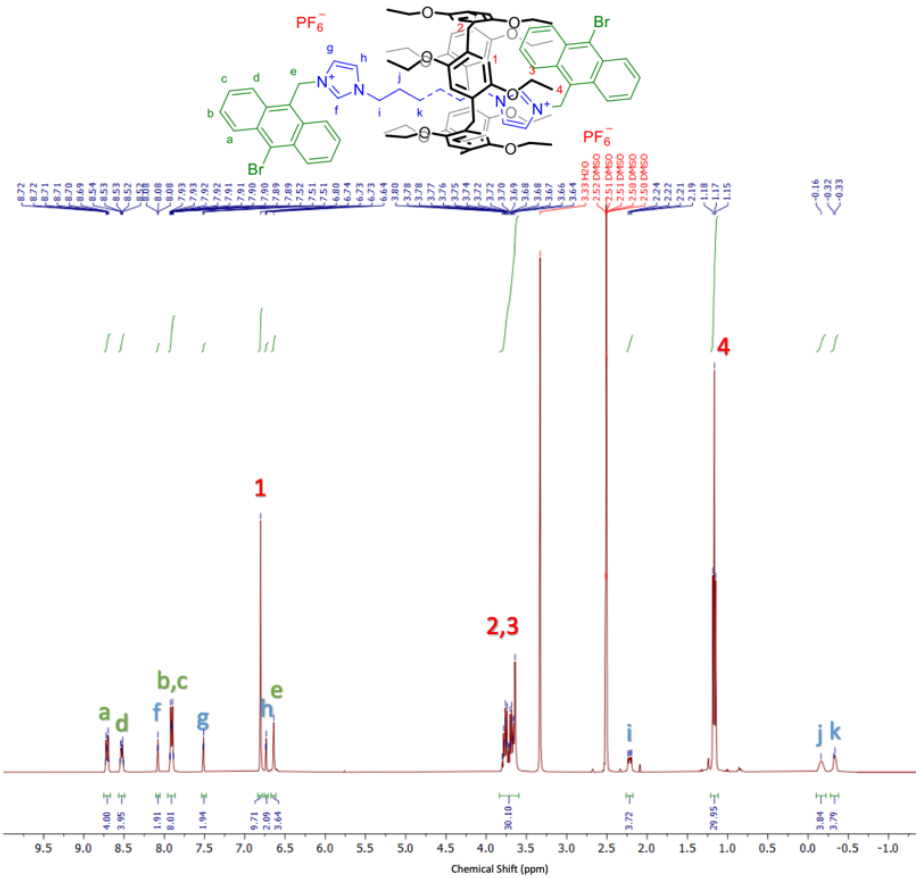

*Figure 7.125. ^{1}H NMR spectrum (400 MHz, DMSO-d_6, 298 K) of **4.17**.*

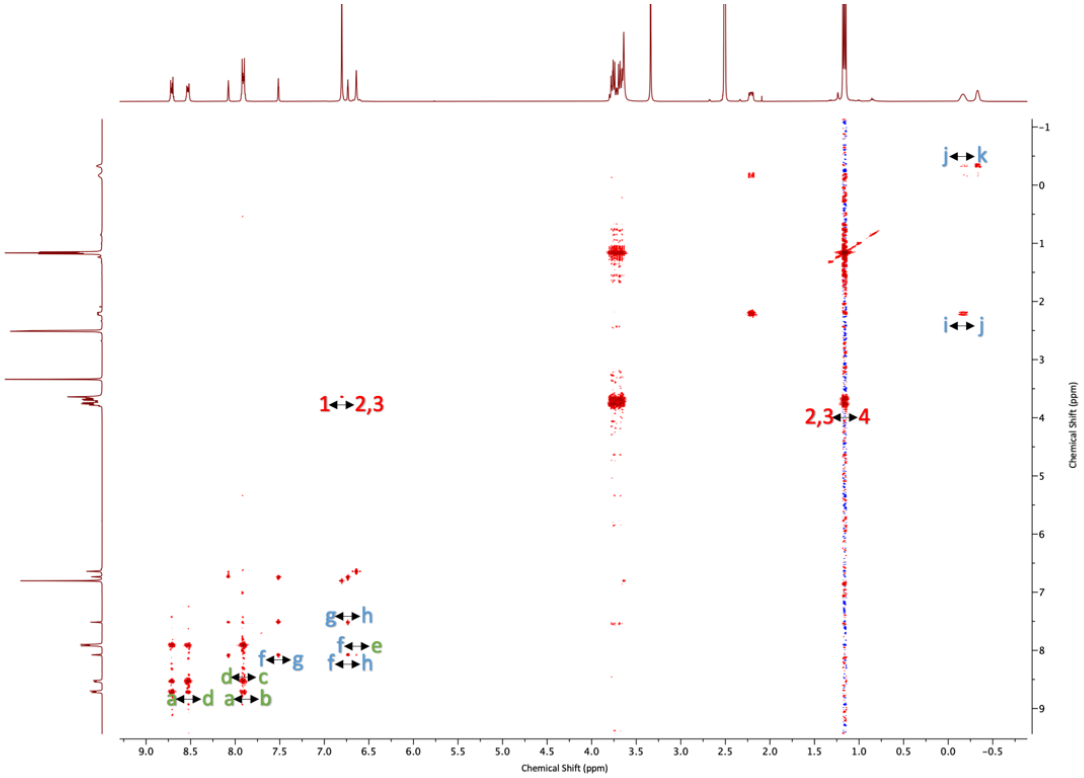

*Figure 7.126. 2D ^{1}H-^{1}H COSY NMR spectrum (400 MHz, DMSO-d_6, 298 K) of **4.17**.*

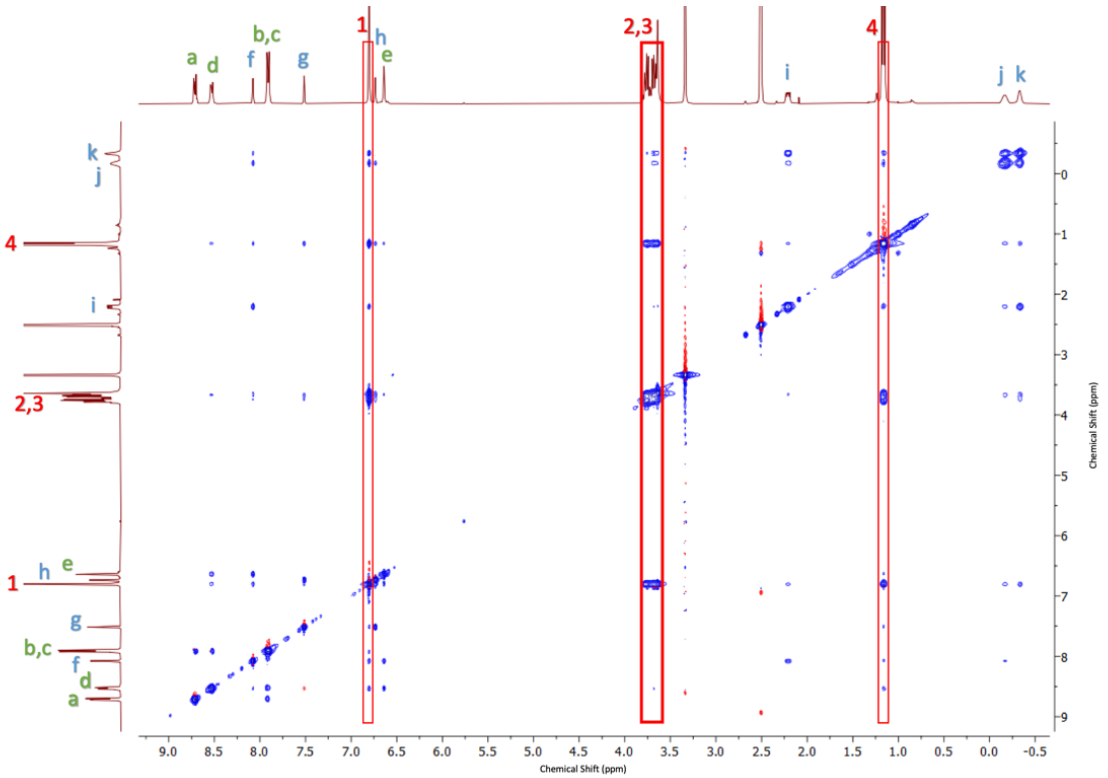

*Figure 7.127. 2D ^{1}H-^{1}H NOESY NMR spectrum (400 MHz, DMSO-d_6, 298 K) of **4.17**.*

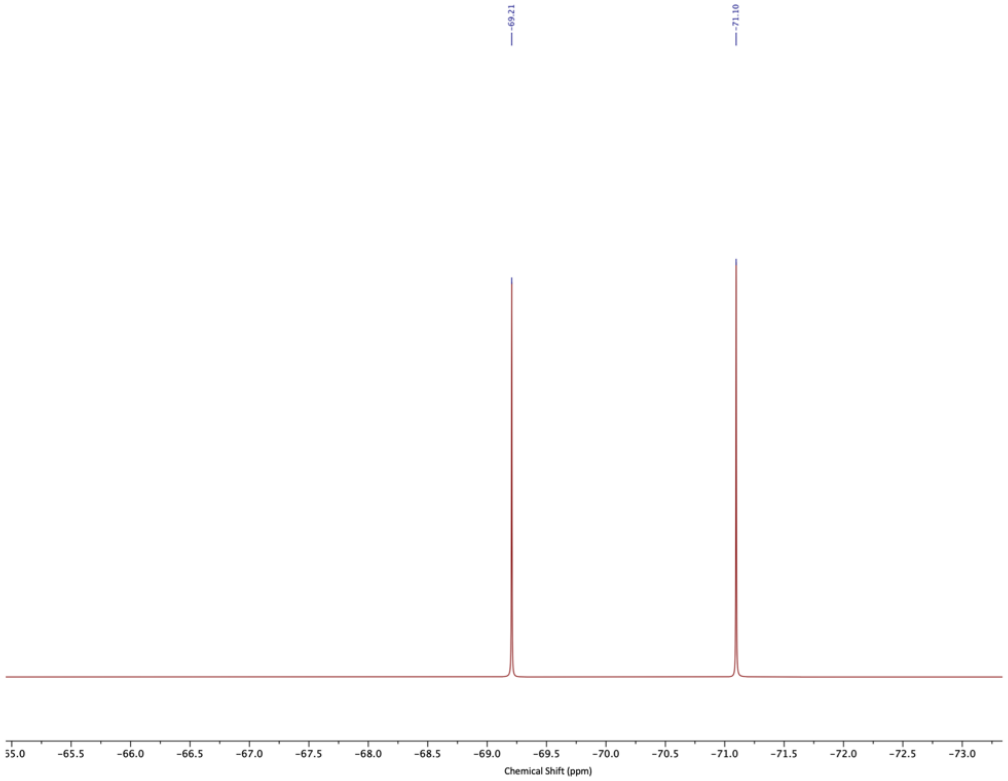

*Figure 7.128. ^{19}F NMR spectrum (376 MHz, DMSO-d_6, 298 K) of **4.17**.*

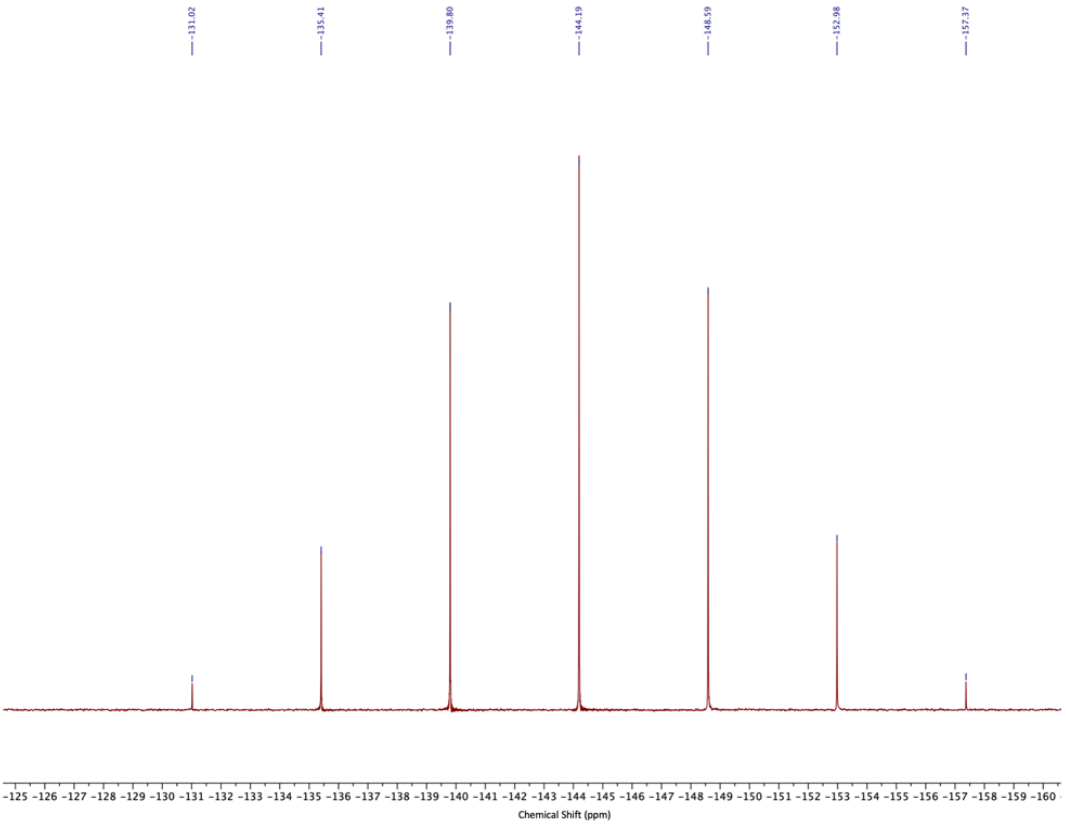

*Figure 7.129. ^{31}P NMR spectrum (162 MHz, DMSO-d_6, 298 K) of **4.17**.*

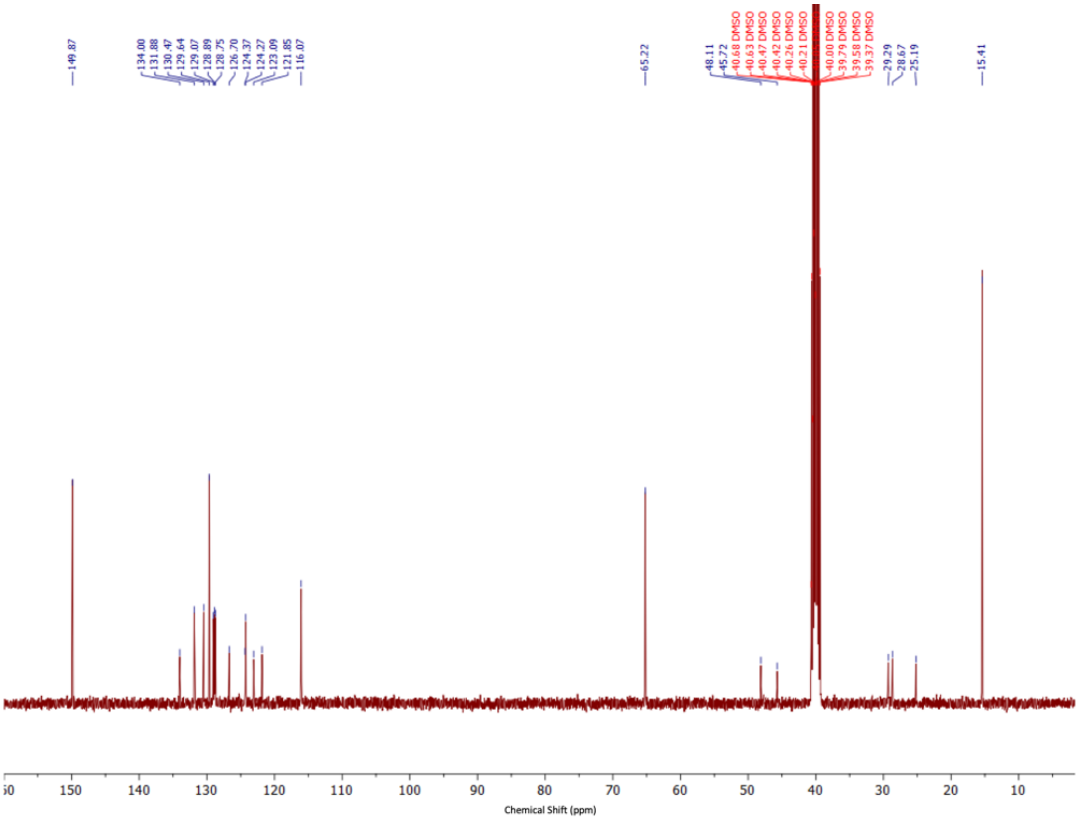

*Figure 7.130. ^{13}C NMR spectrum (101 MHz, DMSO-d_6, 298 K) of **4.17**.*

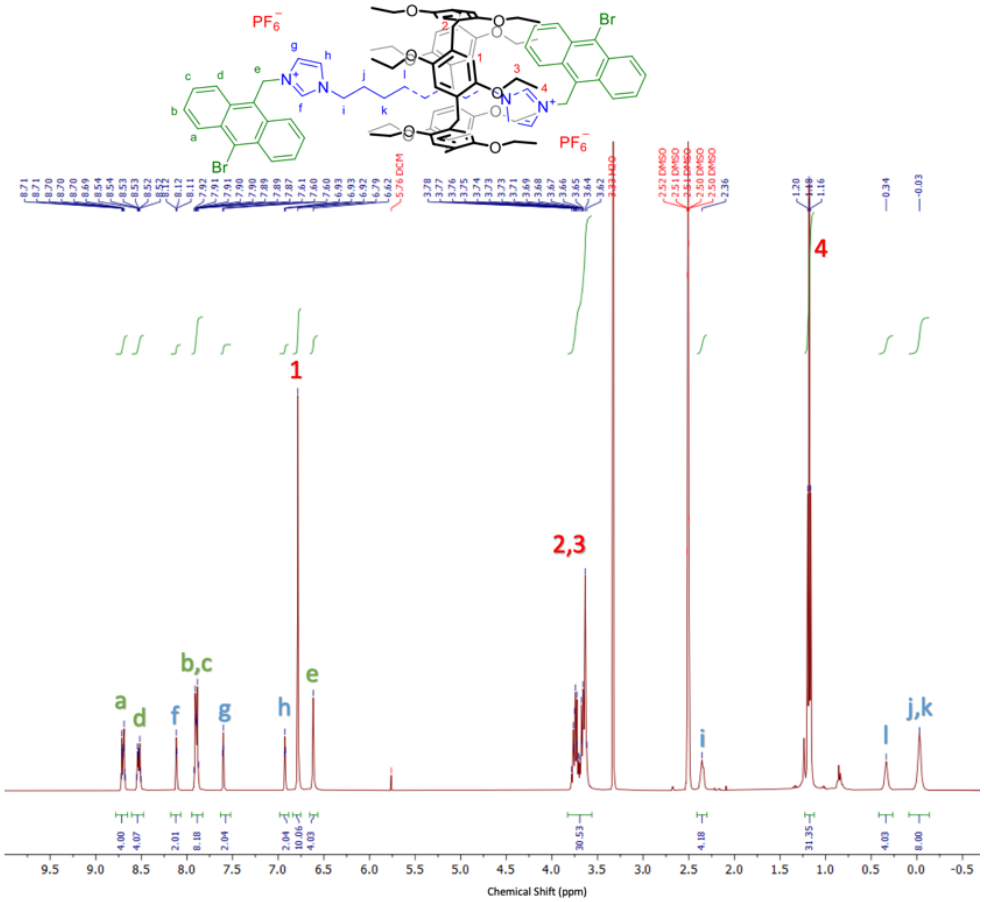

*Figure 7.131. ^{1}H NMR spectrum (400 MHz, DMSO-d_6, 298 K) of **4.18**.*

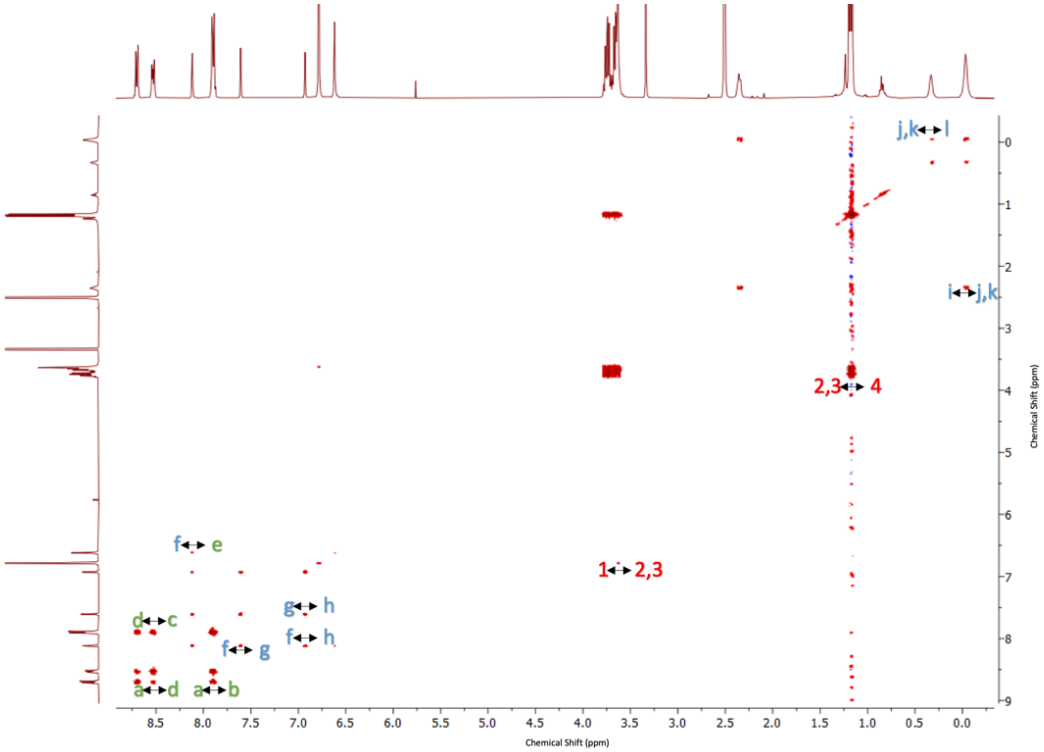

*Figure 7.132. 2D ^{1}H-^{1}H COSY NMR spectrum (400 MHz, DMSO-d_6, 298 K) of **4.18**.*

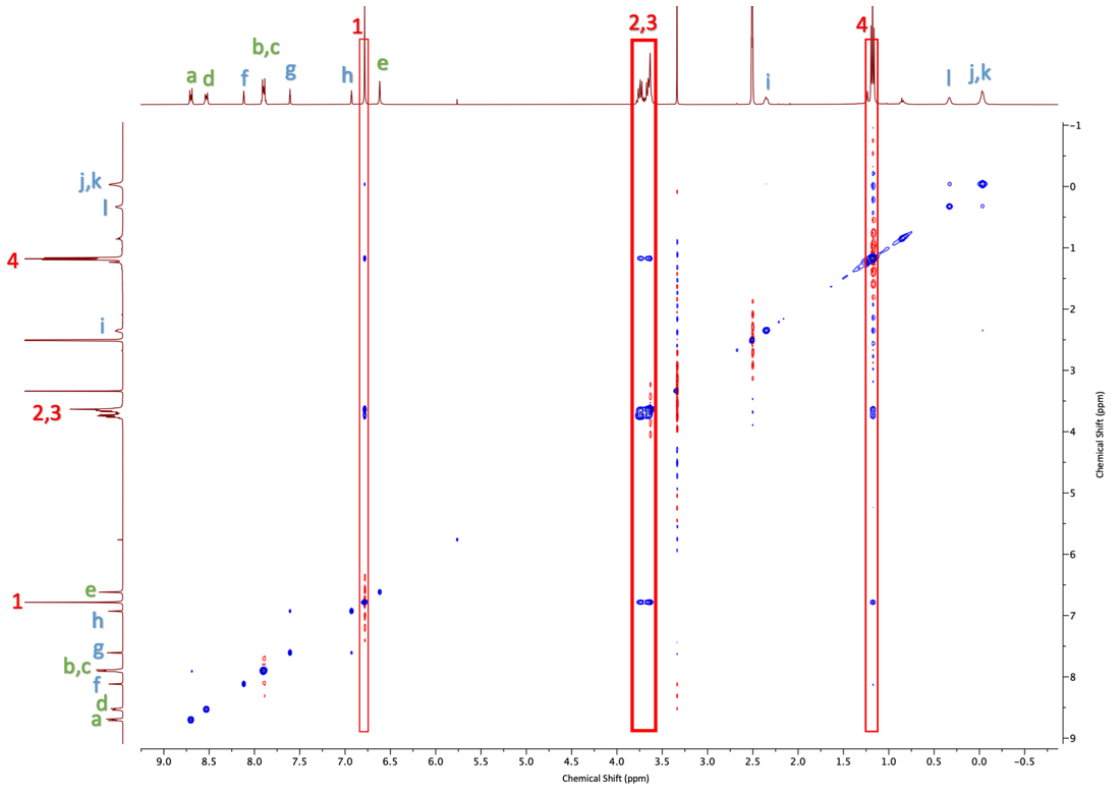

*Figure 7.133. 2D ^{1}H-^{1}H NOESY NMR spectrum (400 MHz, DMSO-d_6, 298 K) of **4.18**.*

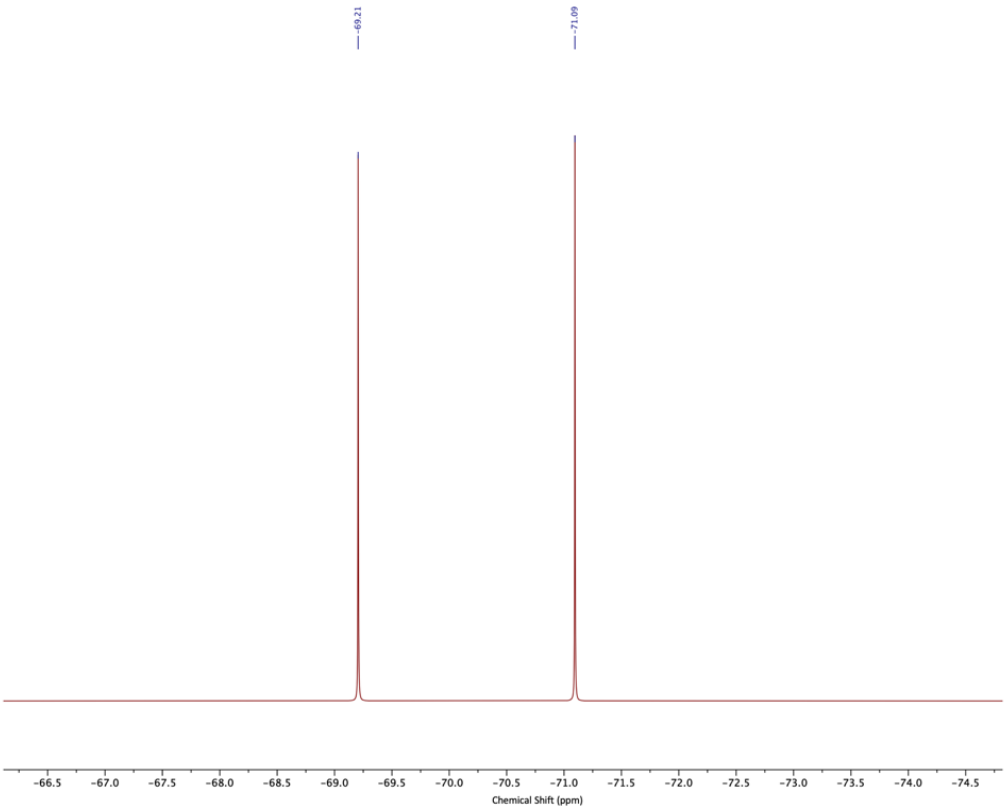

*Figure 7.134. ^{19}F NMR spectrum (376 MHz, DMSO-d_6, 298 K) of **4.18**.*

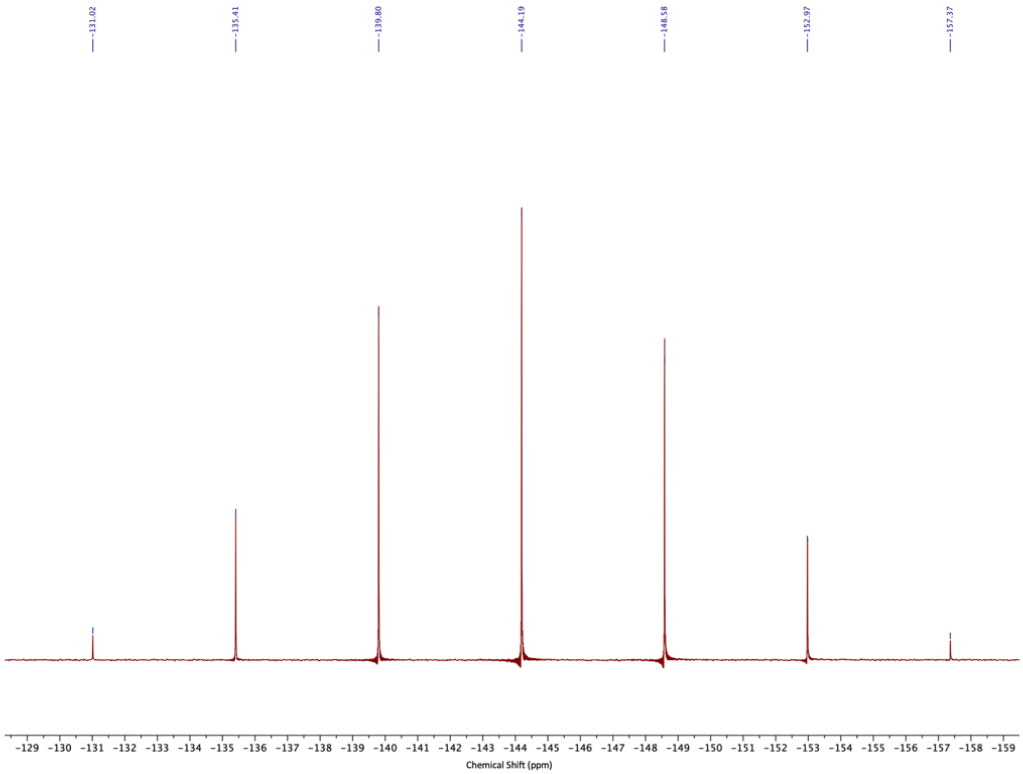

*Figure 7.135. ^{31}P NMR spectrum (162 MHz, DMSO-d_6, 298 K) of **4.18**.*

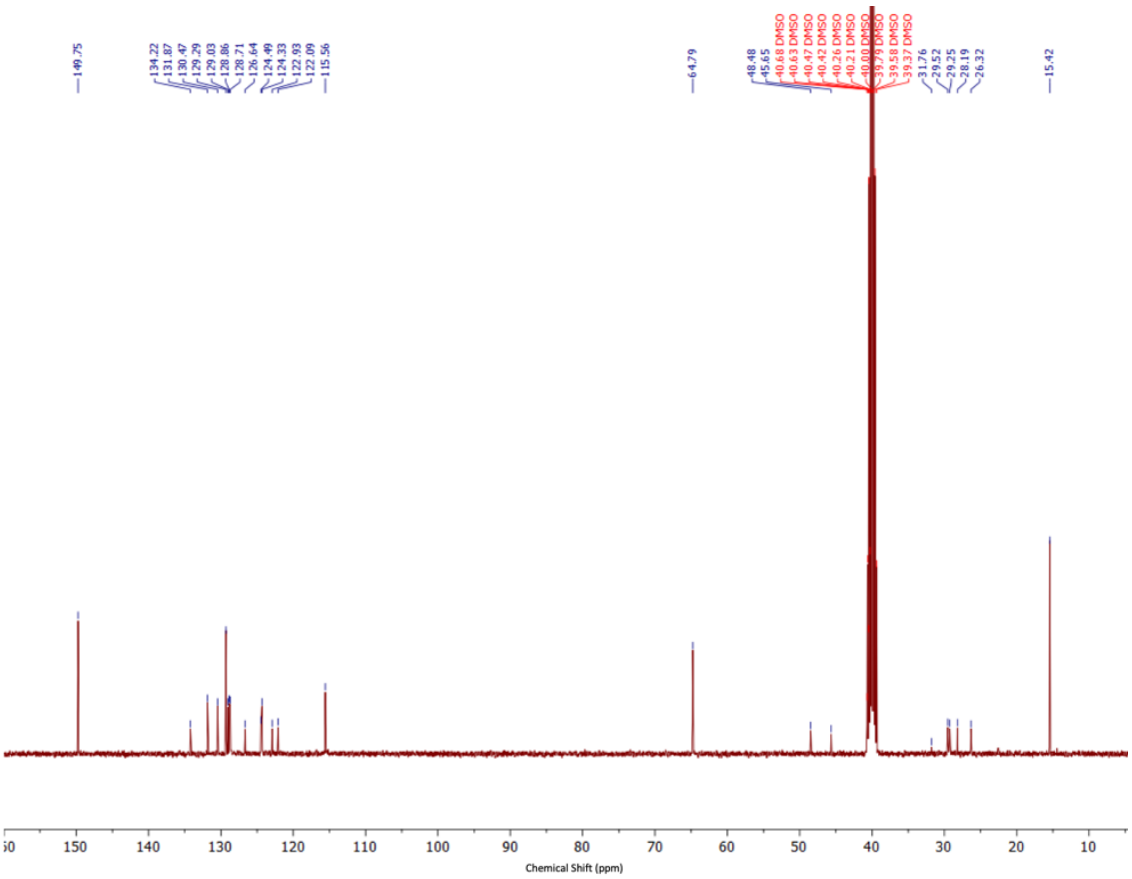

*Figure 7.136. ^{13}C NMR spectrum (101 MHz, DMSO-d_6, 298 K) of **4.18**.*

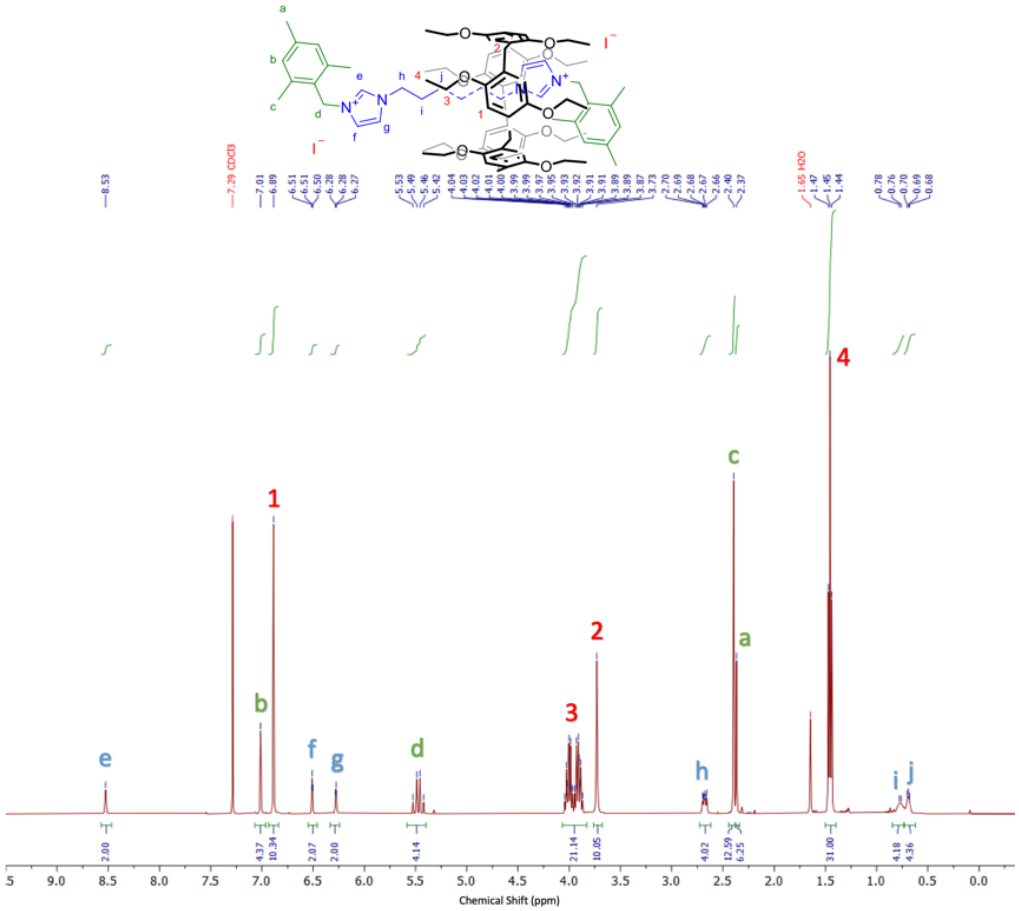

*Figure 7.137. ^{1}H NMR spectrum (400 MHz, $CDCl_3$, 298 K) of **4.19**.*

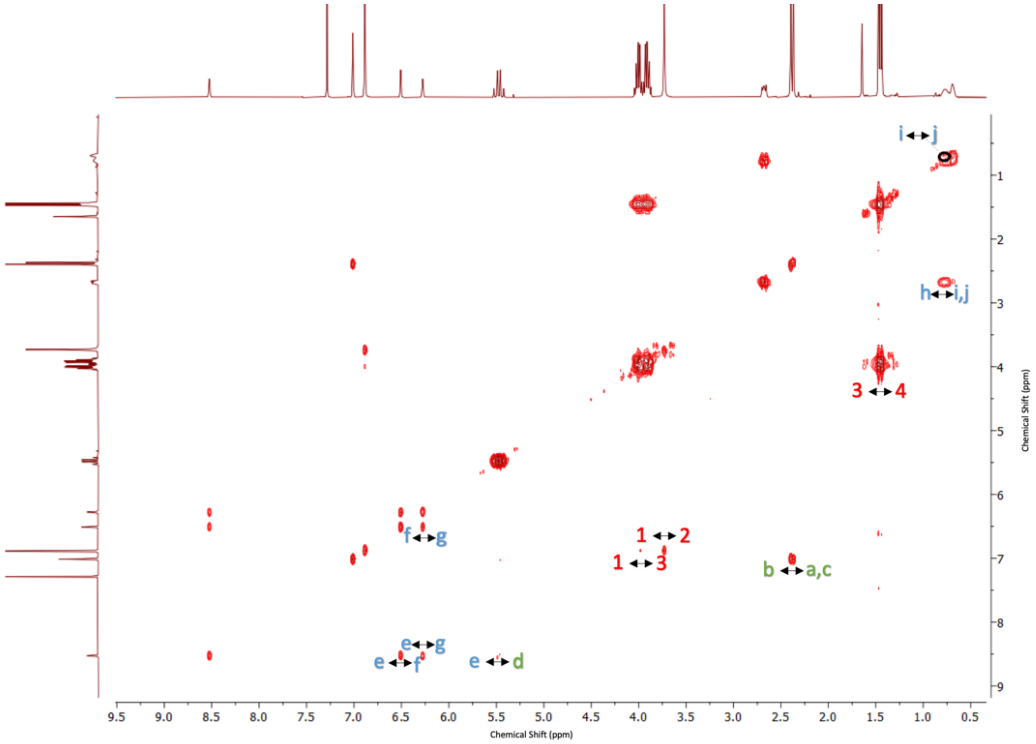

*Figure 7.138. 2D ^{1}H-^{1}H COSY NMR spectrum (400 MHz, $CDCl_3$, 298 K) of **4.19**.*

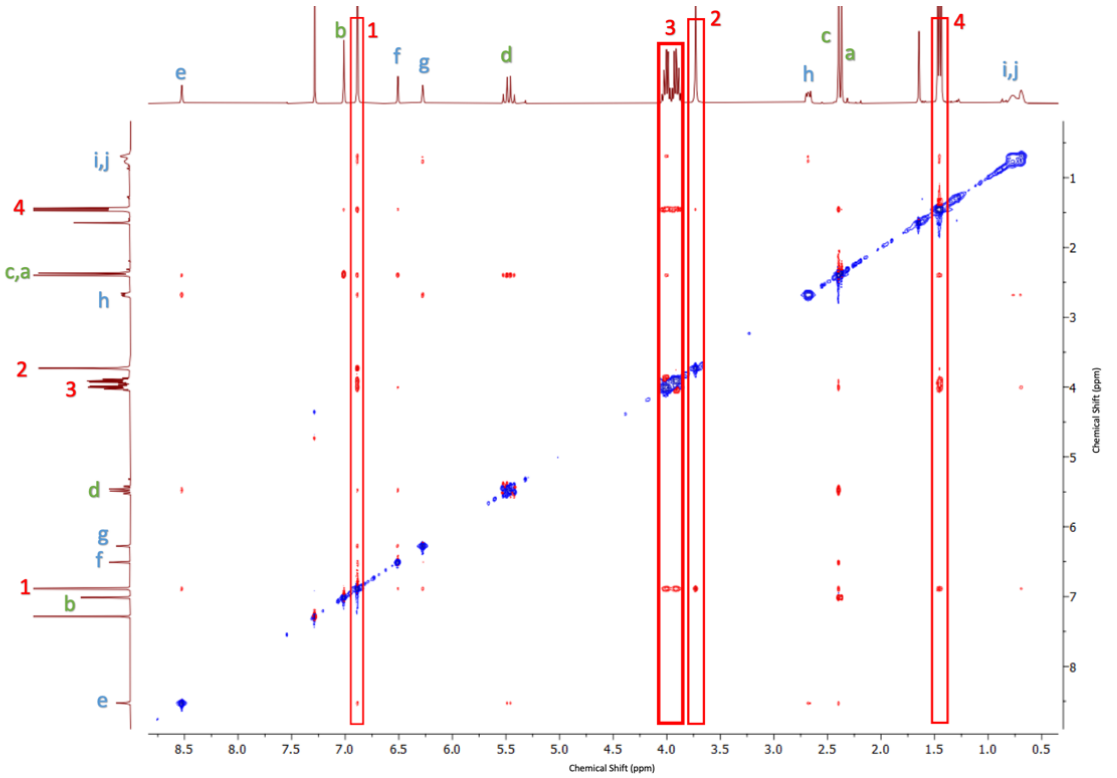

*Figure 7.139. 2D ^{1}H-^{1}H NOESY NMR spectrum (400 MHz, $CDCl_3$, 298 K) of **4.19**.*

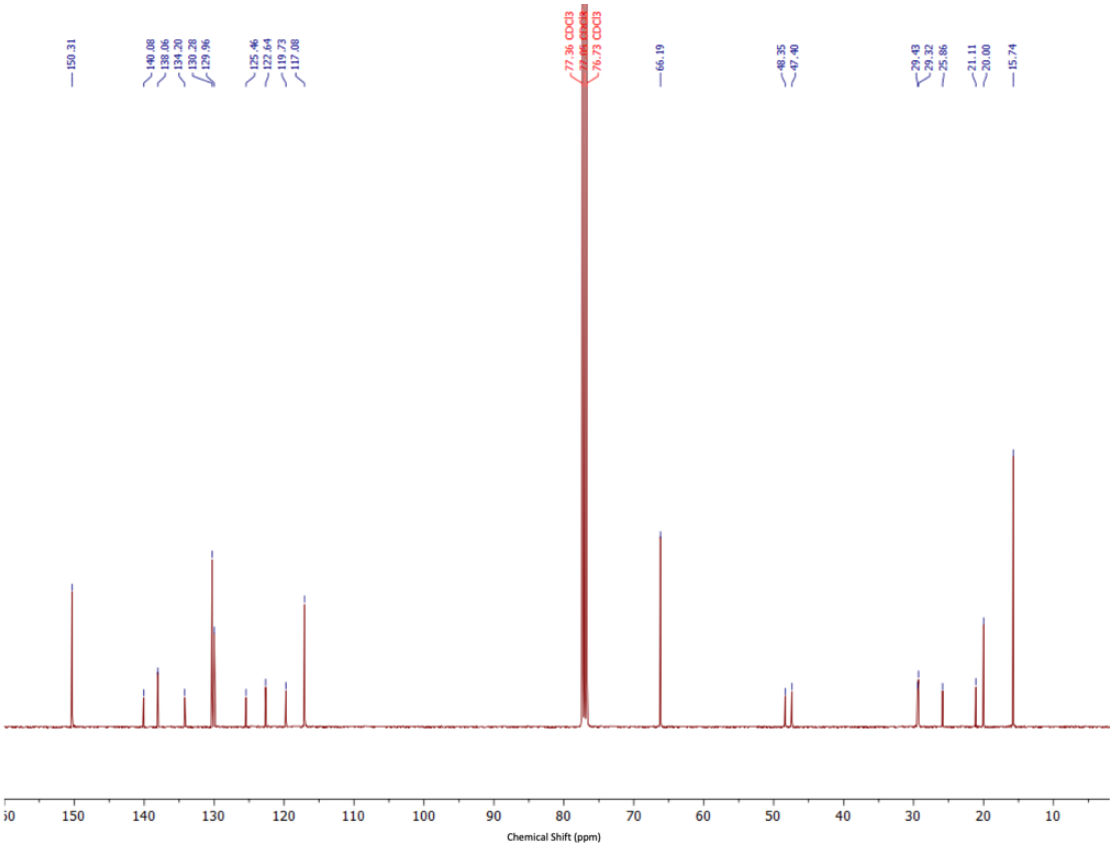

*Figure 7.140. ^{13}C NMR spectrum (101 MHz, $CDCl_3$, 298 K) of **4.19**.*

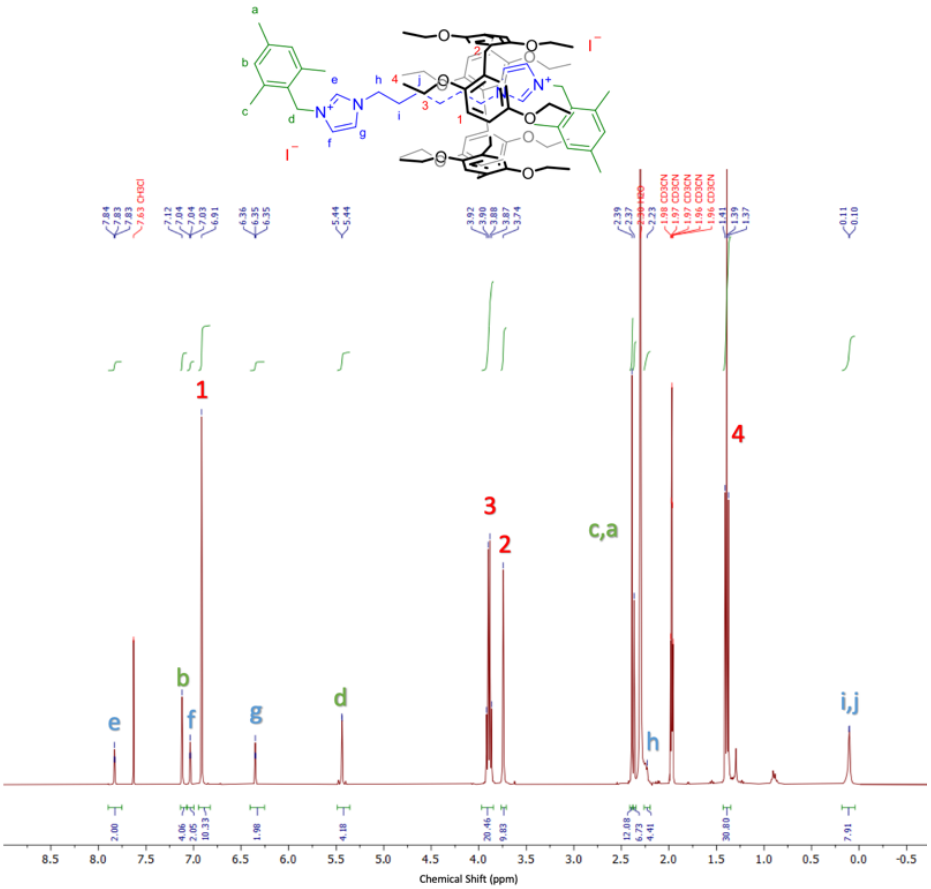

*Figure 7.141. ^{1}H NMR spectrum (400 MHz, CD_3CN, 298 K) of **4.19**.*

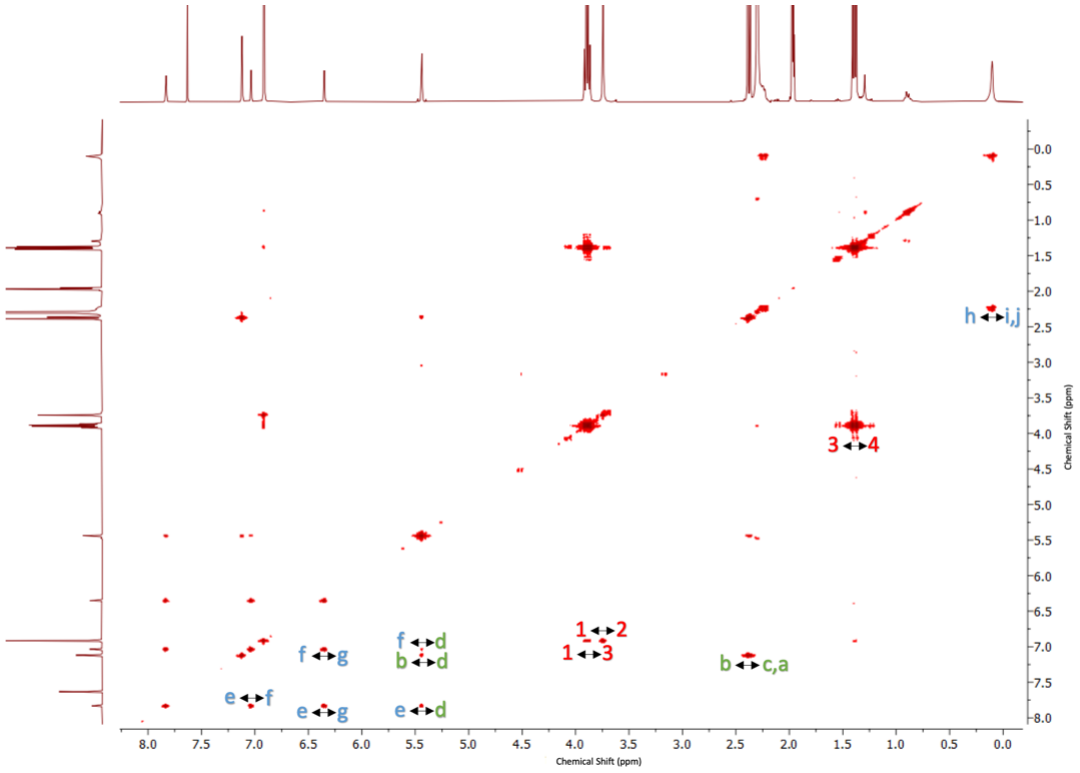

*Figure 7.142. 2D ^{1}H-^{1}H COSY NMR spectrum (400 MHz, CD_3CN, 298 K) of **4.19**.*

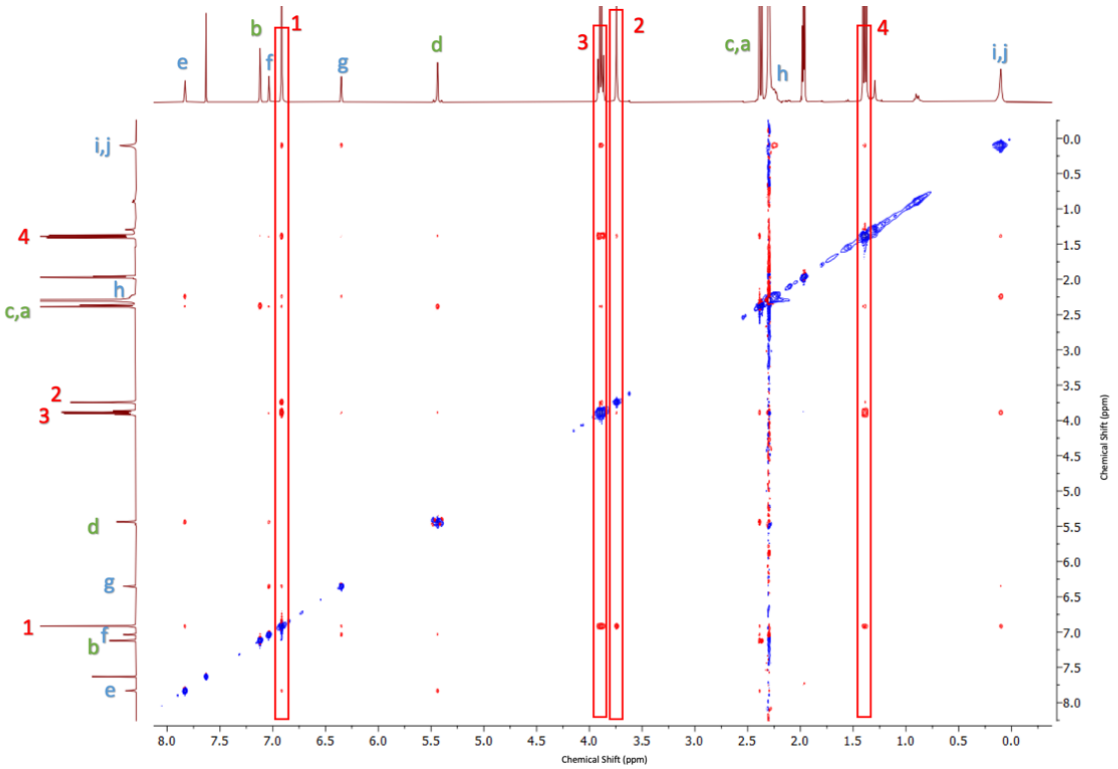

*Figure 7.143. 2D ^{1}H-^{1}H NOESY NMR spectrum (400 MHz, CD_3CN, 298 K) of **4.19**.*

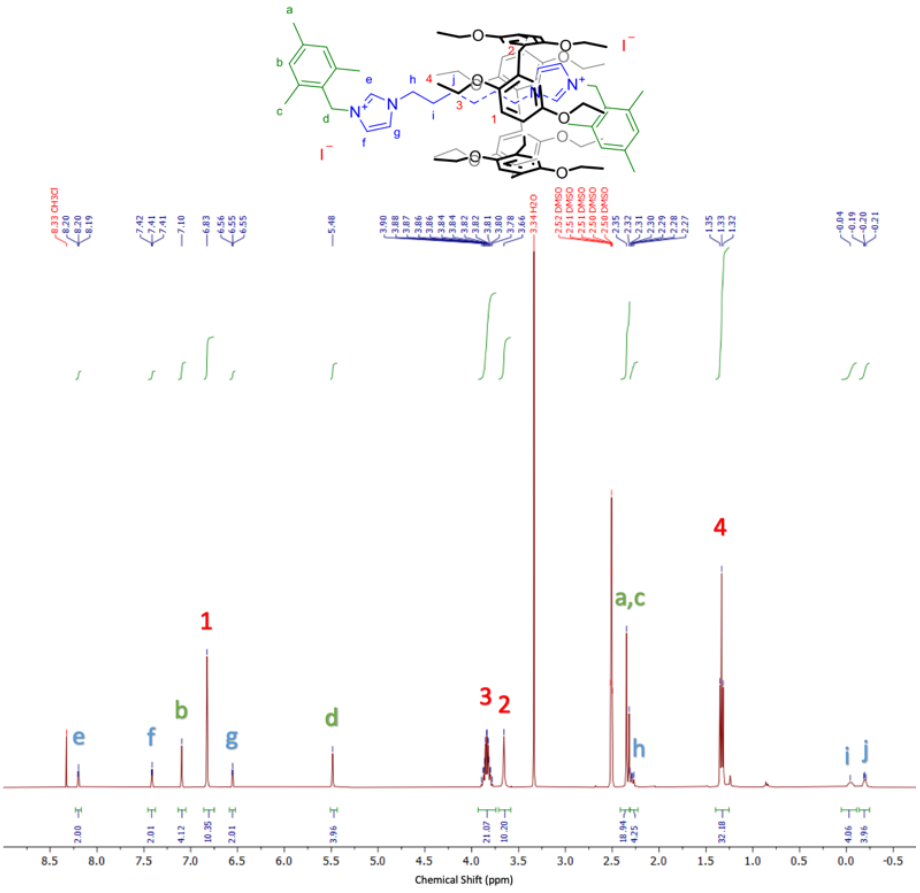

*Figure 7.144. ^{1}H NMR spectrum (400 MHz, DMSO-d_6, 298 K) of **4.19**.*

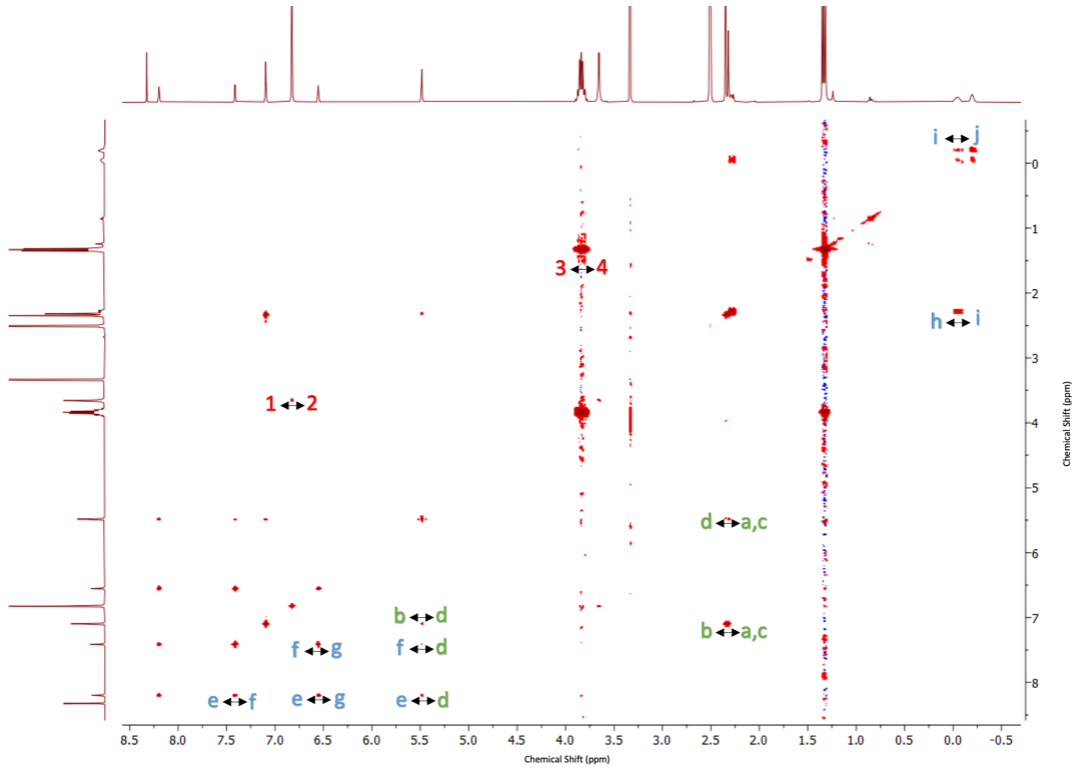

*Figure 7.145. 2D ^{1}H-^{1}H COSY NMR spectrum (400 MHz, DMSO-d_6, 298 K) of **4.19**.*

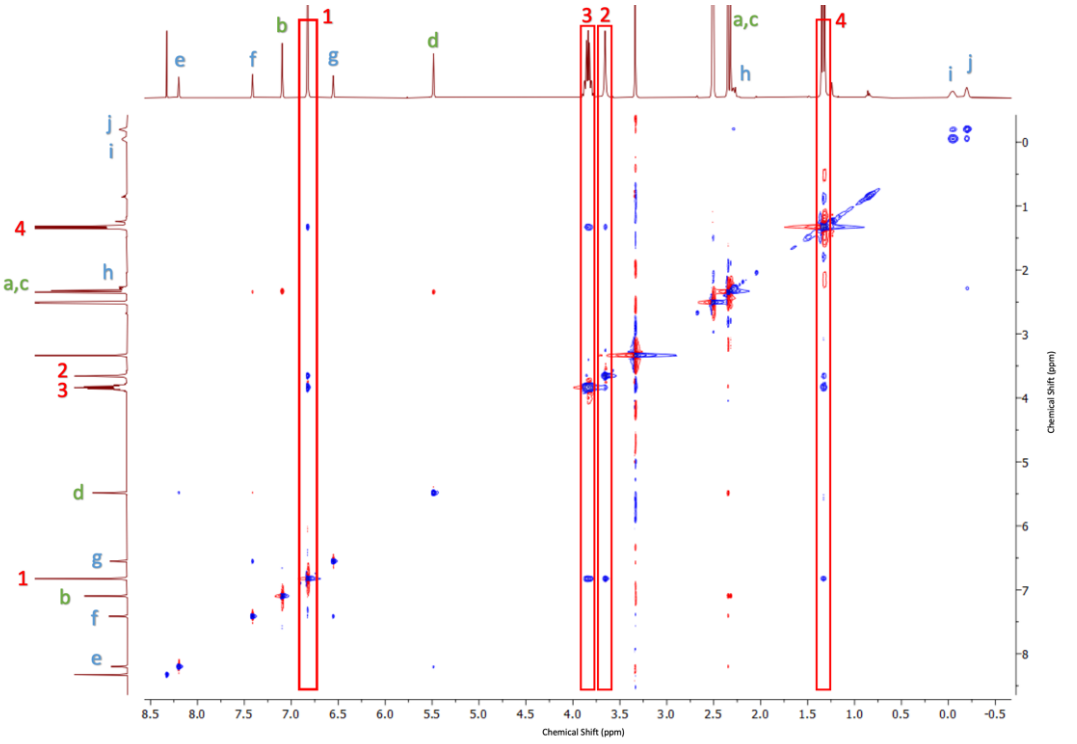

*Figure 7.146. 2D ^{1}H-^{1}H NOESY NMR spectrum (400 MHz, DMSO-d_6, 298 K) of **4.19**.*

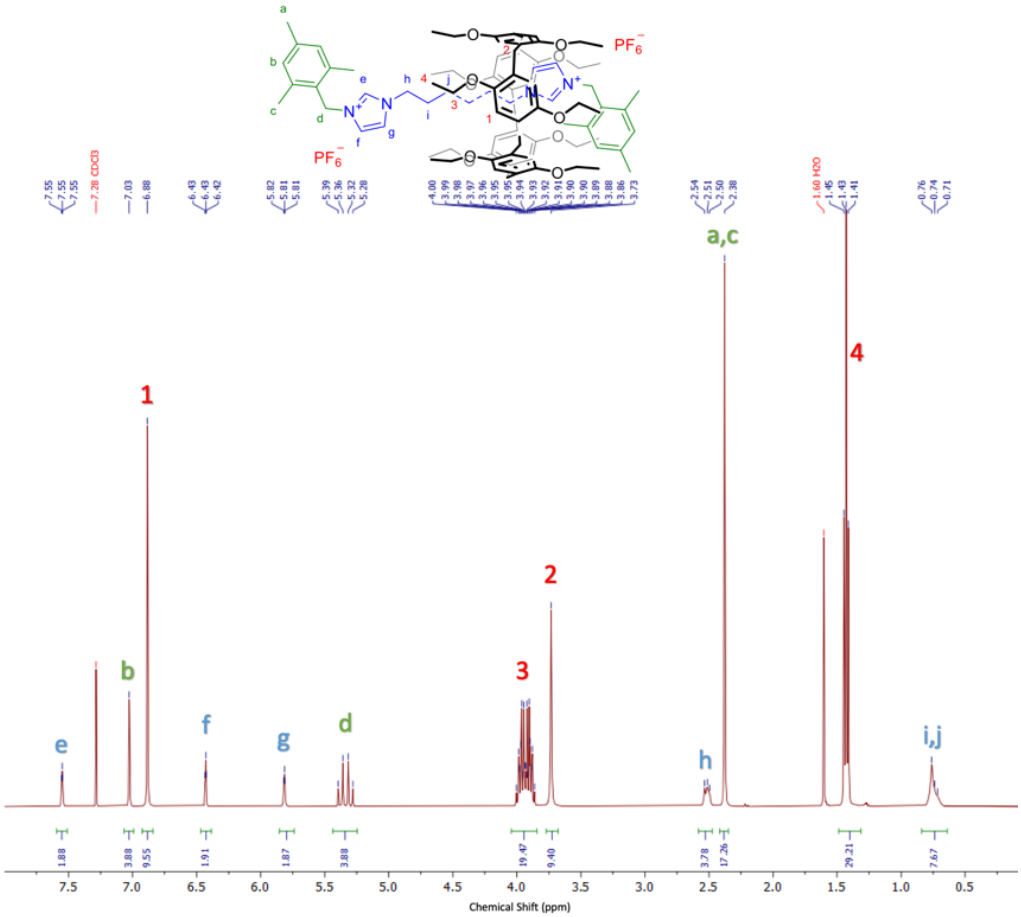

*Figure 7.147. ^{1}H NMR spectrum (400 MHz, $CDCl_3$, 298 K) of **4.20**.*

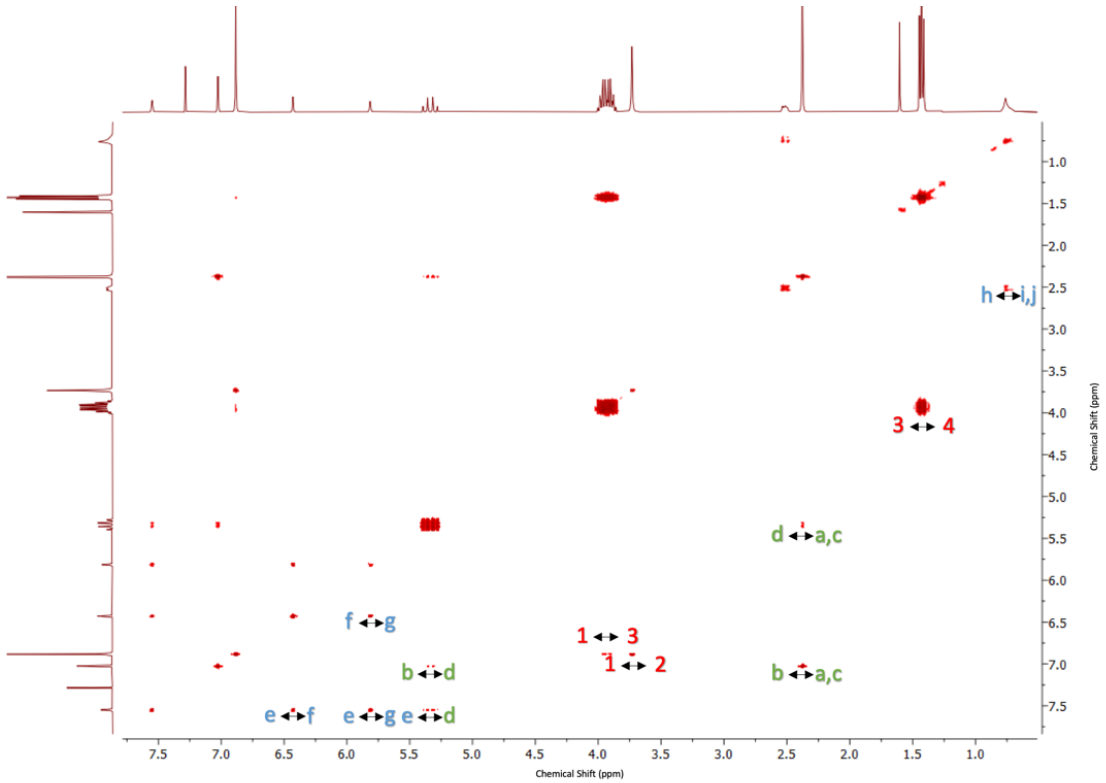

*Figure 7.148. 2D ^{1}H-^{1}H COSY NMR spectrum (400 MHz, $CDCl_3$, 298 K) of **4.20**.*

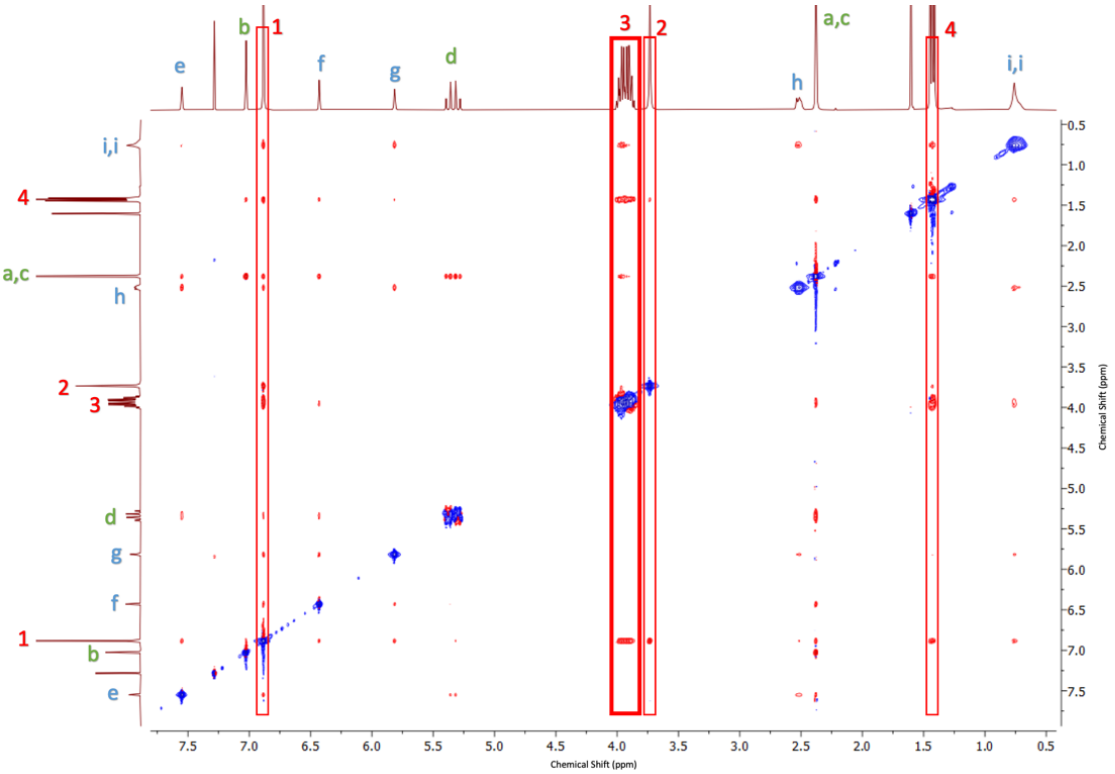

*Figure 7.149. 2D ^{1}H-^{1}H NOESY NMR spectrum (400 MHz, $CDCl_3$, 298 K) of **4.20**.*

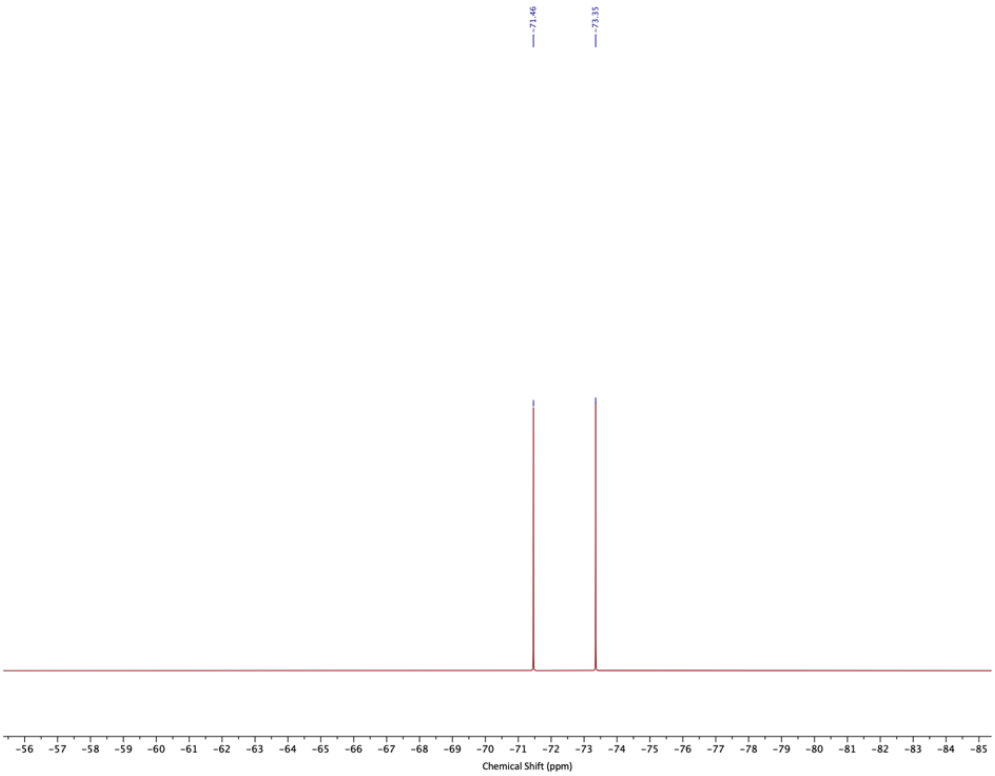

*Figure 7.150. ^{19}F NMR spectrum (376 MHz, $CDCl_3$, 298 K) of **4.20**.*

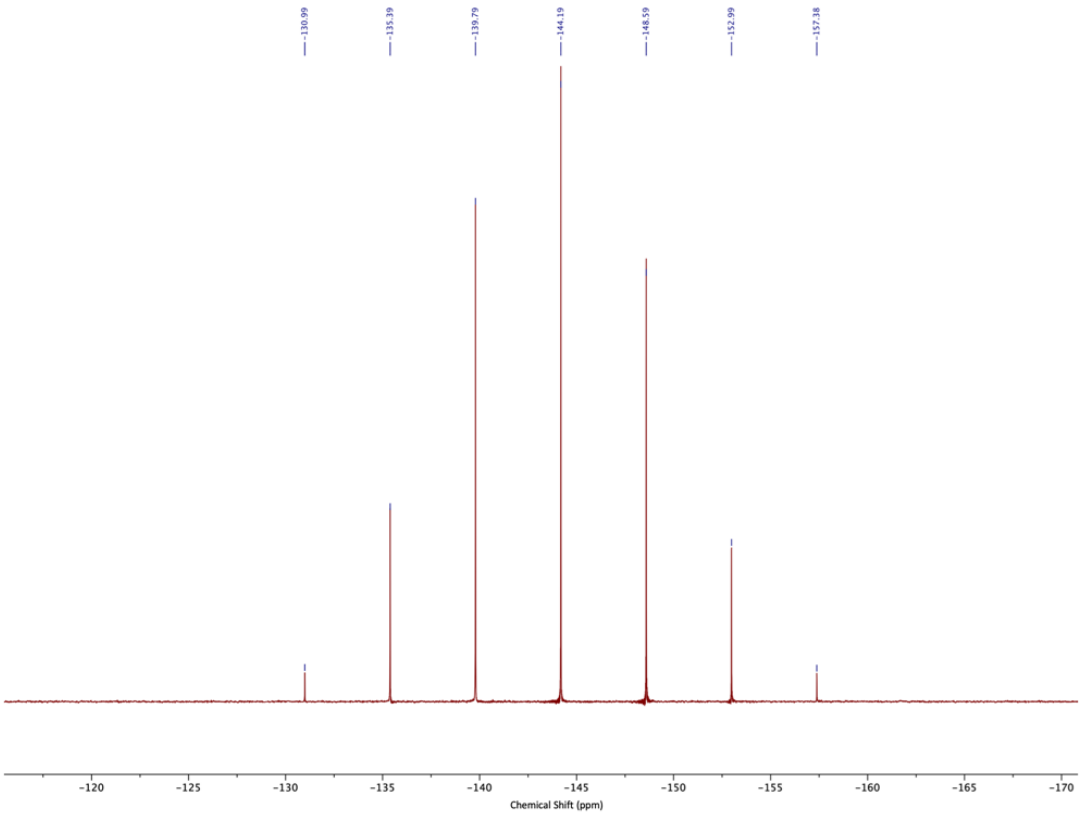

*Figure 7.151. ^{31}P NMR spectrum (162 MHz, $CDCl_3$, 298 K) of **4.20**.*

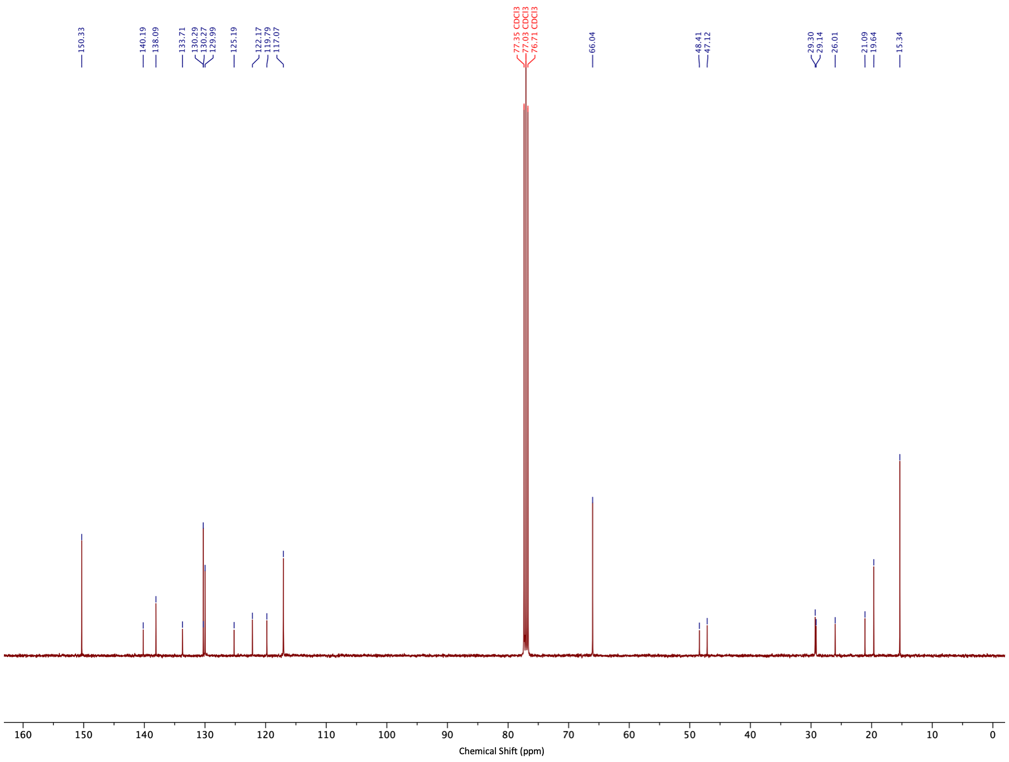

*Figure 7.152. ^{13}C NMR spectrum (101 MHz, $CDCl_3$, 298 K) of **4.20**.*

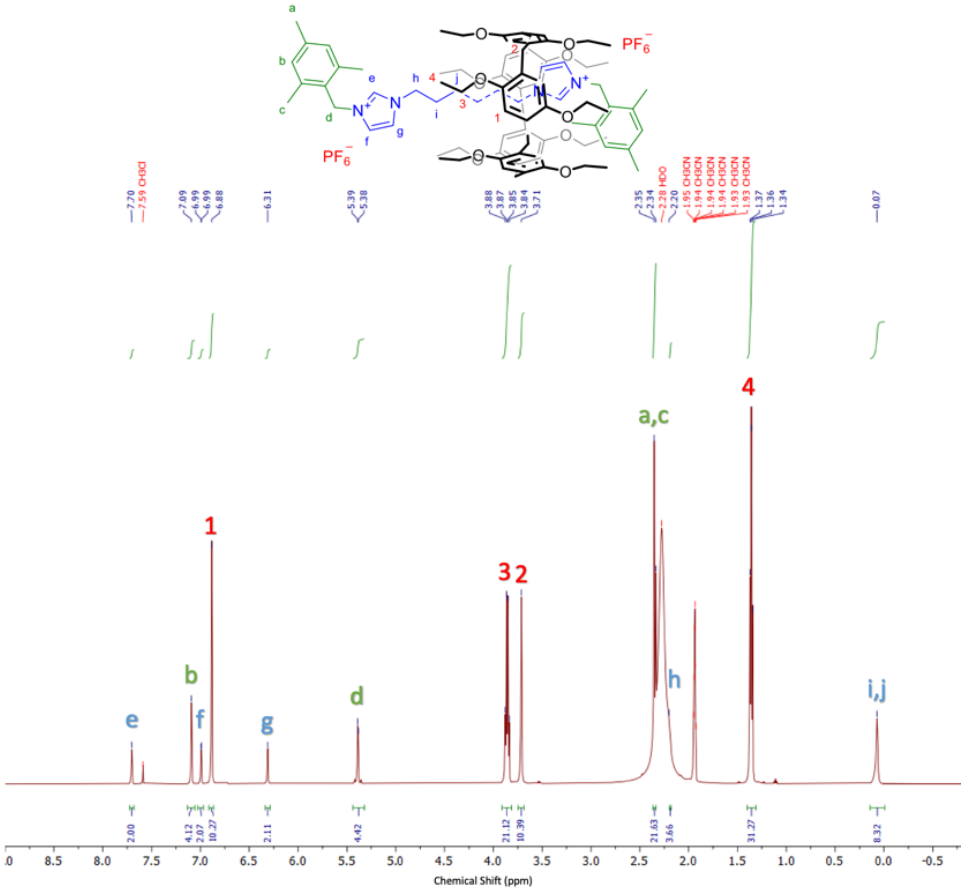

*Figure 7.153. ^{1}H NMR spectrum (400 MHz, CD_3CN, 298 K) of **4.20**.*

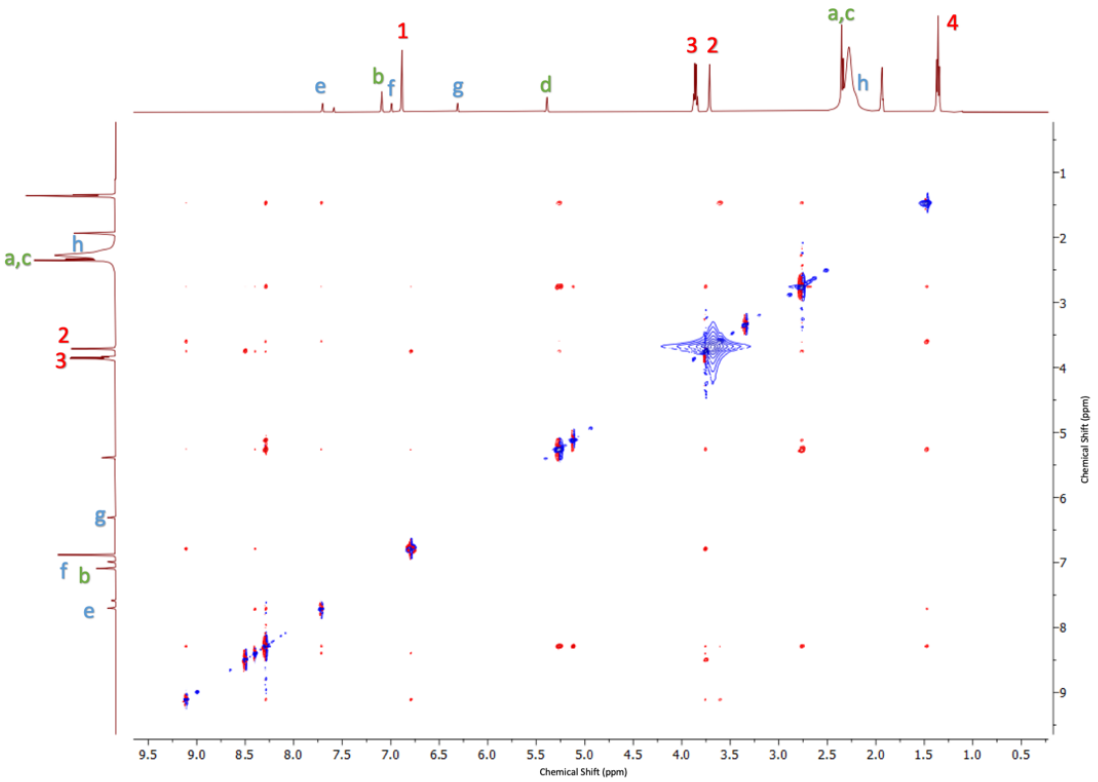

*Figure 7.154. 2D ^{1}H-^{1}H NOESY NMR spectrum (400 MHz, CD_3CN, 298 K) of **4.20**.*

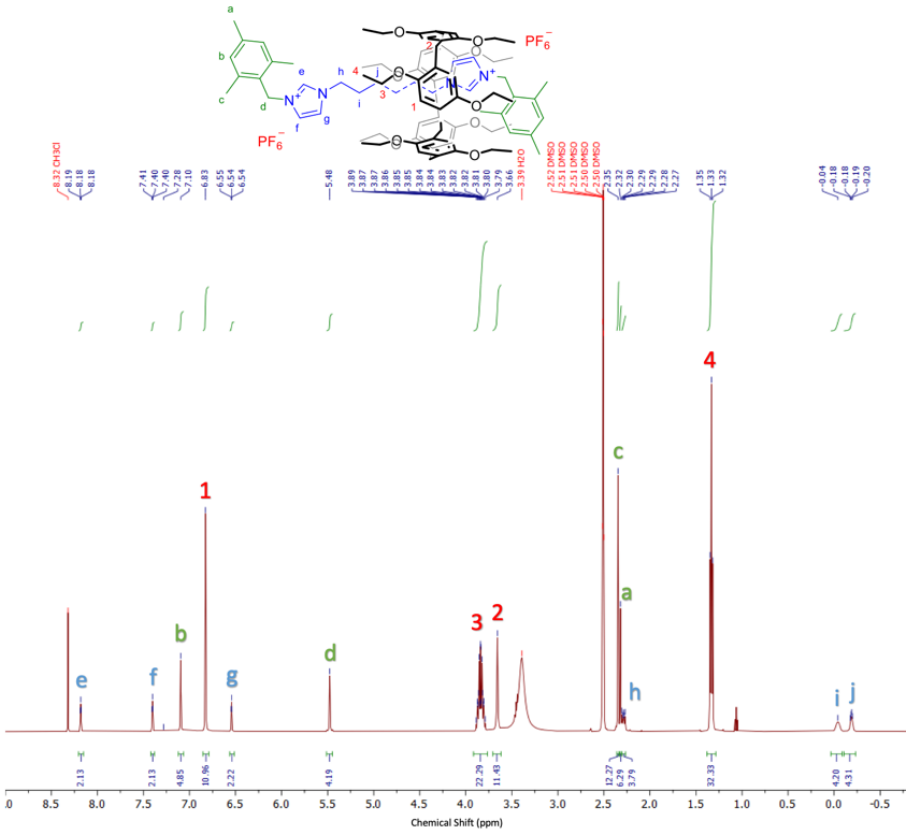

*Figure 7.155. ^{1}H NMR spectrum (400 MHz, DMSO-d_6, 298 K) of **4.20**.*

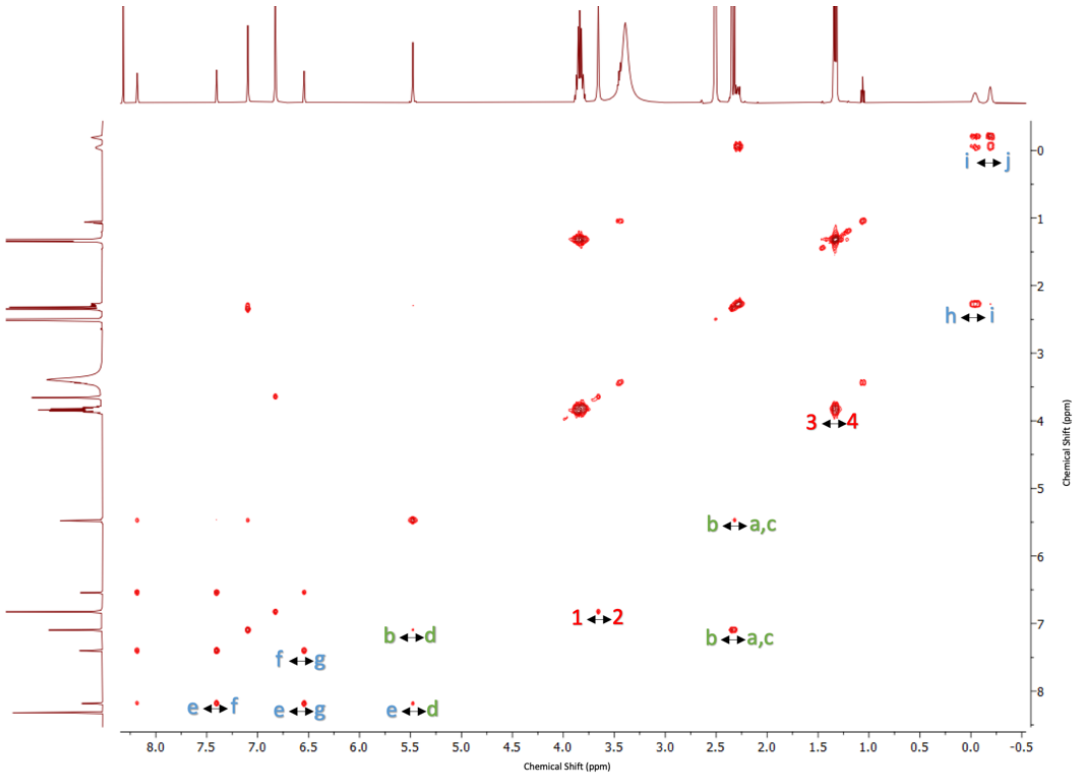

*Figure 7.156. 2D ^{1}H-^{1}H COSY NMR spectrum (400 MHz, DMSO-d_6, 298 K) of **4.20**.*

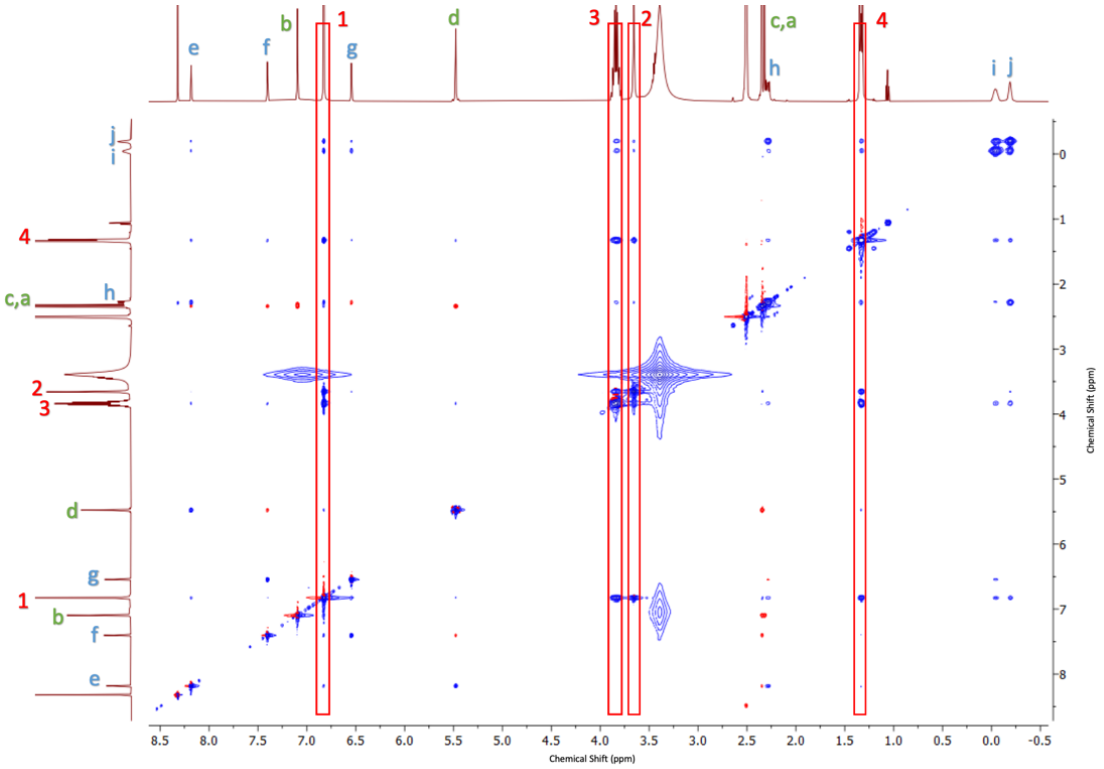

*Figure 7.157. 2D ^{1}H-^{1}H NOESY NMR spectrum (400 MHz, DMSO-d_6, 298 K) of **4.20**.*

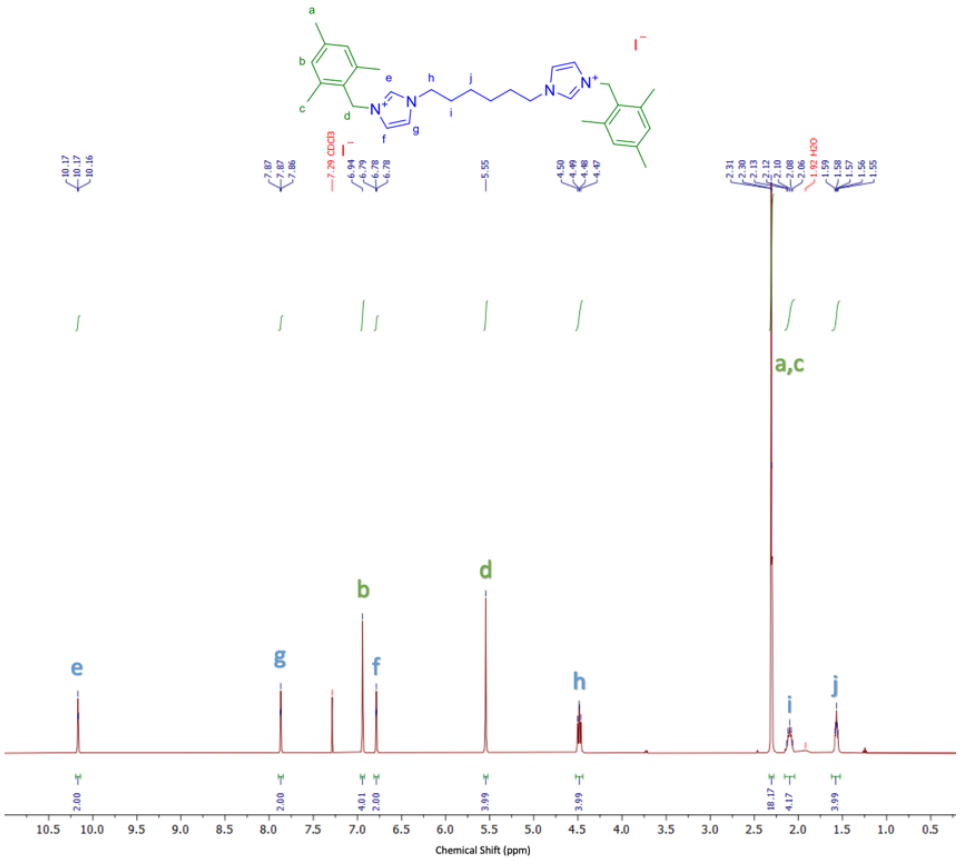

*Figure 7.158. ^{1}H NMR spectrum (400 MHz, $CDCl_3$, 298 K) of **4.21**.*

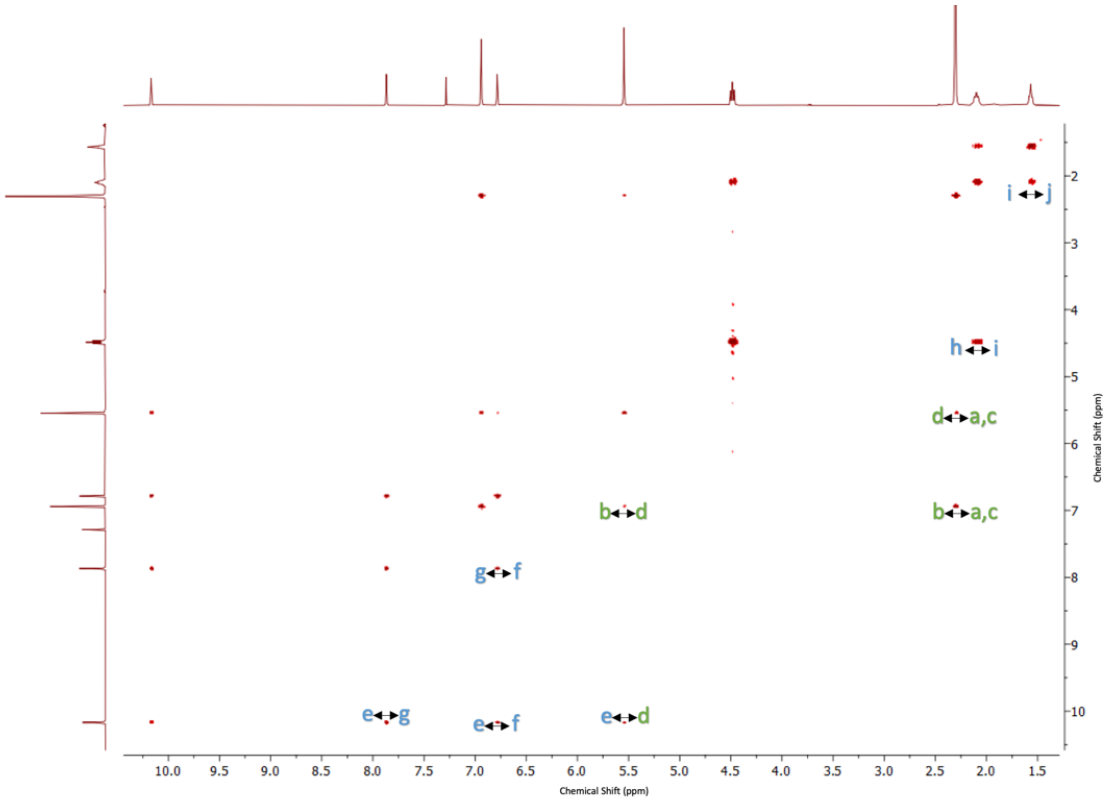

*Figure 7.159. 2D ^{1}H-^{1}H COSY NMR spectrum (400 MHz, $CDCl_3$, 298 K) of **4.21**.*

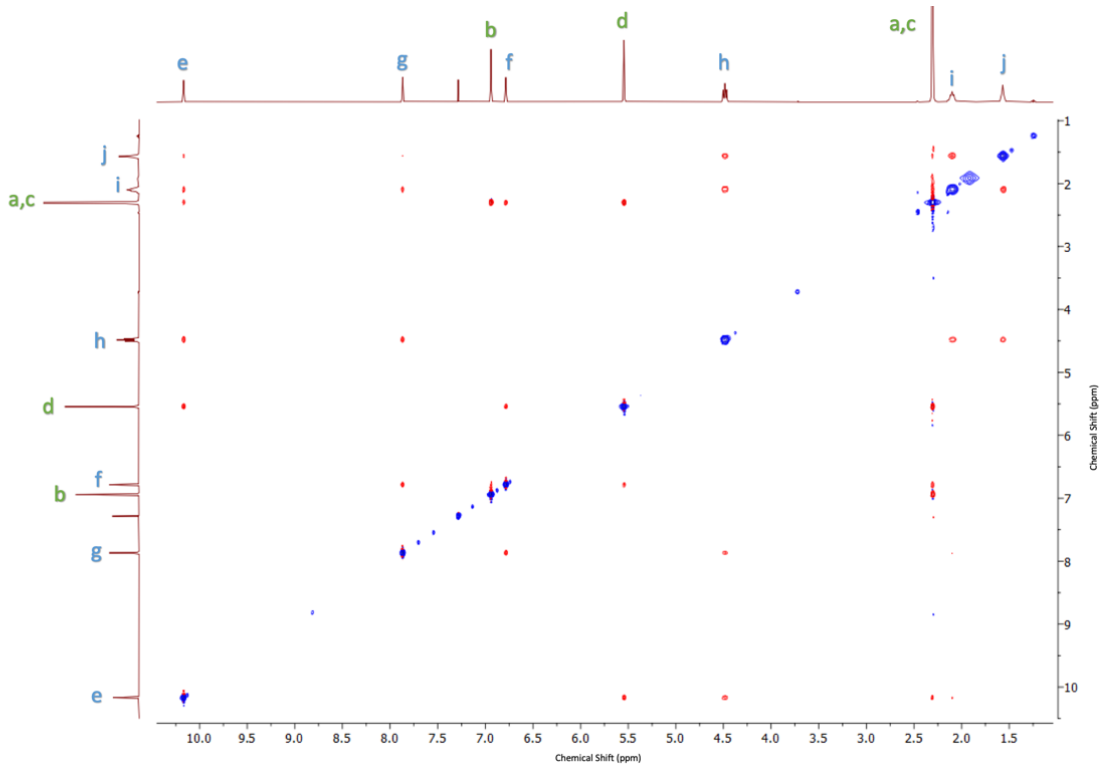

*Figure 7.160. 2D ^{1}H-^{1}H NOESY NMR spectrum (400 MHz, $CDCl_3$, 298 K) of **4.21**.*

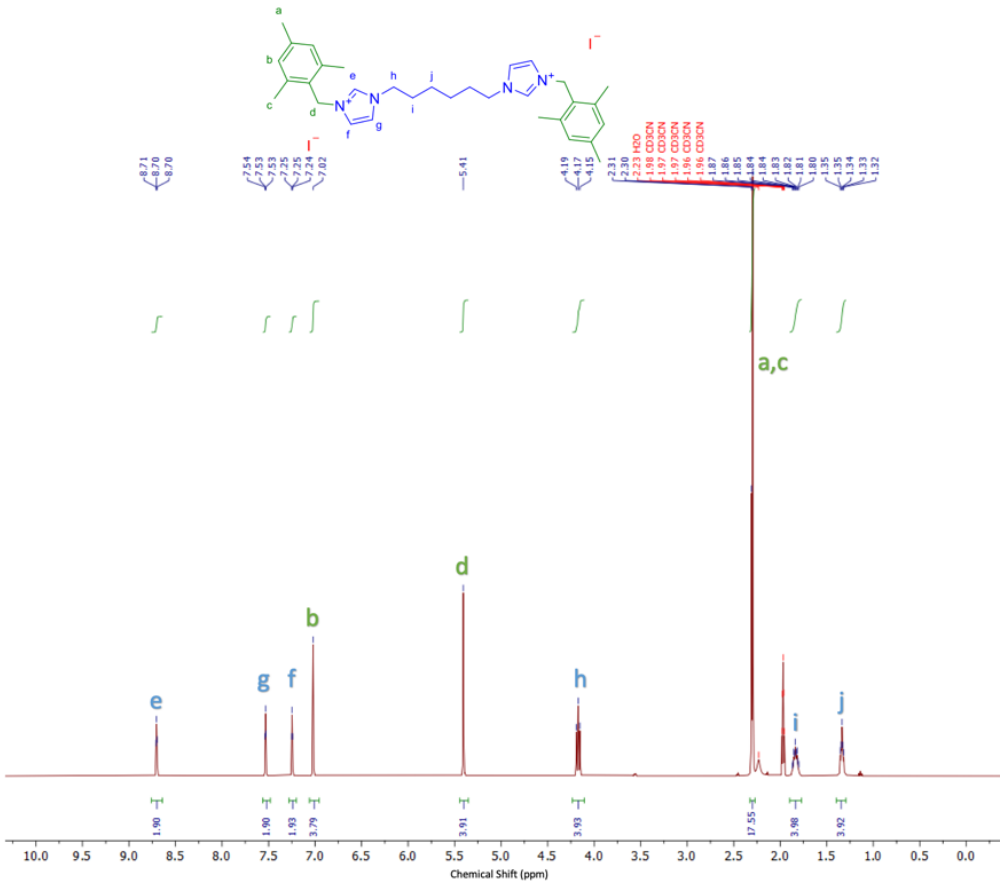

*Figure 7.161. ^{1}H NMR spectrum (400 MHz, CD_3CN, 298 K) of **4.21**.*

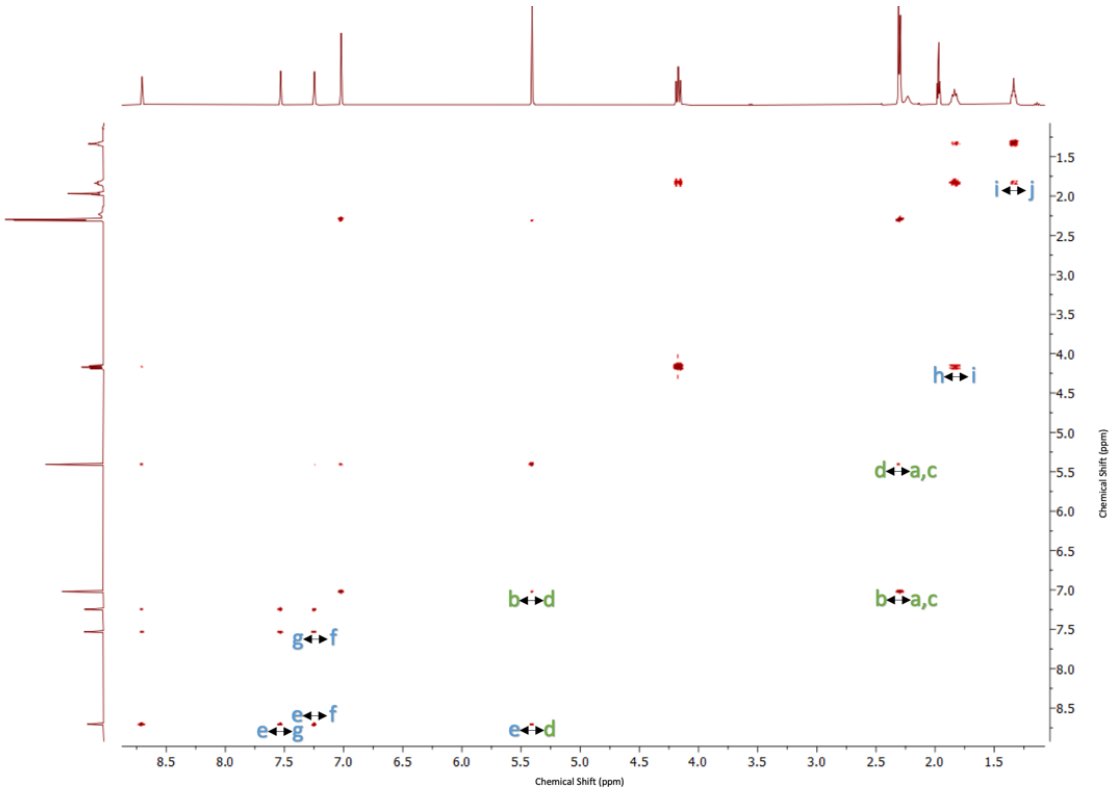

*Figure 7.162. 2D ^{1}H-^{1}H COSY NMR spectrum (400 MHz, CD_3CN, 298 K) of **4.21**.*

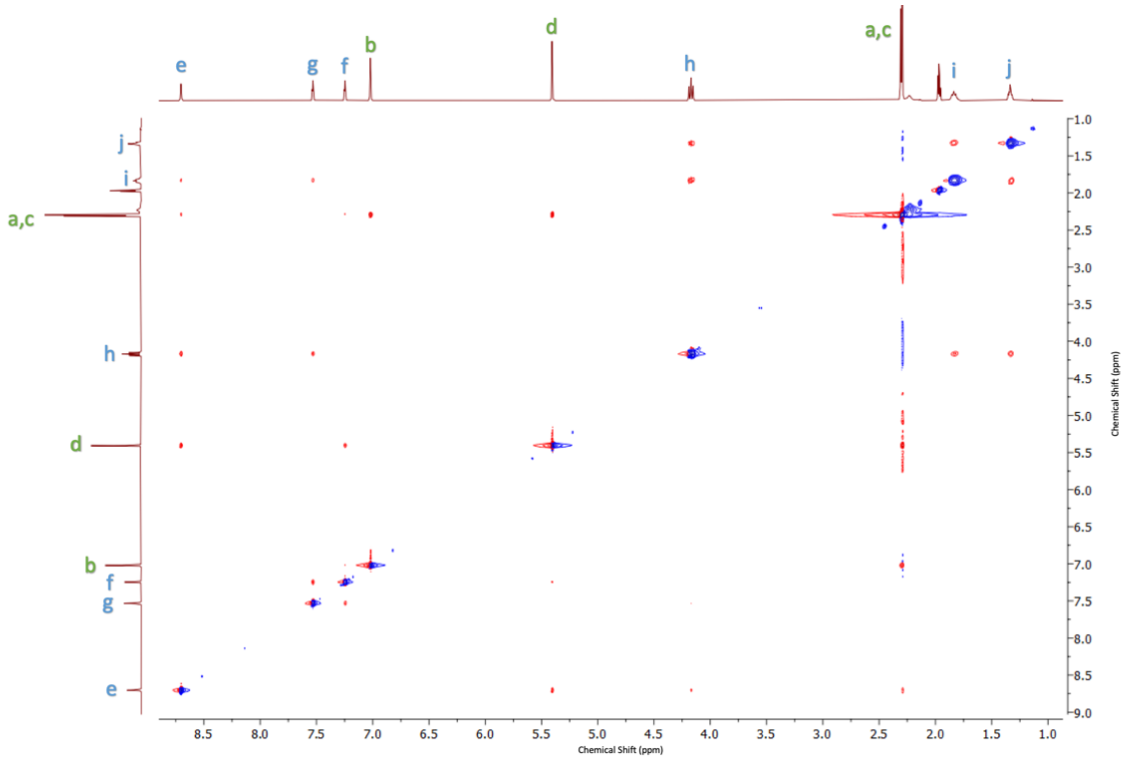

*Figure 7.163. 2D ^{1}H-^{1}H NOESY NMR spectrum (400 MHz, CD_3CN, 298 K) of **4.21**.*

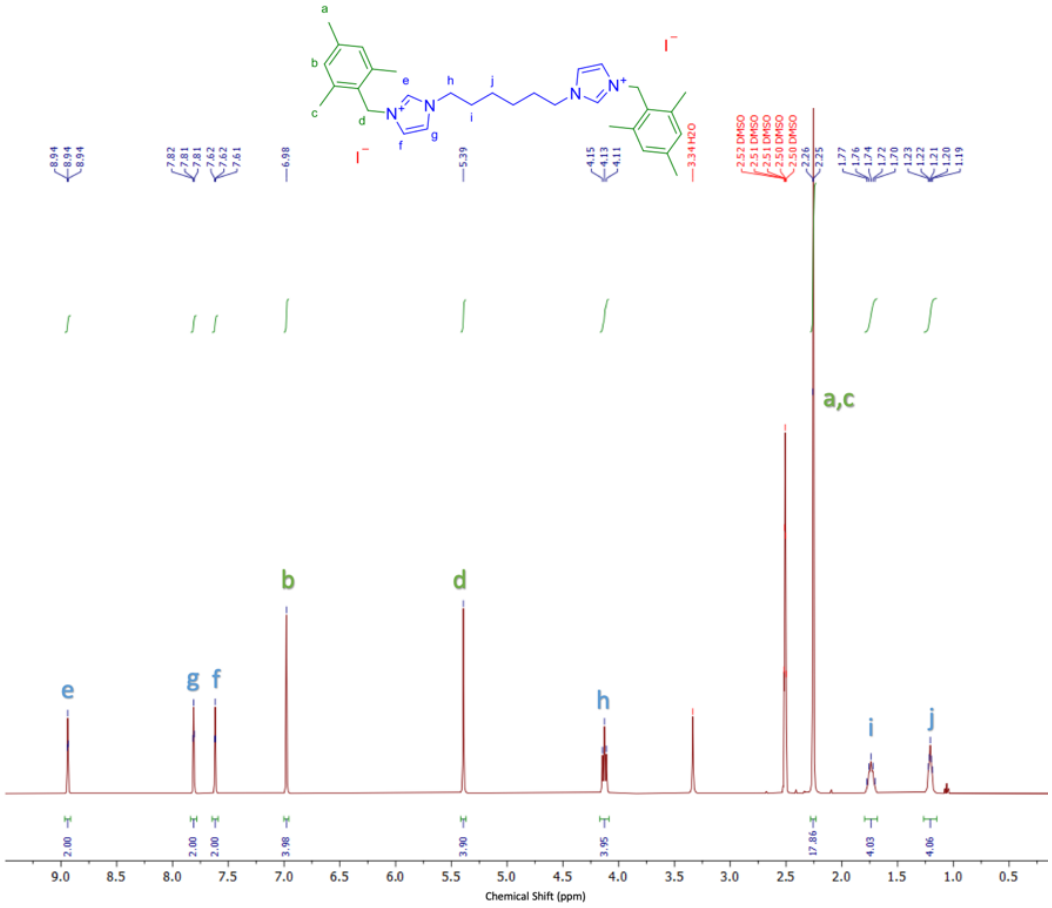

*Figure 7.164. ^{1}H NMR spectrum (400 MHz, DMSO-d_6, 298 K) of **4.21**.*

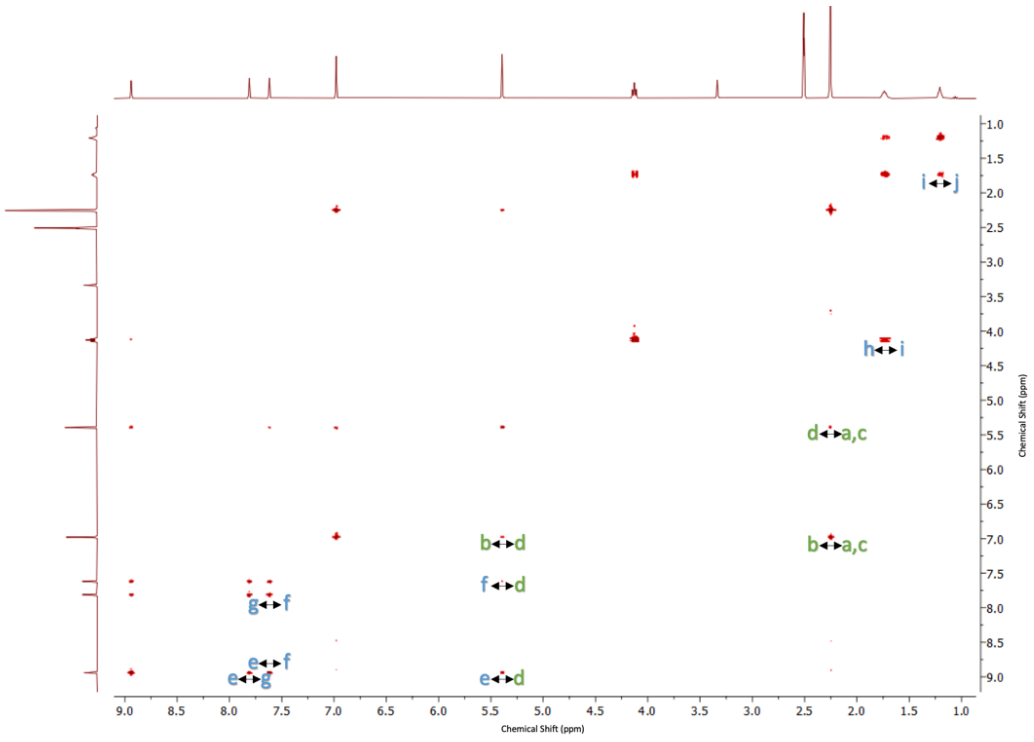

*Figure 7.165. 2D ^{1}H-^{1}H COSY NMR spectrum (400 MHz, DMSO-d_6, 298 K) of **4.21**.*

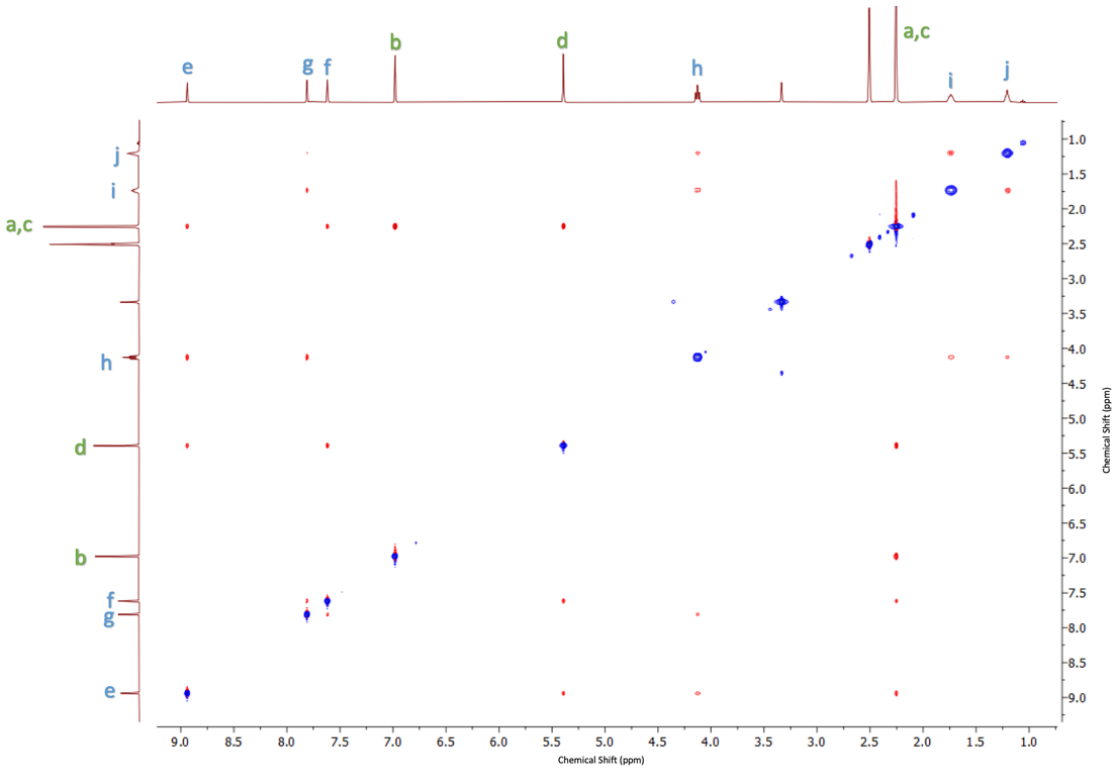

*Figure 7.166. 2D ^{1}H-^{1}H NOESY NMR spectrum (400 MHz, DMSO-d_6, 298 K) of **4.21**.*

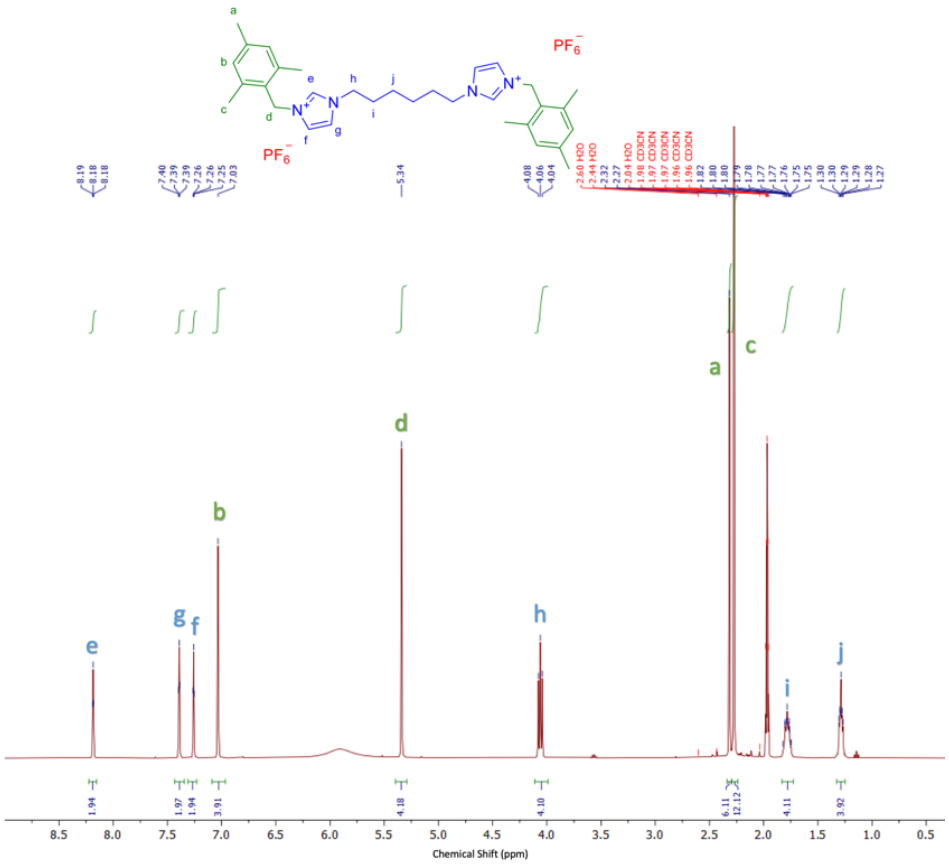

*Figure 7.167. ^{1}H NMR spectrum (400 MHz, CD_3CN, 298 K) of **4.22**.*

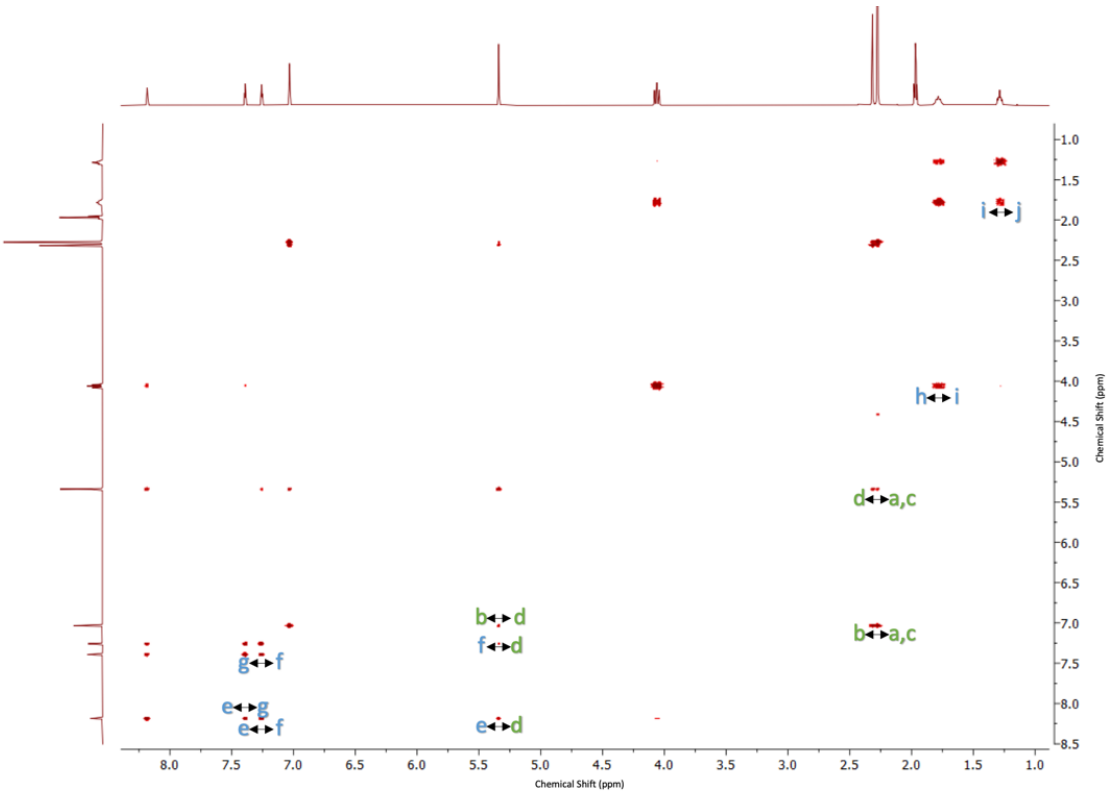

*Figure 7.168. 2D ^{1}H-^{1}H COSY NMR spectrum (400 MHz, CD_3CN, 298 K) of **4.22**.*

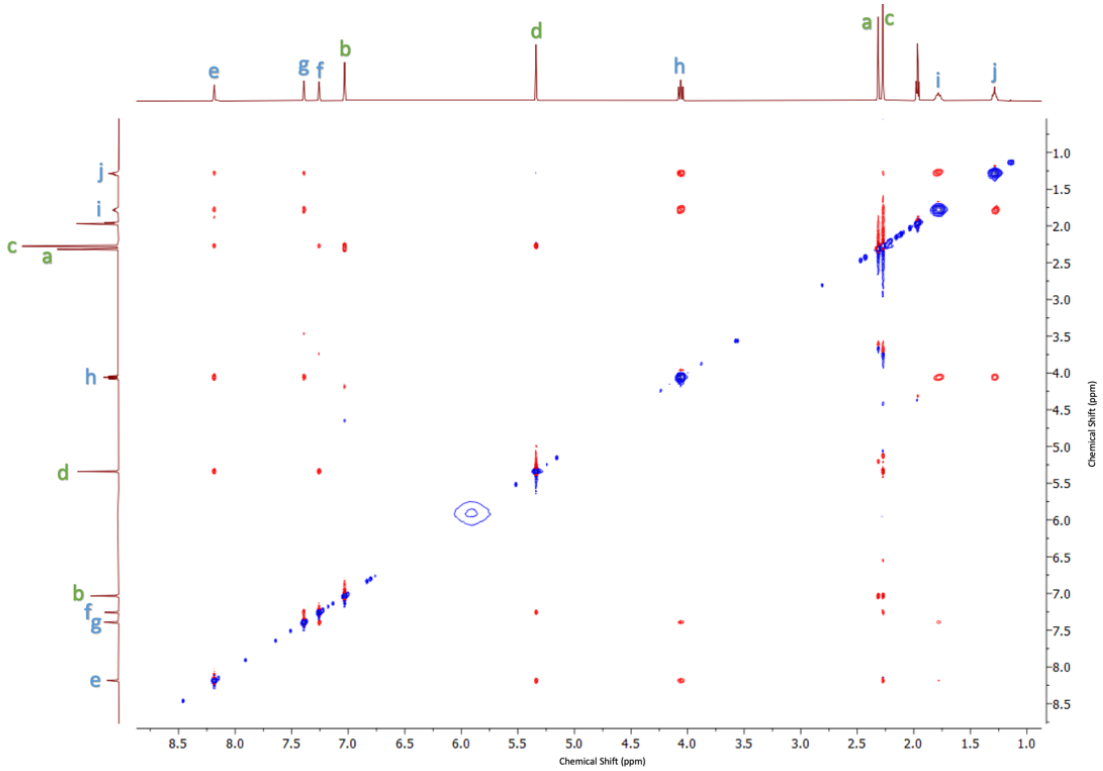

*Figure 7.169. 2D ^{1}H-^{1}H NOESY NMR spectrum (400 MHz, CD_3CN, 298 K) of **4.22**.*

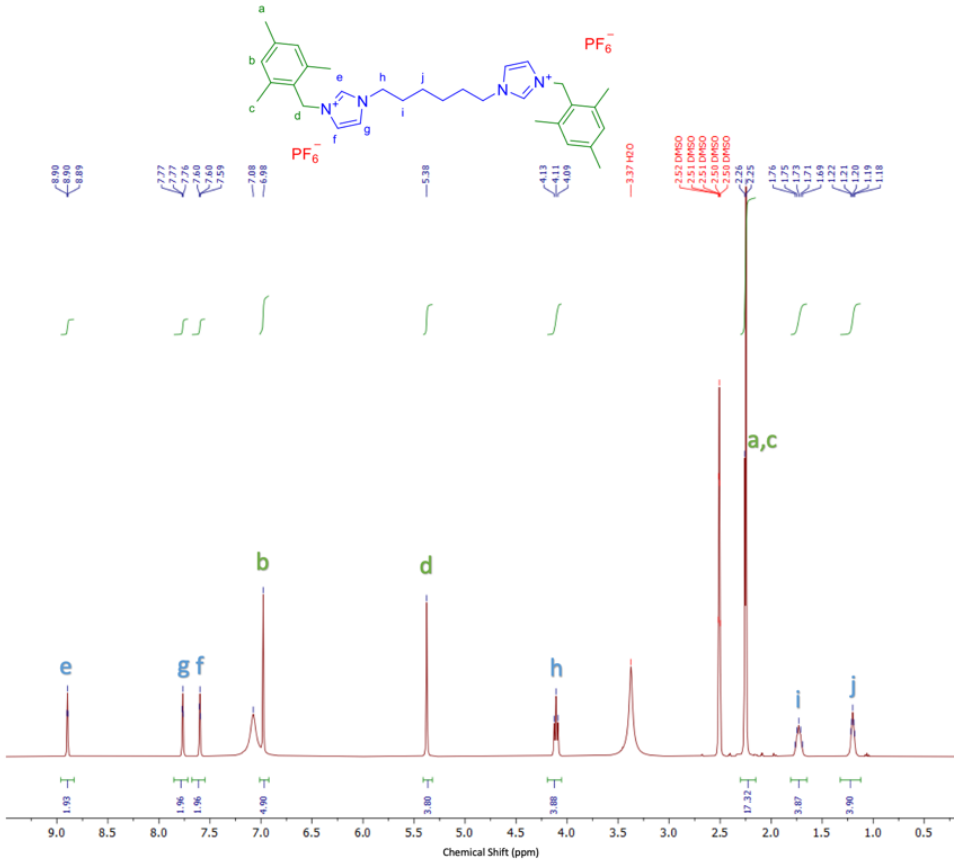

*Figure 7.170. ^{1}H NMR spectrum (400 MHz, DMSO-d_6, 298 K) of **4.22**.*

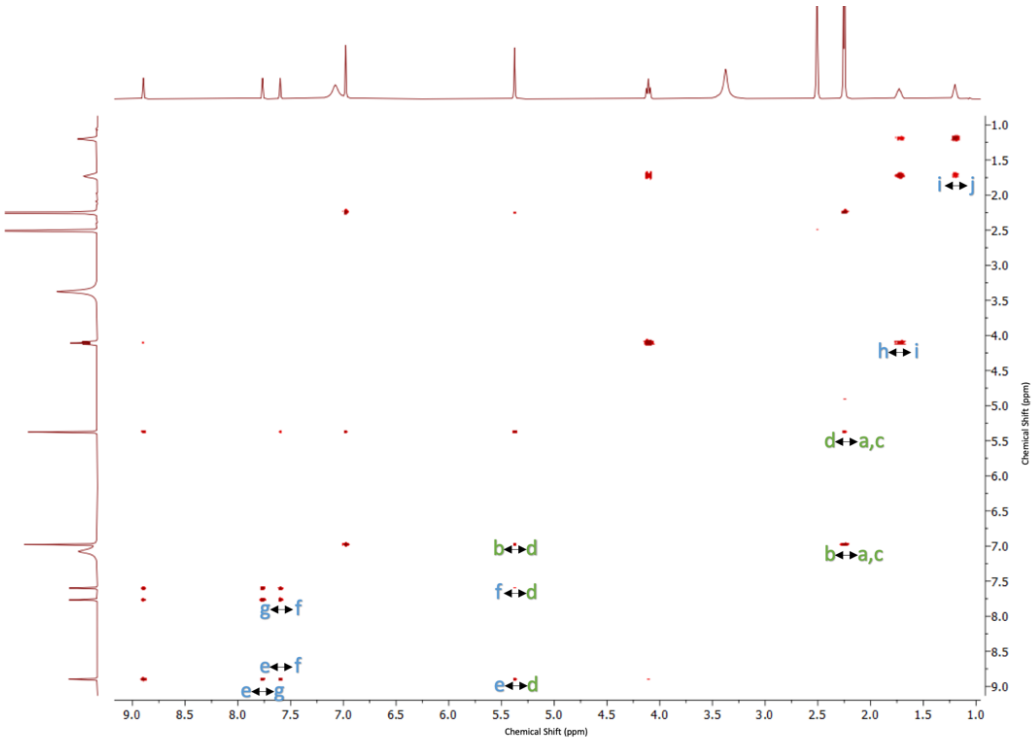

*Figure 7.171. 2D ^{1}H-^{1}H COSY NMR spectrum (400 MHz, DMSO-d_6, 298 K) of **4.22**.*

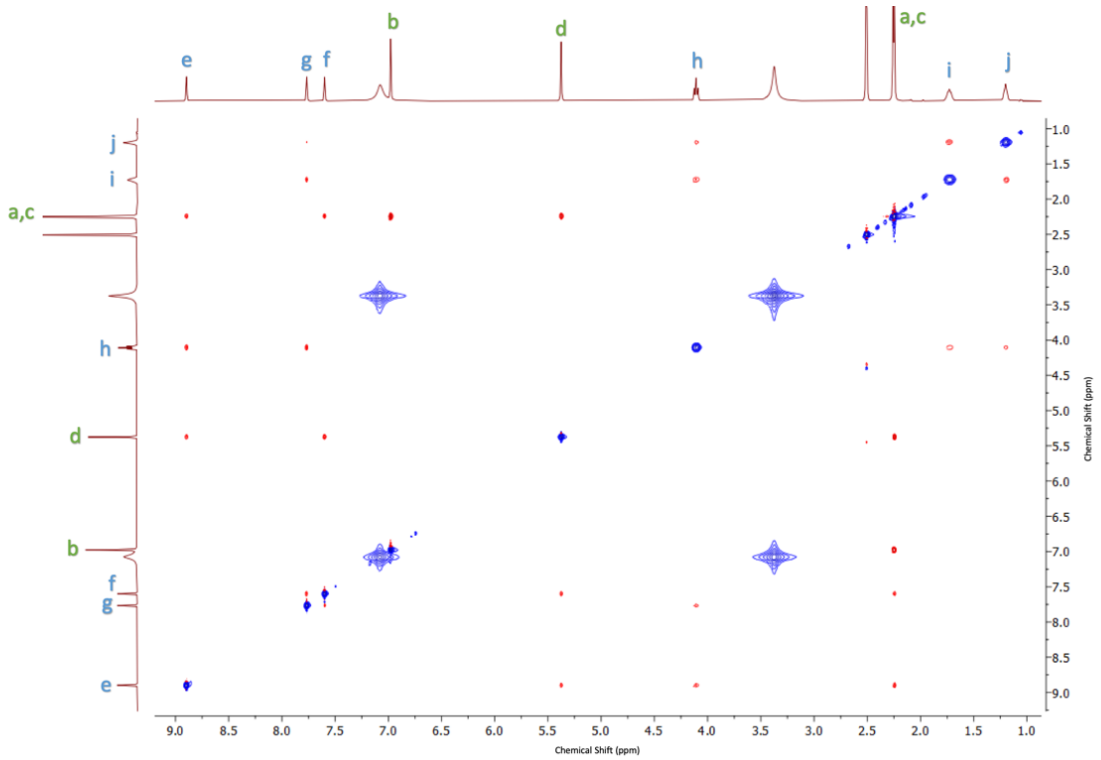

*Figure 7.172. 2D ^{1}H-^{1}H NOESY NMR spectrum (400 MHz, DMSO-d_6, 298 K) of **4.22**.*

7.2 Mass spectrometry

Mass spectrum after stopper **4.5** and axle **4.2** were refluxed in acetonitrile overnight.

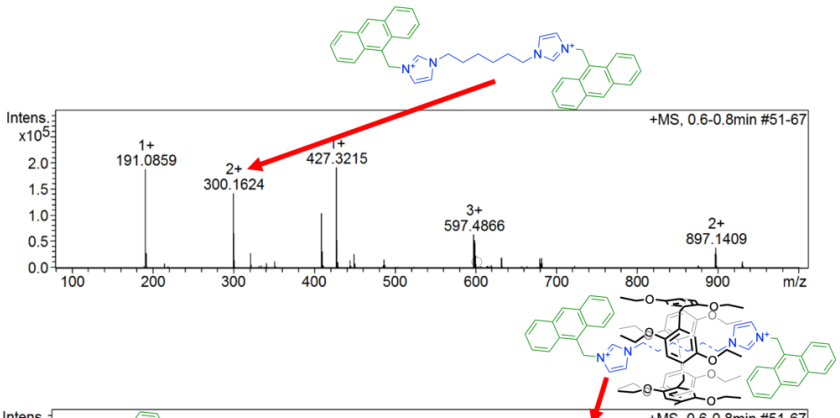

Mass spectrum of reaction mixture of stopper **4.5**, DEP5A **2.7** and axle **4.2** in chloroform at room temperature after 72 hours.

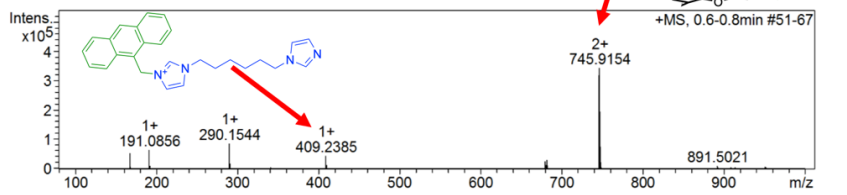

*Figure 7.173. ESI-Mass spectra of (above) reaction mixture after **4.5** and **4.2** had refluxed overnight in acetonitrile and (below) the reaction mixture after **4.5**, **4.2** and **2.7** had reacted for 72 hours in chloroform at room temperature.*

7.3 UV/vis absorption spectroscopy

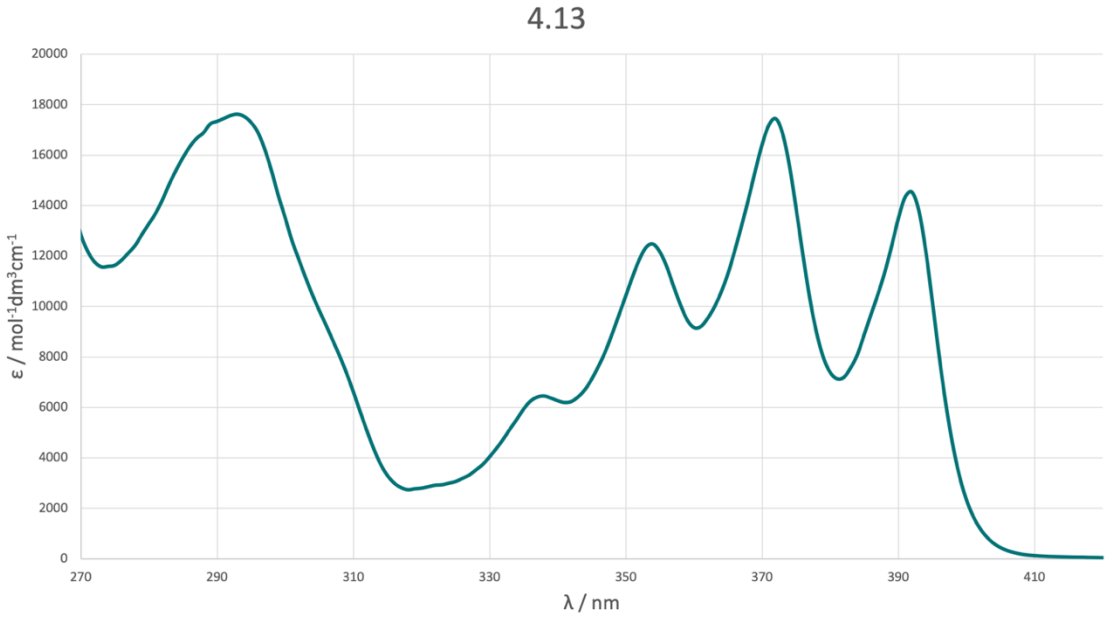

*Figure 7.174. UV/vis absorption spectrum of **4.13** in DCM where the concentration is 4.9 x 10^{-5} mol dm^{-3}.*

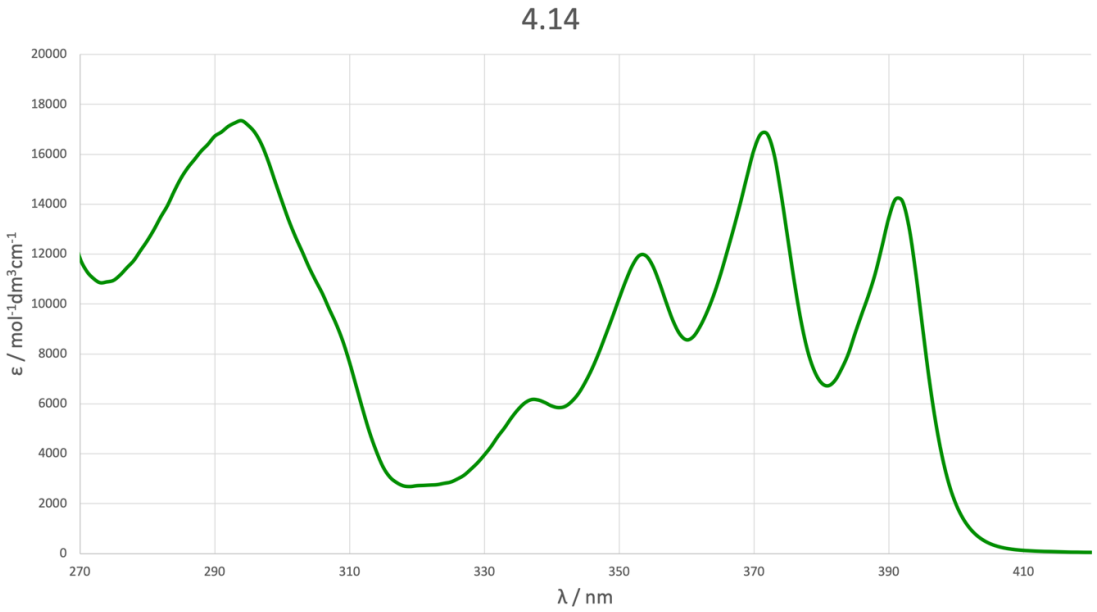

*Figure 7.175. UV/vis absorption spectrum of **4.14** in DCM where the concentration is 5.1 x 10^{-5} mol dm^{-3}.*

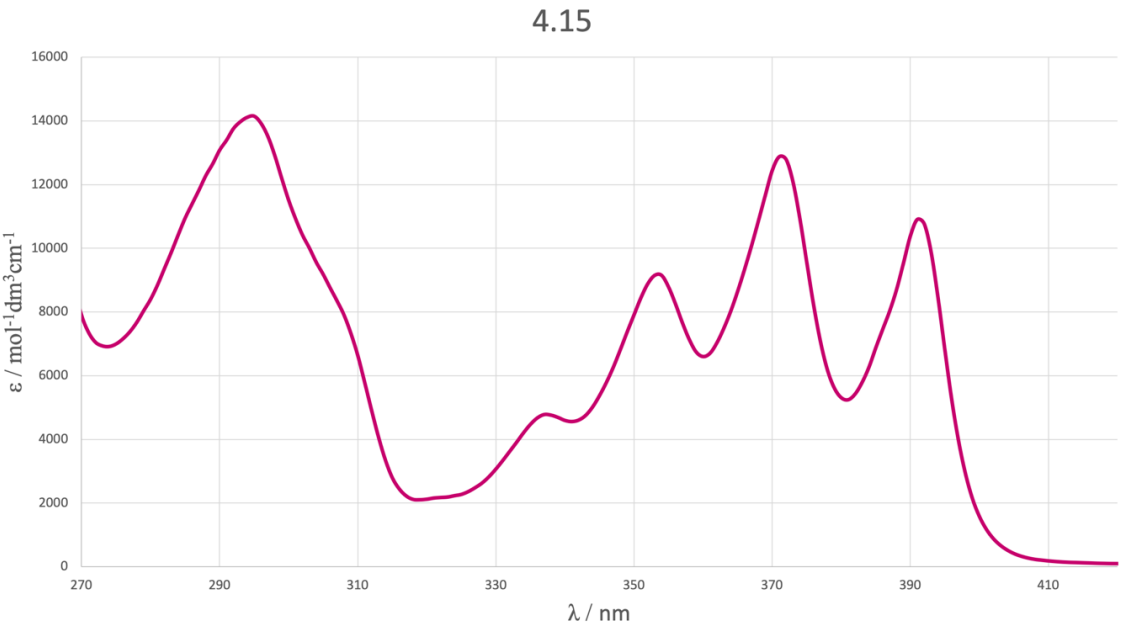

*Figure 7.176. UV/vis absorption spectrum of **4.15** in DCM where the concentration is 6.4 x 10^{-5} mol dm^{-3}.*

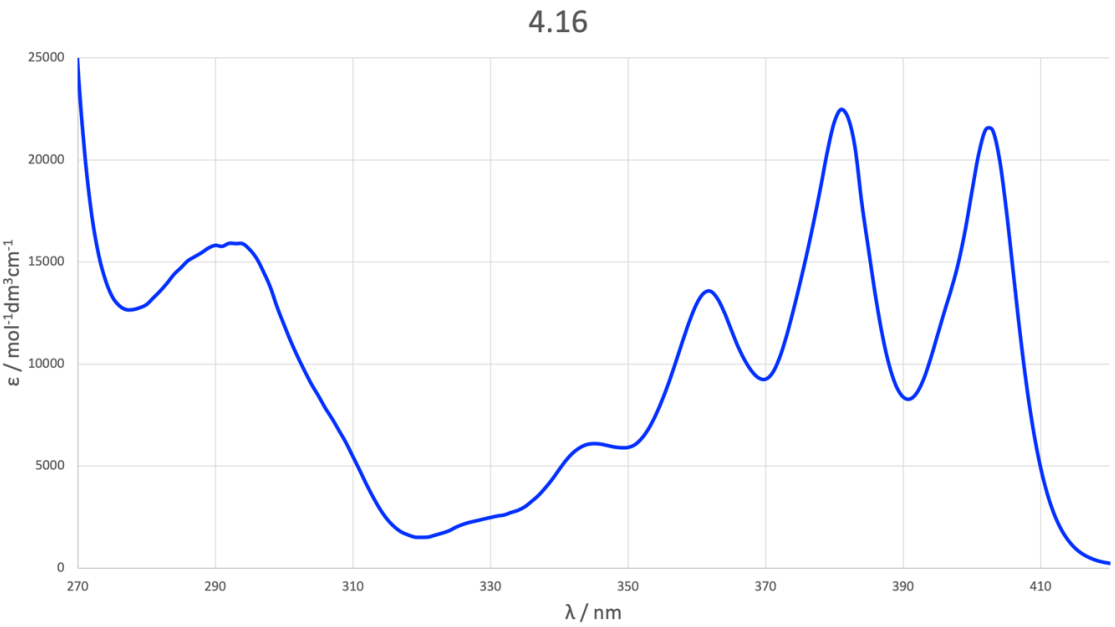

*Figure 7.177. UV/vis absorption spectrum of **4.16** in DCM where the concentration is 4.2 x 10^{-5} mol dm^{-3}.*

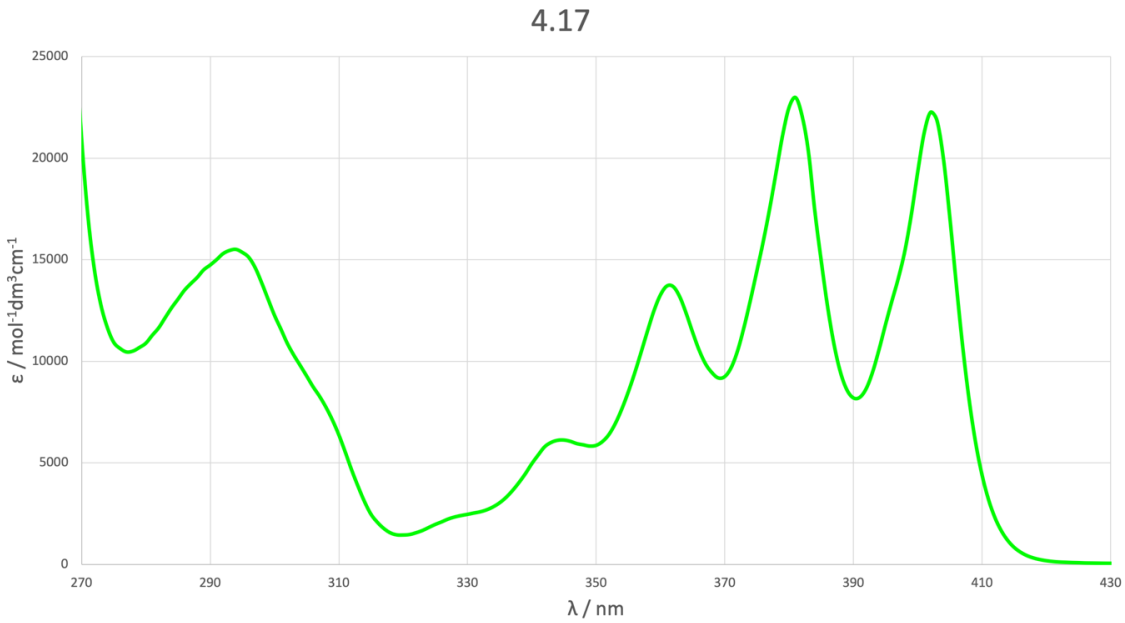

*Figure 7.178. UV/vis absorption spectrum of **4.17** in DCM where the concentration is 3.8 x 10^{-5} mol dm^{-3}.*

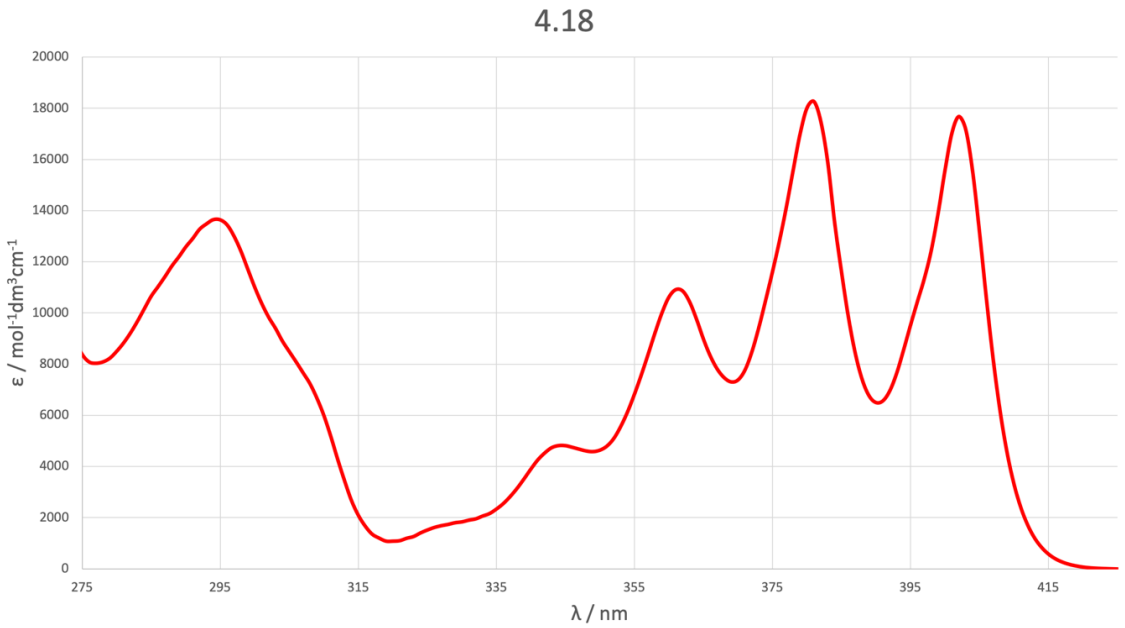

*Figure 7.179. UV/vis absorption spectrum of **4.18** in DCM where the concentration is 5.1 x 10^{-5} mol dm^{-3}.*

7.4 X-Ray crystallography

4.8 – OAPALF

4.11 – OAPALG

4.10 – OAPALI

4.9 – OAPALJ

2.13 - OAPALL